THE HYDROGEN BOND / I

Recent developments in theory and experiments

THEORY

Edited by
P. Schuster, G. Zundel
and C. Sandorfy

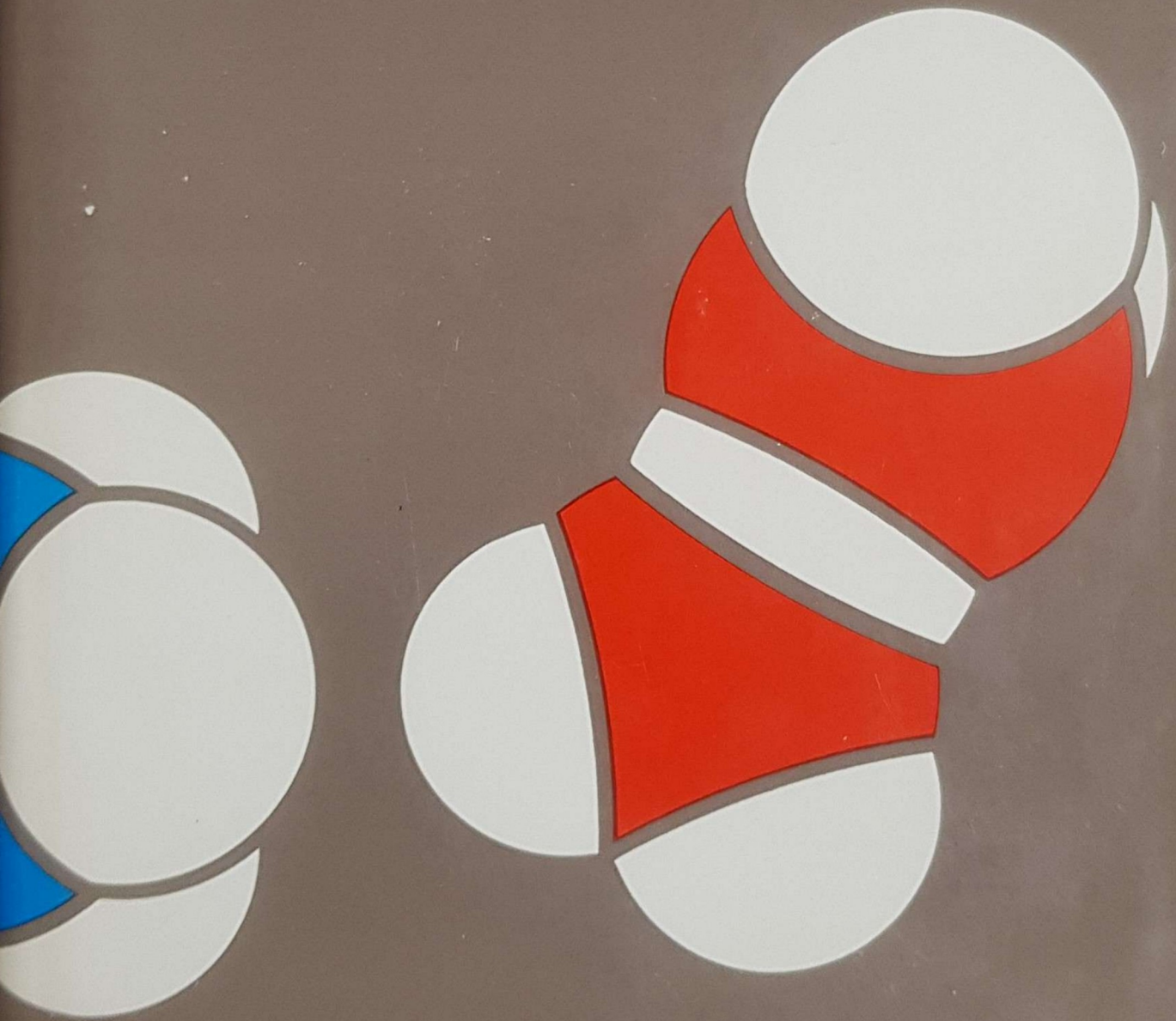

NORTH-HOLLAND

ISBN 0-7204-0315-4

THE HYDROGEN BOND
RECENT DEVELOPMENTS IN THEORY AND EXPERIMENTS
(in 3 volumes)
edited by P. SCHUSTER, G. ZUNDEL *and* C. SANDORFY

The past decade has seen a massive increase in the amount of data on hydrogen bonding. This three-volume work provides, for the first time, a truly comprehensive survey of the field, comprising hitherto unpublished original work, together with relevant material previously scattered throughout the literature. As no successful summary can be expected from any one scientist in this broad field, the twenty-nine chapters contained in this work are each written by a specialist in the particular discipline. Collectively, they cover the various approaches towards an understanding of hydrogen bonds.

Volume I - Theory contains an introduction and six chapters reflecting the present stage of theory. Starting from energy surfaces of hydrogen bonds, calculations of vibrational spectra, proton motion, dynamics of proton networks and hydrogen bond statistics are treated extensively.

In **Volume II - Structure and Spectroscopy,** experimental results on structure and stereochemistry of hydrogen bonds in crystals and liquids are described. Five chapters provide detailed insight into the current state of infrared and long wave length vibrational spectroscopy. Nuclear magnetic resonance studies are reported, especially results obtained from solids.

Volume III - Dynamics, Thermodynamics and Special Systems presents a survey of experimental results on hydrogen bond dynamics as studied by incoherent neutron scattering, dielectric methods, spin-lattice and chemical relaxation techniques. Two chapters deal with hydrogen bonded ferroelectrics and the subsequent contributions report thermodynamic results and their correlation with spectral data. The other chapters present results on hydrogen bonding in surface chemistry, water and ice, as well as in studies by the matrix isolation technique.

"The Hydrogen Bond" constitutes a valuable and up-to-date source of information and will be of interest to those concerned with all fields of molecular science.

The Hydrogen Bond

The Hydrogen Bond

Recent developments in theory and experiments

I. Theory

Экз. чит. зала

P. Schuster
Institut für Theoretische Chemie und Strahlenchemie der Universität Wien

G. Zundel
Institut für Physikalische Chemie der Universität München

C. Sandorfy
Département de chimie, Université de Montréal

1407-in
ЦНИИБ
БИБЛИОТЕКА

1976

NORTH-HOLLAND PUBLISHING COMPANY
AMSTERDAM · NEW YORK · OXFORD

© North-Holland Publishing Company - 1976.
All rights reserved. No part of this publication may be reproduced, stored in a retrieval system, or transmitted, in any form of by any means, electronic, mechanical, photocopying, recording or otherwise, without the prior permission of the copyright owner.

North-Holland ISBN: 0 7204 0315 4
American Elsevier ISBN: 0 444 10805 X

Published by:

North-Holland Publishing Company - Amsterdam, New York, Oxford

Sole distributors for the U.S.A. and Canada:

American Elsevier Publishing Company, Inc.
52 Vanderbilt Avenue
New York, N.Y. 10017

PRINTED IN THE NETHERLANDS

EDITORS' PREFACE

The methods and techniques applied to studies of hydrogen bonding have reached a high degree of refinement and specialization and have branched into a variety of different fields. Consequently it has become almost impossible for an individual or a small group of scientists to give a comprehensive and detailed review on this subject. Fifteen years ago, Pimentel and McClellan covered all the material that was then available. In the series of volumes we present, almost forty scientists contribute their most recent results and ideas in their own fields, surveying the present stage of knowledge on the nature and properties of the hydrogen bond.

One of the editors' aims was to combine findings and views of experimentalists and theoreticians. Whereas only modest advance could be made towards a unified theory covering all of the interesting aspects and the various results in this widespread field, we hope that the treatise presented will initiate and encourage discussions and cooperation between scientists working in the various fields.

The Reader familiar with the subject, will probably notice the absence of two of the many important and promising approaches. Both of these fields are developing extremely fast and we therefore felt that at this time it would be inappropriate to prepare an extensive survey on these. We are referring to hydrogen bonding in excited states and to the application of relaxation kinetics to hydrogen bond systems which have been covered only briefly.

Our present volumes do not include investigations with a strong tie-in to biology. On the one hand, interpretation of experimental facts is often very difficult in molecular biophysics and, further, at the present time views are changing much faster than in other fields. On the other hand, an impressive amount of important material has been already accumulated on hydrogen bonds in biology, in sufficient quantity as to be presented in a separate volume.

Wien/München/Montréal,
September 1975

P. Schuster
G. Zundel
C. Sandorfy

CONTENTS

Preface v

Volume I. Theory

Ch. 1. Introduction, E. Lippert 1

PART A. THEORY OF THE HYDROGEN BOND 23

Ch. 2. Energy surfaces for hydrogen bonded systems, P. Schuster. 25
Ch. 3. Calculated vibrational spectra of hydrogen bonded systems, P. Janoschek 165
Ch. 4. Proton motions in hydrogen bonds, J. Brickmann . . 217
Ch. 5. Model studies on proton correlations in hydrogen bonds, E. Weidemann 245
Ch. 6. Dynamical properties of hydrogen bonded systems, G.L. Hofacker, Y. Maréchal and M. Ratner 295
Ch. 7. Hydrogen bond statistics, J.W. Perram. 359

Volume II. Structure and spectroscopy

PART B. INVESTIGATIONS ON STRUCTURE AND STEREOCHEMISTRY. . 391

Ch. 8. X-Ray and neutron diffraction studies of hydrogen bonded systems, I. Olovsson and P.-G. Jönsson . . . 393
Ch. 9. Neutron diffraction studies of hydrogen bonding in α-amino acids, Th.F. Koetzle and M.S. Lehmann . . 457
Ch. 10. The hydrated proton in solids, J.-O. Lundgren and I. Olovsson 471
Ch. 11. The angular dependence of hydrogen bond interactions, W.A.P. Luck 527

PART C. VIBRATIONAL AND RESONANCE SPECTROSCOPIC STUDIES. . 563

Ch. 12. Vibrational spectroscopy of the hydrogen bond, D. Hadži and S. Bratos 565

Ch. 13. Anharmonicity and hydrogen bonding, C. Sandorfy . 613
Ch. 14. Spectroscopic studies of hydrated proton species, $H^+(H_2O)_n$, in crystalline compounds, J.M. Williams . 655
Ch. 15. Easily polarizable hydrogen bonds – Their interactions with the environment – IR continuum and anomalous large proton conductivity, G. Zundel . . 683
Ch. 16. Long wave length vibrational spectroscopy of hydrogen bonding, W.G. Rothschild 767
Ch. 17. High resolution nuclear magnetic resonance studies of hydrogen bonding, E.E. Tucker and E. Lippert . . . 791
Ch. 18. Magnetic resonance studies of hydrogen bonding in solids, R. Blinc 831

Volume III. Dynamics, thermodynamics and special systems

PART D. DYNAMICS OF HYDROGEN BONDED SYSTEMS 889

Ch. 19. Incoherent neutron scattering experiments on hydrogen bonded systems, J.A. Janik 891
Ch. 20. Dielectric properties of hydrogen bonded systems, L. Sobczyk, H. Engelhardt and K. Bunzl 937
Ch. 21. Nuclear magnetic relaxation in hydrogen bonded liquids, H.G. Hertz and M.D. Zeidler 1027

PART E. MATRIX ISOLATION TECHNIQUE 1063

Ch. 22. Matrix-isolation studies of hydrogen bonding, H.E. Hallam 1065

PART F. INVESTIGATIONS ON FERROELECTRICS WITH HYDROGEN BONDS 1107

Ch. 23. Ferroelectric hydrogen bonded systems, V.H. Schmidt. 1109
Ch. 24. Coherent neutron scattering for observations on collective proton motions in systems of hydrogen bonds, H. Stiller 1169

PART G. THERMODYNAMICS OF HYDROGEN BONDED SYSTEMS . . . 1197

Ch. 25. Spectroscopic and calorimetric studies of hydrogen bonding, A.D. Sherry 1199

Ch. 26. Vapor pressure studies on hydrogen and deuterium bonding, H. Wolff 1225

PART H. HYDROGEN BONDING AND ADSORPTION ON SURFACES . . . 1261

Ch. 27. Hydrogen bonds in systems of adsorbed molecules, H. Knözinger 1263

PART I. WATER AND ICE 1365

Ch. 28. Hydrogen bonds in liquid water. W.A.P. Luck . . . 1367
Ch. 29. The hydrogen bond in ice, E. Whalley 1425

Author index 1471

Subject index *(also included, without pagination, at the end of volumes I and II)* 1529

ШНИИБ. 19.06.84г. Заказ № 1537. Тираж 1экз.

"THE HYDROGEN BOND",

CHAPTER 1

INTRODUCTION

ERNST LIPPERT

Iwan N. Stranski-Institut für Physikalische und Theoretische Chemie der Technischen Universität Berlin, Berlin (West), FRG

Contents

1.1. What is a hydrogen bond? 3
1.2. The historical development 5
1.3. About this book 6
1.4. Hydrogen bonds in excited states 8
1.4.1. Changes in the charge distribution 8
1.4.2. Charge transfer effects 9
1.4.3. Electronic structure and intramolecular tautomeric equilibria 11
1.4.4. Constants of ionization 12
1.4.5. The β–naphthol problem 13
1.5. Applications of laser techniques 15
1.5.1. Methods 15
1.5.2. 4-methylumbelliferone 16
1.5.3. Tunable 4-MU-lasers 18
Note added in proof 18
References 20

The hydrogen bond – recent developments in theory and experiments
Eds. P. Schuster et al. © *North-Holland Publ. Co., Amsterdam, 1976*

1.1. What is a hydrogen bond?

A H-bond exists if one hydrogen atom H is bonded to more than one other atom, for instance, to two atoms named X and Y. In this case X and Y are connected with each other along H. If the two bonds of H to X and Y have different strengths the stronger bond will be written X–H and termed a *normal* XH-bond, but the weaker bond will be written H···Y and termed a *hydrogen bond* (abbreviated *H-bond* in this book).

In this case the strength of H···Y is identical with the dissociation energy of the *complex* X–H···Y. From the point of view of a complex chemist the H-bond that forms the complex is said to be a *symmetrical* or an *unsymmetrical* one, depending on whether the energy surface for the proton between X and Y is symmetric or not. In the vapor phase the anion $[HF_2]^-$ and the cation $[H_5O_2]^+$, for instance, possess symmetrical H-bonds with a *one-minimum* or a *two-minima* potential function, respectively, whereas HOH···NH_3 possesses an unsymmetrical single-minimum potential.

The H-bond is said to be *intra*-molecular, e.g. in salicylaldehyde and in diborane, or *inter*-molecular, e.g. in carboxylic acid dimers, that is if the atoms X and Y belong to the same molecule or not. For making this distinction the term "molecule" has to be taken in its chemical sense. From the physical point of view each intermolecular H-bond forms a larger molecule, a *complex*, which possesses its own force constants, chemical reactivities, etc., because of its characteristic structural properties in its nuclear configuration as well as in its electronic structure.

In the case of intermolecular association one distinguishes between *self*-association ("Eigenassoziation") and *mixed* association ("Mischassoziation") if the complexing molecules are of the same type (water) or different type (adenine with thymine), respectively.

H-bonding gives rise to a *specific* interaction between atoms or functional groups in which: the strength is higher than that of dispersion forces alone; it is directed along a hydrogen atom; and demonstrates some

characteristic angular dependencies. A H-bond exists, therefore, and has been verified if such properties have been substantiated; but it no longer seems reasonable to establish a definition for a lower limit of the H-bonding enthalpy, as long as the experimental methods for the detection of H-bonding are still in the process of becoming more accurate and sensitive.

The recent developments in theory made it possible to define certain contributions to H-bond energies. Estimates on the relative importance of forces of different origin (coulomb, exchange, polarization, dispersion forces etc.) became accessible in both perturbation theory and MO methods. Quantum theory is able, nowadays, to give a fairly correct description of isolated dimers or in some cases also trimers. It fails, however, to deal with larger clusters as they occur in condensed phases. But recently calculations became possible for infinitely extended systems.

The weaker a H-bond is and the higher the temperature of the associate or of the system to which it belongs, the shorter is the *lifetime* of that complex. In liquids thermal motion is the origin for a continuous *dynamic reorientation* of the partners. But it is now possible to obtain evidence for or against the presence of complexes, with well defined geometries and formation constants, as well as for the accurate determination of reorientational axes, of the friction from surrounding molecules, of characteristic correlation functions and correlation times, etc.

A chemical reaction is faster with higher force constants, smaller moving masses, and shorter distances along the reaction coordinate.

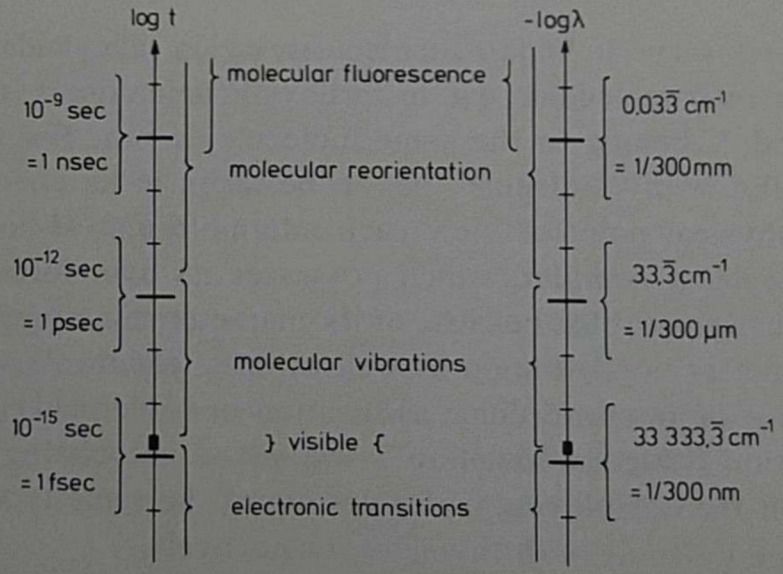

Fig. 1.1. Ranges of processes in solutions of H-bonding systems along a time scale (left) and a wave length scale (right).

Proton transfer reactions along H-bonds, therefore, belong to the fastest chemical reactions. But even here $\tilde{\nu}(XH) \approx 3333\ cm^{-1}$, which corresponds to $\tau_c \approx 10\ fs \equiv 0.01\ ps$ (fig. 1.1), i.e. a time interval which is next to the shortest mode locked laser pulses and in principle could be measured directly. But almost all other experimental techniques reveal *mean* values and mean structures only.

1.2. The historical development

The historical development started when Werner [1902] revealed that ammoniumhydroxyde is the addition product of ammonia and water

$$H_3N \cdots H\text{–}OH \longrightarrow H_3N\text{–}H \cdots OH$$

("Nebenvalenzbindung wird im folgenden stets durch einen punktierten Strich angedeutet" [l.c., p. 277].)

Hantzsch [1910] described the structure of acetoaceticacidester

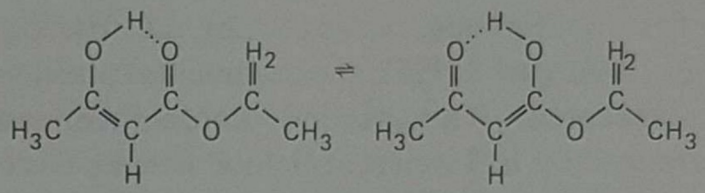

("ältestes und wichtigstes Tautomerie-Problem" [l.c., p. 3054]) as an intramolecular complex salt formation. Pfeiffer [1914] discovered the structure

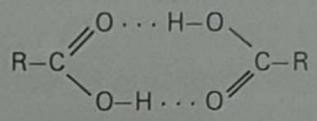

of carboxylic acid dimers. Huggins [1919] applied Lewis' octet theory to the hydrogenbifluoride anion, and Latimer and Rodebush [1920] stated that if the hydrogen nucleus is held between 2 octets then a weak bond is constituted. They also mentioned a chains and quasicrystalline network model: water "may be made up of large aggregates of molecules continually breaking up and reforming under the influence of thermal agitation". This is almost all one could say about the nature of H-bonding before the development of quantum chemistry.

Later on it became clear that *lone-pair* electrons at the basic site Y play an important role. That such lone-pair electrons are affected we can see from effects of H-bonding on $\pi^* \leftarrow n$ transition shifts (Kasha [1950]).

Neutron and X-ray scattering experiments (especially for ferroelectric crystals) show that the protons tend to be situated on the lone-pair orbital axis. The X–H group is therefore called the "proton donor" as well as the "electron acceptor" group. Of course, the interaction between the proton donor X–H and the proton acceptor Y is higher, the stronger the electric dipole moments of the X–H bond due to its bond character and of the atom Y due to its lone-pair charge distribution. Hence the strongest H-bonds are formed between atoms C, N, O and F acting as X and Y. The distance between X and Y in these cases is shorter than about 3 Å. The higher the strength and the shorter the length of the H-bond, the higher is the orbital overlap, so that electronic charge transfer structures also contribute to the electronic structure of the complex. The first charge transfer absorption band, if any, of carboxylic acid dimers and related complexes, is to be expected in the spectral region of 150 to 200 nm (Jentschura and Lippert [1971]).

The further progress in the last two decades became obvious at the three international conferences on H-bonding which have been held to date. At the first conference, arranged by D. Hadži at Ljubljana, Yugoslavia, July 29–August 3, 1957, the arguments mentioned above were fairly widely accepted. The second conference, an EUCHEM-Conference, arranged by E. Lippert at Schloß Elmau, Germany, on April 16–21, 1967, was devoted to the nature of the H-bond. In discussing the contour of IR absorption bands of proton stretching vibrations along H-bonds, more attention was given to the dynamic behaviour of H-bond associates. At the third conference, arranged by H. J. Bernstein at Ottawa, Canada, on August 21–25, 1972, it became evident that present commercial instruments allow detection of very weak H-bonds in liquids, even if their strength equals kT, the energy of thermal motion, and how large computers can be used for better calculations (see ch. 2).

1.3. About this book

Even though this book consists of three volumes and the overlap of the contents of the different chapters is rather small due to the thorough work of the editors, and even though all chapters contain results not yet published in recent books and review articles* on H-bonding or even

* See special lists of references at the end of this chapter.

elsewhere, there are three extensive areas which are treated only occasionally but not presented in special chapters in these volumes.

(i) H-bonding in *excited* states, and photochemical *proton transfer* reactions, which are due to the fact that the acidity and the basicity of functional groups are changed with each electronic transition of the molecule to which a group belongs because of the change in the electronic structure of the molecule. These effects are especially important e.g. for some biochemical reaction mechanisms like that of photosynthesis. For recent theoretical studies see section 2.9, and for further very recent and significant or characteristic work see sections 4 and 5 of this introductory chapter.

(ii) *Anionic* H-bonds like those in diborane in which the bridging proton

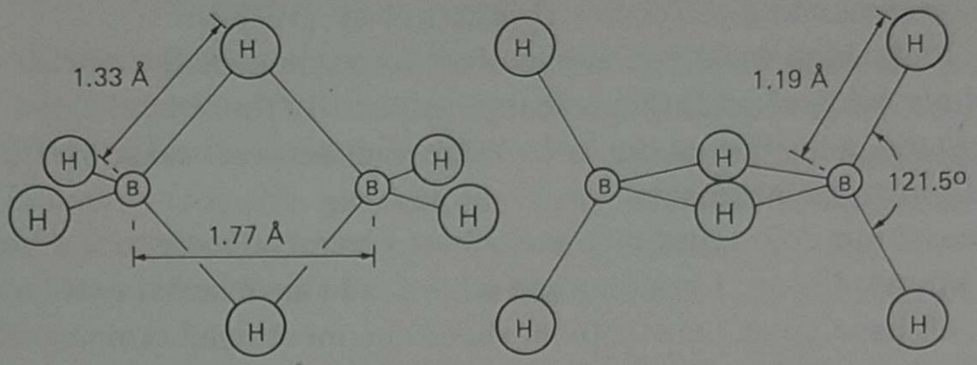

carries a negative charge which is larger than unity (see Pimentel and McClellan [1960], p. 203ff.). There is an analogy between anionic H-bonds and fluorine bridging in the fluoroxenon cations and their salts such as $(XeF)^+(Sb_2F_{11})^-$ and $(XeF_3)^+(SbF_6)^-$. Gillespie et al. [1974] have proposed that the lengths and stretching frequencies of these bridge bonds are closely related to the acceptor or acid strength of the fluoro cation forming the bridge and it is concluded that their acid strength increases in the series $(XeF_5)^+ < (XeF_3)^+ < (XeF)^+$ whereas it had been previously supposed, on the basis of rather little evidence, that the order was $(XeF_5)^+ < (XeF)^+ < (XeF_3)^+$. However, this book deals mostly with X–H···Y bonds of the cationic type in which the dipole moment of the X–H bond is directed with its positive end towards the H-atom.

(iii) *Very weak* H-bonding like that in H_3 which is well known to be the possible intermediate state in the high temperature ortho/para hydrogen conversion reaction. This book deals mostly with complexes, the dissociation energy of which is higher than the historical limit of about 2 kcal/mole. None-the-less, a number of theoretical investigations on very weak H-bonding-like interactions are included in section 2.4.1.

Weak H-bonds are most easily studied by IR or NMR techniques. The ν(OH) valence vibrational IR absorption band of monomeric phenol in mixtures of hydrocarbon solvents with CH_3CCl_3, for instance, is composed of 2 subbands, and the splitting is due to a weak H-bond $R_{ar}O\text{–}H\cdots ClCCl_2CH_3$ to just one of the chlorine atoms of the CCl_3-group, $\Delta H = -1.5$ kcal/mole (Lippert and Schröer [1969]).

For the self-association of acetonitrile, a value of $-\Delta H = 1.43$ kcal/mole (and $K_c = 0.04$ mole/l at 20°C) has been obtained by two methods: by the effect of concentration on the intensity of the ν_a(CH)-stretching mode ν_5; as well as from the wave number differences $\tilde{\nu}_2 - \tilde{\nu}_D \approx 50\ cm^{-1}$ between the ω(CN)-stretching mode ν_2 and a combination band which is due to a vibration mode of the entire molecule in the cage of surrounding molecules (Lippert et al. [1972]).

Due to the high variety of applications of our knowledge on H-bonding in various fields of scientific research (especially those in chemistry and biology) the collection of our knowledge and the production of this book turned out to be necessary.

Some of our colleagues who contributed tremendously to the increase in our knowledge on H-bonding and who should have been contributors to this book have gone. One of them should be mentioned in remembrance to all of them: Walter C. Hamilton of Brookhaven National Laboratories at New York.

1.4. Hydrogen bonds in excited states

1.4.1. Changes in the charge distribution

During an electronic transition the position and the velocity of all atomic nuclei in a given system remain constant (Franck–Condon-principle). With each such transition the physical properties of a molecule are changed, since its electronic charge distribution is altered. In different electronic states, therefore, the nature of the H-bonds is changed, and there are different pK values for the equilibrium

$$BH + H_2O \rightleftarrows B^- + H_3O^+. \qquad (1.1)$$

In the $^1(\pi^*\pi)_1$ state of aromatic compounds, basic sites are often more basic and acidic sites more acidic than in the ground state. If both such functional groups are present, it might occur that a molecule in its fluorescing $(\pi^*\pi)$ state exists either as a cation or as an anion, but there is

no pH value in aqueous solution at which it is neutral, as has been demonstrated for lumazine compounds (Lippert and Prigge [1960], Lippert et al. [1961], Prigge and Lippert [1965] and Lippert [1966, 1970]).

There are, of course, solutions in which H-bond complexes and proton transfer processes occur in excited states only (e.g. Oosterhoff [1967]).

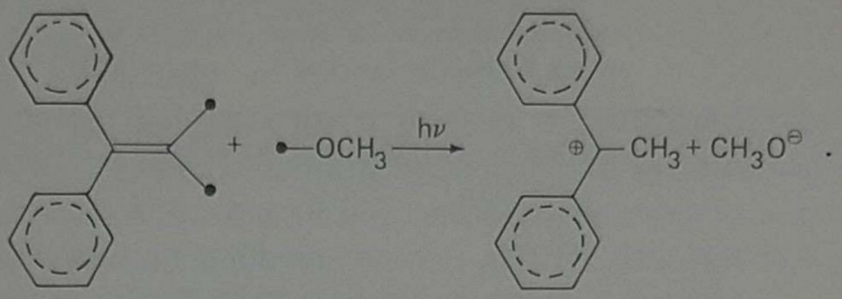

And there might be examples where a carbon atom becomes the proton acceptor by excitation. This has been predicted theoretically by Del Bene (see section 2.9) for formaldehyde after $\pi^* \leftarrow$ n absorption, since negative charge is moved from the nitrogen lone-pair orbital towards the carbon atom, and the molecular structure might become a pyramidal one. This prediction should be checked experimentally, e.g. by laser excitation and ^{13}C-NMR analysis.

1.4.2. Charge transfer effects

With H-bond formation the $S_1 \leftrightarrows S_0$ transitions of a proton donor molecule which possesses a π electronic system next to an OH- or NH-bond undergo bathochromic shifts towards the spectral position of the corresponding transitions of the anion. This is the first evidence for the fact that acidic groups like –OH or >NH are more acidic in S_1 than in S_0 and are better proton donor groups for H-bonding. The same type of bathochromic shifts of $S_1 \leftrightarrows S_0$ transitions with H-bonding toward the spectral position of the corresponding transitions of the cation, is a property of the π electronic system of heteroaromatic compounds.

In both cases the other partner could have a saturated or an unsaturated carbon skeleton. Examples for all four possibilities are given in table 1.1, showing that the constants of association are increased by excitation, $K^* > K$. In all four examples the increase in acidity or basicity, respectively, is so strong that the reaction of association partly proceeds to the formation of the reversed complex, i.e. to the ion pair $X^- \cdots HY^+$; the bridging proton moves to the basic atom Y, leaving an anion behind, of which the basic site X^- now acts as the proton acceptor.

TABLE 1.1

Types of $\pi^*\pi$ excimer formation via H-bonding

No.	Type of formation	Example for $S_1 \rightleftarrows S_0$ red shifts	Association	Fluorescence
1	$D^*_{ar} + A_{al}$	β–naphthol + triethylamine	$K^* > K$	$\eta_{ass} > \eta_{free}$
2	$D^*_{ar} + A_{ar}$	β–naphthylamine + pyridine	$K^* \gg K$	$\eta_{ass} \ll \eta_{free}$
3	$D_{al} + A^*_{ar}$	trichloroaceticacid + acridine	$K^* \gtrsim K$	$\eta_{ass} > \eta_{free}$
4	$D_{ar} + A^*_{ar}$	phenol + 3,6-aminoacridine	$K^* \gtrsim K$	$\eta_{ass} \ll \eta_{free}$

References to no. 1 and 2: Mataga and Kaifu [1963]; and to no. 3 and 4: Mataga and Tsuno [1957].

The electronic structure of such "exciplexes" or "hetero-excimers" has a certain charge transfer character. The electronic charge transfer process proceeds along the H-bond and is the reason for fluorescence quenching by association. In examples no. 2 and 4 in table 1.1, the fluorescence quantum yield η, vanishes because of the univalent redox reactions shown in fig. 1.2. With each absorption process the ionization potential of an electronic system is decreased and the electron affinity is increased. In the left-hand side of fig. 1.2 the molecule with the longest wave length absorption band transfers its promoted electron to the lowest non-occupied π orbital of its complex partner molecule (no. 2 of table 1.1), but in the right-hand side of fig. 1.2 it takes an electron from its partner into

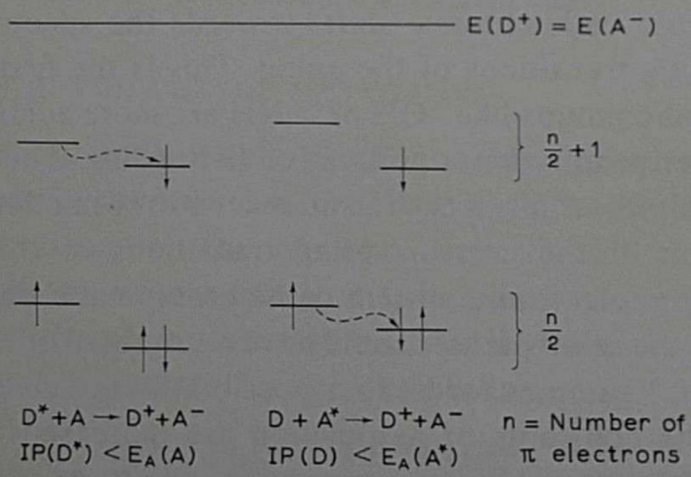

Fig. 1.2. Fluorescence quenching in hetero-excimers by electron transfer processes. Energies of the highest occupied and of the lowest unoccupied molecular orbital, $n/2$ and $(n/2)+1$, respectively, of a π electronic system of n electrons, as measured from the ionisation potential (top line) of the electron donor molecule, D, and of the electron acceptor molecule, A. (See text).

that orbital from where the promoted electron had come (no. 4 in table 1.1). Both processes could also be explained as a radiationless vibronic coupling between the relevant electronic systems. For further literature see Lippert [1959], Mataga and Ezumi [1967], Mataga and Kubota [1970] and Vander Donckt [1970].

1.4.3. Electronic structure and intramolecular tautomeric equilibria

The equilibrium constant for a process of tautomerization along an intramolecular H-bond is extremely sensitive to the electronic structure of the carbon skeleton, e.g. of phenanthrene, possessing an auxochromic group, –OH, and an antiauxochrome, $-NCHC_6H_5$, in *ortho*-position to each other. This is illustrated by the absorption spectra of three isomers of *o*-hydroxy aromatic azomethines as shown in fig. 1.3.

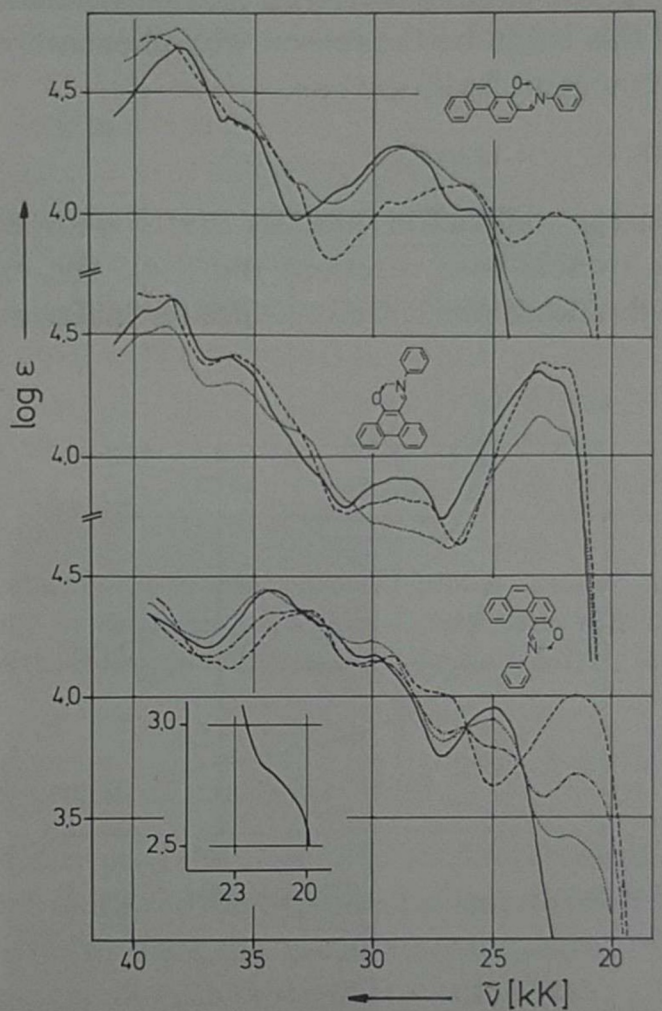

Fig. 1.3. Absorption spectra of 3 isomeric *o*-hydroxyphenanthren aldehydeanils in ——— cyclohexane, ····· acetonitrile, –·–·– ethanol, – – – – acetic acid. (Muszik [1965]).

The absorption spectra of the *3,4-isomer* in different solvents possess isosbestic points due to the lactim/lactam equilibrium. The NH-form possesses a higher dipole moment and the longest wave length absorption band, the intensity of which increases with increasing solvent polarity, and in cyclohexane at 20°C its $K_T = 0.095$, $\Delta H = 252$ cal/mole, and $\Delta S = -3.8$ cal/grad mole.

The *1,2-isomer*, however, still shows the bands of the OH and NH species but no isosbestic points because of secondary reactions and/or the superposition of transitions to the ^1L_a and ^1L_b excited states of the phenanthrene π electronic system which may have different solvent effects.

However, the *9,10-isomer* in all solvents exists only in the NH-form, as could be deduced from the absorption spectrum of the corresponding methoxy compound. The behaviour of the carbon atoms 9 and 10 is more like that of a vinyl group as compared with the real aromatic carbon atoms 1, 2, 3 and 4, and this might be the reason why phenanthrene itself is the smallest size carcinogenic hydrocarbon.

1.4.4. Constants of ionization

An electronic energy relaxation process starts with each electronic transition, e.g., with acid-base reactions (fig. 1.4). The excimer fluorescence shows no vibrational fine structure since its final (ground) state, S_0^{FC},

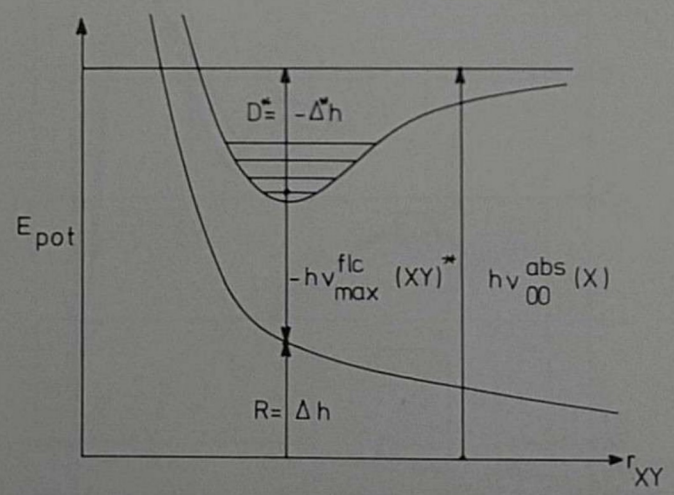

Fig. 1.4. Total potential energy, $E_{pot}(X, Y)$, of 2 molecules, X and Y, as a function of their interacting distance, r_{XY}.

$$(S_1^{eq} - S_0^{eq})_{XY} = h\nu_{00}^{abs} - D = h\nu_{max}^{flc} + R$$

The energy of dissociation, D, has the opposite sign, the energy of repulsion, R, has the same sign, compared to the sign of the corresponding reaction enthalpy ΔH, and $\Delta h \equiv \Delta H / N_L$.

is not stable and possesses, therefore, a minimum of potential energy only at infinite distance.

There are two methods in fluorescence spectroscopy for the determination of $pK(S_1)$ values, i.e., the pK value of the lowest singlet state. Both methods have been reviewed recently (Mataga and Kubota [1970], Vander Donckt [1970] and Lippert [1974]). The *first* method depends on the Förster cycle as shown in fig. 1.5,

$$pK(S_1) = pK(S_0) + hc_0[(\tilde{\nu}_a + \tilde{\nu}_f)_B - (\tilde{\nu}_a + \tilde{\nu}_f)_{BH^+}]/2kT \ln 10,$$

where $\tilde{\nu}_a$ and $\tilde{\nu}_f$ are the wave numbers of the maximum of the absorption band and the corresponding fluorescence band, respectively, and h, c_0, k, N_L are natural constants. In the *second* method the values $\vec{k}$ and $\overleftarrow{k}$ of eq. (1.1) are calculated from measurements of the lifetime and of the fluorescence intensity as a function of the pH value for both species, and $K = \vec{k}/\overleftarrow{k}$ allows calculation of $pK(S_1)$.

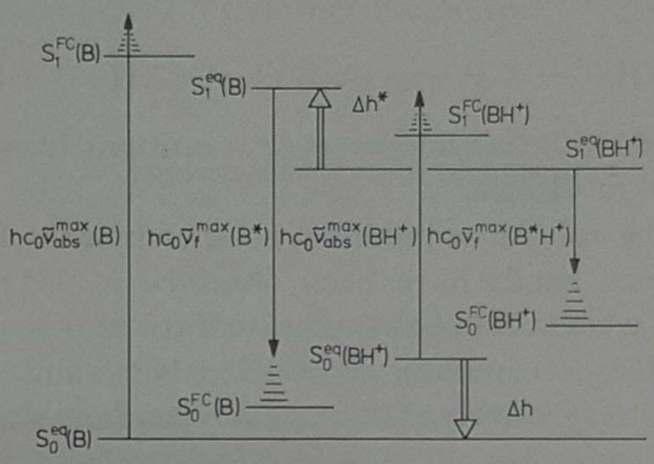

Fig. 1.5. Energy diagram of a photochemical proton transfer reaction in solution. Superscripts FC and eq determine the Franck–Condon-state and the equilibrium state, respectively. ΔH is the enthalpy of reaction (1.1), and $\Delta h \equiv \Delta H/N_L$ (Lippert [1974] section 3.3).

1.4.5. The β–naphthol problem

Förster [1950] discovered the effect of dual fluorescence of β–naphthol in alkaline solutions and gave the explanation that not only does β–naphthol fluoresce, but so also does the β–naphtholate anion. Weller [1955] and many other photochemists then started to examine the effect of pH on the fluorescence spectra of β–naphthol, and the results obtained up to 1967 have been reviewed by Vander Donckt [1970].

At 25°C, β–naphthol has a pK(S_0) of 9.49 so that only the undissociated species is responsible for the absorption of light in the pH range between 2 and 8. In these acid media, fluorescence is emitted by the molecule, BH, in the near UV, and by the anion, B^-, in the visible spectral region. This behaviour clearly shows that in the excited state the equilibrium eq. (1.1) is displaced to the right as compared to the ground state. As indicated by the independence of the relative fluorescence intensities as a function of pH, the proton acceptor is a water molecule and not a hydroxyl anion. Since, in the whole range of pH the total fluorescence intensity remains constant, it can be confirmed that the loss of a proton occurs without deactivation of the excited state ("adiabatic" photoreaction).

Most recently Matsuzaki et al. [1974] investigated, by time-resolved fluorescence spectra, the proton donor-acceptor interactions of β–naphthol, the proton donor, in its first excited singlet state, S_1, with triethylamine, the proton acceptor, in toluene and in acetonitrile at different concentrations. In the non-polar solvent toluene, the normal Förster cycle

$$XH \xrightarrow{h\nu} X^*H \xrightarrow{Y} (X^*HY) \longrightarrow XH + Y + h\nu$$

was reconfirmed, with two fluorescence transitions from X^*H at 355 nm and from X^*HY at 410 nm.

But in the polar solvent acetonitrile, polar complexes are favoured and three fluorescence bands have been observed at 355 nm, 370 nm and 450 nm (fig. 1.6) which could be ascribed to the free β–naphthol molecule, to the H-bonded β–naphthol, R_{ar}–O–H$\cdots$$NR_3$, and to the ion-pair $R_{ar}O^-\cdots HNR_3^+$, respectively, but none to the free naphtholate anion,

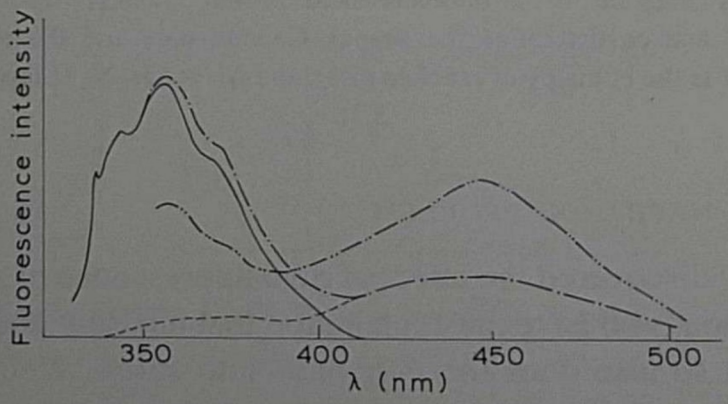

Fig. 1.6. The fluorescence spectra of the β–naphthol-TEA system in acetonitrile at 25°C. The concentrations of TEA are 0, 0.705×10^{-2}, and 3.52×10^{-2} M for curves ———, —·—, and —··—, respectively (Matsuzaki et al. [1974]).

since the back reactions from the ion-pair to the H-bonded β–naphthol and further back to the free β–naphthol molecule cannot be disregarded when evaluating the kinetic data from the experimental results. The authors demonstrate that the ion-pair formation takes place through the H-bond.

But even this simple β–naphthol problem has not yet been completely settled. Klein and Hauser [1974] studied the fluorescence of β–naphthol in sodium lauryl sulfate/water mixtures in which the β–naphthol was only partly dissolved in water, but to a higher extent it was in an intramicellar phase. No photolysis of β–naphthol, and no proton transfer into the water phase was observed, even though water molecules were present in the intramicellar phase, the travelling distance amounted to only about 20 Å and the outer phase was an alkaline medium. Ito and Azumi [1973] observed dissolved electrons in alcoholic solutions of β–naphthol after excitation. Further fluorescence spectroscopic studies on excimer-like complexes in related solutions have also been done in Sapporo (see Kitamura and Baba [1973] for further literature).

1.5. Applications of laser techniques

1.5.1. Methods

There are two methods for the measurement of shortest photochemical rate constants. For the *first* method very intense laser pulses are used, the intensity of which can be altered even above the *laser threshold* of the solution to be studied, and the ratio of the intensities of the various fluorescence bands is determined as a function of the excitation intensity, i.e. as a function of the lifetimes of the fluorescing species (Gronau et al. [1972a, b]). In this method, due to stimulated emission, the lifetimes are shortened and the product fluorescence intensities and the competing chemical reactions are deteriorated. This method is restricted to laser-active media (see Schäfer [1973]). In reversible photochemical reactions the fluorescence band of an adiabatic photoreaction product occurs at longer wave lengths than the primary fluorescence with which it competes, because of energetical reasons (fig. 1.7).

For the *second* method ultrashort light pulses are used for excitation and for the study of the *time-resolved* absorption and fluorescence spectra of the different species (see Rentzepis and Busch [1972]).

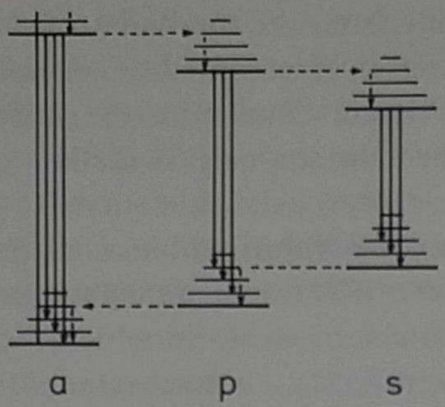

Fig. 1.7. Energies of electronic states of a solution exhibiting *triple fluorescence.* (a) Fluorescence of the absorbing species, (p) fluorescence of the primary adiabatic photoreaction product, and (s) fluorescence of a secondary adiabatic photoreaction product (Lippert [1974]).

1.5.2. 4-Methylumbelliferone

Both methods have been applied to the investigation of radiationless processes in aqueous solutions of 4-methyl-7-hydroxy coumarin (4-MU, fig. 1.8). The phototautomerism in the lowest excited singlet state has especially been studied experimentally (Yakatan et al. [1972]) and theoretically (Huber et al. [1973]). Recent results have been summarised by Bergman and Jortner [1973] and Dienes et al. [1973a, b].

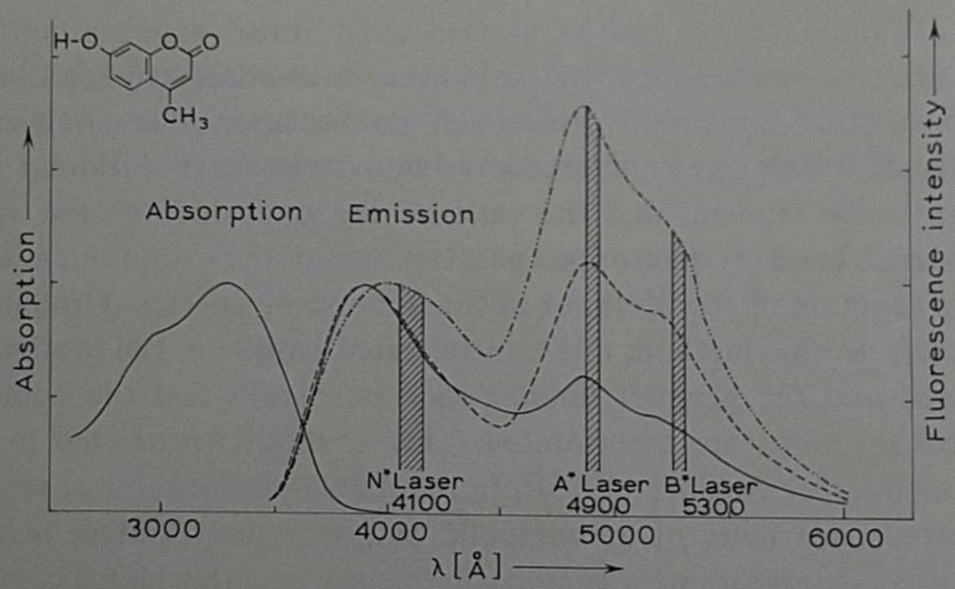

Fig. 1.8. Absorption and emission spectra of HCl-acidified ethanolic 4-MU solutions ($c_{4\text{-MU}} = 10^{-4}$ m/l, with ——— 0.01 m/l, – – – – – – 0.1 m/l, –·–·–·– 1 m/l HCl). The emission spectra were obtained with an excitation wave length of 3472 Å. The height of the first peak of each emission spectrum has been set at the height of the absorption peak (Kindt et al. [1972]).

Groves et al. [1973] recently showed that not all properties of the laser fluorescence emitted from solutions of 4-methylumbelliferone can be explained adequately by different excited state structures of the molecule alone, but that the structural model has to be extended in order to account for the effects of H-bonds with the solvent environment. But even photochemical ring opening reactions on both sides of the ring oxygen atom might contribute to the broad emission spectrum (Fink and Koehler [1970]).

A schematic diagram of solute/solvent interactions via H-bonds of 4-MU in water containing solutions is demonstrated in fig. 1.9. Here the solvent is represented by three water molecules surrounding the solute. The pH value of the solution is assumed to increase from the bottom (cations) to the top (anions). If the solute molecules exist in the electronic ground state S_0, heat is necessary to shift the thermodynamical equilibrium from left to right; but if the solute is in S_1 the contrary might be the case. It must be the case if, e.g., the species $c2$ fluoresces, because $n1$ has absorbed the exciting photon and $S_1(n1) \rightarrow S_1(c1) \rightarrow S_1(c2)$ is a sequence

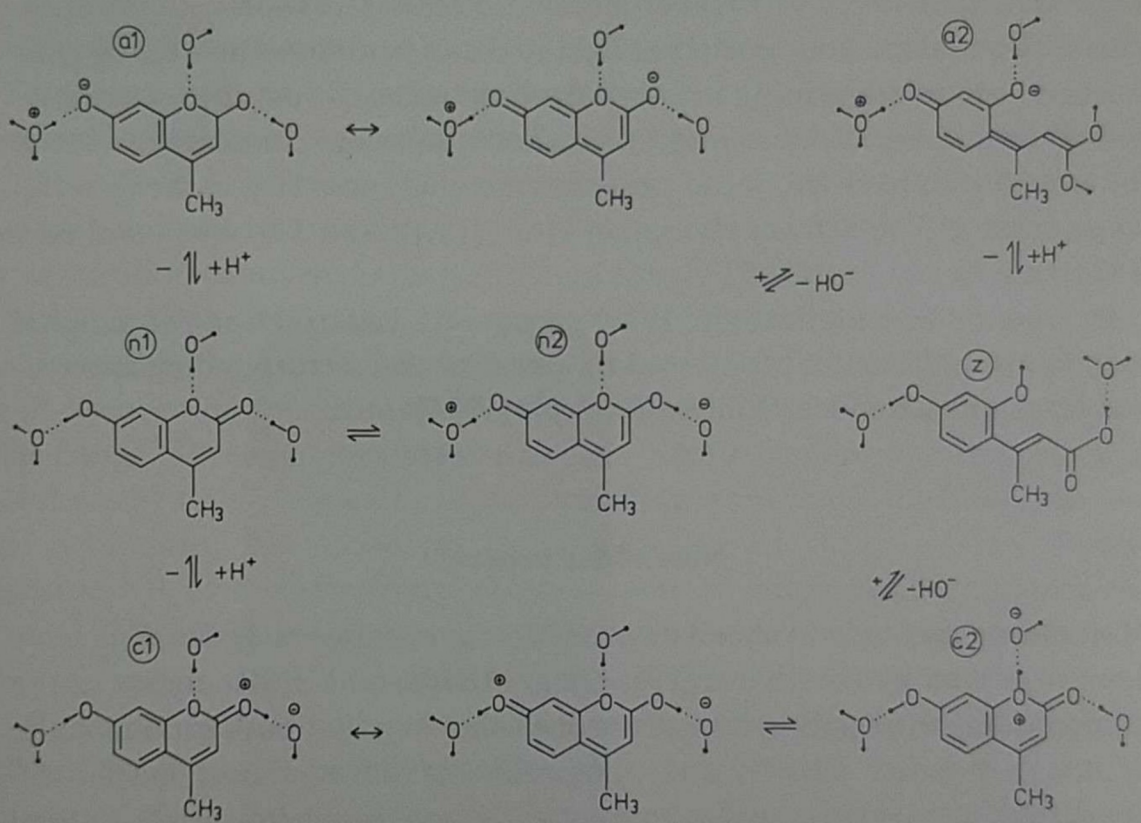

Fig. 1.9. 4-MU in some solvated states, schematically. The bridging protons are indicated by heavy points.

1407-ch
ЦНИИБ
БИБЛИОТЕКА

of adiabatic photoreactions of the system under consideration. (A synopsis of adiabatic photoreactions has been given by Lippert [1974]).

The 4-MU anion *a*1 possesses 3 oxygen atoms each of which can act as a proton acceptor. The neutral form *n*2 can undergo a photochemical ring opening reaction either in alkaline or acidified media via structures *a*2 and *c*2, respectively, yielding 2,4-dihydroxy-α-methyl cinnamic acid, *z*. We leave the question open if the (photochemical) ring opening reactions occur preferably between atoms O_1 and C_2 or O_1 and C_9; but presumably in both cases a cleavage of the bond O_1–C_2 will be dominating (Perst [1971] and Praefke and Simon [1974]). But it should be possible to solve this question by using ^{17}O-water and measuring the relative amount of ^{17}O in both positions after irradiation. There are at least five H-bonded complexes which are laser active, presumably *a* 1, *n* 1, *c* 1, *n* 2 and *z*; also, in very strong acids the doubly protonated species may be laser active (Bergman and Jortner [1973]).

1.5.3. Tunable 4-MU-lasers

In recent years there has been considerable interest in the development of dye lasers as sources of tunable monochromatic radiation (Stokes et al. [1972]). Dye lasers emit polarized light and can be filtered and tuned with a swivel-mounted grating as a reflecting mirror. Just the 4-methylumbelliferone laser consisting in alcoholic solution containing a small amount of water turned out to possess extended tunability in the spectral range from 415 to 558 nm (Bergman et al. [1972] and Takakusa and Itoh [1974]).

Harrington and Malmstadt [1974] proposed a construction for a digital scanning spectrometer for laboratory use. For the corresponding anomalous laser emission see Srinivasan et al. [1974].

Note added in proof

Modulation methods in chemistry and their application to H-bonding have been reviewed by Günthardt [1974], e.g. MEIR and MESR studies of the photooxidation of polyhydroxybenzenes showing that both ground state, hydrogen bonded dimers, and photoradicals follow simple amplitude-phase dependence on modulation frequency from which information about mechanisms and reaction rate constants may be derived.

The role of *inelastic neutron scattering* (I.N.S.), a relatively recent

technique for the investigation of molecular vibrations in H-bonded complexes, has been outlined by J. L. Wood [1973]. There are two features which make I.N.S. of particular interest. First, the symmetry restrictions that apply in infrared or Raman spectra are absent. Second, the amplitude of the H-atom motion is the predominating influence on the band intensity which is either energy gain or loss spectra corresponding to loss or gain of vibrational energy by the sample.

Intermolecular H-bonding is a criterium against *mesomorphism* since its energy keeps the melting point at a higher temperature than the expected transition temperature to the mesophase. Nevertheless *p*-phenylene-di-*p*-amino-benzoate as well as the corresponding -*p*-hydroxy-benzoate exhibit very stable nematic and smectic mesophases. An explanation might be possible on the fact that both compounds supercool phenomenally (Schröder and Schröder [1974]).

The infrared spectra of the mixed associates of imidazole with acetonitrile-d_3, dioxane-d_8, dimethylsulfoxide-d_6, pyridine-d_5, and N-methyl-imidazole exhibit NH stretching vibrational bands at higher wavenumbers than the spectrum of self-associated imidazole. However, additional bands are observed in the spectral range in which the NH stretching band and the subbands of self-associated imidazole are situated. The wavenumbers of these bands are almost the same for the various mixed associates. They are approximately equal to the values found for the subbands of self-associated imidazole with not too advanced a degree of association, and they correspond to the values calculated for the binary combination bands in the same spectral range. The intensities of the bands increase as the NH stretching band, with increasing acceptor basicity, approaches the bands in frequency. The intensities are largest at the self-association spectrum at which the NH stretching band coincides with the bands. These observations do not agree with the current interpretation of the subbands by coupling of the stretching vibration to the intermolecular vibrations. They confirm the explanation of the bands by *Fermi interaction* of the stretching vibration with overtones and combination tones of the frequencies between 1600 and 900 cm^{-1} which are mainly due to ring and bending vibrations (Wolff [1974]).

Systematically, studies of mixed association by H-bonding in the *gas phase* have been started by Millen et al. [1974a, b] which provide a measure of the relative electron donating abilities of, for example, free amines and which allow the determination of thermodynamic parameters from pressure, volume, and temperature measurements.

References

Recent books on H-bonding

Covington, A. K. and P. Jones, Eds., 1968, Hydrogen-Bonded Solvent Systems (Taylor & Francis, London).

Franks, F., Ed., 1972, Water (chs. 1–4) (Plenum Press, New York).

Hadži, D. and H. W. Thompson, Eds., 1959, Hydrogen Bonding. Proceedings of the first International Conference on Hydrogen Bonding, Ljubljana, 1957 (Pergamon Press, London).

Hamilton, W. C. and J. A. Ibers, 1968, Hydrogen Bonding in Solids (Benjamin, New York).

Joesten, M. D. and L. J. Schaad, 1974, Hydrogen Bonding (Marcel Dekker, New York).

Luck, W. A. P., Ed., 1974, Water–As Liquid and Solid (Verlag Chemie, Weinheim).

Pimentel, G. C. and A. L. McClellan, 1960, The Hydrogen Bond (Freeman, San Francisco).

Riehl, N., Ed., 1969, Physics of Ice (Plenum Press, New York).

Sokolov, N. D. and V. M. Chulanovskii, Eds., 1964, Hydrogen Bonding (Akad. Nauk SSSR, Moscow).

Vinogradov, S. N. and R. H. Linnell, 1971, Hydrogen Bonding (Van Nostrand Reinhold, New York).

Zundel, G., 1969, Hydration and Intermolecular Interaction (Academic Press, New York) and 1972 (Mir, Moscow).

Review articles on H-bonding

Bratož, S., 1967, Electronic Theories of H-bonding. Advan. Quantum Chem. **3**, 209.

Huggins, M. L., 1971, 50 Jahre Theorie der Wasserstoffbrückenbindung. Angew. Chem. **83**, 163.

Kollman, P. and L. C. Allen, 1972, The Theory of the Hydrogen Bond. Chem. Rev. **72**, 283.

Morokuma, K., S. Iwata and W. A. Lathan, 1974, Molecular Interactions in Ground and Excited States, in: The World of Quantum Chemistry, Eds. R. Daudel and B. Pullman (D. Reidel, Dordrecht), p. 277.

Murthy, A. S. N. and C. N. R. Rao, 1970, Recent Theoretical Studies of the H-bond. J. Mol. Structure **6**, 253.

Pimentel, G. C. and A. L. McClellan, 1971, Hydrogen Bonding. Am. Rev. Phys. Chem. **22**, 347.

Schuster, P., 1973, Neuere Ergebnisse aus der Theorie der Wasserstoffbrücken und Protonenübergänge. Z. Chem. **13**, 41.

Schuster, P., W. Jakubetz, G. Beier, W. Meyer and B. M. Rode, 1974, Potential Curves for Proton Transfer along Hydrogen Bonds, in: Chemical and Biochemical Reactivity, Eds. E. D. Bergmann and B. Pullman (Academic Press, Jerusalem).

Zimmermann, H., 1970, Wasserstoffbrückenbindungen und ihre Bedeutung in der Biologie. Chemie in unserer Zeit **4**, 69.

Other articles

Bergman, A. and J. Jortner, 1973, J. Luminescence **6**, 390.

Bergman, A., R. David and J. Jortner, 1972, Opt. Comm. **4**, 431.

Dienes, A., R. K. Jain and C. Lin, 1973a, Appl. Phys. Letters **22**, 632.

Dienes, A., C. V. Shank and R. L. Kohn, 1973b, IEEE J. Quant. Electronics **QE-9**, 833.

Fink, D. W. and W. R. Koehler, 1970, Anal. Chem. **42**, 990.
Förster, Th., 1950, Z. Elektrochem. **54**, 42, 531.
R. J. Gillespie, P. Ireland, B. Landa and G. J. Schrobilgen, 1974, Private Communication, presented at the EUCHEM-Conference in Montpellier.
Gronau, B., E. Lippert and W. Rapp, 1972, (a) IEEE J. Quant. Electronics **QE-8.2**, 526; (b) Ber. Bunsenges. Phys. Chem. **76**, 432.
Groves, M. R., S. C. Haydon and O. M. Williams, 1973, Opt. Comm. **9**, 42.
Hantsch, 1910, Ber. **43**, 3049 (for companion: 1911, Ber. **44**, 1771).
Harrington, D. and H. V. Malmstadt, 1974, International Laboratory, May/June, 67.
Huber, J. R., M. Nakashima and J. A. Sousa, 1973, J. Phys. Chem. **77**, 860.
Huggins, M. L., 1919, Laboratory report, inorganic chemistry, University of California, as referred to by Latimer and Rodebusch [1920] and by Huggins [1971].
Ito, M. and Azumi, 1973, Private Communication.
Jentschura, U. and E. Lippert, 1971, Z. Physik. Chem. N.F. **75**, 88.
Kasha, M., 1950, Disc. Faraday Soc. **9**, 14.
Kindt, T., E. Lippert and W. Rapp, 1972, Z. Naturforsch. **27a**, 1371.
Kitamura, M. and H. Baba, 1973, Bull. Chem. Soc. Japan **46**, 3056.
Klein, U. and M. Hauser, 1974, (a) Paper presented at the Annual Conference of the Dt. Bunsengesellschaft on New Methods in Molecular Spectroscopy at Kassel, May 25; (b) Z. Phys. Chem. N.F. **90**, 215.
Latimer, W. M. and W. H. Rodebush, 1920, J. Am. Chem. Soc. **42**, 1419.
Lippert, E., 1959, Der Einfluß von Wasserstoffbrücken auf Elektronenspektren, in: Hadži and Thompson [1959], pp. 217–257 (e.c.).
Lippert, E., 1966, Die Medienabhängigkeit der Fluoreszenzfarbe, in: Optische Anregung Organischer Systeme (2. Internationales Farbensymposium, Elmau, 1964), Ed. W. Foerst (Verlag Chemie, Weinheim), pp. 342–355.
Lippert, E., 1970, Accounts Chem. Res. **3**, 74.
Lippert, E., 1974, Laser-spectroscopic Studies of Reorientation and Other Relaxation Processes in Solution, in: Organic Molecular Photophysics, Vol. 2, ch. 1, Ed. J. B. Birks, in press (Wiley and Sons, London and New York).
Lippert, E. and H. Prigge, 1960, Ber. Bunsenges. Phys. Chem. **64**, 662.
Lippert, E. and Schröer, W., 1969, Ber. Bunsenges. Phys. Chem. **73**, 1027.
Lippert, E., W. Lüder, F. Moll, W. Nägele, H. Boos, H. Prigge and I. Seibold-Blankenstein, 1961, Angew. Chem. **73**, 695.
Lippert, E., H. Mahnke, H. Michel and W. Schröer, 1972, IR-Spectroscopic Investigations of Weak H-bonding and of the Structure of Acetonitrile in its Liquid Phase, in: Abstracts of the 2nd International Conference on Hydrogen Bonding, Ottawa, p. 22.
Mataga, N. and K. Ezumi, 1967, Bull. Chem. Soc. Japan **40**, 1350.
Mataga, N. and Y. Kaifu, 1963, Mol. Phys. **7**, 137.
Mataga, N. and T. Kubota, 1970, Molecular Interactions and Electronic Spectra, ch. 7, (Marcel Dekker, Inc., New York).
Mataga, N. and S. Tsuno, 1957, Bull. Chem. Soc. Japan **30**, 368, 711.
Matsuzaki, A., S. Nagakura and K. Yoshihara, 1974, Bull. Chem. Soc. Japan **47**, 1152.
Muszik, J. A., 1965, Elektronenspektren aromatischer o-Hydroxy-azomethin-Verbindungen. Dissertation, Stuttgart.
Oosterhoff, L. J., 1967, Discussion remark, to "Fast Reaction and Primary Processes in

Chemical Kinetics, Proceedings of the Fifth Nobel Symposium, Ed. S. Claesson (Almquist & Wiksell, Stockholm), p. 162.
Perst, H., 1971, Oxonium Ions in Organic Chemistry (Verlag Chemie, Weinheim), p. 46.
Praefke, K. and H. Simon, 1974, Private Communication (Diplom-Arbeit H. Simon, T.U. Berlin), p. 6ff.
Pfeiffer, P., 1914, Ber. **47**, 1580.
Prigge, H. and E. Lippert, 1965, Ber. Bunsenges. Phys. Chem. **69**, 458.
Rentzepis, P. M. and G. E. Busch, 1972, IEEE Transactions on Instrumentation, **IM-21**, 488.
Schäfer, F. P., Ed., 1973, Dye Lasers (Springer-Verlag, Berlin).
Srinivasan, R., R. J. von Gutfeld, C. S. Angadiyavar and R. W. Dreyfus, 1974, Chem. Phys. Letters **25**, 537.
Stokes, E. D., F. B. Dunning, R. F. Stebbings, G. K. Walters and R. D. Rundel, 1972, Opt. Comm. **5**, 267.
Takakusa, M. and U. Itoh, 1974, Opt. Comm. **10**, 8.
Vander Donckt, E., 1970, Acid-Base Properties of Excited States, in: Progress in Reaction Kinetics, Vol. 5, Ed. G. Porter (Pergamon Press, Oxford).
Weller, A., 1955, Z. Phys. Chem. N.F. **3**, 238.
Werner, A., 1902, Liebigs Ann. **322**, 261, 293.
Yakatan, G. J., R. J. Juneau and S. C. Schulman, 1972, Anal. Chem. **44**, 1044.

Added in proof:

Günthardt, H. H., 1974, Ber. Bunsenges. **78**, 1110.
Millen, D. J. and M. A. Hussein, 1974a, J. Chem. Soc., Faraday Trans. II **70**, 685.
Millen, D. J. and G. W. Mines, 1974b, ibid., **70**, 693.
Schroeder, D. C. and J. P. Schroeder, 1974, J. Amer. Chem. Soc. **96**, 4347.
Wolff, H., Helmuth Müller and Harald Müller, 1974a, Ber. Bunsenges. **78**, 1241.
Wolff, H., Helmuth Müller and Harald Müller, 1974b, J. Chem. Phys. **60**, 2938.
Wood, J. L., 1973, The vibrational spectra of H-bonded complexes, in: Spectroscopy and structure of molecular complexes, Editor J. Yarwood, Plenum Press, London.

PART A

THEORY OF THE HYDROGEN BOND

CHAPTER 2

ENERGY SURFACES FOR HYDROGEN BONDED SYSTEMS*

PETER SCHUSTER

Institut für Theoretische Chemie,
Universität Wien, Währingerstraße 17, A-1090 Wien, Austria

* Dedicated to the late Prof. C. A. Coulson, who long ago explained correctly the nature of hydrogen bonds on the basis of reflection and intuition rather than by extensive numerical computer calculation not accessible in those days.

Contents

2.1. Introduction 27
2.2. Quantum mechanical methods and their application to hydrogen bonds . . . 29
2.2.1. Molecular orbital theory of isolated molecules 30
2.2.2. Perturbation theory of hydrogen bonds 39
2.2.3. Molecular orbital theory of hydrogen bonds 57
2.2.4. Nature and properties of the hydrogen bond 71
2.3. Molecular potentials and the electrostatic energy of interaction 81
2.3.1. Electrostatic potentials in calculations on hydrogen bonds 82
2.3.2. Consistent force field calculations on hydrogen bonds 85
2.3.3. Empirical potentials from associations in the vapor phase 92
2.4. Intermolecular hydrogen bonds 93
2.4.1. Weak interactions between unpolar systems and polar molecules . . . 93
2.4.2. Moderately strong hydrogen bonds 106
2.4.3. Strong intermolecular hydrogen bonds 118
2.5. Intramolecular hydrogen bonds 123
2.6. Stereochemistry of the hydrogen bond 128
2.7. Hydrogen bonds in clusters of molecules and molecular crystals 132
2.7.1. Calculations on small chains of molecules forming hydrogen bonds . . 133
2.7.2. Two- and three-dimensional clusters of molecules forming hydrogen bonds 137
2.7.3. Hydrogen bonded crystals 141
2.8. Hydrogen bonds in excited states 143
2.9. Proton affinities and potential curves for proton transfer 146
2.10. Conclusions 151
Acknowledgements 153
Note added in proof 154
References 155

The hydrogen bond – recent developments in theory and experiments
Eds. P. Schuster et al. © *North-Holland Publ. Co., Amsterdam, 1976*

2.1. Introduction

Associations between molecules containing polar HX-bonds and nonbonding electron pairs are characterized by relatively high energies of interaction and unique geometries. This kind of molecular interaction, generally called H-bond or H-bridge determines the structures of most molecular clusters in all three states of aggregation and hence fascinated theoreticians from the very beginning of theoretical chemistry. Various empirical and quantum mechanical methods were applied more or less successfully to calculate H-bonded structures. No satisfactory results, however, were obtained before extensive calculations of high numerical accuracy became possible. Six years ago Bratož [1967] summarized the various approaches to describe H-bonds. In this article he regretted that almost no accurate quantum mechanical calculations on H-bonded structures had been performed. Due to the rapid development of computational facilities high numerical accuracy is no hindrance any more. Nowadays far more than one hundred papers dealing with numerical calculations on H-bonds are available. Almost exclusively molecular orbital (MO) methods and perturbation theory were applied. Several review articles summarizing the results of calculations on H-bonding from one or the other point of view were published: Murthy and Rao [1970], Kollman and Allen [1972], Rao [1972], Schuster [1973, 1974] and Morokuma et al. [1974]. In this paper emphasis is laid on the calculations of energy surfaces for the interaction of H-bonded molecules and on the structure of molecular clusters. An attempt was made to cover most of the relevant literature from 1968 to 1973.

A successful theory of the H-bond has to be able to explain a number of important properties of H-bonded aggregates for which extensive experimental evidence is available:

1. Molecules forming H-bonds come much closer than the sum of the Van der Waals radii of the nearest atoms would allow. In fig. 2.1 this fact is demonstrated with the aid of two typical H-bonded complexes – $(HF)_2$ and $(H_2O)_2$.

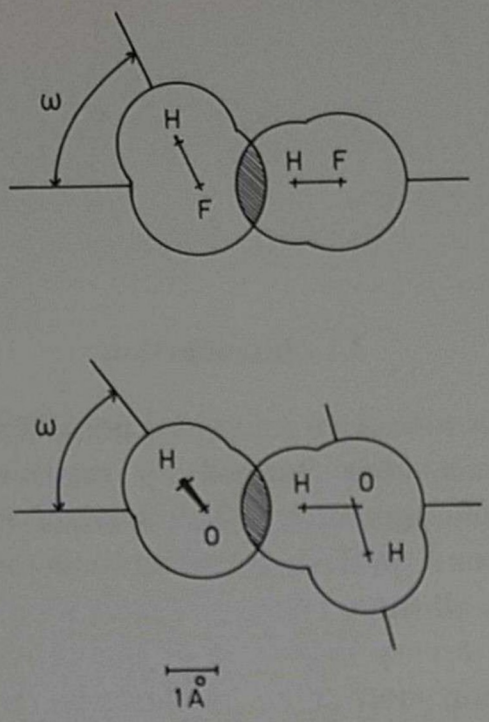

Fig. 2.1. Equilibrium geometry of $(HF)_2$ and $(H_2O)_2$. The circles around the nuclei represent the Van der Waals radii ($R^\circ_H = 1.2$ Å, $R^\circ_F = 1.3$ Å and $R^\circ_O = 1.4$ Å; for the definition of ω see also fig. 2.28).

2. H-bonding increases the polarity of the molecules concerned. The dipole moment of an H-bonded complex is larger than vectorial addition of the monomer moments would suggest.

3. As a consequence of H-bonding the lengths of the HX-bonds concerned are somewhat increased, IR stretching frequencies are shifted to smaller wave numbers and larger integral IR intensities of the corresponding absorption bands are found.

4. Electron densities at the protons involved in H-bonds are decreased and consequently NMR signals are shifted to lower magnetic fields.

Any generalization of the theory of H-bonding leads to the problem of intermolecular interactions. Consequently, we will demand from any general theory of molecular interactions to be able to describe H-bonds. The semiclassical theory* is based on the electrostatic contributions to intermolecular forces. Accordingly, we expect electrostatic models to be most successful in the case of ion/ion interactions, e.g. in the theory of ionic crystals, where electrostatic energy overwhelms by far all the other

* The expression "semiclassical" is used here for any method which is based on a quantum mechanical treatment of electronic structures of individual molecules but on calculations of intermolecular energies and forces by classical mechanics and electrostatics.

contributions. In the case of ion/molecule complexes the relative contribution of the electrostatic energy is much smaller. The electrostatic contribution decreases further if we proceed to interactions between uncharged polar molecules. No reasonably accurate description by semiclassical theories is possible anymore in this case and therefore we have to apply quantum mechanics. In the following section (2.2) a brief outline of quantum mechanical methods which are able to describe intermolecular interactions successfully is presented together with a summary of the actual stage of H-bond theory. Semiclassical and empirical calculations on H-bond energies are discussed in section 2.3 and finally the available theoretical results on H-bonds in various molecular systems are reviewed (sections 2.4–9).

2.2. Quantum mechanical methods and their application to hydrogen bonds

The theory of molecular interactions has been described extensively in the past, e.g. Hirschfelder et al. [1954], Hirschfelder and Meath [1967] and Margenau and Kestner [1971]. In this section only a very brief summary is given in order to present the essential expressions and definitions for an understanding of the following discussion of H-bonding.

Any quantum mechanical description of molecular properties starts from the time-dependent Schrödinger equation (2.1).

$$\hat{\mathcal{H}}\Phi = \mathrm{i}\hbar\frac{\partial\Phi}{\partial t}. \tag{2.1}$$

Neglecting relativistic effects the full Hamiltonian of our system of N atoms and n electrons (2.2) contains the operators for nuclear and electron kinetic energies (T_N and T_E) as well as the operator for the potential energy (V):

$$\hat{\mathcal{H}} = T_N + T_E + V. \tag{2.2}$$

$$T_N = -\frac{\hbar^2}{2}\sum_{k=1}^{N}\frac{1}{M_k}\nabla_k^2, \qquad T_E = -\frac{\hbar^2}{2m_0}\sum_{i=1}^{n}\nabla_i^2,$$

$$V = e_0^2\left\{\sum_{k=1}^{N-1}\sum_{l>k}^{N}\frac{Z_kZ_l}{R_{kl}} + \sum_{i=1}^{n-1}\sum_{j>1}^{n}\frac{1}{R_{ij}} - \sum_{k=1}^{N}\sum_{i=1}^{n}\frac{Z_k}{R_{ki}}\right\}.$$

In this equation R_{ab} represents the distance between the two particles a and b: $R_{ab} = |\boldsymbol{R}_a - \boldsymbol{R}_b| \cdot M_k$, Z_k and $\boldsymbol{R}_k$ are mass, charge and position of the nucleus k, $\boldsymbol{R}_i$ describes the position of electron i and finally m_0, e_0 and $\hbar$

are universal constants representing the mass of the electron, the elementary charge and Planck's constant divided by 2π ($\hbar = h/2\pi$)*. For our purpose we can restrict our interest in stationary states. For interactions between ordinary closed shell molecules the Born–Oppenheimer approximation will certainly be valid within the desired limits of accuracy. A detailed discussion of the separation of nuclear and electronic motion is found in many reviews and text books of quantum mechanics, e.g. Hirschfelder and Meath [1967] or Messiah [1970].

After the separation of the variables we are left with the problem to solve a set of two coupled differential equations:

$$\hat{\mathcal{H}}\Psi_\lambda = E_\lambda(\boldsymbol{R})\Psi_\lambda\,, \qquad \hat{\mathcal{H}} = T_E + V \tag{2.3}$$

and

$$\{T_N + E_\lambda(\boldsymbol{R})\}\chi_\mu^{(\lambda)} = W_{\mu\lambda}\chi_\mu^{(\lambda)}. \tag{2.4}$$

The nuclear coordinates, here summarized as $\boldsymbol{R}$, enter as parameters in the equation for electronic motion (2.3). The energy surface $E_\lambda(\boldsymbol{R})$ for the electronic state λ of the calculated system therefore represents a $3N$ dimensional hypersurface, which has to be calculated point by point since no analytic solutions of equation (2.3) are known. The differential equation for nuclear motion (2.4) can be solved only if $E_\lambda(\boldsymbol{R})$ is already known. $W_{\mu\lambda}$ finally represents the energy of the stationary state characterized by the two quantum numbers μ and λ. Consequently, we have to start with an attempt to solve the stationary Schrödinger equation for electronic motion. In this chapter we will be concerned exclusively in the calculation of energy surfaces $E_\lambda(\boldsymbol{R})$ of H-bonded associates. Nuclear motion will be discussed in the following chs. 3–6.

2.2.1. Molecular orbital theory of isolated molecules

For all molecules and molecular aggregates besides the hydrogen molecular ion (H_2^+) no analytic solution of the electronic Schrödinger equation has been found. Various approximative methods have been developed but unfortunately they all involve extensive numerical calculations. As mentioned before such calculations have to be performed point per point for the whole energy surface $E_\lambda(\boldsymbol{R})$ and therefore an enormous amount of computer time is necessary to obtain the desired information. Among all

* In all the following equations atomic units will be used (see, e.g. Kauzmann [1957]). Therefore m_0, e_0 and $\hbar$ are equal to 1. The two most important conversion factors concern energy and length: 1 a(tomic) l(ength) u(nit) = 0.5292 Å, 1 a(tomic) e(nergy) u(nit) = 27.21 eV = 627.5 kcal/mole.

methods which have been proposed during the development of quantum mechanics, the LCAO–MO* formalism turned out to be most efficient for numerical calculations on small molecules consisting of light atoms (atoms up to approximately the size of Cl or K).

Two degrees of approximation are commonly used in accurate LCAO–MO calculations on molecules. At the lower level of accuracy well known as Hartree–Fock (HF), self-consistent field (SCF) or independent particle approximation, the molecular wave function is represented by a single determinant (Slater determinant). This many electron function is built up from one electron MOs, which describe the uncorrelated motions of single electrons. For the ground state wave function of a closed shell molecule with $2n$ electrons we obtain:

$$\Psi_0 = \frac{1}{\sqrt{2n!}} \begin{vmatrix} \psi_1(1)\psi_1(2)\psi_1(3)\cdots\psi_1(2n) \\ \bar{\psi}_1(1)\bar{\psi}_1(2)\bar{\psi}_1(3)\cdots\bar{\psi}_1(2n) \\ \vdots \\ \bar{\psi}_n(1)\bar{\psi}_n(2)\bar{\psi}_n(3)\cdots\bar{\psi}_n(2n) \end{vmatrix}. \tag{2.5}$$

For the sake of simplicity the spin functions α and β corresponding to the m_s values $+1/2$ and $-1/2$ are already included in the notation, $\psi_k = \psi_k\alpha$ and $\bar{\psi}_k = \psi_k\beta$ respectively. The one electron MOs are constructed as linear combinations of basis orbitals

$$\psi_k = \sum_{i=1}^{m} c_{ik}\phi_k, \qquad m > n. \tag{2.6}$$

The coefficients on this linear combination are determined by a variational calculation leading to the well known eigenvalue (SCF) equations (2.7) derived by Roothaan [1951].

$$\hat{f}\psi_k = \epsilon_k\psi_k \qquad \text{or in matrix formalism:} \quad \mathbf{F}\cdot\mathbf{C} = \mathbf{S}\cdot\mathbf{C}\cdot\boldsymbol{\epsilon}. \tag{2.7}$$

For a detailed introduction to atomic and molecular SCF calculations the reader is referred to the recent monograph by Schaefer [1972]. For trivial mathematical reasons–otherwise the molecular orbitals would not be linearly independent–the number of orbitals in the basis set, m, has to exceed the number of double occupied orbitals, n. Generally, accurate calculations require very large numbers of m. In most cases either Slater (STOs) or Gaussian (GTOs) functions are used. With only few exceptions

* LCAO–MO means: Molecular Orbitals (MOs) built as Linear Combination of Atomic Orbitals (AOs) or basis functions of similar nature.

these orbitals are centered at the nuclei and therefore can be classified by the same symmetry arguments as ordinary atomic orbitals (AOs)*.

Very often the choice of an appropriate basis set is a tricky problem, because most molecular properties depend strongly on the basis sets applied. According to the variational principle the calculated energy represents an upper bound to the exact value and hence is always lowered with an extension of the basis set. In case of other quantities, however, there is no such systematic improvement. This is demonstrated clearly in fig. 2.2 which shows the relation between calculated energies and dipole moments for the water molecule (Clementi and Popkie [1972]). There is no direct correlation between calculated energies and dipole moments. Medium size and even small basis sets can reproduce the dipole moment of water almost correctly although the calculated total energy is rather

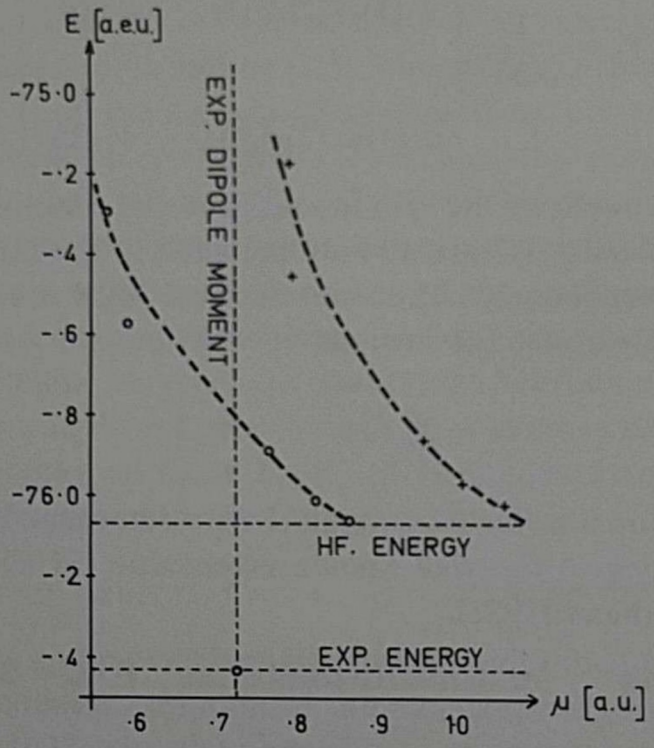

Fig. 2.2. Relation between calculated total energies and dipole moments in ab initio GTO calculations. Basis sets with (○) and without (+) polarization functions (Clementi and Popkie [1972]). All quantities in atomic units: energy unit, 1 au = 627.5 kcal/mole; length, 1 au = 0.5292 Å, dipole moment, 1 au = 2.541 Å.

* The following short notation for basis sets will be applied throughout in this contribution: $(\alpha, \beta, \gamma, \delta/\lambda, \mu, \nu)$ indicates that α s-type, β p-type, γ d-type, δ f-type orbitals are applied for second row atoms and λ s-type, μ p-type and ν d-type functions for H-atoms. The numbers of contracted functions are shown in square brackets: $[\alpha', \beta', \gamma', \delta'/\lambda', \mu', \nu']$.

poor. For very extended basis sets the inverse is usually true. The inclusion of polarization functions–orbitals of different symmetry properties than those occupied in the ground state of the atom, e.g. d- or f-orbitals at the O-atom and p- or d-orbitals at the H-atom–reduces the calculated dipole moments remarkably. With very extended basis sets the calculated molecular quantities become constant. Generally, these values are called HF-energies, HF-dipole moments and HF-force constants etc. The calculated properties do not coincide with the measured values because of the approximations of the independent particle model. At the HF level dipole moments for water and many other polar molecules are obtained too large, a fact which is very important for calculations of intermolecular interactions. To give another example HF-force constants for bond stretching vibrations show systematic errors too. For XH-bonds they are about 10–20% too large (table 2.1). In other cases even larger deviations were obtained.

A more sophisticated stage of approximation in LCAO–MO calculations is the so called nonrelativistic limit of molecular properties, which came within the reach of numerical calculations during the last five years. At this level the electrons are no longer regarded as independently moving particles and hence correlations between the motions of individual electrons have to be taken into account. Recently, Kutzelnigg [1973] presented a detailed review on different methods for the calculation of correlation energies, to which the interested reader is referred. All important methods start from the results of preceding SCF calculations. In general, a wave function Φ consisting of many Slater determinants Ψ_k is able to describe a particular electronic state exactly, provided the configuration interaction (CI) expansion has been extended until convergence and the one electron MO basis $(\psi_1 \cdots \psi_m)$ was complete:

$$\Phi = \gamma_0 \Psi_0 + \sum_{i,a} \gamma_{ia} \Psi_{ia} + \sum_{i<j} \sum_{a<b} \gamma_{ia,jb} \Psi_{ia,jb} + \cdots . \tag{2.8}$$

By Ψ_{ia} we denote here a Slater determinant, which differs from Ψ_0 the original ground state SCF function by replacement of the one electron orbital ψ_i by ψ_a. Accordingly, $\Psi_{ia,jb}$ indicates a double substitution $(\psi_i, \psi_j \rightarrow \psi_a, \psi_b)$. The summation in (2.8) includes also threefold and higher substitutions. The coefficients of this linear combination, γ, are determined by the conventional variation method. In case canonical HF-orbitals as obtained by the usual SCF procedure are used the expansion series shows very slow convergence and hence is not very useful for

TABLE 2.1

Influence of basis sets and electron correlation on the calculated properties of H_2O and HF

H_2O-molecule (z axis = C_2 axis; molecular plane: yz)

Orbitals	Basis set Uncontracted	Contracted	Method	Ref.	E_{tot} (au)	R_e^{OH} (Å)	α_e (°)	Force constants (10^5 dyn/cm)[a] f_{RR}	$f_{RR'}$	$f_{R\alpha}/R_e$	$f_{\alpha\alpha}/R_e^2$	$\mu(D)$	Polarizabilities (Å^3) α_{xx}	α_{yy}	α_{zz}	$\bar{\alpha}$
STO	(2, 1; 1)	[2, 1; 1]	SCF	a	−75.6614							1.63	$\sim 10^{-5}$	1.108	0.419	0.509
STO	(5, 2, 1; 2, 1)	[5, 2, 1; 2, 1]	SCF	a, b	−76.0384							1.93	1.069	1.279	1.162	1.170
GTO	(10, 6, 2; 4, 2)	[5, 3, 2; 2, 1]	SCF	c	−76.044							2.00				
GTO	(10, 6, 2; 4, 2)	[10, 6, 2; 4, 2]	SCF	c	−76.059							2.09				
GTO	(9, 5, 2; 4, 1)	[4, 3, 2; 2, 1]	SCF	d	−76.054	0.941	106.1	9.88	−0.08	0.26	0.88	2.00				
GTO	(11, 7, 2; 5, 1)	[6, 5, 2; 3, 1]	SCF	e	−76.063	0.941	106.6	9.83	−0.08	0.25	0.87	2.03				
GTO	(11, 7, 2; 6, 2)	[7, 4, 2; 4, 2]	SCF	f	−76.062	0.942	106.5	9.31	0.40	0.23	0.82					
GTO	(11, 7, 2; 6, 2)	[7, 4, 2; 4, 2]	IEPA	f	−76.393	0.973	103.3	8.37	−0.55	0.22	0.72					
–	–	–	EXP	b, d, e	−76.436	0.958	104.5	8.45	−0.10	0.23	0.76	1.85				1.456

HF-molecule (z axis = C_∞ axis)

Orbitals	Basis set Uncontracted	Contracted	Method	Ref.	E_{tot} (au)	R_e (Å)	Force constant $f(10^5$ dyn/cm)	μ (D)	Polarizabilities (Å^3) α_{zz}	$\alpha_{xx} = \alpha_{yy}$	$\bar{\alpha}$
GTO	(8, 5, 1; 4, 1)	[5, 4, 1; 3, 1]	SCF	g	−100.0260			2.08	0.653	0.261	0.391
GTO	(8, 5, 1; 4, 1)	[5, 4, 1; 3, 1]	IEPA	g	−100.3020			1.94	0.714	0.296	0.436
GTO	(8, 5, 1; 4, 1)	[5, 4, 1; 3, 1]	CEPA	g	−100.2542			1.99	0.685	0.267	0.406
GTO	(8, 5, 3; 4, 1)	[5, 4, 3; 3, 1]	SCF	g	−100.0282			1.95	0.812	0.609	0.677
GTO	(8, 5, 3; 4, 1)	[5, 4, 3; 3, 1]	IEPA	g	−100.3154			1.73	0.939	0.762	0.821
GTO	(8, 5, 3; 4, 1)	[5, 4, 3; 3, 1]	CEPA	g	−100.2657			1.82	0.879	0.674	0.742
GTO	(11, 7, 3; 6, 1)	[7, 4, 3; 4, 1]	SCF	g	−100.0630	0.900	11.20	1.93	0.848	0.662	0.725
GTO	(11, 7, 3; 6. 1)	[7, 4, 3; 4, 1]	IEPA	g	−100.3444	0.927	9.27	1.78	0.950	0.824	0.865
GTO	(11, 7, 3; 6, 1)	[7, 4, 3; 4, 1]	CEPA	g	−100.2943	0.917	9.92	1.82	0.907	0.725	0.785
–	–	–	EXP	f, g		0.917	9.66	1.82	0.960	0.720	0.800

[a] The definitions of the individual force constants of H_2O are the same as given by Ermler and Kern [1971].

References: **a** = Arrighini et al. [1967]; **b** = Arrighini et al. [1970]; **c** = Neumann and Moskowitz [1968]; **d** = Ermler and Kern [1971]; **e** = Dunning et al. [1972]; **f** = Lischka [1973c]; **g** = Lischka [1974a].

economic calculations of correlation energies. Nevertheless, due to the development of new numerical procedures to calculate the lowest eigenvalues of large CI matrices some authors succeeded to account for 10000 configurations and even more (Nesbet [1965a] and Shavitt [1970]).

Several methods were proposed in order to avoid this tedious and uneffective expansion. Among all these theories of electron correlation only electron pair methods will be used in our further discussion and therefore are mentioned briefly there. Electron pair theories consider pairwise electron correlation. Two closely related methods turned out to be very appropriate for numerical calculations on ground states of small molecules: The independent electron pair approximation (IEPA) originally suggested by Nesbet [1958, 1965b] and Sinanoglu [1962] and further developed for actual numerical calculations by Kutzelnigg [1963], Ahlrichs and Kutzelnigg [1968] and Jungen and Ahlrichs [1970] and the coupled electron pair approximation (CEPA) recently developed by Meyer [1973]. In both methods special orbitals for all individual electron pairs, the so called pair-natural-orbitals (PNOs) are constructed. The correlation energy is obtained by simple addition of the contributions from individual pairs

$$\Delta E_{\mathrm{COR}} = \sum_{i<j} E_{ij}. \tag{2.9}$$

The main difference between both procedures concerns the off-diagonal terms in the Hamiltonian matrix between two electron pairs. In the IEPA method these terms are neglected whereas they are taken into account in CEPA calculations.

In any case calculations including correlation energies are extremely time consuming. Nevertheless, accurate results are available nowadays for many small molecules and some bimolecular associations. For two molecules, which are important in H-bonding, H_2O and HF, the influence of electron correlation on some molecular properties is summarized in table 2.1. From changes in force constants we can conclude that not only the absolute values but also the curvatures of energy surfaces $E(\boldsymbol{R})$ are sensitive to electron correlation. Dipole moments in most cases are reduced to some extent if correlation is taken into account. The excellent agreement between the experimental dipole moment of the HF-molecule and the value calculated by the CEPA method is rather fortuitous since a contribution of singly excited configurations is neglected in this procedure. Exactly this contribution was shown to be of some importance in

case of CO (Grimaldi et al. [1967]) and LiH (Bender and Davidson [1968]). The polarizabilities are remarkably sensitive to correlation effects too. On the whole, table 2.1 clearly demonstrates that HF calculations present a roughly correct description of the molecules and their properties. However, correlation effects have to be considered if accurate values are desired. On the other hand large basis sets are inevitable too, since calculations including electron correlation using small or medium size basis sets do not give results of reasonable accuracy.

The chemist, however, is primarily interested in larger molecules than HF or H_2O. In this case even ab initio calculations with small basis sets require an unrealistic amount of computer time. Therefore many different kinds of semiempirical MO theories have been proposed. In actual calculations, however, the CNDO procedure proposed by Pople et al. [1965] and Pople and Segal [1965, 1966] and a number of variants derived from the original version were applied most frequently. Recent reviews of the CNDO and other semiempirical methods can be found in two books to which the interested reader is referred: Pople and Beveridge [1970] and Murrell and Harget [1972]. Two semiempirical methods–CNDO/2 and INDO–were applied successfully to H-bonded complexes and hence we will summarize here briefly the approximations introduced into the LCAO–MO–SCF formalism by these two procedures:

Approximation 1: Overlap integrals between atomic orbitals, $S_{\mu\nu}$, are neglected and accordingly the whole overlap matrix is replaced by the unit matrix

$$S_{\mu\nu} = \int \phi_\mu^* \phi_\nu \, d\tau = \delta_{\mu\nu}. \tag{2.10}$$

Approximation 2: Differential overlap is neglected in all two electron integrals (zero differential overlap = ZDO approximation)

$$(\mu\nu/\lambda\kappa) = \int\int \phi_\mu^*(1)\phi_\lambda^*(2) \frac{1}{R_{12}} \phi_\nu(1)\phi_\kappa(2) \, d\tau_1 \, d\tau_2 = \delta_{\mu\nu}\delta_{\lambda\kappa}(\mu\mu/\lambda\lambda). \tag{2.11}$$

In the INDO procedure one exception is made for one center two electron exchange integrals, which are taken into account explicitly. INDO: $(\mu\nu/\mu\nu) \neq 0$, if ϕ_μ and ϕ_ν belong to the same atom (Pople et al. [1967]).

Approximation 3: The remaining set of the coulomb type two electron integrals $(\mu\mu/\lambda\lambda)$ is further reduced in order to guarantee rotational invariance of the calculations. All coulomb integrals between two particular atoms are set equal to an average value calculated from s-type

functions: $(\mu\mu/\lambda\lambda) = \gamma_{AB}$, if ϕ_μ belongs to atom A and ϕ_λ to atom B,

$$\gamma_{AB} = \int\int \phi^*_{sA}(1)\phi^*_{sB}(2)\frac{1}{R_{12}}\phi_{sA}(1)\phi_{sB}(2)\,d\tau_1\,d\tau_2. \tag{2.12}$$

Approximation 4: The calculations are restricted to valence shell electrons. Inner shell electrons are neglected. The core potential is represented by point charges under the assumption of complete screening by inner shell electrons: $Z' = Z$ for K-shell atoms (H, He) and $Z' = Z - 2$ for L-shell atoms (Li to Ne).

Approximation 5: The neglect of differential overlap is extended to the core attraction integrals, which are further averaged to conservate rotational invariance

$$(\mu\nu/U_B) = \int \phi^*_\mu(1)U_B(1)\phi_\nu(1)\,d\tau_1 = \delta_{\mu\nu}(\mu\mu/U_B). \tag{2.13}$$

If point charges are used to represent the core ($U_B(1) = -Z'_B/R_{1B}$) these integrals are very easy to evaluate:

$$(\mu\mu/U_B) = -Z'_B\int \phi^*_\mu(1)\frac{1}{R_{1B}}\phi_\mu(1)\,d\tau_1. \tag{2.14}$$

In the CNDO/2 or INDO procedure the electron point charge interaction integrals are replaced by two electron coulomb integrals in order to achieve better agreement with experimental data:

$$(\mu\mu/U_B) \sim -Z'_B\gamma_{AB}. \tag{2.15}$$

We will keep in mind this particular approximation, because it is very important for the interpretation of semiempirical calculations on intermolecular interactions. For the calculation of the nuclear repulsion term, however, the point charges are retained:

$$E_{REP} = \sum_A \sum_{B>A} \frac{Z'_A Z'_B}{R_{AB}}. \tag{2.16}$$

Approximation 6: The off-diagonal elements of the one electron Hamiltonian are introduced empirically:

$$H_{\mu\nu} = \beta^0_{AB}S_{\mu\nu}, \text{ if } \phi_\mu \text{ belongs to atom A and } \phi_\nu \text{ belongs to atom B.} \tag{2.17}$$

The bond parameters β^0 are assumed to be additive and hence only one parameter for each kind of atoms used is necessary:

$$\beta^0_{AB} = \tfrac{1}{2}(\beta^0_A + \beta^0_B). \tag{2.18}$$

In general CNDO/2 and INDO calculations give a roughly correct description of the most important ground state properties of molecules. In table 2.2 the results of semiempirical calculations on some small molecules are compared with experimental data.

Considering the approximations made the agreement is surprisingly good. Bond-stretching force constants are much too large thus indicating that the shape of energy surfaces is reproduced rather poorly. This failure is a result of unbalanced approximations in the attraction and repulsion terms (see also section 2.2.2). Molecular geometries on the other hand are obtained in excellent agreement with the experiment. The only exceptions are polar XH-bonds which in general are calculated somewhat too long. Most calculated dipole moments are too large, but there are some exceptions, e.g. the formaldehyde molecule, where the inverse is found.

2.2.2. Perturbation theory of hydrogen bonds

During the last decade MO theory became by far the best developed quantum mechanical method for numerical calculations on isolated molecules. Calculations of intermolecular interactions generally start from wave functions of the isolated systems. Concerning the treatment of the interaction, however, there is some competition between MO methods and perturbation theory. Therefore, both procedures will be mentioned briefly here.

Intermolecular perturbation theory has been formulated long ago by Eisenschitz and London [1930]. Recently, new formulas were derived, e.g. Murrell et al. [1965] or Murrell and Shaw [1967], which turned out to be very appropriate when discussing small model systems*. This perturbational treatment was applied most frequently to structures with hydrogen bonds (Van Duijneveldt and Murrell [1967], Van Duijneveldt [1968] and Van Duijneveldt-Van de Rijdt and Van Duijneveldt [1968, 1970, 1971]). In intermolecular perturbation theory one of the major

* A more general derivation of intermolecular perturbation theory was given by Musher and Salem [1966] or Musher and Amos [1967]. Their equations include the formalism described here as the first term of an iterative procedure. For the discussion presented here, however, the simpler formalism is sufficient. The interested reader is referred also to two more recent papers: Jeziorski and Piela [1972], Piela and Jeziorski [1972].

TABLE 2.2

Semiempirical MO calculations on small molecules (Pople and Beveridge [1970]; Murrell and Harget [1972])

		Bond stretching						Angular deformation								
		Equilibrium bond length (Å)			Force constant (10^5 dyn/cm)				Equilibrium bond angle			Force constant (10^5 dyn/cm)		Dipole moment (D)[a]		
Molecule	Bond	CNDO/2	INDO	EXP	CNDO/2	INDO	EXP	Angle	CNDO/2	INDO	EXP	CNDO/2	EXP	CNDO/2	INDO	EXP
HO	HO	1.026	1.033	0.971	17.02	16.39	7.8							1.78	1.79	1.660
HF	HF	1.004[c]	1.006	0.917	19.12	18.64	9.66							1.86	1.98	1.820
CO	CO	1.191	1.191	1.128	41.34	40.46	19.0							0.64	0.60	−0.11
H_2O	HO	1.03	1.03	0.958				HOH	107.1[b]	108.6[b]	104.5	0.95	0.69	2.08	2.14	1.85
										104.7						
H_3N	HN	1.066[c]	1.07	1.019				HNH	106.7	109.7	106.6	0.95	0.6	2.08		1.47
H_2CO	HC	1.12[c]	1.12	1.116				HCH		115.0	116.5			1.92[c]		2.37
	CO		1.25	1.208												

[a] Dipole moment with the sign according to $A^+ B^-$ in AB.

[b] Upper value calculated with experimental, lower value calculated with INDO optimized bond length.

[c] Values taken from Schuster [1969a, 1970].

problems concerns the consideration of electron exchange between molecules. In the method described here exchange is limited to single electrons. This simplification is certainly a good approximation at large intermolecular distances. The energy of interaction between the molecules, ΔE^*, is obtained as a sum of first order, second order and higher order contributions:

$$\Delta E = \underbrace{\Delta E_{\mathrm{COU}} + \Delta E_{\mathrm{EX}}^{(1)}}_{\text{1st order terms}} + \underbrace{\Delta E_{\mathrm{POL}} + \Delta E_{\mathrm{DIS}} + \Delta E_{\mathrm{CHT}} + \cdots}_{\text{2nd order terms}}. \qquad (2.20)$$

The less important second order contributions and higher order contributions are not shown explicitly in eq. (2.20). The superscript on the exchange energy indicates that only single electron exchange has been taken into account.

The first order perturbation energy is calculated by the following zeroth-order approximation to the ground state wave function Ψ^0 of the two molecules:

$$\Psi^0 = N(1+P)\Psi_{\mathrm{A}}^0\Psi_{\mathrm{B}}^0. \qquad (2.21)$$

N represents a normalization constant of the wave functions. P takes care of antisymmetric behavior with respect to electron exchange. In the approximation of single electron exchange P can be substituted by

$$P \sim -\sum_{\mu\in\mathrm{A}}\sum_{\nu\in\mathrm{B}} P_{\mu\nu},$$

where $P_{\mu\nu}$ represents a permutation operator interchanging the coordinates of the electrons μ and ν. μ and ν are assumed to belong originally to the molecules A and B respectively. The wave functions of the isolated molecules are denoted by Ψ_{A}^0 and Ψ_{B}^0. They are solutions to the corresponding Schrödinger equations of the Hamiltonians $\hat{\mathscr{H}}_{\mathrm{A}}^0$ and $\hat{\mathscr{H}}_{\mathrm{B}}^0$:

$$\hat{\mathscr{H}}_{\mathrm{A}}^0\Psi_{\mathrm{A}}^0 = E_{\mathrm{A}}^0\Psi_{\mathrm{A}}^0, \qquad \hat{\mathscr{H}}_{\mathrm{B}}^0\Psi_{\mathrm{B}}^0 = E_{\mathrm{B}}^0\Psi_{\mathrm{B}}^0. \qquad (2.22)$$

* ΔE is defined in this paper as energy of complex formation:

$$\mathrm{A}+\mathrm{B}\rightarrow\mathrm{AB}, \qquad \Delta E = E_{\mathrm{AB}} - (E_{\mathrm{A}}^0 + E_{\mathrm{B}}^0). \qquad (2.19)$$

E_{A}^0, E_{B}^0 are the total energies of the isolated molecules–cf. eq. (2.22)–, E_{AB} is the total energy of the association or supermolecule AB. ΔE, of course, is a function of intermolecular distance and relative orientation: $\Delta E = \Delta E(\boldsymbol{R})$.

The total Hamiltonian $\hat{\mathcal{H}}$ of the supermolecule AB is split into $\hat{\mathcal{H}}_0$ and the perturbation $\lambda\hat{\mathcal{H}}'$. In all actual calculations on molecular interactions the intensity parameter λ is set $\lambda = 1$:

$$\hat{\mathcal{H}} = \hat{\mathcal{H}}_0 + \lambda\hat{\mathcal{H}}', \qquad \hat{\mathcal{H}}_0 = \hat{\mathcal{H}}^0_A + \hat{\mathcal{H}}^0_B, \qquad \hat{\mathcal{H}}' = V_{AB}(\boldsymbol{R}). \tag{2.23}$$

V_{AB} represents the potential for intermolecular interaction and accordingly is a function of the distance between the molecules and their relative orientation. Using the expressions given above the first order contribution to the perturbation energy can be deduced without further difficulty (Murrell and Shaw [1967]):

$$\Delta E_{COU} + \Delta E^{(1)}_{EX} = \frac{U_{OO} + U'_{OO}}{1 + S'_{OO}} \sim U_{OO} + U'_{OO} - U_{OO}S'_{OO} - U'_{OO}S'_{OO}. \tag{2.24}$$

The integrals are defined in the following way:

$$U_{OO} = \int (\Psi^0_A\Psi^0_B)^* V_{AB}(\boldsymbol{R})\Psi^0_A\Psi^0_B \, d\tau, \tag{2.25a}$$

$$U'_{OO} = \int (\Psi^0_A\Psi^0_B)^* V_{AB}(\boldsymbol{R})P(\Psi^0_A\Psi^0_B) \, d\tau, \tag{2.25b}$$

$$S'_{OO} = \int (\Psi^0_A\Psi^0_B)^* P(\Psi^0_A\Psi^0_B) \, d\tau. \tag{2.25c}$$

S'_{OO} is exactly, U'_{OO} is roughly proportional to the square of the overlap between the molecules, S_{AB}. The dependence of U'_{OO} on orbital overlap was discussed in detail by Murrell and Teixeira-Dias [1970]. The last term in eq. (2.24), $U'_{OO}S'_{OO}$, is roughly proportional to the fourth power of molecular overlap (S_{AB}) and hence much smaller in magnitude. Therefore, it is usually added to the higher order contributions.

More or less arbitrarily the electrostatic or coulomb energy of interaction ΔE_{COU} is defined directly in the basis of nonorthogonalized molecular orbitals of the isolated molecules. The renormalization correction of the electrostatic energy ($U_{OO}S'_{OO}$) is included in the exchange term $\Delta E^{(1)}_{EX}$.

$$\Delta E_{COU} = U_{OO}, \qquad \Delta E^{(1)}_{EX} = U'_{OO} - U_{OO}S'_{OO}. \tag{2.26}$$

An alternative partitioning, e.g. $\Delta E_{COU} = U_{OO}/(1 + S'_{OO})$ and $\Delta E^{(1)}_{EX} = U'_{OO}/(1 + S'_{OO})$ could be justified as well, because there are no physical

criteria for the preference of one or the other assignment*. The only advantage of eq. (2.26) is that it collects all terms of the same order with respect to molecular overlap.

ΔE_{COU} represents the semiclassical electrostatic energy of interaction and can be obtained directly from intermolecular geometries and charge distributions of the individual molecules. The charge distribution $Q_I(\boldsymbol{R})$ consists of the first order density function $\rho_I(\boldsymbol{R})$ and the nuclear charges;

$$Q_I(\boldsymbol{R}) = -\rho_I(\boldsymbol{R}) + \sum_{k=1,\, k\in I}^{N} Z_k \delta(\boldsymbol{R} - \boldsymbol{R}_k), \tag{2.27}$$

$$\rho_I(\boldsymbol{R}) = \int \cdots \int (\Psi_I^0)^* \Psi_I^0 \, \mathrm{d}\sigma_1 \, \mathrm{d}\tau_2 \cdots \mathrm{d}\tau_n.$$

σ_i represents the spin coordinate, τ_i spin and space coordinates of electron "i". From the charge distribution of the molecules A and B we obtain by classical electrostatics:

$$\Delta E_{\mathrm{COU}} = \int\int \rho_{\mathrm{A}}(\boldsymbol{R}_1)\rho_{\mathrm{B}}(\boldsymbol{R}_2) \frac{1}{R_{12}} \mathrm{d}\boldsymbol{R}_1 \, \mathrm{d}\boldsymbol{R}_2 + \sum_{k\in\mathrm{A}} \sum_{l\in\mathrm{B}} \frac{Z_k Z_l}{R_{kl}}$$

$$- \sum_{k\in\mathrm{A}} \int \rho_{\mathrm{B}}(\boldsymbol{R}_1) \frac{Z_k}{R_{1k}} \mathrm{d}\boldsymbol{R}_1 - \sum_{l\in\mathrm{B}} \int \rho_{\mathrm{A}}(\boldsymbol{R}_1) \frac{Z_l}{R_{1l}} \mathrm{d}\boldsymbol{R}_1. \tag{2.28}$$

Here the absolute values of the distances between two points are denoted by $R_{ij} = |\boldsymbol{R}_i - \boldsymbol{R}_j|$.

For two closed shell molecules A and B the first order exchange contribution always shows positive sign and represents the nonclassical repulsion of the molecules. Actually, it is roughly proportional to the square of the overlap between the molecules and hence falls off exponentially with increasing distance.

The three major second order contributions to the perturbation energy can be interpreted as changes in the energy of interaction due to the first order changes in the wave functions. Usually the changes in the wave functions are described by partial excitations to the unoccupied or virtual

* The difficulty here arises from the nonvanishing overlaps between the molecules. At sufficiently large intermolecular distances overlap and exchange energy become negligibly small and then the electrostatic energy of course is a physically well-defined quantity.

orbitals* of the isolated molecules. Three different cases can be distinguished (fig. 2.3):

1. Polarization of molecule A in the field of molecule B or vice versa polarization of B in the field of A. These two contributions are summed up to the polarization energy ΔE_{POL}.

2. Charge transfer from one molecule to the other is described by partial excitations of an electron from an occupied orbital of one molecule to a virtual orbital of the other. The energetic contribution of this intermolecular delocalization of electrons is called charge transfer energy, ΔE_{CHT}. In H-bonded structures a net electron transfer always occurs from the molecule with the lone pair to the molecule with the HX-bond, because the most important contribution to the charge transfer excites a lone pair electron into the antibonding HX orbital (cf. section 2.2.4).

3. Simultaneous and correlated excitations of electrons in both molecules lead to correlation of electron motions and to a general net

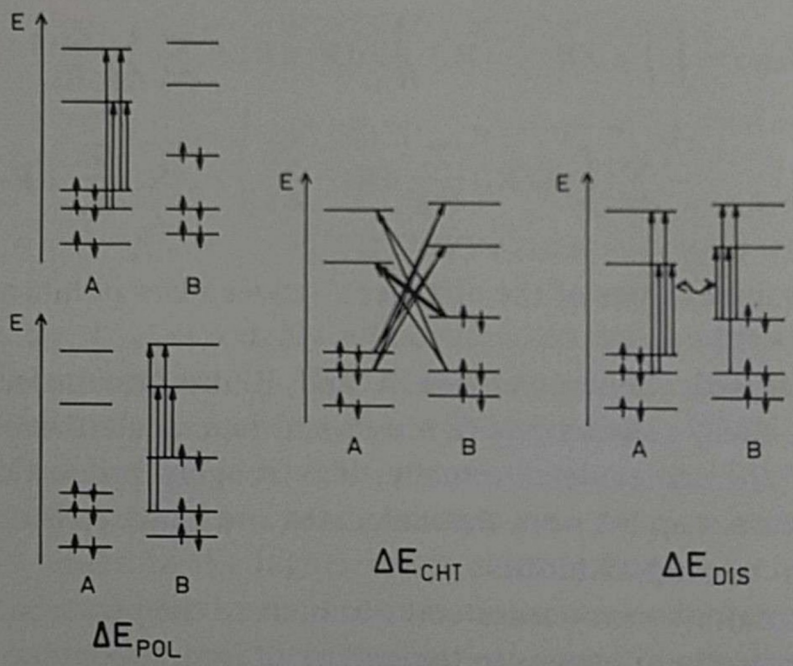

Fig. 2.3. Schematic explanation of different intermolecular contributions to second order perturbation energies by orbital excitations within the frame of the independent particle model.

* Here and in the following considerations we refer more or less to actual calculations than to the rigorous formalism of perturbation theory. For practical reasons the molecular excited states are simulated by raising electrons into the higher, virtual energy levels obtained by the MO–SCF procedure.

stabilization of the complex. This effect is usually attributed to the so called attractive dispersion forces and the corresponding energy is therefore called dispersion energy ΔE_{DIS}.

In general, all three contributions to the second order perturbation energy stabilize the molecular association AB. ΔE_{POL} is the analogue to the classical polarization energy and becomes identical with the function (CR^{-n}) calculated from molecular polarizabilities at large intermolecular distances. ΔE_{CHT}, on the other hand, is roughly proportional to the square of molecular overlap and hence falls off very much more rapidly with increasing distance R than the other two contributions. The dispersion energy ΔE_{DIS}, of course is identical with the London or attractive Van der Waals energy. Again the separation of the second order energy into individual contributions, especially into charge transfer and polarization effects is only free from arbitrariness at large distances where molecular overlap is sufficiently small. It is easy to visualize that in strongly overlapping systems any reasonable distinction between charge transfer and polarization disappears, because in this case all molecular orbitals are more or less extended over the whole complex. For intermediate distances, however, we will keep in mind that the partitioning of perturbation energies into individual contributions always depends to some extent on the model assumptions applied.

In fig. 2.4 the partitioning of the energy of interaction between two molecules forming an H-bond (XH$\cdots$Y) is shown as a function of the distance R_{XY}. The particular numerical values chosen here concern a model for the H-bond in water dimer (OH$\cdots$O). The perturbational treatment was restricted to four electrons forming the OH-bond and the lone pair at the second O-atom (Van Duijneveldt-Van de Rijdt and Van Duijneveldt [1970]). Three orbitals were used in the actual calculations: an O lone pair orbital on molecule A, a bonding and an antibonding orbital describing the OH-bond on molecule B, which participates in the H-bond (fig. 2.5). In a number of closely related calculations (Van Duijneveldt and Murrell [1967], Van Duijneveldt [1968] and Van Duijneveldt-Van de Rijdt and Van Duijneveldt [1968, 1971]) similar restrictions to the XH$\cdots$Y systems were made. The results can be generalized in the following way: around the energy minimum of the complex AB coulomb and charge transfer energy contribute significantly to the stability of the H-bonded association. The first order exchange contribution is of similar absolute magnitude but repulsive. Both polarization and dispersion energies lead to an additional stabilization of the H-bonded complex. They are, however,

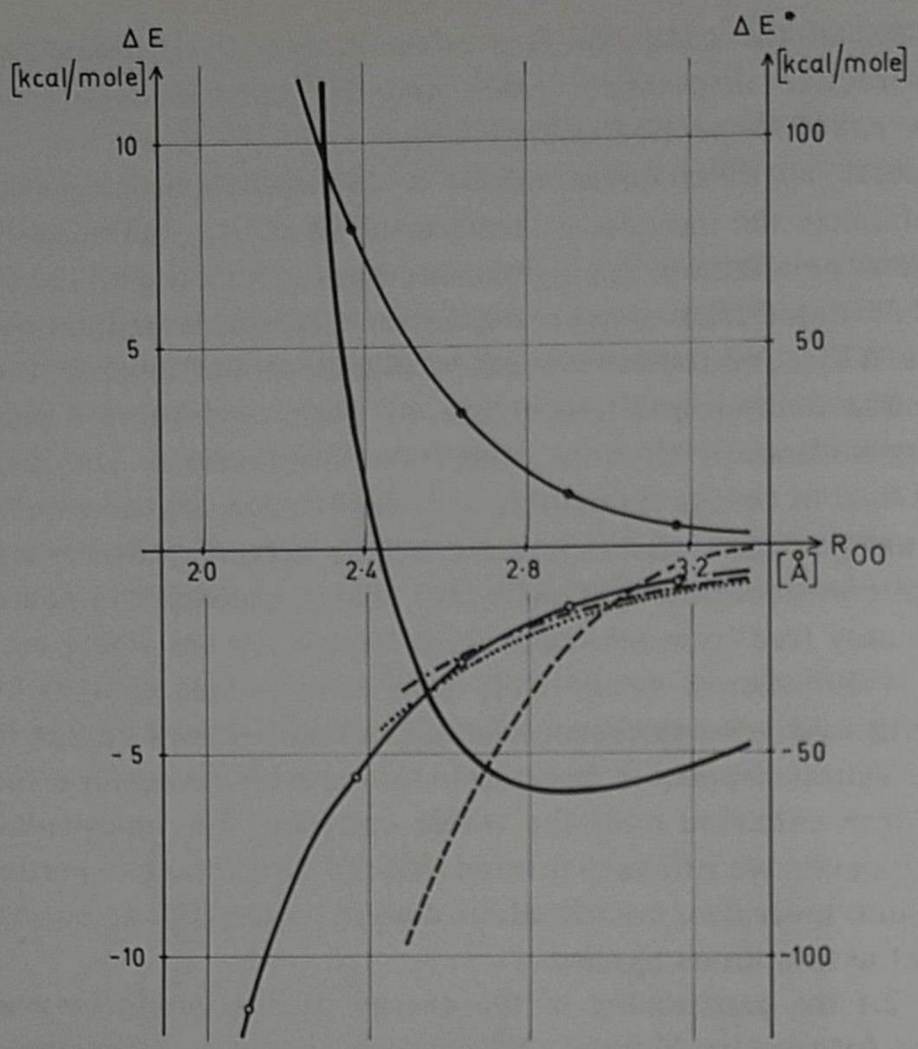

Fig. 2.4. Energy partitioning in $(H_2O)_2$ obtained by intermolecular perturbation theory. The H-bond is simulated by the four-electron fragment shown in fig. 2.5. Left hand calibration of the energy axis for ΔE: ———; ΔE_{POL}: –·–·–·–·–; ΔE_{CHT}: – – – – – and ΔE_{DIS}:· · · · · ·, right hand calibration of the energy axis for ΔE_{COU}: –○–○–○– and $\Delta E^{(1)}_{EX}$: –●–●–●–●–; (Van Duijneveldt-Van de Rijdt and Van Duijneveldt [1970]).

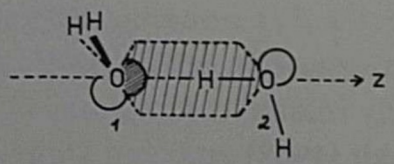

$$lp(O_1):\ \phi_1 = h_1\ ;\ h_1 = N_1\,(\phi^{O_1}_{2s} + \lambda_1\,\phi^{O_1}_{2p_z})$$

$$\sigma(HO_2):\ \phi_2 = N_2\,(\phi^{H}_{1s} + \mu h_2)\ ;\ h_2 = N_2'\,(\phi^{O_2}_{2s} - \lambda_2\,\phi^{O_2}_{2p_z})$$

$$\sigma^*(HO_2):\ \phi_3 = N_3\,(\mu\,\phi^{H}_{1s} - h_2)$$

Fig. 2.5. Orbitals used in the intermolecular perturbation theory to describe the four-electron fragment forming the H-bond in $(H_2O)_2$.

smaller in absolute value and therefore less important. As mentioned above, exchange and charge transfer energy are roughly proportional to the square of molecular overlap, S_{AB}, and hence fall off much faster with increasing distance than the other contributions. As a consequence of this result we have to expect charge transfer to be much more important in strong and hence shorter than in weak H-bonds.

A number of critical comments have been raised against the description of H-bonded structures by the perturbation formalism discussed above. First of all there is no reason to believe that the restriction of the exchange term to single electron exchange between molecules is valid for the structures actually calculated. In general, we would expect this simplification to be reasonably accurate only at large distances. Recently, double exchange contributions to the first order energy of interaction between closed shell systems were calculated by Van Duijneveldt-Van de Rijdt and Van Duijneveldt [1972]. They found in the case of $(He)_2$ that double exchange of electrons becomes important at distances below $R_{HeHe} \sim 2.0$ Å. Therefore, calculations on structures with H-bonds are at least around the limits of reliability of perturbation formalism considering only single exchange of electrons.

A second, serious shortcoming of most applications of this formalism is caused by the restriction to small fragments of both molecules. Only the three atoms and four electrons forming the H-bond were taken into account explicitly (XH···Y). Other parts of the molecules, however, contribute significantly to the electrostatic interaction too. This is clearly shown in table 2.3 where the results of different methods are compared. ΔE_{COU} calculated for the fragment OH···O in water dimer is almost twice as much as the value obtained by other methods for the whole system. Additionally, it seems doubtful if the angular dependence of intermolecular energies can be discussed correctly by this model since the contributions from other parts of the molecules are also changed drastically by rotations.

Another difficulty arises from an evident discrepancy between formalism and actual calculations. In the derivation of expressions for individual energy contributions it was assumed that the exact wave functions of the isolated systems are known, eq. (2.22). In practical calculations, however, we have to start always from approximate wave functions. In the best case SCF orbitals can be used and consequently no correlation effects in the isolated molecules are taken into account. The calculated perturbation energies, on the other hand, include electron correlation at least in part

TABLE 2.3

Comparison of intermolecular energy partitioning in water dimer

R_{OO}(Å)	Method[a]	Ref.	Quantity (kcal/mole) ΔE_{COU}	ΔE_{EX}	ΔE_I[b]	ΔE_{POL}	ΔE_{CHT}	ΔE_{DIS}	ΔE_{II}[b]	ΔE
2.78	PT	a	−7.5	9.2	1.7	−0.5	−5.0	−0.4	−5.7	−4.1
	MO	b	−8.0	9.9	1.9	−0.3	−8.2		−8.5	−6.6
	MO	c			−4.4	−3.2			−3.2	−7.6
	EP	d	−7.2							
2.9	PT, F	e	−12.0	13.1	1.1	−1.5	−1.4	−1.7	−4.6	−3.4
	PT	a	−5.8	5.6	−0.3	−0.4	−3.5	−0.3	−4.0	−4.3
	MO	c			−5.2	−2.3			−2.3	−7.4
	EP	d	−5.6							
3.2	PT, F	e	−7.2	5.0	−2.2	−0.8	−0.3	−1.0	−2.1	−4.3
	PT	a	−3.7	1.6	−2.1	−0.2	−1.3	−0.2	−1.6	−3.7
	MO	c			−5.3	−1.1			−1.1	−6.4
	EP	d	−3.7							

[a] PT = perturbation theory, MO = molecular orbital calculations, EP = electrostatic potential and PT, F = perturbation theory restricted to the four electron fragment XH···Y.

[b] ΔE_I = first order, ΔE_{II} = second order contribution.

References: **a** = Daudey [1974]; **b** = Morokuma [1971]; **c** = Kollman and Allen [1970a]; **d** = Bonaccorsi et al. [1971]; **e** = Van Duijneveldt-Van de Rijdt and Van Duijneveldt [1970].

and no clear separation of inter- and intramolecular contributions is possible. This problem can be discussed best by a double perturbation expansion, which was described in detail by Hirschfelder et al. [1964]. One perturbation series accounts for the intramolecular corrections and the other introduces the external perturbation (Musher [1967]). Until now no calculations of this type on interactions between molecules have been reported in the literature.

Recently, Daudey et al. [1974a] developed a different perturbative procedure for intermolecular interactions. They start directly from SCF wave functions of the isolated molecules and discuss molecular interactions as a CI problem. The lowest eigenvalue of the CI matrix is then obtained by a perturbational procedure. Both intra- and intermolecular correlation effects are taken into account. This method was applied to the interaction between two helium atoms (Daudey et al. [1974b]) and two water molecules (Daudey [1974]). In the second case the whole molecules were included in the calculation contrary to the model studies we discussed above. In this calculation Daudey [1974] used the LCAO–MO–SCF wave function of Morokuma and Winick [1970] for the isolated water molecules. Actually, this is the only example where the same wave function has been used for perturbational treatment and an SCF calculation on an H-bonded complex and hence the results are suitable for a comparison. The energy of interaction is split into different contributions which can be more or less rigorously identified with the quantities derived by Murrell et al. [1965] (fig. 2.6). Qualitatively, intermolecular energy partitioning is very similar to that presented by Van Duijneveldt and Murrell [1967] (fig. 2.4). In this perturbation formalism the correlation effects can be split into an intra- and an intermolecular contribution*. The latter, of course, represents the dispersion energy. Interestingly, the intramolecular contribution of electron correlation is repulsive. This can be explained by the correlation correction to the dipole moment, which as we have seen is obtained too large at the HF limit. Electron correlation therefore reduces its absolute value and consequently the dipole–dipole term of the electrostatic energy becomes smaller as well. Since the dipole–dipole term always stabilizes the H-bonded complex we obtain a net destabilization by intramolecular electron correlation. A more detailed discussion of this effect together with the influence of basis sets on the calculated energies of interaction

* Actually, this is possible only because effects of higher than second order are neglected.

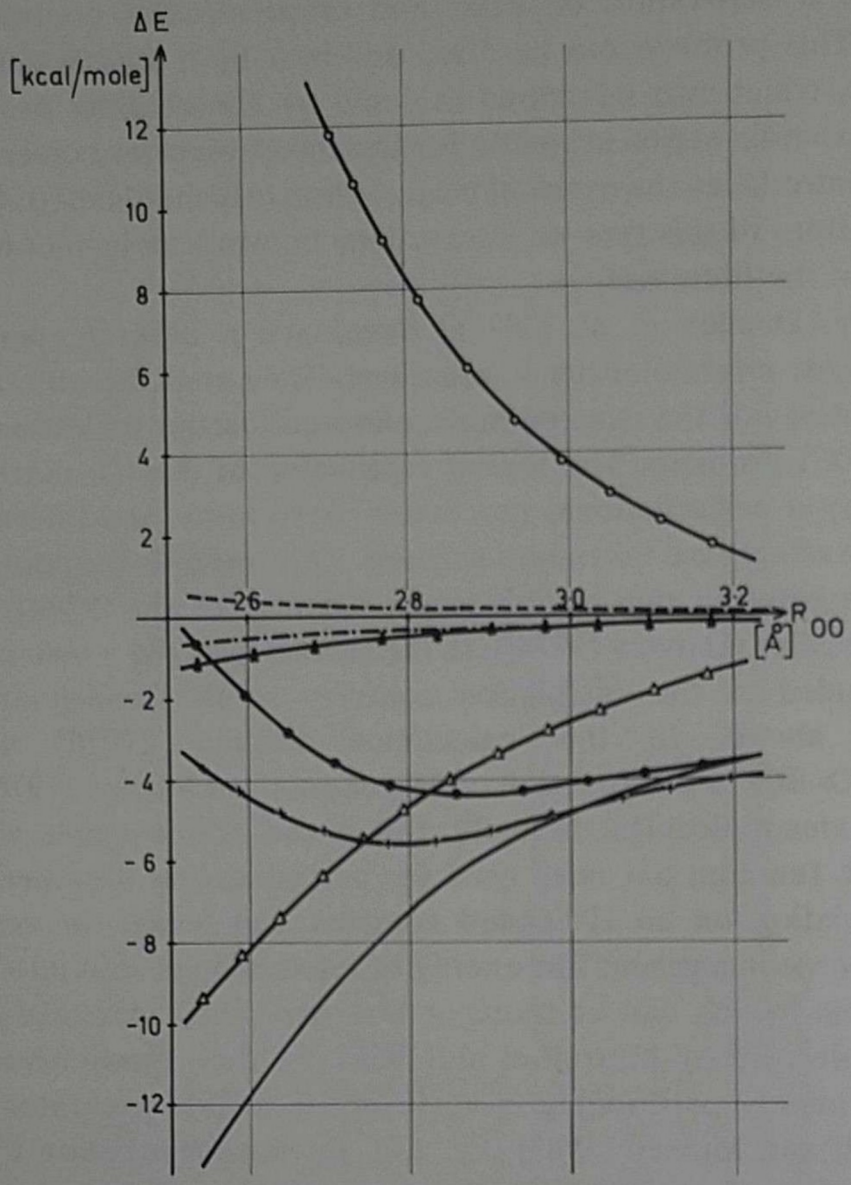

Fig. 2.6. Energy partitioning in $(H_2O)_2$ obtained by perturbational CI calculations (Daudey [1974], $\omega = 0°$), ΔE: -●-●-●-●-, ΔE_{COU}: ———, ΔE_{EX}: -○-○-○-, ΔE_{POL}: -▲-▲-▲-▲-, ΔE_{CHT}: -△-△-△-△-, ΔE_{COR}^{INTER}: -·-·-·-, ΔE_{COR}^{INTRA}: ——, for comparison ΔE_{SCF}: -+-+-+-.

will be presented together with the results of MO calculations on H-bonds. Interestingly, the polarization energy obtained by Daudey [1974] is remarkably small. This might well be an artifact of the small basis set used. We will come back to this problem in the discussion of interactions between noble gas atoms and polar molecules where polarization energy plays a dominating role (section 2.4.1).

An alternative application of perturbation theory to intermolecular interactions introduces the interaction potential as a perturbation into the HF equations. This procedure, usually, called HF or SCF perturbation

theory was developed independently by several groups. A detailed description of the formalism was presented by McWeeny [1962, 1968] and Diercksen and McWeeny [1966]. In a semiempirical (CNDO/2) version this perturbation method was recently applied to the water dimer by Sustmann and Vahrenholt [1973]. The total energy of interaction in this calculation is almost the same as obtained by other methods. The individual contributions, however, strikingly contradict the results of energy partitioning in other perturbational or ab initio MO calculations (fig. 2.7). It was found that the electrostatic energy does not contribute

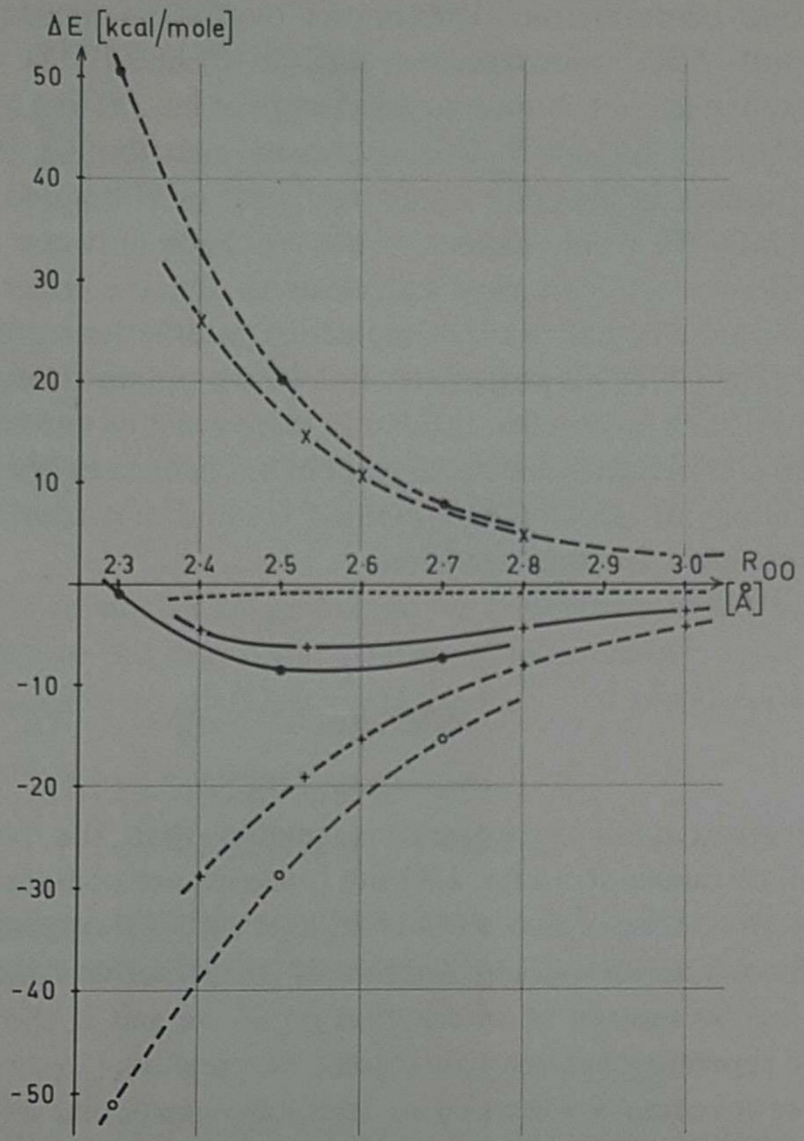

Fig. 2.7. Energy partitioning in $(H_2O)_2$ obtained by CNDO/2 calculations. SCF perturbation theory (Sustmann and Vahrenholt [1973]), ΔE: – + – + – + –, ΔE_{COU}: ———, $\Delta E_{EX}^{(1)}$: – × – × – × –, ΔE_{DEL}: – + – – + – – + –, LCAO–MO calculation (Kollman and Allen [1970a]), ΔE: –●–●–, ΔE_1: – –●– –●– –, ΔE_{DEL}: – –○– –○– –○– –.

significantly to the total energy and the stability of the H-bonded complex is exclusively due to delocalization of mainly charge transfer effects. A similar artificial result was obtained by energy partitioning in CNDO/2–SCF calculations of the whole complex (Kollman and Allen [1970a]) and will be discussed in the following subsection (2.2.3). Therefore, it seems reasonable to attribute this failure to the CNDO/2 method and not to the SCF perturbation theory.

For a better understanding of the limitations of semiempirical calculations it seems interesting to regard energy partitioning in intermolecular CNDO/2 calculations more closely. At the first glance we are confronted with a striking contradiction. Differential overlap is neglected in the CNDO method–ZDO approximation, eqs. (2.10) and (2.11). Therefore, there is no exchange contribution to the energy of interaction in CNDO or INDO calculations, $\Delta E_{EX} = 0$. The exchange contribution in ab initio perturbation theory is the only repulsive term* in H-bonded structures and consequently we would expect no net repulsion between two closed shell molecules in semiempirical calculations. On the other hand, we know from actual calculations that molecular interactions are described fairly well by the CNDO/2 procedure. Indeed we obtain strong repulsion between closed shell molecules. Evidently there must be another approximation which compensates for the neglect of exchange energy. Regarding the simplifications of the CNDO/2 method we find that approximation 5 (2.15) is responsible for the repulsion.

$$\int \phi_a^*(1)\, U_B \phi_a(1)\, d\tau_1 = -Z_B \int \phi_a^*(1) \frac{1}{R_{1B}} \phi_a(1)\, d\tau_1 \sim -Z_B \gamma_{AB}. \qquad (2.29)$$

The two electron coulomb integral is smaller than the point charge integral at all distances R. In fig. 2.8 both integrals are compared with the repulsion energy between two point charges $+e_0^2(1/R)$. Approximation 5, therefore, introduces an underestimation of an attractive contribution to the intermolecular energy of interaction or, if we put it the other way round, a net repulsion between the molecules results.

In any case it seems worthwhile to consider a particular example. For the sake of simplicity we have chosen the interaction between two

* Repulsion due to the nuclear interaction energy, E_{REP}, eq. (2.16) becomes important at much shorter interatomic distances.

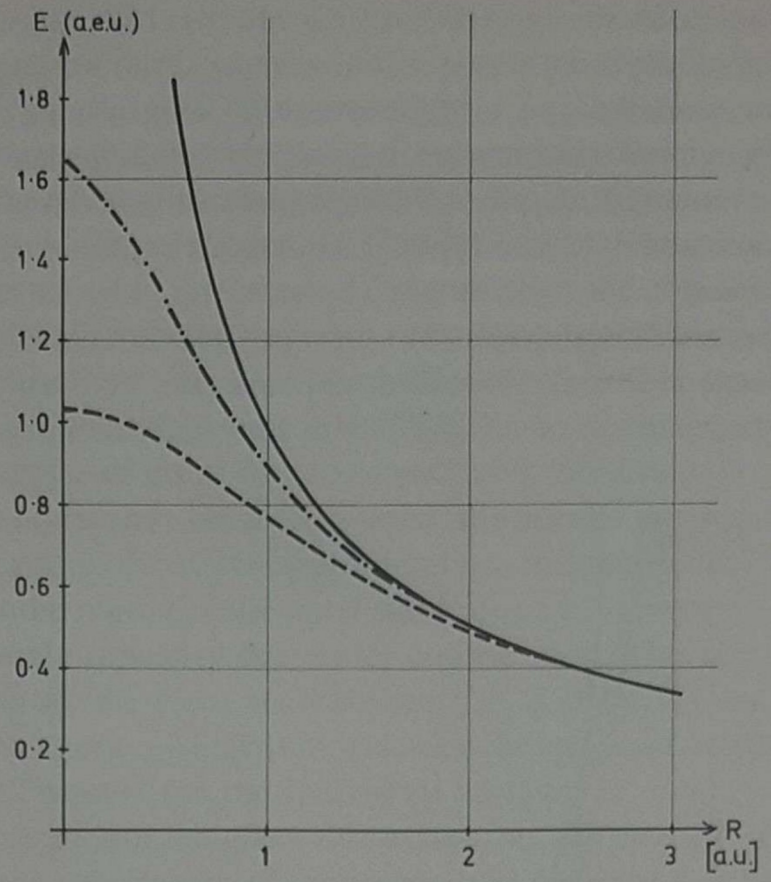

Fig. 2.8. Coulomb type interactions and their dependence on the interatomic distance R. R^{-1}: ———, (aa/R_b^{-1}): –·–·–·– and (aa/bb): – – – –; 1s orbitals a and b, $\xi_a = \xi_b = 1.65$; atomic units, see fig. 2.2.

He-atoms. From eqs. (2.25) and (2.26) we calculate coulomb and exchange contributions to the first order energy of interaction*:

$$\Delta E_{\mathrm{COU}} = 4\{(aa/bb) + (1/R) - 2(aa/r_{\mathrm{B}}^{-1})\}, \tag{2.30}$$

$$\Delta E_{\mathrm{EX}}^{(1)} = 2\{S_{ab}^2[3(aa/bb) - 4(aa/r_{\mathrm{B}}^{-1})] + 2S_{ab}[2(ab/r_{\mathrm{B}}^{-1}) - (aa/ab)] - (ab/ab)\}.$$

Introducing now the approximations of the CNDO/2 procedure we obtain a very simple expression for the first order contributions to the energy of interaction:

$$\Delta E_{\mathrm{COU}}^{\mathrm{CNDO/2}} = 4\{(1/R) - (aa/bb)\}, \qquad \Delta E_{\mathrm{EX}}^{\mathrm{CNDO/2}} = 0. \tag{2.31}$$

* The following short notation for one and two electron integrals is applied here: $S_{ab} = \int \phi_a^*(1)\phi_b(1)\,\mathrm{d}\tau_1$,

$$(ab/r_{\mathrm{B}}^{-1}) = \int \phi_a^*(1)\frac{1}{R_{1\mathrm{B}}}\phi_b(1)\,\mathrm{d}\tau_1, \qquad (ab/cd) = \int\int \phi_a^*(1)\phi_c^*(2)\frac{1}{R_{12}}\phi_b(1)\phi_d(2)\,\mathrm{d}\tau_1\,\mathrm{d}\tau_2.$$

From this expression we can see immediately that the coulomb energy is repulsive at any finite interatomic distance in the CNDO/2 approximation. This is not necessarily true in the "ab initio" expression, eq. (2.30). In order to obtain more information we calculated numerical values at a number of distances, R_{HeHe}, for all four expressions given above. ϕ_a and ϕ_b were represented by Slater type He 1s orbitals centered at the nuclei A and B respectively. The results are shown in fig. 2.9. As we suggested previously the interatomic repulsion term in CNDO/2 calculations is due to approximation 5 and therefore appears in the coulomb energy $\Delta E_{\mathrm{COU}}^{\mathrm{CNDO/2}}$. A comparison of $\Delta E_{\mathrm{COU}}^{\mathrm{CNDO/2}}$ with the total "ab initio" first order

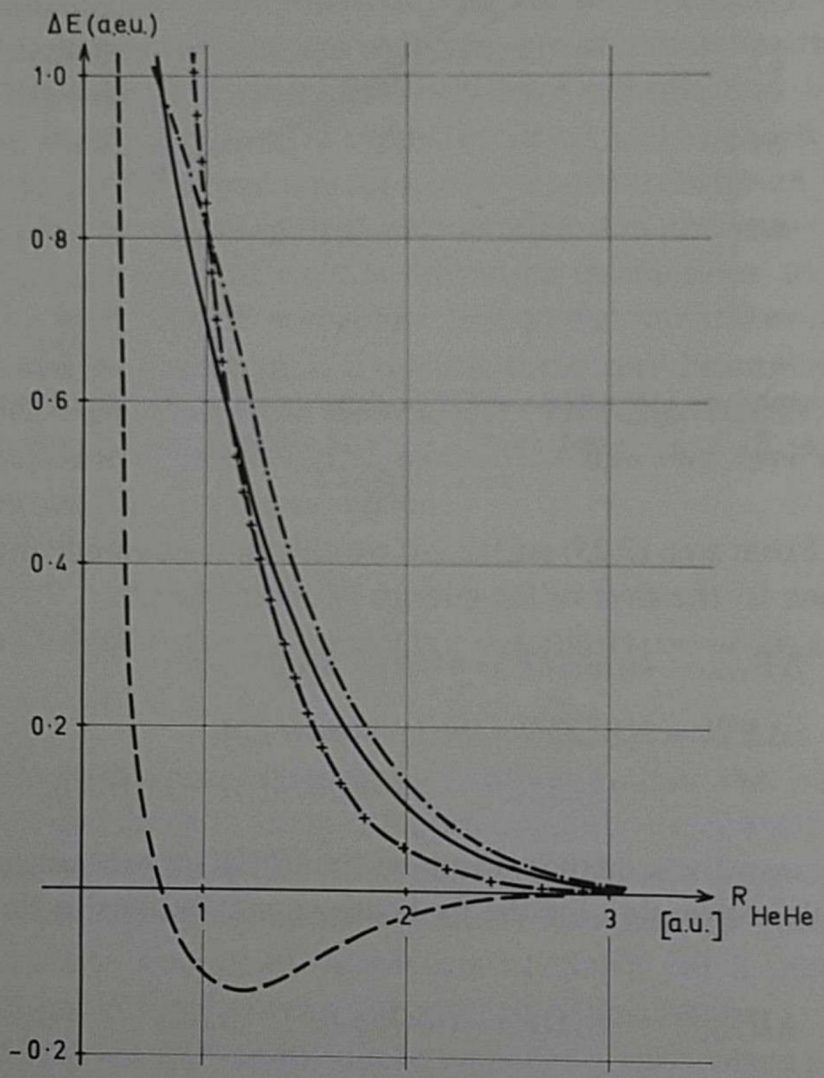

Fig. 2.9. Energy partitioning in $(He)_2$ obtained by first order perturbation theory. Basis set: 1s orbitals, $\xi = 1.65$; exact calculation, ΔE: ———, ΔE_{COU}: – – – –, $\Delta E_{\mathrm{EX}}^{(1)}$: –·–·–·–·–; CNDO/2 approximation, $\Delta E_{\mathrm{EX}}^{\mathrm{CNDO/2}} = 0$, $\Delta E^{\mathrm{CNDO/2}} = \Delta E_{\mathrm{COU}}^{\mathrm{CNDO/2}}$: –+–+–+–; atomic units, see fig. 2.2.

energy, $\Delta E_{COU} + \Delta E_{EX}^{(1)}$, shows that error compensation within the semiempirical method is unexpectedly well and explains at least in part the success of the CNDO/2 procedure in calculations of H-bonded structures. Regarding the two energy curves more closely we find that the curvature of the semiempirical curve is much larger. Because of the different origin of the repulsion the CNDO/2 energy curve increases much faster with decreasing interatomic distance than the ab initio curve does. Most probably approximation 5 also contributes significantly to the wrong curvature in energy curves for bond dissociation which is manifested by the unrealistically large force constants for bond stretching (table 2.2)*.

In the examples of the H-bonded structures, $(HF)_2$ and $(H_2O)_2$ for which energy partitioning has been calculated, the results are somewhat different. The errors of the ZDO approximation and approximation 5 do not cancel out in the region of the most stable complex geometry but lead to a residual strongly repulsive first order contribution. This repulsive term is compensated, as we have seen before (fig. 2.7) by the large attractive delocalization energy, which is more or less determined by the empirically introduced β^0 values for the individual atoms.

A corollary of our detailed discussion on the use of semiempirical methods in the calculation of intermolecular energies can be formulated as follows: CNDO/2 and related calculations might be very useful for the investigation of H-bonded structures. Any agreement with experimental data, however, is brought about by error compensation. Energy partitioning in the framework of perturbation theory based on semiempirical methods, however, has no meaning because at the end the results are determined by approximations and model assumptions of the method itself.

Regarding the "ab initio" contributions in the $(He)_2$ system more closely we find another remarkable result. The coulomb contribution defined according to eq. (2.26) leads to a potential curve with a stable minimum even in the $(He)_2$ system. Additionally, the exchange contribution reaches a maximum at very short distances ($R \approx 0.6$ au) as can be guessed from the (in absolute value) decreasing slope of the corresponding curve in fig. 2.9. The total first order contribution, $\Delta E_{COU} + \Delta E_{EX}^{(1)}$, is repulsive of course at every interatomic distance as it has to be. Any

* Force constants for bond stretching are calculated too large by ab initio SCF calculations as well (table 2.1). This error, due to neglect of electron correlation, however, amounts to only 10–20%.

physical interpretation for the minimum of the electrostatic contribution, ΔE_{COU}, must be very artificial if not impossible at all. The second curious result, the maximum of $\Delta E_{EX}^{(1)}$ can be recognized as an artifact of the calculation itself. According to the limited basis set the electrons of $(He)_2$ are forced to converge to a nonexisting state of the Be-atom at $R = 0$: $(1s^4)$. This example clearly shows that partitioning of intermolecular energies in the framework of perturbation theory is not free from arbitrariness at short distances. For a detailed discussion of the basis set dependence of ΔE_{COU} and $\Delta E_{EX}^{(1)}$ in He_2 see also Conway and Murrell [1972]. Although an extreme situation has been demonstrated by our peculiar example we should regard it as a serious warning to restrict the method to the region of vanishing molecular overlap. There we will not encounter the difficulties mentioned before. Around the Van der Waals minimum ($R = 5.6$ au $= 2.96$ Å, $\Delta E = -21.6$ cal/mole, see, e.g. Bertoncini and Wahl [1970, 1973] or McLaughlin and Schaefer [1971]) the electrostatic energy is negligibly small, the exchange energy represents the only remarkable contribution to the first order energy, which is repulsive as expected. Stabilization of the $(He)_2$ system occurs only by dispersion forces which appear of course in the second order term to perturbation energy.

Finally, another problem of intermolecular perturbation theory should be mentioned briefly. Claverie [1971] showed that ordinary Raleigh–Schrödinger perturbation theory does not reproduce the symmetry of the unperturbed ground state correctly, when it is applied to intermolecular interactions. At the limit $S_{AB} \to 0$ the wave function of the complex does not necessarily converge to separated wave functions of the isolated molecules. Recently a double perturbation theory was proposed by Beretta and Vetrano [1973] in order to overcome this difficulty. With this double parameter expansion they could derive equations which agree with the symmetry conditions of the isolated molecules and the molecular association at all orders including the zeroth-order wave function. Furthermore the equations for the individual contributions obtained do not differ very much from those originally derived by Murrell et al. [1965].

The formalism of intermolecular perturbation theory was developed further during the last few years. The interested reader is referred to two recent papers: Chipman et al. [1973] and Chipman and Hirschfelder [1973].

2.2.3. Molecular orbital theory of hydrogen bonds

In principle direct MO calculations of intermolecular energies are free of almost all the errors mentioned in the preceding subsection. The energy of interaction is obtained as the difference between the total energies of the association and the isolated molecules:

$$\Delta E = E_{AB} - (E_A^0 + E_B^0). \tag{2.32}$$

The energy of the complex, AB, is calculated by approximative solution of the Schrödinger equation exactly in the same way

$$\hat{\mathcal{H}}\Psi_{AB} = E_{AB}\Psi_{AB} \tag{2.33}$$

as for isolated molecules. The major problem, however, arises from the numerical details. The energy of interaction is obtained as a difference between huge numbers. In case of the water dimer it amounts to only 0.005% of the total energy. Hence all kinds of errors, methodical or numerical, might appear largely amplified in the intermolecular energies. No appreciable progress in this field was possible before high accuracy and high speed computers became available. Nowadays MO theory can be applied to molecular interactions at various stages of sophistication. We will mention here three different levels: semiempirical all valence electron calculations, ab initio SCF calculations and ab initio calculations including electron correlation.

An impressive number of accurate SCF calculations on H-bonded structures is available now. In one case, a very detailed study of $(HF)_2$, the influence of electron correlation on various properties of the H-bonded association was investigated thoroughly by Lischka [1974a]. In this section we will compare the results of different MO methods on two typical H-bonded complexes, $(HF)_2$ and $(H_2O)_2$, which have been studied more extensively than all the other molecular associations.

In order to learn more about the nature of H-bonds we will start with partitioning of the total molecular energy, ΔE, into individual contributions similar to those in perturbation theory. Attempts to split ΔE into different parts were undertaken independently by Dreyfus and Pullman [1970a] and Kollman and Allen [1970a]. A little later Morokuma [1971] presented a more detailed scheme of energy partitioning within the

framework of MO theory, which we will discuss here*. This analysis starts from antisymmetrized wave functions of the isolated molecules, Ψ_A^0 and Ψ_B^0, as well as from the complete Hamiltonian $\hat{\mathcal{H}}$ of the interacting complex AB. Four different approximations are used to describe the whole system:

1. A simple Hartree product of the two wave functions:

$$\Psi_1 = \Psi_A^0 \Psi_B^0. \tag{2.34}$$

2. An antisymmetrized (HF) product of the two wave functions

$$\Psi_2 = \mathcal{A}(\Psi_A^0 \Psi_B^0). \tag{2.35}$$

As in the previous subsection, $\mathcal{A}$ represents an antisymmetrizer ($\mathcal{A} = 1 + P$).

3. A product of the two wave functions, which have been optimized individually in the potential field of the other molecule:

$$\Psi_3 = \Psi_A \Psi_B. \tag{2.36}$$

Again Ψ_A and Ψ_B are antisymmetric.

4. The ordinary, antisymmetric and optimized SCF wave function of the complex

$$\Psi_4 = \Psi_{AB}. \tag{2.37}$$

Now expectation values of the energy are calculated from all four wave functions. The individual contributions to the energy of interaction are obtained as differences:

$$\Delta E_i = E_i - (E_A^0 + E_B^0), \qquad E_i = \int \Psi_i^* \hat{\mathcal{H}} \Psi_i \, d\tau. \tag{2.38}$$

Regarding the definitions given above more closely, we find that ΔE_1 is equivalent to the coulomb or electrostatic energy of interaction, ΔE_{COU}, defined in intermolecular perturbation theory cf. eq. (2.26) and becomes identical with it in case the exact solutions of the Schrödinger equations for the isolated molecules are used, eq. (2.22). ΔE_2 on the other hand is the analogue to the complete first order energy of interaction including the exchange contribution. Accordingly, we can define an intermolecular

* Another type of energy partitioning in MO theory was proposed by Clementi [1967a]. This kind of partitioning called "Bond Energy Analysis" (BEA) was found to be particularly useful in larger molecular clusters (Clementi and Popkie [1972] and Popkie et al. [1973]). Since the individual contributions of BEA are not directly related to the quantities we discussed in intermolecular perturbation theory, we will not use Clementi's technique here.

exchange energy within the framework of MO theory:

$$\Delta E_{EX} = \Delta E_2 - \Delta E_1. \tag{2.39}$$

This exchange energy, however, differs somewhat from the exchange contribution in perturbation theory, since in the MO treatment the exchange is not restricted to single electrons.

The one electron MOs in the wave function Ψ_3 account for the field of the other molecule whereas no electron exchange is allowed. Physically we might interpret this contribution as a sum of electrostatic and polarization energy*:

$$\Delta E_{POL} + \Delta E_{COU} = \Delta E_3, \qquad \Delta E_{POL} = \Delta E_3 - \Delta E_1. \tag{2.40}$$

Finally, the remaining difference to the total SCF energy of interaction, ΔE_4, is attributed to a stabilization of the complex in consequence of electron delocalization or charge transfer between the molecules:

$$\Delta E_{CHT} = \Delta E_4 - (\Delta E_{COU} + \Delta E_{EX} + \Delta E_{POL}) = \Delta E_4 + \Delta E_1 - \Delta E_2 - \Delta E_3. \tag{2.41}$$

Partitioning of intermolecular energies within the framework of MO theory represents a possibility to compare results of perturbation theory and MO calculations (table 2.3). The qualitative features of the individual contributions and their dependence on intermolecular distances are roughly the same in all calculations presented.

Looking more closely to the numerical values, however, we find large differences. The major problem, which arises now, is to decide if this disagreement results from different methods–MO or perturbation theory–or from different model assumptions and the use of different basis sets. The same basis set has been used only in one example–the partitioning of intermolecular energies in $(H_2O)_2$ by perturbation theory (Daudey [1974]) and MO calculation (Morokuma [1971]). In this particular case the agreement is fairly good. Perturbation theory underestimates the charge transfer contribution to some extent and hence the total energy is somewhat too small as well. As expected the numerical values for the coulomb energy of interaction agree well with the numbers calculated from molecular electrostatic potentials, which were derived from a

* Morokuma [1971] defined this contribution as a sum of polarization and dispersion energy. In case Ψ_A and Ψ_B are single Slater determinants, as generally in SCF calculations, no correlation effects are taken into account and hence $\Delta E_3 - \Delta E_1$ actually represents only the contribution of electron polarization.

calculation on the water molecule with a similar basis set (Bonaccorsi et al. [1971], see also section 2.3.1). Model calculations limited to a perturbational treatment of the four-electron, three-atom fragment, OH···O, (cf. fig. 2.5) in water dimer lead to very different individual first order contributions. Both coulomb and exchange energy are about twice as large in these model calculations as in ordinary calculations on whole molecules. Additionally, the charge transfer contribution seems to be largely underestimated. To some extent these perturbational calculations on the interaction of molecular fragments, however, are semiempirical in nature, because the orbitals for the four-electron, three-atom fragment have to be chosen at the beginning and remain unchanged throughout the calculations. Therefore, orbital sizes and polarities of the XH-bonds enter as parameters into the calculations (e.g. λ_1, λ_2 and μ in fig. 2.5, see also Van Duijneveldt and Murrell [1967]).

Within the framework of MO theory, on the other hand, the results of energy partitioning depend very much on the basis sets applied. This is shown clearly by a comparison of the results of two calculations by Morokuma and Winick [1970] or Kollman and Allen [1970a] and Morokuma [1971]. Unfortunately, only medium size basis sets have been used in both calculations and hence no really accurate data on energy partitioning became available until now. Afterwards we will discuss the influence of basis sets on calculated energies and other quantities in more detail. However, from the available data we can conclude already the results obtained are much more sensitive to model assumptions or basis sets than to individual procedures of calculation–perturbation or MO theory–provided the same definitions are used for the individual quantities.

As indicated above we have to expect strong dependence of calculated properties on the basis sets applied as long as the basis is not flexible enough. We will regard the available MO calculations and their results on structures with H-bonds more closely now. The most important results on two molecular associations $(HF)_2$ and $(H_2O)_2$ are summarized in the tables 2.4 and 2.5. As a more or less general rule we find that the energy of interaction is obtained too large with small basis sets and decreases gradually when the basis set is extended. Very flat orbitals with small exponents were found to be of particular importance for calculations on intermolecular energies (Popkie et al. [1973] and Lischka [1973a, b; 1974a]). In case of $(HF)_2$ the major differences between calculation **c** ($\Delta E = -4.5$ kcal/mole) and calculation **d** ($\Delta E = -3.5$ kcal/mole) in table 2.4 is

TABLE 2.4

SCF calculations on $(HF)_2$ with different basis sets

Basis set (GTOs)	Ref.	E_{HF}(au)	$E_{(HF)_2}$(au)	ΔE (kcal/mole)	R_{FF}(Å)	γ(°)	ω(°)
(8, 4; 4)→[2, 1; 1][a]	a	−99.27023	−198.54876	−5.2	2.55	4	69
(10, 5; 5)→[3, 1; 1]	b	−99.99578	−199.99638	−4.6	2.88	–	20
(10, 5; 5, 1)→[4, 2; 2, 1]	b	−100.01346	−200.03726	−6.5	2.78	–	20
(9, 5, 1; 4, 1)→[4, 2; 2, 1]	e	−100.0442	−200.0953	−4.63	2.80	5	52
(11, 7, 1; 6, 1)→[5, 4, 1; 3, 1]	c	−100.05638	−200.11989	−4.5	2.85	–	40
(11, 7, 2; 6, 1)→[7, 4, 2; 4, 1]	d	−100.06261	−200.13073	−3.5	2.90	–	–
Exp.	f, g, h	–	–	−6 ± 1.5	2.79	~0	60–70

[a] Minimal Slater basis set; the Slater orbitals are expanded in a set of gaussian orbitals: STO-NG, Hehre et al. [1969] and Ditchfield et al. [1971].

References: **a** = Del Bene and Pople [1971]; **b** = Kollman and Allen [1970b]; **c** = Diercksen and Kraemer [1970a]; **d** = Lischka [1974a]; **e** = Yarkony et al. [1974]; **f** = Dyke et al. [1972]; **g** = Smith [1959]; **h** = Franck and Meyer [1959].

TABLE 2.5

SCF calculations on $(H_2O)_2$ with different basis sets

Basis sets (GTOs)	Ref.	E_{H_2O}(au)	$E_{(H_2O)_2}$(au)	ΔE (kcal/mole)	R_{OO}(Å)	ω(°)
(5, 3; 3)	a	−75.54940	−151.11887	−12.6	2.86	0–15
STO, min	b	−75.70503	−151.42051	−6.6	2.78	54
(8, 4; 4)→[2, 1; 1][a)]	c	−75.50013	−151.00998	−6.1	2.73	58
(10, 5; 5)→[3, 1; 1]	d	−75.97565	−151.95775	−5.3	3.00	25
(10, 5, 1; 4, 1)→[5, 3, 1; 2, 1]	e	−76.04136	−151.09069	−5.0	3.00	40
(11, 7, 1; 6, 1)→[5, 4, 1; 3, 1]	f	−76.05326	−152.11167	−4.8	3.00	–
(13, 8, 2, 1; 6, 2, 1)→[8, 5, 2, 1; 4, 2, 1]	g	−76.06598	−152.13781	−3.7	3.00	–

[a)] STO-4G basis, see footnote to table 2.4.

References: **a** = Morokuma and Pedersen [1968]; **b** = Morokuma and Winick [1970] and Bonaccorsi et al. [1971]; **c** = Del Bene and Pople [1969, 1970]; **d** = Kollman and Allen [1969]; **e** = Hankins et al. [1970a, b; 1973]; **f** = Diercksen [1969, 1971]; **g** = Popkie et al. [1973].

due to the inclusion of a very flat d-function at the F-atom in **d**. A similar effect of very extended functions on the energy of interaction was found in $(H_2O)_2$ too (cf. calculations **f** and **g** in table 2.5). A straightforward analysis of these basis set effects leads to two major contributions, which can be classified as intra- and intermolecular changes. First of all the properties of the isolated systems themselves are changed by an extension of the basis set. The inclusion of polarization functions–d- and f-orbitals at the O- or F-atoms, p- or d-orbitals at the H-atoms–in general reduces the calculated dipole moments $\boldsymbol{\mu}$ and increases the calculated polarizabilities $\boldsymbol{\alpha}$ (table 2.1). Consequently, the coulomb contribution to the energy of interaction is reduced as we can see directly from the classical electrostatic formula:

$$\Delta E_{\mathrm{COU}}^{\mathrm{CL}} = (1/R^3)\{\boldsymbol{\mu}_A \cdot \boldsymbol{\mu}_B - (3/R^2)(\boldsymbol{\mu}_A \cdot \boldsymbol{R})(\boldsymbol{\mu}_B \cdot \boldsymbol{R})\} + \cdots . \qquad (2.42)$$

In case of the contribution of electron polarization an estimate is more difficult because it depends on both $\boldsymbol{\mu}$ and $\boldsymbol{\alpha}$. Regarding the classical approach (2.43) we would expect the polarization energy to remain more or less constant:

$$\Delta E_{\mathrm{POL}}^{\mathrm{CL}} = (1/R^6)\{\alpha_A|\mu_B|^2 + \alpha_B|\mu_A|^2\} + \cdots *. \qquad (2.43)$$

Hence intermolecular changes due to extension of the basis set by polarization functions will reduce the energy of interaction. Intermolecular effects of basis set extensions have to be expected too, but they are somewhat more difficult to explain. In principle any MO calculation will be improved by the addition of functions of appropriate symmetry to this basis set. Orbitals outside the region of high electron density are of course less effective than orbitals inside, but they can lead to nonnegligible lowering of the total energy if small changes are considered. These external orbitals, however, have much more influence on calculations with small basis sets than on extended calculations. Therefore the energy of molecule A is lowered to some extent in presence of the basis set of molecule B and vice versa. Due to this effect we obtain an artificial stabilization of the complex AB, which is expected to be larger if small basis sets are applied. This suggestion has been verified recently by a number of authors: Johansson et al. [1973], Marius [1973], Meunier et al. [1973], Daudey [1974] and Lischka [1974b]. An attempt was made to

* Spherical symmetry of the polarizability tensor has been assumed for this simplified estimate.

correct this error by using different energies for the monomers E_A^{AB} and E_B^{AB}. These energies were obtained by independent calculations of the individual molecules using the basis set of the whole complex AB. Accordingly, these monomer energies are functions of the intermolecular geometry. In general these corrections are larger for smaller basis sets. The corrected energies of interaction again are not completely independent of the basis set applied. Often the corrections are rather sensitive to smaller changes, e.g. the addition of flat polarization functions or slightly different contractions (table 2.6). Comparing the corrected energies with the calculated dipole moments as far as they are available we find the expected parallelism. Hence intermolecular basis set effects were eliminated at least in part by the procedure described above. Since both intra- and intermolecular effects tend to decrease the energy of interaction on an extension of the basis set we have to expect most of the calculated energies to be too large in absolute value.

Finally, we will concentrate on one of the most important questions in intermolecular MO theory, the influence of electron correlation on the SCF energies of interaction. A definite answer to this question was not possible until quite recently a number of papers on this problem were published (Meunier et al. [1973], Daudey [1974] and Lischka [1974a]). In these three papers more or less extended MO calculations including electron correlation were presented for the systems $H_3N\cdots HOH$; $(H_2O)_2$ and $(HF)_2$. The authors of these calculations come to the same conclusions and therefore we will only discuss the last paper, wherein the most extended basis set was applied. In the linear arrangement of $(HF)_2$ the net effects of correlation energy are very small indeed. However, this is only due to cancellation of two contributions with opposite sign (table 2.7). In HF, H_2O and similar molecules intramolecular electron correlation reduces molecular dipole moments and increases polarizabilities. Consequently, the coulomb energy of interaction is decreased. By the same arguments as before the contribution of electron polarization is expected to remain almost unchanged. On the other hand, intermolecular electron correlation will lead to significant lowering of the total energy of the complex since it accounts for stabilization by dispersion forces. As fig. 2.10 shows, these two contributions to correlation energy change cancel each other almost completely in the linear arrangement of $(HF)_2$ at distances around the energy minimum. For other intermolecular geometries ($\omega = 0°$), however, we have to expect the electrostatic contribution to be smaller, since the two dipoles are no longer in the most favorable

TABLE 2.6

Basis set corrections to intermolecular energies of interaction (values taken from SCF calculations Lischka [1974b]: $(HF)_2$ linear, $R_{HF} = 0.917$ Å, $R_{FF} = 2.91$ Å)

Basis set		Energies (in au)				$\Delta E^{b)}$	$\Delta E'^{b)}$	$\mu(D)$
GTOs	Contraction	E_{AB}	$E_0^{a)}$	$E_A^{a)}$	$E_B^{a)}$	(kcal/mole)	(kcal/mole)	calc.
(8, 4, 1; 4, 1)	[5, 3, 1; 3, 1]	−200.03973	−100.01586	−100.01617	−100.01709	−5.03	−4.06	
(8, 5, 1; 4, 1)	[5, 4, 1; 3, 1]	−200.05865	−100.02604	−100.02631	−100.02620	−4.12	−3.85	2.09
(8, 5, 2; 4, 1)	[5, 4, 2; 3, 1]	−200.06152	−100.02787	−100.02805	−100.02817	−3.62	−3.32	1.95
(11, 7, 1; 6, 1)	[7, 4, 1; 4, 1]	−200.12986	−100.06200	−100.06209	−100.06205	−3.68	−3.60	
(11, 7, 1; 6, 1)	[5, 4, 1; 3, 1]$^{c)}$	−200.11556	−100.05452	−100.05517	−100.05477	−4.10	−3.53	
(11, 7, 2; 6, 1)	[7, 4, 2; 4, 1]	−200.13094	−100.06280	−100.06294	−100.06287	−3.35	−3.28	1.95

[a] E_0 is the energy of the isolated monomer calculated with the corresponding basis set. E_A and E_B are energies of the monomers calculated with the whole basis set of the complex; A is the molecule, which contributes the H-atom to the H-bond.

[b] $\Delta E = E_{AB} - 2E_0$; $\Delta E' = E_{AB} - (E_A + E_B)$.

[c] The same contraction and almost the same basis set as that applied by Diercksen and Kraemer [1970a].

TABLE 2.7

Influence of electron correlation on the energy of interaction and other properties of $(HF)_2$ (Lischka [1974a])

Method of calculation	R_{FF}(Å)	R_{HF}[a](Å)	f_{FF} (10^5 dyn cm^{-1})	f_{HF}[a] (10^5 dyn cm^{-1})	ΔE_{COR}^{INTRA} (kcal/mole)	ΔE_{COR}^{INTER} (kcal/mole)	ΔE_{COR}^{TOT}[c] (kcal/mole)	ΔE (kcal/mole)
SCF[b]	2.90	0.902 0.900 0.002	0.095	11.00 11.20 −0.20				−3.46
IEPA	2.89	0.930 0.927 0.003	0.101	9.18 9.27 −0.09	1.01	−0.80	0.20	−3.25
CEPA	2.89	0.919 0.917 0.002	0.104	9.83 9.92 −0.09	0.67	−0.71	0.09	−3.37

[a] Distance and force constant in the HF-molecule, which contributes the H-atom to the H-bond (proton donor). First value: dimer, second value: isolated HF-monomer, third value: change due to formation of the H-bond.

[b] Basis set applied: $(11, 7, 2; 6, 1) \rightarrow [7, 4, 2; 4, 1]$.

[c] In the CEPA method the total correlation energy is not simply a sum of ΔE_{COR}^{INTRA} and ΔE_{COR}^{INTER}.

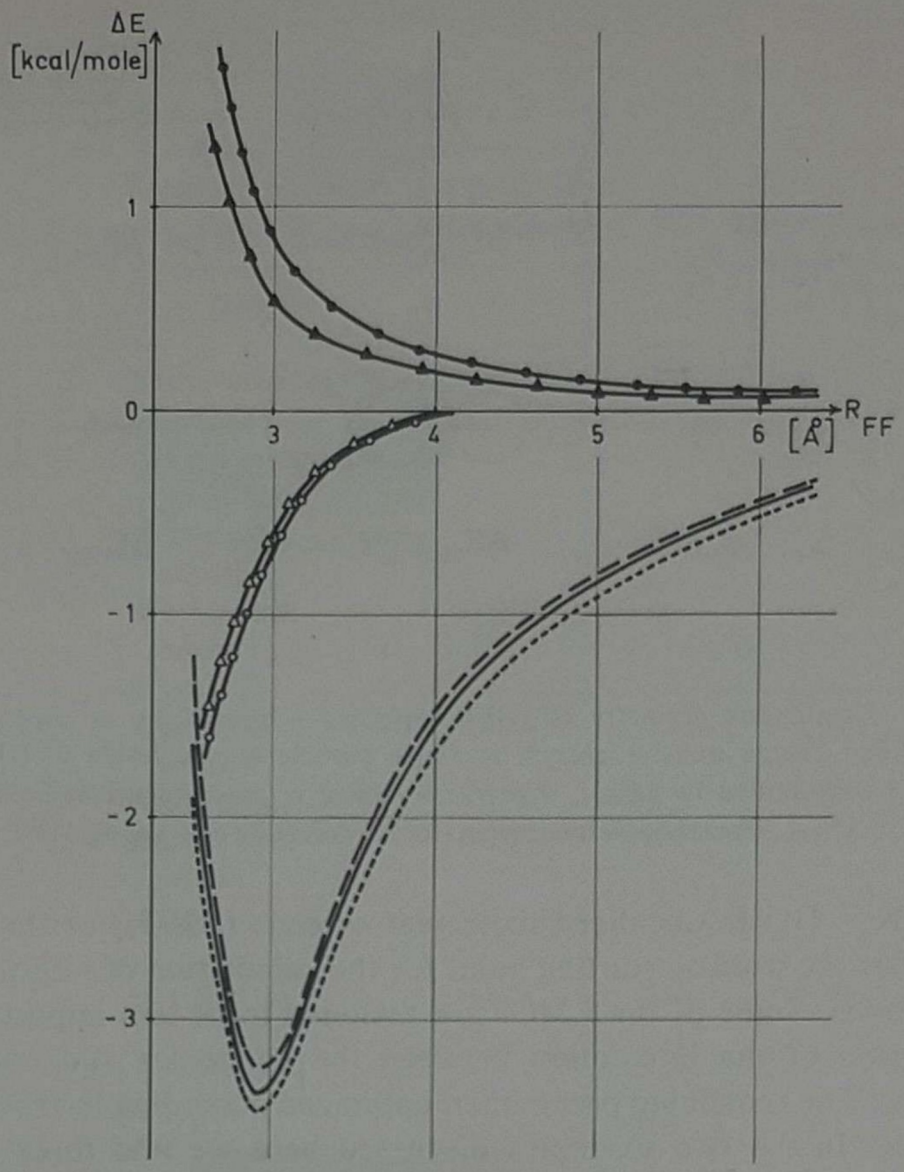

Fig. 2.10. Intermolecular energy and analysis of correlation effects in $(HF)_2$. ΔE_{SCF}: ·····; IEPA calculation, ΔE_{IEPA}: – – – –, ΔE_{COR}^{INTER}: –○–○–○–, ΔE_{COR}^{INTRA}: –●–●–●–; CEPA calculation ΔE_{CEPA}: ———, ΔE_{COR}^{INTER}: –△–△–△–; ΔE_{COR}^{INTRA}: –▲–▲–▲–; (Lischka [1974a]).

arrangement. Hence, the relative contribution of the coulomb energy decreases with increasing values of ω (cf. also fig. 2.11). The two contributions to the change in correlation energy (ΔE_{COR}) will not cancel any more and we obtain a net stabilization of bent geometries by electron correlation. Consequently, we have to expect some influence of correlation energy on the shape of the energy surface of interaction.

A different MO approach to H-bonding was described recently by Von Niessen [1973b, c]. He applied the previously (Von Niessen [1971, 1973a]) developed method of molecules in molecules (MIM) to H-bonds in $(HF)_2$

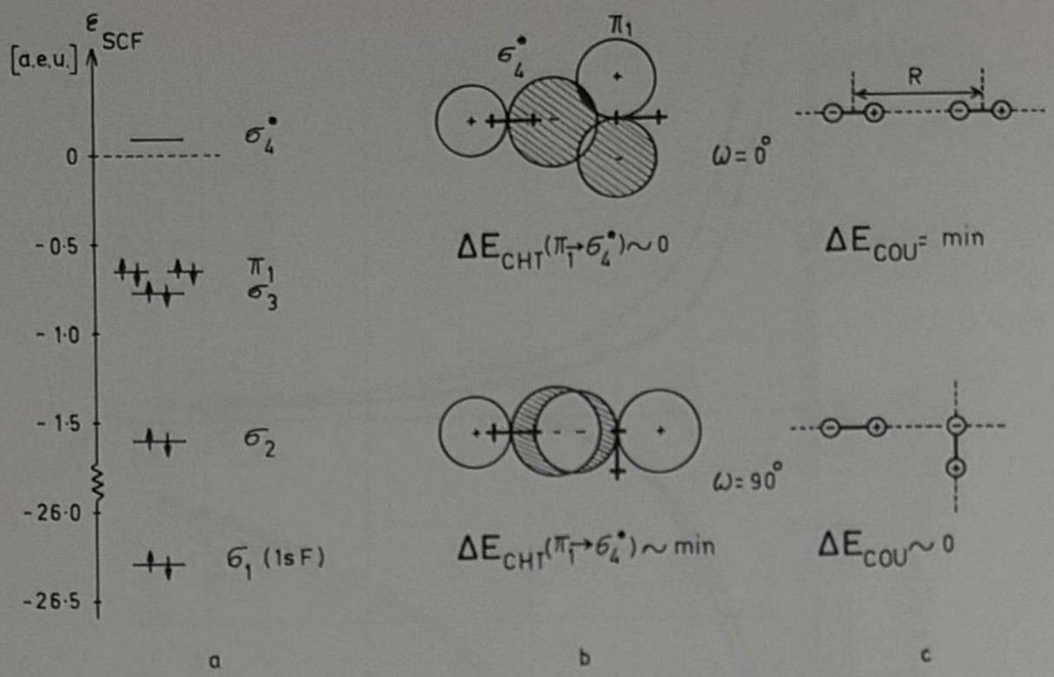

Fig. 2.11. Equilibrium geometry of $(HF)_2$ explained schematically as superposition of coulomb and charge transfer energy. a: single particle energy levels in HF; b: most important contribution to ΔE_{CHT}, $\pi_1 \rightarrow \sigma_4^*$ excitation; c: most important contribution to ΔE_{COU}, dipole/dipole interaction (for the definition of ω see fig. 2.28).

and $H_3N \cdots HOH$. Localized molecular orbitals (LMOs) of the isolated molecules are used as starting point for the calculation of intermolecular interactions. Some of the LMOs are assumed to be less important for a description of the interaction between the molecules and hence kept constant. The remaining part is then optimized according to the variation principle. In the two examples discussed here we find three types of LMOs: inner (K) shell orbitals of the atoms X, XH-bond orbitals and lone pair orbitals of X (X = N, O or F respectively). As a test for the applicability of MIM to H-bonding Von Niessen [1973b, c] optimized each individual LMO in the field of all the others. The corresponding gains in the energy are summarized in table 2.8. The sum of all individual contributions comes very close to the actual SCF energy of interaction. For our purpose this energy partitioning is interesting because it presents some insight into the degree of delocalization in different parts of the complex. Regarding table 2.8 more closely we find that more than 80% of the SCF energy of interaction are obtained if a variation of the smallest reasonable four-electron fragment (two electrons from the XH-bond and two electrons from the lone pair at the atom Y, cf. fig. 2.5) is performed. An optimization of the other valence electron orbitals, however, leads to

TABLE 2.8

Contributions of individual localized MOs to the energy of interaction calculated by the molecules method (Von Niessen [1971, 1973b, c])

	No.	Localized orbital(s) modified	F–H···F–H[a] ΔE(kcal/mole)	%	HO–H···NH$_3$[a] ΔE(kcal/mole)	%
	1	None[b]	−4.60	72.1	−4.13	51.8
Proton donor	2	XH involved in the H-bond	−0.19	3.0	−0.87	10.9
	3	XH not involved in the H-bond	–	–	−0.25	3.1
	4	X lone pair orbitals	−0.24	3.8	−0.62	7.8
	5	X inner shell orbital	−0.014	0.2	−0.048	0.6
Proton acceptor	6	X lone pair orbital	−0.50	7.8	−1.64	20.6
	7	XH-bond(s)	−0.78	12.2	−0.40	5.0
	8	X inner shell orbital	−0.056	0.9	−0.016	0.2
"Four-electron fragment"		(1) + (2) + (6)	−5.29	82.9	−6.64	83.3
		$\sum_{K=1}^{8}(K)$	−6.38	100	−7.97	100
		SCF calculation	−6.0		−7.6	

[a] Basis sets: $(HF)_2$: (9, 5; 4) contracted to [5, 3; 3]; $H_2O\cdots NH_3$: (9, 5; 4) contracted to [5, 3; 2].

[b] This energy corresponds to ΔE_2 of MO energy partitioning or the first order energy $\Delta E_{COU} + \Delta E_{EX}$ of the perturbation treatment.

significant energy lowering too. The restriction to the four-electron system introduces an appreciable error, especially in $(HF)_2$. In this case the contributions of the valence electrons not involved directly in the H-bond are even larger than those of the four electrons mentioned above. As expected, the only contributions which are small enough to be neglected with almost no loss in accuracy come from the inner shell

electrons. Although we have to take into account that the results described by Von Niessen will depend to some extent on the choice of the basis set since he used a rather small one, we can expect the relative importance of individual LMOs to be reproduced fairly well.

A number of semiempirical MO–SCF calculations on H-bonded structures mainly using CNDO/2 or INDO formalism were performed during the last six years. Recently, Murthy and Rao [1970] summarized the results. Interestingly, relative energies of interactions and many other important observable quantities are reproduced very well by these methods as we will see in the following sections (sections 2.4–6). In general the stability of the complex is overemphasized to some extent. The type of energy partitioning in MO theory we applied previously, however, gives more insight into the semiempirical procedure. The more or less correct values are brought about by error compensation. Intermolecular repulsion and electron delocalization are largely overestimated as fig. 2.7 shows (Kollman and Allen [1970a]). This deficiency of CNDO/2 calculations to reproduce the individual contributions to intermolecular energies correctly can be explained from an analysis of the approximations made in the semiempirical method. The argumentation is exactly the same as previously presented for CNDO/2 energy partitioning in the perturbation treatment (section 2.2.2) and hence need not be repeated here.

A critical summary of the data on H-bonds, which have been calculated by different methods and models, leads to the conclusion that correct values for energies of interaction and various other properties can be expected only from MO calculations or extensive perturbation theory starting from very extended basis sets including polarization functions. An appropriate consideration of electron correlation, as in the IEPA or CEPA approach or in perturbational CI calculations, is inevitable. Calculations of this degree of sophistication, however, are possible only for the smallest aggregates, e.g. $(HF)_2$ or $(H_2O)_2$. The chemists, on the other hand, are not only interested in principles of H-bonding but also in the actual energies of interaction between larger molecules, which in most cases are extremely difficult to obtain by experiments too. Nowadays for that purpose theory can offer exclusively a much less accurate ab initio treatment starting from small basis sets or semiempirical methods. These calculations represent a compromise between the size of the molecules and the desired accuracy of the results. Consequently, we can rely at best in relative values for series of calculations on similar molecular aggregates.

2.2.4. Nature and properties of the hydrogen bond

In the two preceding sections (2.2.2 and 2.2.3) we discussed applications of perturbation theory and MO methods to theoretical investigations on H-bonds. Now an attempt is made to summarize the general features of a typical, moderately strong H-bond as it occurs in the dimers $(HF)_2$ or $(H_2O)_2$. Some time ago it had already been suggested by Coulson and Danielson [1955] or Coulson [1957] and independently by Tsubomura [1954] that the main problem in the theory of the H-bond is brought about by a complicated superposition of the five main contributions which are of similar magnitude:

(a) electrostatic or coulomb energy,
(b) exchange repulsion,
(c) polarization energy,
(d) charge transfer energy or covalent contribution, and
(e) dispersion energy.

They thought that the success of the electrostatic models in calculation of H-bond energies is based on an accidental cancellation of the other contributions. The results of recent calculations meet exactly these ideas.

Bowers and Pitzer [1973] performed a model calculation on the individual contributions to the H-bond energy in $(H_2O)_2$ in order to find out their relative weights according to the ideas of Coulson [1957]. They used the same minimal STO basis set and intermolecular geometry as Del Bene and Pople [1970]. This relatively simple procedure is generally called *bond orbital analysis* and uses definitions for the individual intermolecular contributions which are almost identical with those of MO energy partitioning. In fact they obtained similar numerical values (cf. table 2.3): $\Delta E_{COU} = -9.1$, $\Delta E_{EX} = 9.0$, $\Delta E_{POL} = -0.7$ and $\Delta E_{CHT} = -7.4$ kcal/mole. Considering the model character of their studies the total energy of interaction ($\Delta E = -8.1$ kcal/mole) comes closely to the SCF value calculated with the same basis set ($\Delta E_{SCF} = -6.1$ kcal/mole).

Although the numbers obtained by various methods might differ appreciably, all reliable calculations agree in the fact that considerable overlap between the molecules forming the H-bond occurs and the whole phenomenon can be described neither by electrostatic theory nor by weak covalent bonding alone. A nice example demonstrating the superposition of different contributions to the H-bond energy was presented by Kollman [1972]. He explained the stereochemistry of H-bonded structures by a superposition of coulomb and charge transfer energy. To give an example we will apply his arguments to an explanation of the preferred

geometry of $(HF)_2$. In general exchange, polarization and dispersion energies do not depend as much on the intermolecular angle (ω)* as the other two contributions. The stereochemistry of the H-bond is expected therefore to be determined by the angular dependence of ΔE_{COU} and ΔE_{CHT}. In our particular example, $(HF)_2$, we estimate the electrostatic energy of interaction by the largest term of the multipole expansion, which in this case is the dipole–dipole term (fig. 2.11). ΔE_{COU} consequently shows a minimum at $\omega = 0°$ and becomes approximately zero around $\omega = 90°$. The most important contribution to charge transfer energy results from partial excitation from the π_1 lone pair orbital of the proton acceptor HF-molecule into the antibonding σ_4^* orbital of the proton donor HF-molecule. ΔE_{CHT} as we discussed before is roughly proportional to the square of molecular overlap. Figure 2.11 shows that the overlap vanishes at $\omega = 0°$ and reaches a maximum at $\omega = 90°$. ΔE_{CHT} thus favors the perpendicular structure ($\omega = 90°$) in contrast to ΔE_{COU}. In the equilibrium geometry of the actual complex a compromise has to be chosen between the structure stabilized by the electrostatic energy and the most favorable arrangement for charge transfer. Therefore we expect the energy minimum at an intermolecular angle, $0 < \omega < 90°$, and the energy curve, $\Delta E(\omega)$, to be very flat as a consequence of the superposition of two curves with opposite slope. Ab initio calculations (Diercksen and Kraemer [1970a], Kollman and Allen [1970b], Del Bene and Pople [1971], Yarkony et al. [1974] and Lischka [1974a]), CNDO/2 calculations (Schuster [1970] and Kollman and Allen [1970c]: $R_{FF} = 2.44$ Å, $\omega = 45°$, $\Delta E = -9.4$ kcal/mole) and recent experimental data obtained from microwave spectroscopy (Dyke et al. [1972]) confirm this suggestion derived from qualitative arguments very nicely (table 2.4). Similarly, energy partitioning was applied successfully to explain the preferred geometries of many other H-bonded complexes (Kollman [1972]).

Redistribution of electron densities in H-bonded complexes and the amount of charge transferred from one molecule to the other have been discussed very much in the past. Charge transfer in molecular associations, however, is no observable quantity and hence there is no unique way to define exactly what we mean by the amount of electron density transferred. Usually in semiempirical calculations or in ab initio calculations with small basis sets Mulliken population analysis is applied

* A definition of the angles ω, θ and γ, which are used to characterize intermolecular geometries is given in fig. 2.28.

(Mulliken [1955]). In case of calculations using very extended basis sets including polarization orbitals a direct analysis of the first order density matrix is less ambiguous and hence more straightforward (e.g. Diercksen [1971]). All calculations agree qualitatively in two results:

1. The charge redistribution in the complex is shown schematically for $(H_2O)_2$ in fig. 2.12. The results obtained by ab initio calculations with very different basis sets or CNDO/2 calculations are roughly the same. Appreciable differences were only found at the O-atom of the proton acceptor and the H-atom of the proton donor, which is not involved in the H-bond. The electron density at the H-atom participating in the H-bond is reduced on H-bond formation. This general result is not easy to understand. Why should the electron density decrease when lone pair electrons approach? A simple explanation considers electron pair repulsion. The electrons of the HX-bond are pushed back towards the X-atom by the lone pair of atom Y.

$$\Delta\rho(z) = \int_{-\infty}^{+\infty}\int \Delta\rho(\boldsymbol{R})\,\mathrm{d}x\,\mathrm{d}y, \qquad \Delta\rho(\boldsymbol{R}) = \rho_{AB}(\boldsymbol{R}) - \{\rho_A(\boldsymbol{R}) + \rho_B(\boldsymbol{R})\}^{*}. \tag{2.44}$$

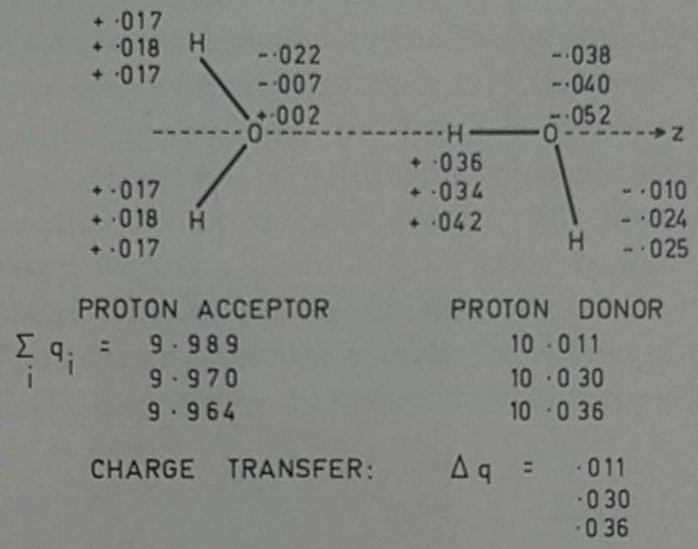

Fig. 2.12. Changes in atomic charges (Δq_i) and charge transfer (Δq) due to H-bond formation in $(H_2O)_2$. Upper values: extended GTO calculation, (10, 5, 1; 4, 1)→[5, 3, 1; 2, 1], (Hankins et al. [1970b]); middle values: minimal basis STO calculation (Morokuma and Winick [1970]), lower values: CNDO/2 calculation (Schuster [1970]).

* For the calculation of the electron density difference function $\Delta\rho(\boldsymbol{R})$ the density functions of the isolated molecules $\rho_A(\boldsymbol{R})$ and $\rho_B(\boldsymbol{R})$ are arranged in the same geometry as in the complex AB.

An integral electron density difference function, $\Delta\rho(z)$ in (2.44), which has been used to discuss the nature of metal oxygen bonds in complexes (Russegger and Schuster [1973], Marius et al. [1975] and Schuster et al. [1974a]) was applied to $(H_2O)_2$ also (fig. 2.13). This integral density

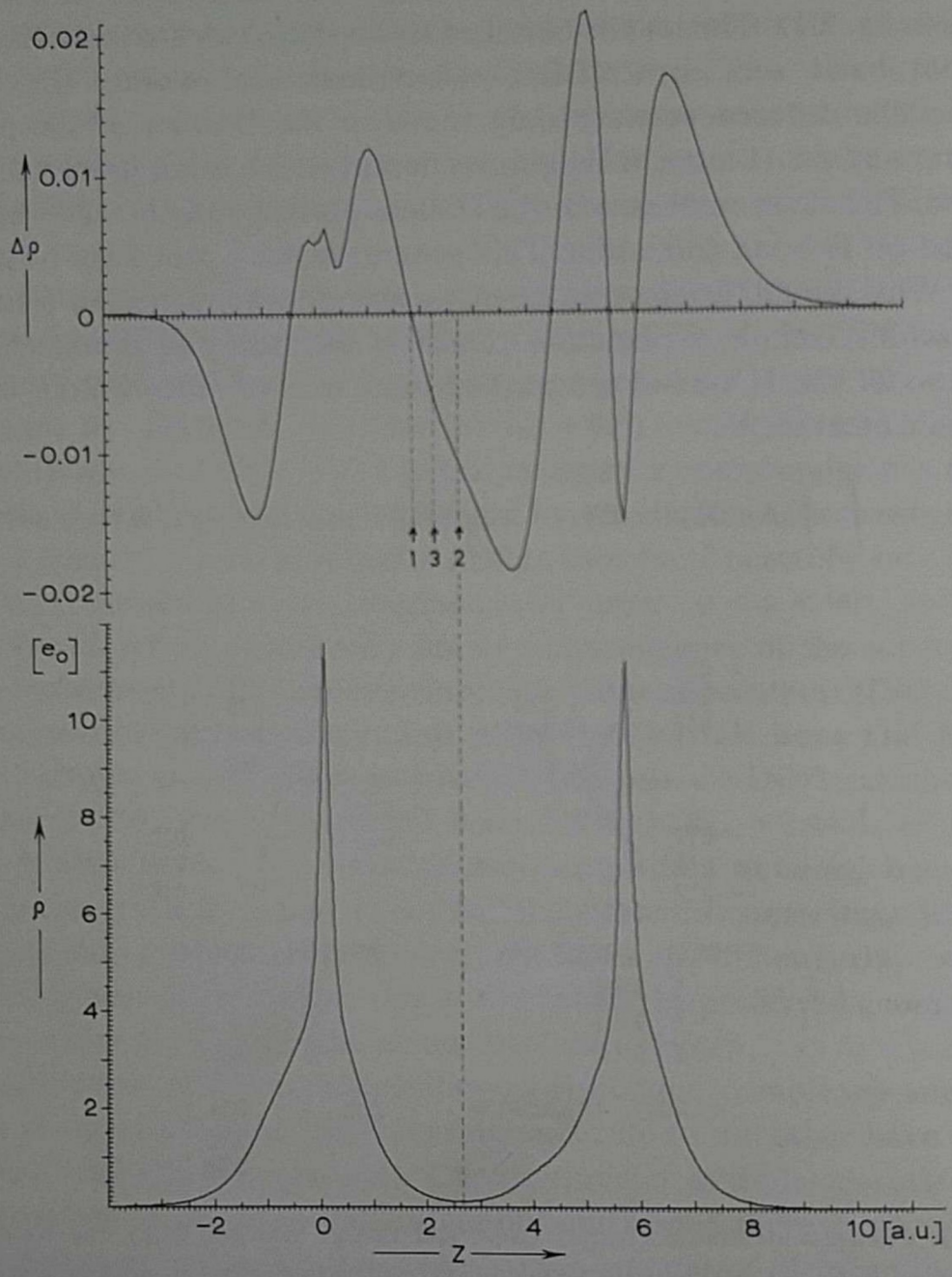

Fig. 2.13. Integral electron density $\rho(z)$ and integral electron density difference $\Delta\rho(z)$ in $(H_2O)_2$. The geometry of $(H_2O)_2$ is the same as shown in fig. 2.12 (O_1 is slightly replaced from the origin: $z(O_1) = 0.1$ au, $z(O_2) = 5.8$ au). The arrows indicate the three choices of a borderline between both molecules: $\mathbf{1} = z_O^{(1)}$, $\mathbf{2} = z_O^{(2)}$ and $\mathbf{3} = z_O^{(3)}$ (see text); atomic units see fig. 2.2.

difference function confirms the interpretation presented above. An equivalent explanation can be given by mutual polarization of the two molecules forming the H-bond. Figure 2.13 nicely shows that the polarization of the H_2O molecule acting as proton donor is remarkably larger. This is a consequence of the fact that the electrostatic field of the proton acceptor in the region of the proton donor is stronger than vice versa. The proton donor molecule is placed around the axis of the acceptor's dipole moment, in a region where the electrostatic field strength of a dipole has its maximum value.

A more detailed discussion of the electron density difference function in $(H_2O)_2$ was presented by Diercksen [1971]. He analyzed also the changes in the individual MOs of both molecules.

2. Regarding the molecules as a whole electron density is transferred from the proton acceptor to the proton donor molecule. Using population analysis the calculated amount of charge transferred varies largely with the method applied. CNDO/2 calculations (Schuster [1970]) and ab initio STO calculations using minimal basis sets (Morokuma and Winick [1970]) find a charge transfer between $0.03e_0$ and $0.04e_0$ in $(H_2O)_2$ (fig. 2.12). In more extended ab initio calculations the amount of charge transferred is remarkably reduced: Kollman and Allen [1972] obtain $0.006e_0$ and Hankins et al. [1970b] $0.011e_0$ for the same complex. In principle charge transfer can be analyzed also by density functions. In this case, however, we are confronted with the problem to define a borderline between the molecules. Again this is not possible without some arbitrariness. Consistent with the analysis by integral density difference functions (2.44) described above, we use a plane perpendicular to the z-axis ($z = z_0$) to divide the three-dimensional space into regions for the individual molecules. The amount of charge transferred is then obtained simply by integration (2.45). $\Delta\rho(z)$ in fig. 2.13 which has been derived originally from

$$\Delta q(z_0) = \int_{z_0}^{\infty} \Delta\rho(z)\,\mathrm{d}z = -\int_{-\infty}^{z_0} \Delta\rho(z)\,\mathrm{d}z \qquad (2.45)$$

an extended ab initio calculation on $(H_2O)_2$ by Diercksen [1971] was integrated starting from three different z_0 values. These values were determined with the aid of plausible arguments:

1. $z_0^{(1)}$ was chosen at the position of zero integral density difference between the molecules: $\Delta\rho(z_0^{(1)}) = 0$, $z_0^{(1)} = 0.93$ Å.

2. $z_0^{(2)}$ was chosen at the position of minimum integral electron density of the complex: $\rho_{AB}(z_0^{(2)}) = \text{min.}$, $z_0^{(2)} = 1.38$ Å,

$$\rho_{AB}(z) = \int\int \rho_{AB}(\boldsymbol{R})\, dx\, dy. \tag{2.46}$$

3. $z_0^{(3)}$ was chosen such that it divides the interatomic distance $R_{O\cdots H}$ according to the ratio of the Van der Waals radii:

$$z_0^{(3)} = 1.14 \text{ Å}.$$

The following values for charge transfer were obtained:

$$\Delta q(z_0^{(1)}) = 0.0032 e_0, \quad \Delta q(z_0^{(2)}) = 0.0079 e_0 \quad \text{and} \quad \Delta q(z_0^{(3)}) = 0.0046 e_0.$$

The values are in fairly good agreement with the previously discussed data derived from population analysis of extended ab initio calculations. Finally we can conclude, that net electron transfer from the proton acceptor to the proton donor molecule is small in $(H_2O)_2$ but certainly not completely zero as long as the usual definitions for charge transfer are applied.

Although the amount of charge transfer differs in calculations of different degree of sophistication, rough agreement is found with respect to a correlation between charge transfer (Δq) and stabilization energy (ΔE) in weak and moderately strong H-bonds (Schuster [1970]). This correlation has been discussed extensively together with a number of other interesting relations between various properties of H-bonds and charge transfer (Ratajczak [1972a, b; 1973] and Ratajczak and Orville-Thomas [1973a, b]). At the end of our discussion on the nature of the H-bond a more critical comment seems to be appropriate. All interpretations of the results presented above are consistent with a particular scheme of intermolecular energy partitioning which converges into the asymptotic expression of classical electrostatic theory at large intermolecular distances. Nevertheless we have seen before (section 2.2.2) that energy partitioning is not free from arbitrariness in the region of appreciable intermolecular overlap. Consequently, our conclusions will also depend to some extent on the particular definitions for the contributions to the energy of interaction we have chosen initially.

The most important properties of H-bonds in $(HF)_2$ and $(H_2O)_2$ are summarized in table 2.9. Most calculated energies for H-bond formation (ΔE) agree well with the ΔH values measured as far as the basis sets applied were large enough and reliable experimental data on dimers are

available. The most extended calculations on $(HF)_2$ (Lischka [1974a]) and $(H_2O)_2$ (Popkie et al. [1973]) on the other hand, lead to significantly smaller ΔE values than those generally accepted. This fact remains unchanged even if the differences between ΔE and ΔH are carefully estimated and taken into account. This point needs some further clarification although we have to admit that error limits are large in both theoretical and experimental values.

The geometry of a typical H-bond is characterized by intermolecular distances which are much smaller than the sum of Van der Waals radii of the atoms concerned. All calculations of sufficient accuracy confirm this experimental result. The most accurately calculated intermolecular distances of H-bonded dimers are larger than those obtained in liquids or solids in perfect agreement with the few available data measured by electron diffraction or microwave spectroscopy in the vapor phase (table 2.9). In crystals with H-bonds we always find remarkably longer HX-bonds than in the isolated monomers. The most reliable calculations, however, show that this elongation is rather small in the isolated dimer. The large differences in length are therefore brought about by interaction with further neighbors in the condensed phase.

All calculations confirm that the polarity of the HX-bond increases on H-bond formation. This is manifested clearly by larger dipole moments found in dimers than those obtained by vectorial addition of the moments for the monomers according to the geometry of the dimer.

The force constant of the HX stretching vibration decreases on H-bond formation. Consequently, the IR absorption is shifted to smaller wave numbers. Again this shift to lower frequencies is much less pronounced in the dimers than in larger aggregates. The intensity of an IR stretching vibration band is roughly proportional to the square of the first dipole moment derivative with the interatomic distance $Q = |\mathrm{d}\mu/\mathrm{d}R_{HX}|$. H-bonding causes a remarkable increase of Q for HX stretching vibrations and hence leads to stronger IR absorption. A comparison of different calculations at the SCF level shows that the calculated values for Q are appreciably basis set dependent. In general the band enhancement is overemphasized if small basis sets are applied. The problem of calculated vibrational spectra in H-bonded structures will be discussed in detail in ch. 3.

Finally, H-bonds are characterized by appreciable down field shifts in proton magnetic resonance spectra. The decrease in magnetic shielding of the protons involved in the H-bond are a good experimental evidence for

TABLE 2.9

Calculated properties of $(HF)_2$ and $(H_2O)_2$ and their comparison with the available experimental data

H_2O and aggregates

Quantity	Calculated values			Experimental data[d]			
	Monomer	Dimer	Ref.	Monomer	Dimer	Liquid water (1 atm, 20°C)	Ice I
R_{OH}(Å)	0.944	0.948	a	0.957			1.01
	0.966	0.976	b				
∢HOH	105.3°		a	104.5°			
R_{OO}(Å)		3.00	a, b, c		2.98 ± 0.04	2.82	2.76
ω		25°	b		$60 \pm 10°$		$54.7 \pm 0.1°$
		30°	c				
ΔE (kcal/mole)		−4.83	a		−5.0[a]	−(1.3–4.5)	−(5.7–6.7)
		−3.90	c				
$\mu(D)$	2.21	4.29 ($\omega = 25°$)	a	1.85	2.60 ($\omega = 60°$)		
$\Delta\mu(D)$[b]		0.32	a		0.49		
f_{OH} (10^5 dyn/cm)	12.45	9.96	b	8.45			
ν_{OH} (cm^{-1})[c]	4020	3806	d	3652	3428[c]		
				3707	3619[c]	3400	3277
$Q = (\partial\mu/\partial R_{OH})_{R\delta_H}(D/Å)$	0.7	2.0	b				
$\{Q[(H_2O)_2]/Q[H_2O]\}^2$		5.3	a		12[a]		
		8.2	b				
f_{OO} (10^5 dyn/cm)		0.18	b				0.17–0.19

σ_H (ppm)	28.55	27.56	e	30.20	25.62	

[a] Highly diluted water vapor in solid N_2 at 20 K (see ch. 22 and Van Thiel et al. [1957]).
[b] Increase in dipole moment with respect to two isolated monomers at the same geometry.
[c] OH stretching mode: upper values wave numbers of the symmetric mode, lower values wave numbers of the decoupled stretching mode.
[d] Experimental data were taken from Eisenberg and Kauzmann [1969]; water dimer in the vapor phase: Dyke and Muenter [1974].

HF and aggregates

	Calculated values[a]			Experimental data[d]			
Quantity	Monomer	Dimer	Ref.	Monomer	Dimer	Cyclic hexamer	Crystal
R_{HF}(Å)	0.900	0.902	f	0.917			
	(0.917)	(0.919)					
R_{FF}(Å)		2.90	f				
		(2.89)			2.79 ± 0.05	2.55	2.49
		2.85	g				
ω		60°	g		60–70°	76°	60°
ΔE (kcal/mole)		−3.46	f				
		(−3.37)			−(6 ± 1)	−6.7	
		−4.5	g				
$\mu(D)$	1.95	4.24[b]	f	1.82	2.99		
		($\omega = 0°$)			($\omega = 70°$)		
$\Delta\mu(D)$[b]		0.34	f				

TABLE 2.9–(*contd.*)
HF and aggregates

Quantity	Calculated values[a]			Experimental data[d]			
	Monomer	Dimer	Ref.	Monomer	Dimer	Cyclic hexamer	Crystal
f_{HF} (10^5 dyn/cm)	11.20 (9.92)	11.0 (9.83)	f	9.66			
$\{Q[(HF)_2]/Q[HF]\}^{2}$ [b]		2.15	f				
f_{FF} (10^5 dyn/cm)		0.095 (0.104)	f				

[a] SCF calculations; values including electron correlation (CEPA method, ref. f) are given in parenthesis.
[b] Dipole moment and increase in dipole moment with respect to the two isolated monomers. The calculated values corresponds to the linear geometry ($\omega = 0°$), which is not the most stable conformation of the dimer.
[c] The same definition for Q as in case of H_2O and $(H_2O)_2$ is applied.
[d] Experimental data were taken from Atoji and Lipscomb [1954], Smith [1958, 1959], Franck and Meyer [1959], Janzen and Bartell [1969] and Dyke et al. [1972].
References: **a** = Diercksen [1971]; **b** = Kollman and Allen [1969]; **c** = Popkie et al. [1973]; **d** = Janoschek [1974] (see also ch. 3) using the energy surface of ref. **a**; **e** = Jaszunski and Sadlej [1972a, b; 1973]; **f** = Lischka [1974a]; **g** = Diercksen and Kraemer [1970a].

the loss in electron density at the proton discussed above. The calculation of chemical shifts, however, is a tricky and involved problem and even for small molecules not completely solved nowadays. In the case of $(H_2O)_2$ chemical shifts for the protons in the complex and in the isolated molecule were calculated. Jaszunski and Sadlej [1972a, b; 1973] used an uncoupled HF variation perturbation procedure developed previously (Karplus and Kolker [1963] and Kolker and Karplus [1964]). They obtained the expected down field shift of the proton involved in H-bonding. The decrease in the shielding constant σ_H, however, is remarkably smaller than experimentally found between H_2O monomer and liquid water.

All important properties of isolated H-bonds as they occur in dimeric associations are described well by the more involved theoretical methods, which have become routine now. The crucial problem to explain the properties of larger aggregates or H-bonds in the liquid or solid state has not been solved in a satisfactory manner until now and still remains a striking challenge to theoreticians.

2.3. Molecular potentials and the electrostatic energy of interaction

There are two main reasons for the recent interest in molecular potentials, which in most cases are simple and easy to calculate. During the last decade more and more experimental information on biological macromolecules became available. Consequently, theoretical methods were developed in order to discuss and to predict stable structures of large molecules and their properties. Secondly, chemists became more and more interested in molecular structures of pure liquids and solutions and were looking for more data on large clusters of molecules and solvation shells. Only in some simple examples direct experimental information could be obtained and hence cooperation of theoreticians and experimentalists is highly necessary in this field. From the very beginning it was evident that all kinds of quantum mechanical calculations on these structures are far beyond our present facilities for numerical computations and most probably will be impossible in the future as well. Drastic simplifications are inevitable therefore and two different types of approach were developed in the last few years.

At first the electrostatic energy has been regarded to be able to represent the total energy in a rough approximation. Electrostatic potentials were calculated and used to predict various molecular properties. In order to give some examples protonations sites of large molecules

(Bonaccorsi et al. [1972a]), preferred geometries in molecular associations (Bonaccorsi et al. [1971]) and orientations of water molecules in hydration shells (Alagona et al. [1973a], Port and Pullman [1973a, b] and Pullman et al. [1974]) were investigated in that way. Recently, an extended review on electrostatic potentials and their applications on chemical problems was presented by Scrocco and Tomasi [1973].

The second type of approach is different in nature. The total energy is not approximated by more or less well founded simplifications of expressions derived by quantum mechanics but by empirical potentials. Analytical functions are introduced and the parameters therein are determined empirically by fitting calculated structures and energies of molecules or crystals to as many experimental data as possible. Both types of methods were applied to H-bonds and will be discussed briefly now.

2.3.1. Electrostatic potentials in calculations on hydrogen bonds

The exact electrostatic potential of a molecule can be calculated without further difficulty provided the wave function or the one particle density matrix of the molecule is known. Starting from a given charge distribution of molecule A, $Q_A(\boldsymbol{R})$, the potential can be obtained directly by integration according to eq. (2.47):

$$V_A(\boldsymbol{R}) = \int \frac{Q_A(\boldsymbol{R}_1)}{|\boldsymbol{R}-\boldsymbol{R}_1|}\,d\boldsymbol{R}_1 = -\int \frac{\rho_A(\boldsymbol{R}_1)}{|\boldsymbol{R}-\boldsymbol{R}_1|}\,d\boldsymbol{R}_1 + \sum_k \frac{Z_k}{|\boldsymbol{R}-\boldsymbol{R}_k|}. \qquad (2.47)$$

The electrostatic molecular potential represents the electrostatic energy of interaction of molecule A with a proton in position $\boldsymbol{R}$. Hence $V_A(\boldsymbol{R})$ is very useful in the discussion of preferred protonation sites and has been used extensively for this purpose (e.g. Bonaccorsi et al. [1970, 1972a, b], Berthier et al. [1972] and Petrongolo and Tomasi [1973]). The calculations of intermolecular electrostatic energies, however, is not facilitated by the concept of molecular potentials at all, because the final expression is exactly the same as in eq. (2.28):

$$\begin{aligned}\Delta E_{COU} &= \int Q_B(\boldsymbol{R})V_A(\boldsymbol{R})\,d\boldsymbol{R} = \int Q_A(\boldsymbol{R})V_B(\boldsymbol{R})\,d\boldsymbol{R} \\ &= \int\int \rho_A(\boldsymbol{R}_1)\rho_B(\boldsymbol{R}_2)\frac{1}{R_{12}}\,d\boldsymbol{R}_1\,d\boldsymbol{R}_2 + \sum_{k\in A}\sum_{l\in B}\frac{Z_kZ_l}{R_{kl}} \\ &\quad - \sum_{k\in A}\int \rho_B(\boldsymbol{R}_1)\frac{Z_k}{R_{1k}}\,d\boldsymbol{R}_1 - \sum_{l\in B}\int \rho_A(\boldsymbol{R}_1)\frac{Z_l}{R_{1l}}\,d\boldsymbol{R}_1. \qquad (2.48)\end{aligned}$$

In order to save computation time further approximations have to be introduced.

Density distributions obtained from semiempirical MO–SCF calculations (CNDO/2 and INDO) were used to calculate molecular electrostatic potentials as well. Giessner-Prettre and Pullman [1972] found that potentials are reproduced fairly well by CNDO/2 densities if the originally orthogonal AO basis has been deorthogonalized by an inverse Löwdin [1950] procedure before*. Previously the same authors (Giessner-Prettre and Pullman [1968] described the improvement of calculated dipole moments by deorthogonalization of CNDO wave function. Looking to the potential maps more closely some systematic deviations of the semiempirical results can be recognized (Giessner-Prettre and Pullman [1974]). In case of large molecules, however, any direct calculation of electrostatic potentials becomes very time consuming in both ab initio and semiempirical procedures after deorthogonalization has been included.

An interesting modification in calculations of molecular electrostatic potentials was proposed by Srebrenik et al. [1973]. They used the Hellman–Feynman theorem to rewrite eq. (2.47) and obtained thereby a Poisson equation for the electronic contribution to the molecular potential

$$\nabla^2 V_{\mathrm{EL}}(\boldsymbol{R}) = -4\pi\rho(\boldsymbol{R}). \tag{2.49}$$

The Poisson equation can be solved analytically if the density function is expressed in Gaussian orbitals (GTOs). Hence, an analytical expression for the potential can be given in terms of the MO coefficients (c_{ik}). Calculations of this type should be much more economic than the direct integration of the potential equation discussed above.

In any case the exact calculation of electrostatic potentials of large molecules remains a tedious problem and consequently different types of approximations are used. Molecular potentials can be described in the conventional way by multipole expansion charge distributions (e.g. Hirschfelder et al. [1954]). The individual coefficients of this expansion are the well known molecular multipole moments. In calculations of intermolecular electrostatic energies multipole expansion is the most

* In a very recent paper, Caballol et al. [1974] discussed the CNDO/2 potential map for the same molecule (H_2CO) using a very similar kind of approximation. In contrast to Giessner-Prettre and Pullman [1972] they distinguished between s- and p-atomic orbitals in the nuclear attraction integrals and obtained a somewhat better result for the orthogonal AO basis set.

efficient way to describe the asymptotic behavior at large intermolecular distances. At short distances the electrostatic model fails in any case, because the other contributions to the energy of interaction become predominant. In the medium range which is most interesting for a discussion of the problems mentioned above the multipole expansion converges rather slowly. Nevertheless, Bonaccorsi et al. [1974] could show that in case of small molecules all moments up to hexadecapoles are sufficient for a reasonably accurate–errors less than 10%–description of the molecular potentials outside the Van der Waals sphere. In case of larger molecules the situation is worse and only a multicenter expansion is able to represent the potential well enough.

Another idea to simplify the calculation of electrostatic potentials is rather old. The molecular charge distribution is simulated by a number of point charges. In these older models, e.g. the water molecule was represented by four (Verwey [1941]) or seven (Pople [1951]) point charges. The corresponding molecular potentials were rather inaccurate. Because of the rapid progress in computational techniques this idea was taken up again recently (Bonaccorsi et al. [1971] and Hall [1973]). A model consisting of 13 point charges for H_2O is already able to give a fairly correct representation of the whole potential outside the Van der Waals radii of the atoms (Bonaccorsi et al. [1971]). The most accurate description of this type was presented by Tait and Hall [1973]. In case of water 27 point charges were used. They succeeded in reproducing the exact molecular potential of H_2O within an accuracy of 1% at a distance of 1.5 Å from the O-atom along the C_2 axis or at 1.0 Å from the H-atom in the OH-bond direction.

Simple point charge models for water were used frequently to calculate the electrostatic part of the pair potential in studies of molecular dynamics. For a recent calculation see Rahman and Stillinger [1971, 1973] and Stillinger and Rahman [1972, 1974]. The computer simulations of liquid water will be discussed in more detail in section 7.3.8. Additionally, point charge models for water were also applied in a slightly different way to fit calculated SCF pair potentials by analytical expressions: Popkie et al. [1973] and Kistenmacher et al. [1973a]. In this case the point charges represent nothing more than empirical parameters for the surface fitting procedure. The potentials obtained in that way were further used for Monte Carlo calculations on liquid water. Examples of empirical point charge potentials will be discussed in sections 2.3.2 and 2.3.3.

A combination of multipole expansion and point charge representation

of molecular potentials was suggested recently (Dreyfus [1970], Port and Pullman [1973a] and Bonaccorsi et al. [1974]). The molecular potential is simulated by a relatively small number of multipole expansions up to the second moments. In case of H_2O five centers were sufficient. The origins of these expansions were chosen at the nuclei and in the middle of covalent bonds. Expansion coefficients are determined from density distribution or from Mulliken [1955] overlap populations. Comparison of exact and approximated molecular potentials shows good agreement at sufficiently large distances.

In the case of $(H_2O)_2$ the total energies of interaction from STO minimal basis set calculations were compared with the electrostatic energies (Bonaccorsi et al. [1971]). Interestingly, at fixed intermolecular distance ($R_{OO} = 2.76$ Å) the angular dependence of the H-bond energy is reproduced reasonably well by the electrostatic model.

Hydration studies were performed on a number of medium size and large molecules: formamide (Alagona et al. [1973a]), formamide dimer (Pullman and Port [1973]), purines and pyrimidines (Port and Pullman [1973a]), alkylammonium groups (Port and Pullman [1973b]) and N-methylacetamide (Pullman et al. [1974]). Approximate electrostatic potentials were used for the calculation of electrostatic energies. In the case of formamide and N-methylacetamide the total energies were calculated using the minimum basis sets (GTO: (7, 3; 3) [2, 1; 1]) also. The comparison of electrostatic and SCF results demonstrates again, that the electrostatic model is able to give a reasonable picture of angular dependences of the total energy of interaction at fixed intermolecular distances. In fig. 2.14 stable hydration sites of formamide are shown.

2.3.2. Consistent force field calculations on hydrogen bonds

Consistent force field (CFF) calculations based on superposition of analytical potential functions were used previously to predict stable conformations, vibrational spectra and heats of formation in the vapor phase and in crystals of hydrocarbons (Bixon and Lifson [1967], Lifson and Warshel [1968], Warshel and Lifson [1970] and Ermer and Lifson [1973]) and various amides (Warshel et al. [1970] and Karplus and Lifson [1971]). The empirical parameters of these potentials were determined by fitting the calculated results to a large number of experimental data mainly stable geometries, dipole moments and energies of several reference

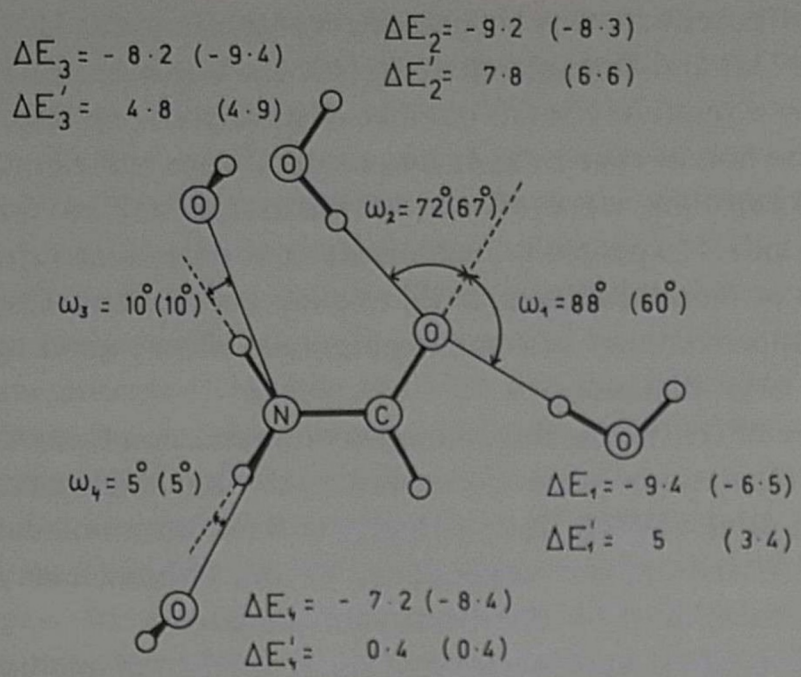

Fig. 2.14. Most important hydration sites of formamide obtained by ab initio SCF calculations and electrostatic potentials. The values from electrostatic calculations are given in parentheses; ΔE_i: energy of hydration; $\Delta E_i'$: activation energy for rotation around the H-bond axis, all energies are given in kcal/mole (Alagona et al. [1973a], for the definition of ω see fig. 2.28).

compounds. Recently, this procedure was applied to H-bonded structures (Hagler et al. [1974a, b] and Hagler and Lifson [1974]). Dipole moments of various amide molecules, geometries and heats of sublimation of amide crystals were used to adjust parameters for the potential functions of the CO···HN bond. Interestingly, the properties of the H-bond can be described successfully by a simple superposition of a Lennard-Jones type potential for nonbonded atoms and an electrostatic contribution, which is represented by the interaction of partial point charges at the atoms concerned:

$$\Delta E = \sum_j \sum_{j>i} \frac{A_{ij}}{(R_{ij})^{12}} - \frac{B_{ij}}{(R_{ij})^6} + \frac{Q_i Q_j e_0^2}{R_{ij}}. \tag{2.50}$$

The summation is extended over all pairs of atoms. The parameters A_{ij} and B_{ij} are calculated from constants for the individual atoms which are summarized in table 2.10.

$$A_{ij} = (A_i A_j)^{1/2}, \qquad B_{ij} = (B_i B_j)^{1/2}. \tag{2.51}$$

The partial point charges were defined in such a way that functional groups as CO, NH, NH_2 or CH_n are neutral. The Lennard-Jones potential

TABLE 2.10

Potential parameters for H-bonds between carbonyl- and aminogroups in amides (Hagler et al. [1974a])

Atom	A (kcal/mole Å^{12})	B (kcal/mole Å^6)	Q (e_0)	ϵ (kcal/mole)	R° Å)	R° (Å)[a]
C[b]	$3022 \cdot 10^3$	1340	+0.38	0.148	2.03	–
O[b]	$275 \cdot 10^3$	502	−0.38	0.228	1.61	1.4
N(H)[c]	$2271 \cdot 10^3$	1230	−0.28	0.167	1.97	1.5
$N(H_2)$[d]	$2271 \cdot 10^3$	1230	−0.83	0.167	1.97	1.5
H[c]	0	0	+0.28	0	0	1.2
H[d]	0	0	+0.41	0	0	1.2
C[e]	$1811 \cdot 10^3$	532		0.039	2.18	
				(0.166)	(1.76)	2.0 (CH_n)
H[e]	$7.15 \cdot 10^3$	32.9	+0.10	0.038	1.38	
				(0.004)	(1.82)	

[a] Conventional Van der Waals radius (Brand and Speakman [1960]).
[b] Atoms of the carbonyl group in amides.
[c] Atoms of an NH group in secondary amides.
[d] Atoms of an NH_2 group in primary amides.
[e] Atoms of CH, CH_2 or CH_3 groups occurring in various amides. The values used in CFF calculations on hydrocarbons (Ermer and Lifson [1973]) are somewhat different and given in parentheses.

of course can be rewritten to give an equivalent expression, with

$$\Delta E - \sum_i \sum_{j>i} \frac{Q_i Q_j e_0^2}{R_{ij}} = \sum_i \sum_{j>i} \epsilon_{ij} \left\{ \left(\frac{R_{ij}^0}{R_{ij}} \right)^{12} - 2 \left(\frac{R_{ij}^0}{R_{ij}} \right)^6 \right\} \tag{2.52}$$

somewhat different combination rules:

$$\epsilon_{ij} = (\epsilon_i \epsilon_j)^{1/2}, \qquad R_{ij}^0 = R_i^0 + R_j^0. \tag{2.53}$$

The parameters R_i^0 are generally well known as Van der Waals radii (e.g. Brand and Speakman [1960]).

The results of the CFF calculations on the preferred geometry of a single amide H-bond are summarized in fig. 2.15. An almost linear arrangement of the three atoms forming the H-bond (NH $\cdots$ O) was found to be most stable. The intermolecular distance $R_{ON} = 2.98$ Å and the energy of interaction $\Delta E = -3.38$ kcal/mole correspond well to the generally accepted values. The few calculated values available indicate a very flat potential curve for the dependence of the H-bond energy on the angle between the functional groups NH and CO (ω). Lattice energies and unit

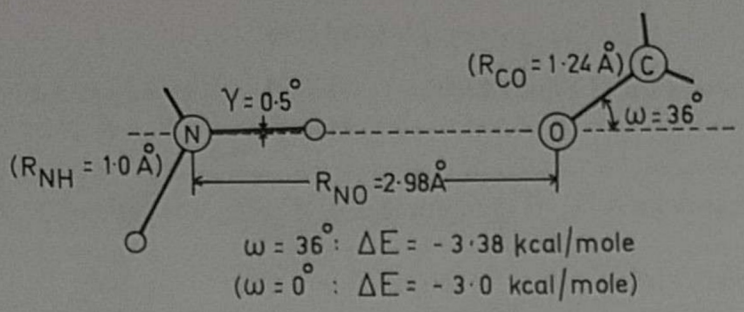

Fig. 2.15. Equilibrium geometry and energy of interaction for H-bonds between carbonyl groups and amino groups obtained by CFF calculations on amide crystals. Assumed bond lengths are given in parentheses (Hagler et al. [1974a, b], Hagler and Lifson [1974], for the definition of γ and ω see fig. 2.28).

cell geometries for ten different amides were determined by CFF calculations using the parameters given before (Hagler and Lifson [1974]). Excellent agreement of calculated and experimental values was obtained.

Initially, in the determination of the H-bond parameters for CFF calculations a conventional three-parameter Morse function (2.54) was incorporated in eq. (2.50) instead of the Lennard-Jones potential for the OH interaction in order to account for covalent H-bond effects.

$$\Delta E_{\mathrm{COV}} = D\{\exp[-2\alpha(R_{\mathrm{OH}} - R^0_{\mathrm{OH}})] - 2\exp[-\alpha(R_{\mathrm{OH}} - R^0_{\mathrm{OH}})\}f(\omega). \quad (2.54)$$

$f(\omega)$ represents an appropriate simulation of the angular dependence of this covalent H-bond energy. The Lennard-Jones potential was removed consequently by an inverse angular dependence, $1 - f(\omega)$. With respect to our previous discussion of intermolecular energy partitioning we are inclined to identify the covalent contribution ΔE_{COV} with the charge transfer term ΔE_{CHT}. Actually, the situation is more complicated because the Morse potential contains part of the intermolecular repulsive energy, which of course does not appear in the charge transfer term according to our definition. In their least squares determination, however, Hagler et al. [1974a] could not find any significant contribution of the covalent potential to the H-bond energy. The parameters obtained were much smaller than their standard deviations except in case of R^0_{OH}. Different functions for the angular dependence, $f(\omega)$, were applied but the covalent contributions remained negligible. Comparing this result with energy partitioning in the most accurate theoretical calculations we are confronted with a striking contradiction which is rather difficult to understand. In order to try an explanation we have to analyse the whole problem in more detail.

As we have seen previously the electrostatic contribution alone is able

to describe the angular dependence of the total energy of interaction fairly well in case of the formamide–water complex provided the intermolecular distance has been fixed to a reasonable value (fig. 2.14). In other molecular associations like $(HF)_2$, however, this was not the case. The dipole moments of the individual monomers present an explanation to this problem:

$$\mu(H_2O) = 1.85D, \qquad \mu(HCONH_2) = 3.22D, \qquad \mu(CO(NH_2)_2) = 4.56D,$$

$$\mu(HF) = 1.82D, \qquad \mu(CH_3CON(CH_3)_2) = 3.79D.$$

Evidently the larger dipole moment of different amides leads to a larger electrostatic energy, which then dominates the angular dependence.

Dreyfus and Pullman [1970a, b] calculated the energy of interaction in the antiparallel dimer of formamide* (cf. fig. 2.16) and its partitioning within the framework of MO theory at a number of intermolecular distances, as well as the angular dependence of the individual contributions. Actually, the angular dependence of the total energy is very well reproduced by the electrostatic contribution alone. Since the charge distribution in the monomer obtained by Mulliken [1955] population analysis from their ab initio wave function is very similar to the point charges applied by Hagler et al. [1974a] direct comparison of ΔE_{COU} from MO energy partitioning and the electrostatic contribution to the CFF energy was possible (fig. 2.16). At large intermolecular distances the

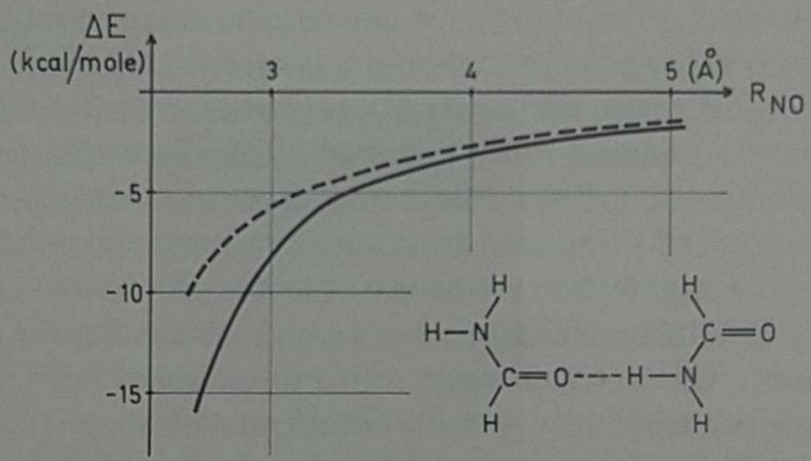

Fig. 2.16. Electrostatic contribution to the energy of interaction in formamide dimer (antiparallel conformation). ΔE_{COU} from the point charge model used in CFF calculations: -------- (Hagler et al. [1974]); ΔE_{COU} from ab initio MO calculations: ———; (Dreyfus and Pullman [1970]).

* These calculations are described in more detail in section 2.4.2.

energy curves start to coincide. In the short distance region around the equilibrium distance ($R_{NO} \approx 3$ Å), however, the point charge model underestimates the electrostatic energy. Since the major attractive contribution in this range comes from O···H interaction along the H-bond, the failure of the point charge expression seems to result at least in part from the poor representation of the O lone pair.

Besides the importance of ΔE_{COU}, Dreyfus and Pullman [1970a, b] found nonnegligible charge transfer in their MO calculations too. At the calculated equilibrium distance, $R_{ON} = 2.85$ Å, a charge of $0.029e_0$ is transferred from one formamide molecule to the other, an amount of electron density very similar to the result on $(H_2O)_2$. Basis set effects might be important since the calculation on formamide dimer was performed with a rather small GTO basis: $(4, 2; 3) \rightarrow [2, 1; 2]$. Nevertheless, we know from very accurate calculations on smaller systems that there is a significant attractive contribution to H-bonds besides electrostatic and dispersion energy.

Now we are left with the problem to look for the contribution in the CFF, wherein charge transfer and polarization energy have disappeared. In order to find an explanation we compared the Lennard-Jones potential with Morse functions of different α values. In any case D or ϵ have to be of the order of one kcal/mole and consequently, we compared potential functions normalized to equal dissociation energy and equilibrium distance. Additionally, it seemed reasonable to assume almost identical repulsive slopes for the purpose of comparison since at short distances the repulsive exchange contribution dominates. In this case the Morse function ($\alpha = 6.4$) falls off much faster with increasing distance and differs from the Lennard-Jones potential by the lack of attractive long range contributions (fig. 2.17). Hence, the Morse potential cannot account for polarization and dispersion forces and, in our opinion, this was the main reason for its rejection by the least squares procedure. Additionally, Hagler et al. [1974a] obtained a zero Van der Waals radius for the H-atom in the H-bond. This unusual result seems to indicate a hidden attractive contribution. Probably the delocalization effects are simulated in the CFF by an extremely small radius for the H-atom. On the whole, however, we feel that any attempt to put too much physical meaning into empirical force field parameters might be dangerous.

The final conclusions we would like to draw from the available CFF results on H-bonds can be formulated as follows. There is no doubt that

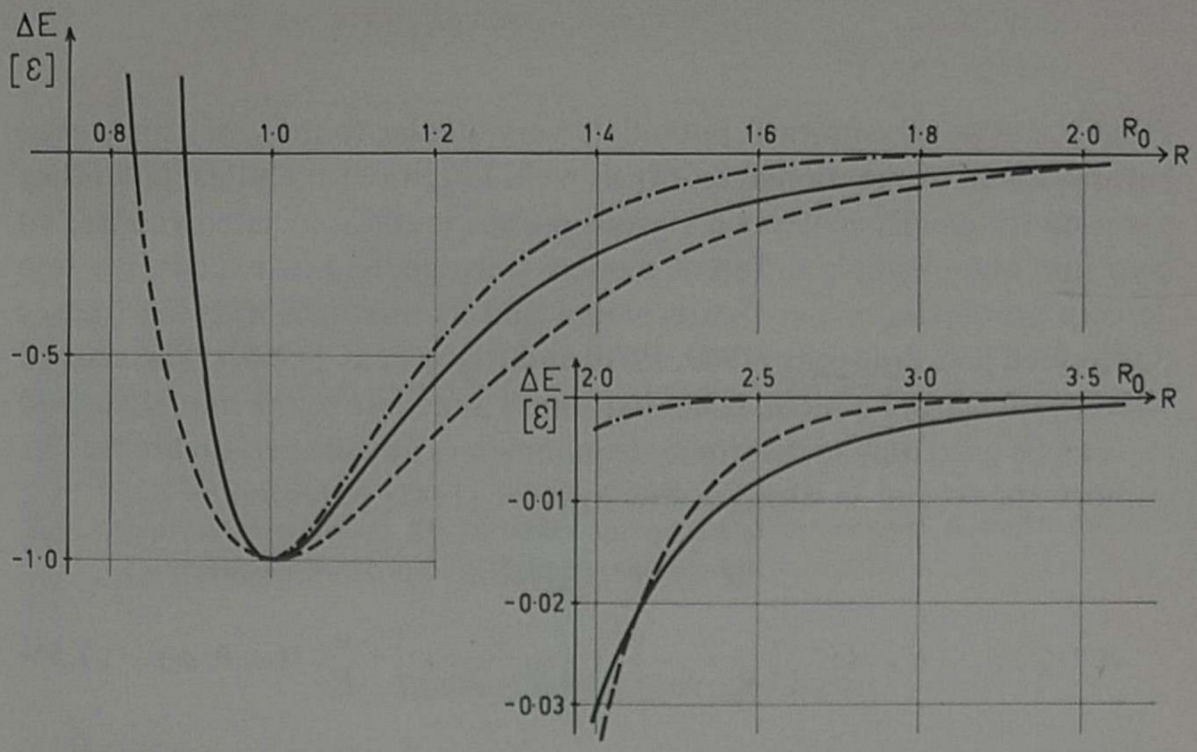

Fig. 2.17. Comparison between Lennard-Jones and Morse potential curves adjusted to equal dissociation energies (ϵ) and equilibrium distances (R_O). Lennard-Jones potential: ———, Morse potentials: $\alpha = 6.4$, chosen to reproduce most closely the repulsive part of the Lennard-Jones function: – · – · – · –, $\alpha = 4.0$: – – – – – –.

CFF calculations on amides and related compounds present an excellent tool for the investigation of structures and spectra of these molecules in the vapor phase and in the crystal. Furthermore, we can expect also highly valuable and interesting results of CFF calculations on peptides and proteins, since the same type of H-bonds occurs most frequently in these macromolecules. Nevertheless, two critical comments should be added at the end. From accurate MO calculations it does not seem likely that the CFF results for the CO···NH bond can be generalized directly to other types of H-bonds, where electrostatic energies are less important. Partitioning of H-bond energies in perturbation or MO theory is not comparable to the relative contributions of different potentials in CFF least squares fitting. In the empirical parameters many effects appear superimposed in a complicated manner. Therefore, the result that the H-bond Morse potential does not contribute significantly to the total CFF energy cannot be translated into MO theory as negligibly small intermolecular delocalization energy.

2.3.3. Empirical potentials from associations in the vapor phase

Finally, a type of empirical potentials very similar to those we discussed before should be mentioned briefly as well. Empirical analytical potentials are used frequently to explain various properties of associated vapors. To give just one example different models were applied to explain the low density properties of pure water vapor and its mixtures with inert gases (O'Connell and Prausnitz [1969, 1970] and Rigby et al. [1969]). The second virial coefficient of course, is not extremely sensitive to the model applied and can be used only to discriminate parameters outside certain limits. The authors succeeded in fitting a Stockmayer [1941] potential

$$R < 2a: \quad \Delta E = \infty,$$

$$R > 2a: \quad \Delta E = 4U_0\left[\left(\frac{\sigma}{R-2a}\right)^{12} - \left(\frac{\sigma}{R-2a}\right)^{6}\right] + \frac{\mu^2}{R^3} f(\omega, \theta, \phi) \qquad (2.55)$$

within the following limits:

$$U_0 < 0.6\ \text{kcal/mole}, \quad 2.6\ \text{Å} < \sigma < 3.0\ \text{Å}, \quad \Delta E(R = R_e) < 6\ \text{kcal/mole}.$$

Within these limits the following values were recommended:

$$U_0 = 0.33\ \text{kcal/mole}, \qquad \sigma = 2.65\ \text{Å} \quad \text{and} \quad 2a/\sigma = 0.1.$$

Moore and O'Connell [1971] compared this empirical potential surface with the most complete MO energy surface of water dimer published until now (364 individual points, Del Bene and Pople [1970]). They found fairly good overall agreement with the exception of two strongly repulsive orientations (fig. 2.18, **a** and **b**) and the most stable H-bonded structures (fig. 2.18, **c** and **d**). In the first case (**a**, **b**) the empirical model underestimates largely the repulsive term, in the latter orientations (**c**, **d**) in contrary MO calculations lead to significantly lower energies. Although it is very risky to make a particular effect like neglect of charge transfer in the electrostatic model responsible for the second type of discrepancies found, it seems at least highly remarkable and represents a good hint for further investigations, that the stability of exactly these structures is underestimated by electrostatic models, to which MO theory attributes the most important covalent contributions.

A similar comparison of empirical and MO potentials for the dimer of ammonia was reported too (Lee et al. [1970]).

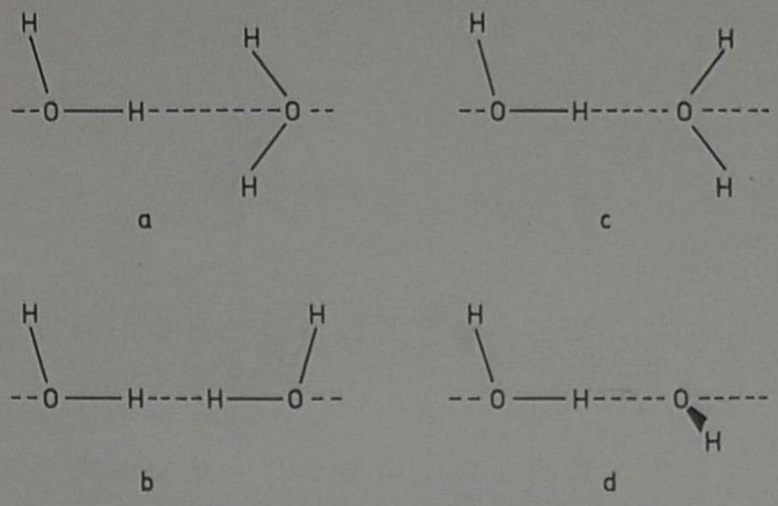

Fig. 2.18. Conformations of $(H_2O)_2$ where the empirical Stockmayer potential failed to reproduce the ab initio MO energy surface with reasonable accuracy.

2.4. Intermolecular hydrogen bonds

For practical reasons it is of advantage to divide the discussion of intermolecular H-bonds into three parts. In the first section we will be concerned with very weak interactions between polar molecules like HF or H_2O and noble gas atoms or unpolar molecules without permanent dipole moments.

Secondly, moderately strong intermolecular interactions, e.g. usual H-bonds are discussed. In the third part calculations on strong intermolecular H-bonds commonly occurring between certain charged and neutral molecules will be summarized.

2.4.1. Weak interactions between unpolar systems and polar molecules

Recently theoreticians became interested in the interaction of HF, H_2O and HCl with noble gas atoms and unpolar molecules like H_2, C_2H_2 and C_2H_4. MO methods were applied to calculate intermolecular geometries and energies (Losonczy et al. [1973], Lischka [1973a, b], Del Bene [1974] and Von Niessen [1974]). Two main questions were raised: Is it possible to discuss weak intermolecular interactions successfully within the limits of SCF calculations? Is there anything like a weak H-bond in these complexes between proton donors and unpolar acceptors? The results of these calculations are summarized in table 2.11.

The energy of interaction between noble gas atoms and polar molecules

TABLE 2.11

Weak intermolecular interactions between polar and unpolar systems

Structure			Basis set				R_{XS}^{e}[b]	ΔE_e (cal/mole)		
Systems	Geom.[a]	Orbitals	Uncontracted	Contracted	Method	Ref.	(Å)	ΔE_{SCF}	ΔE_{DIS}	ΔE_{TOT}
He, HF	a	GTO	(9, 5, 1; 4, 1) He (6, 2)	[5, 4, 1; 3, 1] He [4, 2]	SCF	a	3.45	−41 −31[d] −13[c]		
					IEPA	a	3.17	−15	−136 −89[d] −76[c]	−151
	b				SCF	a	3.11	−47 0[d] −19[c]		
					IEPA	a	2.93	−35	−76 −51[d] −94[c]	−111
He, H_2O	f	GTO	(9, 5, 1; 4, 1) He (6, 2)	[5, 4, 1; 3, 1] He [4, 2]	SCF	a	3.48	−56 −19[d] −15[c]		
					IEPA	a	3.26	−29	−118 −99[d] −72[c]	−147
	g				SCF	a	3.36	−55 −17[d] −13[c]		
					IEPA	a	3.16	−43	−71 −55[d] −55[c]	−141

Ne, H_2O	e	GTO	(10, 5, 1; 4, 1)	[5, 3, 1; 2, 1]	SCF	b	3.63	−170	−135[e)]	−305
	f		Ne (10, 5, 1)	[5, 3, 1]	SCF	b	3.56	−90		
	g				SCF	b	3.47	−50		
	e	GTO	(9, 5; 4)	[5, 3; 3]	SCF	c	3.70	−161		
	f		Ne (9, 5)	[5, 3]	SCF	c	3.70	−86		
	g				SCF	c	3.70	−7		
Ar, H_2O	e	GTO	(10, 5, 1; 4, 1)	[5, 3, 1; 2, 1]	SCF	b	4.45	−20	−174[e)]	−194
			Ar (17, 12, 1)	[5, 4, 1]						
H_2, HF	c	GTO	(9, 5, 1; 4, 1)	[5, 4, 1; 3, 1]	SCF	d	3.15	−357		
			$H(H_2)$: (4, 2)	[3, 2]	IEPA	d	2.90	−288	−326	−614
	d				SCF	d	3.07	−872		
					IEPA	d	2.83	−667	−867	−1534
H_2, H_2O	h	GTO	(9, 5, 1; 4, 1)	[5, 4, 1; 3, 1]	SCF	d	3.12	−581		
			$H(H_2)$: (4, 2)	[3, 2]	IEPA	d	2.81	−394	−651	−1045
	k				SCF	d	3.35	−401		
					IEPA	d	3.10	−298	−448	−746
C_2H_2, HF	l	STO-3G[e)]	(6, 3; 3)	[2, 1; 1]	SCF	e	3.50	−1040		
C_2H_4, HF	m	STO-3G[e)]	(6, 3; 3)	[2, 1; 1]	SCF	e	3.48	−910		
C_2H_2, H_2O	p, $\gamma = 19°$	STO-3G[e)]	(6, 3; 3)	[2, 1; 1]	SCF	e	3.63	−790		
	n, $\gamma = 4°$				SCF	e	3.69	−690		
	p, $\gamma = 52°$				SCF	e	3.85	−770		

TABLE 2.11–(*contd.*)

Structure		Basis set					R^{e}_{XS} [b]	ΔE_e (cal/mole)		
Systems	Geom.[a]	Orbitals	Uncontracted	Contracted	Method	Ref.	(Å)	ΔE_{SCF}	ΔE_{DIS}	ΔE_{TOT}
C_2H_4, H_2O	**o**, $\gamma = 8°$	STO-3G[e]	(6, 3; 3)	[2, 1; 1]	SCF	**e**	3.65	−630		
	q, $\gamma = 8°$				SCF	**e**	3.65	−620		
	o, $\gamma = 52°$				SCF	**e**	3.63	−500		
	q, $\gamma = 52°$				SCF	**e**	3.67	−490		

[a] The geometries are shown in fig. 2.19.

[b] The equilibrium distance R^{e}_{XS} is defined as the distance between the noble gas atom or the center of H_2, C_2H_2 or C_2H_4 and the heavy atom of the polar molecule: S = F or O.

[c] Polarization and dispersion energy calculated from experimental dipole moments polarizabilities and ionization potentials (2.56 and 2.57); only the coefficient d_6 was used.

[d] Polarization and dispersion energy calculated from the asymptotic expression using the coefficients d_6 and d_7 given by Lischka [1973a].

[e] See footnote to table 2.4.

References: **a** = Lischka [1973a]; **b** = Losonczy et al. [1973]; **c** = Von Niessen [1974]; **d** = Lischka [1973b]; **e** = Del Bene [1974] (STO-3G calculations, see footnote to table 2.4).

is characterized by the lack of a classical electrostatic contribution, $\Delta E_{\mathrm{COU}}^{\mathrm{CL}} = 0$. Consequently only electron exchange, polarization and charge transfer contribute to the energy of interaction at the SCF limit. ΔE_{EX} and ΔE_{CHT} fall off with the square of intermolecular overlap. At larger intermolecular distances the only nonvanishing term in the SCF energy of interaction is the polarization energy: $\Delta E_{\mathrm{SCF}}(R \to \infty) = \Delta E_{\mathrm{POL}}$. Dispersion energy ΔE_{DIS}, can be calculated in the IEPA method as the intermolecular contribution to correlation energy, $\Delta E_{\mathrm{COR}}^{\mathrm{INTER}} = \Delta E_{\mathrm{DIS}}$. SCF and IEPA calculations on He···HF and He···H_2O in various geometries shown in fig. 2.19 were recently presented by Lischka [1972a, b]. Additionally, he performed MO energy partitioning according to eqs. (2.34–2.40). His results for the most stable intermolecular orientation of He···HF (**a**) are shown in fig. 2.20. The asymptotic energy of interaction ($R \to \infty$) is given by the following expressions derived from perturbation theory (Margenau

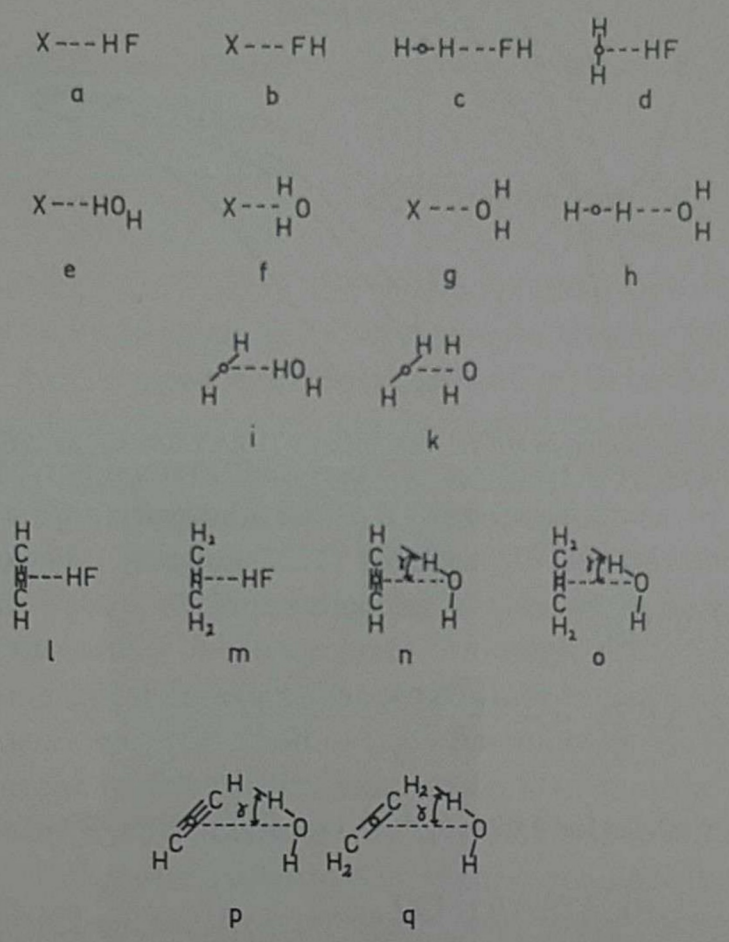

Fig. 2.19. Most important intermolecular geometries for which interaction between atoms or unpolar molecules and dipole molecules has been studied. The center of gravity (M) in unpolar molecules is denoted by "○".

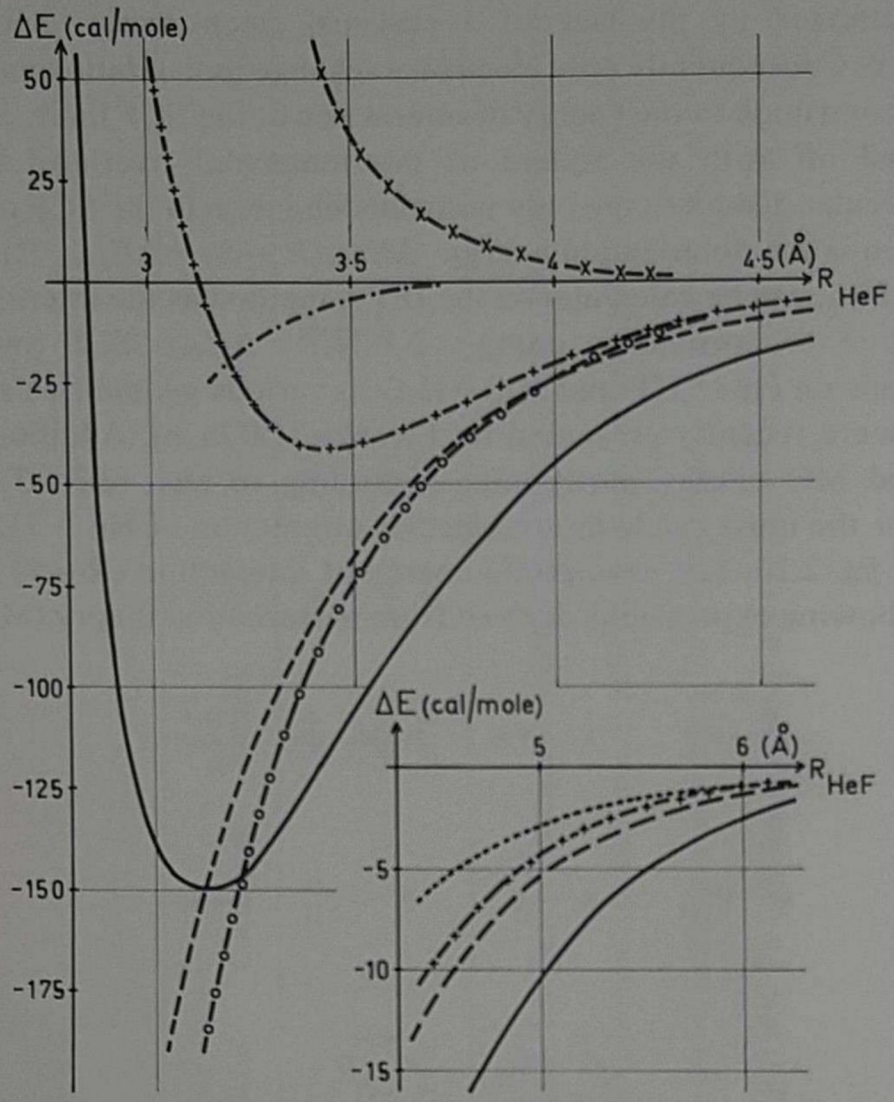

Fig. 2.20. Energy partitioning in He/HF obtained by IEPA calculations. ΔE: ———; ΔE_{SCF}: –+–+–+–+–; $\Delta E_{\mathrm{COR}}^{\mathrm{INTER}} = \Delta E_{\mathrm{DIS}}$: – – – –; ΔE_{COU}: –·–·–·–; ΔE_{EX}: –×–×–×–; ΔE_{POL}: –○–○–○–○–; $\Delta E_{\mathrm{POL}}^{\mathrm{CL}}$: · · · · · ·; (Lischka [1973a, b]).

and Kestner [1971]):

$$\lim_{R\to\infty} \Delta E_{\mathrm{POL}}(\gamma) = \Delta E_{\mathrm{POL}}^{\mathrm{CL}} = -\frac{d_6^{\mathrm{POL}}(\gamma)}{R^6} - \frac{d_7^{\mathrm{POL}}(\gamma)}{R^7} + \cdots, \tag{2.56}$$

$$d_6^{\mathrm{POL}}(\gamma) = \tfrac{1}{2}\alpha_{\mathrm{He}}\mu_{\mathrm{HF}}^2(3\cos^2\gamma + 1), \qquad d_7^{\mathrm{POL}}(\gamma) = 3\alpha_{\mathrm{He}}\mu_{\mathrm{HX}}Q_{\mathrm{HX}}\cos^3\gamma,$$

$$\lim_{R\to\infty} \Delta E_{\mathrm{DIS}}(\gamma) = -\frac{d_6^{\mathrm{DIS}}(\gamma)}{R^6} - \frac{d_7^{\mathrm{DIS}}(\gamma)}{R^7} + \cdots, \tag{2.57}$$

$$d_6^{\mathrm{DIS}}(\gamma) \sim \frac{I_{\mathrm{He}}I_{\mathrm{HF}}}{4(I_{\mathrm{He}} + I_{\mathrm{HF}})}\,\alpha_{\mathrm{He}}\{(5\alpha_{\mathrm{HF}}^{xx} + \alpha_{\mathrm{HF}}^{zz}) + 3(\alpha_{\mathrm{HF}}^{zz} - \alpha_{\mathrm{HF}}^{xx})\cos^2\gamma)\}.$$

This equation for d_6^{DIS} implies already an approximation according to Unsöld theorem, whereby the atomic or molecular ionization potentials are introduced instead of infinite summations over excited states. The expression for d_7^{DIS} is somewhat more complicated (see, e.g. Lischka [1973a]), and will not be used in further detail here. It changes sign like d_7^{POL} if γ is substituted by $180 - \gamma$. The importance of the R^{-7} contribution is well known from IR spectroscopy. Herman [1966] and Bonamy and Robert [1970] pointed out that this term is essential for a correct interpretation of noble gas broadening observed in vibration rotation lines of polar molecules.

The coefficients for the asymptotic expansion calculated from experimental dipole moments, quadrupole moments, ionization energies and polarizabilities using the expression derived by perturbation theory agree very well with values obtained from curve fitting to the points, which were calculated by the MO formalism at large distances:

Asymptotic perturbation theory:	$d_6^{POL}(0) = 1.4$ au,	$d_6^{DIS}(0) = 4.9$ au,
MO calculation (Lischka [1973a]):	$d_6^{POL}(0) = 1.7$ au,	$d_6^{DIS}(0) = 4.2$ au,
	$d_7^{POL}(0) = 10.3$ au,	$d_7^{DIS}(0) = 8.6$ au.

In case of polarization energy the values calculated by MO methods deviate significantly from eq. (2.56) at distances shorter than $R_{HeF} \approx 5$ Å. As expected the asymptotic expressions fail to describe the situation correctly around the energy minimum. In certain examples the calculated polarization energy is more than twice as much as the extrapolated result from the asymptotic formula (table 2.11). Similarly, as in our previous calculations on He_2 (section 2.2.2) Lischka [1973b] obtained a nonzero coulomb contribution at intermolecular distances, where the overlap between the molecules is appreciable, although there is no classical electrostatic energy of interaction between noble gas atoms and polar molecules. Again we see, that energy partitioning is not free from arbitrariness in the region of significant molecular overlap. Additionally, from Lischka's detailed calculations we can conclude that the expressions derived from asymptotic perturbation theory are only useful at large intermolecular distances. Around the energy minimum and at intermediate distances, however, energies and other important properties of the He···HF system cannot be described without a detailed consideration of the electronic structure of the particular complex.

The calculations on $He \cdots H_2O$ (Lischka [1973a]) show roughly the same results as in the case of $He \cdots HF$. Again the structure with the plus end of the dipole pointing towards the He-atom (structure **f** in fig. 2.19) was found to be most stable (table 2.11). A third geometry (**e**) similar to the most favored structures of ordinary H-bonds with a linear $He \cdots H–O$ arrangement was found to be repulsive in an SCF calculation at $R_{OHe} = 3.48$ Å (Lischka [1973b]). At larger distances, of course, we have to expect a weakly bound state because both asymptotic contributions to the total energy are negative.

MO calculations on $Ne \cdots H_2O$ were performed exclusively at the SCF limit (Losonczy et al. [1973] and Von Niessen [1974]). Although very different basis sets were applied, the same relative stabilities of the geometries **e**, **f** and **g** are reported. Contrary to $He \cdots H_2O$ the H-bond-like structure **e** was found to be most stable followed by structure **f** and structure **g**. At the energy minimum the SCF contribution to the energy of interaction again is much larger than the extrapolated value from the asymptotic expression. For this estimate Losonczy et al. [1973] used the dipole moment of H_2O calculated with their basis set and the experimental polarizability of Ne. The difference becomes larger if the calculated polarizability for Ne is used too. The basis sets applied by Losonczy et al. [1973] are rather poor in reproducing atomic and molecular polarizabilities (table 2.12), because they do not contain functions which account appropriately for polarization effects (Marius [1974]). In case of the Ne-atom Marius used the same basis set as Losonczy et al. [1973] but changed the orbital exponent of the d-functions from $\xi = 1.4$ to $\xi = 0.2$. The calculated polarizability increased by a factor of 2.5. Hence, very flat polarization functions are essential for a reasonably correct representation of polarizabilities by SCF calculations. This underestimation of polarizabilities certainly leads to an appreciable error in the asymptotic SCF energies, ΔE^{CL}_{POL}. Additionally, we have to expect that the SCF energies around the energy minima as calculated by Losonczy et al. [1973] are somewhat too small in absolute value as well, since polarization energy contributes significantly in this region of the potential curve as well. The dispersion energy of structure **e** was extrapolated from an asymptotic formula and might include significant errors too (table 2.11). Nevertheless, it seems safe enough to conclude from the results available that SCF and dispersion energy contribute almost equally to the stability of the preferred geometry of $Ne \cdots H_2O$ (**e**).

TABLE 2.12

Polarizabilities and quadrupole moments of noble gas atom and unpolar molecules considered in calculations of intermolecular interactions

Atom or molecule[a]	Method[b]	Polarizability (Å^3) α_{xx}	α_{yy}	α_{zz}	$\bar{\alpha}$	Ref.	Quadrupole moments (10^{-26} esu cm^2) Method	Θ_{xx}	Θ_{yy}	Θ_{zz}	Ref.
He	SCF calc.				0.182	a					
	Exp.				0.216	b					
					0.20	c					
Ne	SCF calc.				0.10	d					
					0.25	e					
	Exp.				0.39	c					
Ar	SCF calc.				0.35	d					
	Exp.				1.63	c					
H_2	SCF calc.	0.54	0.54	0.90	0.66	a	SCF calc.	−0.216	−0.216	0.432	g
		0.68	0.68	0.93	0.77	f		−0.320	−0.320	0.639	a
	Exp.	0.72	0.72	0.93	0.79	b	Exp.	−0.309	−0.309	0.619	h
C_2H_2	Exp.	2.4	2.4	5.1	3.3	b	SCF calc.	−3.57	−3.57	7.14	g
C_2H_4	Exp.				4.3	b	SCF calc.	−3.98	1.97	2.02	g

[a] The cartesian coordinate system was chosen in such a way that the z-axis coincides with the molecular axis in the H_2 or C_2H_2 and with the direction of the CC-bond in C_2H_4. The C_2H_4-molecule lies in the yz-plane.

[b] The basis sets applied in calculation **a** and **d** are shown in table 2.11. In calculation **e** the same basis set as in **d** was used except a change in the orbital exponent of the d-functions. Calc. **f**: very accurate calculation using a complicated many parameter wave function; Calc. **g**: a basis set with "double zeta STO" quality, $(10, 5; 4) \rightarrow [4, 2; 2]$.

References: **a** = Lischka [1973b]; **b** = Landolt-Börnstein [1951]; **c** = Condon and Odishaw [1967]; **d**, **e** = Marius [1974]; **f** = Kolos and Wolniewicz [1967]; **g** = Snyder and Basch [1972]; **h** = McLean and Yoshimine [1966].

Interestingly the results on $Ar\cdots H_2O$ obtained by SCF calculations and an extrapolation of the asymptotic dispersion energy (Losonczy et al. [1973]) again differ very much from the $Ne\cdots H_2O$ case. In the SCF calculation the H-bond-like structure **e** appears hardly bound. The potential curve presented shows only a very flat minimum at a rather large intermolecular distance. Unfortunately, no other geometry was investigated and hence, the obvious conclusion we would like to derive from atomic polarizabilities and molecular dipole moments suggesting a situation similar to the $He\cdots H_2O$ case does not seem to be seriously founded. Additionally, the polarizability of Ar is largely underestimated by the basis set applied (table 2.12) and similar arguments as raised before in the case of $Ne\cdots H_2O$ can be applied to $Ar\cdots H_2O$ as well. Further calculations are necessary as the authors already pointed out.

Contrary to the interaction between noble gas atoms and polar molecules, the electrostatic energy does not vanish in the structures H_2/HX. There is a quadrupole–dipole term, which falls off with the inverse fourth power of the intermolecular distance according to eq. (2.58) in the structures **c** and **h** and according to eq. (2.59) in the structures **d** and **k**:

$$\text{Structures } \mathbf{c}, \mathbf{h}: \quad \Delta E_{\text{COU}}^{\text{CL}} = -3\frac{\mu_{\text{HX}} Q_{\text{H}_2}}{R^4} + \cdots, \qquad (2.58)$$

$$\Delta E_{\text{POL}}^{\text{CL}} = -2\frac{\mu_{\text{HX}}^2 \alpha_{\text{H}_2}^{zz}}{R^6}.$$

$$\text{Structures } \mathbf{d}, \mathbf{k}: \quad \Delta E_{\text{COU}}^{\text{CL}} = -\frac{3}{2}\frac{\mu_{\text{HX}} Q_{\text{H}_2}}{R^4} + \cdots, \qquad (2.59)$$

$$\Delta E_{\text{POL}}^{\text{CL}} = -2\frac{\mu_{\text{HX}}^2 \alpha_{\text{H}_2}^{xx}}{R^6} + \cdots.$$

The asymptotic expressions for the polarization energy, $\Delta E_{\text{POL}}^{\text{CL}}$, of course, are identical with those given before (2.52) if we account for the anisotropy of the polarizability in H_2 and put $\omega = 0°$ or $\omega = 180°$. Lischka [1973b] calculated energy curves for the system H_2/HF and H_2/H_2O and performed MO energy partitioning too. His results on the most favorable structure of H_2/HF (**d**) are shown in fig. 2.21. In comparison to He/HF the total energy of interaction is increased by roughly one order of magnitude and dispersion energy has lost its dominating role. Nevertheless, it remains an important contribution and its consideration is inevitable for any fairly accurate description of the intermolecular potential in H_2/HF.

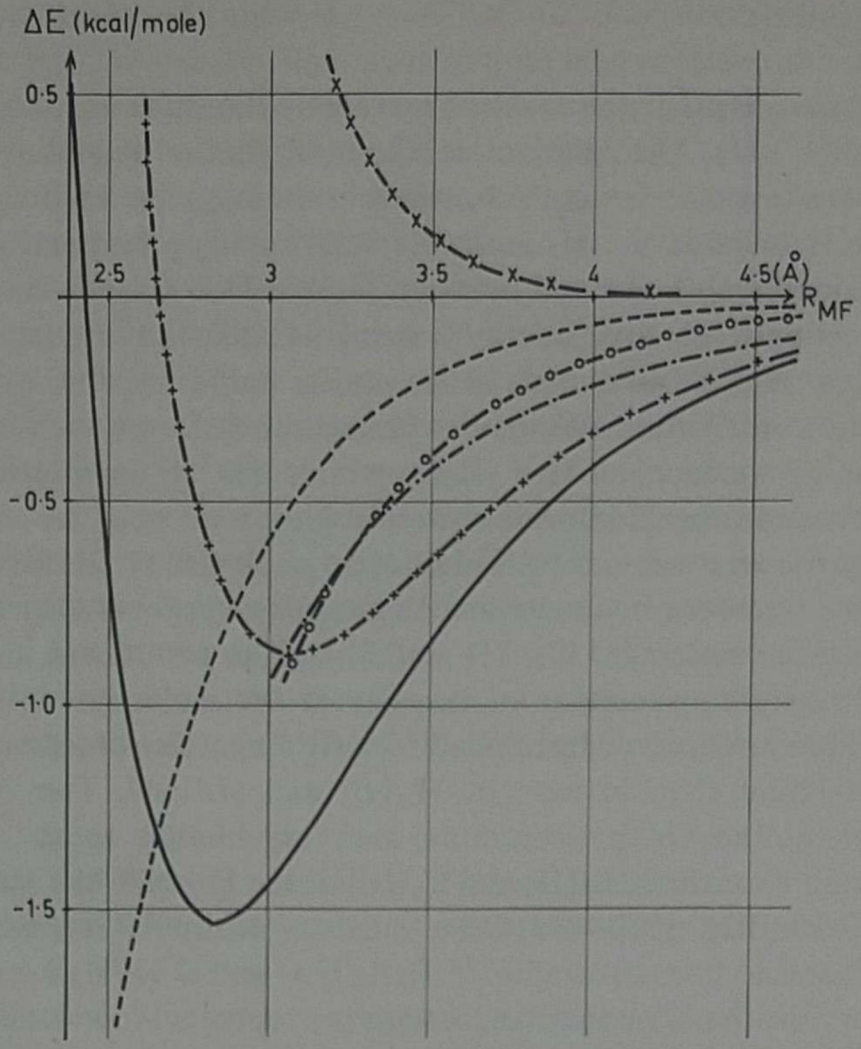

Fig. 2.21. Energy partitioning in H_2/HF obtained by IEPA calculations ΔE: ———; ΔE_{SCF}: –+–+–+–; $\Delta E_{COR}^{INTER} = \Delta E_{DIS}$: – – – –; ΔE_{COU}: –·–·–·–; ΔE_{EX}: –×–×–×–; ΔE_{POL}: –○–○–○–○; (Lischka [1973b]).

Lischka [1973b] tried a comparison of the individual contributions to the total energy of interaction for different intermolecular geometries. Thereby he encountered the additional difficulty of defining an origin inside the heteronuclear molecule for the calculation of intermolecular distances. For different choices he obtained different answers to the question: Which contribution is responsible for the difference in energy between different intermolecular orientations? At large intermolecular distances, $R_{MF} > 5$ Å the electrostatic contribution is by far the most important term and ΔE_{COU}^{CL} of course is a very good approximation to the total energy of interaction. Accordingly, the interaction between unpolar and polar molecules regarded here lies in between the atom–polar

molecule interaction and an ordinary H-bond between two polar molecules.

In the system H_2/H_2O the results are roughly the same as in the case of H_2/HF (table 2.11). The relative stabilities of the individual structures, however, are inverse. Structure **h**, wherein the negative end of the H_2O dipole points towards the H_2 molecule was found to be most stable. A structure simulating a H-bond between H_2 and H_2O (**l**) was investigated too. Interestingly, its total energy lies in between the energies for the structures **h** and **k** predicted to be most stable by the asymptotic electrostatic contribution. We have to expect therefore a local minimum in the energy surface of $H_2 \cdots H_2O$, which lies at an intermolecular geometry near to the H-bonded structure **l**.

Looking for an evidence for H-bonds to π-electrons Del Bene [1974] performed a number of calculations on the interaction between C_2H_2 and C_2H_4 with polar molecules like HF and H_2O. The results are included in table 2.11. As a consequence of the size of the molecules investigated only small basis sets could be applied. The SCF energies of interaction are somewhat larger than in case of H_2/HF and H_2/H_2O. The calculated geometries at the energy minimum are very similar to the previous examples. In case of C_2H_2/HF and C_2H_4/HF the H-bond-like structure is identical with that predicted from quadrupole/dipole interaction and actually found to be most stable. In C_2H_2/H_2O and C_2H_4/H_2O a geometry very near to the H-bond-like structure represents a local energy minimum. Del Bene [1974] carefully investigated the surrounding of the local minima in the energy surface of the two intermolecular complexes. Actually, the regions around these minima are very flat and the energy of interaction is rather intensive to certain rotations of the H_2O molecule (table 2.11).

According to the molecular polarizabilities and quadrupole moments the asymptotic energies ΔE^{CL}_{COU} and ΔE^{CL}_{POL} are significantly larger in C_2H_2/HF, C_2H_4/HF, C_2H_2/H_2O and C_2H_4/H_2O than in the previously discussed complexes H_2/HF and H_2/H_2O. Again we have to expect an important contribution of dispersion energy to the total energy of interaction, which of course was not included in Del Bene's SCF calculations.

Finally, we can conclude that there is some evidence for preferred geometries which indicate a H-bond-like arrangement involving the π-electrons of C_2H_2 and C_2H_4. The same preference, however, was found in our previous example H_2/H_2O, where the σ-electrons interact more

strongly with the local dipole of the HO-bond than with the molecular dipole of H_2O. No really significant differences between the complexes involving σ- or π-electrons were found. Nevertheless, more accurate calculations might modify this conclusion slightly.

Coming back again to our two initial questions we can give the following answer:

1. Calculations at the HF limit on weak intermolecular interactions are not sufficient even if only a rough description is desired. Electron correlation is important in all examples discussed here. As expected its influence is larger in the interaction between neutral atoms and polar molecules than in the interaction between unpolar and polar molecules. At large intermolecular distances the asymptotic expressions for electrostatic polarization and dispersion energies agree well with the results of MO energy partitioning. Since the asymptotic expression fails completely around the energy minima (table 2.11) no accurate description of stable geometries and other important properties of the complex is possible without a detailed calculation of the particular electronic structure.

2. It is more difficult to give an answer to the second question concerning the H-bond character of weak intermolecular interactions. First of all we have to agree to a definition of the H-bond. If we use H-bonding as a synonym for all effects in structures containing polar HX-bonds, which cannot be explained by semiclassical expressions derived from electrostatic theory, the answer is yes. Consequently, we have to concede in this case that semiclassical theory fails to describe other types of intermolecular interactions too, and we have to find a name for these discrepancies as well. Therefore it seems more appropriate to define the concept of an H-bond less embracing. For that purpose we might restrict our definition of H-bonds exclusively to those structures which persist in a more or less linear $Y \cdots HX$ arrangement with relatively strong resistance against deformation, especially in cases where the asymptotic electrostatic energy predicts a different geometry. Now only few candidates remain among the weakly interacting structures studied: $Ne \cdots H_2O$ and the six complexes formed from H_2, C_2H_2 and C_2H_4 with HF or H_2O. In the first example the linear H-bond-like arrangement (**e**) is remarkably more stable in the SCF limit than the other two more symmetric structures **f** and **g**. It seems interesting, that such a hint for an H-bond is found only in $Ne \cdots H_2O$ and seems to be missing in $He \cdots H_2O$ and $Ar \cdots H_2O$. Nevertheless, better evidence for the fact that orbitals of

a certain size have to be provided by the proton acceptor in order to guarantee a stable H-bond will be presented in the next section (2.4.2), wherein H-bonds to second and third row elements are discussed. In the two complexes involving H_2 the evidence for a preferred H-bond-like structure is somewhat weaker. In the first case the energy of structure **i** in $H_2 \cdots H_2O$ lies only in between the two geometries predicted by electrostatics (**l** and **k**). In $He \cdots H_2O$, however, the analogous structure was repulsive. In $H_2 \cdots HF$ the H-bond-like geometry is much more stable than the other structure preferred by the electrostatic contribution. On the remaining four complexes similar results were obtained. In C_2H_2/H_2O and C_2H_4/H_2O local minima near the H-bond-like arrangement were found. The conclusions presented here should be regarded only as first attempt of explanation. In any case more calculations of higher accuracy are needed before a definite answer to this question can be given.

2.4.2. Moderately strong hydrogen bonds

In sections 2.2.2–2.4 the problems arising in calculations on structures with moderately strong H-bonds have been discussed. Now we will present a summary of the most important results obtained in calculations on various structures. As we had seen calculated energies of interaction and, to a smaller extent also, calculated intermolecular geometries depend on the basis sets applied in ab initio calculations. Until now no calculation of H-bonded structures had reached the HF limit and only a few of them came very close to it. Consequently, it has no meaning to compare results of calculations using basis sets of very different size for different molecular associations. We will restrict ourselves therefore to compare ab initio calculations on roughly three levels of extension (see table 2.13): small basis sets (minimal STO basis, STO-3G, STO-4G, small GTO basis), medium size basis sets (double zeta STO basis, 4-31G, GTO basis of Huzinaga [1965] quality, contracted with some flexibility) and large basis sets (Huzinaga and Sakai [1969]) including polarization functions.

Molecules containing one or more polar HX-bonds form dimeric associations which can be classified approximately in three geometric types: linear, bifurcated and cyclic dimers (fig. 2.22). Actually, stable intermediate geometries, e.g. between linear and bifurcated arrangements are possible too, but a classification according to the nearest ideal structure facilitates the discussion enormously. Disregarding stereochemical aspects we might think the cyclic dimer should be favored since two

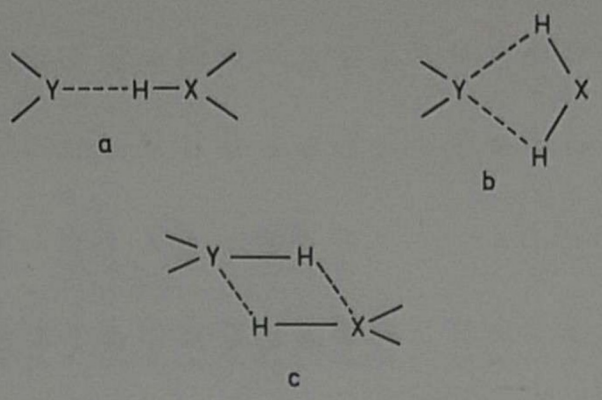

Fig. 2.22. Different types of intermolecular geometries in H-bonded dimers (**a**: linear, **b**: bifurcated and **c**: cyclic dimer).

H-bonds are formed in this case. In reality, however, the most stable dimers between small molecules come very close to the ideal linear arrangement ($\gamma = 0°$, see fig. 2.28). Bifurcated and cyclic dimers are much less stable. Only in exceptional cases of very weak H-bonds like in $(H_2S)_2$ the bifurcated arrangement is practically as stable as in the linear arrangement. The differences in energy between structure **a** and **b** (fig. 2.22) in $(H_2S)_2$ and $(H_2O)_2$ are the following:

$(H_2S)_2$: $E(\mathbf{a}) - E(\mathbf{b}) = -0.04$ kcal/mole (Sabin [1971a]),

$(H_2O)_2$: $E(\mathbf{a}) - E(\mathbf{b}) = -1.41$ kcal/mole (Diercksen [1971]).

In case of larger molecules different atoms can take over the role of proton acceptor and proton donor atom in cyclic dimers and then two efficient linear or almost linear H-bonds between both molecules can be formed without steric constraint. Consequently, these cyclic dimers are much more stable than the corresponding dimers with only one H-bond. The most important calculated ab initio results on linear dimers are summarized in table 2.13. Stable cyclic dimers will be discussed afterwards.

Regarding table 2.13 more closely we find a number of generalizable results. In neutral molecules third row atoms, e.g. Cl or S are very weak lone pair donors in H-bond formation. The energy of interaction in the corresponding associations is rather small. As mentioned above, in $(H_2S)_2$ the bifurcated arrangement, which is favored by the dipole–dipole term of the electrostatic energy, is almost as stable as the typical H-bond structure–the linear dimer. Only weak H-bonds are formed in complexes where HCl acts as proton acceptor.

TABLE 2.13

Ab initio MO–SCF calculations on moderately strong intermolecular H-bonds in linear dimers

Proton acceptor	Proton donor	Basis set[a] Orbitals	Uncontracted	Contracted	Ref.	ΔE (kcal/mole)	R_{XY} (Å)	ΔR_{HX} (Å)	γ (°)	ω (°)
			Calculated Results							
H_2S	HSH	GTO	(12, 9; 3)	[3, 2; 1]	a	−0.71	4.50	–	0	0
CH_3SH	$HSCH_3$	GTO	(6, 4; 2)	[5, 3; 2]	b	−1.40	4.30	–	0[c]	0[c]
			CH_3: (4, 2; 1)	[2, 1; 1]						
HCl	HF	STO-3G[b]	(6, 3; 3)	[2. 1; 1]	c	−1.3	3.50	–	0[c]	68
			Cl (9, 6)	[3, 2]		−1.3	3.50	0.01	0[c]	68
HCl	HCl	STO-3G[b]	(9, 6; 3)	[3, 2; 1]	c	−1.5	3.80	–	0[c]	68
						−1.6	3.80	0.01	0[c]	68
HF	HNH_2	GTO	(10, 5; 5)	[3, 1; 1]	d	−1.27	3.45	–	0[c]	0
H_2O	HNH_2	GTO	(11, 7, 1; 6, 1)	[5, 4, 1; 3, 1]	e	−2.33	3.35	–	0[c]	0[c]
		GTO	(10, 5; 5)	[3, 1; 1]	d	−2.28	3.41	–	0[c])	0
		STO-3G[b]	(6, 3; 3)	[2, 1; 1]	k	−4.3	2.8	–	0	60
H_3N	HNH_2	GTO	(10, 5; 5)	[3, 1; 1]	d	−2.71	3.49	–	0[c]	0
FHO	HOH	STO-3G[b]	(6, 3; 3)	[2, 1; 1]	f	−2.86	2.91	–	1	50
HF	HOH	GTO	(10, 5; 5)	[3, 1; 1]	g	−3.0	3.08	0.004	0[c]	52
CH_2O	HOH	STO-3G[b]	(6, 3; 3)	[2, 1; 1]	h	−3.33	2.88	–	1	61
		STO-3G[b]	(6, 3; 3)	[2, 1; 1]	k	−3.35	2.85	–	0[c]	64[c]
		STO	(2, 1; 1)	[2, 1; 1]	i	−3.42	2.87	–	0	64
H_2O_2	HOH	STO-3G[b]	(6, 3; 3)	[2, 1; 1]	f, j	−3.42	2.85	–	2	46
CH_2O	$HOCH_3$	STO-3G[b]	(6, 3; 3)	[2, 1; 1]	h	−3.49	2.86	–	1	61
HF	HCN	GTO	(10, 5; 5)	[3, 1; 1]	l	−3.58	3.18	–	0[c]	0
HCN	HCN	STO-3G[b]	(6, 3; 3)	[2, 1; 1]	v	−3.7	3.2	–	0[c]	0

H_2NOH	HOH	STO-3G[b]	(6, 3; 3)	[2, 1; 1]	f	−4.03	2.81	–	0	47
CH_2O	$HONH_2$	STO-3G[b]	(6, 3; 3)	[2, 1; 1]	h	−4.19	2.80	–	7	68
FHO	HOF	STO-3G[b]	(6, 3; 3)	[2, 1; 1]	f	−4.24	2.81	–	2	47
CH_2O	HOOH	STO-3G[b]	(6, 3; 3)	[2, 1; 1]	h	−4.39	2.78	–	6	66
HF	HF	GTO	(11, 7, 1; 6, 1)	[5, 4, 1; 3, 1]	m	−4.5	2.85	–	0[c]	40
		GTO	(11, 7, 2; 6, 1)	[7, 4, 2; 4, 1]	n	−3.46	2.91	–	0[c]	0[c]
		GTO	(10, 5; 5)	[3, 1; 1]	g	−4.58	2.88	0.003	0[c]	20
		STO-4G[b]	(8, 4; 4)	[2, 1; 1]	o	−5.2	2.55	–	4	69
		STO-3G[b]	(6, 3; 3)	[2, 1; 1]	c	−5.6	2.55	–	0[c]	65
						−5.6	2.55	0.01	0[c]	65
H_2O	HOH	GTO	(11, 7, 1; 6, 1)	[5, 4, 1; 3, 1]	p	−4.84	3.00	0.004	0[c]	0[c]
		GTO	(13, 8, 2, 1; 6, 2, 1)	[8, 5, 2, 1; 4, 2, 1]	q	−3.67	3.00	–	0[c]	0[c]
		GTO	(10, 5; 5)	[3, 1; 1]	r	−5.27	3.00	0.007	0[c]	25
		STO-4G[b]	(8, 4; 4)	[2, 1; 1]	s	−6.09	2.73	–	0	58
		STO-3G[b]	(6, 3; 3)	[2, 1; 1]	t	−5.88	2.74	–	0	57
		STO	(2, 1; 1)	[2, 1; 1]	u	−6.55	2.78	0.003	0	53.8
CH_2O	HOF	STO-3G[b]	(6, 3; 3)	[2, 1; 1]	h	−5.00	2.77	–	3	60
CH_3OH	HOH	STO-3G[b]	(6, 3; 3)	[2, 1; 1]	t	−5.22	2.77	–	1	48
HCN	HF	GTO	(10, 5; 5)	[3, 1; 1]	l	−5.48	3.05	–	0[c]	0
		STO-3G[b]	(6, 3; 3)	[2, 1; 1]	w	−3.58	3.04	–	0[c]	0
CH_3OH	$HOCH_3$	STO-3G[b]	(6, 3; 3)	[2, 1; 1]	t	−5.57	2.74	–	0	48
H_2O	$HOCH_3$	STO-3G[b]	(6, 3; 3)	[2, 1; 1]	t	−6.26	2.71	–	0	55
H_3N	HOH	GTO	(11, 7, 1; 6, 1)	[5, 4, 1; 3, 1]	x	−6.28	3.07	–	0[c]	0
		GTO	(10, 5; 5)	[3, 1; 1]	d	−5.8	3.12	–	0[c]	0
		STO	NH_3 (4, 2; 1)	[4, 2; 1]	y	−6.44	3.03	–	0[c]	0
			OH_2 (2, 2; 1)	[2. 2; 1]						
		STO-3G[b]	(6, 3; 3)	[2. 1; 1]	z	−5.89	2.91	–	3	4
H_3N	$HOCH_3$	STO-3G[b]	(6, 3; 3)	[2, 1; 1]	z	−6.48	2.87	–	2	3
H_2NCHO[b]	HOH	STO-3G[b]	(6, 3; 3)	[2, 1; 1]	k	−6.4	2.75	–	0	65
H_2NOH	$HONH_2$	STO-3G[b]	(6, 3; 3)	[2, 1; 1]	f	−7.00	2.70	–	10	58

TABLE 2.13–(*contd.*)
Calculated Results

Proton acceptor	Proton donor	Basis set[a] Orbitals	Uncontracted	Contracted	Ref.	ΔE (kcal/mole)	R_{XY} (Å)	ΔR_{HX} (Å)	γ (°)	ω (°)
H_3N	$HONH_2$	STO-3G[b]	(6, 3; 3)	[2, 1; 1]	z	−7.08	2.81	–	3	8
H_2O	$HONH_2$	STO-3G[b]	(6, 3; 3)	[2, 1; 1]	f	−7.30	2.66	–	8	69
H_2O	HNHCHO[d]	STO-3G[b]	(6, 3; 3)	[2, 1; 1]	k	−7.40	2.7	–	0	20
H_2O_2	HOOH	STO-3G[b]	(6.3; 3)	[2, 1; 1]	f, j	−7.56	2.68	–	18	61
H_2O	HOOH	STO-3G[b]	(6, 3; 3)	[2, 1; 1]	f	−7.64	2.67	–	3	58
HF	HCl	STO-3G[b]	(6, 3; 3)	[2, 1; 1]	c	−7.6	2.80	–	0	65
			Cl (9, 6)	[3, 2]		−8.5	2.80	0.05	0	65
H_2NCHO	HNHCHO[d]	GTO	(4, 2; 3)	[2, 1; 1]	aa	−7.95	2.85	–	0[c]	0[c]
		GTO	(7, 3; 3)	[2, 1; 1]	ab	−6.19	2.85	–	0[c]	0[c]
		GTO	(4, 2; 3)	[2, 1; 1]	aa, ac	−9	2.85	0.01	0[c]	60
		STO-3G[b]	(6, 3; 3)	[2, 1; 1]	k	−9.4	2.8	–	0[c]	60[c]
H_3N	HOOH	STO-3G[b]	(6, 3; 3)	[2, 1; 1]	z	−8.01	2.80	–	2	4
H_2O	HOF	STO-3G[b]	(6, 3; 3)	[2, 1; 1]	f	−8.72	2.65	–	3	52
H_2O	HF	GTO	(10, 5; 5)	[3, 1; 1]	g	−9.4	2.72	0.011	0[c]	0
		STO-3G[b]	(6, 3; 3)	[2, 1; 1]	c	−7.7	2.60	0.01	0	35
H_3N	HOF	STO-3G[b]	(6, 3; 3)	[2, 1; 1]	z	−9.80	2.77	–	1	1
H_3N	HF	GTO	(10, 5; 5)	[3, 1; 1]	d	−11.7	2.75	–	0[c]	0
		STO-3G[b]	(6, 3; 3)	[2, 1; 1]	c	−8.5	2.75	–	0[c]	0
						−8.5	2.75	0.01		
H_2O	HCl	STO-3G[b]	(6, 3; 3)	[2, 1; 1]	c	−10.9	2.80	–	0[c]	45
			Cl (9, 6)	[3, 2]		−13.6	2.80	0.07	0[c]	45
H_3N	HCl	STO-3G[b]	(6, 3; 3)	[2, 1; 1]	c	−12.7	3.00	–	0[c]	0
			Cl (9, 6)	[3, 2]		−15.7	3.00	0.09	0[c]	0
		GTO	(11, 7; 6)	[5, 3; 3]	ad	−19.5	2.86	0.03	0[c]	0
			Cl (11, 7)	[5, 4]						

[a] If two third-row elements are involved in the H-bond their basis set is given without further notation. In case of one third-row element the corresponding basis set is shown separately.

[b] See footnote to table 2.4.

[c] Assumed geometry.

[d] Hydration studies on formamide were presented previously (section 2.3.1). Antiparallel geometry was used for the open chain dimer (see fig. 2.16), the parallel dimer shows almost the same energy of interaction (Dreyfus and Pullman [1970a]).

References: **a** = Sabin [1971a]; **b** = Pecul and Janoschek [1974]; **c** = Kollman et al. [1974]; **d** = Kollman and Allen [1971]; **e** = Diercksen et al. [1972]; **f** = Del Bene [1972b]; **g** = Kollman and Allen [1970b]; **h** = Del Bene [1973a]; **i** = Morokuma [1971]; **j** = Del Bene [1972a]; **k** = Johansson and Kollman [1972]; **l** = Johansson et al. [1972a]; **m** = Diercksen and Kraemer [1970a]; **n** = Lischka [1974a]; **o** = Del Bene and Pople [1971]; **p** = Diercksen [1969, 1971]; **q** = Popkie et al. [1973]; **r** = Kollman and Allen [1969]; **s** = Del Bene and Pople [1969, 1970], **t** = Del Bene [1971]; **u** = Morokuma and Winick [1970]; **v** = Johansson et al. [1972b]; **w** = Del Bene and Marchese [1973]; **x** = Diercksen et al. [1972]; **y** = Piela [1972]; **z** = Del Bene [1973b]; **aa** = Dreyfus and Pullman [1970a]; **ab** = Berthod and Pullman [1972]; **ac** = Dreyfus and Pullman [1970b]; **ad** = Clementi [1967b, c] and Clementi and Gayles [1967].

On the other hand HCl is even a better proton donor than HF in H-bond formation. Somehow this result reflects the higher acidity of the HCl molecule compared to HF. Kollman et al. [1974] found another interesting difference in the proton donor properties of HF and HCl. The elongation of the HF bond during H-bond formation is rather small (see tables 2.9 and 2.13) and the corresponding gain in energy due to relaxation of the proton acceptor molecule hardly exceeds the error limits of the calculation. The bond length in HCl, however, is remarkably increased during H-bond formation and relaxation of the HCl molecule leads to a pronounced decrease in the energy of the complex.

The general rule stating that an increase in acidity of the proton donor or basicity of the proton acceptor leads to stronger H-bonds is fulfilled fairly well by moderately strong H-bonds. Especially, Del Bene's papers dealing with the interaction of various ROH model compounds confirm this suggestion (table 2.13).

The energy of interaction in the linear dimer $(HCN)_2$ was calculated also by perturbation theory using a simplified formalism similar to that applied by Murrell et al. [1965]. Starting from a very accurate wave function of HCN (McLean and Yoshimine [1967]) Rae [1969] obtained the following results: $\Delta E = -4.7$ kcal/mole, $R_{NC} = 3.3$ Å, which are in good agreement with STO-3G calculations (table 2.13) and experimental data ($\Delta E = -3.3$ kcal/mole, Pimentel and McClellan [1960]).

In most cases small basis sets lead to exaggerated stabilities of molecular associations. Some examples in table 2.13 involving H_3N as proton acceptor, e.g. $H_3N\cdots HOH$ or $H_3N\cdots HF$, however, show an inverse tendency. The energy of interaction is smaller in some calculations using small basis sets. Most probably a superposition of two effects is responsible for this unusual trend. First of all the dipole moments of H_3N, H_2O and HF calculated by certain minimum basis sets, e.g. STO-3G are much smaller than those obtained by much more extended calculations. Consequently, the electrostatic contribution to the energy of interaction is smaller if small basis sets are used. This difference in electrostatic energies alone, however, cannot account for the trend inversion observed in the series of proton acceptors HF, H_2O, H_3N. The dipole moments of other proton acceptors besides H_3N are obtained much smaller in STO-3G than in very extended near Hartree–Fock ab initio calculations too. The second source of errors concerns this kind of basis set effects we have discussed previously (section 2.2.3). The energy of interaction is obtained too large in absolute value, because mutual

extension of basis sets by the functions of the other molecule in the complex leads to an additional stabilization in MO calculations with small basis sets. This effect was found to be more important in molecules with a smaller ratio of basis functions to electrons as we can see from the numerical data on $(HF)_2$, $(H_2O)_2$ and $(HCN)_2$ reported by Johannson et al. [1973]. In the series HF, H_2O and H_3N this ratio increases steadily and consequently basis set effects of the second type are expected to be much more important in complexes of HF than in those of H_3N. The difference in relative importance of mutual basis set extension is nicely demonstrated in the extreme case of interaction with free protons which is represented by proton affinities, ΔE_{PA}:

$$X + H^+ \rightleftharpoons [XH]^+ \qquad \Delta E_{PA} = E_{[XH]^+} - \{E_X + E_{H^+}\}. \tag{2.60}$$

Small basis sets overemphasize the proton affinity of HF much more than the corresponding energy of H_3N. In calculations with minimum basis sets even the relative basicity in the series HF, H_2O and H_3N is inverted and HF is calculated to be a stronger base than H_3N (Hopkinson et al. [1968] and Schuster [1970]; see also section 2.9). In complexes involving H_3N as proton acceptor, therefore, the electrostatic effect of calculated dipole moments determines the influence of the size of the basis set applied, whereas in the other examples the effect of mutual basis set extension dominates.

Semiempirical MO methods were applied extensively to moderately strong H-bonds. In most cases the results of CNDO/2 calculations turned out to be very satisfactory. Only in one example, $(HCN)_2$, a wrong intermolecular geometry was predicted (Johannson et al. [1972b]). Since the results of CNDO calculations on H-bonded structures have been summarized in several review articles (Murthy and Rao [1970], Kollman and Allen [1972] and Schuster [1973]) we need not repeat here the individual numbers. In fig. 2.23 a comparison between energies of interaction calculated by medium size basis sets and the CNDO/2 procedure is shown. The calculated intermolecular distances are compared in fig. 2.24. In general the energies of interaction obtained by CNDO/2 calculations are somewhat too short. Both figures show, however, that relative values are reproduced correctly by CNDO/2 calculations on this kind of H-bonds. Hence the CNDO/2 method represents a reliable and relatively cheap procedure of interpolation for unknown structures within a series of known molecular associations. Consequently, it is very useful for an estimate of interactions between large molecules, where accurate calcula-

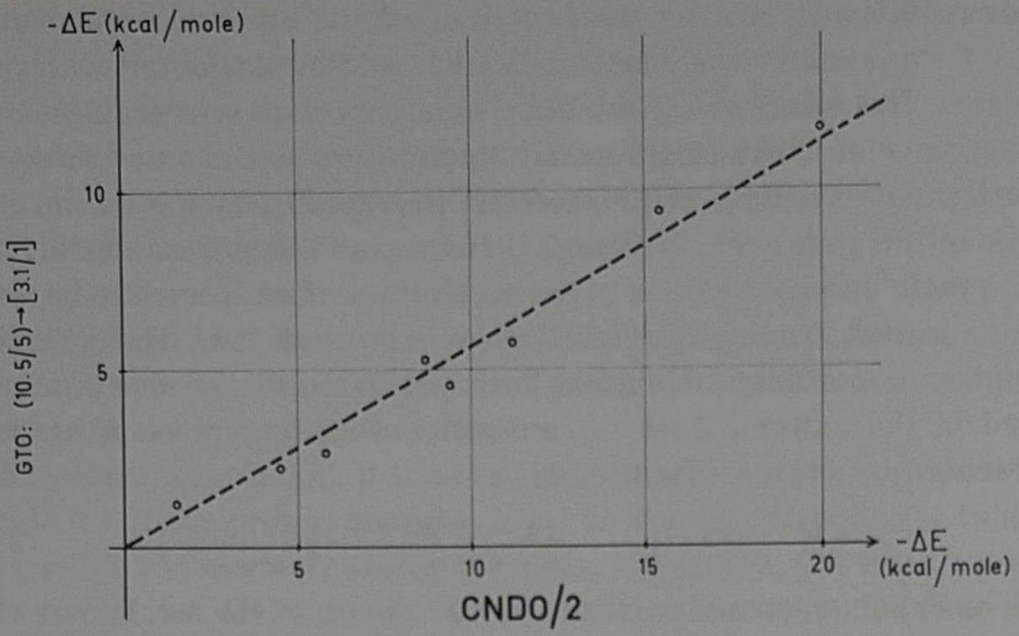

Fig. 2.23. Correlation of H-bond energies in linear dimers calculated by CNDO/2 and medium size ab initio MO calculations (Schuster [1973]).

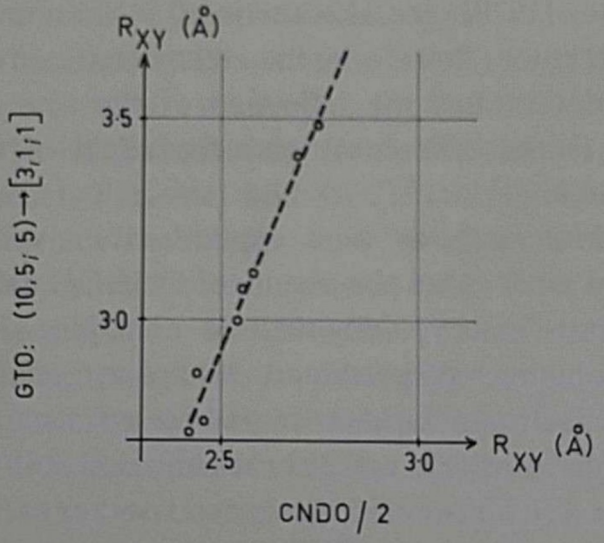

Fig. 2.24. Correlation of intermolecular equilibrium distances (R_{XY}) in linear dimers calculated by CNDO/2 and medium size ab initio MO calculations (Schuster [1973]).

tions are far outside the range accessible by our present computational facilities. Interestingly, CNDO/2 calculations at fixed experimental geometries reproduce the available experimental enthalpies of association very well (Schuster [1969a]).

At attempt to compare calculated and experimental data for the associations considered here is shown in fig. 2.25. Regarding this comparison we have to keep in mind that a correct experimental determination of

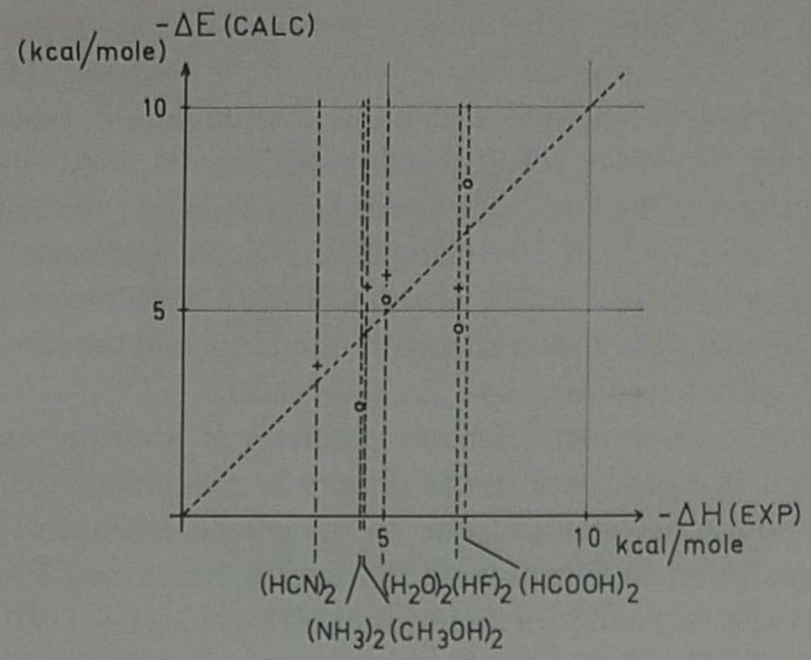

Fig. 2.25. Correlation between calculated and experimental H-bond energies. STO-3G calculations: +; medium size basis sets, e.g. (10, 5/5)→[3, 1/1]: ○; see also tables 2.13, 2.14.

H-bond enthalpies and intermolecular geometries is a very tricky problem too. Only in a few exceptional cases reliable vapor phase enthalpies are available. In case of hydrogen fluoride stable dimers were identified in the vapor phase (Smith [1959] and Dyke et al. [1972]) and reliable information on its structure was obtained by microwave spectroscopy. Additionally, higher polymers were found, e.g. stable cyclic hexamers (Smith [1958]). In case of water vapor the situation is even more difficult. Only very recently Dyke and Muenter [1974] reported microwave data for free $(H_2O)_2$ (see table 2.9). Previously, $(H_2O)_2$ has been investigated by matrix isolation technique at very low temperatures (cf. ch. 30). Considering the difficulties in both theoretical and experimental determinations the values obtained agree fairly well. As long as sufficiently large basis sets were used the calculated energies of interaction are very similar to the generally accepted experimental enthalpies (Pimentel and McClellan [1960]). Interestingly, the relative strength of H-bonds is reproduced very well by STO-3G calculations too, which do not require such an enormous amount of computer time as extended ab initio calculations (fig. 2.25). Between theory and experiment there is only one major discrepancy: In almost all calculations using comparable basis sets the energy of interaction in $(HF)_2$ was obtained slightly smaller in absolute value than in $(H_2O)_2$, whereas the experimental data favor an opposite relative strength.

A number of stable cyclic dimers between larger molecules were investigated by both ab initio and semiempirical methods. Their results are summarized and compared with experimental data in table 2.14. The comparison of ab initio results and experimental data shows good agreement as long as the basis sets applied were flexible enough. CNDO/2 results agree well, only if the calculations were performed at frozen experimental geometries. Again at the CNDO/2 equilibrium geometries the calculated energies of interaction are too large and the intermolecular distances too short (see also figs. 2.23 and 2.24).

As long as the same local H-bond geometry is used the energy for a single H-bond in cyclic and linear dimers is essentially the same. No remarkable additional stability due to the cyclic arrangement of both H-bonds was found in formic acid dimers (Schuster and Funck [1968] and Schuster [1969a]) and formamide dimer (Dreyfus et al. [1970], Dreyfus and Pullman [1970a, b] and Berthod and Pullman [1972]).

The energy surface for proton motion in the cyclic dimer of formamide was recently calculated in detail by Janoschek [1973b]. He used this surface for an analysis of nuclear motion around the energy minimum and calculated frequencies and intensities of the corresponding vibrational bands (see also ch. 3).

A detailed CNDO/2 investigation on acetic acid dimer and its tri-, hexafluoro and trichloro derivatives was recently reported by Rode et al. [1973]. These semiempirical calculations reproduce correctly the H-bond strengths in cyclic dimers of carboxylic acids (table 2.14): $\Delta H(\mathrm{HCOOH})_2 < \Delta H(\mathrm{CF_3COOH})_2 < \Delta H(\mathrm{CH_3COOH})_2$ (Pimentel and McClellan [1960]). A careful analysis of the experimental error limits was performed by Clague and Bernstein [1969]. They ended with the conclusion that the standard deviations are much larger than most authors concede. Actually, they found differences between the individual energies of interaction which are not much larger than the error limits determined.

An ab initio calculation on the bicyclic dimer between guanine and cytosine well known as the Watson–Crick-GC base pair (fig. 2.26) was performed by Clementi et al. [1971]. They used a small GTO basis set: $(7, 3; 3) \rightarrow [2, 1; 1]$. Most probably this is the largest computation on an electronic molecular structure which has been performed until now. From their data and the previously reported total energies of the monomeric bases (Clementi et al. [1969]) we calculated an energy of interaction of $\Delta E = -37$ kcal/mole at the experimental geometry. Although no reliable experimental data on the energy of dimerization of the GC base pair in the

TABLE 2.14

MO–SCF calculations and experimental data on stable cyclic intermolecular H-bonded dimers

Structure	Method of calculation	Ref.	ΔE (kcal/mole)	R_{XY}(Å)	R_{HX}(Å)	$\Delta H^{a)}$ (kcal/mole)	$R_{XY}{}^{a)}$(Å)	Ref.
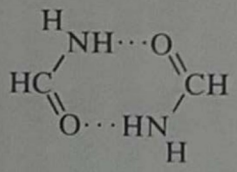	GTO: (7, 3; 3)→[2, 1; 1]	a	−14	2.94[b)]	1.0[b)]	−14(s)		h
	GTO: (4, 2; 3)→[2, 1; 2]	a	−19	2.94[b)]	1.0[b)]		2.94(s)	i
	CNDO/2	b	−12	2.94[b)]	1.0[b)]			
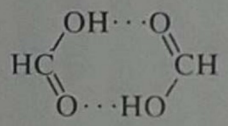	GTO: (9, 5, 1; 4, 1)	c	−16.2	2.73	0.98	−14.1 + 0.4(v)	2.73(v)	j
	GTO: (8, 3; 4)→[3, 1; 2]	d	−13.8	2.73[b)]	0.98[b)]		2.58(s)	j
	CNDO/2	e, f	−16.0	2.73[b)]	0.98[b)]	−13.7 + 0.7(v)		k
		f	−34	2.40	1.07			
		f	−22.1	2.70[b)]	1.05			
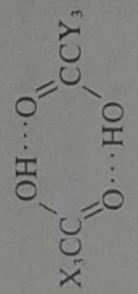 X=Y=H	CNDO/2	g	−25.0	2.70[b)]	1.057	−15.4 + 0.1(v)	2.76(v)	j
						−14.8 + 1.0(v)	2.61(s)	j
						−14.8 + 1.0(v)		k
X=Y=F	CNDO/2	g	−22.6	2.70[b)]	1.057	−14(v)		j
X=H, Y=F	CNDO/2	g	−24.8	2.70[b)]	1.054	−15.0 ± 1.0(v)		k
					1.063			
X=H, Y=Cl	CNDO/2	g	−24.4	2.70[b)]	1.054			
					1.063			

[a)] Measurements in the vapor phase are indicated by (v), those performed on crystals by (s).

[b)] Assumed geometric input data.

References: **a** = Dreyfus et al. [1970]; **b** = Pullman and Berthod [1968]; **c** = Clementi et al. [1971]; **d** = Ady and Brickmann [1971]; **e** = Schuster and Funck [1968]; **f** = Schuster [1969a]; **g** = Rode et al. [1973]; **h** = Poland and Scheraga [1967]; **i** = Ladell and Post [1954]; **j** = Pimentel and McClellan [1960]; **k** = Clague and Bernstein [1969].

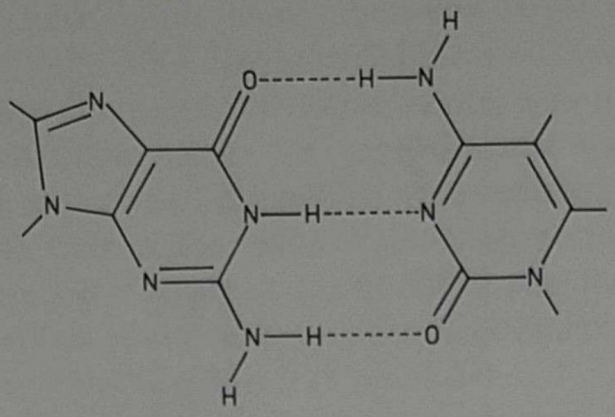

Fig. 2.26. Intermolecular geometry of the Watson–Crick guanine-cytosine base pair.

vapor phase are available the calculated result for ΔE seems to be too large in absolute value. To end up with such an energy of interaction each of the three H-bonds in the GC pair would have to be almost twice as strong as one H-bond in formic acid or formamide dimer.

2.4.3. Strong intermolecular hydrogen bonds

Intermolecular interactions between ions and neutral molecules have been investigated by theoretical methods for a very long time. In some cases strong intermolecular H-bonds were postulated. Consequently, the interest of theoreticians and experimentalists was concentrated around the best known example, the $[FHF]^-$ ion, which was found to occur as a more or less independent entity in ionic crystals. The first quantum mechanical calculations on $[FHF]^-$ were performed by Clementi [1961], Clementi and McLean [1962] and McLean and Yoshimine [1967]. They used STO basis sets of different size. All these calculations resulted in a symmetric equilibrium geometry of this anion with equal distances R_{HF}. Later on structural data on various other systems with strong H-bonds, e.g. $[H_5O_2]^+$, became available and theoretical investigations on these structures were encouraged. It turned out that these ionic complexes are more or less flexible units and show different structures in different environments although the enthalpies of formation are rather large in absolute values: $\Delta H([FHF]^-) = -60$ kcal/mole, $\Delta H([H_5O_2]^+) = -32$ kcal/mole. Even in case of $[FHF]^-$ the proton can be shifted significantly towards one F-atom by a suitable crystal field. In a recent neutron diffraction study of p-toluidinium bifluoride crystals the following distances were obtained: $R_{HF_1} = 1.235$ Å, $R_{HF_2} = 1.205$ Å (Williams and Schneemeyer [1973]). Many structural data on crystals with solvated

protons demonstrate the variability of $[H_5O_2]^+$ and derived cations (see chs. 10 and 14). The influence of electrostatic crystal fields on the structure of small molecules or ions was investigated by Almlöf et al. [1972] and Almlöf and Wahlgren [1973] using ab initio methods. The crystal field was simulated by a number of point charges. Interestingly, the results obtained for $[H_3O]^+$ indicate that the deformations of the cation in the electrostatic field of the crystal are very similar to those we would expect in case linear H-bonds are formed to the ligands (Almlöf and Wahlgren [1973]). Further structural data on strong H-bonds were presented together with an interpretation of the typical vibrational spectra of these compounds by Hadži [1972] (see also ch. 12).

The strong H-bonds we are going to discuss here represent interactions between ions and dipole molecules. Accordingly, the electrostatic contribution is very important and determines the asymptotic R^{-2} dependence of the energy of interaction. Nevertheless, the energy minima are encountered at a linear or almost linear arrangement of the three atoms XHY indicating a strong H-bond. In most examples (table 2.15) the energies of interaction amount to 30 kcal/mole or more in absolute values. Regarding the energies of formation these complexes fall into the range of usual intermolecular interactions between dipole–molecules and ordinary chemical bonds.

A number of calculated equilibrium geometries are symmetric ($R_{HX} = R_{HY}$). In this case it is impossible to recognize individual components of the complex or in other words to find out which part of the association stems from the HX- or Y-molecule. In some other examples the proton in the H-bond does not occupy an equilibrium position exactly in the middle between the atoms X and Y, but one of two more or less equivalent positions very near to it. Again appreciable differences between the equilibrium geometries of the individual subunits in the complex and the free molecules or ions are found.

The only remarkable exception in table 2.15 is represented by the complex $Cl^- \cdots H_2O$. In this case the equilibrium structure deviates significantly from the linear arrangement of the three atoms participating in the H-bond. Furthermore, the H_2O-molecule bound to Cl^- is very flexible against partial rotation around the O-atom. According to calculations of Piela [1973] the linear $Cl^- \cdots H–OH$ arrangement is only slightly more stable than the complex with C_{2v} symmetry, the geometry which is preferred by simple electrostatics. Contrary to $Cl^- \cdots H_2O$ the H-bond in $F^- \cdots H_2O$ is rather rigid. This was recently proved experimentally by

TABLE 2.15

Ab initio MO–SCF calculations and experimental data on strong intermolecular H-bonds

Proton acceptor	Proton donor	Basis set[a] Orbitals	Uncontracted	Contracted	Ref.	ΔE (kcal/mole)	R_{XY} (Å)	R_{HX}[b] (Å)	γ (°)	ΔH_{exp}[b] (kcal/mole)	Ref.
HS^-	HSH	GTO	(12, 9; 3)	[3, 2; 1]	a	−31.2	3.49	1.743		−14(s)	p
HO^-	HOH	GTO	(11, 7, 1; 6, 1)	[5, 4, 1; 3, 1]	b	−24.3	2.51	1.16		−22.5(s)	q
		4-31G[d]	(8, 4; 4)	[3, 2; 2]	c	−40.7	2.45	1.11		(−34.6(v))	r
F^-	HF	GTO	(11, 7; 5, 1)	[5, 3; 2, 1]	d	−40	2.22	1.11		−60.2(v)	s, y
		GTO	(9, 5, 1; 4, 1)	[4, 2, 1; 2, 1]	e	−51	2.246	1.123			
		GTO	(10, 5; 5)	[4, 2; 2]	f	−52.2	2.285	1.143			
F^-	HOH	GTO	(11, 7, 1; 6, 1)	[5, 4, 1; 3, 1]	h, i	−24.1	2.41	0.96[c]		−23.3(v)	f
		GTO	(11, 7, 2; 6, 2)	[4, 3, 2; 2, 2]	j, k	−23.7	2.51	1.0	4.5		
			F^-(13, 8, 2)	[7, 4, 2]							
Cl^-	HOH		(11, 7, 2; 6, 2)	[4, 3, 2; 2, 2]	j, k	−11.9	3.31	0.964	16.6	−13.1(v)	
			Cl^-(17, 11, 2)	[9, 6, 2]							
		STO	(3, 2; 2)	[3, 2; 2]	g	−19.5	3.04	1.02	0[c]		
			Cl^-(5, 4)	[5, 4]		−15.7	3.18	0.97[c]	54.3[c]		
H_3N	$[HNH_3]^+$	GTO	(10, 5; 5)	[3, 1; 1]	l_α	−25.9	2.65	1.18		−24.8(v)	x
		GTO	(10, 5; 5)	[4, 2; 1]	l_α	−32.0	2.70	1.08			
			H_7 (5, 1)	[2, 1]	l_β	−36.0	2.71	1.08			

H_2O	$[HOH_2]^+$	GTO	(11, 7, 1; 6, 1)	[5, 4, 1; 3, 1]	m	−32.2	2.39	1.14	−31.6(v)	v
		GTO	(10, 5; 5)	[4, 2; 2]	f	−35.3	2.38	1.19	−36(v)	u
		4-31G[d]	(8, 4; 4)	[3, 2; 2]	c	−43.9	2.36	1.18	−32.3(v)	w
		STO	(4, 2; 2)	[2, 1; 1]	n	−44.4	2.36[c]	1.18[c]		
HF	$[HFH]^+$	GTO	(11, 7, 1; 6, 1)	[5, 4, 1; 3, 1]	o	−30.7	2.26	1.13		

[a] See footnote to table 2.13. H_7 (ref. l) represents the H-bond.

[b] R_{HX} represents the distance between the proton in the H-bond and the atom X, which lies nearer.

[c] Assumed geometric input data.

[d] 4-31G and related basis sets were described by Ditchfield et al. [1971] and Hehre et al. [1972].

[e] Vapor phase enthalpies determined by mass spectroscopy (v) or values calculated from lattice energies (s). If more than one value is shown less reliable data are given in parentheses.

References: **a** = Sabin [1971b]; **b** = Kraemer and Diercksen [1972a]; **c** = Newton and Ehrenson [1971]; **d** = Noble and Kortzeborn [1970]; **e** = Almlöf [1972]; **f** = Kollman and Allen [1970d]; **g** = Piela [1973]; **h** = Diercksen and Kraemer [1970b]; **i** = Kraemer and Diercksen [1972b]; **j** = Kistenmacher et al. [1973a]; **k** = Kistenmacher et al. [1973b]; **l** = Merlet et al. [1972] (α = nonequivalent NH_3 subunits, β = equivalent NH_3 subunits); **m** = Kraemer and Diercksen [1970]; **n** = Alagona et al. [1973b]; **o** = Diercksen et al. [1973]; **p** = McDaniel and Evans [1966]; **q** = Arshadi and Kebarle [1970]; **r** = De Paz et al. [1970]; **s** = Dixon et al. [1972]; **t** = Arshadi et al. [1970]; **u** = Kebarle et al. [1967]; **v** = Cunningham et al. [1972]; **w** = De Paz et al. [1969]; **x** = Payzant et al. [1973]; **y** = Neckel et al. [1971].

Hertz and Rädle [1973] (see also ch. 21). A further investigation in this field was published very recently (Hertz et al. [1974]). This result demonstrates again that third row atoms are rather weak acceptors in H-bond formation.

Corresponding to the higher energies of interaction the two atoms X and Y come very close at the equilibrium geometries. As expected the shortest distances were obtained for the strongest symmetric or almost symmetric H-bonds in $[FHF]^-$, $[H_3F_2]^+$ and $[H_5O_2]^+$ as shown in table 2.15.

The calculated energies of interaction depend strongly on the basis sets applied. Similar to our previous experience the intermolecular energies decrease in absolute value if basis sets are extended. The most accurate calculations available now reproduce fairly well the experimental vapor phase enthalpies or the data extrapolated from crystal energies. The experimental values in their turn are difficult to obtain and also not free from errors.

In case of $[H_3S_2]^-$ only one calculation using a rather small and highly contracted GTO basis set was performed (Sabin [1971b]). In this calculation a strong H-bond was obtained: $\Delta E = -31$ kcal/mole. According to the results of other calculations in table 2.15 we have to expect a much smaller energy of interaction in this case as it was actually determined from crystal energies.

Correlation effects in structures with strong H-bonds might well be important. Until now no extensive calculations, including electron correlation, were performed with only one exception (Meyer et al. [1973]). In this study on $[H_5O_2]^+$, however, the influence of electron correlation on the shape of the potential curve for proton transfer was investigated (see section 2.9) and no calculation at the equilibrium geometry was performed. Estimates of correlation energies based on a statistical model for electron correlation on the other hand, indicate only a negligible influence of correlation energies on the calculated ΔE values of $F^- \cdots H_2O$ and $Cl^- \cdots H_2O$ (Kistenmacher et al. [1973a]).

Semiempirical calculations on strong H-bonds and other kinds of ion–molecule interactions were not very successful, because the stability of the complexes is largely overemphasized (Schuster [1973] and references therein). In some cases the energies of interaction calculated by the CNDO/2 method are three times as large as the most reliable values.

The energy surface $E = E(R_{OO}, R_{OH})$ in $[H_5O_2]^+$ was calculated by Janoschek et al. [1972, 1973]. Afterwards they performed a detailed investigation on vibrational spectra of this cation in the free state and in

the electric field of its environment in condensed phases. A number of other model studies on molecular motion in $[FHF]^-$ (Almlöf [1972]) and other, less common systems with strong H-bonds were reported. In the latter case, it is not possible to present an estimate on the H-bond strength because no values for total energies of interaction were given in these papers: $[ClHCl]^-$, $[H_3Cl_2]^+$ (Janoschek [1973a]) and $[HCNHNCH]^+$ (Güdel [1972]).

Finally, an attempt to fit an analytical potential surface, $\Delta E = E(R_{XY}, R_{HX})$, to the available energies calculated by ab initio MO methods should be mentioned: $[FHF]^-$ (Jiang and Anderson [1973]) and $[H_5O_2]^+$ (Anderson and Jiang [1973]). In both cases linearity of the H-bond ($\gamma = 0°$) was assumed. The energy surfaces were used to calculate vibrational spectra of these ions. Furthermore, they are rather flat around the energy minima and thereby present an explanation for the structural variability of these units in different crystals. The electrostatic potentials in the solid state are able to shift energy minima to significantly different values of R_{HX} and to change the intermolecular distance R_{XY} to some extent too. Since the energy surface is much less steep than in ordinary molecules the effects observed in these ions are larger than in those calculated for $[H_3O]^+$ (Almlöf and Wahlgren [1973]) and H_2O (Almlöf et al. [1972]).

2.5. Intramolecular hydrogen bonds

Intramolecular H-bonds are discussed frequently in order to explain thermodynamic data, spectra and reactivities of certain organic molecules. In polypeptides or proteins intramolecular H-bonds are considered as one of the most important factors determining stable structures in crystals and in solution. Nevertheless, only a very few extensive and systematic theoretical studies have been performed on this type of H-bonds. Even the smallest model compounds which are able to form intramolecular H-bonds contain a rather large number of electrons. With only one exception (Morokuma et al. [1974]) no results of medium size ab initio calculations are available. Furthermore, there are many degrees of conformational freedom in these molecules, which make any systematic minimization of the energy very expensive. A few ab initio calculations using extremely small basis sets were performed (Christoffersen [1972], Shipman and Christoffersen [1972, 1973a, b]). Additionally, various semiempirical methods like PCILO (Diner et al. [1969a, b], Malrieu et al. [1969]), CNDO or INDO were applied.

A large number of model calculations on protein conformations has been performed by several groups. Usually conformational maps of small oligopeptides (mainly dipeptides) using fixed bond lengths and valence angles were calculated. The importance of intramolecular H-bonds in stable conformations of these molecules has been stressed by a number of authors (e.g. Momany et al. [1971], Shipman and Christoffersen [1972] and Pullman and Maigret [1973]) and was verified experimentally (e.g. Cung et al. [1973]). During the last few years a number of review articles (Ramachandran and Sasisekharan [1968], Scheraga [1968, 1971] and Pullman [1971]) and an extensive contributed volume (Bergmann and Pullman [1973]) appeared, and consequently, we will not discuss any details of these calculations and their results here. For further references the interested reader is referred to these summaries.

Extensive semiempirical CNDO or INDO calculations were performed on the structures shown in fig. 2.27. Their results are presented in table 2.16. It is by no means trivial to define the energy of intermolecular H-bonds uniquely. Schuster [1969c] suggested to use the structure with least changes in molecular geometry besides a cleavage of the H-bond as

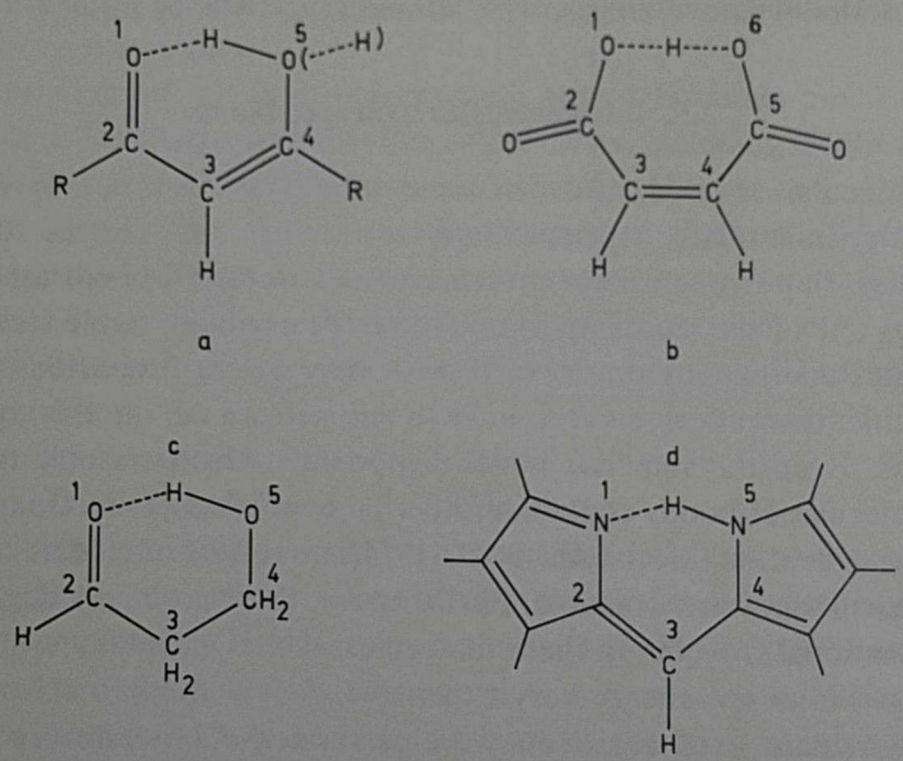

Fig. 2.27. Structures with intramolecular H-bonds. The reference state for an appropriate definition of intramolecular H-bond energies is shown in parentheses (structure a, Schuster [1969c]).

TABLE 2.16

Semiempirical (CNDO/2) calculations on intramolecular H-bonds

Structure	Ref.	Calculated equilibrium geometry R_{XH}(Å)	R_{YH}(Å)	R_{XY}(Å)	∢RXH	∢YHX	ΔE (kcal/mole)
H_2O	a, b	1.03	–	–	107°	–	–
$H_2CO\cdots HOH$	b	1.04	1.51	2.55	107°[a]	180°	−7.2
c	c	1.05	1.47	2.45[a]	105.17°	164.83°	−5.1[c]
a, R=H	c	1.09	1.39	2.42[a]	102.33°	167.67°	−14.7[c]
a, R=H[b]	c, h	1.13	1.33	2.42[a]	100.17°	169.83°	−19.0[c]
a, R=F	d	1.22	1.22	2.42[a]	97.51°	172.49°	−24.0[c]
a, R=CH_3	e	1.174	1.174	2.279	106.2°	152.18°	
a, R=CF_3	e	1.167	1.186	2.284	103.95°	152.17°	
b	f	1.2	1.2	2.4		180°	−29.8[d]
d	g	1.07	1.86	2.61	–		−4.6[d]

[a] Assumed geometrical input data.

[b] This structure contains a symmetric molecular backbone $R_{23} = R_{34}$ and $R_{12} = R_{45}$. It does not correspond to a local energy minimum of the whole energy surface.

[c] H-bond energy defined as the difference in energy between the two planar configurations of **a** or **c** as indicated in fig. 2.26.

[d] H-bond energy defined as the difference in energy between *cis*- and *trans*-isomer according to a rotation around the bond C_3–C_4.

References: **a** = Pople and Beveridge [1970]; **b** = Schuster [1969a]; **c** = Schuster [1969c]; **d** = Russegger and Schuster [1974]; **e** = Gordon and Koob [1973]; **f** = Murthy et al. [1970]; **g** = Falk et al. [1974]; **h** = Schuster [1969b].

reference state (see fig. 2.27, structure **a**). This reference state differs from the H-bonded structure by a rotation of 180° around the CO-bond and need not be a local minimum of the energy surface. In the case of the maleate anion Murthy et al. [1970] used a different reference state. They compared the energy of the H-bonded maleate anion with the energy of fumarate anion, which differs from it by a rotation around the CC-double bond. Falk et al. [1974] similarly used the transconfiguration of pyrromethene as a reference state for structure **d** with the intramolecular H-bond (in this case no other reference state defined according to the previously mentioned criteria is possible). The second choice of the reference state has the advantage that this state corresponds to an energy minimum of the molecular energy surface. Nevertheless, the former definition seems to be more appropriate in cases where it can be applied, because it does not mix a large energy of isomerization into the H-bond

energy. Furthermore, we can see that any splitting of the change in total energy into "pure" isomerization and H-bond energy is artificial and it is not possible to define an intramolecular H-bond energy uniquely.

In table 2.16 we can distinguish two different types of intramolecular H-bonds. In the first case (fig. 2.27, **c**) proton donor and proton acceptor groups are separated at least by one sp^3 hybridized C-atom which prevents π-electron delocalization along the molecular backbone from one group to the other. Intramolecular H-bonds in oligopeptides or proteins are other examples of this type. There is no significant difference between this kind of intramolecular H-bonds and intermolecular H-bonds besides a certain stereochemical restriction. A compromise between the most favored H-bond geometry and the most stable structure of the molecular backbone has to be found. Consequently, these intramolecular H-bonds are somewhat weaker than intermolecular H-bonds between the same functional groups.

The other kind of intramolecular H-bonds discussed here (fig. 2.27, **a**, **b** and **d**) is characterized by a planar π-electron system which connects both functional groups forming the H-bond. Charge transfer along H-bonds in these structures can be compensated by an inverse electron flow along the π-electron system. As we can see from table 2.16 these intramolecular H-bonds are much stronger than their intermolecular analogs. Besides the rather high energies for the H-bonds, which depending on the definition chosen, of course, are somewhat arbitrary, we observe a much more pronounced elongation of the OH-bond. Additionally, the deformation of the $\measuredangle$RXH valence angle, which increases with increasing bond strength, is larger in these compounds. According to CNDO/2 calculations the most stable structure of the enol form of malonic dialdehyde (**a**, R = H) does not show C_{2v} symmetry (Schuster [1969b, c] and Schuster et al. [1974b]). This structure of higher symmetry corresponds to a saddle point of the energy surface. The most stable geometry of the molecules is planar with alternating CC- and CO-bond lengths. The equilibrium position of the H-atom is significantly displaced from the bisector of the connection line between the O-atoms. Interestingly, at the equilibrium geometry the H-bond is much weaker than in the structure with a symmetric molecular backbone ($R_{12} = R_{54}$; $R_{23} = R_{34}$, see fig. 2.27).

Substitution of F instead of H (**a**, R = F) increases the H-bond energy (Russegger and Schuster [1974]). The most stable geometry of the enol form of malonyl fluoride shows C_{2v} symmetry. Consequently, we conclude that the electron donating mesomeric (+M) and electron withdraw-

ing inductive (−I) effect of the F-atom together increase the H-bond strength–at least in these CNDO/2 model calculations reported. As expected the calculated proton affinity of the unsubstituted enolate anion of malonic dialdehyde $\Delta E_{PA}([C_3H_3O_2]^-) = -523$ kcal/mole is larger in absolute value than the proton affinity of its bifluoro derivative $\Delta E_{PA}([C_3F_2HO_2]^-) = -504$ kcal/mole. In absolute values the proton affinities obtained by CNDO/2 calculations are appreciably too large (Schuster [1970], section 2.9). Relative values, however, were found to be fairly reliable.

CNDO/2 calculations on hydrogen maleate anion (**b**) led to a structure with C_{2v} symmetry and a very strong linear H-bond (Murthy et al. [1970]). Somewhat later Morita and Nagakura [1972] proposed a modified CNDO/2 procedure with other approximations for molecular integrals than those used in the original formalism. A calculation on hydrogen maleate anion gave essentially the same results. The most stable geometry shows C_{2v} symmetry with an equilibrium position of the H-atom in the middle between the two O-atoms involved in the H-bond.

A very recent STO-3G calculation on hydrogen maleate anion (**b**, Morokuma et al. [1974]) gave essentially the same results. Again the most stable geometry of the anion shows C_{2v} symmetry. Interestingly, a very high H-bond energy of $\Delta E = -52.1$ kcal/mole was obtained for the first definition of a reference state given here (rotation of 180° around the CO-bond).

Only a less extensive study is available for the much larger structure of pyrromethene (**d**). Falk et al. [1974] found that the most stable geometry of this molecule is characterized by alternating bond lengths and an unsymmetric position of the H-atom in the H-bond.

Gordon and Koob [1973] performed extensive INDO calculations on acetylacetone (**a**, $R = CH_3$) and its hexafluoro derivative (**a**, $R = CF_3$). According to previous investigations on H_2CO/HF (Schuster [1970]) INDO calculations overemphasize the strength of H-bonds:

$$\begin{aligned} H_2CO\cdots HF: \quad \Delta E(\text{CNDO/2}) &= -13.2 \text{ kcal/mole}, \\ \Delta E(\text{INDO}) &= -21.2 \text{ kcal/mole}. \end{aligned}$$

Consequently, it is not unexpected that a symmetric equilibrium geometry of the enol of acetylacetone was predicted by these INDO calculations. In the enol of hexafluoroacetyl acetone the H-bond is weaker and a slightly asymmetric structure was found. As expected the electron withdrawing inductive (−I) effect of the CF_3 group reduces the H-bond strength.

2.6. Stereochemistry of the hydrogen bond

The concept of stereochemistry in H-bonded complexes includes various angular dependences of H-bond energies, which determine the directional properties of H-bonds in molecular associations. Since potential surfaces for H-bonded aggregates are extremely important in many fields, numerous attempts were made to calculate them either directly or by model assumptions.

In general the geometry of a dimeric association of linear molecules is characterized by an intermolecular distance R and three angles Θ_1, Θ_2 and ϕ (fig. 2.28). For our purpose, however, it is more appropriate to define

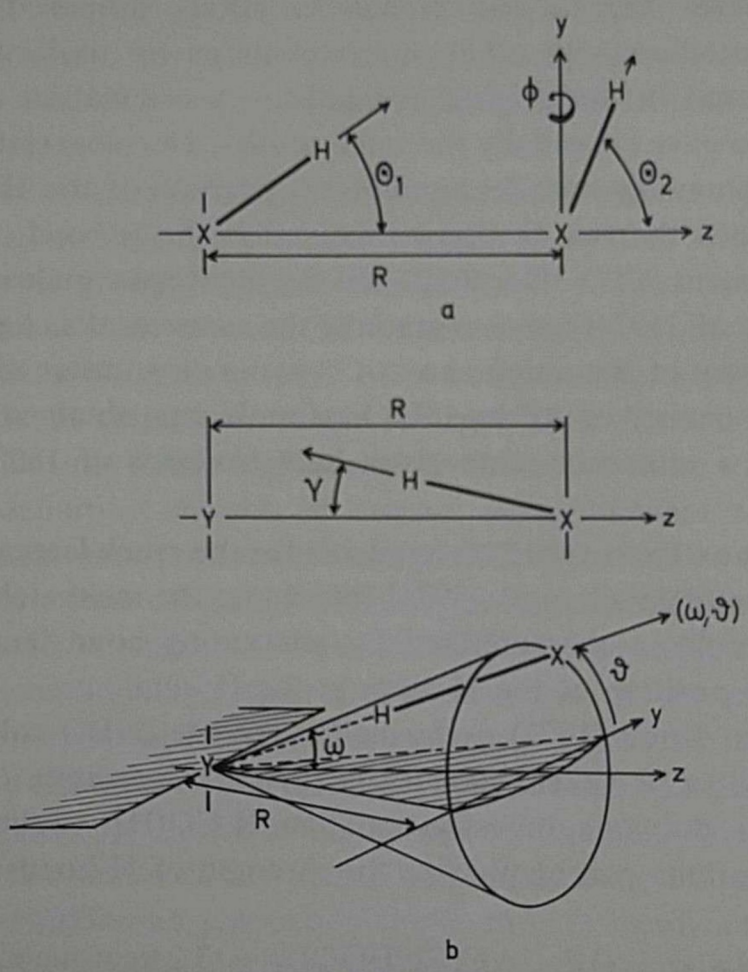

Fig. 2.28. Choice of coordinates for a discussion of the angular dependence of H-bond energies (a: conventional definition of three angles describing relative orientations of two linear molecules; b: set of angles proposed by Schuster [1970] in order to describe H-bonded dimers; γ describes deviations from linear H-bonds, X–H···Y; ω and θ characterize relative orientations of the two functional groups forming the H-bond, z coincides with a global or local n-fold symmetry axis of the proton acceptor molecule Y, e.g. C_2 in H_2O, H_2CO or pyridine, C_3 in H_3N, C_∞ in HF; θ is defined according to a plane of global or local symmetry in Y ($\theta = 0°$), which contains the highest number of σ-bonds ending in Y).

characteristic angles for H-bonded associations in a different way (Schuster [1970]). Now in case of small deviations from linearity (XHY), a generalization to nonlinear monomers is much easier, because the additional degrees of freedom are less important for our discussion. As we can see in fig. 2.28, γ characterizes the deviation from linearity of the H-bond. In the most stable intermolecular geometry ω and θ represent the directional properties of the molecule providing the lone pair electrons.

Directional properties of H-bonds were discussed long ago before accurate quantum mechanical calculations became available (Schneider [1955]). He used a concept of hybridized lone pair orbitals to explain the preferred geometries of H-bonded associations. With simple point charge models simulating bonds and lone pairs he interpreted the linearity of H-bonds ($\gamma = 0°$) by strong interactions of local dipoles. Additionally, some other directional properties, e.g. the preferred ω, θ values were predicted correctly in a few representative examples. Nevertheless, the accuracy of electrostatic calculations of this type is not sufficient for the requirements of today.

An illustrative model for the discussion of stereochemical properties of H-bonded associations considering electrostatic and charge transfer effects was proposed by Kollman [1972]. We used his concept already to demonstrate the importance of both contributions for correct predictions of intermolecular geometries (section 2.2.4).

Now an impressive number of perturbational and MO calculations on angular dependences of H-bond energies became available. We will make an attempt to generalize the most important results. The most extended ab initio calculations were performed on $(HF)_2$–294 individual points, Yarkony et al. [1974]–and on $(H_2O)_2$–190 individual points, Popkie et al. [1973]. Many other less extensive ab initio studies on angular dependences of H-bond energies were published. Additionally, semiempirical CNDO/2 calculations were applied in order to facilitate a classification of different types of H-bonds (Schuster [1970]). Perturbation theory was used as well to calculate directional properties of H-bonds in small aggregates (Van Duijneveldt-Van de Rijdt and Van Duijneveldt [1971]).

Results obtained by all kinds of theoretical methods confirm that linear H-bonds with the atoms Y, H and X on a straight line are most stable. The only exceptions are structures in which H-bonds and other strong intermolecular interactions compete at the energy minimum. In molecules with intramolecular H-bonds a compromise between preferred H-bond geometries (linear Y–H–X arrangement) and equilibrium bond lengths and bond angles in the molecular backbone has to be made. Deviations from

linearity in various other intermolecular complexes are caused, e.g. by strong electrostatic forces resulting from other polar groups which are not involved in the H-bond (see table 2.13).

Some years ago Luck [1965a, b; 1967] (see also ch. 11) investigated angular dependences of H-bond strength in molecular aggregates by comparison of various experimental data. From IR bands of the HX stretching vibration he derived an empirical potential curve for H-bond bending. This energy curve shows a minimum at the linear arrangement ($\gamma = 0°$) and agrees well with the results of recent LCAO–MO calculations.

The general dependence of the H-bond energy on the intermolecular angles ω and θ was investigated in detail by Schuster [1970]. He performed extended CNDO/2 calculations on intermolecular energies at fixed intermolecular distances (R_{XY}) and linear H-bond geometry ($\gamma = 0°$). HF was chosen as proton donor molecule in order to avoid additional degrees of freedom in the complex. Furthermore, the directional properties of the proton acceptor molecule can be studied more easily in this case because there is no superposition of the H-bond energy and the energy of interaction with other bond moments in the proton donor molecule. The general rules obtained in these calculations can be summarized as follows. The stereochemistry of these H-bonded complexes depends on the number of lone pairs and π-electrons at the atom in the proton acceptor molecule, which is involved in the H-bond. In case this atom contains only one lone pair and does not take part in a π-electron system stable H-bonds can be formed exclusively in a small range around the preferred intermolecular orientation. This orientation coincides with the direction of the lone pair as it is defined by the concept of localized hybrid orbitals. Examples for this type of restricted angular flexibility are H-bonds to saturated amines. All calculations performed on structures of this kind lead to the same result that the energy of interaction decreases strongly with increasing angles ($\omega > 0°$).

Two lone pairs at the proton acceptor atom Y are found in most cases where Y is represented by the O-atom. H-bonds to these atoms are characterized by flexibility with respect to angular variations in one plane. H_2O is a good example for this type of proton acceptor molecules. For $\delta = 0°$ we find a rather steep parabolic curve $E(\omega)$ with a minimum at $\omega = 0°$. A rather flat curve $E(\omega)$ showing two shallow minima around $\omega = \pm 30°$ or one at $\omega = 0°$ was obtained in different calculations for $\delta = 90°$. Similar angular dependences were found in calculations on H-bonds to other proton acceptor molecules with two lone pairs at the

atom Y. Consequently, we can rotate the proton donor molecule in the plane determined by the directions of the two lone pairs without an appreciable loss in the energy of interaction as long as ω does not exceed a certain value ($|\omega| < 70°$).

Proton acceptors with three lone pairs at the atom involved in H-bond formation (e.g. HF) finally show the least pronounced angular dependence in H-bonding. High flexibility for variation of the angles ω, δ in two dimensions is obtained in all calculations available. Only at large deviations from the linear arrangement of all four atoms concerned ($|\omega| > 70°$) the H-bond loses its stability.

The angular dependence of H-bonds to proton acceptor molecules with π-electron systems is predicted somewhat differently by semiempirical and ab initio methods. Semiempirical calculations on H_2CO/HF, H_2O or HNH_2 (Schuster [1969a, 1970]) or pyridine/HF, H_2O or HNH_2 (Schuster [1969a, 1970]) or pyridine/HF (Jakubetz and Schuster [1971]) give almost equal stabilities for H-bonds to lone pairs or π-electrons. Consequently, calculated H-bond energies are less sensitive to angular deformations than in saturated compounds with the same proton acceptor atoms. In these calculations the energy surface $E(\omega, \theta)$ of pyridine/HF is very similar to that of H_2O/HF. H_2CO/HF resembles, somewhat, the system HF/HF as long as angular dependences of H-bond energies are concerned. More accurate ab initio calculations (Morokuma [1971] and Del Bene [1974]), however, lead to much smaller energies of interaction for H-bonds to π-electron systems. The CNDO/2 method in general overemphasizes the stability of bridged, nonclassical structures. We have to expect, therefore, that the angular flexibility of H-bonding to lone pair donors with π-electron systems predicted by these semiempirical calculations is not as pronounced in reality. On the other hand, ab initio calculations using small basis sets as those mentioned above underestimate stabilities of bridged structures involving π-electrons. This has been demonstrated most clearly in calculations of nonclassical and classical carbocations. A comparison of various calculations on bridged and classical structures of ethyl and vinyl carbocations was recently presented by Griengl and Schuster [1974]. They reported that the results of the most accurate calculations including correlation effects lie somewhere in between the results of semiempirical and small basis set ab initio calculations. Hence, we expect a realistic energy of H-bonding to π-electrons to represent a compromise between the results of semiempirical and ab initio calculations available now.

Electron correlation effects on CNDO/2 calculations of H-bond ener-

gies in H_2CO/HOH were recently investigated by second order perturbation theory (Tapia et al. [1974]). A comparison with conventional CNDO/2 calculations (Schuster [1969a]) showed only slight differences in the shape of potential curves for angular variations, $E(\omega)$.

The stereochemistry of $(HF)_2$ was analyzed recently in a slightly different way by extended ab initio calculation (Yarkony et al. [1974]). They tried to answer the question if the most stable arrangement of $(HF)_2$ is planar or not at a given value of R_{FF}. The equilibrium geometry, $R_{FF} = 2.80$ Å, was found to be planar in agreement with other calculations. At smaller intermolecular distances, however, nonplanar structures are energetically favored.

2.7. Hydrogen bonds in clusters of molecules and molecular crystals

Many properties of molecules forming intermolecular H-bonds like intermolecular distances, vibrational frequencies and proton chemical shifts change significantly with the degree of aggregation, e.g. in the series: dimer, oligomer, pure liquid, crystal. Additionally, the energies of interaction deviate remarkably from pairwise additivity in higher aggregations and consequently, statistical mechanics of H-bonded molecules is full of problems very hard to solve (see ch. 7).

Properties of H-bonded molecules in higher aggregations were investigated by both theoretical and experimental methods. Calculations on complexes containing many molecules showed an increase of H-bond energies with cluster size and the formation of large H-bonded complexes is a cooperative process with respect to the energy of formation. The scientific intermezzo concerning polywater encouraged studies on H-bonding in structures involving many molecules at various intermolecular geometries even more. After its rapid decline the interest in nonadditivity of H-bond energies remained and nowadays an impressive number of semiempirical and ab initio studies on higher complexes is available.

In general there are two problems in theoretical calculations on energy surfaces of larger molecular aggregations. First of all the supermolecule which has to be calculated within the SCF–MO formalism is larger than the previously discussed examples of dimeric aggregations, because it consists of more monomeric units. Consequently, the calculation of the individual point of the energy surface requires much more computer time. Furthermore, the configurational freedom is much larger in higher aggregations and increases enormously if further molecules are added to the

complex. Therefore it is not possible to calculate the whole energy surface for trimers or even higher aggregations. Usually, only the regions around local energy minima were investigated in detail. In almost all cases the geometry of the monomeric unit was assumed to remain unchanged in higher aggregates. In the following sections investigations on small chains of neutral molecules, two- or three-dimensional clusters and crystals will be discussed separately.

2.7.1. Calculations on small chains of molecules forming hydrogen bonds

Finite chains of molecules forming H-bonds were calculated directly by semiempirical and ab initio MO methods. $(H_2O)_n$ and $(HF)_n$ were investigated most frequently. Only for the first members in the series very accurate calculations are available $(H_2O)_3$: Hankins et al. [1970a, b; 1973], $(H_2O)_3$ and $(H_2O)_4$: Lentz and Scheraga [1973]). The results of Hankins et al. are summarized schematically in fig. 2.29. At most geometries of $(H_2O)_3$ the calculated energy of trimerization ΔE_3 differs appreciably from

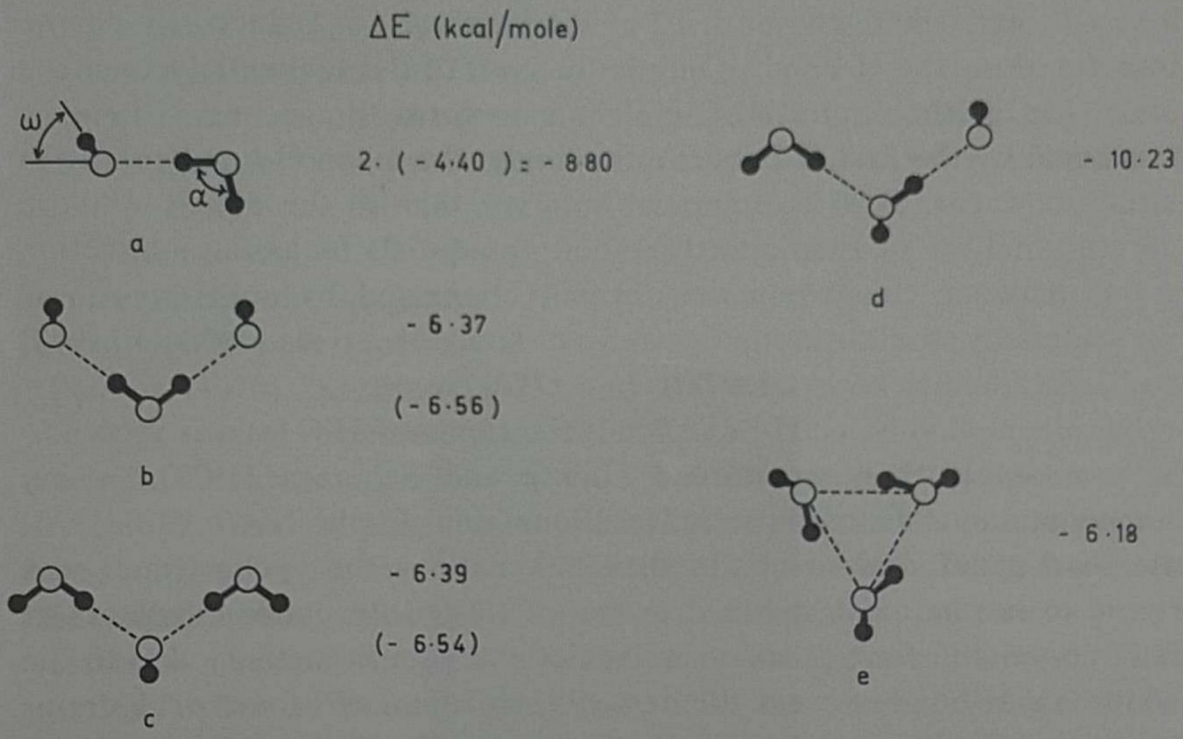

Fig. 2.29. Nonadditivity of H-bond energies in $(H_2O)_3$. Four types of trimer geometries are distinguished: **b** = double donor, **c** = double acceptor, **d** = sequential and **e** = cyclic trimer; for comparison the dimer in its most stable geometry is shown too, **a** (Hankins et al. [1970a, b; 1973]). $R_{OO} = 3.0$ Å, corresponding to the most stable geometry of **d**; in case of **b** and **c** the values in parentheses correspond to the energy minimum at $R_{OO} = 3.15$ Å.

the value calculated for two isolated H-bonds at the equilibrium geometry of the dimer. Additionally, a striking difference in energy is found for the three possible combinations (**b**, **c** and **d**) of H-bonds to the central H_2O-molecule. Characteristically, these structures are called double donor (**b**), double acceptor (**c**) and sequential (**d**) trimer. In both double acceptor and double donor trimer, the energy of interaction is appreciably smaller than in the sequential trimer and even smaller than twice the H-bond energy of the dimer. Besides, the repulsion of the two H_2O-molecules not connected by an H-bond, repulsive three-body energies were obtained at intermolecular distances slightly smaller than the equilibrium value ($R_{OO} = 3.15$ Å). In the sequential trimer **d** the three-body energies are attractive. This fact can be explained by charge transfer arguments. The first H-bond in the double acceptor trimer increases the electron density at the central H_2O-molecule. Hence the proton not involved in the first H-bond is less acidic and consequently forms a weaker H-bond to the third H_2O-molecule. After electron rearrangement we finally obtain two equivalent H-bonds which are weaker than the H-bond in the dimer. Analogous arguments can be used in case of the double donor trimer, where the basicity of the lone pairs is reduced by charge transfer along the H-bonds. Only in the case of the sequential trimer the capability of the central H_2O-molecule to form the second H-bond is increased by the first H-bond. Accordingly, the mean H-bond energy in structure **d** (fig. 2.29) is appreciably larger than in the dimer. A more careful analysis of two- and three-body potentials including interaction terms between the two molecules not connected by an H-bond was presented by the authors themselves (Hankins et al. [1970a, b; 1973] and Lentz and Scheraga [1973]).

Despite an additional H-bond the cyclic trimer of H_2O (**e**) was shown to be less stable than structure **d** (Lentz and Scheraga [1973]). Using somewhat smaller basis sets Del Bene and Pople [1969, 1970, 1973] obtained a different result. In their calculations the cyclic trimer was found to be the most stable structure of $(H_2O)_3$. In cyclic oligomers of H_2O containing four or more molecules the gain in stability due to the additional H-bond exceeds the destabilizing effect of geometrical strains brought about by ring closure. Consequently, the cyclic structure of the oligomers $(H_2O)_{n\geq 4}$ are the most stable ones. Again no special effect which does not occur in open chain structures besides the additional H-bond was found to stabilize cyclic oligomers (cf. section 2.4.2).

The influence of basis sets on calculated deviations from pairwise additivity of energies in $(H_2O)_3$ has been studied by Del Bene and Pople

[1973]. As expected the nonadditivity depends on the basis sets chosen. Similar to the energies of dimerization the three-body energies decrease somewhat if more extended basis sets are applied.

Calculations on small oligomers of HF produced analogous results as in the case of $(H_2O)_n$ (Del Bene and Pople [1971]). Again sequential oligomers were found to represent the most stable open chain structures. Nonadditivity of H-bond energies indicates the existence of a cooperative effect in the formation of higher, H-bonded aggregates. Contrary to $(H_2O)_n$ cyclic oligomers of HF show rather high stability. Especially cyclic tetra-, penta- and hexamers are energetically favored and might occur together with monomers and dimers at higher pressure in the vapor phase. Experimental evidence for the existence of higher aggregates, especially cyclic hexamers, in HF vapor was presented by several authors (Smith [1958], Franck and Meyer [1959] and Janzen and Bartell [1969]).

Two further calculations on trimers fit well into the results on $(H_2O)_3$ and $(HF)_3$ discussed above. In the linear trimer of HCN ($R_{NC} = 3.2$ Å, Johansson et al. [1972b]) the energy of trimerization ($\Delta E_3 = -8.1$ kcal/mole) is significantly larger than twice the energy of dimer formation ($2 \cdot \Delta E_2 = -7.4$ kcal/mole). The complex $H_2CO \cdot 2H_2O$ as calculated by Morokuma [1971] represents an example for a double acceptor trimer. Due to repulsion between the H_2O-molecules and charge transfer effects the energy of interaction in the trimer ($\Delta E_3 = -5.9$ kcal/mole) is smaller than twice the dimerization energy ($2 \cdot \Delta E_2 = -6.8$ kcal/mole).

Semiempirical CNDO/2 calculations on chains of H_2O- and HF-molecules in the sequential H-bond geometry were extended up to nonamers in order to be able to extrapolate to infinite chain lengths (Plesser [1970], Karpfen [1973] and Karpfen et al. [1974]). CNDO/2 results on small oligomers are essentially the same as those obtained by ab initio calculations besides the fact that the energies of interaction are overemphasized to some extent. In case experimental geometries are used for the monomers and the intermolecular geometries were fixed near the experimental values, the calculated energies agree well with the results of more accurate calculations or available experimental data (cf. section 2.4.2 or Schuster [1969a]). In fig. 2.30 the results of these CNDO/2 calculations are summarized. In order to find out how many neighbors contribute significantly to the increase of H-bond energy the average H-bond energy $\overline{\Delta E}_n$ (2.61) was plotted against n, the number of monomers in the chain.

$$\overline{\Delta E}_n = \frac{E[(HX)_n] - nE[HX]}{m}. \tag{2.61}$$

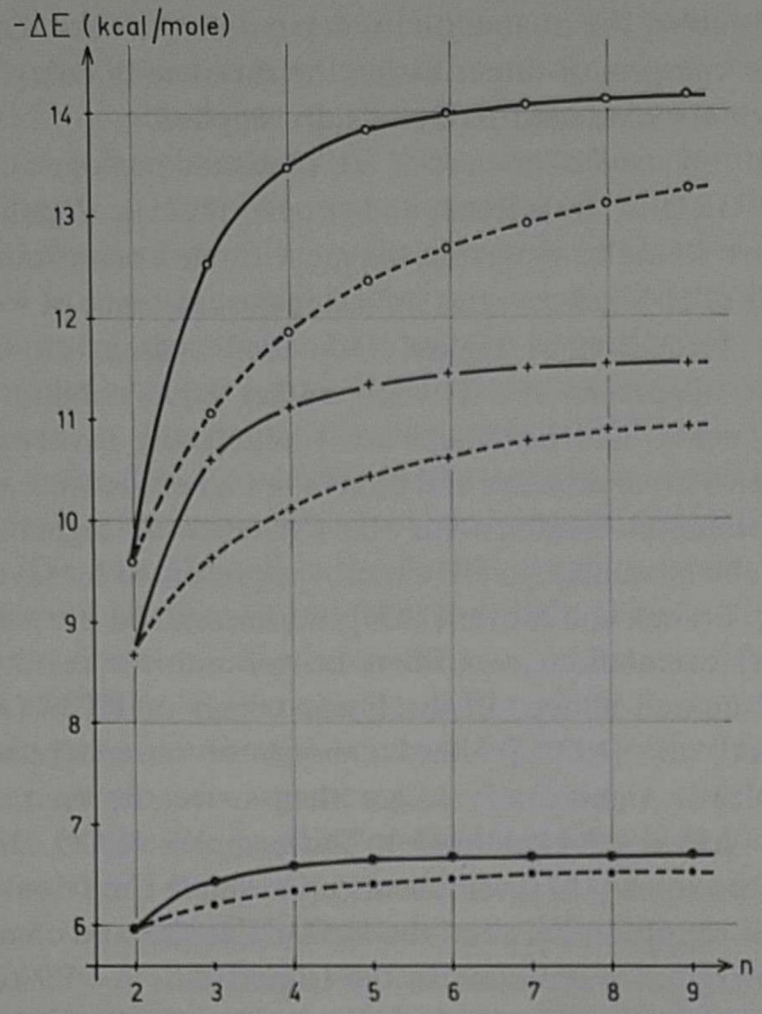

Fig. 2.30. Convergence of H-bond energies in one-dimensional chains of molecules. Mean H-bond energies $\overline{\Delta E}_n$: ----; "last" H-bond energies, $\Delta E_{n-1,n}$: ———; $(H_2O)_n$, experimental geometries: ●; $(H_2O)_n$, CNDO/2 minimum geometries: +; $(HF)_n$, CNDO/2 minimum geometries: ○; (Karpfen et al. [1974]).

The number of H-bonds, in our examples always $n-1$, is denoted by m. It turned out, however, that $\overline{\Delta E}_n$ is not an appropriate measure for this purpose, because the relative importance of end effects is different in chains of different lengths. This is also the reason for the slow convergence of this quantity with increasing chain lengths (fig. 2.30). More suitable for our purpose is the energy of the "last" H-bond, which describes the insertion of a monomer into the middle of an already existing chain ($\Delta E_{n-1,n}$), eq. (2.62). In all cases this quantity converges much faster than $\overline{\Delta E}_n$.

$$\Delta E_{n-1,n} = E[(HX)_n] - \{E[(HX)_{n-1}] + E[HX]\}. \qquad (2.62)$$

In the case of infinite chains, of course, $\overline{\Delta E_n}$ and $\Delta E_{n-1,n}$ have to become identical. Regarding fig. 2.30 more closely we can draw two conclusions: Nonadditivity of H-bond energies is more important in $(HF)_n$ than in $(H_2O)_n$. Important contributions to the mean H-bond energy come from up to the fifth neighbors in $(H_2O)_n$ and reach slightly further in $(HF)_n$.

2.7.2. Two- and three-dimensional clusters of molecules forming hydrogen bonds

Three-dimensional clusters of neutral H_2O-molecules are of primary importance in discussion of all properties of liquid water and ice. Consequently, calculations on three-dimensional aggregates of H_2O-molecules were performed. The smallest reasonable model consists of five H_2O-molecules (fig. 2.31). According to the geometry of ice I the central H_2O-molecule is surrounded by four neighbors forming four H-bonds with pseudo-tetrahedral geometry. Perturbation theory (Guidotti et al. [1972]) semiempirical (Hoyland and Kier [1969], Russegger et al. [1972] and Karpfen et al. [1974]) and ab initio MO methods (Del Bene and Pople [1969, 1970]) were applied to calculate the energy and other properties of tetrahedral $(H_2O)_5$.

Both kinds of MO methods gave the same qualitative results for the average H-bond energy in the tetrahedral structure of $(H_2O)_5$ (table 2.17): $\overline{\Delta E_5}$ is somewhat larger than the H-bond energy in the dimer (ΔE_2) but significantly smaller than the mean H-bond energy in the open chain sequential trimer or pentamer. This result can be explained easily if we consider the structure of the tetrahedral pentamer more closely. We can recognize six trimeric subunits in the pentamer: four sequential trimers, one double donor and one double acceptor trimer (fig. 2.31). In these

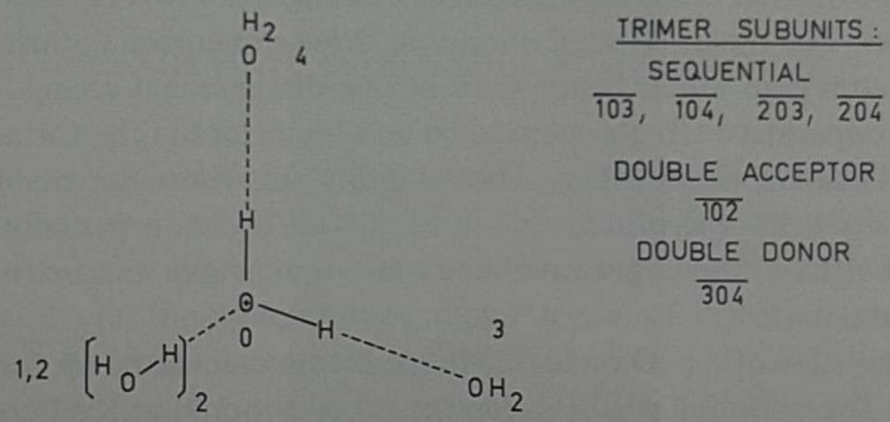

Fig. 2.31. Geometry of tetrahedral clusters of $(H_2O)_5$. Six trimeric subsystems can be recognized.

TABLE 2.17

Hydrogen bond energies in tetrahedral aggregates of water molecules

n	m	Structure	$\overline{\Delta E}$ (kcal/mole) SCF calc.[a]	CNDO/2, min[b]	CNDO/2, exp.[b]
2	1	Sequential	−6.10	−8.7	−4.8(−6.0)
3	2	oligomers	−7.33	−9.6	(−6.2)
4	3	(fig. 2.29)	−8.19	−10.1	(−6.3)
5	4	1	−7.28	−9.00	−5.81
8	7	2		−9.15	
11	10	3 Tetrahedrons (fig. 2.31)		−9.25	
14	13	4		−9.30	
17	16	5		−9.30	

[a] STO-4G calculations by Del Bene and Pople [1970].

[b] CNDO/2 calculations using the geometry of the CNDO/2 energy minimum ("min") or experimental values ("exp"; $R_{OH} = 0.96$ Å, $R_{OO} = 2.72$ Å, $\alpha = 107.1°$; values in parentheses correspond to the geometry of Ice I: $R_{OH} = 1.02$ Å, $R_{OO} = 2.72$ Å and $\alpha = 109.5°$). The energy values are taken from Hoyland and Kier [1969] and Karpfen et al. [1974].

contributions to the mean H-bond energy of the complex some of the individual three-body energies compensate each other and consequently, the average H-bond strength in the tetrahedral pentamer of H_2O is smaller than in the open chain sequential trimer, $(H_2O)_3$.

CNDO/2 calculations on larger aggregates of H_2O-molecules were performed by Karpfen et al. [1974]. They investigated clusters consisting of some tetrahedrons with up to 17 H_2O-molecules. The clusters were constructed in such a way that they had one edge, i.e. two H_2O-molecules in common. The mean H-bond energy in three-dimensional clusters was found to converge much faster than in one-dimensional chains. Consequently, cooperative effects seem to be less important in the formation of three-dimensional aggregates. The stability of three-dimensional H-bonded networks therefore, does not result from especially strong H-bonds but from the larger number of H-bonds which can be formed in three dimensions.

The properties of a H_2O molecule in ice I were calculated by Guidotti et al. [1972]. They applied perturbation theory to a model of ice I consisting of four peripheral H_2O-molecules surrounding a central H_2O-molecule in pseudo-tetrahedral geometry (fig. 2.31). The electrostatic potential of the

four H_2O-molecules is introduced as a perturbation into the Hamiltonian of the central H_2O-molecule. The electrostatic potential of the peripheral molecules is derived from an SCF calculation using a minimal STO basis set, whereas an extended STO basis set has been applied for the central molecule. Electrostatic and polarization effects were taken into account, but exchange, charge transfer and dispersion contributions were neglected. By this rather simple model an H-bond energy of $\Delta E = -9.2$ kcal/mole was calculated, a value which is somewhat too large. Furthermore, the increase in dipole moment ($\Delta\mu(H_2O) = 0.61\ D$) and the change in proton chemical shifts ($\Delta\sigma_H = -3.81$ ppm) with respect to the isolated molecule were predicted in reasonable agreement with the available experimental data. A second hydration shell was included in another calculation and Guidotti et al. [1972] could show that the agreement with experimental data is significantly improved by this enlargement of the surrounding.

H-bonding plays an important role in the theory of hydration of cations and anions as well. Since recent developments in the theory of ion solvations will be discussed extensively in a forthcoming review article (Schuster et al. [1974a]) we will mention here only studies on the hydration of the two most important ions in water: $[H_3O]^+$ and $[OH]^-$.

Aggregates of $[H_3O]^+$ and $[OH]^-$ with up to four H_2O-molecules were studied by Newton and Ehrenson [1971]. They performed ab initio calculations using a 4-31G basis set, which was shown to overemphasize energies of interaction to some extent (cf. table 2.15). Consequently, the calculated intermolecular energies $\Delta E_{n-1,n}$ are expected to be too large in absolute value and the intermolecular distances to be somewhat too short. In case of ion hydration the energy differences $\Delta E_{n-1,n}$ is defined appropriately by eq. (2.63). The calculated values are shown in table 2.18.

$$\Delta E_{n-1,n} = E[X(H_2O)_n] - \{E[X(H_2O)_{n-1}] + E[H_2O]\}, \qquad X = H^+, OH^-. \tag{2.63}$$

As expected the H-bond energy, $\Delta E_{n-1,n}$ decreases gradually with increasing number of H_2O-molecules in the hydration shell (n). The calculated ΔE values are compared with experimental enthalpies (ΔH) obtained from the temperature dependence of equilibrium constants measured by mass spectroscopy (Kebarle et al. [1967], Arshadi and Kebarle [1970] and Cunningham et al. [1972]). The relative values are reproduced very well by these calculations using medium size basis sets. The OO distance becomes longer and longer in case more H_2O-molecules

TABLE 2.18

Ab initio MO–SCF calculations and experimental data on the hydration of hydroxonium and hydroxide ions

n	Structure	Symmetry	R_{OO}(Å)	$\Delta E_{n-1,n}$ (kcal/mole)	Ref.	$\Delta H_{n-1,n}$ (kcal/mole)	Ref.
2	$[H_5O_2]^+$: $H^+(OH_2)_2$	C_{2v} (D_{2d})	2.39	−32.2	a	−31.6	d
		D_2	2.36	−43.9	b	−36	e
3	$[H_7O_3]^+$: $HOH_2^+(OH_2)_2$	C_{2v}	2.46	−30.9	b	−19.5	d
						−22.3	e
4	$[H_9O_4]^+$: $OH_3^+(OH_2)_3$	C_{3v}	2.54	−26.1	b	−17.5	d
						−17	e
5	$[H_{11}O_5]^+$: $H_9O_4^+ \cdot H_2O$	C_s	2.54[a] 2.70[a]	−17.7	b	−15.3	d
1	$[H_3O_2]^-$: $HO^- \cdot H_2O$	C_s	2.51	−24.3	c	−22.5	f
			2.45	−40.7	b		
2	$[H_5O_3]^-$: $HO^-(H_2O)_2$	C_{2v}	2.53	−30.5	b	−16.4	f
3	$[H_7O_4]^-$: $HO^-(H_2O)_2$	C_{3v}	2.61	−23.1	b	−15.1	f
4	$[H_9O_5]^-$: $H_7O_4^- \cdot H_2O$	C_s	2.61[b] 2.70[b]	−20.7	b	−14.2	f

[a] The shorter distance corresponds to the $[H_9O_4]^+$ subsystem, the large value represents the intermolecular distance between O-atoms of the first and second hydration shell.

[b] The shorter distance corresponds to the $[H_7O_4]^-$ subsystem, which prefers a cyclic arrangement in $[H_9O_5]^-$. The larger value represents the intermolecular distance between O-atoms of the first and second hydration shell.

References: **a** = Kraemer and Diercksen [1970]; **b** = Newton and Ehrenson [1971]; **c** = Kraemer and Diercksen [1972a]; **d** = Cunningham et al. [1972]; **e** = Kebarle et al. [1967]; **f** = Arshadi and Kebarle [1970].

are bound to the central ion. This result is in good agreement with data on crystal structures of various salts containing hydrated protons (cf. chs. 10 and 14). An interesting question concerns relative stabilities of the highly symmetric structures $[H_9O_4]^+$ and $[H_7O_4]^-$ which have been postulated as the predominant ionic species in liquid water. In the vapor phase no unusual stability of these ions was found. The energies for ion hydration decrease gradually and no sharp break in the series is obtained. A more careful analysis of experimental ΔG values (Grimsrud and Kebarle [1973]) indicates a slight preference of $[H_4O_9]^+$ in the series of hydrated cations $H^+(H_2O)_n$.

2.7.3. Hydrogen bonded crystals

A number of different methods to calculate crystal structures was developed during the last ten years. Two of them were used to discuss band structures, unit cell geometries and mean intermolecular energies in H-bonded crystals. Both methods have been described extensively in the literature and therefore we can restrict ourselves here to present only the most important results of these calculations.

Bacon and Santry [1971, 1972] developed an SCF perturbation theory for molecular crystals based on localized orbitals of the molecules in the unit cell. A CNDO/2 version of this intermolecular perturbation theory was applied to $(HF)_2$ and $(HCN)_2$. Good agreement with direct CNDO/2 calculations was obtained in case the perturbation treatment was extended to third order contributions. This CNDO perturbation method was applied at first to one-dimensional chains of HF-molecules and actual three-dimensional HF-crystals. The total energies of unit cells and the geometry of the molecules in the crystal was reproduced satisfactorily in these calculations. The mean H-bond energy in the one-dimensional crystal ($\Delta E = -12.8$ kcal/mole) was found to be appreciably larger than in the dimer ($\Delta E_2 = -9.54$ kcal/mole) thus indicating the presence of cooperative effects in sequential chains of HF-molecules. These zig-zag $(HF)_\infty$ chains can be packed in two ways to form three-dimensional crystals: The parallel arrangement of the chains with all HF-dipoles pointing in the same direction usually called "polar HF-crystal" or a second arrangement, where the individual HF-dipoles compensate each other in part. Consequently, the second structure is called the "nonpolar HF-crystal". The nonpolar HF-crystal was found to be slightly more stable ($\Delta E = -13.1$ kcal/mole) than the polar structure ($\Delta E = -11.1$ kcal/mole). The latter is even slightly less stable than the one-dimensional chains. The energy of interaction between unit cells is obtained as a sum of individual contributions in perturbation theory, ΔE_{COU}, ΔE_{POL}, etc. Since the CNDO/2 approximation was used in these calculations the individual contributions show exactly the same systematic errors as we have discussed previously in the case of some dimers (cf. section 2.2.2). Further calculations using perturbation theory in the CNDO/2 version were performed on ice I in its hexagonal modification (Santry [1972, 1973]) and on urea (Middlemiss and Santry [1973]). Recently a generalized version of this method, which can be applied also to

structures with more than one type of molecules in the unit cell, was published (Crowe and Santry [1973]). With this generalization it became possible to calculate reasonably accurate H-bond energies for cubic and hexagonal ice I and to describe deformations of the molecules by the crystal field accurately.

The second type of approach to describe molecular crystals can be interpreted as a straightforward application of MO–SCF theory to infinite systems. It is usually called crystal orbital (CO) method and was originally formulated by Del Re et al. [1967] and André [1969]. The whole crystal is treated as a supermolecule and translational symmetry is introduced by the Born–Von Karman periodic boundary condition. In most cases of actual calculations only interactions with nearest neighboring elementary cells were taken into account. The approximations of several semiempirical MO methods were introduced in the CO formalism. Recently a CNDO/2 version (Ladik and Biczó [1971]) was applied to calculate band structures and energies of infinite one- or two-dimensional structures of $(HF)_\infty$ and $(H_2O)_\infty$ (Karpfen et al. [1974]). In order to obtain fairly correct mean H-bond energies interactions up to the fifth neighbors had to be included. In this case the calculated mean H-bond energies for the zig-zag $(HF)_\infty$ chain ($\Delta E = -16$ kcal/mole) and for the $(H_2O)_\infty$ chain ($\Delta E = -15.3$ kcal/mole) are somewhat larger in absolute value than the results obtained by extrapolation of direct CNDO/2 calculations. H-bonding in two-dimensional formamide networks has been studied by the CNDO–CO method as well (Suhai and Ladik [1972]).

Finally, it should be mentioned briefly that the tight binding approximation based on ab initio SCF orbitals of the isolated HF-molecule was applied to calculate band structures of HF-crystals as well (Bassani et al. [1973]).

Although much progress has been made in the field of molecular crystals during the last few years one feels that many further investigations are necessary before definite conclusions can be drawn. It has been shown in the case of polyene and polyethylene that the band structures calculated by ab initio, CNDO/2 and extended Hueckel (EHM) CO method differ largely (André et al. [1971]). Additionally, the calculation of energy band derivatives was found to be important for a reasonable discussion of the meaning of band structures (André et al. [1972]). Almost all calculations on H-bonded crystals available now were performed within the framework of semiempirical methods. Consequently, it is very difficult to realize possible sources of errors, which might result from the

approximation of the semiempirical procedure or from the CO formalism and its approximations or from both. Since more accurate ab initio calculations on H-bonded crystals seem to be within the range of problems which can be solved with the present computational facilities we can expect further progress in this field in the near future.

2.8. Hydrogen bonds in excited states

In contrast to the great variety and large number of calculations on H-bonds between molecules in their ground states only a few examples of H-bonds in excited states have been investigated. Less than ten papers were published on this subject during the last three years. Most calculations performed until now concentrate on H-bonds to carbonyl groups in their first excited states ($n \rightarrow \pi^*$ excitation). The major problem in these calculations concerns the technique to obtain reliable energy surfaces and wave functions for excited states. Unlike in calculations on closed shell ground states of molecules and molecular aggregations there is no generally accepted best method for a description of open shell systems.

In the first two papers on H-bonds in the lowest excited states of H_2CO/H_2O (De Jeu [1970]) and $H_2CO/HOCH_3$, $(CH_3)_2CO/H_2O$ and $(CH_3)_2CO/HOCH_3$ (Rao and Murthy [1971]) the unrestricted Hartree–Fock (UHF) method within the framework of the CNDO/2 formalism was used. Some features of H-bonding to the $n \rightarrow \pi^*$ excited state of the carbonyl group were predicted correctly, e.g. the fact that H-bonds in excited states are much weaker than in the corresponding ground states or that H-bonding causes an appreciable blue shift of the $n \rightarrow \pi^*$ absorption bands of carbonyl groups. Nevertheless, these calculations turned out to be of very limited value only. The CNDO/2 formalism is characterized by serious limitations in the description of excited states. Since the essential integrals are neglected in the CNDO approximation singlet and triplet $n \rightarrow \pi^*$ states are energetically degenerate. Consequently, the semiempirical calculations correspond somehow to an average of both states.

More recently a detailed CNDO/Cl investigation of solvent effects on $n \rightarrow \pi^*$ and $\pi \rightarrow \pi^*$ absorption bands of carbonyl compounds and some nitrogen containing heterocycles was presented by Cremaschi et al. [1973]. They applied up to six H_2O-molecules in order to simulate a protic solvent around the chromophoric group and varied the intermolecular distance. At reasonable distances they could reproduce experimental

frequency shifts of $n \rightarrow \pi^*$ and $\pi \rightarrow \pi^*$ bands within certain limits of error. Interestingly, one H_2O-molecule corresponding to the most simple H-bond model for solvent effects was not enough to account for the experimentally well known hypsochromic $n \rightarrow \pi^*$ and bathochromic $\pi \rightarrow \pi^*$ shifts appropriately (cf. also p. 145 and Morokuma et al. [1974]). A model containing more H_2O-molecules seems inevitable.

The most detailed ab initio calculation on the geometry of H_2CO/H_2O in the $n \rightarrow \pi^*$ excited singlet and triplet states was performed by Del Bene [1973c]. She used an STO-3G basis set. Excited states were obtained by CI calculations based on canonical virtual orbitals. The equilibrium geometry obtained in these calculations is shown schematically in fig. 2.32. The resulting H-bonding geometry is somewhat unexpected. In both $n \rightarrow \pi^*$ states the C-atom acts as proton acceptor. At the equilibrium geometry of the ground state complex only a very weak interaction in the excited state was found. Previously, almost the same equilibrium geometry was predicted for the excited states in a less extended calculation using another method to describe excited states (Iwata and Morokuma [1973]). The energy of interaction in the excited states is somewhat smaller (fig. 2.32) than in the ground state ($\Delta E = -3.35$ kcal/mole, $R_{CO} = 2.85$ Å, see table 2.13). Accordingly, the intermolecular distances are somewhat larger in the excited states. The

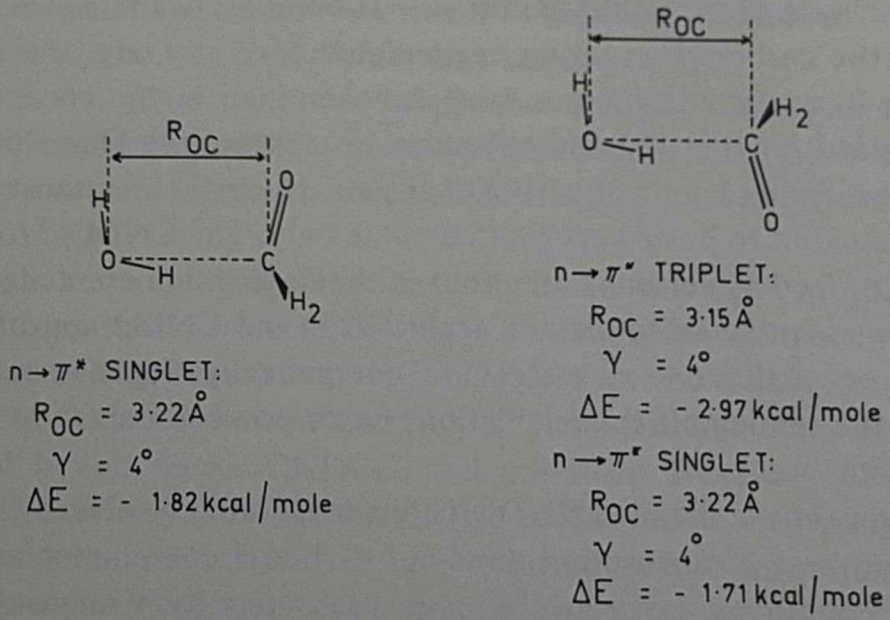

Fig. 2.32. Equilibrium geometry of H_2CO/H_2O in the first excited $n \rightarrow \pi^*$ singlet and triplet states (Del Bene [1973c]).

experimentally well known hypsochromic shift of $n \rightarrow \pi^*$ bands in the electronic spectra of carbonyl compounds, which occurs if one changes from aprotic to protic solvents, is reproduced very well by STO-3G calculations (Del Bene [1973d]). According to the Franck–Condon principle the geometry of the complex remains unchanged during electron excitation. At the ground state geometry the H-bond in the excited state is very weak. Therefore, the hypsochromic shift in protonic solvents is caused by the difference in energy which is necessary to compensate for H-bonds between the H_2CO-molecule in its ground state and the solvent molecules. STO-3G calculations were performed on various other systems H_2CO/HOR in $n \rightarrow \pi^*$ excited singlet and triplet states as well. Similar hypsochromic shifts of the absorption bands were obtained in all cases (Del Bene [1973d]).

A different procedure for calculations on excited states was proposed by Morokuma and Iwata [1972]. They called their method electron-hole-potential (EHP) theory. The EHP method starts again from ground state SCF calculations. Energies and wave functions of the excited states are improved by an iterative procedure. The EHP method was applied to calculations on excited states of the H-bonded complexes: H_2CO/H_2O (Iwata and Morokuma [1972]), $H_2CO/2H_2O$, $H_2C{=}CH{-}CHO/H_2O$, formic acid dimer and hydrogen maleate anion (Morokuma et al. [1974]). As mentioned above the calculated equilibrium geometry of the $n \rightarrow \pi^*$ excited state of H_2CO/H_2O is essentially the same as that obtained by Del Bene [1973c].

In case of $\pi \rightarrow \pi^*$ excitations in H_2CO/H_2O agreement between theory and experiment is not as good as for $n \rightarrow \pi^*$ excitations. Morokuma et al. [1974] used a number of small and medium size basis sets but they were not able to reproduce the experimentally well established bathochromic shifts of $\pi \rightarrow \pi^*$ bands of carbonyl compounds in protic solvents. It is somewhat encouraging, however, that they could find a small bathochromic shift at least between the $\pi \rightarrow \pi^*$ bands of acrolein and its complex with H_2O.

Regarding the results on H-bonds in excited states available now we are attempted to conclude that this interesting field is in a promising first stage of development. Further improvement of methods to calculate molecular complexes in excited states and more results on different structures are necessary before definite general answers to the open questions can be given.

2.9. Proton affinities and potential curves for proton transfer

Proton transfer represents a fairly simple but nevertheless very important type of chemical reactions. In most cases the following general three-step mechanism was found to explain experimental data on intermolecular proton transfer fairly well:

$$\underset{}{AH + B \rightleftarrows \underset{(N)}{AH \cdots B} \rightleftarrows \underset{(I)}{A^- \cdots HB^+} \rightleftarrows A^- + HB^+}. \tag{2.64}$$

Consequently, any method, which can be expected to describe potential curves for proton transfer reasonably well, has to reproduce proton affinities and potential curves for ionic dissociation (2.65) with reasonable accuracy.

$$AH^+ \rightarrow A + H^+. \tag{2.65}$$

Ionic dissociation is not a very frequent process but it occurs in ions like $[H_3O]^+$* or $[H_2F]^+$. Both ions have been investigated extensively by very accurate calculations ($[H_2F]^+$: Diercksen et al. [1973], $[H_3O]^+$: Kollman and Bender [1973] and Lischka and Dyczmons [1973]). We will restrict our discussion here to calculated proton affinities and the influence of correlation energy on the potential curve of ionic dissociation in $[H_3O]^+$.

Proton affinities were found to represent a crucial test for the capability of quantum chemical methods to reproduce energy differences between differently charged molecules or ions correctly (table 2.19). Schuster [1970] showed that CNDO/2 calculations can only produce reliably relative values in a series of equally charged molecules or ions. In absolute values all calculated proton affinities are much too large. In the series of neutral molecules the error is somewhat smaller than in the case of anions. Relative to neutral molecules CNDO/2 calculations overestimate the stability of cations and underestimate even more the stability of anions. In case of ab initio calculations using minimal basis sets the situation is even worse (Hopkinson et al. [1968]). Even relative proton affinities within a series of molecules were obtained incorrectly, e.g. HF

* In $[H_3O]^+$ the situation is a little more complicated because the first ionization potential of H_2O ($I_1(H_2O) = 12.6$ eV) is smaller than the ionization energy of H ($I(H) = 13.6$ eV). $I_1(H_2O)$, however, corresponds to a removal of an electron from the π-lone pair. The OH-bond in $[H_3O]^+$, on the other hand, is formed to a very large extent by the σ-lone pair of H_2O, which is represented by the second ionization potential of H_2O ($I_2(H_2O) = 14.7$ eV). Therefore we have to expect crossing of two states with different spatial symmetry in the correlation diagram of $H_2O + H^+$ or $[H_2O]^+ + H$ respectively.

TABLE 2.19

Calculated and experimental proton affinities (ΔE_{PA})

Molecule or ion	Calculated proton affinity: ΔE_{PA} (kcal/mole)								Experimental proton affinity ΔH_{PA} (kcal/mole)	
	CNDO/2	(3, 1; 1)	(10, 6; 4)	SCF calculations (11, 7, 1; 6, 1)	(11, 7, 2; 6, 2)	HF limit	IEPA calculations (11, 7, 1; 6, 1)	(11, 7, 2; 6, 2)	exp. det.[a]	spectr.[b]
	Ref. a	Ref. b	b	c	c	c	c	c	b	c
HF	−182	−401	−108	−121.8	−122.5		−121.8	−120.8		
H_2O	−246	−345	−181	−176.6	−175.6		−174.0		−(151–181)	
H_3N	−299	−303	−220						−(200–206)	
F^-	−598	−1022	−387	−380.9	−382.1	−383.5	−374.3	−372.9	−(361–368)	−388.6
HO^-	−608	−785	−403	−406.4	−407.5	−408.0	−396.2	−396.4	−(370–392)	−411.1
H_2N^-	−625	−627	−427						−380	

[a] Values obtained by various methods.

[b] Values obtained from spectroscopically determined total energies.

References: a = Schuster [1970]; b = Hopkinson et al. [1968]; c = Lischka [1973c].

was found to be a stronger base than H_3N. Near the HF limit, however, SCF calculations reproduce experimental proton affinities very well. Consequently, the contribution of electron correlation to the calculated values of proton affinities is expected to be rather small. Recently this assumption has been verified by Lischka [1973c].

Encouraged by the results obtained in case of proton affinities many theoretical chemists hopefully thought that electron correlation is not very important for the whole potential curve of ionic dissociation. This assumption, however, was found to be wrong (Meyer et al. [1973]). In the intermediate range of the potential curve for ionic dissociation in $[H_3O]^+$ there is an appreciable contribution of correlation energy to the total energy of the ion (fig. 2.33). The correlation energy reaches a maximum at $R_{OH} = 1.40$ Å and decreases again at larger distances. An explanation of this somewhat unexpected behavior can be given if we regard the size of the σ-lone pair orbital during the process of bond dissociation more closely. For the sake of simplicity the size of the lone pair orbital is characterized by the center of charge (fig. 2.34). At first the center of charge of the electrons in the OH-bond follows the leaving proton. The

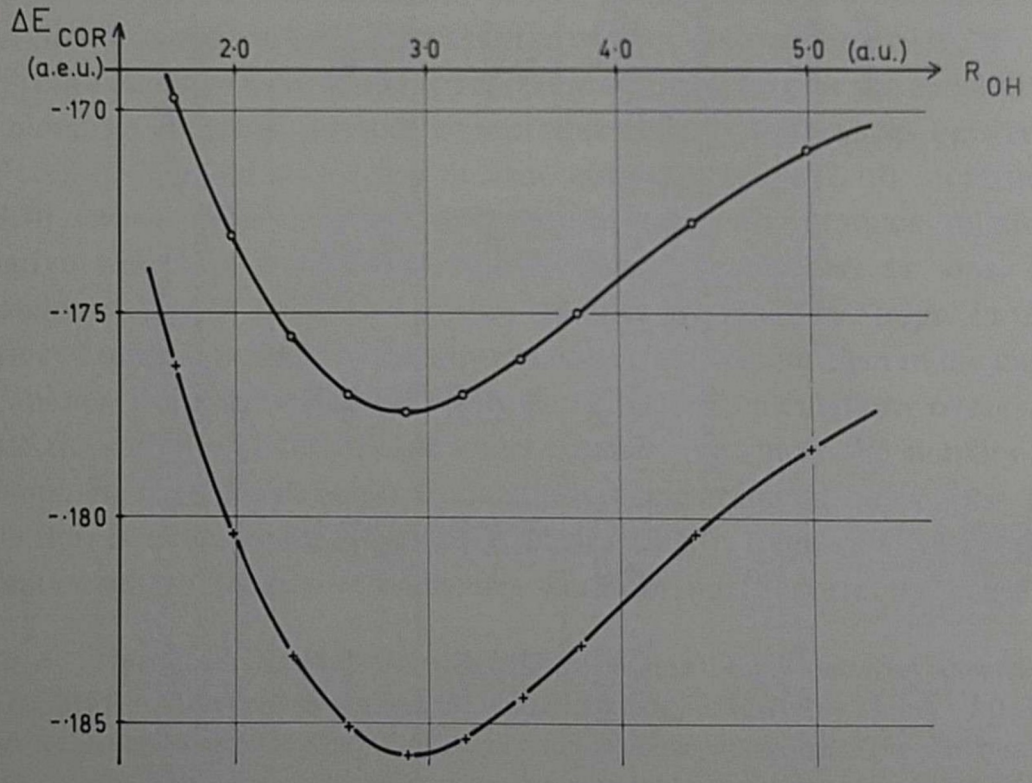

Fig. 2.33. Contribution of electron correlation to the potential curves of ionic dissociation $H_3O^+ \rightarrow H_2O + H^+$. CEPA calculation: –+–+–+–+–; PNO-CI calculation: –○–○–○–; (Meyer et al. [1973], atomic units see fig. 2.2).

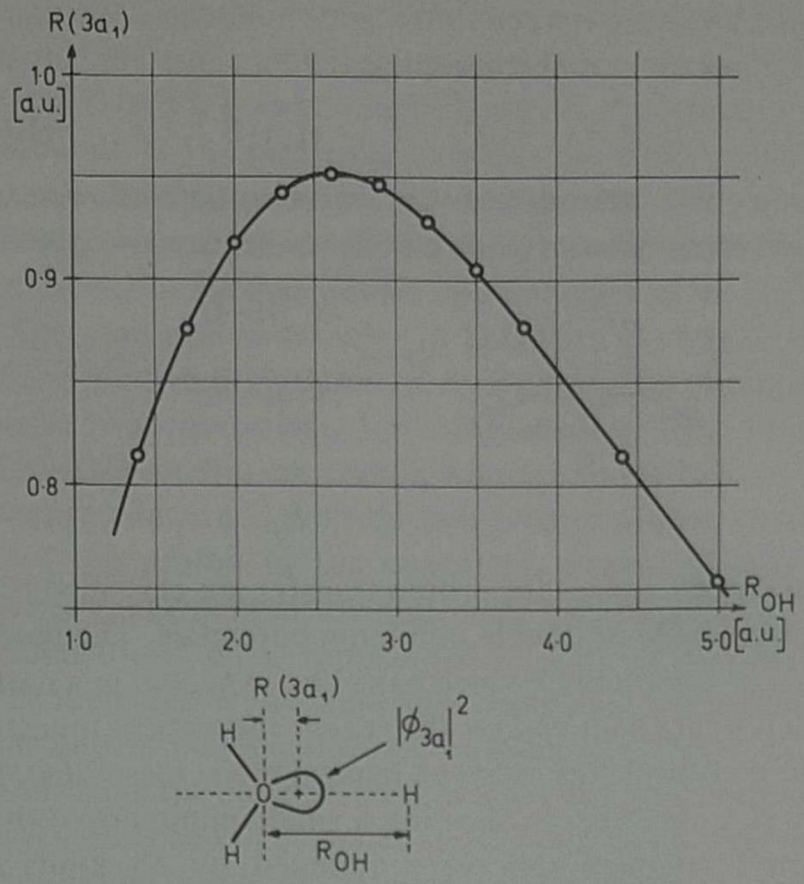

Fig. 2.34. Size of the HO-bond or lone pair orbital ($3a_1$) during the course of ionic dissociation in H_3O^+. The orbital size is represented here simply as the distance between the center of electronic charge and the O-nucleus (Meyer et al. [1973], Schuster et al. [1974b]).

process starts in a completely analogous way as the dissociation of any covalent bond. At a certain stage of bond elongation, however, the orbital size reaches a maximum and at still larger values of R_{OH} the proton leaves and the lone pair collapses to its original size in the isolated H_2O-molecule. Since ionic dissociation starts off very similar to covalent bond dissociation we find the same increase of correlation energy in the first part of the potential curve.

Recently a review article on calculated potential curves of proton transfer along H-bonds was published (Schuster et al. [1974b]). Therefore we will restrict ourselves here to a very brief summary of the most important results and some new calculations. It was found appropriate to distinguish three cases of proton transfer processes:

1. Proton transfer between neutral molecules forming a H-bonded ion pair (2.66),

$$AH \cdots B \rightleftarrows A^- \cdots HB^+. \qquad (2.66)$$

2. Proton transfer between ions and molecules without a drastic change in the polarity of the complex (2.67),

$$AH^+\cdots B \rightleftarrows A\cdots HB^+ \quad \text{or} \quad AH\cdots B^- \rightleftarrows A^-\cdots HB. \qquad (2.67)$$

3. Intramolecular proton transfer or simultaneous transfer of two protons between molecules with mobile π-electrons, e.g.

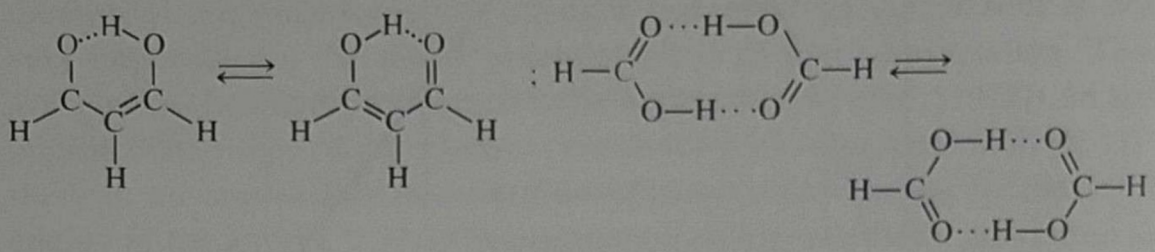

In general energy curves for proton transfer are classified as symmetric or asymmetric, single or double minimum potentials. The lengthy discussion on the kind of potential which has to be expected in a particular case was finally brought to an end by the recent theoretical investigations. In case of isolated complexes between neutral molecules (2.64), exclusively asymmetric potential curves showing a single minimum at the geometry of the neutral complex (**N**) were obtained by all kinds of reliable calculations, CNDO/2 and ab initio (Fang and De la Vega [1970], Kollman and Allen [1971] and Clementi et al. [1971] etc.). Consequently, the ionic complex (**I**) does not exist in the vapor phase and proton transfer occurs via a two-step mechanism (2.68).

$$AH + B \rightleftharpoons AH\cdots B \rightleftharpoons A^- + HB^+. \qquad (2.68)$$

Solvent molecules are able to stabilize the ionic complex. In CNDO/2 calculations simulating a first hydration shell of six water molecules in the system $H_3N\cdots HF$ a double minimum potential was found indeed (Schuster et al. [1974b]). Another type of model studies was applied to solvent effects on $H_3N\cdots HF$ as well (Yamabe et al. [1973]). The same qualitative results were obtained.

Proton transfer between molecules and ions of the type shown in eq. (2.67) leads to symmetric or slightly asymmetric potential curves depending on the nature of the subsystem A and B. In case A and B are identical, symmetric single or double minimum potentials were obtained according to the intermolecular distance. At distances sufficiently large–in some cases like $[H_3N\cdots HNH_3]^+$ already at the equilibrium distance (Merlet et al. [1972])–the two minima are separated by an energy barrier. For $[H_5O_2]^+$ a barrier of $\Delta E^+ = 9.5$ kcal/mole was calculated at $R_{OO} = 2.74$ Å

by Meyer et al. [1973] with a rather extended basis set. Additionally, they investigated the influence of electron correlation on the height of the barrier and found that it is appreciably lowered, if correlation effects are taken into account. In the particular example the CEPA calculation gave $\Delta E^+ = 7.0$ kcal/mole. This result is not unexpected if we remember the influence of electron correlation on the energy curve of ionic dissociation mentioned above. For further details see Schuster et al. [1974b], where hydration effects on proton transfer in $H_5O_2^+$ are discussed as well. The influence of the relative orientation of A and B on the potential curve for proton transfer was investigated by Ingraham [1972]. He performed extensive CNDO/2 studies on proton transfer in $[H_7N_2]^+$.

Finally, we are concerned with the last type of proton transfer, where the motion of the proton or the concerted motion of two protons is coupled to a rearrangement of the molecular backbone. In this case very extensive calculations on a representative part of the whole energy surface of the molecule or the molecular complex are inevitable. For two examples, the enol of malonic dialdehyde (Schuster [1969b, c] and Schuster et al. [1974b]) and the dimer of formic acid (Ady and Brickmann [1971], Clementi et al. [1971] and Schuster et al. [1974b]), an attempt was made to approach the minimum energy pathway for the whole process. In both cases proton transfer does not occur completely synchronized with the relaxation of the molecular backbone. The initial and final period of the reaction is characterized by relatively large changes in backbone geometry whereas proton motion predominates along the minimum energy path around the transition state.

Certainly more and more detailed calculations on proton transfer and its coupling to other molecular modes are necessary before final conclusions on the detailed shape of the energy surfaces can be drawn. Nevertheless, the results obtained until now show that this field promises to be very appropriate for applications of chemical dynamics in order to obtain a detailed picture of the mechanisms of proton transfer.

2.10. Conclusions

Typical H-bonds between neutral molecules do not differ in principle from other types of intermolecular interactions. Some factors stabilizing particular intermolecular geometries coincide in case of linear H-bonds and therefore H-bonds are stronger than most other intermolecular forces between neutral molecules. Because of this unusual strength intermolecu-

lar distances in H-bonded complexes are shorter than in other associations and the electron distribution of both molecules overlap significantly. In the conventional type of energy partitioning the two major stabilizing contributions are intermolecular electrostatic and charge transfer energies. At relatively short intermolecular distances the local dipole of the HX-bond dominates the electrostatic energy and favors the linear arrangement.

Intermolecular energy partitioning, on the other hand, is not free from arbitrariness in the region of appreciable overlap. Therefore, we can easily imagine various other possibilities to define the individual contribution to the total energy of interaction. All our conclusions on the relative importance of certain contributions to the intermolecular energy depend on the particular definitions we have chosen. One should keep in mind this difficulty, although most calculations reported in the literature use the same definitions with respect to energy partitioning.

Ab initio MO–SCF methods were developed to a stage which in principle allows a detailed description of intermolecular forces. Energies of interaction and equilibrium geometries can be calculated very accurately as long as the individual systems are small enough. Nevertheless, these calculations require a large amount of computer time on large computers since very extended basis sets including polarization functions are inevitable and electron correlation has to be taken into account. No extension of these calculations to larger systems seems to be within our present capabilities for numerical calculations. From the energy surfaces force constants can be derived or frequencies for IR absorption bands can be calculated directly (see chs. 3 and 6). As far as reliable data for comparison are available the most accurate calculations reproduce force constants very well. A number of quantities were calculated from the wave functions of H-bonded complexes. Only the three most important ones will be mentioned: increase in dipole moment, increase in dipole moment derivatives (related to IR intensities) and decrease of proton chemical shifts. In all three examples the qualitative trends are reproduced correctly by the calculations. On the other hand, any comparison of the numbers obtained is more or less academic since almost no reliable experimental information is available for isolated dimers.

A number of difficulties arises when ab initio MO–SCF methods are applied to aggregates of more than two molecules. First of all the computer time necessary for accurate calculations increases tremendously even for a single point on the energy surface of the whole complex. Furthermore, the configurational freedom is much larger and the point by

point approach very soon leads to astronomic amounts of computer time required. Consequently, only very few examples were investigated in some detail and this only in regions around the expected energy minima. The results of these calculations show, that in principle the changes in physical properties between isolated dimers and larger clusters are predicted correctly by the theory. Nevertheless, much more results are necessary before quantitatively reliable estimates on the properties of larger aggregates can be made.

Investigations on H-bonds in excited states are still in a more or less preliminary state. Further development of ab initio MO–SCF methods for excited states is inevitable, but we can expect rapid progress and interesting results in this field for the near future.

Energy surfaces for proton transfer represent the basis of further theoretical investigations. Only the vibrational spectra and the dynamics of proton transfer reactions (see ch. 4) shall be mentioned here. Unlike equilibrium geometries and proton affinities, potential barriers for proton transfer and therefore the energy surfaces on the whole change significantly if electron correlation is taken into account. Accordingly, more accurate energy surfaces have to be calculated. Furthermore some improvement of the methods applied is necessary, because theoretical techniques, which are most efficient around equilibrium geometries, can no longer be used reasonably well at larger bond distances. In any case the results obtained from the solution of the electronic Schrödinger equation have to be selected carefully before further calculations are performed. Otherwise the finally calculated numbers will be useful only for qualitative discussions, which can be undertaken equally well on the basis of empirical potential surfaces.

Acknowledgements

The author is indebted to many colleagues for sending their most recent results prior to publication. Numerous discussions with Dr. H. Lischka, who also carefully read large parts of the manuscript, and the help with some numerical calculations by Dipl. chem. W. Marius are gratefully acknowledged. Financial support for our investigations in this field has been provided by the Austrian "Fonds zur Förderung der wissenschaftlichen Forschung" (Projekt Nr. 1217) and the "Th. Körner Stiftungsfonds". Finally, the assistance of our technical staff, Mrs. J. Dura and Mr. J. Schuster, with the preparation of the manuscript is gratefully acknowledged.

Note added in proof

Since the manuscript of this review had been sent to the publishers, a number of papers dealing with energy-calculations on H-bonded systems became available. We will mention here only a review article in a recent monograph, Joesten and Schaad [1974] and two publications on energy partitioning and intermolecular correlation energy in water dimer: Beyer et al. [1975] and Diercksen et al. [1975]. As it has been already suggested on p. 60 the results on partitioning of intermolecular energies according to the scheme proposed by Morokuma [1971] are rather sensitive to changes in the basis sets applied. Therefore, the calculation on $(H_2O)_2$ was repeated by Beyer et al. [1975] using an extended basis set of roughly the same size as that applied by Diercksen [1971]. In fact, at the energy minimum the results obtained by the procedure of partitioning differ significantly from those given by Morokuma [1971], which for convenience are shown here in parentheses: $\Delta E = -4.7$ (-6.6); $\Delta E_{COU} = -7.3$ (-8.0), $\Delta E_{EX} = 4.6$ (9.9), $\Delta E_{POL} = -0.7$ (-0.3) and $\Delta E_{CHT} = -1.2$ (-8.2) kcal/mole. The decrease in absolute value of the coulomb contribution and the small increase in polarization energy can be explained easily by the changes in dipole moment and polarizability of the isolated H_2O molecules on basis set extension. The most drastic changes, however, are found in the charge transfer and the exchange contribution. These changes are much more difficult to explain and a comparison of energy partitioning in different intermolecular complexes is inevitable before a better understanding of these contributions caused by electron exchange can be achieved (Beyer et al. [1975]). Nevertheless, the charge transfer contribution although largely reduced in absolute value remains the second important stabilizing contribution of the H-bonded complex.

Diercksen et al. [1975], finally, presented a very extended calculation on $(H_2O)_2$, wherein they included interaction with 56267 excited configurations in order to account for correlation effects. As expected the contribution of electron correlation to the stability of the dimeric complex is rather small. At the energy minimum of the SCF calculation ($R_{OO} = 3.00$ Å) Diercksen et al. [1975] obtained: $\Delta E_{COR} = -0.87$ kcal/mole. As a consequence of this stabilizing effect the energy minimum is shifted somewhat to smaller distances ($R_{OO} = 2.92$ Å). In general the results on $(H_2O)_2$ correspond very well to those obtained in case of $(HF)_2$ (Lischka [1974a]), where we have seen, that the net effect of electron correlation is a result of the compensation of two contributions (pp. 64–67). Finally

Diercksen et al. [1975] performed a type of energy partitioning within the framework of MO theory, which is somewhat different from Morokuma's method. A comparison and discussion of both schemes can be found in Beyer et al. [1975].

References

Ady, E. and J. Brickmann, 1971, Chem. Phys. Letters **11**, 302.

Ahlrichs, R. and W. Kutzelnigg, 1968, J. Chem. Phys. **48**, 1819.

Alagona, G., A. Pullman, E. Scrocco and J. Tomasi, 1973a, Intern. J. Peptide Protein Res. **5**, 251.

Alagona, G., R. Cimiraglia and H. Lamanna, 1973b, Theoret. Chim. Acta **29**, 93.

Almlöf, J., 1972, Chem. Phys. Letters **17**, 49.

Almlöf, J. and U. Wahlgren, 1973, Theoret. Chim. Acta **28**, 161.

Almlöf, J., J. Lindgren and J. Tegenfeldt, 1972, J. Mol. Struct. **14**, 427.

Anderson, G. R. and G. J. Jiang, 1973, J. Phys. Chem. **77**, 2560.

André, J. M., 1969, J. Chem. Phys. **50**, 1536.

André, J. M., G. S. Kapsomenos and G. Leroy, 1971, Chem. Phys. Letters **8**, 195.

André, J. M., J. Delhalle, G. Kapsomenos and G. Leroy, 1972, Chem. Phys. Letters **14**, 485.

Arrighini, G. P., M. Maestro and R. Moccia, 1967, Chem. Phys. Letters **1**, 242.

Arrighini, G. P., C. Guidotti and O. Salvetti, 1970, J. Chem. Phys. **52**, 1037.

Arshadi, M. and P. Kebarle, 1970, J. Phys. Chem. **74**, 1483.

Arshadi, M., R. Yamdagni and P. Kebarle, 1970, J. Phys. Chem. **74**, 1475.

Atoji, M. and W. N. Lipscomb, 1954, Acta Cryst. **7**, 173.

Bacon, J. and D. P. Santry, 1971, J. Chem. Phys. **55**, 3743.

Bacon, J. and D. P. Santry, 1972, J. Chem. Phys. **56**, 2011.

Bassani, F., L. Pietronero and R. Resta, 1973, J. Phys. C: Solid State Phys. **6**, 2133.

Bender, C. F. and E. R. Davidson, 1968, J. Chem. Phys. **49**, 4222.

Beretta, E. and F. Vetrano, 1973, Intern. J. of Quantum Chem. **7**, 333.

Bergmann, E. D. and B. Pullman, Eds., 1973, Conformation of Biological Molecules and Polymers (Academic Press, Jerusalem).

Bertagnolli, H., J. U. Weidner and H. W. Zimmermann, 1974, Ber. Bunsenges. Physik. Chem. **78**, 1.

Berthier, G., R. Bonaccorsi, E. Scrocco and J. Tomasi, 1972, Theoret. Chim. Acta **26**, 101.

Berthod, H. and A. Pullman, 1972, Chem. Phys. Letters **14**, 217.

Bertoncini, P. J. and A. C. Wahl, 1970, Phys. Rev. Letters **25**, 991.

Bertoncini, P. J. and A. C. Wahl, 1973, J. Chem. Phys. **58**, 1259.

Bixon, M. and S. Lifson, 1967, Tetrahedron **23**, 769.

Bonaccorsi, R., E. Scrocco and J. Tomasi, 1970, J. Chem. Phys. **52**, 5270.

Bonaccorsi, R., C. Petrongolo, E. Scrocco and J. Tomasi, 1971, Theoret. Chim. Acta **20**, 331.

Bonaccorsi, R., A. Pullman, E. Scrocco and J. Tomasi, 1972a, Chem. Phys. Letters **12**, 622.

Bonaccorsi, R., A. Pullman, E. Scrocco and J. Tomasi, 1972b, Theoret. Chim. Acta **24**, 51.

Bonaccorsi, R., R. Cimiraglia, E. Scrocco and J. Tomasi, 1974, Theoret. Chim. Acta **33**, 97.

Bonamy, J. and D. Robert, 1970, Chem. Phys. Letters **6**, 591.

Bowers, M. J. T. and R. M. Pitzer, 1973, J. Chem. Phys. **59**, 163.
Brand, J. C. D. and J. C. Speakman, 1960, Molecular Structure–the Physical Approach (E. Arnold, London), p. 244ff.
Bratož, S., 1967, Electronic Theories of Hydrogen Bonding, in: Advances in Quantum Chemistry, Vol. **3**, Ed. P. O. Löwdin (Academic Press, New York), pp. 209–237.
Caballol, R., R. Gallifa, M. Martin and R. Carbo, 1974, Chem. Phys. Letters **25**, 89.
Chipman, D. M. and J. O. Hirschfelder, 1973, J. Chem. Phys. **59**, 2838.
Chipman, D. M., J. D. Bowman and J. O. Hirschfelder, 1973, J. Chem. Phys. **59**, 2830.
Christoffersen, R. E., 1972, Ab initio Calculations on Large Molecules, in: Advances in Quantum Chemistry, Vol. **6**, Ed. P. O. Löwdin (Academic Press, New York), pp. 333–393.
Clague, A. D. H. and H. J. Bernstein, 1969, Spectrochim. Acta **25A**, 593.
Claverie, P., 1971, Intern. J. of Quantum Chem. **5**, 273.
Clementi, E., 1961, J. Chem. Phys. **34**, 1468.
Clementi, E., 1967a, J. Chem. Phys. **46**, 3842.
Clementi, E., 1967b, J. Chem. Phys. **46**, 3851.
Clementi, E., 1967c, J. Chem. Phys. **47**, 2323.
Clementi, E. and J. N. Gayles, 1967, J. Chem. Phys. **47**, 3837.
Clementi, E. and A. D. McLean, 1962, J. Chem. Phys. **36**, 745.
Clementi, E. and H. Popkie, 1972, J. Chem. Phys. **57**, 1077.
Clementi, E., J. M. André, M. C. André, D. Klint and D. Hahn, 1969, Acta Phys. Acad. Sci. Hung. **27**, 493.
Clementi, E., J. Mehl and W. Von Niessen, 1971, J. Chem. Phys. **54**, 508.
Condon, E. U. and H. Odishaw, Eds., 1967, Handbook of Physics, 2nd ed. (McGraw-Hill, New York, pp. 7–40.
Conway, A. and J. N. Murrell, 1972, Mol. Phys. **23**, 1143.
Coulson, C. A., 1957, Research **10**, 149.
Coulson, C. A. and U. Danielson, 1955, Arkiv Fysik **8**, 205.
Cremaschi, P., A. Gamba and M. Simonetta, 1973, Theoret. Chim. Acta **31**, 155.
Crowe, R. W. and D. P. Santry, 1973, Chem. Phys. **2**, 304.
Cung, M. T., M. Marraud and J. Neel, 1973, Experimental Study of Conformation of Dipeptides, in: Conformation of Biological Macromolecules and Polymers, Eds. E. D. Bergmann and B. Pullman (Academic Press, Jerusalem), pp. 69–86.
Cunningham, A. J., J. D. Payzant and P. Kebarle, 1972, J. Am. Chem. Soc. **94**, 7627.
Daudey, J. P., 1974, Intern. J. Quantum Chem. **8**, 29.
Daudey, J. P., P. Claverie and J. P. Malrieu, 1974a, Intern. J. Quantum Chem. **8**, 1.
Daudey, J. P., J. P. Malrieu and O. Rojas, 1974b, Intern. J. Quantum Chem. **8**, 17.
De Paz, M., J. J. Leventhal and L. Friedman, 1969, J. Chem. Phys. **51**, 3748.
De Paz, M., A. Guidoni-Giardini and F. Friedman, 1970, J. Chem. Phys. **52**, 687.
De Jeu, W. H., 1970, Chem. Phys. Letters **7**, 153.
Del Bene, J. E., 1971, J. Chem. Phys. **55**, 4633.
Del Bene, J. E., 1972a, J. Chem. Phys. **56**, 4923.
Del Bene, J. E., 1972b, J. Chem. Phys. **57**, 1899.
Del Bene, J. E., 1973a, J. Chem. Phys. **58**, 3139.
Del Bene, J. E., 1973b, J. Am. Chem. Soc. **95**, 5460.
Del Bene, J. E., 1973c, Chem. Phys. Letters **23**, 287.

Del Bene, J. E., 1973d, J. Am. Chem. Soc. **95**, 6517.
Del Bene, J. E., 1974, Chem. Phys. Letters **24**, 203.
Del Bene, J. E. and F. T. Marchese, 1973, J. Chem. Phys. **58**, 926.
Del Bene, J. E. and J. A. Pople, 1969, Chem. Phys. Letters **4**, 426.
Del Bene, J. E. and J. A. Pople, 1970, J. Chem. Phys. **52**, 4858.
Del Bene, J. E. and J. A. Pople, 1971, J. Chem. Phys. **55**, 2296.
Del Bene, J. E. and J. A. Pople, 1973, J. Chem. Phys. **58**, 3605.
Del Re, G., J. Ladik and G. Biczó, 1967, Phys. Rev. **155**, 997.
Diercksen, G. H. F., 1969, Chem. Phys. Letters **4**, 373.
Diercksen, G. H. F., 1971, Theoret. Chim. Acta **21**, 335.
Diercksen, G. H. F. and W. P. Kraemer, 1970a, Chem. Phys. Letters **6**, 419.
Diercksen, G. H. F. and W. P. Kraemer, 1970b, Chem. Phys. Letters **5**, 570.
Diercksen, G. H. F. and R. McWeeny, 1966, J. Chem. Phys. **44**, 3554.
Diercksen, G. H. F., W. P. Kraemer and W. Von Niessen, 1972, Theoret. Chim. Acta **28**, 67.
Diercksen, G. H. F., W. Von Niessen and W. P. Kraemer, 1973, Theoret. Chim. Acta **31**, 205.
Diner, S., J. P. Malrieu and P. Claverie, 1969a, Theoret. Chim. Acta **13**, 1.
Diner, S., J. P. Malrieu, F. Jordan and M. Gilbert, 1969b, Theoret. Chim. Acta **13**, 101.
Ditchfield, R., W. J. Hehre and J. A. Pople, 1971, J. Chem. Phys. **54**, 724.
Dixon, H. P., H. D. B. Jenkins and T. C. Waddington, 1972, J. Chem. Phys. **57**, 4388.
Dreyfus, M., 1970, These 3é Cycle, University of Paris.
Dreyfus, M. and A. Pullman, 1970a, Theoret. Chim. Acta **19**, 20.
Dreyfus, M. and A. Pullman, 1970b, Compt. Rend. Acad. Sci. (Paris) **271**, 457.
Dreyfus, M., B. Maigret and A. Pullman, 1970, Theoret. Chim. Acta **17**, 109.
Dunning, Th. H. Jr., R. M. Pitzer and S. Aung, 1972, J. Chem. Phys. **57**, 5044.
Dyke, T. R. and J. S. Muenter, 1974, J. Chem. Phys. **60**, 2929.
Dyke, T. R., B. J. Howard and W. Klemperer, 1972, J. Chem. Phys. **56**, 2442.
Eisenberg, D. and W. Kauzmann, 1969, The Structure and Properties of Water (Clarendon Press, Oxford).
Eisenschitz, H. and F. London, 1930, Z. Physik **60**, 491.
Ermer, O. and S. Lifson, 1973, J. Am. Chem. Soc. **95**, 4121.
Ermler, W. C. and C. W. Kern, 1971, J. Chem. Phys. **55**, 4851.
Falk, H., O. Hofer and H. Lehner, 1974, Mh. Chem. **105**, 995.
Fang, Y. and J. R. De la Vega, 1970, Chem. Phys. Letters **6**, 117.
Franck, E. U. and F. Meyer, 1959, Z. Elektrochem. **63**, 577.
Giessner-Prettre, C. and A. Pullman, 1968, Theoret. Chim. Acta **11**, 159.
Giessner-Prettre, C. and A. Pullman, 1972, Theoret. Chim. Acta **25**, 83.
Giessner-Prettre, C. and A. Pullman, 1974, Theoret. Chim. Acta **33**, 91.
Gordon, M. S. and R. D. Koob, 1973, J. Am. Chem. Soc. **95**, 5863.
Griengl, H. and P. Schuster, 1974, Tetrahedron **30**, 117.
Grimaldi, F., A. Lecourt and C. Moser, 1967, Intern. J. Quantum Chem. **15**, 153.
Grimsrud, E. P. and P. Kebarle, 1973, J. Am. Chem. Soc. **95**, 7939.
Güdel, H. U., 1972, J. Chem. Phys. **56**, 4984.
Guidotti, C., U. Lamanna and M. Maestro, 1972, Theoret. Chim. Acta **26**, 147.
Hadži, G., 1972, Chimia **26**, 7.
Hagler, A. T. and S. Lifson, 1974, J. Am. Chem. Soc. **96**, 5327.
Hagler, A. T., E. Huler and S. Lifson, 1974a, J. Am. Chem. Soc. **96**, 5319.

Hagler, A. T., E. Huler and S. Lifson, 1974b, J. Am. Chem. Soc., in press.
Hall, G. G., 1973, Chem. Phys. Letters **20**, 501.
Hankins, D., J. W. Moskowitz and F. H. Stillinger, 1970a, Chem. Phys. Letters **4**, 527.
Hankins, D., J. W. Moskowitz and F. H. Stillinger, 1970b, J. Chem. Phys. **53**, 4544.
Hankins, D., J. W. Moskowitz and F. H. Stillinger, 1973, J. Chem. Phys. **59**, 995.
Hehre, W. J., R. F. Stewart and J. A. Pople, 1969, J. Chem. Phys. **51**, 2657.
Hehre, W. J., R. Ditchfield and J. A. Pople, 1972, J. Chem. Phys. **56**, 2257.
Herman, R. M., 1966, J. Chem. Phys. **44**, 1346.
Hertz, H. G. and C. Rädle, 1973, Ber. Bunsenges. Physik. Chem. **77**, 521.
Hertz, H. G., M. Holz, R. Klute, G. Stalidis and H. Versmold, 1974, Ber. Bunsenges. Physik. Chem. **78**, 24.
Hirschfelder, J. O. and W. J. Meath, 1967, The Nature of the Intermolecular Forces, in: Advances in Chemical Physics, Vol. **12**, Ed. J. O. Hirschfelder (Interscience Publ., New York), pp. 3–106.
Hirschfelder, J. O., Ch. F. Curtiss and R. B. Bird, 1954, Molecular Theory of Gases and Liquids (Wiley, New York), pp. 835–1103.
Hirschfelder, J. O., W. Byers Brown and S. T. Epstein, 1964, Recent Developments in Perturbation Theory, in: Advances in Quantum Chemistry, Vol. **1**, Ed. P. O. Löwdin (Academic Press, New York), pp. 284–298.
Hopkinson, A. C., N. K. Holbrook, K. Yates and I. G. Csizmadia, 1968, J. Chem. Phys. **49**, 3596.
Hoyland, J. R. and L. B. Kier, 1969, Theoret. Chim. Acta **15**, 1.
Huzinaga, S., 1965, J. Chem. Phys. **42**, 1293.
Huzinaga, S. and Y. Sakai, 1969, J. Chem. Phys. **50**, 1371.
Ingraham, L. L., 1972, Biochem. Biophys. Acta **279**, 8.
Iwata, S. and K. Morokuma, 1973, Chem. Phys. Letters **19**, 94.
Jakubetz, W. and P. Schuster, 1971, Tetrahedron **27**, 101.
Janoschek, R., 1973a, Theoret. Chim. Acta **29**, 57.
Janoschek, R., 1973b, Theoret. Chim. Acta **32**, 49.
Janoschek, R., 1974, unpublished results.
Janoschek, R., E. G. Weidemann, H. Pfeiffer and G. Zundel, 1972, J. Am. Chem. Soc. **94**, 2387.
Janoschek, R., E. G. Weidemann and G. Zundel, 1973, J. Chem. Soc., Farad. Trans. II, **69**, 505.
Janzen, J. and L. S. Bartell, 1969, J. Chem. Phys. **50**, 3611.
Jaszunski, M. and A. J. Sadlej, 1972a, Chem. Phys. Letters **15**, 41.
Jaszunski, M. and A. J. Sadlej, 1972b, Theoret. Chim. Acta **27**, 135.
Jaszunski, M. and A. J. Sadlej, 1973, Theoret. Chim. Acta **30**, 257.
Jeziorski, B. and L. Piela, 1972, Acta Physiol. Polon. **A42**, 177.
Jiang, G. J. and G. R. Anderson, 1973, J. Phys. Chem. **77**, 1764.
Johansson, A. and P. A. Kollman, 1972, J. Am. Chem. Soc. **94**, 6197.
Johansson, A., P. A. Kollman and S. Rothenberg, 1972a, Chem. Phys. Letters **16**, 123.
Johansson, A., P. A. Kollman and S. Rothenberg, 1972b, Theoret. Chim. Acta **26**, 97.
Johansson, A., P. A. Kollman and S. Rothenberg, 1973, Theoret. Chim. Acta **29**, 167.
Jungen, M. and R. Ahlrichs, 1970, Theoret. Chim. Acta **17**, 339.
Karpfen, A., 1973, Thesis (1st deg.), Univ. of Vienna.

Karpfen, A., J. Ladik, P. Russegger, P. Schuster and S. Suhai, 1974, Theoret. Chim. Acta **34**, 115.
Karplus, M. and H. J. Kolker, 1963, J. Chem. Phys. **38**, 1263.
Karplus, S. and S. Lifson, 1971, Biopolymers **10**, 1973.
Kauzmann, W., 1957, Quantum Chemistry (Academic Press, New York), p. 729.
Kebarle, P., S. K. Searles, A. Zolla, J. Scarborough and M. Arshadi, 1967, J. Am. Chem. Soc. **89**, 6393.
Kistenmacher, H., H. Popkie and E. Clementi, 1973a, J. Chem. Phys. **59**, 5842.
Kistenmacher, H., H. Popkie and E. Clementi, 1973b, J. Chem. Phys. **58**, 5627.
Kolker, H. J. and M. Karplus, 1964, J. Chem. Phys. **41**, 1259.
Kollman, P. A., 1972, J. Am. Chem. Soc. **94**, 1837.
Kollman, P. A. and L. C. Allen, 1969, J. Chem. Phys. **51**, 3286.
Kollman, P. A. and L. C. Allen, 1970a, Theoret. Chim. Acta **18**, 399.
Kollman, P. A. and L. C. Allen, 1970b, J. Chem. Phys. **52**, 5085.
Kollman, P. A. and L. C. Allen, 1970c, J. Am. Chem. Soc. **92**, 573.
Kollman, P. A. and L. C. Allen, 1970d, J. Am. Chem. Soc. **92**, 6101.
Kollman, P. A. and L. C. Allen, 1971, J. Am. Chem. Soc. **93**, 4991.
Kollman, P. A. and L. C. Allen, 1972, Chem. Rev. **72**, 283.
Kollman, P. A. and C. F. Bender, 1973, Chem. Phys. Letters **21**, 271.
Kollman, P. A., A. Johansson and S. Rothenberg, 1974, Chem. Phys. Letters **24**, 199.
Kolos, W. and L. Wolniewicz, 1967, J. Chem. Phys. **46**, 1426.
Kraemer, W. P. and G. H. F. Diercksen, 1970, Chem. Phys. Letters **5**, 463.
Kraemer, W. P. and G. H. F. Diercksen, 1972a, Theoret. Chim. Acta **23**, 398.
Kraemer, W. P. and G. H. F. Diercksen, 1972b, Theoret. Chim. Acta **27**, 265.
Kutzelnigg, W., 1963, Theoret. Chim. Acta **1**, 327.
Kutzelnigg, W., 1973, Electron Correlation and Electron Pair Theories, in: Topics in Current Chemistry, Vol. **41**, Ed. F. Boschke (Springer-Verlag, Berlin), p. 31.
Ladell, J. and B. Post, 1954, Acta Cryst. **7**, 559.
Ladik, J. and G. Biczó, 1971, Acta Chim. Acad. Sci. Hung. **67**, 397.
Landoldt-Börnstein, 1951, Zahlenwerte und Funktionen, 6. Aufl. Springer, Berlin, Vol. 1/3, p. 511.
Lee, C. S., J. P. O'Connell, C. D. Myrat and J. M. Prausnitz, 1970, Can. J. Chem. **48**, 2993.
Lentz, B. R. and H. A. Scheraga, 1973, J. Chem. Phys. **58**, 5296.
Lifson, S. and A. Warshel, 1968, J. Chem. Phys. **49**, 5116.
Lischka, H., 1973a, Chem. Phys. Letters **20**, 448.
Lischka, H., 1973b, Chem. Phys. **2**, 191.
Lischka, H., 1973c, Theoret. Chim. Acta, **31**, 39.
Lischka, H., 1974a, J. Am. Chem. Soc. **96**, 4761.
Lischka, H., 1974b, unpublished results.
Lischka, H. and V. Dyczmons, 1973, Chem. Phys. Letters **23**, 167.
Losonczy, M., J. W. Moskowitz and F. H. Stillinger, 1973, J. Chem. Phys. **59**, 3264.
Löwdin, P. -O., 1950, J. Chem. Phys. **18**, 365.
Luck, W. A. P., 1965a, Naturwissenschaften **52**, 25.
Luck, W. A. P., 1965b, Naturwissenschaften **52**, 49.
Luck, W. A. P., 1967, Naturwissenschaften **54**, 601.
Malrieu, J. P., P. Claverie and S. Diner, 1969, Theoret. Chim. Acta **13**, 18.

Margenau, H. and N. R. Kestner, 1971, Theory of Intermolecular Forces, 2nd ed. (Pergamon Press, Oxford), pp. 15–298.
Marius, W., 1973, Thesis (1st deg.), Univ. of Vienna.
Marius, W., 1974, Thesis (2nd deg.), Univ. of Vienna.
Marius, W., P. Schuster, H. Berthod and A. Pullman, 1975, submitted for publication.
McDaniel, D. H. and W. G. Evans, 1966, Inorg. Chem. **5**, 2180.
McLaughlin, D. R. and H. F. Schaefer III, 1971, Chem. Phys. Letters **12**, 244.
McLean, A. D. and M. Yoshimine, V, 1966, J. Chem. Phys. **45**, 3676.
McLean, A. D. and M. Yoshimine, 1967, IBM J. Res. Develop. Suppl. **11**, Tables of Linear Molecules, pp. 163 and 169.
McWeeny, R., 1962, Phys. Rev. **126**, 1028.
McWeeny, R., 1968, Chem. Phys. Letters **1**, 567.
Merlet, P., S. D. Peyerimhoff and R. J. Buenker, 1972, J. Am. Chem. Soc. **94**, 8301.
Messiah, A., 1970, Quantum Mechanics, Vol. **2** (North-Holland Publ. Co., Amsterdam), pp. 781–793.
Meunier, A., B. Levy and G. Berthier, 1973, Theoret. Chim. Acta **29**, 49.
Meyer, W., 1973, J. Chem. Phys. **58**, 1017.
Meyer, W., W. Jakubetz and P. Schuster, 1973, Chem. Phys. Letters **21**, 97.
Middlemiss, K. M. and D. P. Santry, 1973, Chem. Phys. **1**, 128.
Momany, F. A., R. F. McGuire, J. F. Yan and H. A. Scheraga, 1971, J. Phys. Chem. **75**, 2286.
Moore, L. S. and J. P. O'Connell, 1971, J. Chem. Phys. **55**, 2605.
Morita, H. and S. Nagakura, 1972, Theoret. Chim. Acta **27**, 325.
Morokuma, K., 1971, J. Chem. Phys. **55**, 1236.
Morokuma, K. and L. Pedersen, 1968, J. Chem. Phys. **48**, 3275.
Morokuma, K. and J. R. Winick, 1970, J. Chem. Phys. **52**, 1301.
Morokuma, K. and S. Iwata, 1972, Chem. Phys. Letters **16**, 192.
Morokuma, K., S. Iwata and W. A. Lathan, 1974, Molecular Interactions in Ground and Excited States, in: The World of Quantum Chemistry, Eds. R. Daudel and B. Pullman. Proceedings of the First International Congress of Quantum Chemistry, Menton, France, 1973 (D. Reidel Publ. Co., Dordrecht, Holland), pp. 277–316.
Mulliken, R. S., 1955, J. Chem. Phys. **23**, 1833, 1841, 2338 and 2343.
Murrell, J. N. and A. J. Harget, 1972, Semi-empirical Self-consistent-field Molecular Orbital Theory of Molecules (Wiley-Interscience, London).
Murrell, J. N. and G. Shaw, 1967, J. Chem. Phys. **46**, 1768.
Murrell, J. N. and J. J. C. Teixeira-Dias, 1970, Mol. Phys. **19**, 521.
Murrell, J. N., M. Randić and D. R. Williams, 1965, Proc. Roy. Soc. London, **A284**, 566.
Murthy, A. S. N. and C. N. R. Rao, 1970, J. Mol. Struct. **6**, 253.
Murthy, A. S. N., S. N. Bhat and C. N. R. Rao, 1970, J. Chem. Soc. (London) A, 1251.
Musher, J. I., 1967, J. Chem. Phys. **46**, 369.
Musher, J. I. and A. T. Amos, 1967, Phys. Rev. **164**, 31.
Musher, J. I. and L. Salem, 1966, J. Chem. Phys. **44**, 2943.
Neckel, A., P. Kuzmany and G. Vinek, 1971, Z. Naturforsch. **A26**, 569.
Nesbet, R. K., 1958, Phys. Rev. **109**, 1632.
Nesbet, R. K., 1965a, J. Chem. Phys. **43**, 311.
Nesbet, R. K., 1965b, Electron Correlation in Atoms and Molecules, in: Advances in Chemical Physics, Vol. **9**, Ed. I. Prigogine (Interscience, New York), p. 321ff.

Neumann, D. and J. W. Moskowitz, 1968, J. Chem. Phys. **49**, 2056.
Newton, M. D. and S. Ehrenson, 1971, J. Am. Chem. Soc. **93**, 4971.
Noble, P. N. and R. N. Kortzeborn, 1970, J. Chem. Phys. **52**, 5375.
O'Connell, J. P. and J. M. Prausnitz, 1969, Ind. Eng. Chem. Fundamentals **8**, 453.
O'Connell, J. P. and J. M. Prausnitz, 1970, Ind. Eng. Chem. Fundamentals **9**, 579.
Payzant, J. D., A. J. Cunningham and P. Kebarle, 1973, Can. J. Chem. **51**, 3242.
Pecul, K. and R. Janoschek, 1974, Theoret. Chim. Acta **36**, 25.
Petrongolo, C. and J. Tomasi, 1973, Chem. Phys. Letters, **20**, 201.
Piela, L., 1972, Chem. Phys. Letters **15**, 199.
Piela, L., 1973, Chem. Phys. Letters **19**, 134.
Piela, L. and B. Jeziorski, 1972, Acta Physiol. Polon. **A42**, 185.
Pimentel, G. C. and A. L. McClellan, 1960, The Hydrogen Bond (W. H. Freeman, San Francisco), pp. 211–212, pp. 266–270 and p. 348ff.
Plesser, T., 1970, unpublished results.
Poland, D. and H. A. Scheraga, 1967, Biochemistry **6**, 3791.
Popkie, H., H. Kistenmacher and E. Clementi, 1973, J. Chem. Phys. **59**, 1325.
Pople, J. A., 1951, Proc. Roy. Soc. **A205**, 163.
Pople, J. A. and D. L. Beveridge, 1970, Approximate Molecular Orbital Theory (McGraw-Hill Book Co., New York).
Pople, J. A. and G. A. Segal, 1965, J. Chem. Phys. **43**, S 136.
Pople, J. A. and G. A. Segal, 1966, J. Chem. Phys. **44**, 3289.
Pople, J. A., D. L. Beveridge and P. A. Dobosh, 1967, J. Chem. Phys. **47**, 2026.
Pople, J. A., D. P. Santry and G. A. Segal, 1965, J. Chem. Phys. **43**, S 129.
Port, G. N. J. and A. Pullman, 1973a, FEBS Letters **31**, 70.
Port, G. N. J. and A. Pullman, 1973b, Theoret. Chim. Acta **31**, 231.
Pullman, B., 1971, Etudes Conformationelles on Biochimie Quantique, Eds. R. Daudel and B. Pullman, Aspects de la Chimie Quantique Contemporaine (C.N.R.S., Paris), pp. 261–301.
Pullman, A. and A. M. Armbruster, 1974, to be published.
Pullman, A. and H. Berthod, 1968, Theoret. Chim. Acta **10**, 461.
Pullman, B. and B. Maigret, 1973, The Dipeptide Model–Its Significance and Limitations, Eds. E. Bergmann and B. Pullman, Conformation of Biological Macromolecules and Polymers, (Academic Press, Jerusalem), pp. 13–40.
Pullman, A. and G. N. J. Port, 1973, C. R. Acad. Sci. Paris **D227**, 2269.
Pullman, A., G. Alagona and J. Tomasi, 1974, Theoret. Chim. Acta **33**, 87.
Rae, A. I. M., 1969, Mol. Phys. **16**, 257.
Rahman, A. and F. H. Stillinger, 1971, J. Chem. Phys. **55**, 3336.
Rahman, A. and F. H. Stillinger, 1973, J. Am. Chem. Soc. **95**, 7943.
Ramachandran, G. N. and V. Sasisekharan, 1968, Conformation of Polypeptides and Proteins, in: Advances in Protein Chemistry, Vol. **23**, Eds. C. B. Anfinsen, M. L. Anson, J. T. Edsall and F. M. Richards (Academic Press, New York), pp. 283–437.
Rao, C. N. R., 1972, Theory of Hydrogen Bonding in Water, in: Water, Vol. **1**, Ed. F. Franks (Plenum Press, New York), pp. 93–114.
Ratajczak, H., 1972a, J. Phys. Chem. **76**, 3000.
Ratajczak, H., 1972b, J. Phys. Chem. **76**, 3991.
Ratajczak, H., 1973, J. Mol. Struct. **17**, 431.

Ratajczak, H., and W. J. Orville-Thomas, 1973a, J. Chem. Phys. **58**, 911.
Ratajczak, H. and W. J. Orville-Thomas, 1973b, J. Mol. Struct. **19**, 237.
Rigby, M., J. P. O'Connell and J. M. Prausnitz, 1969, Ind. Eng. Chem. Fundamentals **8**, 460.
Rode, B. M., A. Engelbrecht and W. Jakubetz, 1973, Chem. Phys. Letters **18**, 285.
Roothaan, C. C. J., 1951, Rev. Mod. Phys. **23**, 69.
Russegger, P. and P. Schuster, 1973, Chem. Phys. Letters **19**, 254.
Russegger, P. and P. Schuster, 1974, in preparation.
Russegger, P., H. Lischka and P. Schuster, 1972, Theoret. Chim. Acta **24**, 191.
Sabin, J. R., 1971a, J. Am. Chem. Soc. **93**, 3613.
Sabin, J. R., 1971b, J. Chem. Phys. **54**, 4675.
Santry, D. P., 1972, J. Am. Chem. Soc. **94**, 8311.
Santry, D. P., 1973, Molecular–Orbital Studies on Ice Ih, in: Physics and Chemistry of Ice, Eds. E. Whalley, S. J. Stones and L. W. Gold (Royal Society of Canada, Ottawa), pp. 19–22.
Schaefer III, F. H., 1972, The Electronic Structure of Atoms and Molecules (Addison-Wesley Publ. Co., Reading, Mass.), pp. 4–83.
Scheraga, H. A., 1968, Calculations of Conformations of Polypeptides, in: Advances in Physical Organic Chemistry, Vol. **6**, Ed. V. Gold (Academic Press, London), pp. 103–179.
Scheraga, H. A., 1971, Chem. Rev. **71**, 195.
Schneider, W. G., 1955, J. Chem. Phys. **23**, 26.
Schuster, P., 1969a, Intern. J. Quantum Chem. **3**, 851.
Schuster, P., 1969b, Chem. Phys. Letters **3**, 433.
Schuster, P., 1969c, Mh. Chem. **100**, 2084.
Schuster, P., 1970, Theoret. Chim. Acta **19**, 212.
Schuster, P., 1973, Z. Chem. **13**, 41.
Schuster, P., 1974, Theory of Hydrogen Bonding in Water and Ion Hydration, in: Water–As Liquid and Solid, Ed. W. A. P. Luck. Proceedings of the International Symposium: Structures of Water and Aqueous Solutions, Marburg (Lahn), 19–28.7.1973 (Verlag Chemie, Weinheim), pp. 141–167.
Schuster, P. and T. Funck, 1968, Chem. Phys. Letters **2**, 587.
Schuster, P., W. Marius and W. Jakubetz, 1974a, Molecular Models on the Solvation of Small Ions and Polar Molecules, in: Topics in Current Chemistry, Ed. F. Boschke (Springer-Verlag, Berlin), in press.
Schuster, P., W. Jakubetz, G. Beier, W. Meyer and B. M. Rode, 1974b, Potential Curves for Proton Transfer along Hydrogen Bonds, in: Chemical and Biochemical Reactivity, Eds. E. D. Bergmann and B. Pullman (Academic Press, Jerusalem), pp. 257–282.
Scrocco, E., and J. Tomasi, 1973, The Electrostatic Molecular Potential as a Tool for the Interpretation of Molecular Properties, in: Topics in Current Chemistry, Vol. **42**, Ed. F. Boschke (Springer-Verlag, Berlin), pp. 95–170.
Shavitt, I., 1970, J. Comp. Phys. **6**, 124.
Shipman, L. L. and R. E. Christoffersen, 1972, Proc. Natl. Acad. Sci. U.S.A. **69**, 3301.
Shipman, L. L. and R. E. Christoffersen, 1973a, J. Am. Chem. Soc. **95**, 1408.
Shipman, L. L. and R. E. Christoffersen, 1973b, J. Am. Chem. Soc. **95**, 4733.
Sinanoglu, O., 1962, J. Chem. Phys. **36**, 706 and 3198.
Smith, D. F., 1958, J. Chem. Phys. **28**, 1040.

Smith, D. F., 1959, J. Mol. Spectr. **3**, 473.
Snyder, L. C. and H. Basch, 1972, Molecular Wave Functions and Properties (Wiley, New York), pp. T2, T26 and T56.
Srebrenik, S., H. Weinstein and R. Pauncz, 1973, Chem. Phys. Letters **20**, 419.
Stillinger, F. H. and A. Rahman, 1972, J. Chem. Phys. **57**, 1281.
Stillinger, F. H. and A. Rahman, 1974, J. Chem. Phys. **60**, 1545.
Stockmayer, W. H., 1941, J. Chem. Phys. **9**, 398.
Suhai, S. and J. Ladik, 1972, Theoret. Chim. Acta **28**, 27.
Sustmann, R. and F. Vahrenholt, 1973, Theoret. Chim. Acta **29**, 305.
Tait, A. D. and G. G. Hall, 1973, Theoret. Chim. Acta **31**, 311.
Tapia, O., A. Nogales and P. Campano, 1974, Chem. Phys. Letters **24**, 401.
Tsubomura, M., 1954, Bull. Chem. Soc. Japan **27**, 445.
Van Duijneveldt, F. B., 1968, J. Chem. Phys. **49**, 1424.
Van Duijneveldt, F. B. and J. N. Murrell, 1967, J. Chem. Phys. **46**, 1759.
Van Duijneveldt-Van de Rijdt, J. G. C. M. and F. B. Van Duijneveldt, 1968, Chem. Phys. Letters **2**, 565.
Van Duijneveldt-Van de Rijdt, J. G. C. M. and F. B. Van Duijneveldt, 1970, Theoret. Chim. Acta **19**, 83.
Van Duijneveldt-Van de Rijdt, J. G. C. M. and F. B. Van Duijneveldt, 1971, J. Am. Chem. Soc. **93**, 5644.
Van Duijneveldt-Van de Rijdt, J. G. C. M. and F. B. Van Duijneveldt, 1972, Chem. Phys. Letters **17**, 425.
Van Thiel, M., E. D. Becker and G. Pimentel, 1957, J. Chem. Phys. **27**, 486.
Verwey, E. J. W., 1941, Rec. Trav. Chim. Pays-Bas Belg. **60**, 887.
Vinogradov, S. N. and R. H. Linnell, 1971, Hydrogen Bonding (Van Nostrand Reinhold, New York), pp. 121–123.
Von Niessen, W., 1971, J. Chem. Phys. **55**, 1948.
Von Niessen, W., 1973a, Theoret. Chim. Acta **31**, 111.
Von Niessen, W., 1973b, Theoret. Chim. Acta **31**, 297.
Von Niessen, W., 1973c, Theoret. Chim. Acta **32**, 13.
Von Niessen, W., 1974, unpublished results.
Warshel, A. and S. Lifson, 1970, J. Chem. Phys. **53**, 582.
Warshel, A., M. Levitt and S. Lifson, 1970, J. Mol. Spectr. **33**, 84.
Williams, J. M. and L. F. Schneemeyer, 1973, J. Am. Chem. Soc. **95**, 5780.
Yamabe, S., S. Kato, H. Fujimoto and K. Fukui, 1973, Theoret. Chim. Acta **30**, 327.
Yarkony, D. R., S. V. O'Neill, H. F. Schaefer III, C. P. Baskin and C. F. Bender, 1974, J. Chem. Phys. **60**, 855.

Added in proof:

Beyer, A., H. Lischka and P. Schuster, 1975, submitted for publication.
Diercksen, G. H. F., W. P. Kraemer and B. O. Roos, 1975, Theoret. Chim. Acta **36**, 249.
Joesten, M. D. and L. V. Schaad, 1974, Hydrogen Bonding (Marcel Dekker, New York) pp. 53–154.

CHAPTER 3

CALCULATED VIBRATIONAL SPECTRA OF HYDROGEN BONDED SYSTEMS

R. JANOSCHEK

Institut für Theoretische Chemie, Universität Stuttgart, D-7000 Stuttgart-Vaihingen, FRG

Contents

3.1. Introduction 167
3.2. Theory of vibrational spectra of H-bonds and computational methods 168
3.2.1. Normal coordinates of H-bonds 169
3.2.2. Theory of vibrational states of H-bonds 171
3.2.3. Theory of IR absorption intensities 177
3.2.4. H-bonds and external electrostatical fields 179
3.2.5. Effects of deuteration 181
3.2.6. Simultaneous proton motions in H-bonds 181
3.3. Applications 182
Acknowledgements 214
References 214

The hydrogen bond – recent developments in theory and experiments
Eds. P. Schuster et al. © *North-Holland Publ. Co., Amsterdam, 1976*

3.1. Introduction

The principles for the calculation of vibrational spectra have been known since the early days of quantum mechanics. In spite of this fact, only now have the first investigations of vibrational spectra of H-bonded systems been performed. On the one hand one has had to wait for the development of accurate high speed computers in order to treat the extensive numerical problems; on the other hand one has had to collect experience of the analytical as well as of the numerical methods. The stage has now been reached when the theory has been sufficiently well tested as to permit one to proceed in the calculation of spectroscopic properties, with reasonable assurance that meaningful results will be obtained. However, in the study of H-bonds it is found that the rules commonly employed in vibrational spectroscopy are not always applicable.

What does one mean by the expression "calculated" vibrational spectra? What kind of starting data are used? It is sometimes considered that the most desirable theory is one which incorporates the least possible fundamental data or laws. Here the initial data consists of Planck's constant h, the charge e and the mass m of the electron, the mass M of the proton whilst, in addition, Pauli's principle is invoked. Methods of calculation which are based upon only a few fundamental constants and laws, and which do not use any further experimental results or arbitrary assumptions will be called ab initio methods. From these ab initio methods it becomes possible for a calculation of vibrational spectra to be performed. In this chapter the theory for vibrational spectra of H-bonds and the appropriate ab initio methods are to be delineated.

Besides the ab initio methods already mentioned there will also be considered a specific kind of approximation which deliberately gives up the accuracy of ab initio calculations, in order to have the advantage that the results may be expressed in analytical form. A well known method of this kind arises out of second order perturbation theory.

Besides this type of calculation the term "calculation" is used in quite a

different sense. The initial data are measured spectra which are interpolated by means of certain analytical expressions containing free parameters. These interpolation formulas are then used to recalculate vibrational spectra. The value of these results is certainly poor because the resulting data can only be the same as the starting data at best. In contrast to the ab initio methods which permit accurate predictions to be made, the empirical calculations can only provide predictions in the sense of an interpolation. For example one may consider the relation between the length of a H-bond AH···B and the AH wave number shift. A useful example is the "measurement" of potential parameters by such a procedure.

Finally a further kind of theoretical technique stems from studies on models. For example, the classical electrostatic model for H-bonds or the bare proton model belong to this category. Since the rise of ab initio methods such studies have become less important. However, sometimes the conjunction of good models with experimental facts can, on occasions, be most useful.

3.2. Theory of vibrational spectra of H-bonds and computational methods

The behaviour of a many particle system may be described in terms of the time dependent Schroedinger equation

$$H\Psi = \mathrm{i}\partial\Psi/\partial t \tag{3.1}$$

where H is the Hamiltonian, Ψ is the wave function of the system, i is the imaginary unit and t is the time. Should one adopt the Born–Oppenheimer approximation then a simplification of the time dependent Schroedinger equation results. The assumption that the nuclei move more slowly than the electrons (adiabatic approximation) permits the electron motion and the motion of nuclei to be treated independently. Under such conditions

$$\Psi(r, \boldsymbol{R}, t) = \psi(r, \boldsymbol{R})\varphi(\boldsymbol{R}, t) \tag{3.2}$$

$$H\psi(r, \boldsymbol{R}) = E(\boldsymbol{R})\psi(r, \boldsymbol{R}) \tag{3.3}$$

$$[T + E(\boldsymbol{R})]\varphi(\boldsymbol{R}, t) = \mathrm{i}\partial\varphi(\boldsymbol{R}, t)/\partial t. \tag{3.4}$$

Equation (3.3) is the time independent Schroedinger equation for the electron motion and eq. (3.4) is the time dependent Schroedinger equation for the nuclear motion. The approximate solution of eq. (3.3) provides the total energy $E(\boldsymbol{R})$ of the system in question as an energy hypersurface in the $\boldsymbol{R}$-space. On this surface chemical reactions can be discussed. For the

specific case of stationary states as they appear with vibrations,

$$\varphi(\boldsymbol{R}, t) = \chi(\boldsymbol{R})\, \mathrm{e}^{-\mathrm{i}\lambda t}. \tag{3.5}$$

The amplitude $\chi(\boldsymbol{R})$ then results from the time independent Schroedinger equation for the nuclear motion

$$[T + E(\boldsymbol{R})]\chi(\boldsymbol{R}) = \lambda\chi(\boldsymbol{R}) \tag{3.6}$$

where T is the operator of the kinetic energy of the nuclei and λ are the energy eigenvalues of the vibrational states. The methods for the solution of eq. (3.3) are treated in ch. 2. In the following the total energy $E(\boldsymbol{R})$ resulting from eq. (3.3) is considered as known and will be denoted by V in order to solve eq. (3.6). A second fundamental result from eq. (3.3) is that the total dipole moment $\boldsymbol{\mu}(\boldsymbol{R}) = \langle\psi(r, \boldsymbol{R})|\sum_k Q_k \boldsymbol{R}_k - \sum_i r_i|\psi(r, \boldsymbol{R})\rangle$ is a function only of nuclear position.

3.2.1. Normal coordinates of H-bonds

If one disregards extreme cases of intramolecular H-bonds, such bonds tend to be linear. In general a H-bond consists of three units

$$\mathrm{A}\cdots\mathrm{H}\cdots\mathrm{B}$$

where A and B may be any atoms or molecules or the corresponding ions. For the description of the nuclear motion of this system four internal coordinates are necessary. They are the distances AH and HB, the angle AHB and an angle measured around the AB axis. There exists, therefore, four vibrational modes in the harmonic approximation, namely two linear modes and two angular modes. These are degenerate in the case of axial symmetry. In the following a normal coordinate analysis will be taken as a first approximation for the system $\mathrm{A}\cdots\mathrm{H}\cdots\mathrm{B}$.

Starting with the Lagrange equations

$$\frac{\mathrm{d}}{\mathrm{d}t}\left(\frac{\partial T}{\partial \dot{q}_i}\right) + \frac{\partial V}{\partial q_i} = 0 \tag{3.7}$$

where q_i are arbitrary coordinates of motion. The kinetic energy T and the potential energy V have to be represented in common coordinates. Considering the two linear modes of the system $\mathrm{A}\cdots\mathrm{H}\cdots\mathrm{B}$, these being the most strongly interacting, the potential energy in the harmonic approximation is of the form

$$V = \tfrac{1}{2} f_{\mathrm{AH}} R_{\mathrm{AH}}^2 + \tfrac{1}{2} f_{\mathrm{HB}} R_{\mathrm{HB}}^2 + f_{\mathrm{AH,HB}} R_{\mathrm{AH}} R_{\mathrm{HB}} \tag{3.8}$$

where R_{AH}, R_{HB} are the changes of the internal coordinates and f represents the respective force constants. The kinetic energy may be represented at first only in cartesian coordinates as

$$T = \tfrac{1}{2}m_A\dot{x}_A^2 + \tfrac{1}{2}m_H\dot{x}_H^2 + \tfrac{1}{2}m_B\dot{x}_B^2. \tag{3.9}$$

Further use of the harmonic approximation gives rise to linear relations between the cartesian coordinates and internal coordinates.

$$\begin{aligned} R_{AH} &= x_H - x_A \\ R_{HB} &= x_B - x_H. \end{aligned} \tag{3.10}$$

The first derivative with respect to the time in matrix notation is

$$\begin{pmatrix} \dot{R}_{AH} \\ \dot{R}_{HB} \\ 0 \end{pmatrix} = \begin{pmatrix} -1 & 1 & 0 \\ 0 & -1 & 1 \\ m_A & m_H & m_B \end{pmatrix} \begin{pmatrix} \dot{x}_A \\ \dot{x}_H \\ \dot{x}_B \end{pmatrix} \tag{3.11}$$

where the third relation means that the total momentum of the system shall be zero. On inversion

$$\begin{pmatrix} \dot{x}_A \\ \dot{x}_H \\ \dot{x}_B \end{pmatrix} = \begin{pmatrix} -(m_H + m_B)/M & -m_B/M & 1/M \\ m_A/M & -m_B/M & 1/M \\ m_A/M & (m_A + m_H)/M & 1/M \end{pmatrix} \begin{pmatrix} \dot{R}_{AH} \\ \dot{R}_{HB} \\ 0 \end{pmatrix} \tag{3.12}$$

where $M = m_A + m_H + m_B$. Substituting this relation between internal coordinates and cartesian coordinates in the kinetic energy T in eq. (3.9) one obtains the Lagrange equations (3.7) in the form

$$\begin{aligned} &m_A/M^2(m_H^2 + 2m_Hm_B + m_B^2 + m_Am_H + m_Am_B)\ddot{R}_{AH} + m_A/(2M^2) \\ &\quad \times (2m_B^2 + 2m_Am_B + 2m_Hm_B)\ddot{R}_{HB} + f_{AH}R_{AH} + f_{AH,HB}R_{HB} = 0 \\ &m_B/M^2(m_H^2 + 2m_Am_H + m_A^2 + m_Hm_B + m_Am_B)\ddot{R}_{HB} + m_A/(2M^2) \\ &\quad \times (2m_B^2 + 2m_Am_B + 2m_Hm_B)\ddot{R}_{AH} + f_{HB}R_{HB} + f_{AH,HB}R_{AH} = 0. \end{aligned} \tag{3.13}$$

This coupled system of linear second order differential equations has solutions

$$\begin{aligned} R_{AH} &= C_{AH}\cos 2\pi\nu t \\ R_{HB} &= C_{HB}\cos 2\pi\nu t. \end{aligned} \tag{3.14}$$

As the result of a secular problem two vibrational frequencies ν are obtained and two corresponding eigenvectors $\boldsymbol{C}$ which describe the modes.

The most important quantities arising out of the analysis are the

eigenvectors $\boldsymbol{C}$ which approximately describe the kind of vibration. In general the pure harmonic approximation is not very good for calculating the vibrational wave numbers of H-bonds. However, if one uses the normal modes as a first approximation, continued by further computational improvements the real vibrational motions are able to be characterised in most cases by means of the terminology of the normal modes.

In contrast to eq. (3.6) it should be noted that eq. (3.7) is classical in origin and so does not provide vibrational states. Only the fundamental vibrations in the harmonic approximation are common to both classical and quantum mechanics.

3.2.2. Theory of vibrational states of H-bonds

In solving eq. (3.6) the use of Jacobian coordinates is advantageous. In the case of unsymmetrical H-bonds AH···B which are in general neutral and weak, experience suggests that the atomic distances AH and AB may be used as normal coordinates, if a one-dimensional treatment for the vibrations is applied. The third term in eq. (3.8) is then negligibly small and the transformation from internal Jacobians to normal coordinates may be neglected. In spite of this one has to take care with the corresponding reduced masses which will be stated later in eq. (3.16). The notion "unsymmetrical" H-bond is referred to the shape of the potential energy for the proton, so that the system AH···A may have an unsymmetrical H-bond. The water dimer is an example.

In the case of symmetrical H-bonds $A_1\cdots H\cdots A_2$ which are ionic and strong bonds, the normal coordinates are as follows:

$$\begin{pmatrix} q_1 \\ q_2 \end{pmatrix} = \begin{pmatrix} \frac{1}{2} & -\frac{1}{2} \\ 1 & 1 \end{pmatrix} \begin{pmatrix} R_{A_1H} \\ R_{A_2H} \end{pmatrix} \tag{3.15}$$

where q_1 measures the proton shift from the middle of the bridge and q_2 is the A_1A_2 distance. Now the middle of the bridge is the centre of mass and therefore q_1, q_2 are Jacobian coordinates. The notion symmetrical H-bonds implies identical units A_1, A_2.

The reciprocal reduced masses are

$$\begin{aligned} 1/m_{q_1} &= 1/m_H + 1/(m_A + m_B) \\ 1/m_{q_2} &= 1/m_{AH} + 1/m_B \end{aligned} \quad \text{and} \quad \begin{aligned} 1/m_{q_1} &= 1/m_H + 1/(m_{A_1} + m_{A_2}) \\ 1/m_{q_2} &= 1/m_{A_1} + 1/m_{A_2} \end{aligned} \tag{3.16}$$

for the unsymmetrical and the symmetrical case, respectively. Hence in the Schroedinger equation (3.6) no coupled terms in q_1 and q_2 appear in

the kinetic energy. In atomic units this equation has the form

$$\left[-\frac{1}{2}\left(\frac{1}{m_H}+\frac{1}{m_A+m_B}\right)\frac{\partial^2}{\partial q_1^2}-\frac{1}{2}\left(\frac{1}{m_{AH}}+\frac{1}{m_B}\right)\frac{\partial^2}{\partial q_2^2}+V(q_1,q_2)\right]\chi(q_1,q_2) = \lambda\chi(q_1,q_2) \quad (3.17)$$

Numerous authors have treated eq. (3.17) particularly for a simple one-dimensional case $m_A = m_B = \infty$, $q_2 =$ constant, where different analytical representations of the potential energy $V(q_1)$ have been tried. Some of these methods will now be outlined.

Manning [1935] has shown, that using the potential energy

$$V = -C\ \mathrm{sech}^2(q_1/2\rho) + D\ \mathrm{sech}^4(q_1/2\rho), \quad (3.18)$$

where C, D and ρ are parameters, eq. (3.17) can be solved in an analytical exact manner. The parameters C, D and ρ are varied, so that the measured doublets due to the inversion of the NH_3 molecule are reproduced. In such a way the height of barrier of the double well potential energy of the NH_3 inversion has been obtained. Wall and Glockler [1937] have investigated the NH_3 inversion using the potential energy

$$V = \tfrac{1}{2}k(|q_1| - l)^2, \quad (3.19)$$

which is certainly a poor approximation in the range of the energy barrier. Indeed, the NH_3 inversion has no relation to H-bonds; but the double well potential energy of the inversion as it is assumed in specific cases for the proton motion in H-bonds, is a useful object for testing different representations of the potential energy.

Baker [1954] has used two Morse curves which represent the potential energy for the proton in the H-bond. The parameters contained in this function are taken from experimental data. Lippincott and Schroeder [1955] have added a repulsion term and a term to describe the electrostatic interaction.

$$V = D\{1-\exp[-n(\Delta r)^2/2r]\} + D^*\{1-\exp[-n^*(R-r-r_0^*)^2/2(R-r)]\} - D^* + A\exp(-bR) - B/R^m. \quad (3.20)$$

$R = O\cdots O$ and $r = OH$ are atomic equilibrium distances in the system $OH\cdots O$. The authors discuss the relations $r(R)$ and $\Delta\omega(R)$, where $\Delta\omega$ is the wave number shift of the OH group. Reid [1959] has used a similar potential function

$$V = U(r) + U'(R-r) + W_R. \quad (3.21)$$

The functions U, U' are Morse curves and W_R describes the O···O interaction. Haas and Hornig [1960] have shown that the calculation of the tunneling wave number requires the consideration of the O···O vibration by means of the distribution function

$$F(R) = (\beta/\pi)^{1/2} \exp\left[-\beta(R - R_0)^2\right], \tag{3.22}$$

where $\beta = 4\pi^2\mu\nu_0/h$. Hence the tunneling frequency is

$$\Delta\nu = \nu \int_0^\infty F(R) \exp\left\{-2\int_a^b \hbar^{-1}[2m(V-E)]^{1/2}\,\mathrm{d}x\right\}\mathrm{d}R. \tag{3.23}$$

An investigation of the symmetrical double well potential using a polynomial representation has been made by Gerson [1961].

$$V(q_1) = q_1^6 - v_2 q_1^2. \tag{3.24}$$

The Schroedinger equation has been solved approximately by means of a variational method using a linear combination of mutually orthogonal oscillator functions $u_n(q_1)$.

$$\chi(q_1) = \sum_{n=0}^{N-1} c_n u_n(q_1), \tag{3.25}$$

where $N = 120$ and n is a quantum number. Somorjai and Hornig [1962] have also used a polynomial representation

$$V(q_1) = v_2 q_1^2 + v_3 q_1^3 + v_4 q_1^4, \tag{3.26}$$

with v_2, v_3, v_4 as variational parameters. Brickmann and Zimmermann [1966, 1967, 1969] have also performed model calculations using a potential energy of the type (3.26). Further model treatments of this kind have been conducted by Heilbronner et al. [1956, 1959]. Ibers [1964] was the first to use an energy surface for the potential energy including the proton motion (q_1) as well as the H-bond stretching vibration (q_3). This surface has the form

$$V(q_1, q_3) = a_1 q_1^2 + a_3 q_3^2 + a_4 q_3^4 + a_{13} q_1 q_3^2, \tag{3.27}$$

where the parameters a_n have been adjusted to fit experimental data. The Schroedinger equation is solved by means of eq. (3.25), with the basis functions taken as products of oscillator functions

$$u_k(q_1) v_l(q_3). \tag{3.28}$$

Marechal and Witkowski [1968] have examined unsymmetrical weak

H-bonds XH···Y under the condition that $\nu_{XH} \gg \nu_{X\cdots Y}$ which allows the adiabatic approximation to be adopted for these two vibrations. Starting from the Hamiltonian

$$H(q, Q) = (P^2/2M) + (p^2/2m_H) + U(q, Q) = P^2/2M + h(q, Q) \tag{3.29}$$

where q, Q are the XH distance and the X···Y distance, respectively, the eigenfunctions Ψ have the form

$$\Psi = \sum_n \alpha_n(Q)\, \phi_n(q, Q). \tag{3.30}$$

The wave functions $\phi_n(q, Q)$ describe the q-motion, when Q is fixed, and satisfy the following Schroedinger equation

$$h\, \phi_n(q, Q) = E_n(Q)\, \phi_n(q, Q). \tag{3.31}$$

The harmonic potential energy is of the form

$$U(q, Q) = \tfrac{1}{2}k(Q)[q - q_0(Q)]^2 + U'(Q). \tag{3.32}$$

Hence the XH equilibrium distance q_0 as well as the XH force constant k are functions of the X···Y distance Q. The wave functions α_n^l, which describe the X···Y motion, where l is the quantum number of this motion, satisfy the Schroedinger equation

$$H_n\alpha_n^l = [P^2/2M + E_n(Q) + \langle \phi_n(q, Q)|P^2/2M|\phi_n(q, Q)\rangle_q]\alpha_n^l = E_n^l\alpha_n^l. \tag{3.33}$$

The total wave function Ψ in the adiabatic form in eq. (3.30) is

$$\Psi_n^l = \alpha_n^l(Q)\, \phi_n(q, Q). \tag{3.34}$$

The difference between the two Hamiltonians H_1 and H_0 from eq. (3.33) may be obtained by developing $\omega_H(Q)$ and $q_0(Q)$ in powers of Q.

$$H_1 - H_0 \approx \text{const} + (\mathrm{d}\omega_H/\mathrm{d}Q)_{Q_0}Q + (\mathrm{d}q_0/\mathrm{d}Q)_{Q_0}Q + \cdots \tag{3.35}$$

The quantities ω_H, $\omega_{X\cdots Y}$, $(\mathrm{d}\omega_H/\mathrm{d}Q)_{Q_0}$, $(\mathrm{d}^2\omega_H/\mathrm{d}Q^2)_{Q_0}$ and $(\mathrm{d}q_0/\mathrm{d}Q)_{Q_0}$ are taken from measured spectra.

Singh and Wood [1968] have performed model studies using a potential energy of the form (3.27). Their expansion (3.25) runs up to 144 basis functions. The effect of vibrational coupling is outlined in detail. This coupling due to the cross term in the potential energy (3.27) influences the resulting vibrational states and their transition wave numbers, and even

generates new types of transition. Brickmann and Zimmermann [1971] have calculated by means of the model potential

$$V(q_1, q_3) = \sum_{l=0}^{4} (\alpha_l + \beta_l q_3^2) q_1^l \tag{3.36}$$

proton states in the two-dimensional double well potential. Here q_1 is the proton coordinate in the direction of the H-bond and q_3 is the coordinate of the bending vibration which is perpendicular to q_1. The Schroedinger equation has been solved approximately with 112 basis functions of the type (3.28) and $k = 0, \ldots, 27$; $l = 0, \ldots, 3$.

The first H-bonded system for which the Schroedinger equation (3.6) has been solved in detail is the dihydrated proton $(H_2OHOH_2)^+$ (Janoschek et al. [1972]). The main difference between that calculation and the model studies just discussed is that the potential energy is no longer assumed in an analytical expression, but is obtained from a solution of eq. (3.3). This essential difference between model studies and ab initio calculations is emphasised by the fact that none of the potential representations so far used is useful for the interpolation of the numerical potential energy in the range of motion of the proton. For that reason the potential energy was taken into account by numerical methods (piecewise polynomial approximation). This procedure is only useful in the case of one-dimensional problems (potential curves). Including more than one dimension (potential surfaces) the global polynomial approximation is indispensable.

The Schroedinger equation (3.6) can be solved approximately using a linear combination of oscillator functions (3.25), or in the case of more dimensions by means of corresponding products of oscillator functions (3.28). The solutions will then be said to be exact, if the expansion (3.25) arrives at the limit of convergence of the resulting eigenvalues. Singh and Wood [1968] have used 144 basis functions for two dimensions and so the number of basis functions seems to be the limiting factor for more extensive computations, and in particular for three dimensions. For that reason Janoschek et al. [1972] have introduced non-orthogonal basis functions in order to accelerate the convergence of the vibrational states with increasing number of basis functions. In the case of symmetrical or slightly unsymmetrical double well potentials the oscillator functions are localised in the potential minima, which is a better starting approximation than orthogonal functions in the region of the energy barrier. The expansion coefficients c_r in the linear combination (3.25) for the descrip-

tion of the vibrational states satisfy the secular equations

$$\sum_{r=1}^{N} (H_{sr} - \lambda S_{sr}) c_r = 0 \tag{3.37}$$

where H_{sr} is an energy matrix element and S_{sr} is an overlap matrix element of the basis functions s and r. After diagonalising first S and then H the resulting energy levels λ_t are obtained and the corresponding eigenfunctions

$$\chi_t = \sum_{r=1}^{N} c_{rt} u_r. \tag{3.38}$$

Besides accelerating the convergence, the use of non-orthogonal basis functions has a further advantage. Especially in the case of slightly unsymmetrical energy curves or surfaces, an identification of the vibrational states is easily found from the resulting expansion coefficients in the eigenfunctions, which allow one to estimate the number and the shape of the node lines of χ_t. The oscillator functions are of the form

$$u_j^{ni}(q - q_i) = \sqrt{\frac{1}{2^n n!}} \sqrt{\frac{\alpha_j}{\pi}} \exp\left[\tfrac{1}{2}\alpha_j (q - q_i)^2\right] \times \left(-\frac{1}{\sqrt{\alpha_j}}\right)^n \frac{\mathrm{d}^n \exp\left[-\alpha_j (q - q_i)^2\right]}{\mathrm{d}(q - q_i)^n} \tag{3.39}$$

where n is the quantum number and α_j, q_i are free parameters. Janoschek et al. [1973] has also extended the use of non-orthogonal basis functions to the treatment of H-bonds including two dimensions. In the case of single minimum potentials the basis ordered in a triangular scheme

$$\begin{array}{llll} u_1^0 u_2^0 & u_1^0 u_2^1 & \cdots & u_1^0 u_2^N \\ u_1^1 u_2^0 & u_1^1 u_2^1 & \cdots & \\ \vdots & & & \\ u_1^N u_2^0 & & & \end{array} \tag{3.40}$$

satisfies the convergence as well as a full rectangular $N \times N$ scheme. The upper indices indicate the quantum numbers (Janoschek [1973b]). All these improvements are able to give consistent results up to the second overtones within a two-dimensional problem.

So far the method of energy variation has been described in order to solve the Schroedinger equation. This method is able to give us exact results if a sufficiently large number of basis functions is taken. Sandorfy

[1972] has examined the relations between measured spectra and the anharmonicity using the second order perturbation theory. Starting with the harmonic oscillator, the anharmonicity in the potential energy

$$V'(q) = k_3 q^3 + k_4 q^4 \tag{3.41}$$

is considered as a small perturbation (ch. 13). However, there is some uncertainty in the application of the perturbation theory on H-bonds, because the assumption of a small anharmonicity is no longer valid for the case of moderately strong H-bonds.

Janoschek [1973b] and Weidemann et al. [1974] have examined the validity of the perturbation approach by comparing such results with those from exact calculations.

3.2.3. Theory of IR absorption intensities

The fundamental quantity in the calculation of vibrational states and wave numbers is the potential energy $E(\boldsymbol{R})$ of the nuclear motion. The corresponding function for the calculation of IR absorption intensities of vibrational transitions is the dipole moment as a function of the nuclear positions $\boldsymbol{\mu}(\boldsymbol{R})$. The use of dipole moments in the context of H-bonds has been neglected considerably in the past. Since the dipole moments are readily accessible such neglect is unwarranted. Knowledge of the dipole moment provides a clarification of many important effects, such as the increase of intensity of the AH fundamental transition or the decrease of intensity of the corresponding overtone on the formation of a H-bond AH···B.

Bertie and Millen [1965] have shown that there must be a so called electrical anharmonicity in the dipole moment function which is an analogy of the mechanical anharmonicity in the potential energy. Both of them are necessary in discussing spectral properties of H-bonds. The term "electrical anharmonicity" refers to all non-linear terms in the dipole moment. For a two-dimensional problem the dipole moment is represented by the expansion

$$\boldsymbol{\mu}(q_1, q_2) = \sum_{k,l} b_{kl} q_1^k q_2^l. \tag{3.42}$$

By means of $\boldsymbol{\mu}(q_1, q_2)$ and the eigenfunctions χ_i in eq. (3.38) the dipole transition moments are obtained as

$$\boldsymbol{\mu}_{ij} = \langle \chi_i | \boldsymbol{\mu}(q_1, q_2) | \chi_j \rangle \tag{3.43}$$

when the relative transition probabilities are

$$A_{ij} = \bar{\nu}_{ij} \boldsymbol{\mu}_{ij}^2 \tag{3.44}$$

where $\bar{\nu}_{ij}$ is the wave number of the transition $i \to j$. The relative absorption intensity at the temperature T is given by

$$I_{ij} = A_{ij} \exp(-\lambda_i/kT) \Big/ \sum_n \exp(-\lambda_n/kT). \tag{3.45}$$

Gerson [1961] has calculated transition moments $\langle \chi_i | q_1 | \chi_j \rangle$ and the corresponding IR absorption intensities with the assumption of rigid electrons during the proton motion, which is not valid as will be shown later (bare proton model). Singh and Wood [1968] have used a dipole moment in their model of the form (3.42)

$$\boldsymbol{\mu}(q_1, q_3) = b_{10} q_1 + b_{11} q_1 q_3 \tag{3.46}$$

while Janoschek et al. [1972, 1973] have calculated IR absorption intensities of several H-bonds by means of a pointwise given dipole moment resulting from eq. (3.3). The only possible form of representation was found to be

$$\boldsymbol{\mu}(q_1, q_2) = b_{10} q_1 + b_{30} q_1^3 + b_{11} q_1 q_2 \tag{3.47}$$

for symmetrical H-bonds, whilst a parabolical interpolation was sufficient in the case of weak unsymmetrical H-bonds.

As a general result it should be emphasized, that H-bonded systems hold an exceptional position in vibrational spectroscopy, since the force constant f by itself is unsuitable for discussing vibrational wave numbers $\bar{\nu}$, and the first derivatives of the dipole moment with respect to the coordinates of motion $\partial \boldsymbol{\mu} / \partial q_i$ are improper for the prediction of intensities I. This means, that the familiar relationships

$$\nu \sim \sqrt{f} \qquad \text{and} \qquad I \sim (\partial \boldsymbol{\mu} / \partial q)^2 \tag{3.48}$$

are no longer valid for strong H-bonds.

Perturbation theory also provides analytical expressions for IR intensities which contain the parameters of the potential energy (3.41) as well as those of the dipole moment (3.42) (ch. 13, eq. (3.22)). Sandorfy [1972] has used that formalism in order to get potential and dipole moment constants by fitting experimental data. The results provide a good insight into the effects of mechanical and electrical anharmonicity upon intensities.

Marechal and Witkowski [1968] and Leviel and Marechal [1971] have used in their model a linear dipole moment function for weak H-bonds and have fitted measured spectra in the fundamental range. The dipole transition moments are then given by

$$P_l^{l'} = |\langle \Psi_0^{l'}(q, Q)|cq + c'Q|\Psi_1^{l}(q, Q)\rangle_{q,Q}|^2 \tag{3.49}$$

which simplifies to be

$$P_l^{l'} = c^2|\langle \alpha_0^{l'}(Q)|\alpha_1^{l}(Q)\rangle|^2$$

when eq. (3.34) is used.

3.2.4. H-BONDS AND EXTERNAL ELECTROSTATICAL FIELDS

Besides the calculation of IR intensities the dipole moment surface (3.42) is of further importance for the H-bond. An electrical field $\boldsymbol{F}$ leads to an additional term in the Hamiltonian of the type

$$\boldsymbol{F}\left(\sum_i r_i - \sum_k Q_k \boldsymbol{R}_k\right). \tag{3.50}$$

Here r_i is the position vector of the ith electron and $\boldsymbol{R}_k$ is the position vector of the kth nucleus. Solving eq. (3.3), including the contribution (3.50) yields the induced dipole moment of the electron distribution as a function of nuclear positions $\boldsymbol{R}$ and the field $\boldsymbol{F}$.

$$\boldsymbol{\mu}_{\text{ind}}^{\text{el}}(\boldsymbol{R}, \boldsymbol{F}). \tag{3.51}$$

For the case of molecules with valence bonds the effect of fields up to $5 \cdot 10^7$ V/cm on the equilibrium geometry is negligible, so that eq. (3.51) alone represents the induced dipole moment and hence the operator for vibrational Raman transitions. For H-bonded systems, however, the situation can be precisely the opposite. Namely, an electrical field can change the equilibrium position of the proton very strongly, so that the induced dipole moment will be caused mainly by the proton shift, whereas that of the electrons (3.51) is negligible. In the second case the term in the potential energy due to the field now appears only in eq. (3.6) as

$$-\boldsymbol{\mu}(\boldsymbol{R}) \cdot \boldsymbol{F}. \tag{3.52}$$

This means that the effect of an electrical field on the electrons may be negligible in contrast to the effect of the moving proton on the electrons (Janoschek et al. [1972]). This fact makes the computation of induced

dipole moments considerably simpler, because $\boldsymbol{\mu}(\boldsymbol{R})$ in eq. (3.52) results when eq. (3.3) is solved without an external field.

The exceptional origin for the induced dipole moment of H-bonds may have an influence upon vibrational Raman transitions. Consider a symmetrical H-bond A···H···A, for which the symmetrical H-bond stretching vibration and the antisymmetrical proton vibration are liable to the frequency condition $\nu_a \gg \nu_s$; under the adiabatic approximation the operator for Raman transitions for the symmetrical vibration is

$$\boldsymbol{\mu}^{a}_{ind}(q_s, \boldsymbol{F}) \tag{3.53}$$

where the integration with respect to q_a has already been performed. This "nuclear" Raman effect may be important for H-bonds, because $\boldsymbol{\mu}^{a}_{ind}$ may be occasionally high which implies a comparably high Raman intensity of the H-bond stretching vibration (Janoschek [1973a]).

The occasionally high polarisability of H-bonds is responsible for the induction interaction with the surrounding molecules or ions, as will be discussed later in section 15.5.

Besides Raman spectroscopy the effect of electrical fields has a further spectroscopic importance in that surrounding ions cause strong wave number and IR intensity shifts in H-bonds. This can easily be seen in applying the Stark effect on the two lowest proton states. As a result of a second order perturbation treatment for the shift of two non-degenerate levels we get λ_0 and λ_1 with $\lambda_1 > \lambda_0$, and for a sufficiently small field strength $\boldsymbol{F}$ we get

$$\Delta\lambda_{0,1} = \pm \frac{\boldsymbol{\mu}^{2}_{01}\boldsymbol{F}^2}{\lambda_0 - \lambda_1} \tag{3.54}$$

where the plus sign is correlated with $\Delta\lambda_0$ and the minus sign with $\Delta\lambda_1$; $\boldsymbol{\mu}_{01}$ is the dipole transition moment of the states 0 and 1. For most systems, such as molecules, the Stark effect in the sense of eq. (3.54) plays no important role. Equation (3.54), however, implies the importance of the Stark effect when applied to proton states in H-bonds. Namely, for the two lowest proton states 0 and 1 the denominator in eq. (3.54) is small compared with other molecules, and furthermore the square of the transition moment $\boldsymbol{\mu}^{2}_{01}$ in the denominator may be much higher than that which is usually found (Janoschek et al. [1972]). By means of the relation

$$\Delta E = \tfrac{1}{2}\alpha F^2 \tag{3.55}$$

where ΔE is the change of energy and α is the polarisability, eq. (3.54)

contains the polarisabilities in the form

$$\alpha_{0,1} = \pm \frac{2\mu_{01}^2}{\lambda_0 - \lambda_1}. \tag{3.56}$$

Hence the two lowest proton states will be polarised in two opposite directions, which is true even for small field strengths. Weidemann and Zundel [1970] have discussed the polarisability

$$\alpha(T) = (2\mu_{01}^2/h\Delta\bar{\nu}) \tanh(h\Delta\bar{\nu}/2kT) \tag{3.57}$$

as a function of the temperature T within the model of the symmetrical double well potential, where $\Delta\bar{\nu} = (\lambda_1 - \lambda_0)/h$ is the tunneling wave number. Equation (3.57) is seen to be a result of thermal averaging of the polarisabilities in eq. (3.56).

Considering eq. (3.54) and taking more than two states into account should result in numerous level crossings due to the opposite directions of polarisability, but this is prevented by the non-crossing rule. On approach of the energy levels, Fermi resonances are caused in which more than two states can also participate. Janoschek et al. [1973] have shown that Fermi resonance is one of the possible origins of the complicated structure of H-bond spectra.

3.2.5. Effects of deuteration

Comparing the spectra of weak unsymmetrical H-bonds with the spectra of the corresponding D-bonds to a first approximation, a frequency ratio of $\nu_H/\nu_D = \sqrt{2}$ is explained by the dominating harmonicity of the potential energy of the proton to the deuteron. Bertie and Millen [1965] have examined, in their model studies, the influence of deuteration on the change of combination transitions which are caused by the two kinds of anharmonicity. More distinct effects appear in the case of strong symmetrical H- and D-bonds. Some results shall be discussed later where wave number and intensity shifts due to deuteration are of interest.

A further effect of deuteration of H-bonds concerns the change of the H-bond length. Singh and Wood [1969] have shown by means of a two-dimensional model, that this effect has a dynamical origin and is caused by the coupling of the two stretching vibrations.

3.2.6. Simultaneous proton motions in H-bonds

In many cases, when only a single H-bond is taken into account, the spectroscopic behaviour of H-bonds is not explained sufficiently. Di

Paolo et al. [1972] have shown in model studies, that in some cases the intensity distribution can only be explained by means of interactions between several H-bonds. Weidemann and Zundel [1967] have assumed proton dispersion forces between H-bonds and have performed model calculations, which will be presented in ch. 5. A global account of the environment of a H-bond by means of a specific range of an electrical field and a range of equilibrium H-bond lengths have been used in an ab initio treatment by Janoschek et al. [1972], where in place of line spectra more real broad bands result. A two-particle ab initio treatment of the simultaneous proton motions of two H-bonds has also been investigated by Janoschek [1973b]. The strength of the coupling can be discussed by the calculated spectra in comparing with that of an isolated H-bond.

Hartmann [1972] has shown that the Hartree equations for two coupled linear harmonic oscillators may be solved exactly, but the resulting wave function is identically equal to that of the uncoupled problem. Therefore the Hartree method alone is not a useful method for solving eq. (3.6). Accordingly, only a "nuclear" CI calculation (configuration interaction) will provide a satisfactory solution of eq. (3.6). Using 120 configurations of the form (3.28) convergence may be achieved upon the six lowest states, labeled by the quantum numbers 00, 10, 01, 20, 11, 02.

3.3. Applications

Within this section only those calculations on H-bonds which yield vibrational wave number intensities or at the least potential parameters are considered.

$(HeHHe)^+$. For this system eq. (3.3) has been solved approximately by means of pure Gaussians (SCF–MO–LCGO method), where linear symmetric, linear asymmetric and bent configurations have been taken into account. The equilibrium geometry is found to be linear and symmetric with an HeH distance of 0.939 Å. The H-bond binding energy corresponding to the dissociation products HeH^+ and He respectively is 7.9 kcal/mole. The complete set of normal wave numbers has been obtained using the harmonic approximation; 1105 cm^{-1} (Σ_g^+), 1312 cm^{-1} (Σ_u^-), 1259 cm^{-1} (Π_u) (Swanstrom et al. [1969]).

$(BeHBe)^+$. In this case eq. (3.3) has been solved again by means of the above method. The calculated equilibrium geometry is linear and symmetric with a BeH distance of 1.609 Å. The H-bond binding energy corresponding to BeH^+ and Be is found to be 7.0 kcal/mole. The normal wave

numbers within the harmonic approximation are 436 cm^{-1} (Σ_g^+), 619 cm^{-1} (Σ_u^-), 1627 cm^{-1} (Π_u) (Janoschek et al. [1968]).

$(FHF)^-$. This system represents the strongest of all H-bonds as yet discovered. Due to the numerous measurements upon this H-bond it provides a useful test for many theoretical investigations.

The first theoretical treatment of the normal frequencies using the harmonic approximation has been performed by Hartmann [1966]. However, crude simplification was used to solve eq. (3.3) and the calculated data have lost the desired accuracy. For instance the H-bond energy corresponding to FH and F^- of 263 kcal/mole exceeds the measured value of 58 kcal/mole by more than a factor four. The following wave numbers have been obtained: 995 cm^{-1} (Σ_g^+), 2948 cm^{-1} (Σ_u^-), 2003 cm^{-1} (Π_u). Comparison with the measured wave numbers 600, 1450 and 1222 cm^{-1} (Ketelaar and Vedder [1951]) shows enormous discrepancies. However, these deviations are not caused by the different environments of the H-bonds, that is, the calculated system is an isolated H-bond whereas the measurements are made on a crystal; the already mentioned approximations which have been used in eq. (3.3) and the harmonic approximation, drastically effect the vibrational frequencies.

The best proof for this assertion are the ab initio calculations of Almlöf [1972] which are based on an accurate SCF–MO–LCGO treatment. A set of 27 linear configurations for the system $(FHF)^-$ yields the following potential energy:

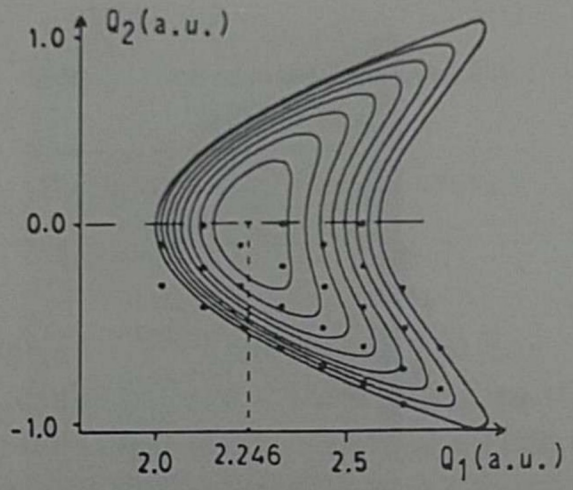

Fig. 3.1. Potential energy surface for the bifluoride ion. The energy levels are drawn at 2(2)16 kcal/mole. The dots indicate geometries for which the energies were calculated.

TABLE 3.1

Coefficients for the potential surface polynomial

m	n	a_{mn} (au)
1	0	0.00000
2	0	0.0939
3	0	−0.0520
0	2	0.0323
0	4	0.2083
0	6	0.0447
1	2	−0.2829
2	2	0.2139
1	4	−0.2283

The potential energy is of the form $V = \Sigma_{m,n} a_{mn} q_1^m q_2^n$ where $q_1 = \boldsymbol{R}_{F(1)H} + \boldsymbol{R}_{HF(2)}$ and $q_2 = \boldsymbol{R}_{F(1)H} - \boldsymbol{R}_{HF(2)}$. Equation (3.6) has been solved by the use of 160 basis functions of the form eq. (3.28) which were ordered in a 10×16 rectangular scheme similar to that of (3.40). The equilibrium geometry corresponds to a F···F distance of 2.246 Å which is in reasonably good agreement with the measured value of 2.28 Å, with the proton found to be in the middle of the bond. The set of calculated frequencies is in very good agreement to the corresponding observed wave numbers for the crystal (Ketelaar [1941]).

TABLE 3.2

Calculated and observed wave numbers of $(FHF)^-$

Calculated (cm^{-1})	Observed (cm^{-1})
660	595, 604
1497	1450
2070	2045
2632	2618
3226	3126
3916	3825
4750	4830
5157	5099

Jiang and Anderson [1973] have interpolated ab initio results using a potential energy of the form eq. (3.20). Starting with the calculations of Almlöf [1972] the symmetric as well as the asymmetric nuclear motion has been treated as a one-dimensional problem. By this approximation a loss of accuracy of the resulting wave numbers is noticed. Also all transitions which are caused by the coupling of the motions involved are lost in one-dimensional treatments. In spite of this fact it is interesting to note the frequencies of the asymmetric stretching vibration:

$$\bar{\nu}_a = 1490\ \mathrm{cm}^{-1}, 2\bar{\nu}_a = 5650\ \mathrm{cm}^{-1}.$$

These data show a ratio of 3.8 between the first overtone and the fundamental which is caused by the extreme anharmonicity.

Noble and Kortzeborn [1970] have examined the importance of the anharmonicity in the potential energy. Starting with the representation

$$V = a_{02}q_2^2 + a_{20}q_1^2 + a_{40}q_1^4 + a_{21}q_1^2q_2 + a_{03}q_2^3 + a_{04}q_2^4$$

where q_1, q_2 have the same meaning as in eq. (3.15) the following potential parameters have been obtained:

TABLE 3.3

Coefficients for several potential surface polynomials

	a_{02}	a_{20}	a_{40}	a_{21}	a_{03}	a_{04}
(a)	1.37	0.15	0.50	−1.72	−0.95	2.55
(b)	1.655	0.11	0.74	−2.08		
(c)	1.235	0.001	19.0	−10.2	0.99	22.9
(d)	1.495	0.47	11.77	−8.78		
(e)	1.41	1.47				
(f)	1.425	2.14	15.2	61.0		
(g)	1.02	0.325	4.90	−1.73		
(h)	1.32	0.28	8.37	−5.52		

All parameters are measured in units mdyne and Å or the corresponding combinations. The results (a) and (b) are based on the calculations of McLean and Yoshimine [1967] using 21 points; (c) and (d) are the results of Noble and Kortzeborn [1970] using 10 and 9 points, respectively; (e) and (f) are those of 6 points. The potential (g) is that of the earlier mentioned empirical estimation of Ibers [1964] and which has been

corrected by Delaplane and Ibers [1968]; (h) are the results of Kollman and Allen [1970a].

Table 3.3 shows that the potential parameters for different analytical representations of an energy surface are only of little importance. This fact is also true for the force constants a_{02} and a_{20}. Furthermore the same analytical representations such as (a) and (c) are unable to be compared. For instance the small value of a_{20} in (c) may be compensated by the large values of a_{40} and a_{21} so that at the end both representations of the potential energy may have comparably the same accuracy. We can draw the conclusion that only the calculated vibrational frequencies are able to yield a global judgement for the accuracy of the representation. In other words, the assignment of wave numbers which are integral quantities, to the potential parameters which are differential quantities, is ambiguous in the case of more than one independent variable.

Recently calculated vibrational transition intensities have not been available for the system $(FHF)^-$.

$(FDF)^-$. This system has been investigated within the harmonic approximation by Hartmann [1966]. The neglect of vibrational coupling gives exactly the same F···F vibration as in the system $(FHF)^-$. The wave numbers of the D vibration are 2112 cm^{-1} (Σ_u^-), 1434 cm^{-1} (Π_u). Ketelaar and Vedder [1951] have observed 1046 and 891 cm^{-1}. The agreement of the calculated with the observed ratio $\bar{\nu}_H/\bar{\nu}_D$ of the corresponding vibrations shows that the energy surface has a distinct single minimum.

Almlöf [1972] has calculated several wave numbers which are in good agreement with the observed values. Due to the vibrational coupling the totally symmetric vibration shows a slightly different wave number when compared with $(FHF)^-$ (table 3.4). The empirical treatment of Ibers [1964] yields wave numbers which are all smaller than the observed values although the potential energy has been adjusted via the observed wave numbers of $(FHF)^-$.

$(ClHCl)^-$. For this system ab initio calculations have been performed by Janoschek [1973a]. Nibler and Pimentel [1967] have stated different wave numbers for different kinds of the surrounding cations. In contrast to $(FHF)^-$ this H-bond is a relatively weak bond so that the cations are able to influence the vibrational structure. Janoschek [1973a] has tried to take the environment into account, so that besides the isolated system $(ClHCl)^-$ the two systems $H^+(ClHCl)^-H^+$ as well as $H(ClHCl)^-H$ have been examined. The two additional protons in the two latter systems have

TABLE 3.4
Calculated and observed wave numbers of $(FDF)^-$

Calculated (cm^{-1})	Observed (cm^{-1})
666	631
1038	1046
1628	1597
2194	2070
2756	2744–2767
3371	3300
3547	3561
4088	4115
4144	—
5011	5099

been fixed at distances of 2 Å, respectively, from the neighbouring chlorine atoms. The energy and dipole moment surfaces for the free H-bond and the first stated protonated H-bond are almost superimposable, whereas the latter protonated H-bond shows essential deviations when compared with the isolated $(ClHCl)^-$. These are mainly concerned with the Cl···Cl distance and with the slope of the dipole moment. The different behaviour of the dipole moment is illustrated in fig. 3.4. This behaviour of the dipole moment can be interpretated in terms of the electron density along the H-bond axis. In the first case the shift of the electrons is opposite in direction to the proton shift, whilst in the second case the electron density shift follows the proton motion (fig. 3.5).

For all the above mentioned systems vibrational spectra have been calculated by means of the potential energy in fig. 3.2 and the dipole moment in fig. 3.3. In addition the influence of external electrostatic fields on these spectra has been examined. For the latter double protonated H-bond, a region of absorption in the range of 1600–2700 cm^{-1} results. The calculated wave numbers and absorption intensities as functions of the temperature and the field strength are represented in table 3.5.

The totally symmetric Cl···Cl vibrations have Raman intensities listed in table 3.6 as obtained by the use of eq. (3.53). According to these results the latter double protonated H-bond should have a comparably high vibrational Raman intensity for the motion involved. Table 3.7 is a summary of theoretical results and crystal data (last column, Nibler and

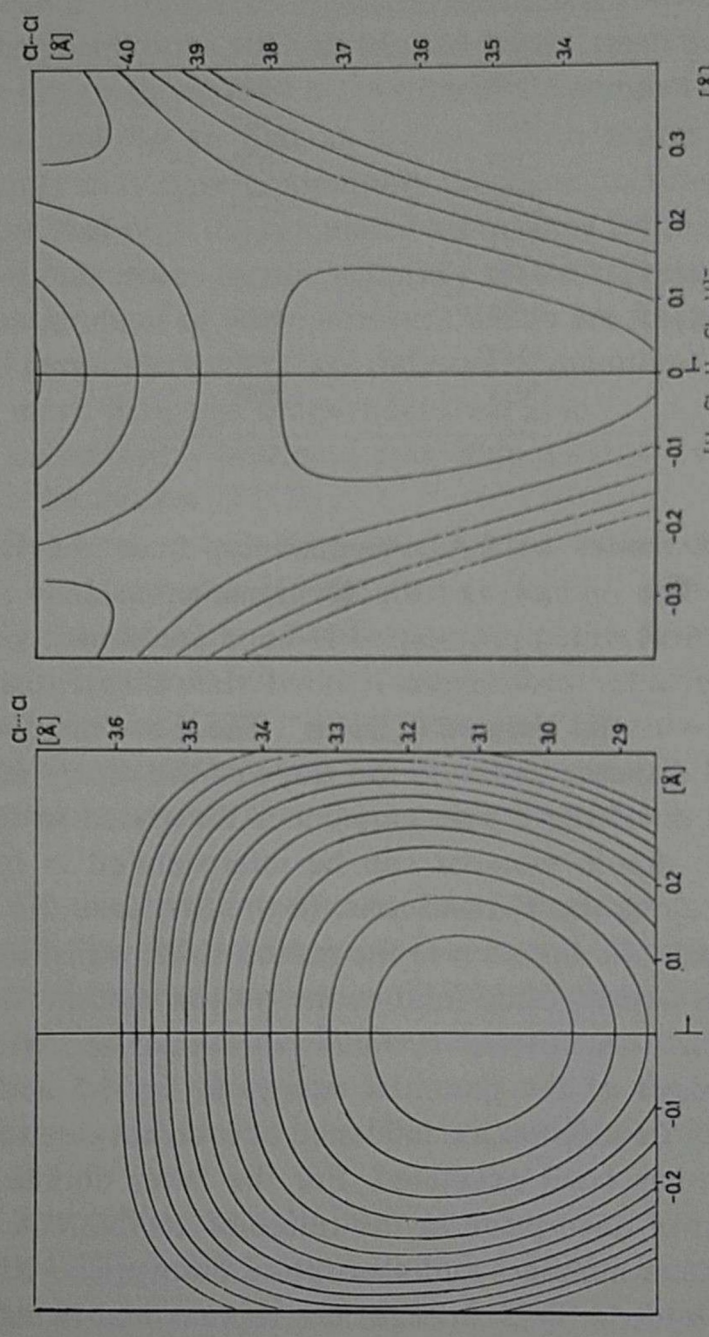

Fig. 3.2. Potential energy surfaces for the systems $H^+(ClHCl)^-H^+$ and $H(ClHCl)^-H$, respectively.

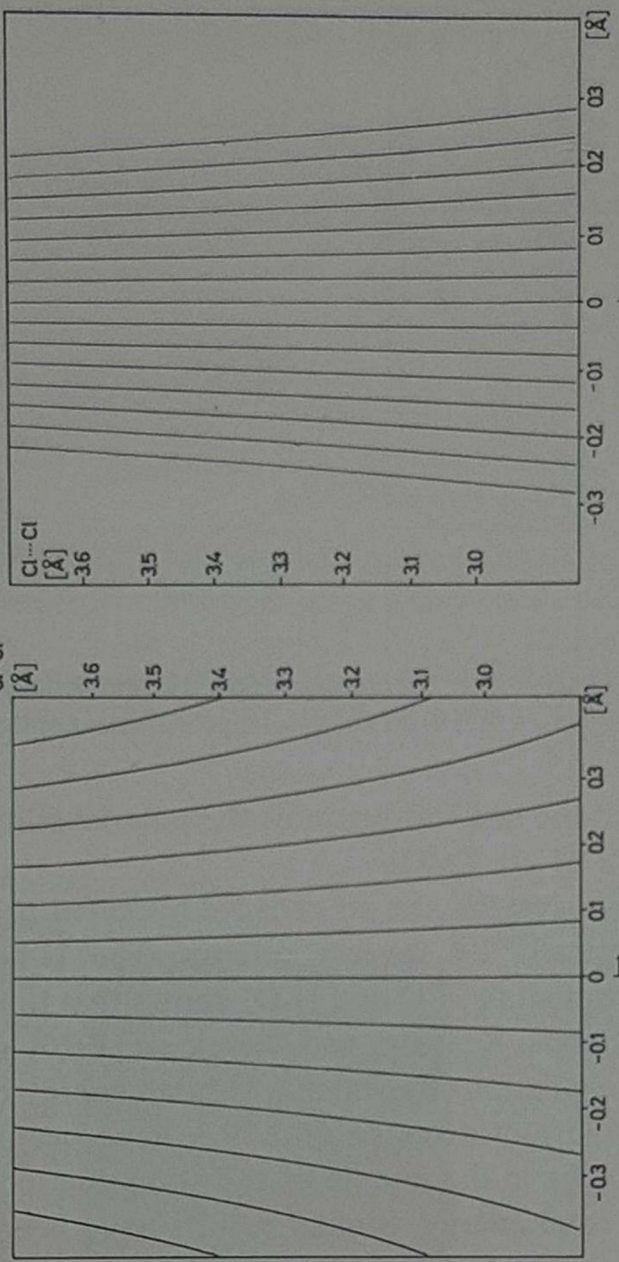

Fig. 3.3. Dipole moment surfaces for the systems $H^+(ClHCl)^-H^+$ and $H(ClHCl)^-H$, respectively.

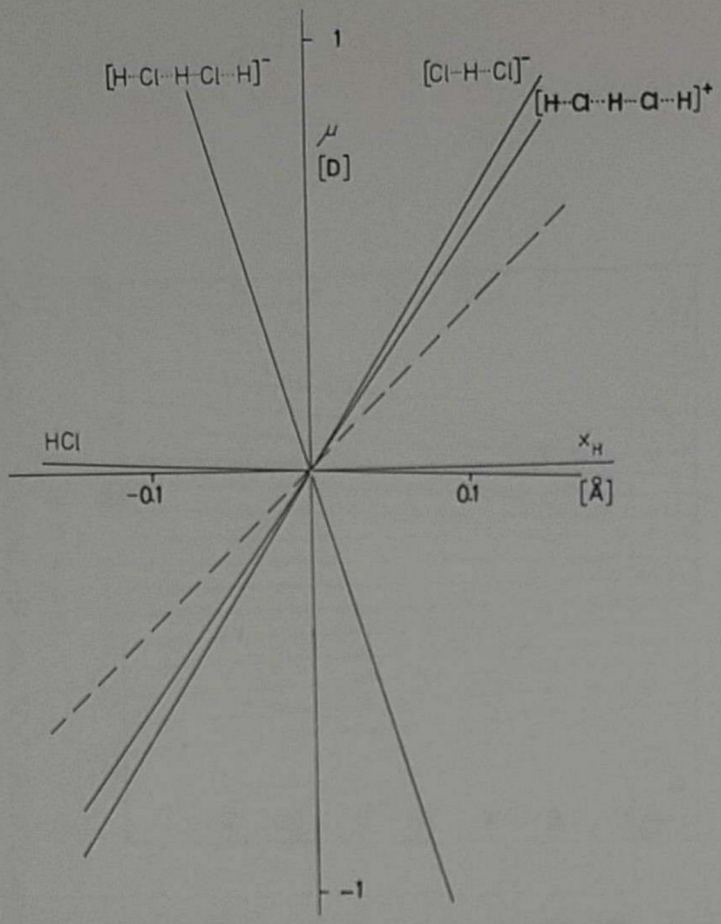

Fig. 3.4. Dipole moment curves over the proton motion. The dipole moment for HCl in the equilibrium geometry ($x_H = 0$) is 0.441 au; (– – –) dipole moment of the bare proton.

Pimentel [1967]) and the last row contains the polarisability of the proton using the formalism of eq. (3.52).

$(H_2OHOH_2)^+$. This system, the so called dihydrated proton, has been investigated theoretically by several authors. The H-bond energy of 36 kcal/mole with respect to H_2O and H_3O^+ shows that this system is one of the strongest H-bonds. Kraemer and Diercksen [1970] have performed accurate ab initio calculations by which a H-bond energy of 32 kcal/mole and an O···O equilibrium distance of 2.39 Å have been obtained. The proton was found to be in the middle of the bond due to a very shallow single minimum of total energy. Similar results have been obtained also by Newton and Ehrenson [1971] and Alagona et al. [1973] which reproduce the well known experimental facts in the gas phase quite well.

In addition, Kollman and Allen [1970a] have discussed the shape of the potential energy surface for the symmetric O···O stretching motion and for the asymmetric motion of the proton. Analogous to the results stated in table 3.3 they have obtained the following potential parameters:

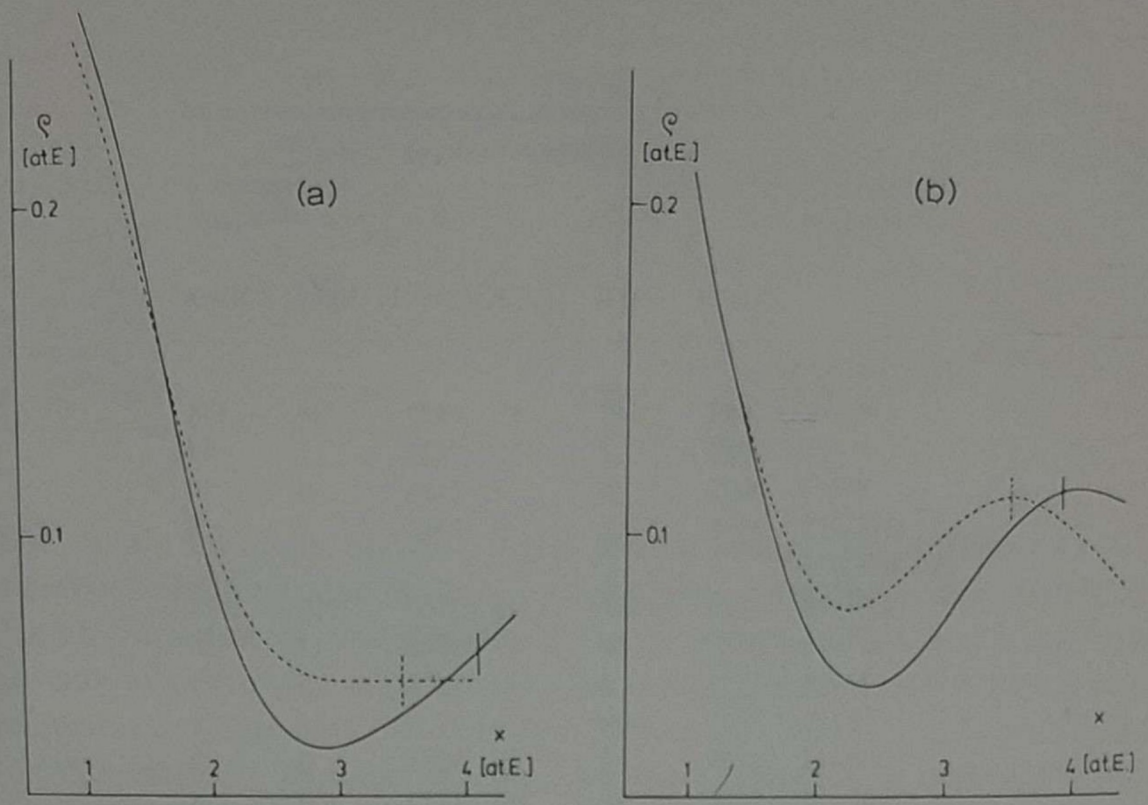

Fig. 3.5. Electron density in the H-bond axis for the systems $H^+(ClHCl)^-H^+$ (a) and $H(ClHCl)^-H$ (b), respectively. The Cl atoms are situated at $x = 0$ and $x = 7$ au, respectively. (a) (– – –) proton in the middle of the bond; (——) proton shifted to the right by 0.6 au; (b) (– – –) proton in the middle of the bond; (——) proton shifted to the right by 0.4 au.

a_{02}	a_{20}	a_{40}	a_{21}
1.06	0.10	2.12	−2.12

where the units are mdyne and Å.

Janoschek et al. [1972] have tried to perform ab initio calculations on the isolated $(H_5O_2)^+$ in such a way that the spectroscopic behaviour of aqueous solutions might be explained. O···O distances between 2.4 and 2.8 Å, as found on experimental investigations (see section 15.4), have been used to calculate the energy curves for the proton rather than working at the total energy minimum at about 2.4 Å. The calculated energy curves represented in fig. 3.6 have the following minimum total energies, respectively:

O···O (Å)	E (au)
2.5	−151.55929
2.6	−151.55358
2.7	−151.54690
2.8	−151.53938

TABLE 3.5

Calculated wave numbers $\tilde{\nu}_{ij}$ and relative absorption intensities I_{ij}. (I: asymmetric vibration, II: combination transitions, III: symmetric vibration)

Transition	$F = 0$			$F = 5.14 \times 10^7$ V/cm		
	$\tilde{\nu}_{ij}$ (cm^{-1})	I_{ij} 100 K	300 K	$\tilde{\nu}_{ij}$ (cm^{-1})	I_{ij} 100 K	300 K
$H^+(ClHCl)^-H^+$						
I 00–10	2098	545	481	2133	544	478
01–11	2089	1	55	2124	1	57
02–12	2095	0	7	2134	0	7
II 00–11	2531	11	9	2562	9	8
$H(ClHCl)^-H$						
I 00–10	1879	1881	1342	2100	2938	2478
01–11	2083	54	319	2285	13	385
02–12	2325	2	132	2474	0	51
II 00–11	2303	948	676	2659	45	38
00–12	2809	37	26	3263	0	0
01–10	1658	41	243	1725	0	8
01–12	2589	25	145	2888	0	12
02–11	1818	1	40	1870	0	2
III 00–01	221	0	0	375	17	14
00–02	485	0	0	789	4	3

TABLE 3.6

Calculated wave numbers and relative Raman intensities of the Cl···Cl vibration

Cl···Cl vibration	Wave number (cm^{-1})	Relative Raman intensity
$H^+(ClHCl)^-H^+$		
00–01	447	1.0
00–02	892	0.07889
00–03	1336	0.00178
$H(ClHCl)^-H$		
00–01	221	5.14968
00–02	485	4.79458
00–03	866	0.22878

TABLE 3.7

Calculated and observed data of $(ClHCl)^-$

	$H^+(ClHCl)^-H^+$	$(ClHCl)^-$	$H(ClHCl)^-H$	$(ClHCl)^-$ (cryst.)
$Cl\cdots Cl$ (Å)	3.109	3.155	3.532	3.16
ω_s (cm^{-1})	447	483	221	210–240
ω_a (cm^{-1})	2098	2133	1879	730–1660
ω_b (cm^{-1})	—	1061	—	1050–1185
α (10^{-24} cm^3)	1.89	2.21	11.30	

The dipole moment curves for the proton motion for different $O\cdots O$ distances are illustrated in fig. 3.7 where again, as in the system $(ClHCl)^-$, a high variation of this quantity is to be noticed. This has been used already as one of the main reasons for the explanation of the increase of IR absorption intensity on the H-bond formation. More exactly the reason for this intensity increase are the transition moments in table 3.8 which show that in general the variation of the dipole moment may not be separated from the transition moment in the general form of eq. (3.43). This is demonstrated by comparing the transition $0+\rightarrow 1-$ in the case $O\cdots O = 2.5$ Å with the transition $0+\rightarrow 0-$. There exists no common ratio between the average values $\langle q\rangle$ (values in parenthesis) and $\langle \mu(q)\rangle$. Figure 3.8 illustrates the strong variation in vibrational states and wave numbers with the change of the $O\cdots O$ distance.

Figure 3.6 together with table 3.8 which contains the dipole transition moments provide a sensitivity probe to the IR absorption spectrum in external electrical fields. Electrical fields have been taken into account using eq. (3.52). The influence of the field on the energy levels is shown in fig. 3.9 which will be discussed later in sections 15.4 and 15.5 (fig. 15.13).

Figure 3.10 shows that the non-linear shape of the induced dipole moment implies besides the polarisability α, the introduction of a further quantity for the description of the influence of a field. The hyperpolarisability β defined by

$$\mu(F) = \mu(F_0) + \alpha(F - F_0) + \tfrac{1}{2}\beta(F - F_0)^2$$

may play an important role, where F_0 is an arbitrary fixed fieldstrength. Further details will be represented in section 15.4 (fig. 15.2).

The calculations on the system $(H_2OHOH_2)^+$ have been extended also by Janoschek et al. [1973] by the coupling of the symmetric $O\cdots O$

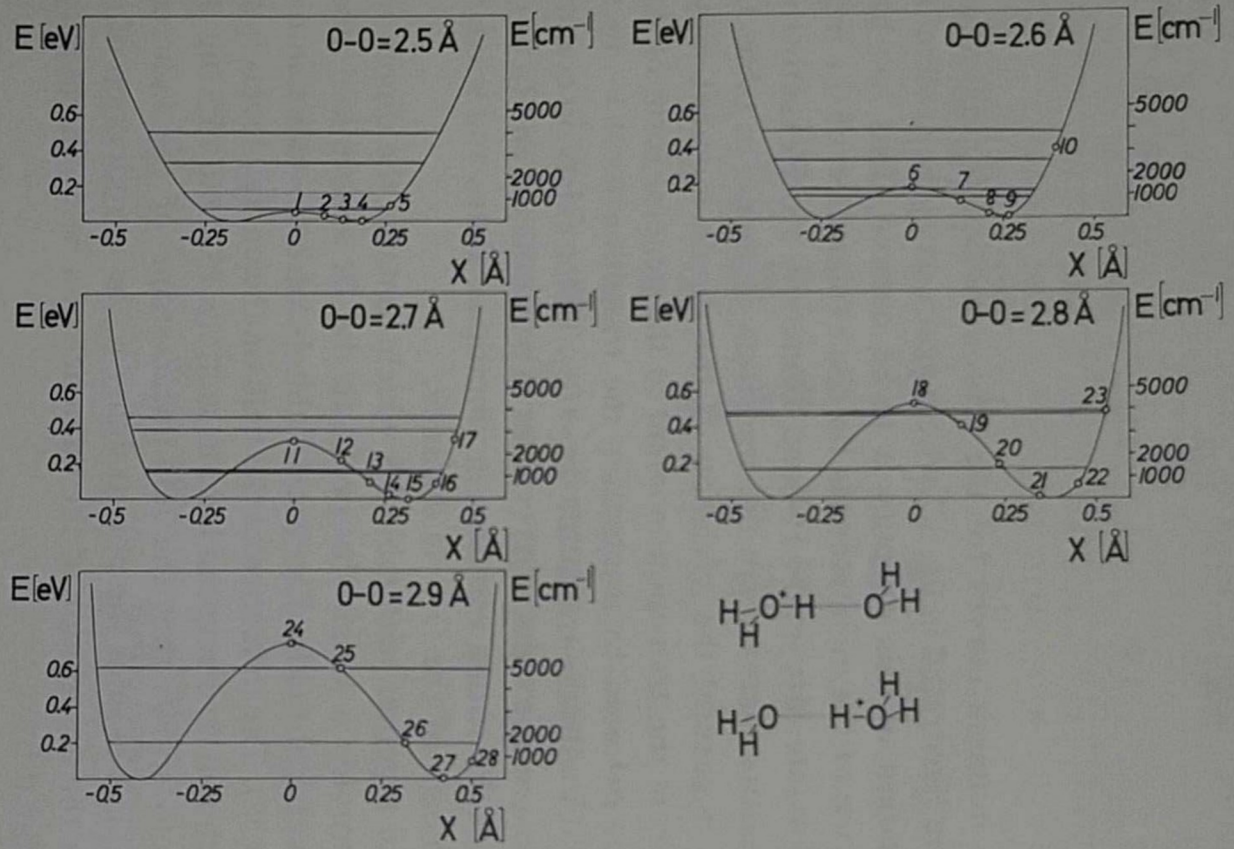

Fig. 3.6. Potential wells for various O···O distances with the four lowest proton states of the system $H_5O_2^+$.

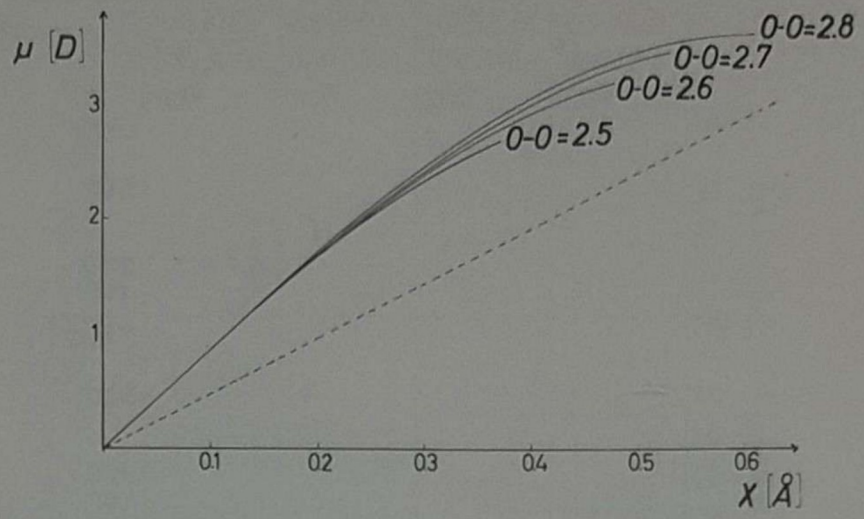

Fig. 3.7. Dipole moment of $H_5O_2^+$ as a function of the displacement of the proton from the middle of the bond for various O···O distances (Å); (– – –) contribution of the bare proton.

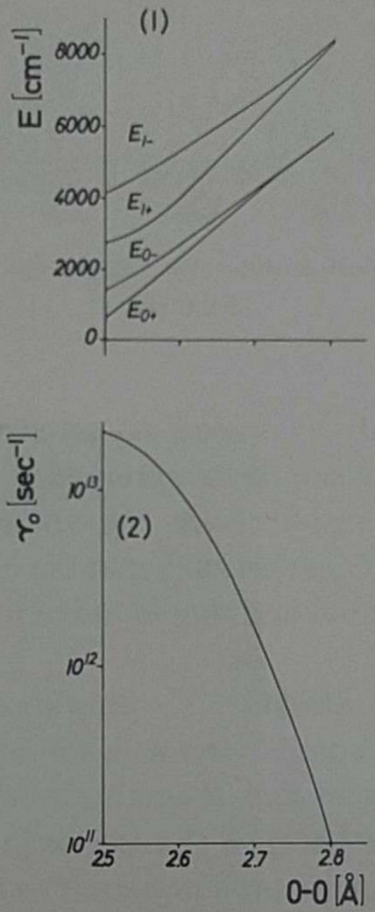

Fig. 3.8. Vibrational states of the proton in the system $H_5O_2^+$ and the tunnelling wave number $\bar{\nu}_0$ as a function of the O···O distance.

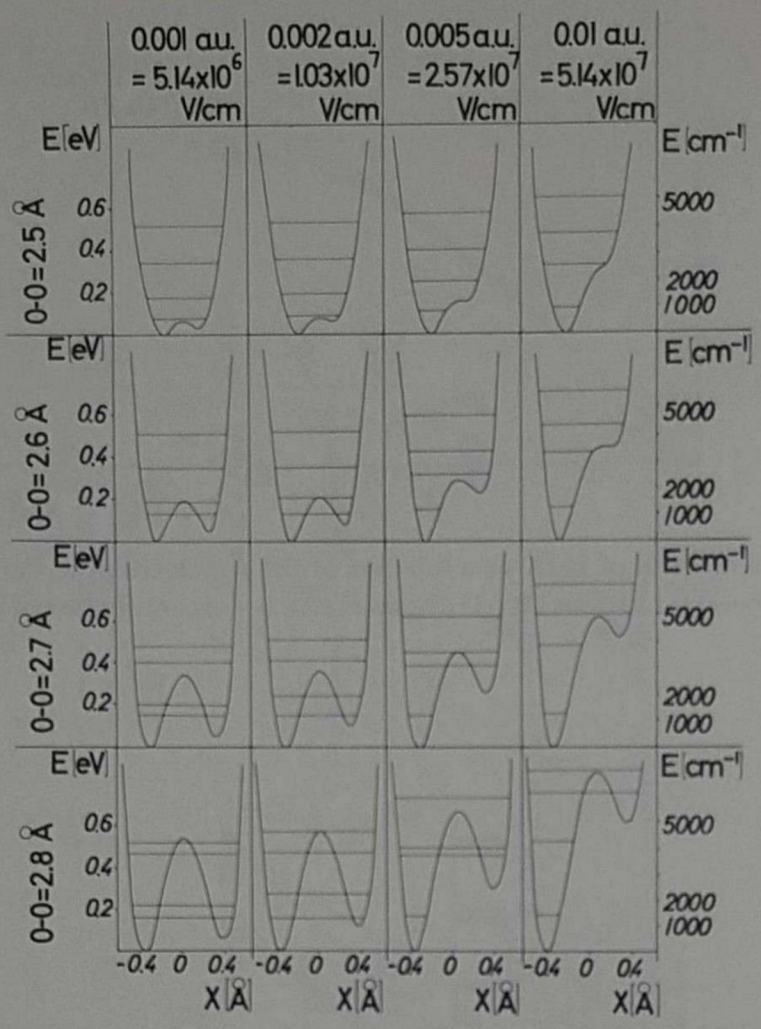

Fig. 3.9. Potential wells and proton states for various field strengths and various O···O distances.

vibration with the already examined asymmetric proton motion. Figure 3.11 shows the energy surface for an assumed O···O equilibrium distance of 2.5 Å. This surface results from the ab initio calculations by the superposition of a linear function such that the observed O···O distances are simulated. The potential and dipole moment parameters are given in the following table 3.9.

The influence of the coupled O···O vibration on the proton motion is to be seen in fig. 3.12. The comparison with the one-dimensional treatment shows that the coupling of the H-bond stretching vibration generates numerous new transitions. In fig. 3.12 and also in fig. 3.13 the energy levels are marked by a pair of quantum numbers. The first of them indicates the state of the proton motion whereas the second quantum number is referred to the O···O vibration. The resulting transitions may be clas-

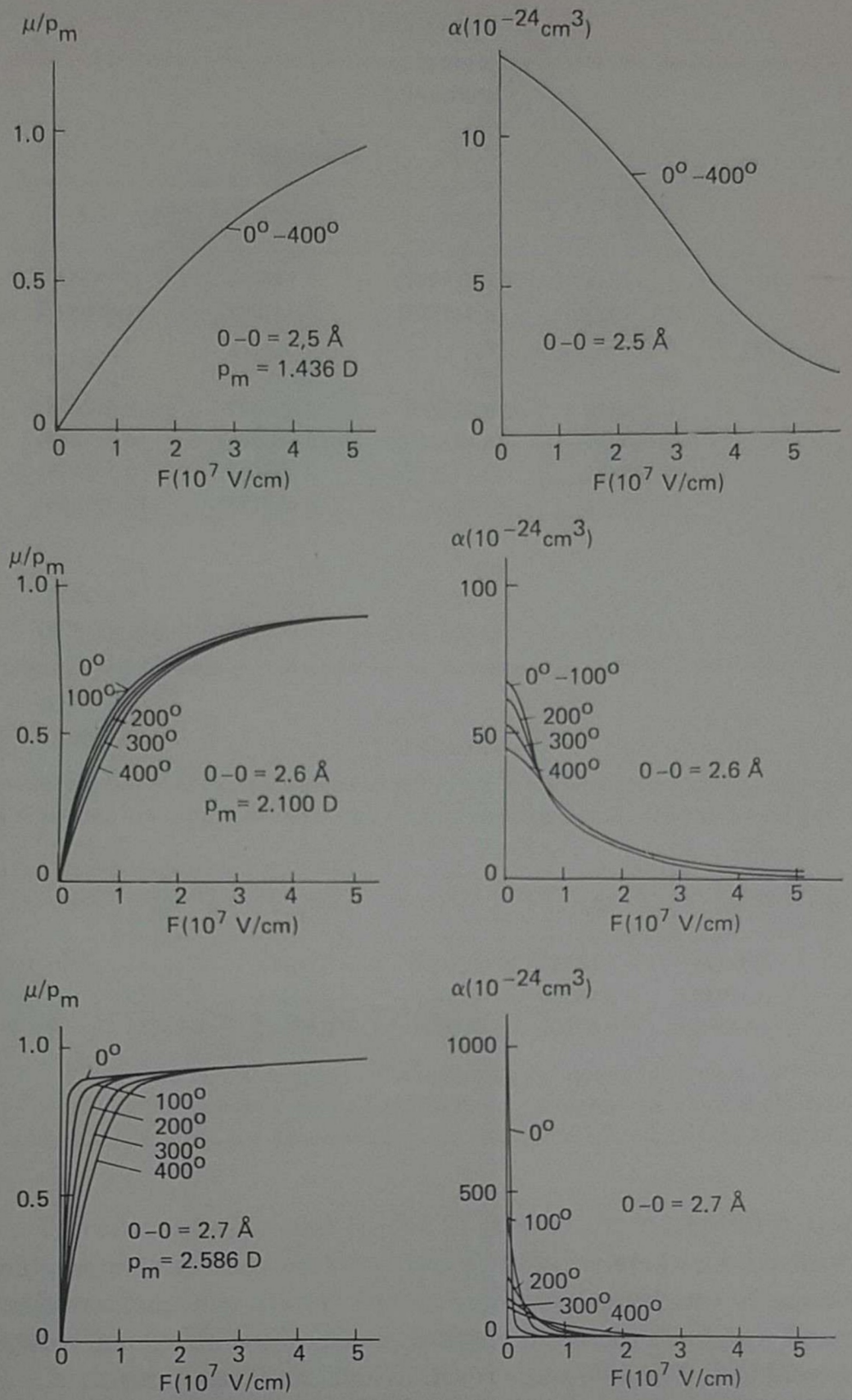

Fig. 3.10. Induced dipole moments and polarisabilities over the field strengths for various temperatures (K). p_m is the dipole moment of the proton boundary structure.

TABLE 3.8

Dipole transition moments (D); values in parentheses represent contribution of the proton alone

Transition	O···O distance (Å)			
	2.5	2.6	2.7	2.8
0+ → 0−	1.211544	1.615994	2.248941	2.745533
	(0.697917)	(0.942583)	(1.347881)	(1.690592)
0+ → 1+	0	0	0	0
	(0)	(0)	(0)	(0)
0+ → 1−	0.054589	0.221868	0.455492	0.472658
	(0.068271)	(0.171842)	(0.332266)	(0.377284)
0− → 1+	1.233623	1.133918	0.738665	0.501114
	(0.751234)	(0.693602)	(0.489774)	(0.391680)
0− → 1−	0	0	0	0
	(0)	(0)	(0)	(0)
1+ → 1−	1.426379	1.412764	1.735601	2.314677
	(0.903192)	(0.866166)	(1.060280)	(1.437222)

TABLE 3.9

Coefficients a_{kl} of the representation of the potential energy surface (au) and coefficients b_{kl} of the representation of the dipole moment surface (au). The dipole moment surface is given for O···O = 2.7 Å

O···O (Å)	a_{00}	a_{20}	a_{40}	a_{01}	a_{21}	a_{02}
2.5	0.00196	−0.04033	0.20749	−0.00981	0.10341	0.03893
2.6	0.00958	−0.08560	0.19125	−0.02314	0.10339	0.03893
2.7	0.01338	−0.07206	0.09701	−0.01941	0.05226	0.03893
	b_{10}	b_{30}	b_{11}			
	1.863	−0.520	0.060			

sified as follows:

I. Transitions whereby only the first quantum number changes, that is, transitions in which the excitation of the O···O vibration remains the same and which are already known from the one-dimensional treatment of the problem. These are again subdivided into two groups:

Ia. Transitions of type $0n$–$3n$ and $1n$–$2n$ which may be interpreted as OH stretching vibrations.

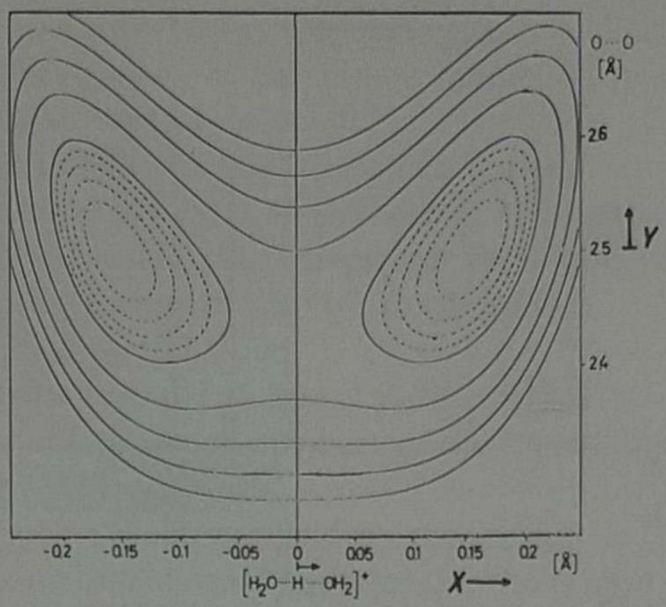

Fig. 3.11. Potential energy surface for the system $H_5O_2^+$ for an assumed O···O distance of 2.5 Å.

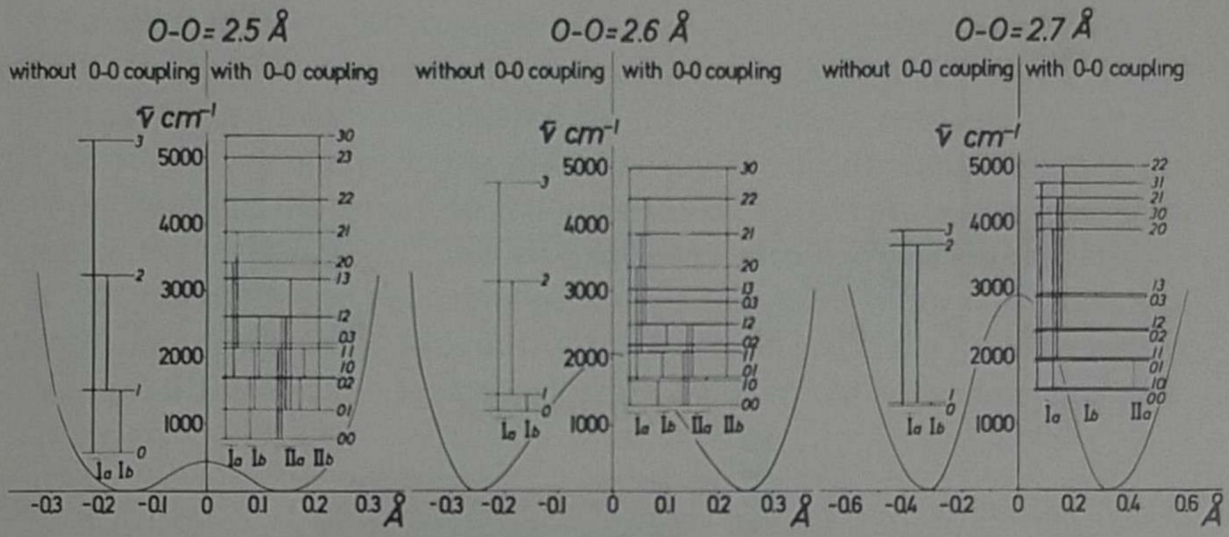

Fig. 3.12. Cross-section of the energy surface through the potential minima. Left-hand side: energy levels of the one-dimensional treatment of the proton motion. Right-hand side: energy levels of the two-dimensional treatment. (a) O···O = 2.5 Å; (b) 2.6; (c) 2.7.

Ib. Transitions $0n-1n$ and $2n-3n$. In general, these transitions occur at considerably smaller wave numbers than those of group Ia. They are called tunnelling transitions. Pure O···O transitions $mn-mn'$ are not permitted in the IR due to the symmetry of the H-bond.

II. Combined transitions, that is, transitions whereby the states of the OH stretching vibration and of the O···O vibration change simultaneously. Two causes exist for these combined transitions. Firstly the term

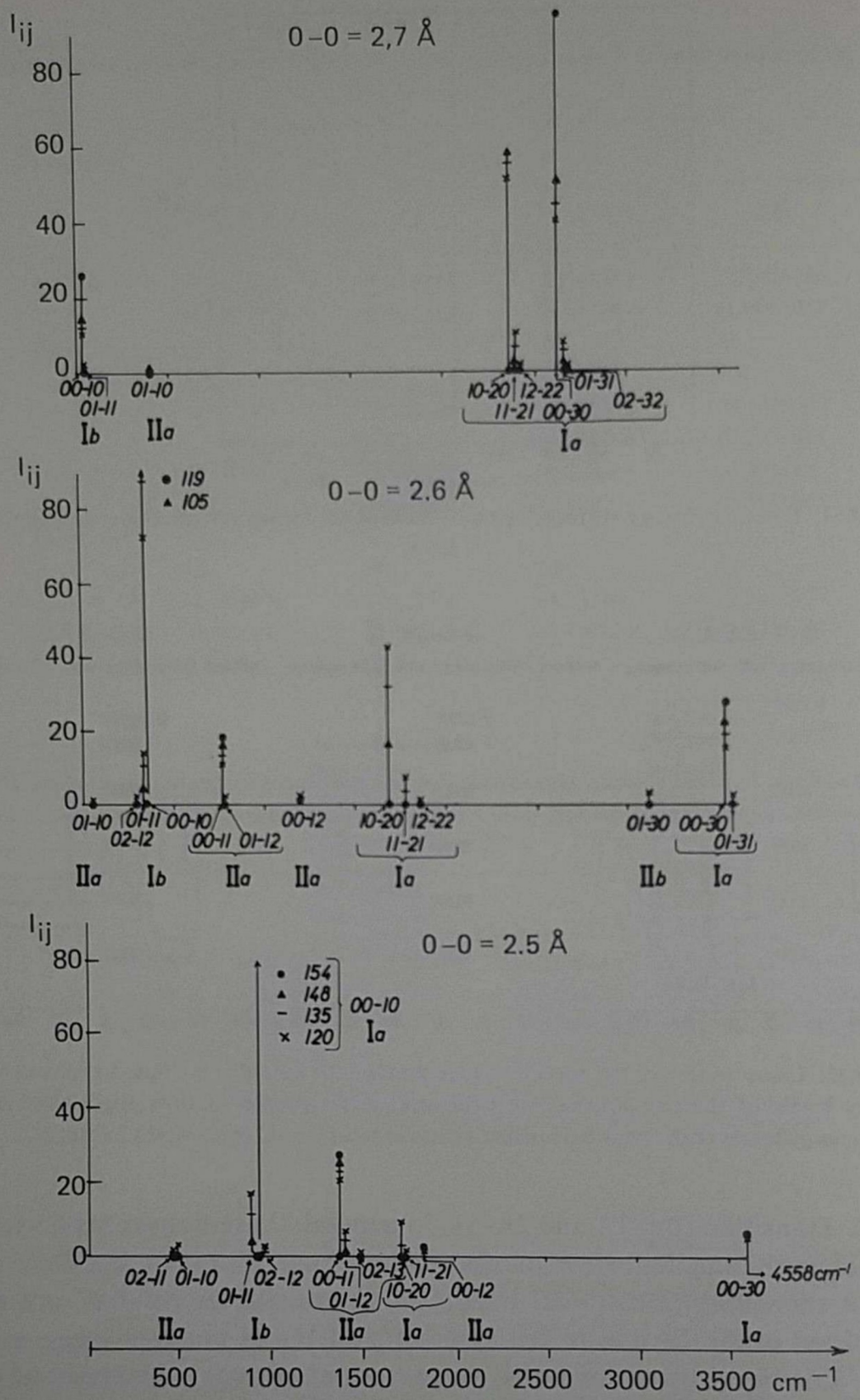

Fig. 3.13. Relative absorption intensities for various temperatures. (●: 0; ▲: 200; —:300; ×: 400 K). (a) O···O = 2.7 Å; (b) 2.6; (c) 2.5.

$a_{21}q_1^2q_2$ in the potential energy provides a mechanical coupling, and secondly the term $b_{11}q_1q_2$ in the dipole moment causes an electrical coupling. Two subgroups again occur:

IIa. Combined transitions $0n$–$1n'$, which are transitions whereby the tunnelling transition is involved. In the case of $n < n'$ an O···O vibration is excited simultaneously with the proton transition, and in the case $n > n'$ the excitation energy of the O···O vibration is used at least in part to excite the tunnelling transition.

IIb. The transitions $0n$–$3n'$ and $1n$–$2n'$, which are composed by adding or subtracting the wave numbers of the transitions from Ia and of the forbidden O···O transitions.

The influence of an electrical field on the energy levels shows differences when the one-dimensional treatment of the proton motion and the two-dimensional treatment are compared. This is a conclusion obtained by comparing fig. 15.13 with fig. 3.14. With increasing field the assignment of quantum numbers to the energy levels is only possible as long as the field-induced level shift is small with respect to level distances without a field. If the field continues to increase, numerous energy levels would intersect were they not hindered by the interaction between the levels. Due to the symmetry being disturbed by the field, transitions are not forbidden and the levels do not cross over. However, in the regions in which the levels interact, the assignment of the quantum numbers to the levels can no longer be maintained, since the states in these regions mix with one another. This will cause Fermi resonances. If the field strength is increased further, the levels can again be assigned to certain quantum

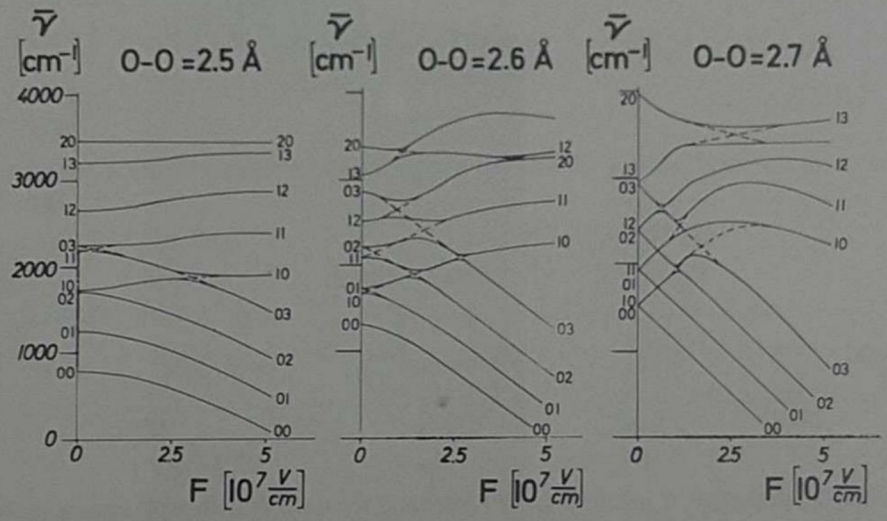

Fig. 3.14. Vibrational states over the field strength. (a) O···O = 2.5 Å; (b) 2.6; (c) 2.7.

numbers if their distance has again become large when compared with the minimum distance. The assignment must then be made as if the levels had intersected, as consideration of the nodal behaviour of the wave function shows. The apparent crossings are indicated by dashed lines.

The transitions as functions of the field strength are represented in fig. 3.15. The figs. 3.14 and 3.15 show the importance of Fermi resonance in

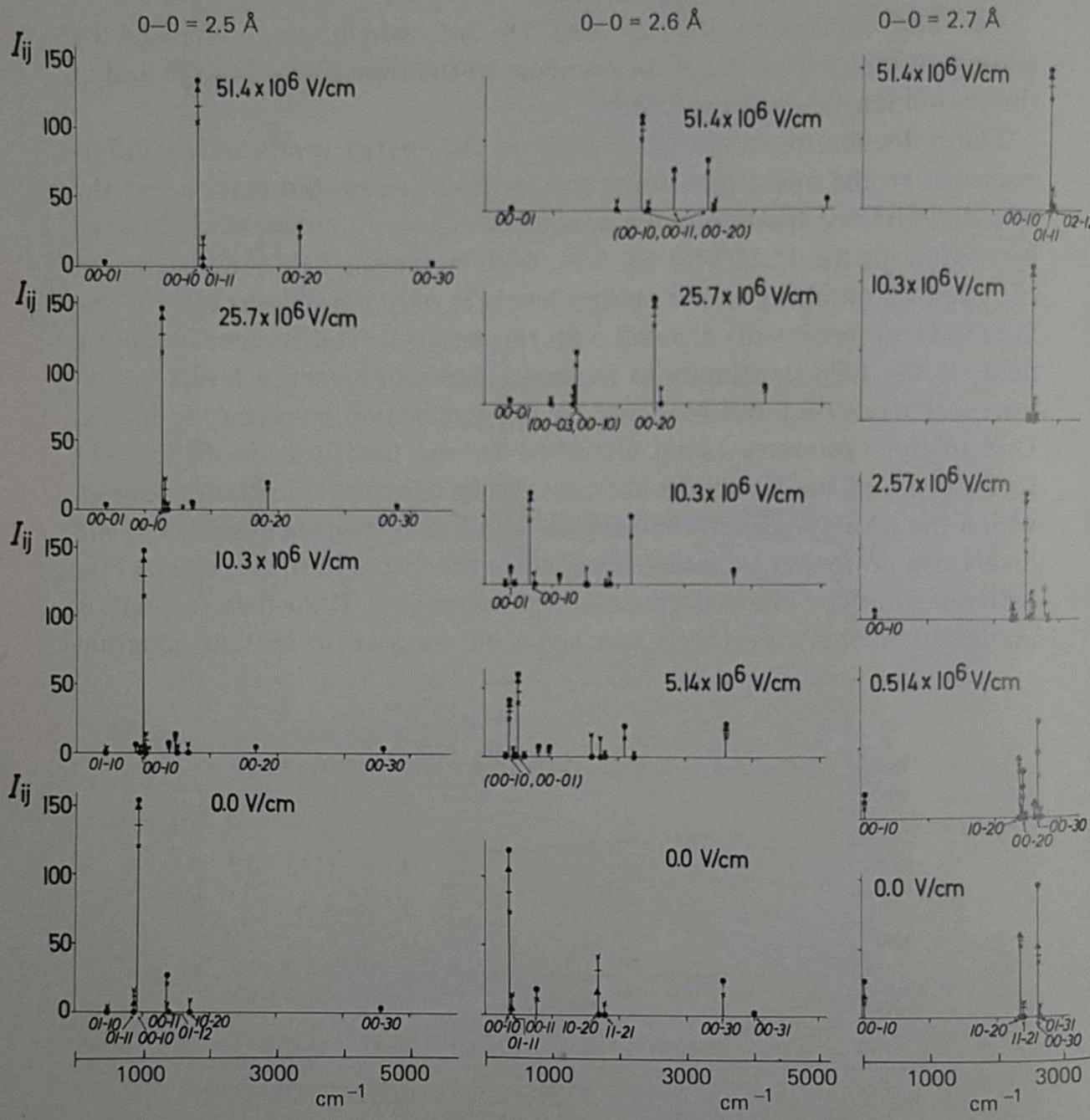

Fig. 3.15. Relative absorption intensities for various field strengths and temperatures. (●: 0; ■: 100; ▲: 200; —: 300; ×: 400 K). (a) O···O = 2.5 Å; (b) 2.6; (c) 2.7.

particular for the case of an O···O distance of 2.6 Å when non-monotonic wave number shifts may occur.

Anderson and Jiang [1973] have used a potential representation similar to that of eq. (3.20) and by means of ab initio results already mentioned, together with empirical data, the H-bond stretching vibration and the asymmetric proton vibration have been examined within a one-dimensional treatment. Accordingly no combination transitions may be included. Some semi-empirical results which are obtained for the absolute minimum of total energy are: $\bar{\nu}_H = 1783\ cm^{-1}$, $2\bar{\nu}_H = 3850\ cm^{-1}$, $3\bar{\nu}_H = 6060\ cm^{-1}$, $\bar{\nu}_{O\cdots O} = 480 \pm 120\ cm^{-1}$. A comparison with observed data $\bar{\nu}_H = 1700–1900\ cm^{-1}$, $\bar{\nu}_{O\cdots O} = 412\ cm^{-1}$ shows a good agreement (Pavia and Giguere [1970]).

$(H_2ODOH_2)^+$. The dihydrated deuteron has been examined by Janoschek [1972] for an assumed O···O equilibrium distance of 2.5 Å using the potential energy in fig. 3.11 and the dipole moment in fig. 3.7. The most significant results of a two-dimensional treatment are compared with the corresponding results of the dihydrated proton in table 3.10. The high loss of intensity of the combination transition 00–11 due to deuteration has been explained already by Bertie and Millen [1964].

Anderson and Jiang [1973] report a wave number of $1242\ cm^{-1}$ for the asymmetric stretching vibration of the deuteron where an O···O distance of 2.407 Å is used. Pavia and Giguere [1970] have observed the range $1250–1400\ cm^{-1}$ in the gas phase.

$(HOHF)^-$. This system represents the strongest unsymmetric H-bond. Diercksen and Kraemer [1970] have obtained from an accurate ab initio calculation a H-bond energy of 24 kcal/mole referred to H_2O and F^-, and an O···F equilibrium distance of 2.51 Å with the H-bond assumed to be linear.

TABLE 3.10

Wave numbers and transition probabilities for the dihydrated proton and deuteron

Transition	$(H_2OHOH_2)^+$ $\bar{\nu}$ (cm^{-1})	A (eq. (3.44))	$(H_2ODOH_2)^+$ $\bar{\nu}$ (cm^{-1})	A (eq. (3.44))
00–01	449.7	0	440.9	0
00–10	930.9	154.291	534.3	85.597
00–30	4557.9	3.427	2836.7	3.717
10–20	1709.3	335.167	1105.8	172.126
00–11	1374.1	26.603	970.6	9.714

Kistenmacher et al. [1973] have found by means of accurate ab initio calculations an O···F distance of 2.51 Å, and an equilibrium geometry which deviates from linearity by about 4.5°. The OH distance increases up from 0.950 to about 1.0 Å on the formation of the H-bond.

Weidemann et al. [1974] have performed ab initio calculations for the O···F distances 2.2, 2.3, 2.4, 2.5, 2.6 Å for which the corresponding energy curves for the proton motion have been calculated. Taking the increase of the OH distance into account an O···F equilibrium distance of 2.31 Å has been obtained. The OH distance of 0.953 Å (O···F = 2.6 Å) increases to 0.960 Å (O···F = 2.3 Å).

The potential energy is approximated as

$$V = \tfrac{1}{2}\omega q^2 + k_3 q^3 + k_4 q^4 \tag{3.58}$$

where the dimensionless quantity q is introduced by the unit of length

$$\sqrt{\frac{\hbar}{2\pi c}}\sqrt{\frac{1}{m\omega}}. \tag{3.59}$$

For the case of O···F = 2.3 Å the following potential parameter should be noted

$$\omega = 3658.5\ \mathrm{cm}^{-1},\ k_3 = -527.4\ \mathrm{cm}^{-1},\ k_4 = 61.3\ \mathrm{cm}^{-1}.$$

The dipole moment is approximated by

$$\mu(q) = \mu_0 + \mu_1 q + \mu_2 q^2$$

where only the component in the direction of the H-bond is a dominating contribution. For ions, the parameter μ_0 is meaningless; the other two parameters for the case of O···F = 2.3 Å are $\mu_1 = 0.46011$ and $\mu_2 = 0.04590$ D. Some results concerning the potential energy are reported in table 3.11. Comparing the wave numbers within the harmonic approximation ω_{OH} with those which are obtained from eq. (3.6) $\bar{\nu}_{OH}$, the breakdown of the harmonic approximation is apparent. The OH force constant shows a monotonic increase with increasing O···F distance whereas the wave number $\bar{\nu}_{OH}$ of the OH stretching vibration shows a distinct minimum for an O···F distance of 2.3 Å due to the maximum of the anharmonicity X. The anharmonicity X is of the form

$$X = \tfrac{15}{4}k_3^2/\omega - \tfrac{3}{2}k_4 \tag{3.60}$$

within the second order perturbation theory.

TABLE 3.11
OH wave numbers in the harmonic approximation ω_{OH}, and by eq. (3.58) $\bar{\nu}_{OH}$; X: anharmonicity

O···F (Å)	ω_{OH} (cm^{-1})	$\bar{\nu}_{OH}$ (cm^{-1})	X (cm^{-1})
2.2	3642.2	3412	162.6
2.3	3658.5	3295	193.2
2.4	3773.6	3372	188.6
2.5	3859.2	3484	171.9
2.6	3878.5	3524	175.3

The second order perturbation theory of eq. (3.41) shows essential differences to the exact results obtained with eq. (3.6) particularly for the overtones. The intensities of the corresponding transitions show that the results from the second order perturbation theory are no longer useful for the discussion of the overtones (tables 3.12, 3.13).

$(HODF)^-$. This D-bond has been examined by Weidemann et al. [1974]. Without going into detail, only some specific spectroscopic properties will be listed where an O···F distance is taken to be 2.3 Å. The following parameters for the potential energy are obtained: $\omega = 2586.9\,\text{cm}^{-1}$, $k_3 = -313.6\,\text{cm}^{-1}$, $k_4 = 30.6\,\text{cm}^{-1}$. The anharmonicity X using eq. (3.60) was calculated to be $96.6\,\text{cm}^{-1}$ (table 3.14).

TABLE 3.12
Wave numbers for the fundamental and first overtone, second order perturbation theory in parentheses

O···F (Å)	$\bar{\nu}_{OH}$ (cm^{-1})	$2\bar{\nu}_{OH}$ (cm^{-1})
2.2	3412	6750
	(3286)	(6180)
2.3	3295	6322
	(3253)	(6081)
2.4	3372	6330
	(3385)	(6369)
2.5	3484	6540
	(3508)	(6655)
2.6	3524	6715
	(3517)	(6658)

TABLE 3.13

Relative absorption intensities for the fundamental and first overtone, second order perturbation theory in parentheses

O···F(Å)	$I(\tilde{\nu}_{OH})$	$I(2\tilde{\nu}_{OH})$
2.2	352	2.4
	(343)	(3.5)
2.3	302	1.9
	(294)	(5.1)
2.4	254	1.1
	(248)	(5.1)
2.5	190	0.03
	(185)	(5.7)
2.6	145	0.04
	(140)	(5.9)

TABLE 3.14

Wave numbers and relative absorption intensities, second order perturbation theory in parentheses

$\tilde{\nu}_{OD}$ (cm^{-1})	$2\tilde{\nu}_{OD}$ (cm^{-1})	$I(\tilde{\nu}_{OD})$	$I(2\tilde{\nu}_{OD})$
2399	4629	146.7	0.66
(2387)	(4567)	(144.9)	(0.99)

$(H_2O)_2$. The water dimer is the most widely studied of H-bonds. Most of the theoretically obtained H-bond binding energies are found to be 4–5 kcal/mole which give a weak H-bond.

Morokuma and Pedersen [1968] have examined the structure and the increase of the OH distance due to H-bond formation. Later Morokuma and Winick [1970] calculated an O···O stretching force constant of $0.21 \cdot 10^5$ dyne/cm and an O···O distance of 2.778 Å. In addition, an increase of the OH distance of 0.0026 Å and an OH stretching force constant of $10.1 \cdot 10^5$ dyne/cm are given; this is 6% smaller than that of the monomeric system.

Kollman and Allen [1969] have examined the water dimer structure. They have found an increase of the OH distance of 0.010 Å, and the OH stretching force constant is found to be 20% smaller than that of the water molecule, whereas the wave number of the bending vibration increases by

2%. By means of the first derivatives of the dipole moment with respect to the OH distance they have tried to explain the increase of absorption intensity of the OH stretching mode. However, the results are only of crude qualitative character because no normal modes have been taken into account; furthermore, the quantity $(\partial|\boldsymbol{\mu}|/\partial q)^2$ has been used for discussion instead of $(\partial\boldsymbol{\mu}/\partial q)^2$.

Hankins et al. [1970] have calculated an O···O distance of 3.00 Å, but no increase of the OH distance is found. The same result has been obtained by Diercksen [1971] by means of an accurate ab initio treatment. The calculated increase of the OH distance of 0.004 Å is considered to be outside the range of the numerical accuracy. In spite of the extensive potential curves which are given, no attempt has been made to calculate spectroscopic data. However, the dipole moment derivative is again used erroneously: on the one hand the symmetric H_2O stretching vibration is employed, which is weak in IR intensity, in order to discuss the observed intensity increase due to H-bond formation and on the other hand the quantity $(\partial|\boldsymbol{\mu}|/\partial q)^2$ is discussed, which in general is quite meaningless.

The calculated total energies and dipole moments from Diercksen [1971] have been used by Janoschek [1973c] in order to obtain the spectroscopic data summarised in table 3.15. According to $X = (\bar{\nu}_{OH} - 2\bar{\nu}_{OH})/2$ the anharmonicity for the bonded OH stretching is more than three times that of the symmetric stretching mode in the non-bonded species. The wave number shift is reproduced quite well but the wave numbers themselves show considerable deviations from observed data

TABLE 3.15

Wave numbers and IR intensities for the monomeric and the dimeric water; observed values in parentheses

	H_2O	$(H_2O)_2$
$\bar{\nu}_{OH}$ (cm^{-1})	4020 (sym.)	3806
	(3652)	(3428)
$2\bar{\nu}_{OH}$	7987	7436
	(—)	(—)
$3\bar{\nu}_{OH}$	11920	10897
	(10867)	(—)
I $(\bar{\nu}_{OH})$	5.08788	61.37072
I $(2\bar{\nu}_{OH})$	0.11524	0.97405
I $(3\bar{\nu}_{OH})$	0.00349	0.17727

even for accurate calculations. The origin of the high wave numbers is due to the wrong asymptotic behaviour of the total energy with the dissociation products $O^{2-} + 2H^+$, this being a failing of the closed shell Hartree–Fock method. The wave number of the O···O vibration is found to be in good agreement with the observed value of 160 cm^{-1} in the liquid state (Walrafen [1966]). $\bar{\nu}_{O\cdots O} = 152\,cm^{-1}$, $2\bar{\nu}_{O\cdots O} = 288\,cm^{-1}$, $3\bar{\nu}_{O\cdots O} = 408\,cm^{-1}$, $I(\bar{\nu}_{O\cdots O}) = 0.023$, $I(2\bar{\nu}_{O\cdots O}) = 0.002$, $I(3\bar{\nu}_{O\cdots O}) = 0$. The IR intensities are so small as to be almost unobservable.

H_2O *in solid hydrates.* Almlöf et al. [1972] have treated the water molecule in the free state as well as in crystal fields of the two oxalates $LiHC_2O_4$ and $NaHC_2O_4$, respectively. However, the term ab initio calculation only refers to the water molecule, the crystal field being simulated by suitably chosen point charges. Accordingly no charge transfer is allowed for the H-bonded water molecule. In spite of this restriction some results deserve to be mentioned.

Total energy representations containing 19 potential parameters for different states of the water molecule are given. The normal coordinates and the spectra are summarised in table 3.16.

These ab initio calculations on the water molecule are of intermediate

TABLE 3.16

Normal modes, wave numbers (cm^{-1}) and the square of dipole moment derivatives for the water molecule in different environments

	H_2O	$NaHC_2O_4 \cdot H_2O$	$LiHC_2O_4 \cdot H_2O$
q_1	0.6837	0.3201	0.9620
	−0.6837	−0.9140	−0.1389
	0	−0.0048	0.0115
q_2	0.6947	0.9199	0.1559
	0.6947	0.3374	0.9646
	0.0346	0.0026	0.0164
q_3	0.0028	0.0380	0.0189
	0.0028	0.0311	0.0182
	0.6454	0.6541	0.6597
ω_1	4212	4024	3925
ω_2	4117	3900	3746
ω_3	1693	1791	1767
$(\partial\boldsymbol{\mu}/\partial q_1)^2$	0.530	2.98	4.14
$(\partial\boldsymbol{\mu}/\partial q_2)^2$	0.282	3.16	4.17
$(\partial\boldsymbol{\mu}/\partial q_3)^2$	1.50	2.79	3.56

accuracy, hence there are noticeably higher wave numbers for the stretching vibrations when compared with observed data. But the main feature of this table should be seen in the changes of spectra due to H-bond formation. The normal coordinates show a high decoupling of the OH stretching which arises with increasing disturbance; the wave numbers of the stretching modes decrease and split more and more; the wave number of the bending mode shows a slight increase. The absorption IR intensities are discussed correctly by means of $(\partial\mu/\partial q)^2$. Table 3.16 shows that even small disturbances cause an increase of intensity of both stretching modes by about the same magnitude.

Formamide, cyclic dimer. The simultaneous NH stretching motions in the two interacting H-bonds in the cyclic dimer of formamide has been examined by Janoschek [1973b]. This ab initio investigation is restricted by an intermediate accuracy and by the neglect of other coupled vibrations. But the changes of spectra of the NH_2 stretching modes with respect to H-bond formation and the H-bond–H-bond interaction are the main features.

TABLE 3.17

Spectra of the NH_2 stretching in formamide and of the simultaneous NH stretching in the cyclic formamide dimer

Transition	Wave number (cm^{-1})	Relative IR absorption (300 K)
NH_2 stretching in formamide		
00–10 (sym.)	2967	8.612
00–01 (asym.)	3211	7.284
00–20	5943	0.006
00–11	6143	0.312
00–02	6411	0.141
NH stretching in the cyclic formamide dimer		
00–10 (in phase)	1701	0.001
00–01 (antiphase)	2254	1210.043
00–20	3086	0
00–11	3885	0.569
00–02	4382	0.009
10–01	553	0.022
10–11	2184	0.499
01–02	2128	0.007

The fundamental quantities for the calculation of spectra are illustrated in fig. 3.16. The importance of anharmonicity is quite well illustrated. The potential energy shows an essential deviation of the level lines from elliptical shapes which is particularly marked for high amplitudes (overtones); the dipole moment shows an electrical anharmonicity owing to the curvature of the level lines. Some results are summarised in table 3.17. The

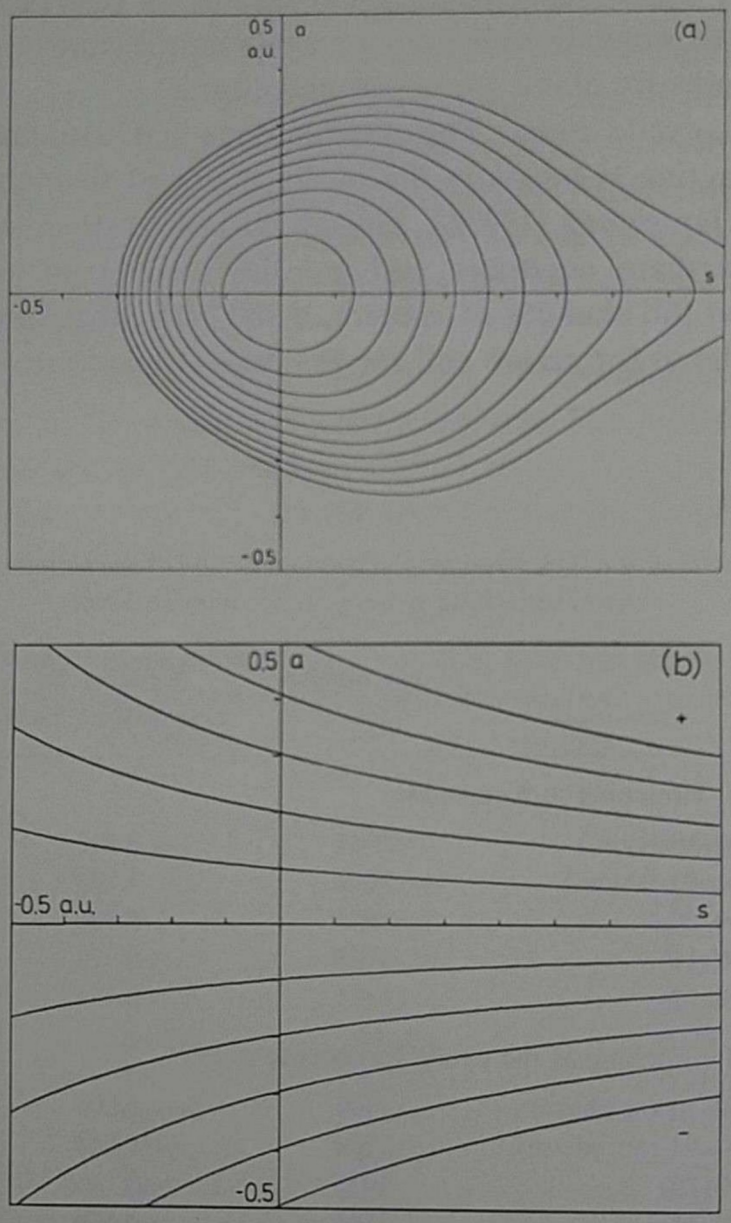

Fig. 3.16. (a) Potential energy surface for the coupled motion of H-bonded protons in the cyclic dimer of formamide. The levels are drawn at 400(400)4000 cm^{-1}. (s in phase-, a antiphase-coordinate). (b) Dipole moment surface of the component parallel to the CN bond for the coupled motion of H-bonded protons in the cyclic dimer of formamide. The levels are drawn at $-1.27(0.254)1.27$ D; the zero level line is the s-axis.

first part of table 3.17 is in good qualitative agreement with observed data (Evans [1954]). The NH stretching spectrum of the cyclic dimer of formamide, disregarding the two non-bonded NH groups, shows a distinct absorption near 2250 cm^{-1}. With respect to two monomeric species the absorption intensity of the cyclic dimer is increased by a factor forty.

HCN *with various acceptors.* The HCN molecule is able to play the role of a proton donor and therefore weak H-bonds are formed. Botschwina [1973] has calculated numerous ab initio potential curves with various acceptors. By the use of the already described formulas which are based on the second order perturbation theory some spectroscopic results concerning the HC stretching are listed in table 3.18 and H-bond stretching properties are given in table 3.19. The H-bond stretching vibration is based on the harmonic approximation. Table 3.18 lists some

TABLE 3.18

Spectroscopic properties of the HC bond in HCN being a proton donor

		Acceptor			
	HCN	HCN	H_2CNH	NH_3	H_2O
H-bond energy (kcal/mole)	—	4.4	6.7	8.5	7.0
HC(Å)	1.068	1.078	1.084	1.095	1.078
ω_{HC} (cm^{-1})	3491	3444	3180	3013	3295
k_3 (cm^{-1})	−334	−354	−379	−388	−362
k_4 (cm^{-1})	44.6	43.1	50.0	57.2	47.7
X (cm^{-1})	52.7	71.5	94.1	102	77.7
$\bar{\nu}_{HC}$ (cm^{-1})	3376	3291	2978	2790	3127
$\Delta\bar{\nu}$ (cm^{-1})	—	−84	−398	−586	−249
(observed)		(−101)	(−293)		

TABLE 3.19

H-bond stretching properties with the donor HCN

	Acceptor			
	HCN	H_2CNH	NH_3	H_2O
X···C (Å)	3.203	3.057	3.001	2.947
$\bar{\nu}$ (cm^{-1})	128	176	224	208

well known relations for H-bonds, and it may be seen that water occupies an anomalous position.

$(CH_3SH)_2$. The potential energy and dipole moment surfaces for the H-bond SH···S in the dimeric methanethiol is calculated by the SCF–MO–LCGO method (Pecul and Janoschek [1974]) which are represented in tables 3.20 and 3.21. The present H-bond is found to be

TABLE 3.20

Parameter a_{kl} for the potential energy surface $\Sigma_{k,l} a_{kl} q_1^k q_2^l$ with $q_1 = \mathrm{SH}$, $q_2 = \mathrm{S}\cdots\mathrm{S}$; parameter after the transformation to normal coordinates in parentheses

l \ k	0	1	2	3	4
0	0.0	0.0	0.10489	−0.08954	0.05467
	(0.0)	(0.0)	(0.10490)	(−0.08954)	(0.05466)
1	0.0	−0.00162	0.00066		
	(0.0)	(0.0)	(−0.00140)		
2	0.00133	−0.00272			
	(0.00132)	(−0.00271)			
3	−0.00087				
	(−0.00089)				
4	0.00025				
	(0.00025)				

TABLE 3.21

Parameter b_{kl} for the dipole moment surface $\Sigma_{k,l} b_{kl} q_1^k q_2^l$. The second component corresponds to the direction of the H-bond

l \ k	0	1	2
	0.00636	0.00217	0.00265
0	−1.29129	0.03204	−0.09670
	−0.74358	−0.00023	0.02953
	−0.00291	−0.00250	
1	0.12718	0.14648	
	−0.01740	−0.01752	
	0.00049		
2	−0.03270		
	0.00565		

extremely weak with an H-bond binding energy of 1.4 kcal/mole. The theoretical treatment suggests, that the SH distance and the potential curve for the SH stretching are practically unchanged upon H-bond formation. Therefore, the wave number shift of the SH mode to smaller wave numbers is solely caused by the increasing reduced mass. The anharmonic coupling of the SH mode with the S···S mode is found to be

TABLE 3.22

Calculated wave numbers and absorptions for $(CH_3SH)_2$ at 20 K

		With coupling		Without coupling	
	Transition	$\tilde{\nu}$ (cm^{-1})	log I	$\tilde{\nu}$ (cm^{-1})	log I
S···S	00–01	48	4.23477	52	4.21956
	01–02	44	2.98363	49	2.86153
	02–03	41	1.71600	47	1.44716
	03–04	40	0.47712	46	0.0
	00–02	92	3.13258	101	3.04139
	01–03	85	2.10037	97	1.88081
	02–04	81	0.95424	94	0.60206
	00–03	132	2.07918	148	1.79934
	01–04	124	1.17609	143	0.77815
	00–04	172	1.07918	195	0.60206
SH	00–10	2309	4.52004	2312	4.12707
	01–11	2301	3.40722	2312	2.51587
	02–12	2290	2.22789	2312	0.95424
	03–13	2284	1.00000	2312	<0
	00–11	2348	4.27448		
	01–12	2334	2.71265		
	02–13	2325	0.95424		
	03–14	2326	0.0		
	00–12	2382	3.62829		
	01–13	2369	2.71096		
	02–14	2367	1.50515		
	00–13	2417	2.57403		
	01–14	2411	1.69897		
	00–14	2459	0.0		
	01–10	2261	3.12352		
	02–11	2257	2.22272		
	03–12	2250	1.25527		
	02–10	2217	<0		
	03–11	2216	0.0		
	03–10	2176	<0		
	00–20	4599		4606	

the origin for band broadening and structuration of the absorption band in the range of the SH stretching mode (table 3.22). The wave number for the S···S stretching vibration seems to coincide with the SH wave number shift of 26 cm^{-1} (Barnes et al. [1972]).

Many theoretical investigations on H-bonds are not yet exploited with respect to vibrational spectra. As an interesting example the systems $(HF)_2$, H_2OHF and HFHOH, examined by Kollman and Allen [1970b], should be mentioned. Another example is the $(HOHCl)^-$ which shows a bent H-bond with an angle of 14.6° (Kistenmacher et al. [1973]). As an example of biological interest the ab initio investigation of the Guanine–Cytosine pair should be mentioned for which energy curves for the proton motion are available (Clementi et al. [1971]).

The application of the method for the reconstitution of H-bond spectra using experimental data suggested by Marechal and Witkowski [1968], Bournay and Marechal [1971], Leviel and Marechal [1971], and Excoffon and Marechal [1972] is found in ch. 6. The theory may, however, yield wrong results, as shown by recent experimental investigations. Wolff et al. [1974, 1974a] have shown that the splitting of the NH stretching vibration band of imidazol is caused by Fermi resonance with overtones and not by coupling of NH stretching and N–N bond vibrations.

Acknowledgements

The author wishes to express his thanks to Dr. B. Webster for many useful discussions and for reading the manuscript.

References

Alagona, G., R. Cimiraglia and U. Lamanna, 1973, Theoret. Chim. Acta **29**, 93.
Almlöf, J., 1972, Chem. Phys. Letters **17**, 49.
Almlöf, J., J. Lindgren and J. Tegenfeldt, 1972, J. Mol. Struct. **14**, 427.
Anderson, G. R. and G. J. Jiang, 1973, J. Phys. Chem. **77**, 2560.
Baker, A. N., 1954, J. Chem. Phys. **22**, 1625.
Barnes, A. J., H. E. Hallam and J. D. R. Howells, 1972, Faraday Transactions II **68**, 737.
Bertie, J. E. and D. J. Millen, 1965, J. Chem. Soc., 514.
Botschwina, P., 1973, Diplom work, Universität Stuttgart.
Bournay, J. and Y. Marechal, 1971, J. Chem. Phys. **55**, 1230.
Brickmann, J. and H. Zimmermann, 1966, Ber. Bunsenges. Phys. Chem. **70**, 157, 521.
Brickmann, J. and H. Zimmermann, 1967, Ber. Bunsenges. Phys. Chem. **71**, 160.

Brickmann, J. and H. Zimmermann, 1969, J. Chem. Phys. **50**, 1608.
Brickmann, J., A. Licha and H. Zimmermann, 1971, Ber. Bunsenges. Phys. Chem. **75**, 1324.
Clementi, E., J. Mehl and W. von Niessen, 1971, J. Chem. Phys. **54**, 508.
Delaplane, R. G. and J. A. Ibers, 1968, J. Chem. Phys. **48**, 539.
Diercksen, G. H. F., 1971, Theoret. Chim. Acta **21**, 335.
Diercksen, G. H. F. and W. P. Kraemer, 1970, Chem. Phys. Letters **5**, 570.
Di Paolo, T., C. Bourderon and C. Sandorfy, 1972, Can. J. Chem. **50**, 3161.
Evans, J. C., 1954, J. Chem. Phys. **22**, 1229.
Excoffon, P. and Y. Marechal, 1972, Spectrochim. Acta **28A**, 269.
Gerson, F., 1961, Helv. Chim. Acta **44**, 471.
Haas, C. and D. F. Hornig, 1960, J. Chem. Phys. **32**, 1763.
Hankins, D., J. W. Moskowitz and F. H. Stillinger, 1970, J. Chem. Phys. **53**, 4544.
Hartmann, H., 1966, Theoret. Chim. Acta **6**, 20.
Hartmann, H., 1972, Theoret. Chim. Acta **27**, 147.
Heilbronner, E., H. H. Günthard and R. Gerdil, 1956, Helv. Chim. Acta **39**, 1171.
Heilbronner, E., H. Rutishauser and F. Gerson, 1959, Helv. Chim. Acta **42**, 2286, 2304.
Ibers, J. A., 1964, J. Chem. Phys. **41**, 25.
Janoschek, R., 1972, (unpublished results).
Janoschek, R., 1973a, Theoret. Chim. Acta **29**, 57.
Janoschek, R., 1973b, Theoret. Chim. Acta **32**, 49.
Janoschek, R., 1973c, unpublished results.
Janoschek, R., G. Diercksen and H. Preuß, 1968, Intern. J. Quantum Chem. **2**, 159.
Janoschek, R., E. G. Weidemann, H. Pfeiffer and G. Zundel, 1972, J. Am. Chem. Soc. **94**, 2387.
Janoschek, R., E. G. Weidemann and G. Zundel, 1973, Faraday Transactions II **69**, 505.
Jiang, G. J. and G. R. Anderson, 1973, J. Phys. Chem. **77**, 1764.
Ketelaar, J. A. A., 1941, Rec. Trav. Chim. **60**, 523.
Ketelaar, J. A. A. and W. Vedder, 1951, J. Chem. Phys. **19**, 654.
Kistenmacher, H., H. Popkie and E. Clementi, 1973, J. Chem. Phys. **58**, 5627.
Kollman, P. A. and L. C. Allen, 1969, J. Chem. Phys. **51**, 3286.
Kollman, P. A. and L. C. Allen, 1970a, J. Am. Chem. Soc. **92**, 6101.
Kollman, P. A. and L. C. Allen, 1970b, J. Chem. Phys. **52**, 5085.
Kraemer, W. P. and G. H. F. Diercksen, 1970, Chem. Phys. Letters **5**, 463.
Leviel, J. L. and Y. Marechal, 1971, J. Chem. Phys. **54**, 1104.
Lippincott, E. R. and R. Schroeder, 1955, J. Chem. Phys. **23**, 1099.
Manning, M. F., 1935, J. Chem. Phys. **3**, 136.
Marechal, Y. and A. Witkowski, 1968, J. Chem. Phys. **48**, 3697.
McLean, A. D. and M. Yoshimine, "Tables of Linear Molecule Wave Functions" IBM Research, San Jose, Calif. 1967.
Morokuma, K. and L. Pedersen, 1968, J. Chem. Phys. **48**, 3275.
Morokuma, K. and J. R. Winick, 1970, J. Chem. Phys. **52**, 1301.
Newton, M. D. and S. Ehrenson, 1971, J. Am. Chem. Soc. **93**, 4971.
Nibler, J. W. and G. C. Pimentel, 1967, J. Chem. Phys. **47**, 710.
Noble, P. N. and R. N. Kortzeborn, 1970, J. Chem. Phys. **52**, 5375.
Pavia, A. C. and P. A. Giguere, 1970, J. Chem. Phys. **52**, 3551.
Pecul, K. and R. Janoschek, 1974, Theoret. Chim. Acta **36**, 25.

Reid, C., 1959, J. Chem. Phys. **30**, 182.
Sandorfy, C., 1972, Can. J. Spect. **17**, 24.
Singh, T. R. and J. L. Wood, 1968, J. Chem. Phys. **48**, 4567.
Singh, T. R. and J. L. Wood, 1969, J. Chem. Phys. **50**, 3572.
Somorjai, R. L. and D. F. Hornig, 1962, J. Chem. Phys. **36**, 1980.
Swanstrom, P., R. Janoschek and H. Preuß, 1969, Intern. J. Quantum Chem. **3**, 115.
Wall, F. T. and G. Glockler, 1937, J. Chem. Phys. **5**, 314.
Walrafen, G. E., 1966, J. Chem. Phys. **44**, 1546.
Weidemann, E. G. and G. Zundel, 1967, Z. Phys. **198**, 288.
Weidemann, E. G. and G. Zundel, 1970, Z. Naturforsch. **25a**, 627.
Weidemann, E. G., R. Janoschek and G. Zundel, 1974, unpublished results.
Wolff, H., Helmuth Müller and Harald Müller, 1974, Ber. Bunsenges. Phys. Chem. **78**, 1241.
Wolff, H. and Helmuth Müller, 1974a, J. Chem. Phys. **60**, 2938.

CHAPTER 4

PROTON MOTIONS IN HYDROGEN BONDS

J. BRICKMANN

Fachbereich Chemie, Universität D775 Konstanz, West Germany

Contents

4.1. Introduction 219
4.2. Model approach 220
4.3. Tunneling in a one-dimensional double well potential 221
4.3.1. Time independent Hamiltonian 221
4.3.2. Vibrational coupling 224
4.3.3. Choice of the initial proton states 227
4.3.4. Two-level system 230
4.4. Calculation of proton transition rates 235
4.4.1. The medium time approximation 235
4.4.2. Time–energy uncertainty relation 239
4.4.3. Quasiclassical approximation 240
Acknowledgements 241
References 242

The hydrogen bond – recent developments in theory and experiments
Eds. P. Schuster et al. © *North-Holland Publ. Co., Amsterdam, 1976*

4.1. Introduction

One of the most interesting viewpoints of H-bonds is their participation in transfer phenomena (Riehl [1966]). The velocity of proton transfer is of general importance for time dependent processes in H-bonded solids (Fischer et al. [1967, 1969, 1970], Hofacker et al. [1975] and Stiller [1975]), in chemical reactions (Eigen [1963], Zimmermann [1964] and Schuster [1975a, b]) and in connection with biological problems as the isomerization rates of base pairs in nucleic acids and their consequences on the reduplication of DNA (Löwdin [1965] and Pullman [1972]). As has been reviewed in the contribution of Schuster [1975a], the proton in some single H-bonds occupies, in some sense, different sites between the two adjacent atoms, say X and Y, near to one or the other of them, and it can interchange between these sites according to a formal "reaction equation" $XH\cdots Y \rightleftharpoons X\cdots HY$. A good example for the proton transfer of this type is the rearrangement of the enol form of malonic aldehyde (I) (Schuster et al. [1973, 1975a, b]).

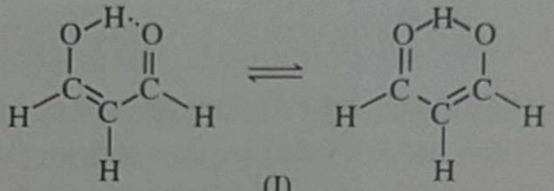

(I)

The rearrangement between the two possible "protomeric" structures (Zimmermann [1964]) is mostly connected not only with a pure proton displacement but with a change of the positions of the other nuclei in the molecular complex (Hofacker et al. [1975] and Schuster [1975a, b]). In many cases, as in the base pairs of DNA or the analogous structure of the dimer of formic acid (II) an isomerization between protomeric structures is only possible by simultaneous proton motion in parallel H-bonds (Ady and Brickmann [1971], Clementi et al. [1971] and Schuster et al. [1973, 1975a, b]).

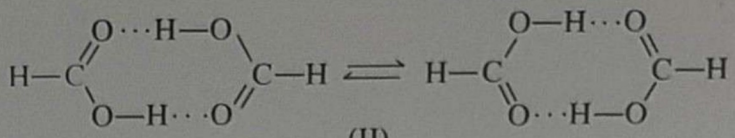

(II)

Contrary to earlier calculations (Rein et al. [1964a, b, 1965a, b] and Löwdin [1965]) a single proton motion in one of the H-bonds does not lead to two quasistable protomeric structures here. The isomerization effected by a proton transfer in one H-bond or the simultaneous proton motion in some coupled H-bonds can be described in terms of the motion of a particle along a rearrangement coordinate ξ which is often correlated to the vibration coordinate of a X–H stretching mode of a H-bond. The velocity of the proton rearrangement in H-bonds is affected by the shape of the effective potential energy as a function of ξ on one hand (Conway et al. [1956, 1964], Zimmermann [1964] and Brickmann and Zimmermann [1969]) and couplings to other nuclear motions on the other hand (Fischer et al. [1967, 1969, 1970], Rösch [1971], Brickmann [1973a] and Hofacker et al. [1975]). In this paper we will restrict our considerations mainly to the first point, i.e. we will review the methods for calculating proton transition rates in H-bonds from the motion of a particle, represented by a quantum-mechanical wave packet, in an effective double well potential.

4.2. Model approach

Considering the validity of the Born–Oppenheimer approximation, the internal nuclear motion of the molecular supercomplex is governed by the time dependent Schrödinger equation

$$H_{\text{tot}}(\{x\}, t)\, \Psi(\{x\}, t) = \mathrm{i}\hbar\, (\partial/\partial t)\, \Psi(\{x\}, t) \tag{4.1}$$

where H_{tot} is the Hamiltonian of the system, $\{x\}$ is a complete set of coordinates for the internal nuclear motion. For an isolated complex, the Hamiltonian is not explicitly time dependent and we have

$$H_{\text{tot}} = T(\{x\}) + V(\{x\}) \tag{4.2}$$

with the kinetic term $T(\{x\})$ and the potential energy or "energy surface" $V(\{x\})$ (see the contribution of Schuster [1975a]). We restrict our consideration to the case where this energy surface has two minima separated by a potential wall and where the coordinate change going from one well to another is mainly governed by a change of the coordinate of a proton in a H-bond. The adiabatic rearrangement between the two protomeric struc-

tures (Zimmermann [1964]) can then be described by a coordinate ξ following the path of steepest descent from one well to the other across a saddle point. The coordinate ξ in general is neither a straight line nor is it exactly identical with one of the vibrational normal coordinates of the system as has been shown by numerous authors (Stepanov [1945, 1946a, b], Bratož and Hadži [1957], Haas and Hornig [1959], Marechal and Witkowski [1967, 1968], Singh and Wood [1968], Janoschek et al. [1972, 1973, 1975], Rice and Wood [1973] and Hofacker et al. [1975]). Nevertheless, in many cases one can describe the proton motion in a H-bond with a one-dimensional model (Zimmermann et al. [1961, 1964, 1965], Löwdin [1963, 1964, 1965], Brickmann and Zimmermann [1966a, b, 1968, 1969] and Carbonell and Kostin [1973]). The coordinate ξ can often be identified with the XH-stretching mode. In the next section, we will analyze the motion of a wave packet representing a proton in a one-dimensional double well potential.

4.3. Tunneling in a one-dimensional double well potential

4.3.1. Time independent Hamiltonian

If the coupling between the proton motion along the coordinate ξ and the other coordinates is very weak, we can neglect this coupling in a first approximation. This restricts the problem of the proton movement to the quantum dynamics of a one-dimensional wave packet. Proton states with respect to a one-dimensional double well potential have been investigated by a large number of authors (Lippincott and Schroeder [1955a, b, 1956, 1957a, b], Heilbronner et al. [1956, 1959], Samorjai and Hornig [1962] and Brickmann and Zimmermann [1969]). In these works, the main point has been the calculation of eigenvalues E_i and eigenfunctions $\varphi_i(\xi)$ which are solutions of the time independent Schrödinger equation

$$H(\xi)\,\varphi_i(\xi) = E_i\,\varphi_i(\xi) \tag{4.3}$$

with the time independent Hamiltonian

$$H(\xi) = \frac{\hbar^2}{2m}\frac{\mathrm{d}^2}{\mathrm{d}\xi^2} + V(\xi) \tag{4.4}$$

and the potential energy function $V(\xi)$. The latter is identical with a cut of the energy surface $V(\{x\})$ (eq. (4.2)) along the coordinate ξ. A graph of $V(\xi)$ and some characteristic potential parameters are given in fig. 4.1.

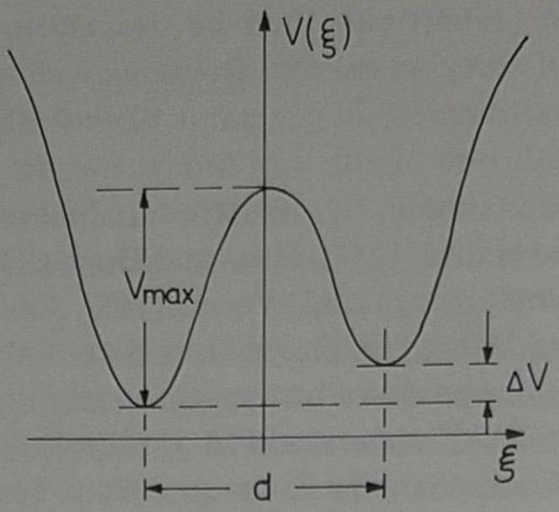

Fig. 4.1. Double minimum potential V and characteristic potential parameters V_{max}, ΔV and d (schematically).

In classical physics, a proton would stay in one of the wells unless it has sufficient energy to pass the potential barrier separating the two minima. However, a quantum-mechanical particle, may leak through the potential barrier from one classically permitted region to another. This phenomenon is known as the "tunnel effect". This effect has been first discussed independently by Gamow [1928a, b] and Gurney and Condon [1929] in order to explain the radiative decay of instable nuclei. The tunnel effect of a proton was first used to explain the inversion of the pyramidal ammonia molecule (Dennison and Uhlenbeck [1931], Morse and Stückelberg [1931], Rosen and Morse [1932], Manning [1935], Wall and Glockner [1937] and Herzberg [1960]). The consequence of the possibility of proton tunneling on the spectroscopic properties of H-bonds has been discussed intensely, but only a few articles exist on the time dependent phenomena of proton tunneling (Bell [1933], Conway et al. [1956], Löwdin [1965], Brickmann and Zimmermann [1966a, b, 1968, 1969], Hofacker [1968], Brickmann [1970], Rösch [1971], Brickmann [1973a] and Carbonell and Kostin [1973]). Instead of eq. (4.4), we have to solve the time dependent Schrödinger equation

$$H(\xi)\,\psi(\xi, t) = \mathrm{i}\hbar\,(\partial/\partial t)\,\psi(\xi, t) \tag{4.5}$$

with respect to a given initial condition $\psi(\xi, 0)$. $\psi(\xi, 0)$ is a wave packet, representing the proton at a given initial time $t = 0$. The probability of finding the proton in the space interval between ξ and $\xi + \mathrm{d}\xi$ is then given by

$$W(\xi)\,\mathrm{d}\xi = |\psi(\xi, 0)|^2\,\mathrm{d}\xi. \tag{4.6}$$

We choose the zero point of the ξ-scale so that the maximum of the barrier is located at $\xi = 0$. If we identify the left well (L) with the protomeric structure XH$\cdots$Y, and the right one (R) with X$\cdots$HY, all initial wave packets $\psi_L(\xi, 0)$ with

$$\int_{-\infty}^{0} |\psi_L(\xi, 0)|^2 \, d\xi = 1 \tag{4.7}$$

represent a proton state of the protomeric structure XH$\cdots$Y. From the normalization condition

$$\int_{-\infty}^{\infty} |\psi_L(\xi, 0)^2| \, d\xi = 1, \tag{4.8}$$

it follows, that the probability of finding the proton in the right area is then identically equal to zero. The initial wave packet can be expanded in a series solution with respect to the eigenfunction $\varphi_i(\xi)$ of the Hamiltonian $H(\xi)$ (eq. (4.4)):

$$\psi(\xi, 0) = \sum_i c_i \varphi_i(\xi) \tag{4.9}$$

with the (in general complex) coefficients c_i. The values $p_i = |c_i|^2$ are the probabilities of finding the system in a quantum state $\varphi_i(\xi)$. One has

$$\sum_i |c_i|^2 = \sum_i p_i = 1. \tag{4.10}$$

The time evolution of the system, i.e. the solution $\psi(\xi, t)$ of the time dependent Schrödinger eq. (4.5) can be given in terms of the unitary evolution operator $U(t, t_0) = \exp[-(i/\hbar) H(t - t_0)]$ (Messiah [1965c])

$$\begin{aligned} \psi(\xi, t) &= \exp\left(-\frac{i}{\hbar} Ht\right) \psi(\xi, 0) = \sum_i c_i \exp\left(-\frac{i}{\hbar} E_i t\right) \varphi_i(\xi) \\ &= \sum_i p_i^{1/2} \exp(i\alpha_i) \exp\left(-\frac{i}{\hbar} E_i t\right) \varphi_i(\xi) \end{aligned} \tag{4.11}$$

when we use the probabilities p_i and the "initial phases" α_i (Carbonell and Kostin [1973]) instead of the coefficient c_i.

The probability density $W(\xi, t)$ to find the proton at time t in the space limits of ξ and $\xi + d\xi$ is given by (Brickmann and Zimmermann [1968, 1969] and Carbonell and Kostin [1973]):

$$\begin{aligned} W(\xi, t) &= \psi^*(\xi, t) \, \psi(\xi, t) = \sum_i p_i |\varphi_i(\xi)|^2 \\ &\quad + 2 \sum_{i>j} \sum_j (p_i p_j)^{1/2} \varphi_i(\xi) \, \varphi_j(\xi) \cos(\alpha_i - \alpha_j - \omega_{ij} t) \end{aligned} \tag{4.12}$$

with

$$\omega_{ij} = (E_i - E_j)/\hbar. \tag{4.13}$$

Here we used the relation $\cos\gamma = \frac{1}{2}(e^{i\gamma} + e^{-i\gamma})$.

The probability $W_L(t)$ of finding the proton in the left well at any time t is given in analogy to eq. (4.7) as an integral over the left half space.

$$W_L(t) = \int_{-\infty}^{0} W(\xi, t)\, d\xi = \sum_i p_i w_{ii} + 2 \sum_{i>j} \sum_j (p_i p_j)^{1/2} w_{ij} \cos(\alpha_i - \alpha_j - \omega_{ij} t) \tag{4.14}$$

with

$$w_{ij} = \int_{-\infty}^{0} \varphi_i^*(\xi)\, \varphi_j(\xi)\, d\xi. \tag{4.15}$$

This function is quasiperiodic around the time average

$$\bar{W}_L = \sum_i p_i w_{ii}. \tag{4.16}$$

The rate r of proton transfer $XH\cdots Y \rightarrow X\cdots HY$ can easily be calculated from the probability (eq. (4.14))

$$r = (d/dt)\, W_L(t). \tag{4.17}$$

This function is once again periodic or quasiperiodic. We will restrict our further considerations to a time scale which is much shorter than the "reoccurrence time" τ_{rev}, i.e. the time where $W_L(\tau_{rev})$ is for the first time approximately equal to its initial value $W_L(0) = 1$.

4.3.2. Vibrational coupling

In the previous section we replaced the influence of the large number of intramolecular and intermolecular degrees of freedom by special constraints. As has been shown by many authors both theoretically (for a review see the contributions of Hofacker et al. [1975], Janoschek [1975] and Schuster [1975a]) and experimentally (Arnold and Millen [1965a, b], Bertie and Millen [1965a, b], Millen and Zabicky [1965], Millen and Samsonov [1965], Grimm et al. [1970] and Stiller [1975]), this coupling between the proton motion along ξ and thermal vibrations along the other coordinates, cannot be neglected in all cases. In principle, we can extend the formalism outlined above to more than one degree of freedom. One is then encountered with the problem of calculating the eigenvalues and eigenfunctions of a Hamiltonian, which depends on more than one coordinate. Although significant progress has been made in the develop-

ment of methods of solving the respective stationary Schrödinger equation (Stepanov [1946a, b], Reid [1959], Ibers [1964], Singh and Wood [1968], Brickmann et al. [1971] and Janoschek et al. [1972, 1975]), it is impossible to include all degrees of freedom of the molecular supercomplex explicitly. Hofacker [1965, 1968] introduced a coarse graining procedure to reduce the large number of energy levels. This leads to a non-Markovian master equation for a reduced density matrix instead of the time dependent Schrödinger equation for the wave functions (Hofacker [1965, 1968] and Rösch [1971, 1972]), i.e. we have an irreversible behavior of the probability functions $W(\xi, t)$ and $W_L(t)$. Another formalism in taking the coupling of a large number of freedoms into account is given by the transport theory: Rösch [1971] discussed a statistical model for the proton transition in a symmetrical H-bond, where the proton motion is strongly coupled to the H-bond vibration (X···Y vibration), which itself is coupled to a heath of harmonic oscillators, representing the rest of the vibrational degrees of freedom. For certain values of the coupling constants, the time dependence of $W_L(t)$ is no longer governed by the phase relations between the eigenfunctions $\varphi_i(\xi)$, but mainly by these couplings. An extensive discussion of coupling phenomenons with respect to the quantum statistics of proton motions in H-bonds will be given in the contribution of Hofacker [1975].

Here we will restrict the discussion to the solutions of the time dependent Schrödinger equation. An interesting model to take thermal vibrations into account has recently been given by Carbonell and Kostin [1973]. The authors used an additional fluctuating potential $v(\xi, t)$ for the vibrations which have not been explicitly considered. Instead of eq. (4.5) one has the time dependent Schrödinger equation

$$H'(\xi, t)\,\psi'(\xi, t) = i\hbar\,(\partial/\partial t)\,\psi'(\xi, t) \tag{4.18}$$

with

$$H'(\xi, t) = H(\xi) + v(\xi, t). \tag{4.19}$$

In analogy to eq. (4.11) we can expand the solutions of eq. (4.18) with respect to the eigenfunctions $\varphi_i(\xi)$ of the time independent Hamiltonian $H(\xi)$

$$\psi'(\xi, t) = \sum_i c_i(t) \exp\left(-\frac{i}{\hbar} E_i t\right) \varphi_i(\xi) \tag{4.20}$$

with time dependent coefficients $c_i(t)$. These coefficients can be obtained

in closed form, if one assumes that the quantities

$$v_{ik}(t) = \int \varphi_i^*(\xi)\, v(\xi, t)\, \varphi_k(\xi)\, \mathrm{d}\xi \tag{4.21}$$

are equal to zero for $i \neq k$, i.e. that no transitions between different states $\varphi_i(\xi)$ and $\varphi_k(\xi)$ will be induced by the perturbation $v(\xi, t)$. In general, this restriction is much too strong as has been shown for the case where the proton motion along the XH-stretching mode is coupled to the H-bond vibration (Rösch [1971] and Brickmann [1973]). One can avoid this difficulty by introducing "relevant" and "nonrelevant" degrees of freedom (Brickmann [1973a]): we replace the coordinate ξ by a set of coordinates–which we call relevant coordinates–so that the respective elements $v_{ik}(t)$ become approximately diagonal. Here we will follow the ideas of Carbonell and Kostin. With the restriction described above, we obtain

$$c_i(t) = \exp\left[-\mathrm{i}\beta_i(t)\right] c_i(0) \tag{4.22}$$

with

$$\beta_i(t) = \frac{1}{\hbar} \int_0^t v_{ii}(t')\, \mathrm{d}t' \tag{4.23}$$

and the probability density $W(\xi, t)$ results in (Carbonell and Kostin [1973])

$$W(\xi, t) = \sum_i p_i |\varphi_i(\xi)|^2 + 2 \sum_{i<j} \sum_j (p_i p_j)^{1/2} \varphi_i(\xi)\, \varphi_j(\xi) \cos\left[\alpha_i - \alpha_j - \omega_{ij} t - \beta_{ij}(t)\right] \tag{4.24}$$

with the phase term

$$\beta_{ij}(t) = \beta_i(t) - \beta_j(t) = \frac{1}{\hbar} \int_0^t \left[v_{ii}(t') - v_{jj}(t')\right] \mathrm{d}t'. \tag{4.25}$$

In general, the fluctuating potential $v(\xi, t)$ is not explicitly known. If one treats $v(\xi, t)$ as a stochastic variable in the form

$$v(\xi, t) = X(t)\, L(\xi) \tag{4.26}$$

with the position-dependent function $L(\xi)$ and the stationary random process $X(t)$ (Carbonell and Kostin [1973]), and assumes that the integral

$$G_{ij}(\tau) = \frac{1}{\hbar} \int_t^{t+\tau} \left[v_{ii}(t') - v_{jj}(t')\right] \mathrm{d}t' \tag{4.27}$$

is a stochastic quantity with a Gaussian distribution, one obtains with random initial phases for the averaged probability distribution (Carbonell and Kostin [1973])

$$\bar{W}(\xi, t) = \sum_i p_i |\varphi_i(\xi)|^2 + 2 \sum_{i>j} \sum_j (p_i p_j)^{1/2} \varphi_i(\xi)\ \varphi_j(\xi) \exp(-D_{ij} t)$$

$$\times [\overline{\cos \alpha_{ij}} \cos(\omega_{ij} t) + \overline{\sin \alpha_{ij}} \sin(\omega_{ij} t)] \tag{4.28}$$

with

$$D_{ij} = \frac{L_{ii} - L_{jj})^2}{\hbar^2} \int_0^\infty \langle X(0)\, X(t') \rangle \, \mathrm{d}t' \tag{4.29}$$

and

$$L_{ii} = \int \varphi_i^*(\xi)\, L(\xi)\, \varphi_i(\xi)\, \mathrm{d}\xi. \tag{4.30}$$

The quantity $\langle X(0)\, X(t') \rangle$ is the correlation coefficient of the stochastic variable $X(t)$.

Contrary to the case described in section 4.3.1, the probability distribution $\bar{W}(\xi, t)$ (eq. (4.28)) is now no longer a periodic or quasiperiodic function. As $t \to \infty$, $\bar{W}(\xi, t)$ approaches the steady state value

$$\bar{\bar{W}}(\xi) = \sum_i p_i |\varphi_i(\xi)|^2. \tag{4.31}$$

The time evolution of the probability amplitudes $W(\xi, t)$, $\bar{W}(\xi, t)$, $W_L(t)$ and $W_R(t)$ is dependent on the initial wave packet $\psi(\xi, 0)$ as has been shown above. Hence the question arises, what types of wave packets are able to represent physically meaningful nonstationary proton states and what are not. We will distinguish between two types of initial wave packets which we call the "spectroscopic initial state" and the "thermodynamic initial state". The physical meaning of this notation will be discussed in the following section.

4.3.3. Choice of the initial proton states

As has been stated above, one can describe the protomeric structures XH···Y and X···HY by wave packets $\psi_L(\xi, 0)$ or $\psi_R(\xi, 0)$ which are localized on the negative or positive half space respectively:

$$\int_{-\infty}^0 |\psi_R(\xi, 0)|^2 \, \mathrm{d}\xi = 0, \qquad \int_0^\infty |\psi_L(\xi, 0)|^2 \, \mathrm{d}\xi = 0. \tag{4.32}$$

However, this localization is not unique. One needs additional conditions to construct physically meaningful proton states. If we restrict our

consideration for a moment to the case where the energy

$$E = \int \psi^*(\xi, 0)\, H\, \psi(\xi, 0)\, \mathrm{d}\xi \tag{4.33}$$

associated with the wave packet, is lower than V_{max}, then the proton can change from one protomeric structure to the other with energy conservation only by quantum-mechanical tunneling. The situation is similar to the radiative α-decay of a nucleus (Gamow [1928a, b]). We describe the initial proton by a quasistationary state, i.e. a state which is localized on one of the two space regions considered, and is moreover the best approximation to the eigenstates of H in that region (Brickmann and Zimmermann [1969]) (see fig. 4.2). We can characterize the localization procedure in terms of projection operators P_L and P_R which we use to classify the protomeric structures XH···Y and X···HY (Hofacker [1965, 1968], Brickmann and Zimmermann [1968, 1969], Golden [1969] and Brickmann [1973a]). We have

$$\begin{aligned} P_L|\psi_L(0)\rangle &= |\psi_L(0)\rangle, \qquad P_L|\psi_R(0)\rangle = 0|\psi_R(0)\rangle = 0 \\ P_R|\psi_R(0)\rangle &= |\psi_R(0)\rangle, \qquad P_R|\psi_L(0)\rangle = 0|\psi_L(0)\rangle = 0 \end{aligned} \tag{4.34}$$

and

$$P_L^2 = P_L, \quad P_R^2 = P_R, \quad P_L P_R = P_R P_L = 0, \quad P_L + P_R \approx 1, \tag{4.35}$$

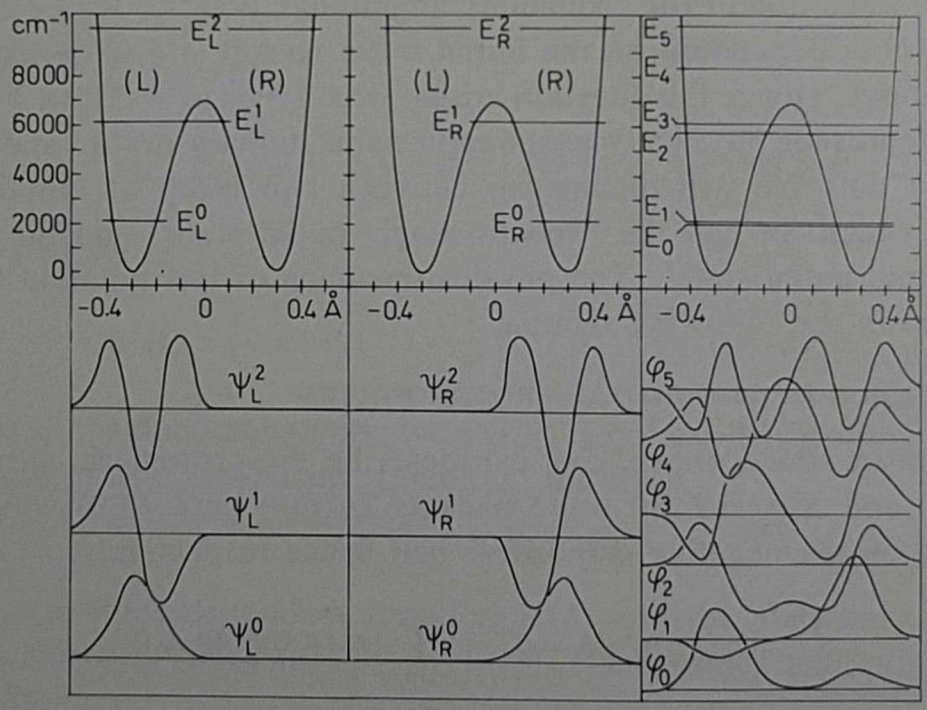

Fig. 4.2. Potential, eigenvalues and eigenfunction of the Hamiltonians H_L, H_R and H. Potential parameters: $V_{max} = 7000\ \mathrm{cm}^{-1}$, $\Delta V = 20\ \mathrm{cm}^{-1}$, $d = 0.7$ Å.

where we used the Dirac notation $|\psi_L(0)\rangle$ and $|\psi_R(0)\rangle$ for the localized states:

$$\psi_R(\xi, 0) = \langle \xi | \psi_R(0) \rangle, \quad \psi_L(\xi, 0) = \langle \xi | \psi_L(0) \rangle. \tag{4.36}$$

The operators P_L and P_R can be given formally by the relations (Brickmann [1973a])

$$P_L = \int_{-\infty}^{0} |\xi\rangle \, d\xi \, \langle \xi|, \qquad P_R = \int_{0}^{\infty} |\xi\rangle \, d\xi \, \langle \xi| \tag{4.37}$$

and one can show that the initial states $|\psi_L(0)\rangle$ or $|\psi_R(0)\rangle$ are eigenstates of an operator H_L or H_R respectively (Brickmann and Zimmermann [1969] and Brickmann [1973a])

$$H_L = P_L H P_L, \qquad H_R = P_R H P_R \tag{4.38}$$

$$H_L |\psi_L^i\rangle = E_L^i |\psi_L^i\rangle, \qquad H_R |\psi_R^i\rangle = E_R^i |\psi_R^i\rangle. \tag{4.39}$$

The states $|\psi_L^i\rangle$ and $|\psi_R^i\rangle$ are pure eigenstates of a Hamiltonian for the proton motion in one of the two wells. To distinguish between these states and superpositions of such states, we call the $|\psi_R^i\rangle$ and $|\psi_L^i\rangle$ "spectroscopic initial states". If the eigenstates $|\varphi_i\rangle$ of the Hamiltonian H are known, the coefficients c_j can be easily calculated, e.g.

$$|\psi_L^i\rangle = \sum_j |\varphi_j\rangle\langle\varphi_j|\psi_L^i\rangle = \sum_j c_j^i |\varphi_j\rangle. \tag{4.40}$$

These coefficients are fully determined within a simultaneously complex phase.

For the matrix elements of H with respect to the localized states, one has

$$\langle \psi_L^i | H | \psi_L^i \rangle = \langle \psi_L^i | P_L H P_L | \psi_L^i \rangle = E_L^i \delta_{ij} \tag{4.41}$$

where we used the property of the projection operator $P_L^+ = P_L$ and the relations of eq. (4.34). For the states $|\psi_R^i\rangle$ we have analogous relations. From eq. (4.40), it follows directly that there is no direct coupling between the states associated to one protomeric structure. The decay of a "quasistationary state" (Landau and Lifshitz [1959a]), $|\psi_L^i\rangle$ or $|\psi_R^i\rangle$ respectively, is related directly to the proton transition from one well to the other.

Instead of pure eigenstates of the one well Hamiltonian H_L and H_R, Carbonell and Kostin [1973] used a superposition of such states as an initial state. In taking the temperature into consideration, they started with the assumption, that the absolute values of the coefficients c_i in eq.

(4.9) are given by the probabilities p_i (see eq. (4.11)) with respect to a Boltzmann distribution

$$p_i = Q^{-1} \exp(-E_i/kT) \tag{4.42}$$

(T: absolute temperature, k: Boltzmann's constant) and that the localization of the wave packet is affected by the choice of the phases α_i. In eq. (4.31), Q is the partition function

$$Q = \sum_i \exp(-E_i/kT). \tag{4.43}$$

To indicate that these initial wave packets are functions of temperature, we use the term "thermodynamic initial state" $\psi_L(\xi, 0) = \psi_L(\xi, T, 0)$ or $|\psi_L(0)\rangle = |\psi_L(T, 0)\rangle$. All such states belonging to one well region can be expanded with respect to the "spectroscopic states" of the same region e.g.

$$|\psi_L(T, 0)\rangle = \sum_i d_{Li} |\psi_L^i\rangle \tag{4.44}$$

with

$$d_{Li} = \langle \psi_L^i | \psi_L(T, 0)\rangle. \tag{4.45}$$

In the case, where the oscillatory proton motion is damped by the stochastic potential $v(\xi, t)$, a protonic system which is described at $t = 0$ by a thermodynamic initial state approaches equilibrium for $t \to \infty$.

4.3.4. Two-level system

For the low temperature region, only the ground states of the XH-stretching mode or the YH-stretching mode are occupied with probability close to unity, and we can neglect the influence of the higher states on the time evolution of the system (Brickmann and Zimmermann [1969] and Brickmann [1970]). In many cases the two states can be identified with the ground states $|\psi_L^0\rangle$ and $|\psi_R^0\rangle$ of the one well Hamiltonians H_L and H_R respectively (see fig. 4.2). If the energy difference of the respective eigenvalues E_L^0 and E_R^0 is much less than the difference between the energies of the ground state and the first excited state of a stretching mode i.e.

$$|E_L^0 - E_R^0| < 1500\ \mathrm{cm}^{-1} \tag{4.46}$$

then the eigenfunctions $\varphi_0(\xi)$ and $\varphi_1(\xi)$ of H belonging to the lowest two eigenvalues E_0 and E_1 can be approximated as linear combinations of $\psi_L^0(\xi) = \langle \xi | \psi_L^0 \rangle$ and $\psi_R^0(\xi) = \langle \xi | \psi_R^0 \rangle$ (Brickmann [1970], Weidemann and

Zundel [1970] and Janoschek [1975]) and vice versa

$$\varphi_0(\xi) = c_1\psi_L^0(\xi) + c_2\psi_R^0(\xi), \qquad \varphi_1(\xi) = c_2\psi_L^0(\xi) - c_1\psi_R^0(\xi) \tag{4.47}$$

with

$$c_1^2 + c_2^2 = 1. \tag{4.48}$$

In this case (two-level systems), the absolute values of the coefficients c_1 and c_2 are fixed and it is not possible to construct a thermodynamic initial state localized in the region of one well. Inversion of the system of (4.48) gives

$$\psi_L^0(\xi) = c_1\varphi_0(\xi) + c_2\varphi_1(\xi), \qquad \psi_R^0(\xi) = c_2\varphi_0(\xi) - c_1\varphi_1(\xi). \tag{4.49}$$

If the proton is in the left well at $t = 0$ i.e. we have the protomeric structure X–H$\cdots$Y, the probability density $W(\xi, t)$ (eq. (4.12)) takes the form

$$W(\xi, t) = c_1^2|\varphi_0(\xi)|^2 + c_2^2|\varphi_1(\xi)|^2 + 2c_1c_2\,\varphi_0(\xi)\,\varphi_1(\xi)\cos\omega t. \tag{4.50}$$

If the potential $V(\xi) = V_0(\xi)$ is symmetrical with respect to $\xi = 0$, representing the proton motion XH$\cdots$X$\rightleftharpoons$X$\cdots$HX in a symmetrical H-bond, then the coefficients c_1 and c_2 have the same absolute value. One can choose

$$c_1 = c_2 = 1/\sqrt{2} \tag{4.51}$$

if we assume without restriction of generality that all functions are real. In the symmetrical case, one obtains

$$\begin{aligned} W(\xi, t) &= \tfrac{1}{2}[\varphi_0^2(\xi) + \varphi_1^2(\xi)] + \varphi_0(\xi)\,\varphi_1(\xi)\cos\omega_s t \\ &= \tfrac{1}{2}[\psi_L^2(\xi) + \psi_R^2(\xi)] + [\psi_L^2(\xi) - \psi_R^2(\xi)]\cos\omega_s t \end{aligned} \tag{4.52}$$

i.e. the probability density oscillates with angular frequency ω_s, which is proportional to the splitting of the degenerate energies E_L^0 and E_R^0 (see fig. 4.3)

$$\omega_s = (E_1 - E_0)/\hbar. \tag{4.53}$$

If the potential $V(\xi)$ is no longer symmetrical but can be represented as a sum of a symmetrical double well potential $V_S(\xi)$ and antisymmetrical part $V_A(\xi) = -V_A(-\xi)$

$$V(\xi) = V_S(\xi) + V_A(\xi), \tag{4.54}$$

the coefficients c_1 and c_2 can be calculated by perturbation theory (Brickmann [1970] and Weidemann and Zundel [1970]). The function

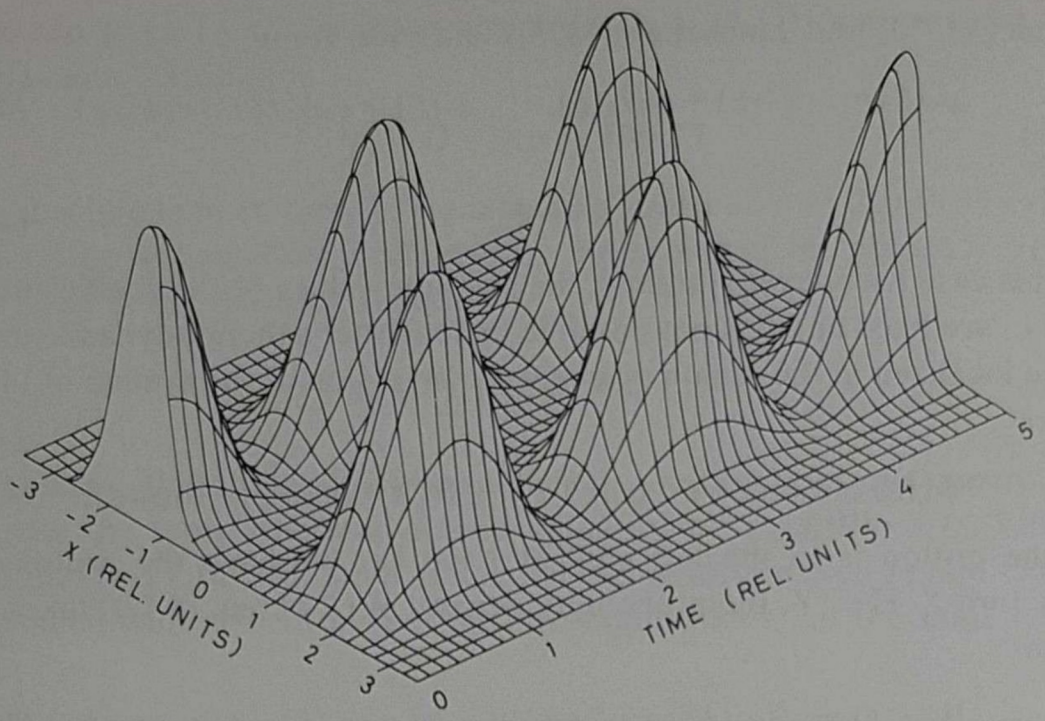

Fig. 4.3. Probability distribution function $W(\xi, t)$ for a proton in a symmetrical H-bond. At $t = 0$ the proton is described by the vibrational ground state of the left well (schematically).

$V_A(\xi)$ can be interpreted as the effect of an electrical field on a symmetrical potential (Weidemann and Zundel [1970]), but the applied formalism can be used more generally for a larger class of nonsymmetrical H-bonds (Brickmann [1970]). Defining

$$\omega = (E_1 - E_0)/\hbar \tag{4.55}$$

where E_0 and E_1 are now eigenvalues belonging to the Hamiltonian with potential energy function $V(\xi)$ (see fig. 4.2), perturbational calculations result in (Brickmann [1970])

$$\begin{aligned} c_1 &= \frac{1}{2}\left[\left(1+\frac{\omega_s}{\omega}\right)^{1/2} + \left(1-\frac{\omega_s}{\omega}\right)^{1/2}\right] \\ c_2 &= \frac{1}{2}\left[\left(1+\frac{\omega_s}{\omega}\right)^{1/2} - \left(1-\frac{\omega_s}{\omega}\right)^{1/2}\right] \end{aligned} \tag{4.56}$$

where ω_s is given by relation eq. (4.53) with respect to the symmetrical potential. The difference ω results in this approximation:

$$\omega = [\omega_s^2 + 4\langle\psi_L|V_A|\psi_L\rangle^2/\hbar^2]^{1/2}. \tag{4.57}$$

The probability function $W(\xi, t)$ remains unequal to zero in the initial

region at all times i.e. only a part of the probability is periodic with frequency ω (see fig. 4.4).

Using the approximation coefficients of eq. (4.56) we obtain

$$W(\xi, t) = \psi_L^2(\xi) - (\omega_s/\omega)^2[\psi_L^2(\xi) - \psi_R^2(\xi)] \sin^2 \tfrac{1}{2}\omega t. \qquad (4.58)$$

If the proton motion is damped by a damping constant D (see eq. (4.29)), the probability density of a two-level system follows from eq. (4.28):

$$\bar{W}(\xi, t) = c_1^2|\varphi_0(\xi)|^2 + c_2^2|\varphi_1(\xi)|^2 2c_1c_2\varphi_0(\xi)\,\varphi_1(\xi) \exp(-Dt) \cos \omega t \qquad (4.59)$$

or in analogy to eq. (4.57)

$$\bar{W}(\xi, t) = \psi_L^2(\xi) - \tfrac{1}{2}(\omega_s/\omega)^2[\psi_L^2(\xi) - \psi_R^2(\xi)][1 - \exp(-Dt) \cos \omega t]. \qquad (4.60)$$

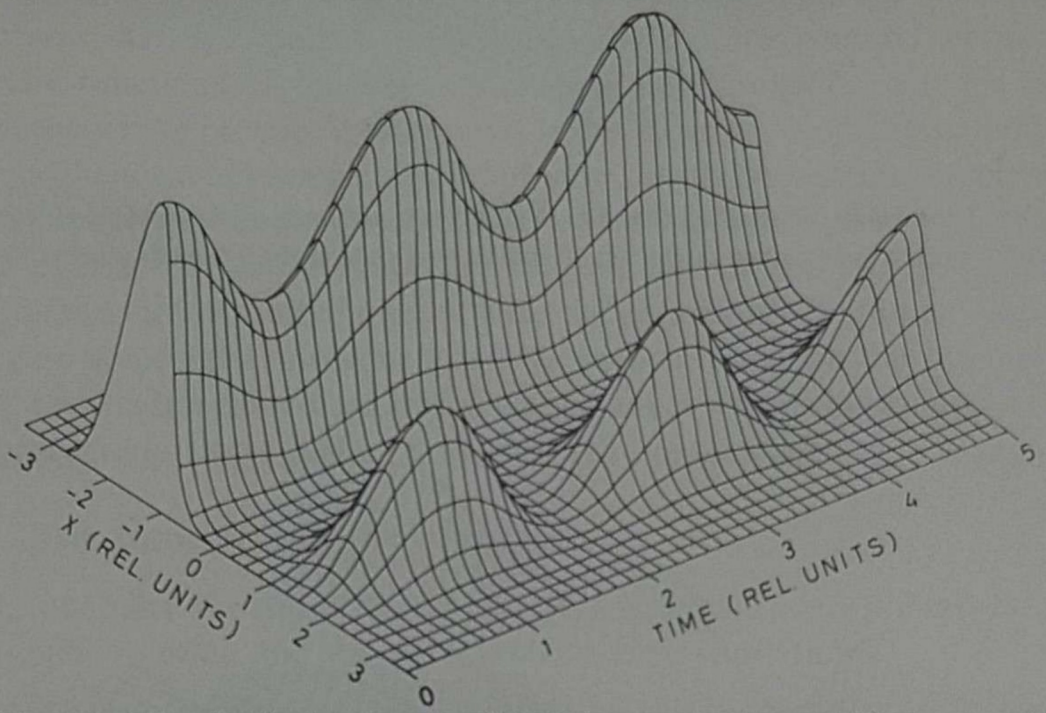

Fig. 4.4. Probability distribution function $W(\xi, t)$ for a proton in a weakly unsymmetrical H-bond. At $t = 0$ the proton is described by the vibrational ground state of the left well (schematically).

In figs. 4.5 and 4.6, the influence of the damping on the probability distribution can be seen schematically for the case of a symmetrical potential (fig. 4.5) and a weakly unsymmetrical one (fig. 4.6). Here it was assumed that the damping constant D is in the same order of magnitude as the frequency ω. For $D \gg \omega$, the time dependency of $\bar{W}(\xi, t)$ is mainly governed by an exponential decay law and the rate of proton transfer is no longer dependent on the energy levels of the one-dimensional double minimum potential. In the latter case, where the damping plays the dominant role, the model of a fluctuating additional potential $v(\xi, t)$ with

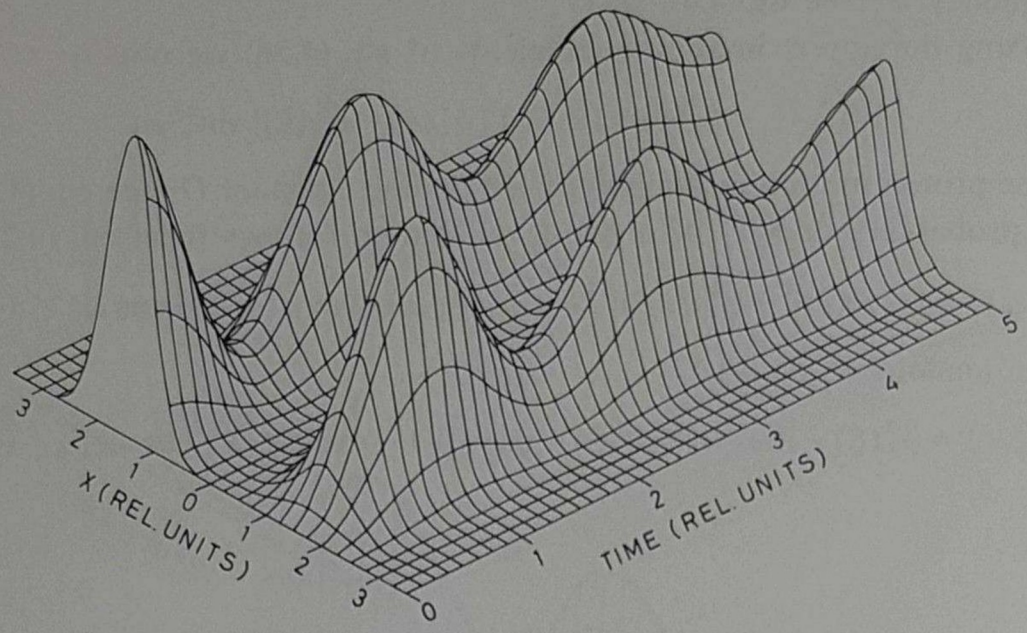

Fig. 4.5. Probability distribution function $\bar{W}(\xi, t)$ for a proton in a symmetrical H-bond. At $t = 0$ the proton is described by the vibrational ground state of the left well (schematically).

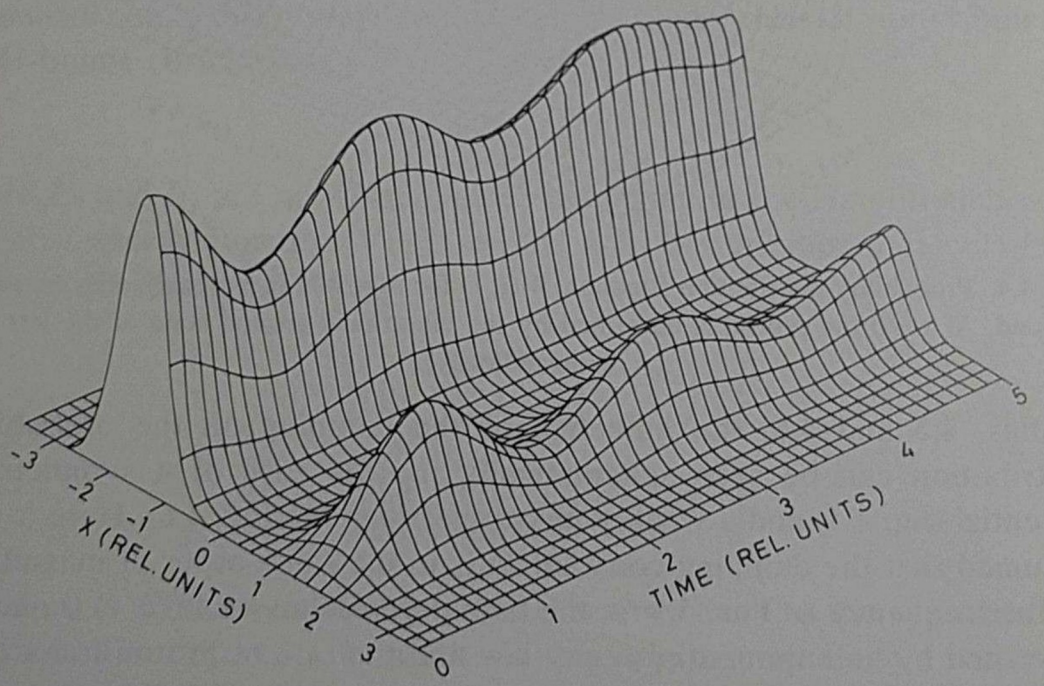

Fig. 4.6. Probability distribution function $\bar{W}(\xi, t)$ for a proton in a weakly unsymmetrical H-bond. At $t = 0$ the proton is described by the vibrational ground state of the left well (schematically).

the simplified assumption of Carbonell and Kostin [1973] can no longer be the basis of our calculations. One has to analyze in detail the mechanism of the coupling between the different degrees of freedom. In the following section we will review some methods to obtain approximations for the rate of proton transfer i.e. the life times of the protomeric structures XH···Y and X···HY based on the model discussed above. We will restrict our discussion to the case where $D \lesssim \omega$.

4.4. Calculation of proton transition rates

In section 4.3, we have demonstrated that in the weakly damped case, the probability amplitudes $W_L(t)$ and $W_R(t)$ to find one of the protomeric structures XH···Y and X···HY respectively, are periodic or quasi-periodic functions of time. The rate of proton transition, i.e. the time derivative of the probability functions is therefore a periodic function too. From a chemical or biological point of view, one is not so much interested in the explicit time dependence of $W(t)$. The interesting point is to obtain some estimate of the average life time of one of the two protomeric structures as a function of a set of external parameters. In this section we will give some relations which can be used to estimate the "tunneling time" i.e. the life time of an initial wave packet which represents one of the protomeric states XH···Y or X···HY respectively.

4.4.1. The medium time approximation

The probability functions $W_L(t)$ and $W_R(t)$ include both processes, the "left–right"-motion and the reversal. For very short times

$$t \approx \tau_{min} = (\omega_{max})^{-1} \tag{4.61}$$

where ω_{max} is the largest frequency giving a significant contribution to the probability functions $W(\xi, t)$ or $\bar{W}(\xi, t)$, eqs. (4.12) and (4.28) respectively, we can neglect the reverse process. We can expand the functions in a series in t. For $t < \tau_{min}$, the time dependence of $W(\xi, t)$ is mainly governed by the t^2-term while in $\bar{W}(\xi, t)$ the linear term dominates the time evolution for $D \approx \omega_{max}$.

For $t \gg \tau_{rev}$, where τ_{rev} is the reoccurrence time of the function considered, the probability becomes periodic or quasiperiodic. τ_{rev} can be approximately identified with

$$\tau_{rev} \approx (\omega_{min})^{-1} \tag{4.62}$$

where ω_{min} is the smallest frequency contributing significantly to $W(\xi, t)$ or $\bar{W}(\xi, t)$. We choose a time scale, which is limited by τ_{min} and τ_{rev}

$$\tau_{min} < t < \tau_{rev}. \tag{4.63}$$

Without further restriction, we assume that we have the structure XH$\cdots$Y at $t = 0$, represented by a wave packet $\psi_L(\xi)$. As an approximation (Brickmann and Zimmermann [1968, 1969] and Brickmann [1970]), we can interpolate the probability function $W_L(t)$ linearly between $t = 0$ and $t = t'$–the time when $W_L(t)$ for the first time equals the average value $\bar{\bar{W}}_L$. For $t < t'$ we can neglect the reverse process and obtain approximately for the rate of proton transfer from left to right

$$r_{L\to R} = \frac{dW_L(t)}{dt} \approx \frac{W_L(0) - W_L(t')}{t'} = \frac{W_L(0) - \bar{\bar{W}}_L}{t'} \tag{4.64}$$

or, if we denote the inverse rate or lingering time in the left well as "tunneling time" τ_L, and assume that $W_L(0) = 1$:

$$\tau_L = t'/W_R(t') = t'/\bar{\bar{W}}_R. \tag{4.65}$$

Here we used the completeness relation for $\bar{\bar{W}}_L$ and $\bar{\bar{W}}_R$, the probabilities to realize the protomeric structure XH$\cdots$Y and X$\cdots$HY respectively:

$$\bar{\bar{W}}_L + \bar{\bar{W}}_R = 1. \tag{4.66}$$

In the two-level systems (section 4.3.4), $\bar{\bar{W}}_R$, $\bar{\bar{W}}_L$ and t' can easily be calculated (Brickmann [1970] and Weidemann and Zundel [1970]). According to eqs. (4.50) and (4.59) we obtain

$$\bar{\bar{W}}_L = 1 - 2c_1^2c_2^2, \qquad \bar{\bar{W}}_R = 2c_1^2c_2^2 \tag{4.67}$$

and

$$t' = \pi/2\omega. \tag{4.68}$$

The tunneling time is therefore given by the relation

$$\tau_L = \pi/4\omega c_1^2 c_2^2 \tag{4.69}$$

or if we use eqs. (4.56)

$$\tau_L = \frac{\pi}{\omega}\left(\frac{\omega}{\omega_s}\right)^2 = \frac{\pi}{\omega_s}\frac{\omega}{\omega_s} = \tau_0\frac{\omega}{\omega_s} \tag{4.70}$$

where ω_s is defined by eq. (4.53) and τ_0 is the tunneling time in the symmetrical case. τ_0 is identical with half the oscillation period of the probability functions $W_L(t)$ and $\bar{W}_L(t)$. It is easy to calculate τ_L if we

know the energy difference $E_1 - E_0$ (see eq. (4.53)) for the symmetrical and unsymmetrical case. If the potential $V(\xi)$ is given as in eq. (4.54), ω and ω_s can be obtained directly from the potential parameters.

The main effect of the additional potential $V_A(\xi)$ is to get an unsymmetrical potential function $V(\xi)$ for the proton motion. One can show (Brickmann [1970]) that the energy difference ΔV of the two minima of the potential (see fig. 4.1) can be calculated from the matrix element of $V_A(\xi)$ with respect to one of the localized states in the two-level approximation. We obtain

$$\Delta V \approx 2\langle \psi_L | V_A | \psi_L \rangle. \tag{4.71}$$

Considering the definition of ω (eq. (4.49)) this gives immediately the relation

$$\omega = [\omega_s^2 + (\Delta V/\hbar)^2]^{1/2} \tag{4.72}$$

and from eq. (4.70)

$$\tau_L = \tau_0[1 + (\Delta V/\hbar\omega_s)^2]^{1/2}. \tag{4.73}$$

In order to calculate the energy splitting $\hbar\omega_s$ for an arbitrary shape of the barrier separating the two wells of the potential function, one can use the quasiclassical WKB-approximation (Landau and Lifshitz [1959a], Berry [1960] and Brickmann and Zimmermann [1966a])

$$\omega_s = \frac{\omega_0}{\pi} \exp\left\{-\frac{1}{\hbar}\int_a^b |\{2m[V(\xi) - E]\}^{1/2}| \, d\xi\right\} \tag{4.74}$$

where ω_0 is the angular frequency of classical proton vibration in one of the two wells, a and b are the classical turning points on the left and the right side of the barrier respectively and $E = \frac{1}{2}(E_1 + E_0)$ is the average energy of the two states $\varphi_0(\xi)$ and $\varphi_1(\xi)$ considered. Introducing the quasiclassical penetration coefficient (Landau and Lifshitz [1959a])

$$D = \exp\left\{-\frac{2}{\hbar}\int_a^b |\{2m[V(\xi) - E]\}^{1/2}| \, d\xi\right\} \tag{4.75}$$

for a plane wave of energy E hitting the barrier $V(\xi)$, one obtains using the formulae (eqs. (4.70, (4.73) and (4.74)) (Brickmann [1970])

$$\tau_L = \frac{\pi^2}{\omega_0} D^{-1/2}\left[1 + \left(\frac{\pi \Delta V}{\hbar\omega_0}\right)^2 D^{-1}\right]^{1/2}. \tag{4.76}$$

If the barrier is parabolic at its top, one can easily evaluate the integral in (eq. (4.75))

$$D = \exp\{-(\pi/2\hbar)(b-a)[2m(V_{\max}-E)]^{1/2}\} \tag{4.77}$$

or if we introduce the characteristic potential parameters d, ΔV and $V_{\max}$ (see fig. 4.1):

$$D = \exp\left\{-\frac{\pi}{2\hbar}\left[d - 2\left(\frac{\hbar}{m\omega_0}\right)^{1/2}\right]\{2m[V_{\max} - \tfrac{1}{2}(\hbar\omega_0 + \Delta V)]\}^{1/2}\right\}. \tag{4.78}$$

In fig. 4.7, τ_L is drawn as a function of the difference d of the two potential wells and the energy gap ΔV between the two minima. The numerical values are obtained using eqs. (4.76) and (4.78). The XH-stretching mode has been chosen at $\omega_0 = 3000\ \mathrm{cm}^{-1}$, and for the maximum $V_{\max}$ of the barrier we have set $V_{\max} = 7000\ \mathrm{cm}^{-1}$. In table 4.1 we have listed some numerical estimates of τ_L for some special values of the characteristic potential parameters $V_{\max}$, ΔV and d with $\omega_0 = 3000\ \mathrm{cm}^{-1}$.

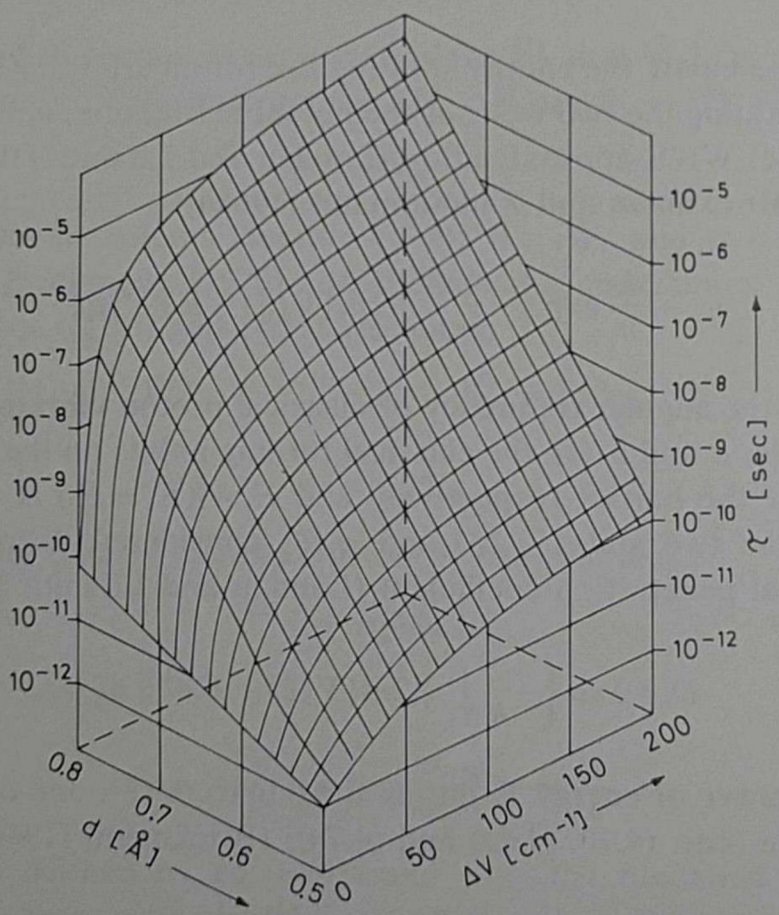

Fig. 4.7. Tunneling time τ as a function of d and ΔV, calculated with respect to eqs. (4.76) and (4.78) ($V_{\max} = 7000\ \mathrm{cm}^{-1}$, $\omega_0 = 3000\ \mathrm{cm}^{-1}$).

TABLE 4.1
Life times τ_L of protomeric structures as a function of potential parameters V_{max}, ΔV and d (calculated with respect to eqs. (4.76) and (4.78), $\omega_0 = 3000\ cm^{-1}$)

V_{max} (cm^{-1})	ΔV (cm^{-1})	τ_L (s)			
		$d = 0.5$ Å	$d = 0.6$ Å	$d = 0.7$ Å	$d = 0.8$ Å
5000	0	5×10^{-13}	1×10^{-12}	4×10^{-12}	1×10^{-11}
	10	5×10^{-13}	2×10^{-12}	4×10^{-11}	9×10^{-10}
	100	4×10^{-12}	1×10^{-10}	3×10^{-9}	8×10^{-8}
	500	6×10^{-11}	2×10^{-9}	4×10^{-8}	1×10^{-6}
7000	0	1×10^{-12}	4×10^{-12}	2×10^{-11}	7×10^{-11}
	10	1×10^{-12}	3×10^{-11}	2×10^{-9}	1×10^{-7}
	100	4×10^{-11}	3×10^{-9}	2×10^{-7}	1×10^{-5}
	500	8×10^{-10}	5×10^{-8}	3×10^{-6}	2×10^{-4}
9000	0	2×10^{-12}	1×10^{-11}	6×10^{-11}	3×10^{-10}
	10	5×10^{-12}	5×10^{-10}	7×10^{-8}	1×10^{-5}
	100	3×10^{-10}	4×10^{-8}	6×10^{-6}	9×10^{-4}
	500	6×10^{-9}	9×10^{-7}	1×10^{-4}	2×10^{-2}

τ_L is not very sensitive with respect to changes of ω_0. The qualitative and quantitative behavior of τ_L as a function of the given parameters is in good agreement with values obtained earlier (Brickmann and Zimmermann [1969]) where more extensive work was employed.

The approximation of τ_L (eq. (4.76)) with the transmission coefficient given in eq. (4.78) enables us to calculate the life times of the protomeric structures XH···Y and X···HY only from a few potential parameters and without extensive quantum-mechanical manipulations. In the following subsections, we will give some other possibilities to approximate τ_L.

4.4.2. TIME–ENERGY UNCERTAINTY RELATION

As has been shown in section 4.3.3 the initial states $\psi_L(\xi, 0)$ and $\psi_R(\xi, 0)$, representing the protomeric structures XH···Y and X···HY respectively are quasistationary states: they behave stationary only in a certain time interval of duration Δt. This time is correlated with some uncertainty ΔE of the energy of the system by the time–energy uncertainty relation (Messiah [1965a])

$$\Delta t\ \Delta E \geqslant \hbar. \tag{4.79}$$

If $\psi_L^i(\xi, 0)$ is a spectroscopic initial state (see section 4.3.3), it can only decay into spectroscopic states $\psi_R^j(\xi)$ associated to the right well and we can identify Δt to be the mean life time τ_L of the structure XH$\cdots$Y in a certain vibrational state of the XH-stretching vibration: we obtain a lower bound for the tunneling time

$$\tau_L \gtrapprox \hbar/\Delta E. \tag{4.80}$$

For times $t \ll \tau_L$ the measurement of the energy will give $E = E_L^i$ an eigenvalue of the Hamiltonian H_L. For $t \gg \tau_L$, a respective measurement will result in the identification of eigenstates of H. We will find $E = E_K$, if $\varphi_K(\xi)$ corresponds to $\psi_L^i(\xi)$ in an adiabatic change (Messiah [1965b]) of the Hamiltonian between H and H_L. Therefore we can identify ΔE to be the energy difference

$$\Delta E = |E_K - E_L^i|. \tag{4.81}$$

In the two-level approximation (section 4.3.4), we can obtain an approximate relation for this energy difference (Brickmann [1970]) using eq. (4.57)

$$\Delta E = \tfrac{1}{2}\hbar[\omega - (\omega^2 - \omega_s^2)^{1/2}] \tag{4.82}$$

or for $\omega \gg \omega_s$

$$\Delta E \approx \tfrac{1}{4}\hbar\omega_s(\omega_s/\omega) \tag{4.83}$$

and we can estimate τ_L from eq. (4.80)

$$\tau_L^{\Delta} \approx \frac{4}{\omega_s}\frac{\omega}{\omega_s} \tag{4.84}$$

where the index Δ indicates that this value was obtained from the time–energy uncertainty relation. Comparison of eqs. (4.84) and (4.70) shows, that the two relations obtained by different methods lead to nearly identical results.

4.4.3. Quasiclassical approximation

In contrast to the wave mechanical description of a proton, moving in a well of a double minimum potential, one can treat this motion by means of classical mechanics if the de Broglie wavelength of the proton is small compared with characteristic changes of the potential energy function (Landau and Lifshitz [1959b]). This has been done by several authors (Bell [1933], Conway et al. [1956] and Löwdin [1965]). Although the restricting condition is not fulfilled in the classical forbidden region and in

the neighborhood of the classical turning points the proton can be described in the well region as a classically oscillating particle (Löwdin [1965]). If we assume that the potential well is approximately harmonic, the angular frequency ω_0 of this oscillation is the same as in eq. (4.74). For energies $E < V_{max}$, the proton hits the barrier

$$\nu_0 = \omega_0/2\pi \tag{4.85}$$

times per second. In the neighborhood of the barrier it no longer behaves as a classical particle, i.e., it can penetrate the barrier and appears in the other well region. The probability for such a process results from the penetration coefficient D (Landau and Lifshitz [1959a] and Löwdin [1965]) which is given in quasiclassical approximation by eq. (4.75). In this approximation the rate of proton transfer can simply be calculated from the relation

$$r_{QC} = \nu_0 D \tag{4.86}$$

and the tunneling time results in (Löwdin [1965])

$$\tau_{QC} = (2\pi/\omega_0)D^{-1} \tag{4.87}$$

The tunneling times obtained from eq. (4.87) differ from the values determined with respect to the formalism described in sections 4.4.1 and 4.4.2 both quantitatively and qualitatively as has been shown (Brickmann and Zimmermann [1968, 1969] and Brickmann [1970]). The main reason for this fact is that, it is impossible in this quasiclassical approximation to take resonance effects into consideration: the proton in one well "does not know" whether there is an "allowed" energy term in the other well. It has been shown earlier (Brickmann [1970]) that even in the case of term resonance the life time of the protomeric structures XH···Y and X···HY is drastically shortened.

Acknowledgements

The author would like to thank Prof. Dr. H. Zimmermann for many stimulating discussions and Dr. P. Russegger for the evaluation of some numerical results and the checking of the formulas. Thanks also go to Mrs. M. Scherer, Dipl. Chem. Ch. Nehrkorn and Cand. Chem. B. John for their help in producing the manuscript. The author is indebted to Mrs. I. Ziegert for carefully drawing the figures.

References

Ady, E. and J. Brickmann, 1971, Chem. Phys. Letters **11**, 302.
Arnold, J. and D. J. Millen, 1965a, J. Chem. Soc. 503.
Arnold, J. and D. J. Millen, 1965b, J. Chem. Soc. 510.
Bell, R. P., 1933, Proc. Roy. Soc., London, **A139**, 466.
Berry, R. S., 1960, J. Chem. Phys. **32**, 933.
Bertie, J. E. and D. J. Millen, 1965a, J. Chem. Soc. 497.
Bertie, J. E. and D. J. Millen, 1965b, J. Chem. Soc. 514.
Bratož, S. and D. Hadži, 1957, J. Chem. Phys. **27**, 991.
Brickmann, J., 1970, Ber. Bunsenges. Phys. Chem. **74**, 331.
Brickmann, J., 1973a, Z. Naturforsch. **28A**, 1759.
Brickmann, J., 1973b, Intern. J. Quantum Chem., Proceedings of the 1973 Sanibel symp. 7, 427.
Brickmann, J. and H. Zimmermann, 1966a, Ber. Bunsenges. Phys. Chem. **70**, 157.
Brickmann, J. and H. Zimmermann, 1966b, Ber. Bunsenges. Phys. Chem. **70**, 521.
Brickmann, J. and H. Zimmermann, 1968, Z. Naturforsch. **23A**, 11.
Brickmann, J. and H. Zimmermann, 1969, J. Chem. Phys. **50**, 1608.
Brickmann, J., A. Licha and H. Zimmermann, 1971, Ber. Bunsenges. Phys. Chem. **75**, 1324.
Bushfield, W. K., M. P. Ennis and I. Y. Macewen, 1973, Spectrochim. Acta **19A**, 1259.
Carbonell, R. G. and M. D. Kostin, 1973, Intern. J. Quantum Chem. **7**, 319.
Clementi, E., J. Mehl and W. von Niessen, 1971, J. Chem. Phys. **54**, 508.
Conway, B. E., 1964, in: Modern Aspects of Electrochemistry, Eds. J. O'M. Bockris and B. E. Conway (Butterworths Publishers, London), pp. 43–148.
Conway, B. E., J. O'M. Bockris and H. Linton, 1956, J. Chem. Phys. **24**, 834.
Dennison, D. M. and G. E. Uhlenbeck, 1932, Phys. Rev. **41**, 313.
Eigen, M., 1963, Angew. Chemie **75**, 489; Angew. Chemie Intern. Edit. **3**, 1 (1964).
Fischer, S. F., 1967, Intern. J. Quantum Chem. **1S**, 745.
Fischer, S. F., G. L. Hofacker and M. A. Ratner, 1969, in: Physics of Ice, Eds. N. Riehl et al. (Plenum Press, New York), p. 385.
Fischer, S. F., G. L. Hofacker and M. A. Ratner, 1970, J. Chem. Phys. **52**, 1934.
Gamow, G. 1928a, Z. Physik **51**, 204.
Gamow, G. 1928b, Z. Physik **52**, 510.
Golden, S., 1969, Quantum Statistical Foundation of Chemical Kinetics (Oxford University Press, London), p. 106.
Grimm, H., H. Stiller and T. Plesser, 1970, Phys. stat. sol. **42**, 207.
Gurney, R. W. and E. U. Condon, 1929, Phys. Rev. **33**, 127.
Haas, C. and D. F. Hornig, 1959, J. Chem. Phys. **32**, 1763.
Heilbronner, E., H. H. Günthard and R. Gerdil, 1956, Helv. Chim. Acta **39**, 1171.
Heilbronner, E., H. Rutishauser and F. Gerson, 1959, Helv. Chim. Acta **42**, 2304.
Herzberg, G., 1960, Molecular Spectra and Molecular Structure, Vol. 2 (Van Nostrand Publishing Company, New York), p. 61.
Hofacker, G. L., 1965, J. Chem. Phys. **41**, 208.
Hofacker, G. L., 1968, in: Chemische Elementarprozesse, Ed. H. Hartmann (Springer Verlag, Berlin, Heidelberg, New York), p. 78.
Hofacker, G. L., Y. Marechal and M. A. Ratner, 1975, this work, ch. 6.

Ibers, J. A., 1964, J. Chem. Phys. **41**, 25.
Janoschek, R., 1975, this work, ch. 3.
Janoschek, R., D. G. Weidemann, H. Pfeiffer and G. Zundel, 1972, J. Amer. Chem. Soc. **94**, 2387.
Janoschek, R., E. G. Weidemann and G. Zundel, 1973, Faraday Transactions II, **69**, 505.
Landau, L. D. and E. M. Lifshitz, 1959a, Quantum Mechanics, 2nd ed. (Pergamon Press, London, Paris), p. 150.
Landau, L. and E. M. Lifshitz, 1959b, ibid. chapter VII.
Lippincott, E. R., 1955, J. Chem. Phys. **23**, 603.
Lippincott, E. R., 1957, J. Chem. Phys. **26**, 1678.
Lippincott, E. R. and R. Schroeder, 1955, J. Chem. Phys. **23**, 1099.
Lippincott, E. R. and R. Schroeder, 1956, J. Am. Chem. Soc. **78**, 517.
Lippincott, E. R. and R. Schroeder, 1957, J. Phys. Chem. **61**, 921.
Löwdin, P. O., 1963, Rev. Mod. Phys. **35**, 724.
Löwdin, P. O., 1964, Biopolymers Symp. **1**, 161.
Löwdin, P. O., 1965, Quantum Genetics and the Aperiodic Solid. in: Advances in Quantum Chemistry, Vol. 2, Ed. P. O. Löwdin (Academic Press, New York, London), pp. 213–360.
Manning, M., 1935, J. Chem. Phys. **3**, 136.
Marechal, Y. and A. Witkowski, 1967, Theoretica Chem. Acta **9**, 116.
Marechal, Y. and A. Witkowski, 1968, J. Chem. Phys. **48**, 3697.
Messiah, A., 1965a, Quantum Mechanics, Vol. 1 3rd ed. (North-Holland Publishing Company, Amsterdam), pp. 135–138 and ch. VIII, section 13.
Messiah, A., 1965b, Quantum Mechanics, Vol. 2 3rd ed. (North-Holland Publishing Company, Amsterdam), pp. 739–761.
Messiah, A., 1965c, Vol. 1, pp. 310–323.
Millen, D. J. and O. A. Samsonov, 1965, J. Chem. Soc. 3085.
Millen, D. J. and J. Zabicky, 1965, J. Chem. Soc. 3080.
Morse, P. M. and E. C. G. Stückelberg, 1931, Helv. Phys. Acta **4**, 335.
Pullman, B. and A. Pullman, 1972, Adv. Heterocyclic Chemistry, **13**, 77.
Reid, C., 1959, J. Chem. Phys. **30**, 182.
Rein, R. and F. E. Harris, 1964, J. Chem. Phys. **41**, 3393.
Rein, R. and F. E. Harris, 1965a, J. Chem. Phys. **42**, 2177.
Rein, R. and F. E. Harris, 1965b, J. Chem. Phys. **43**, 4415.
Rein, R. and J. Ladik, 1964, J. Chem. Phys. **40**, 2466.
Rice, S. A. and J. L. Wood, 1973, Faraday Transactions II, **69**, 91.
Riehl, N., 1966, Energy and Charge Transfer over Hydrogen Bridges, in: Energy Transfer in Radiation Processes, Ed. G. O. Phillips (Elsevier Publishing Company, Amsterdam), pp. 95–104.
Rösch, N., 1971, Dissertation, TH Munich.
Rösch, N., 1972, Z. Naturforsch. **27A**, 526.
Rosen, N. and P. M. Morse, 1932, Phys. Rev. **42**, 210.
Samorjai, R. L. and D. F. Hornig, 1962, J. Chem. Phys. **36**, 1980.
Schuster, P., 1973, Z. Chemie **13**, 41.
Schuster, P., 1975a, this work, ch. 2.
Schuster, P., W. Jakubetz, G. Baier, W. Mayer and B. M. Rode, 1975b, to be published.

Singh, T. R. and J. L. Wood, 1968, J. Chem. Phys. **48**, 4567.
Stepanov, B. I., 1945, Zhur. fiz. Khim **19**, 507.
Stepanov, B. I., 1946a, Zhur. fiz. Khim **20**, 408.
Stepanov, B. I., 1946b, Nature **157**, 808.
Stiller, H., 1975, this work, ch. 24.
Wall, F. T. and G. Glockner, 1937, J. Chem. Phys. **5**, 314.
Weidemann, E. G. and G. Zundel, 1970, Z. Naturforsch. **25A**, 627.
Zimmermann, H., 1961, Ber. Bunsenges, Phys. Chem. **65**, 821.
Zimmermann, H., 1964, Angew. Chemie **76**, 1; Angew. Chemie Intern. Edit. **3**, 157.
Zimmermann, H. and J. Rudolph, 1965, Angew. Chemie **77**, 65; Angew. Chemie Intern. Edit. **4**, 40.

CHAPTER 5

MODEL STUDIES ON PROTON CORRELATIONS IN HYDROGEN BONDS

E. G. WEIDEMANN

Sektion Physik, Universität München, 8 München 2, Theresienstr. 37, West Germany

Contents

5.1. Introduction 247
5.2. Polarizability of symmetrical hydrogen bonds with double-minimum potential wells 249
5.3. Correlation of tunnelling protons 253
5.3.1. Energy levels of a pair of coupled protons 253
5.3.2. Influence of coupling on the intensities of IR transitions 256
5.3.3. Correlation functions 259
5.4. Influence of the molecular environment on proton correlations 263
5.4.1. Polarizability of hydrogen bonds with an asymmetrical double-minimum potential 263
5.4.2. Influence of a polar medium on proton tunnelling 265
5.4.3. Proton–anion interaction in a polar medium 267
5.4.4. Interaction of two protons and two anions in a polar medium 271
5.4.5. Modification of the potential curve by the reaction field 273
5.4.6. Discussion of numerical results 275
5.4.7. Correlation of protons 285
5.4.8. Changes in tunnelling frequency 288
5.5. Conclusion 291
References 292

The hydrogen bond – recent developments in theory and experiments
Eds. P. Schuster et al. © *North-Holland Publ. Co., Amsterdam, 1976*

5.1. Introduction

H-bonds of the type $(BH\cdots B)^+$ and $(BH\cdots B)^-$ in acid and base solutions are discussed. It is assumed that the oscillations of the proton or defect proton in such bonds take place in a double-minimum potential; most of the results are also valid in a very broad single-minimum potential. Potentials of this kind were postulated to explain a continuous IR absorption observed in many systems (Zundel [1969]; see also ch. 15). Double-minimum potential wells were proved to exist in some crystals by neutron diffraction (Will [1969]). Ab initio SCF calculations by Merlet et al. [1972] yielded such potentials for the case of $N_2H_7^+$. The anomalous isotope effect of the Curie temperature in some H-bonded ferroelectric crystals was, for example, explained by double-minimum potentials (Blinc and Ribarič [1963], Tokunaga [1966] and Tokunaga and Matsubara [1966]). Such potentials were also considered in studies on the mobility of structural defects in H-bonded solids by Fischer and Hofacker [1969] and by Fischer et al. [1969a, b]. The motion of a proton in a double-minimum potential well, the energy levels, transition probabilities and lingering times in both wells were investigated by Somorjai and Hornig [1962] and by Brickmann and Zimmermann [1966, 1967, 1969] for the first time considering the proton motion in H-bonds. The extremely high polarizability of H-bonds with a symmetrical double-minimum potential is decisive for the influence of the molecular environment on the proton motion and on the coupling of protons in adjacent H-bonds. The polarizability is caused by the displacement of the proton along the bond and it could be shown (Weidemann and Zundel [1970] and Janoschek et al. [1972]) that it is 1–2 orders of magnitude greater than usual electron polarizabilities which are not associated with considerable nuclear displacements.

The high polarizability can be explained very easily. Its dependence on the tunnelling frequency, the temperature and the transition moment between the two lowest levels which are split by the tunnelling motion of

the proton is calculated in section 5.2. Analytical formula can be given in the tunnelling approximation which consists in replacing the whole level scheme of the proton by the two lowest levels.

The high polarizability causes strong induction effects of such H-bonds by ions and dipoles of the molecular environment. Induction effects also occur between adjacent H-bonds and are very important because the H-bonds polarize each other mutually. This is especially true for the charged H-bonds considered here. In electrically neutral H-bonds, induction effects, of course, occur only if the bonds have a non-vanishing dipole moment since the influence of higher moments will be negligible. Hence, induction effects are of importance for neutral bonds only if the bonds are unsymmetrical, or if proton acceptor and donator are of the same kind, but the symmetry is disturbed by the molecular environment. Because of the induced dipole interaction between two adjacent H-bonds, the position of the proton in one bond is no longer independent of the position of the proton in the other bond, i.e. the mean charge distributions in both bonds are correlated. The tunnelling motions of the protons in adjacent H-bonds are also correlated to some extent. The correlated proton motion gives rise to proton dispersion forces analogous to the usual London dispersion forces (Weidemann and Zundel [1967, 1973] and Zundel and Weidemann [1970]).

Polar solvents have a strong influence on the proton motion in H-bonds because of the high polarizability. The electric fields of the solvent molecule dipoles, as well as the anion fields, change the potentials of the H-bond protons and destroy their symmetry. Thereby the tunnelling frequency is changed and, hence, the interaction between the protons is influenced, too. The interactions between two adjacent H-bonds are discussed in section 5.3 as well as the correlations caused thereby. The effects in polar solvents are treated in section 5.4.

All these effects cause great changes in the IR spectra of acid and base solutions in which the symmetrical H-bonds, considered here, occur. They give rise to considerable frequency shifts, great changes in intensities and new bands. The positions of the bands are determined by the spatial arrangement of the interacting H-bonds and of the ions. Since the arrangement in solutions varies statistically, instead of bands, a continuous absorption is observed in a broad frequency range. The intensity of the continuum depends on the proton or defect proton concentration (see ch. 15).

5.2. Polarizability of symmetrical hydrogen bonds with double-minimum potential wells

We consider the motion of the proton in a charged H-bond $(BH\cdots B)^+$ along the bond and neglect the coupling of this motion with the stretching and bending vibration of the H-bond. We assume that the proton moves in a symmetrical double-minimum potential, schematically shown in fig. 5.1. The wave functions in a symmetrical potential are known to be even or odd functions of the displacement from the midpoint; the wave functions of the ground state 0+ and of the first excited state 0− are shown qualitatively in fig. 5.1. In both states, the proton occurs with equal probability in either well. Hence, the mean charge distribution is symmetric and the mean dipole moment is equal to zero.

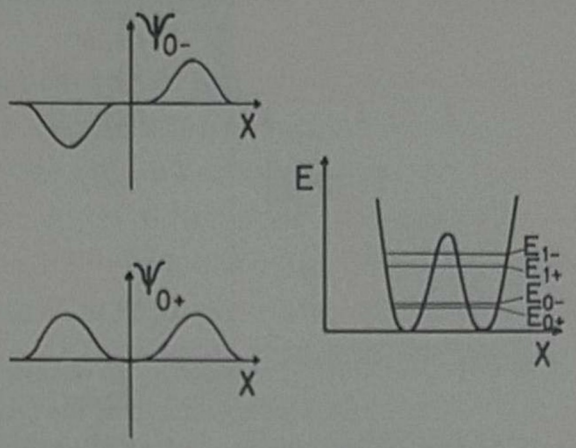

Fig. 5.1. Lowest energy levels and wave functions in a double-minimum potential.

A dipole moment different from zero arises when the symmetry of the potential is disturbed, e.g. by an outer electric field with a non-vanishing component in the bond axes. The potential well in the field direction is lowered and the wave functions become asymmetrical, too. In the ground state, the position probability becomes greater in the lower well than in the higher well; the H-bond is polarized in field direction. In the first excited state, however, the position probability increases in the higher well; the H-bond is polarized in the negative field direction (see fig. 5.2).

The wave functions are extremely sensitive to disturbances of the symmetry of the potential. A small displacement of the potential wells relative to each other is sufficient to localize the proton in the deeper well in the ground state and in the higher well in the first excited state almost

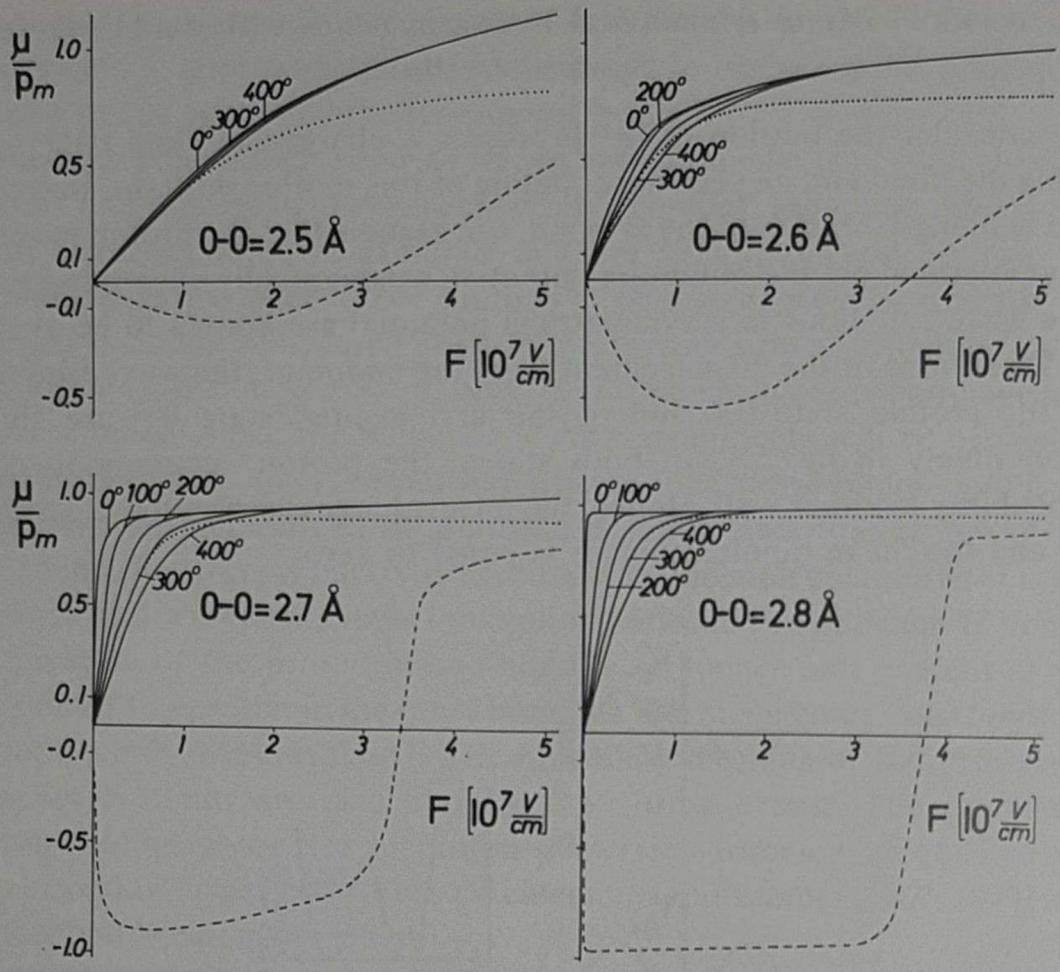

Fig. 5.2. Dipole moment of a H-bond in $H_5O_2^+$ induced by an electric field F for various O–O distances and temperatures, in units of the dipole moment of the proton boundary structure; ------ dipole moment of the first excited state, ····· tunnelling approximation at 300 K.

completely. The reason for the sensitivity of the wave functions on the symmetry can immediately be seen from the level scheme in fig. 5.1. The lowest levels penetrating the potential barrier lie pairwise close to each other. To each pair of levels belongs a state of even and a state of odd parity. The wave functions in an unsymmetrical potential can be thought of as a superposition of the states in a symmetrical potential. A small field or a weak asymmetry is sufficient to cause a considerable superposition of the almost degenerate states, ie. the pair of states the levels of which lie close to each other, and to give rise to an asymmetrical charge distribution. This is the main reason for the extremely high polarizability of symmetrical H-bonds with a double-minimum potential.

In order to complete the argument, we have to consider the displacement of the electrons connected with the displacement of the proton in the H-bond. Until now we have tacitly assumed that the H-bond develops

a non-vanishing dipole moment if the proton is displaced from the midpoint, i.e. we have assumed that the derivative of the dipole moment with respect to the proton coordinate is different from zero. This is not entirely trivial, since the electrons follow the proton adiabatically and could possibly compensate the contribution of the proton to the dipole moment (Janoschek [1973]). Usually, however, the electron displacements will enhance the dipole moment of the H-bond (Janoschek et al. [1972]). Hartree–Fock calculations have shown that usually less than one electron charge is dragged by the proton. The most important contribution to the dipole moment is caused by the electron shifts in the proton acceptor and donator. The electrons are shifted in a direction opposite to that of the proton and thus enhance the dipole moment caused by the proton displacement. Hence, the derivative of the dipole moment with respect to the proton displacement is usually greater than one proton charge.

Analytic formula for the polarizability can be derived (Weidemann and Zundel [1970]) in a simple approximation called tunnelling approximation in solid state physics (Narajanamurti and Pohl [1970]). It is a two-level approximation; the level scheme of the proton is replaced by the two lowest levels $0+$ and $0-$. Since the pair of states is almost degenerate, the properties of the proton in these states are approximated very well. The omitted levels become important with interactions comparable in strength with the distance between the lowest pair of levels $0+$, $0-$ and the next higher pair of levels $1+$, $1-$. The approximation is called tunnelling approximation since the superposition of the two retained states with equal amplitudes, yields a state in which the proton moves periodically from one well to the other with a frequency corresponding to the separation of the two levels.

The Hamiltonian for the proton motion along the H-bond with a homogeneous electric field, F, applied in the direction of the bond, is given by

$$H = \frac{1}{2m}\frac{\mathrm{d}^2}{\mathrm{d}x^2} + V(x) - \mu(x)\,F. \tag{5.1}$$

m is the reduced mass of the valence bond vibration which may be taken as the proton mass in many cases, x is the displacement of the proton from the center of the H-bond, $V(x)$ is the double-minimum potential and $\mu(x)$ is the component of the total dipole moment parallel to the H-bond as given by the Born–Oppenheimer approximation. Diagonalizing H in

the space of states $0+$ and $0-$, which are the stationary states of the system with $F = 0$, the eigenvalues and eigenfunctions of the system with the electric field applied are obtained as the solutions of a simple quadratic secular equation.

$$E_{\pm} = \mp \tfrac{1}{2} h\nu_0 \sqrt{1+\zeta^2}, \tag{5.2}$$

$$\psi_{\pm} = c_{1\pm}\psi_{0+} + c_{2\pm}\psi_{0-}. \tag{5.3}$$

The amplitudes $c_{1\pm}$, $c_{2\pm}$ are given by the following relations:

$$c_{1\pm} = -\frac{\zeta}{N_{\pm}}, \qquad c_{2\pm} = \frac{1 \mp \sqrt{1+\zeta^2}}{N_{\pm}} \tag{5.4}$$

with the normalization constants

$$N_{\pm} = \sqrt{\zeta^2 + (1 \mp \sqrt{1+\zeta^2})^2} = \sqrt{2\sqrt{1+\zeta^2}(\sqrt{1+\zeta^2} \mp 1)}. \tag{5.5}$$

$\nu_0 = (E_{0-} - E_{0+})/h$ is the tunnelling frequency in the symmetrical potential. The dimensionless parameter

$$\zeta = 2pF/h\nu_0, \qquad p = |\langle 0+|\mu|0-\rangle|, \tag{5.6}$$

containing the transition dipole moment between the two lowest states determines the level shifts and the degree of mixing of the two states in the approximation applied.

With high field strengths, eqs. (5.2) and (5.6) yield the energy of a dipole of magnitude p which is orientated in the field direction in the ground state $|+\rangle$ and which is orientated opposite to the field direction in the first excited state $|-\rangle$. The modulus p of the transition moment $\langle 0-|\mu|0+\rangle$ is the maximum value of the dipole moment which can be induced, since the mean dipole moment

$$\bar{\mu}_{\pm} = -\frac{\mathrm{d}E_{\pm}}{\mathrm{d}F} = \pm p\frac{\zeta}{\sqrt{1+\zeta^2}} \tag{5.7}$$

is obtained from eqs. (5.3) or (5.2) by calculating the expectation values $\langle \pm|\mu|\pm\rangle$ or, more simply, by taking the derivative of the energy values $E_{\pm}$ with respect to F. Assuming a Boltzmann distribution in the two states, the thermal average results in a dipole moment in the field direction of magnitude

$$\bar{\mu}(F, T) = p\frac{\zeta}{\sqrt{1+\zeta^2}} \tanh\left(\frac{h\nu_0}{2kT}\sqrt{1+\zeta^2}\right). \tag{5.8}$$

The polarizability is the derivative of the dipole moment with respect to the field strength.

$$\alpha(T) = \left(\frac{\partial \bar{\mu}(F, T)}{\partial F}\right)_{F=0} = \frac{2p^2}{h\nu_0} \tanh \frac{h\nu_0}{2kT}. \tag{5.9}$$

Hence, small tunnelling frequencies, high transition moments and low temperatures favor high polarizabilities.

The transition dipole moment p can be calculated starting from SCF calculations which yield the potential and the dipole moment as a function of the proton coordinates, by solving the Schroedinger equation for the proton motion in the self-consistent potential, numerically. This was done, for instance, for the system $H_5O_2^+$ (Janoschek et al. [1972, 1973]). Values of 1–3 debye were obtained for the transition dipole moment p whereby the value of p depends on the H-bond length. A rough estimate of p can also be given without such a detailed calculation. By definition, p is the dipole moment of the function $\psi_{0+}(x)\,\psi_{0-}(x)$, which is qualitatively of the same shape as the function $\psi_{0-}(x)$ (see fig. 5.1). p is roughly equal to the dipole moment obtained if the proton is considered to be fixed in one minimum, i.e. p is equal to the dipole moment of a proton boundary structure. This estimation is especially good if the maxima and minima of the wave functions are sharp and if the barrier in the double-minimum potential is high and broad.

Equation (5.9) results in a polarizability of $95.8 \times 10^{-24}\,\mathrm{cm}^3$ taking a transition moment of 2 debye, a tunnelling frequency of $100\,\mathrm{cm}^{-1}$, and a temperature of 300 K. The value of the polarizability obtained is 1–2 orders of magnitude greater than usual electron polarizabilities not associated with larger nuclear displacements. The result is not changed essentially by the coupling of the proton motion with the stretching vibration of the H-bond. This was shown for the H-bond in $H_5O_2^+$ by Janoschek et al. [1973].

5.3. Correlation of tunnelling protons

5.3.1. Energy levels of a pair of coupled protons

The high polarizability of symmetrical H-bonds with a double-minimum potential implies not only that such systems are extremely sensitive to applied electric fields and to the fields of ions and dipole moments of polar molecules in the surroundings. It implies also that such H-bonds are strongly polarized by the electric fields of protons tunnelling in adjacent

H-bonds of the same type. This results in correlations of protons in adjacent H-bonds: Charged H-bonds polarize each other mutually resulting in a correlation of the polarization directions. Moreover, the proton tunnelling will no longer take place independently but is more or less correlated. The correlated proton motion gives rise to dispersion forces analogous to the usual London dispersion forces. Hence, they are called proton dispersion forces. They are a special type of charge fluctuation forces, a general theory of which was developed by Lifshitz [1955] and Dzyaloshinskii et al. [1961]. In molecular biophysics, charge fluctuation interactions are discussed by Jehle [1963, 1969] and by Jehle et al. [1958, 1965].

In order to investigate the question concerning the effect of the coupling between H-bond protons on the IR spectra of systems containing such H-bonds, the changes in the level scheme of a pair of symmetrical H-bonds with double-minimum potentials were calculated. First of all the H-bonds were assumed to be either electrically neutral, or it was assumed that the charge of the H-bond $(BH\cdots B)^+$ is compensated by a counterion in such a position that the symmetry of the potential is not disturbed. Moreover, the usual approximations were used: Expansion of the charge distributions in the H-bonds in multipole moments and perturbation theory up to second order (Weidemann and Zundel [1967]). Later on perturbation theory was abandoned and the Hamiltonian of a pair of H-bond protons was diagonalized in the state space consisting of the products of the four lowest states of each proton (Kremer et al. [1974]). The dipole–dipole approximation of the interaction operator was initially retained. In this approximation, the interaction operator is given by

$$W(x_1, x_2) = 1/\epsilon R^3 \{\boldsymbol{\mu}_1(x_1) \cdot \boldsymbol{\mu}_2(x_2) - 3[\boldsymbol{\mu}_1(x_1) \cdot \boldsymbol{n}][\boldsymbol{\mu}_2(x_2) \cdot \boldsymbol{n}]\}. \tag{5.10}$$

x_1, x_2 are the proton coordinates along the H-bonds 1 and 2 (measured from the centers of the bonds), $\boldsymbol{\mu}_1(x_1)$, $\boldsymbol{\mu}_2(x_2)$ are the corresponding dipole moments and $\boldsymbol{n}$ is a unit vector in the direction of the straight line connecting the centers of the bonds. Introducing the product states

$$\langle x_1 x_2 | \alpha\beta \rangle = \psi_\alpha(x_1)\, \psi_\beta(x_2), \qquad (\alpha, \beta = 0+, 0-, 1+, 1-), \tag{5.11}$$

the matrix elements of W are reduced to the dipole matrices of the individual bonds

$$\langle \alpha\beta | W | \gamma\delta \rangle = 1/\epsilon R^3 \langle \alpha | \mu_1 | \gamma \rangle \langle \beta | \mu_2 | \delta \rangle g, \tag{5.12}$$

$$g = n_1 \cdot n_2 - 3(n_1 \cdot n)(n_2 \cdot n). \tag{5.13}$$

n_1, n_2 are the unit vectors in direction of μ_1, μ_2, i.e. in direction of the two H-bonds. Hence, the factor g is determined by the mutual orientation of the bonds. The value of g lies in the range $-2 \leqslant g \leqslant 2$.

In order to obtain reasonable values for the dipole-moment matrix elements, the values were taken from calculations on the particular system $H_5O_2^+$ (Janoschek et al. [1972]). The proton states in a self-consistent potential were expanded in harmonic oscillator functions. The proton levels were also taken from this paper. Hence, the energy matrix of a pair of H-bonds is known as a function of the distance R and the mutual orientation of the bonds.

Diagonalizing the energy matrix in the space of the 16 functions (5.11), the energy levels in fig. 5.3 were obtained as a function of the distance R for the case of two collinear bonds, and as a function of the orientation (factor g of eq. (5.13)) for the case of two bonds at distance $R = 4$ Å. The dipole matrix and the energy levels of the isolated H-bonds were taken from the paper of Janoschek et al. [1972] for an O–O distance of 2.6 Å in the system $H_5O_2^+$. The levels, part of which are double degenerate, are increasingly split and displaced with decreasing distance, i.e. with increas-

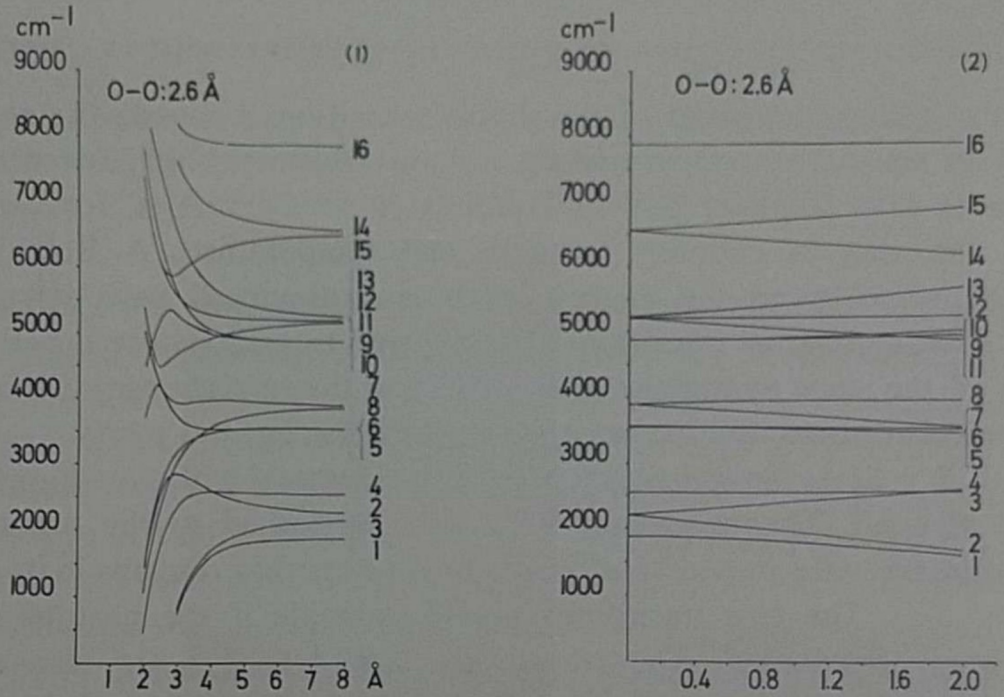

Fig. 5.3. Proton levels for the case of two collinear H-bonds in $H_5O_2^+$ as a function of (1) separation R and (2) mutual orientation of the H-bonds (determined by the factor g in eq. (5.13)) with $R = 4$ Å.

ing coupling strength. A considerable displacement can be seen at distances as large as 6–7 Å, especially at the degenerate levels. The wave functions are even more strongly influenced than the energy levels, and hence the intensities of the transitions are more sensitive to the coupling than the frequencies.

Intersections of energy levels occur at smaller distances. This is no contradiction to the well-known rule that energy levels do not cross but avoid each other, if they correspond to states between which the matrix element of the interaction operator is different from zero. For with the applied dipole–dipole approximation, the 16×16 energy matrix separates into a 6×6 matrix, two 4×4 matrices and a 2×2 matrix because of the symmetry of the interaction

$$W(x_1, x_2) = W(x_2, x_1) = W(-x_1, -x_2), \tag{5.14}$$

which is evident from eq. (5.10), since $\mu(-x) = -\mu(x)$. The states belonging to the four submatrices differ in their symmetry with respect to the interchange of the two proton coordinates and with respect to their total parity. The states belonging to the same submatrix behave according to the crossing rule: The corresponding energy levels avoid each other when they are approaching, and Fermi resonances are observed in the spectra.

5.3.2. Influence of coupling on the intensities of IR transitions

The absorption intensities of the dipole transitions between the energy levels of fig. 5.3 are shown in fig. 5.4, in arbitrary units, for various distances of a collinear pair of H-bonds ($g = -2$), that is, for various cases differing in coupling strength and temperature. A Boltzmann distribution between the energy levels was assumed. Selection rules reduce the number of transitions. The allowed transitions occur between states of the same symmetry with respect to the interchange of the two proton coordinates and between states differing in total parity.

With $R = 12$ Å, the transitions are almost identical with transitions in a single H-bond. The transitions 1–3, 3–4 correspond to the tunnelling transition $0+ \rightarrow 0-$ in one bond while the other proton remains in its state ($0+$ or $0-$). The two transitions would coincide if the protons were completely decoupled. The transitions 3–6, 4–8, 2–5 are transitions $0- \rightarrow 1+$ of one proton, with an unchanged state ($0+$ or $0-$) of the other proton. The transitions 3–11, 1–10 are transitions $0+ \rightarrow 1-$ of one proton, with an unchanged state ($0+$ or $0-$) of the other proton. With increasing

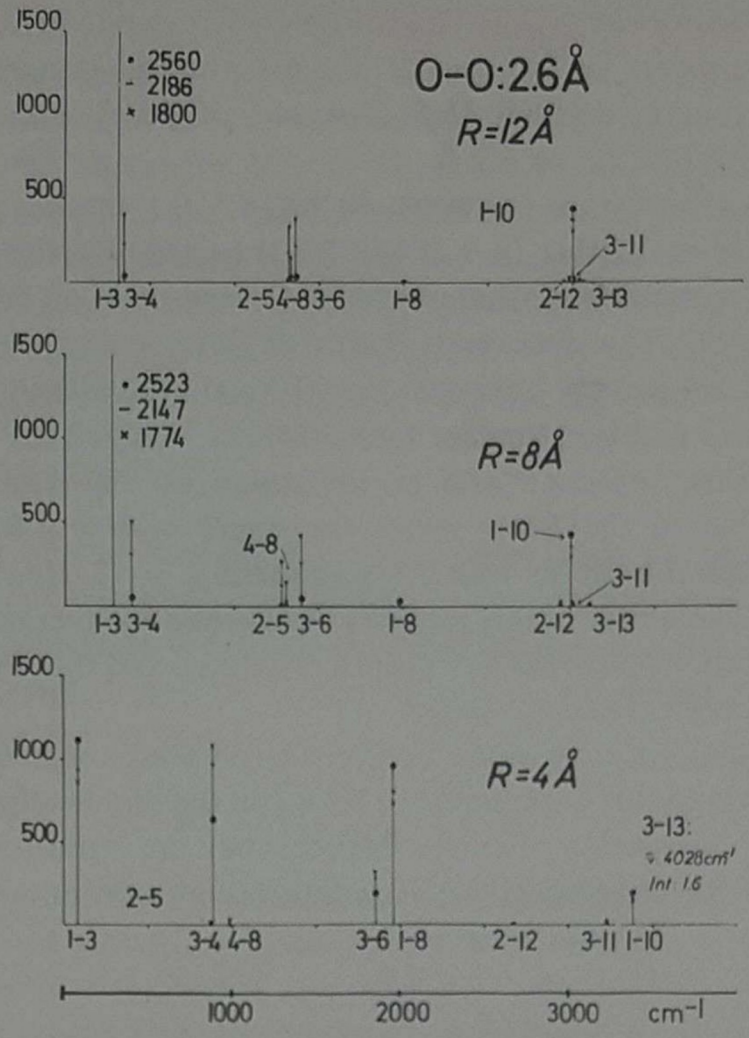

Fig. 5.4. Intensities of the absorptive dipole transitions (in arbitrary units) between the energy levels of fig. 5.3 for various separations R of an interacting collinear pair of H-bonds ($g = -2$) and various temperatures: ·, −, × for $T = 100, 200, 300$ K.

coupling of the protons, the frequencies and intensities of the transitions are changed considerably. The coupling gives rise to only one combined transition 1–8 or $|0+0+\rangle \rightarrow |0-1+\rangle$, in which one proton makes a tunnelling transition while the other proton is lifted from level 0+ to level 1+.

In order to get an impression of the appearance of the IR spectrum if the motion of the H-bond protons were coupled only pairwise and if the other interactions with the molecular environment were negligible, the transmittance was calculated as a function of the frequency (Hayd et al. [1974]). A mean distance between the H-bonds of 5.5 Å was chosen. Gaussian profiles $\exp\{-[(\bar{\nu} - \bar{\nu}_0)/\alpha]^2\}$ were selected for the superimposed bands with a line breadth determined by $\alpha = 300\,\mathrm{cm}^{-1}$. Moreover, the energy levels and dipole-moment matrices were taken from SCF calcula-

tions on $H_5O_2^+$, not only for the case of an O–O distance of 2.6 Å but also for an O–O distance of 2.5 and 2.7 Å. An average transmittance was calculated assuming that an O–O distance of 2.6 Å occurs twice as frequently as O–O = 2.5 or 2.7 Å.

The resulting spectrum is shown in fig. 5.5 for the case of parallel H-bonds beside each other ($g = 1$) and for the case of collinear H-bonds ($g = -2$). For comparison, the spectrum for the case of no interaction ($g = 0$) is plotted. The deviations from the latter curve thus show the effect of the interaction between the H-bonds. Evidently, deviations occur with wave numbers smaller than 3000 cm^{-1} only. They are particularly large below 400 cm^{-1} and in the range of 800–1300 cm^{-1}. It is noteworthy that in the latter range the curve with $g = 0$ lies almost midway between the curves with $g = 1$ and with $g = -2$. Hence, it is to be expected that the effect in this range is diminished by averaging over the various orientations between the pair of H-bonds, and that the effect can be observed below 400 cm^{-1} only.

These results, however, must be considered with some reservations: The calculations in this paragraph are based on the dipole–dipole approximation of the interaction operator. Hence, they are valid for uncharged H-bonds, and for charged H-bonds with a counterion in the immediate

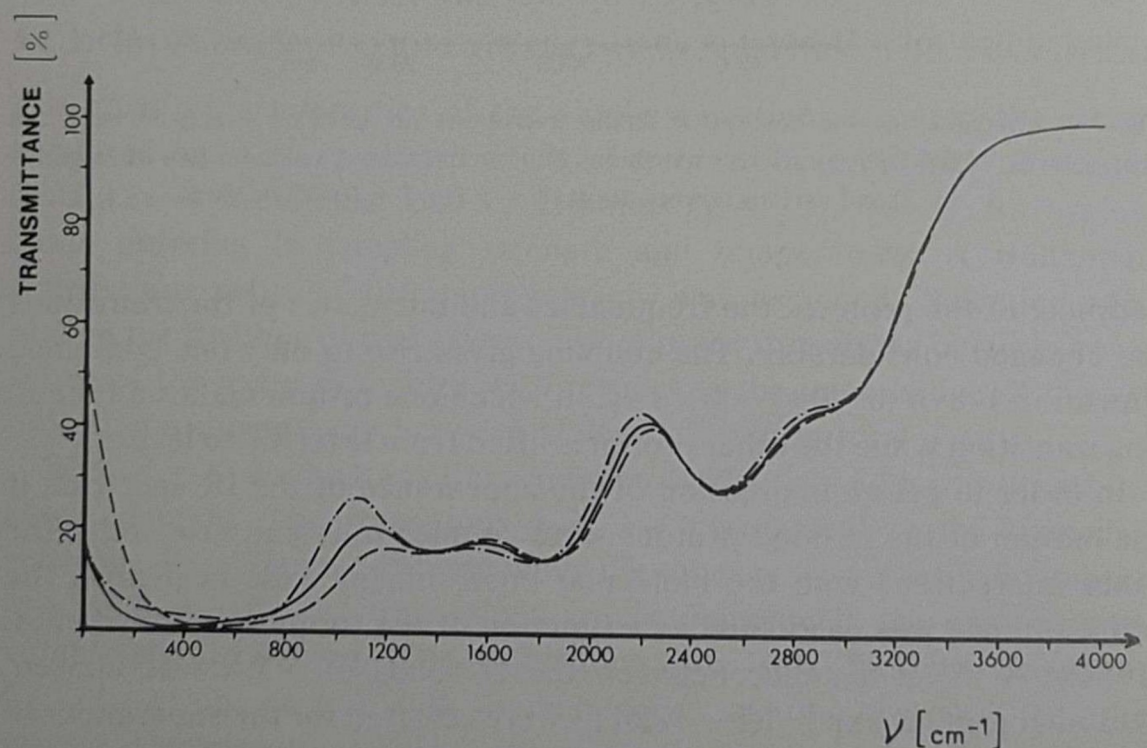

Fig. 5.5 Transmittance for a system of pairwise interacting H-bonds, —— $g = 0$, ------ $g = 1$, –·–·–·– $g = -2$; layer thickness 5μ; average separation of pairs 5.5 Å.

neighborhood providing for the electrical neutrality. Moreover, a symmetrical double-minimum potential was assumed. Hence, the dipole moment vanishes in the ground state as well as in the excited states of the isolated system. Therefore with these assumptions, no induced dipole interactions occur between H-bonds, but dispersion and resonance interactions only (see section 5.4.7 for the discussion of the resonance interaction). In general however, the induced dipole interaction predominates, in particular with charged H-bonds; this interaction is discussed in section 5.4 together with the influence of polar solvents.

5.3.3. Correlation functions

The coupling of the tunnelling protons observable by changes in the energy levels and transition probabilities cause correlations of the protons in adjacent H-bonds. In order to investigate the correlations in the various states of a coupled pair of H-bond protons, we define a correlation function K_ψ in the state ψ by

$$K_\psi = N\langle\psi|x_1x_2|\psi\rangle n_1 \cdot n_2. \tag{5.15}$$

As before, x_1 and x_2 are the coordinates of the protons along the H-bonds, the directions of which are given by the unit vectors n_1, n_2. Since the dipole moment of a H-bond is approximately proportional to the elongation xn of the proton from the center of the H-bond, K_ψ is essentially the expectation value of the scalar product between the dipole moments of the two bonds in the state ψ. N is a normalization factor chosen in such a way that $|K_\psi| = 1$ with strict correlation.

A simple analytical expression can be given for the correlation functions in the tunnelling approximation. Since the two lowest levels of the isolated systems are only taken into account in this approximation, four proton states are to be considered for a pair of H-bonds. The states are denoted by $|+\rangle = |0+0+\rangle$, $|-\rangle = |0-0-\rangle$, $|s\rangle = |0+0-, s\rangle$, $|a\rangle = |0+0-, a\rangle$. In the states $|+\rangle$ or $|-\rangle$, both protons are in the ground state $0+$ or in the first excited state $0-$. One proton is in the ground state whereas the other proton is excited in the states $|s\rangle$ and $|a\rangle$; in fact the symmetrical or antisymmetrical states with respect to interchange of the proton coordinates must be taken. Calculating the four stationary states of the pair of coupled protons in the tunnelling approximation and in the dipole–dipole approximation (5.10) for the interaction operator, and substituting them in eq. (5.15), the following formulas are obtained for the correlation func-

tions in these states (Weidemann and Zundel [1973])

$$K_{\pm} = \mp z/\sqrt{1+z^2}, \qquad K_{s,a} = \pm 1 \tag{5.16}$$

with the abbreviation

$$z = p^2 g/h\nu_0 \epsilon R^3, \tag{5.17}$$

whereby p and ν_0 have the same meaning as in eq. (5.6) and whereby g is the orientation factor of eq. (5.13). The correlation functions are plotted in fig. 5.6.1 as a function of the dimensionless parameter z which includes the total dependence of the correlation with distance, orientation and tunnelling frequency. In choosing the values of the tunnelling frequency ν_0 and the transition moment p, as they are obtained for the particular system $H_5O_2^+$ with an O–O distance of 2.6 Å, one gets the dependence on the distance R, as plotted in fig. 5.6.2, for the case of two parallel H-bonds ($g = 1$). Figure 5.6 shows that the correlation increases with increasing z or decreasing R in the states $|+\rangle$ and $|-\rangle$. The sign of the correlation functions indicates whether the dipole moments of the two H-bonds are orientated preferably parallel or antiparallel to one another. The correlation functions do not decrease with increasing distance R in the states $|s\rangle$ and $|a\rangle$; the reason for this unrealistic behavior is that the calculation is based on stationary states which are adapted to the symmetry of the interaction–irrespective of how small the interaction may be. Of course in reality, the correlation decreases in all states with distances R at which the neglected interactions disturbing the symmetry are no longer small compared with the interaction taken into account.

The simple picture (fig. 5.6) of the correlation functions is valid in the tunnelling approximation only, i.e. in the interaction of two-level systems. The picture gets more complicated when the omitted proton levels are taken into account. Substituting in eq. (5.15) the eigenfunctions obtained by diagonalizing the energy matrix of two H-bonds with four proton levels in each bond, results in fig. 5.7, whereby the energy levels and dipole-moment matrices of the single H-bond were again taken from the paper of Janoschek et al. [1972] for the particular system $H_5O_2^+$ and various O–O distances. The left-hand column contains the correlation functions of the four lowest states of the pair of H-bonds in which both protons preferably occupy the states $0+$ or $0-$. The right-hand column applies to the states of the upper level group in which both protons are in states $1+$ or $1-$. Finally, the middle column contains the states in which one proton is in state $0+$ or $0-$, the other one in state $1+$ or $1-$. The

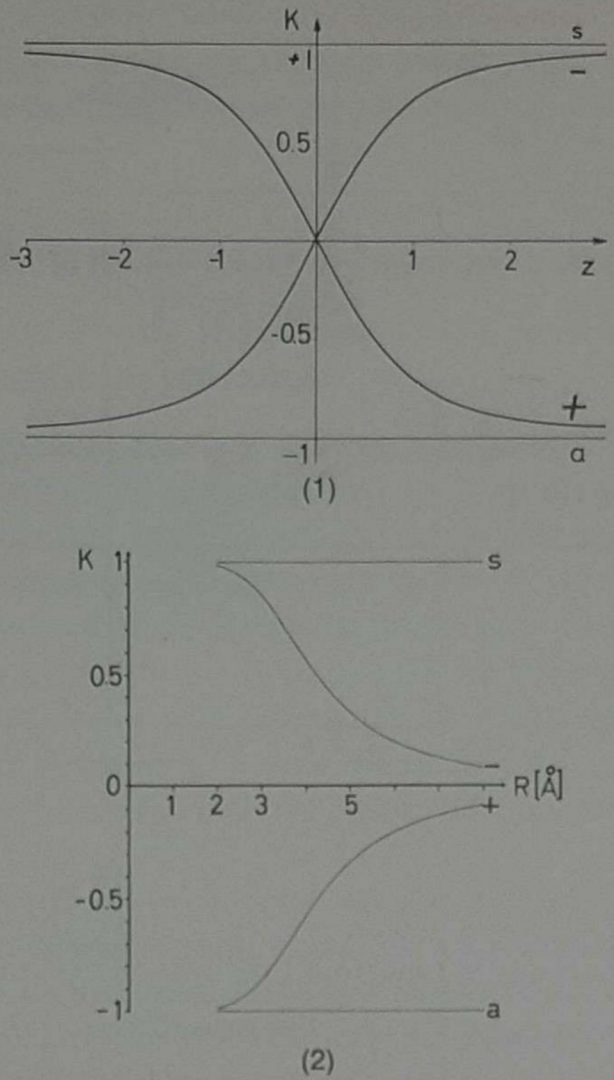

Fig. 5.6. Correlation functions for the four lowest states of a pair of interacting H-bonds in the tunnelling approximation as a function of (1) the dimensionless parameter z defined in eq. (5.13) and (2) the separation R of two parallel H-bonds.

schematic picture of the tunnelling approximation, as shown in fig. 5.6.2, can be recognized in the left-hand and right-hand columns of fig. 5.7, in fact it is the more easily recognizable, the greater the O–O distance. The reason for this behavior is evident. As the O–O distance increases, the potential barrier in the double-minimum potential also increases and the lowest levels in this potential move together pairwise. Thus the interactions between these level pairs exceed the interactions with the other levels. The sudden changes in the sign of the correlation functions, occurring particularly in the double-minimum potentials with a high barrier at certain distances, indicate Fermi resonances. At these distances, two energy levels of the same symmetry and parity repel each

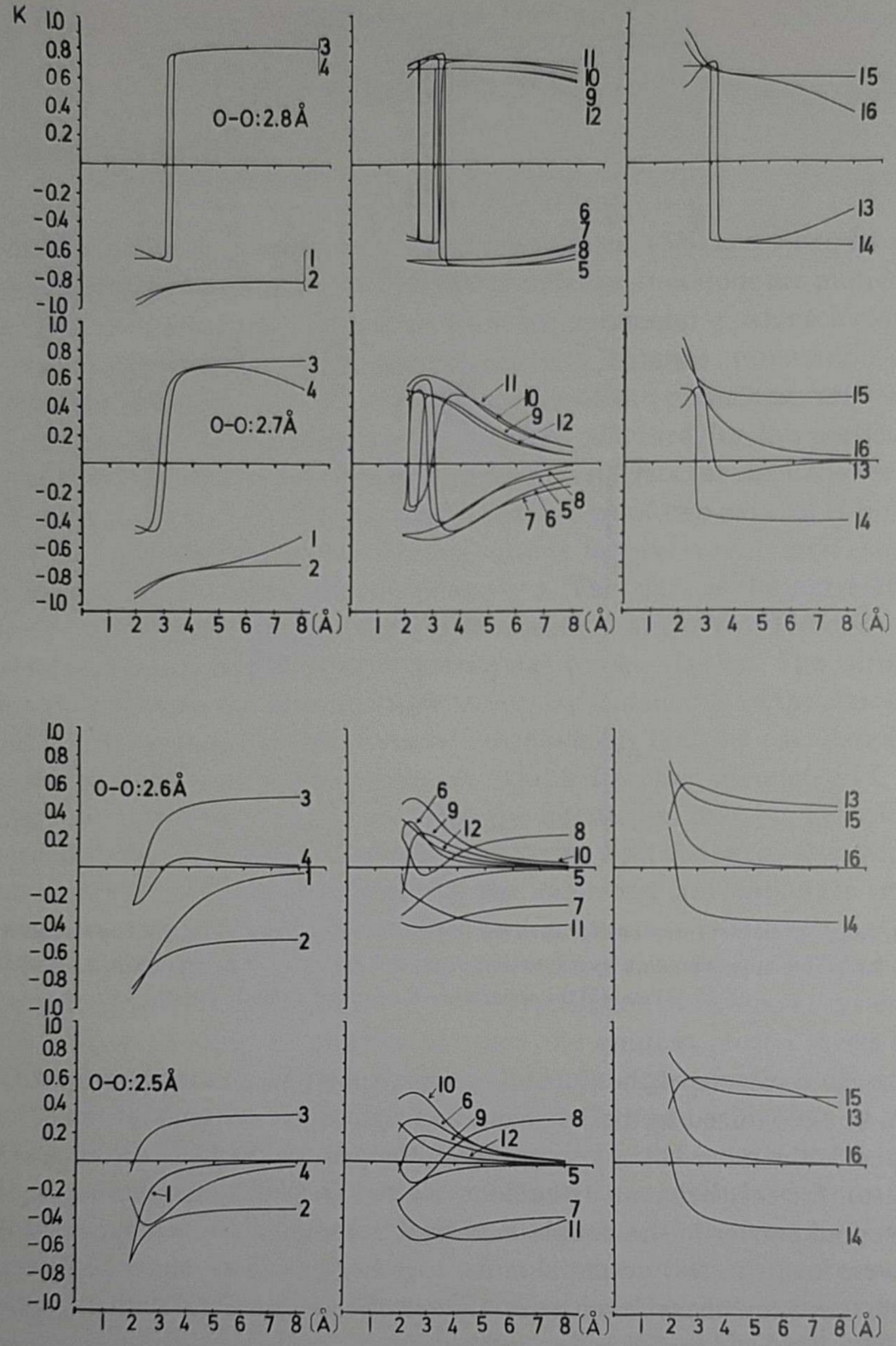

Fig. 5.7. Correlation functions for the 16 lowest states of two parallel H-bonds in $H_5O_2^+$ beside each other for various O–O distances plotted as a function of the separation of the H-bonds.

other because of the crossing rule already mentioned, and the wave functions of the two states are strongly mixed. Therefore, the intensities of the transitions involving one of the two levels as initial or final state are also changed suddenly.

5.4. Influence of the molecular environment on proton correlations

5.4.1. Polarizability of hydrogen bonds with an asymmetrical double-minimum potential

Until now only single-charged symmetrical H-bonds or pairs of such bonds isolated from their environment were considered. In many systems of interest, however, such bonds occur in polar solvents having a considerable influence on the potential of the H-bond proton. In particular, the symmetry of the potential is disturbed. The symmetry is also disturbed in general by the anion compensating the charge of the H-bonds $(BH\cdots B)^+$ which was neglected until now. An asymmetry of the potential gives rise to a decreasing polarizability and to a weakening of all interactions mediated by electric fields. Hence, the correlations are weakened too.

The influence of an asymmetry on the polarizability can be easily calculated in the tunnelling approximation by using eq. (5.8). We think of the asymmetry as produced from the symmetrical case by applying a homogeneous electric field of strength F_0. The field F_0 gives rise to an energy difference in the potential wells given by

$$\Delta V = 2\mu(x_0)\, F_0, \tag{5.18}$$

whereby x_0 is the distance of the minima from the middle of the H-bond, in which the influence of the field F_0 is neglected. The polarizability in the asymmetrical case is then given by the polarizability of the H-bond already polarized by the field F_0, i.e. it is given by the derivative of eq. (5.8) with respect to the field at $F = F_0$.

$$\alpha = \frac{2p^2}{h\nu_0} \tanh\left(\frac{h\nu_0}{2kT}\sqrt{1+\zeta_0^2}\right)\frac{1}{1+\zeta_0^2} \times\left(\frac{1}{\sqrt{1+\zeta_0^2}} + \frac{(h\nu_0/kT)\,\zeta_0^2}{\sinh\left[(h\nu_0/kT)\sqrt{1+\zeta_0^2}\right]}\right). \tag{5.19}$$

The dimensionless parameter ζ_0 is given by

$$\zeta_0 = 2pF_0/h\nu_0 \approx \Delta V/h\nu_0, \tag{5.20}$$

whereby eq. (5.18) and $p \approx \mu(x_0)$ was used. $p \approx \mu(x_0)$ is approximately valid since, because of eq. (5.7), p is the maximum inducible dipole moment which is–within a high degree of approximation–the same as the dipole moment obtained if the proton is localized in one potential well. The polarizability of the asymmetrical H-bond is plotted as a function of ζ_0 in fig. 5.8 with $\bar{\nu}_0 = 100\ \mathrm{cm}^{-1}$ and $p = 2$ debye for various temperatures. The polarizability decreases rapidly with increasing asymmetry, but even with an asymmetry of $\Delta V = 500\ \mathrm{cm}^{-1}$ ($\zeta_0 = 5$), it is a factor of 30 greater than the usual polarizabilities, at room temperature.

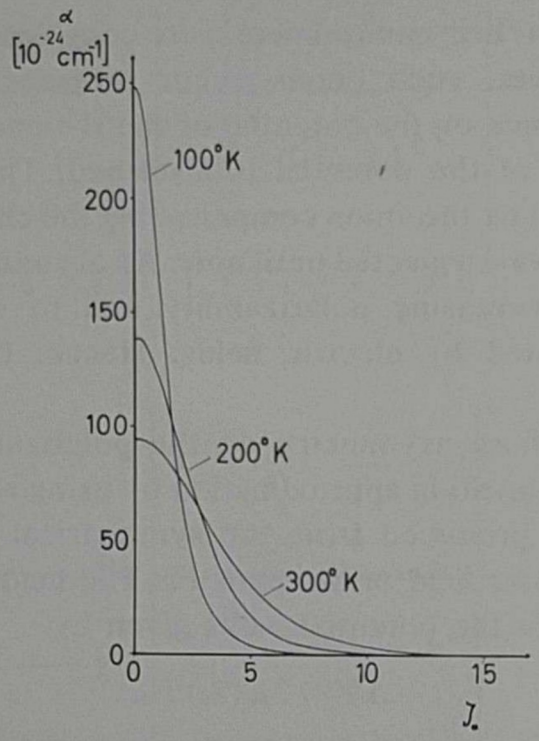

Fig. 5.8. Average polarizability α of an unsymmetrical H-bond plotted as a function of the asymmetry parameter $\zeta_0 = \Delta V/(h\nu_0)$ for the temperatures $T = 100, 200, 300$ K.

The polarizability of the symmetrical H-bond indeed decreases with rising temperature; the high polarizability, however, is maintained up to higher degrees of asymmetry. This behavior is caused by the protons in the first excited state in which state the protons are shifted opposite to the field direction. The contribution of these protons is the reason why the dipole moment rises less rapidly in the thermal average, and hence also why the saturation value is reached at higher field strengths.

The influence of the molecular environment on the polarizability of a single H-bond, however, is not determined by the quantities averaged

over a thermal equilibrium distribution, but by the polarizabilities in the various stationary states, in particular in the ground state. Hence, the polarizability α_0 of a single H-bond in the direction of the bond axis is plotted as a function of the asymmetry parameter ζ_0 in fig. 5.9, for various tunnelling frequencies in the symmetrical potential, assuming that the proton is in its ground state. The polarizability α_0 is given by eq. (5.19) in the limit $T \to 0$. The polarizability is larger for smaller tunnelling frequencies. Of course, this is true only as long as the assumption on which the calculation is based is valid, i.e. as long as the potential can be considered

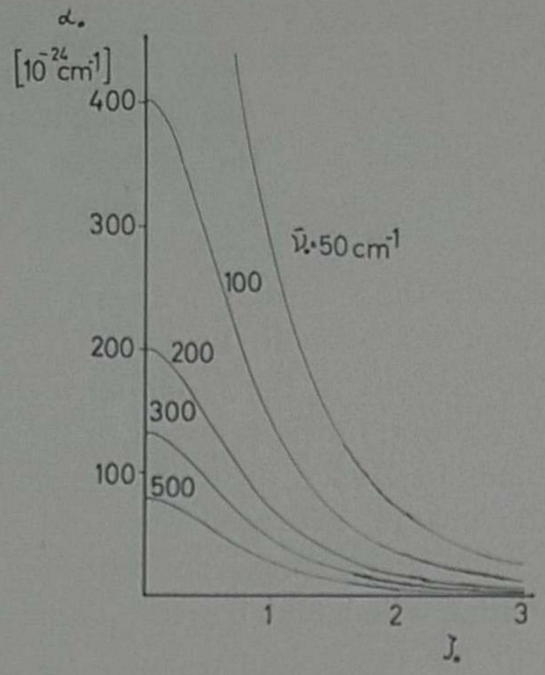

Fig. 5.9. Polarizability α_0 of an unsymmetrical H-bond in the ground state plotted as a function of the asymmetry parameter $\zeta_0 = \Delta V/(h\nu_0)$ for various tunnelling frequencies ν_0.

as constant during several tunnelling motions. Hence, the lingering times in both potential wells have to be small compared with time constants relevant to the reorientation of the dipole moments of the medium and to the motion of the anions. Finally, it must be borne in mind that the H-bonds themselves have a finite lifetime in fluids and that they break and reform from time to time. Hence, the lingering times have to be short compared with the lifetime, too.

5.4.2. Influence of a polar medium on proton tunnelling

The influence of a polar medium on the tunnelling of protons in H-bonds is of great importance in H-bonded ferroelectrics. Blinc and Ribarič

[1963], for instance, explain the anomalous isotope effect of the Curie temperature in KH_2PO_4 by a coupling of this kind, an idea which was taken up by several authors later on, e.g. by Tokunaga [1966] and Tokunaga and Matsubara [1966]. Usually, these calculations are also carried out in the tunnelling approximation, i.e. with restriction to two-level systems rendering the application of the quasi spin formalism which greatly simplifies the calculations. The influence of a polar medium is also discussed in treatments on proton transfer reactions, e.g. by J. L. Kurz and L. C. Kurz [1972] and by Vorotyntsev et al. [1973].

The situation in fluids is usually expressed by correlation functions of a small number of particles. In order to take a first step in this direction, pairs of H-bonds of type $(BH\cdots B)^+$ with two anions compensating the excess charge were considered in various geometrical configurations. The anions polarize the H-bonds and the H-bonds polarize each other mutually. In addition, the proton motion is coupled to the polar medium influencing the polarization effects decisively.

In order to investigate the interplay between all these interactions, some crude approximations have to be used. It is assumed that the lingering times of the protons in the potential wells are always small compared with the relaxation times, relevant to the reorientation of the dipoles of the polar medium. Hence, the dipoles orientate themselves with respect to the proton charge, averaged over the proton motion. The proton charge distribution itself, being concentrated in both wells in a double-minimum potential with a high barrier, is approximated by Dirac's δ-functions located in the two minima. Since the total charge in the H-bond is the charge of one proton, the charge distribution is described by a single parameter in the approximation considered here, i.e. by the average charge in one of the two wells. This parameter must be determined self-consistently, for the mean charge distribution depends on the potential and vice versa. The Schroedinger equation is solved for a given potential; the wave function $\psi(x)$ yields the charge density $\rho(x) = e\,\psi^*(x)\,\psi(x)$ along the bond axis, and the dipole moments of the medium orientate themselves with respect to the charge density and modify the potential.

In order to simplify the calculation, the continuous charge density $\rho(x)$ is replaced by two point charges e' and e'' located in the potential wells at $x = +\frac{1}{2}d$ and $-\frac{1}{2}d$. The two point charges result from the charge density by integrating over the individual wells.

$$e' = \int_{-\infty}^{0} \rho(x)\,dx, \qquad e'' = \int_{0}^{\infty} \rho(x)\,dx, \qquad e' + e'' = e. \tag{5.21}$$

Here, the origin $x = 0$ is taken to be the center of the potential barrier. The continuous charge density is then replaced by discrete charges according to

$$\rho(x) \to \bar{\rho}(x) = e'\,\delta(x + \tfrac{1}{2}d) + e''\,\delta(x - \tfrac{1}{2}d). \tag{5.22}$$

The influence of the polar medium on the potential can also be described in a crude approximation only, retaining, however, the essential factors. The medium in which the H-bonds are embedded, is described by a continuous polarization divided into two parts: One part of the polarization follows the proton tunnelling motion instantaneously and is described by a dielectric constant ϵ_ν, i.e. by the dielectric constant at the tunnelling frequency. This polarization is caused mainly by the displacement of the electrons. The other part of the polarization does not follow the proton motion at all. It is orientated with respect to the mean charge distribution ρ, averaged over the proton oscillations.

Describing the polar medium by a macroscopic dielectric constant is, of course, rather crude, since we are interested in the interaction of neighboring protons and anions. With very short distances, the electric field strength becomes so high that saturation of the polarization has to be taken into account. This is done by introducing a dielectric constant into the interaction between two point charges, depending on the distance r between the charges and approaching 1 in the limit $r \to 0$. The approximate shape of the function $\epsilon(r)$ can be derived from empirical data on the interaction between ions (Landis and Schwarzenbach [1969]).

5.4.3. Proton–anion interaction in a polar medium

In order to explain the Hamiltonian on which the numerical calculations are based, we consider at first the interaction of a proton in a single H-bond with an anion in a dielectric medium whose polarization consists of one "active" part, which follows the proton motion without retardation, and of another "inert" part, orientated in the field of the mean charge distribution in the bond and in the ion field.

In order to distinguish between these two parts, we start from the well-known relation

$$\boldsymbol{F} = \boldsymbol{D} - 4\pi\boldsymbol{P} \tag{5.23}$$

between the electric field strength $\boldsymbol{F}$, the dielectric displacement $\boldsymbol{D}$ and

the polarization $\boldsymbol{P}$. The polarization is divided into the active part $\boldsymbol{P}_\nu$ and the inert part $\boldsymbol{P}_0$

$$\boldsymbol{P} = \boldsymbol{P}_\nu + \boldsymbol{P}_0. \tag{5.24}$$

Accordingly, the electric field strength is divided into two parts,

$$\boldsymbol{F} = \boldsymbol{F}_\nu + \boldsymbol{F}_0, \tag{5.25}$$

whereby

$$\boldsymbol{F}_\nu = \boldsymbol{D} - 4\pi\boldsymbol{P}_\nu \tag{5.26}$$

is the electric field of the charges surrounded by the medium with the active polarization and the dielectric constant ϵ_ν, and whereby

$$\boldsymbol{F}_0 = -4\pi\boldsymbol{P}_0 \tag{5.27}$$

is the electric field strength caused by the inert polarization.

For a given charge distribution with density $\rho(r)$, the field strengths $\boldsymbol{F}$, $\boldsymbol{F}_\nu$ and $\boldsymbol{F}_0$ and their potentials ϕ, ϕ_ν and ϕ_0 can easily be written. As a consequence of eq. (5.25),

$$\phi = \phi_\nu + \phi_0. \tag{5.28}$$

Since

$$\phi(r) = \int \frac{\rho(r')\,\mathrm{d}^3r'}{\epsilon|r - r'|} \tag{5.29}$$

is the potential of a charge distribution ρ in a dielectric medium with dielectric constant ϵ,

$$\phi_\nu(r) = \int \frac{\rho(r')\,\mathrm{d}^2r'}{\epsilon_\nu|r - r'|} \tag{5.30}$$

is the potential in the medium containing the active polarization and described by a dielectric constant ϵ_ν. Consequently, using eq. (5.28),

$$\phi_0(r) = -\int \frac{\rho(r')\,\mathrm{d}^3r'}{\hat{\epsilon}|r - r'|} \tag{5.31}$$

with the abbreviation

$$\frac{1}{\hat{\epsilon}} = \frac{1}{\epsilon_\nu} - \frac{1}{\epsilon}. \tag{5.32}$$

Since the dielectric constant at the tunnelling frequency is smaller than the static dielectric constant, $\epsilon_\nu < \epsilon$, the dielectric constant $\hat{\epsilon}$ defined by eq. (5.32), is positive: $\hat{\epsilon} > 0$.

In the case of one proton and one anion, considered here initially, the

charge density is given by

$$\rho(r) = \rho_P(r) - e\,\delta(r - r_A). \tag{5.33}$$

Here, $\rho_P(r) = e|\psi(r)|^2$ is the mean charge distribution of the proton and r_A is the position of the anion with charge $-e$. Hence, the potential of the inert polarization, orientated with respect to this charge distribution, is given by

$$\phi_0(r) = -\int \frac{\rho_P(r')\,d^3r'}{\hat{\epsilon}|r - r'|} + \frac{e}{\hat{\epsilon}|r - r_A|}. \tag{5.34}$$

Applying the approximation (5.22), ϕ_0 is the potential of two negative point charges, located in the wells of the double-minimum potential, and one positive point charge at the position of the anion in a medium with dielectric constant $\hat{\epsilon}$.

In order to obtain the Hamiltonian for the motion of the H-bond proton in the field of the anion and influenced by the dielectric medium, the energy necessary to produce the inert polarization, orientated with respect to the charge distribution of the proton and the anion, is calculated. This is accomplished in two steps: In the first step, the charge distribution $\rho(r)$ is built up in the dielectric medium; in the second step, the charge distribution is removed, but with the inert polarization considered fixed.

The energy to form a charge density $\rho(r)$ out of infinitesimal charge elements in the infinite, is known to be

$$W_1 = \tfrac{1}{2}\int \rho(r)\,\phi(r)\,d^3r. \tag{5.35}$$

Here, $\phi(r)$ is the potential at point r produced by the charge density itself. $\phi(r)$ is divided into the two parts, $\phi_\nu(r)$ and $\phi_0(r)$, given by eqs. (5.30) and (5.31).

$$W_1 = \tfrac{1}{2}\int \rho(r)\,\phi_\nu(r)\,d^3r + \tfrac{1}{2}\int \rho(r)\,\phi_0(r)\,d^3r. \tag{5.36}$$

In order to remove the charge distribution with the inert polarization fixed, i.e. with constant $\phi_0(r)$, the energy

$$W_2 = -\tfrac{1}{2}\int \rho(r)\,\phi_\nu(r)\,d^3r - \int \rho(r)\,\phi_0(r)\,d^3r \tag{5.37}$$

must be supplied. Hence, the energy

$$W_0 = W_1 + W_2 = -\tfrac{1}{2}\int \rho(r)\,\phi_0(r)\,\mathrm{d}^3r \tag{5.38}$$

is necessary to produce the inert polarization.

In the case of one proton and one anion considered here,

$$W_0 = -\tfrac{1}{2}\int \rho_P(r)\,\phi_0(r)\,\mathrm{d}^3r + \tfrac{1}{2}e\,\phi_0(r_A) \tag{5.39}$$

results, using eq. (5.33). Substituting the potential (5.34) of the inert polarization, the energy

$$W_0 = \frac{1}{2}\int \frac{\rho_P(r)\,\rho_P(r')\,\mathrm{d}^3r\,\mathrm{d}^3r'}{\hat{\epsilon}|r-r'|} - \int \frac{e\,\rho_P(r)\,\mathrm{d}^3r}{\hat{\epsilon}|r-r_A|} \tag{5.40}$$

necessary to produce this polarization is obtained. We have omitted an infinite term which occurs because of the idealization of representing the anion charge by a point charge. This term arises because of the well-known infinite self-energy necessary to build up a point charge from infinitesimal charge elements.

Finally, the proton and the anion together with their active polarization fields are moved to their positions r_P and r_A, respectively. Hence, in order to produce the final situation, the energy

$$W = W_0 + V(r_P) + e\,\phi_0(r_P) - e^2/(\epsilon_\nu|r_P - r_A|) - e\,\phi_0(r_A) \tag{5.41}$$

must be supplied. We have denoted the double-minimum potential by $V(r_P)$, i.e. the potential in which the proton would move without the influence of the dielectric medium. $e\,\phi_0(r_P)$ is the modification of this potential by the inert part of the polarization. The fourth term is the attractive force between the charges shielded by the active polarization. $-e\,\phi_0(r_A)$ is the energy necessary to move the anion to its position in the field of the inert polarization. Substituting in eq. (5.41) for W_0 and ϕ_0, from eqs. (5.40) and (5.34), and combining terms of the same kind,

$$W = V(r_P) + e\,\phi_R(r_P) - \frac{e^2}{\epsilon|r_P - r_A|} + \frac{1}{2}\int \frac{\rho_P(r)\,\rho_P(r')\,\mathrm{d}^3r\,\mathrm{d}^3r'}{\hat{\epsilon}|r-r'|} \tag{5.42}$$

results with the abbreviation

$$\phi_R(r_P) = -\int \frac{\rho_P(r)\,\mathrm{d}^3r}{\hat{\epsilon}|r_P - r|}. \tag{5.43}$$

Comparing eq. (5.43) with eqs. (5.31) or (5.34) shows that $\phi_R(r_P)$ is the potential of the inert polarization, orientated with respect to the charge distribution ρ_P at the position of the proton producing this polarization. This potential is usually called the reaction potential. By means of the compensation of several terms, the full static dielectric constant shows up in the third term of eq. (5.42), and the second term of eq. (5.40) has dropped out. The last term in eq. (5.42) is, according to eqs. (5.38) and (5.31), the energy which is stored in the inert polarization field, orientated with respect to the charge distribution of the proton.

If one is merely interested in the displacement of the proton levels in the field of the anion, only the three first terms in eq. (5.42) are of importance, since these terms alone depend on the momentary position r_P of the proton. The last term is an additive constant in the Hamiltonian in the solution of the wave equation. It is to be noted, however, that this constant depends on the proton state $\psi(r)$ with respect to which the inert polarization is orientated, because of $\rho_P(r) = e|\psi(r)|^2$. The discussion of the effects caused thereby, and also of the problems connected with the calculation of the reaction potential (5.43), and of the last term in eq. (5.42), is deferred to section 5.4.5.

5.4.4. Interaction of two protons and two anions in a polar medium

Turning now to the case of two positively charged H-bonds with their corresponding anions, an important case concerning the correlations. The density of the charge distribution, with respect to which the inert polarization is orientated, is in this case given by

$$\rho(r) = \rho_1(r) + \rho_2(r) - e\,\delta(r - r_{A_1}) - e\,\delta(r - r_{A_2}), \tag{5.44}$$

whereby ρ_1 and ρ_2 are the mean charge distributions of the two protons. Hence, the potential of the inert polarization, according to eq. (5.31), is given by

$$\phi_0(r) = -\int \frac{\rho_1(r')\,\mathrm{d}^3r'}{\hat{\epsilon}|r - r'|} - \int \frac{\rho_2(r')\,\mathrm{d}^3r'}{\hat{\epsilon}|r - r'|} + \frac{e}{\hat{\epsilon}|r - r_{A_1}|} + \frac{e}{\hat{\epsilon}|r - r_{A_2}|}. \tag{5.45}$$

Substituting eq. (5.44) in eq. (5.38), the energy necessary to produce the inert polarization field is obtained.

$$W_0 = -\tfrac{1}{2}\int [\rho_1(r) + \rho_2(r)]\,\phi_0(r)\,\mathrm{d}^3r + \tfrac{1}{2}e\,\phi_0(r_{A_1}) + \tfrac{1}{2}e\,\phi_0(r_{A_2}). \tag{5.46}$$

The total energy of the charge distribution in the dielectric medium is hence, by analogy with eq. (5.41), given by

$$W = W_0 + V(r_{P_1}) + V(r_{P_2}) + e\,\phi_0(r_{P_1}) + e\,\phi_0(r_{P_2}) - e\,\phi_0(r_{A_1}) - e\,\phi_0(r_{A_2}) + \frac{e^2}{\epsilon_\nu}\left(\frac{1}{r_{P_1P_2}} + \frac{1}{r_{A_1A_2}} - \frac{1}{r_{P_1A_1}} - \frac{1}{r_{P_1A_2}} - \frac{1}{r_{P_2A_1}} - \frac{1}{r_{P_2A_2}}\right). \tag{5.47}$$

For simplicity $r_{P_1P_2} = |r_{P_1} - r_{P_2}|$ etc. Again, many terms compensate each other by substituting the potential ϕ_0 in eqs. (5.47) and (5.46).

The result is the following

$$\begin{aligned} W = {} & V(r_{P_1}) + e\,\phi_{R1}(r_{P_1}) - \int \frac{e\,\rho_2(r)\,d^3r}{\hat{\epsilon}|r_{P_1} - r|} - \frac{e^2}{\epsilon}\left(\frac{1}{r_{P_1A_1}} + \frac{1}{r_{P_1A_2}}\right) \\ & + V(r_{P_2}) + e\,\phi_{R2}(r_{P_2}) - \int \frac{e\,\rho_1(r)\,d^3r}{\hat{\epsilon}|r_{P_2} - r|} - \frac{e^2}{\epsilon}\left(\frac{1}{r_{P_2A_2}} + \frac{1}{r_{P_2A_1}}\right) \\ & + \frac{e^2}{\epsilon_\nu r_{P_1P_2}} + \frac{e^2}{\epsilon r_{A_1A_2}} + \int \frac{\rho_1(r)\,\rho_2(r')}{\hat{\epsilon}|r - r'|}\,d^3r\,d^3r' \\ & + \frac{1}{2}\int \frac{\rho_1(r)\,\rho_1(r')}{\hat{\epsilon}|r - r'|}\,d^3r\,d^3r' + \frac{1}{2}\int \frac{\rho_2(r)\,\rho_2(r')}{\hat{\epsilon}|r - r'|}\,d^3r\,d^3r', \end{aligned} \tag{5.48}$$

where the reaction potential $\phi_{Ri}(r)$ $(i = 1, 2)$ is formed, as in eq. (5.43), with ρ_i instead of ρ_P. The full static dielectric constant shows up in the interactions of the protons and anions, whereas the dielectric constant at the tunnelling frequency occurs in the interaction of the two protons as expected. The third term in the first and second lines of eq. (5.48) is the interaction of each proton with the polarization field produced by the other one. No problems arise in calculating these terms, particularly if the approximation (5.22) is used. The same applies to the third term in the third row, which is to be interpreted as the interaction energy of the inert polarization fields of both charge distributions, ρ_1 and ρ_2. The calculation of the last two terms, the energies of the polarization fields orientated with respect to ρ_1 or ρ_2, respectively, and the calculation of the reaction potential gives rise to difficulties already mentioned in the discussion of eq. (5.42).

Equation (5.48) also provides the correct result if both protons are localized in a potential well by means of the interaction. For in that case, the mean charge distribution of the protons coincides with the momentary proton positions, neglecting the oscillations in the individual wells, and the total polarization is orientated with respect to the momentary positions. This can be seen in eq. (5.48) by replacing ρ_i by $e\,\delta(r - r_{P_i})$. The

third terms in the first three lines become the same, except for the signs, and add up to $-e^2/(\hat{\epsilon} r_{P_1P_2})$. Together with the first term in the third line, this yields $e^2/(\epsilon r_{P_1P_2})$ because of eq. (5.32), i.e. the repulsion of the protons in a medium of the full static dielectric constant ϵ.

5.4.5. Modification of the potential curve by the reaction field

Before the discussion of the numerical results, we turn to the question of how to calculate the reaction potential $\phi_R(r_P)$, introduced by eq. (5.43). In fact, this equation cannot be used to calculate the reaction potential because there is not even approximately a homogeneous isotropic medium in the immediate neighborhood of the charge distribution producing the reaction potential, as was assumed in eq. (5.43). The molecular structure of the environment and the saturation of the polarization has to be taken into account.

The problem of how to calculate the reaction potential or the inner electric field in a dielectric medium, has been known for a long time and is the main problem in calculating the dielectric constant from the polarizabilities of the molecules. Two methods were adopted in solving this problem: Either the concept of a medium with a continuous polarization was maintained and a spherical cavity in the surrounding of the molecule was introduced, or the field of the molecular environment was treated by methods of statistical mechanics.

In our case, both methods yield essentially the same result, particularly since only the values of the reaction potential in the two minima of the double-minimum potential $V(r_P)$ are of importance. The problem is simplified in this way because of the approximation applied to the wave functions of the proton. In eq. (5.22), the charge densities $\rho_i = e|\psi_i|^2$ are approximated by δ-functions located in the potential wells. The same approximation is applied to the transition densities $\rho_{ik} = e\,\psi_i^* \psi_k$ taking the parity of the wave functions into account. Hence, in calculating the matrix elements of the interaction operator $W(r_{P_1}, r_{P_2})$ between the stationary states of the uncoupled case according to eq. (5.48), only the values of the operator are of importance, which correspond to the case of both protons being localized in a potential well. Therefore, only the difference in the energy of the two wells, arising from the reaction potentials ϕ_{R1} and ϕ_{R2} in eq. (5.48), are relevant for the results.

In applying the cavity method, it must be clarified which dielectric constant has to be assigned to the medium outside the cavity. It is shown by a simple consideration that the dielectric constant is not $\hat{\epsilon}$, but $\tilde{\epsilon}$

defined by

$$\frac{1}{\tilde{\epsilon}} = 1 - \frac{1}{\hat{\epsilon}} = 1 - \frac{1}{\epsilon_\nu} + \frac{1}{\epsilon}. \tag{5.49}$$

For the polarization potential $\tilde{\phi}$, in a medium with dielectric constant $\tilde{\epsilon}$, is given by eqs. (5.31) and (5.32) with $\epsilon_\nu = 1$ and $\epsilon = \tilde{\epsilon}$ according to the discussion in section 5.4.3. Hence, it is given by

$$\tilde{\phi}(r) = -\int \left(1 - \frac{1}{\tilde{\epsilon}}\right) \frac{\rho(r')\,\mathrm{d}^3 r'}{|r - r'|}. \tag{5.50}$$

In order that $\tilde{\phi}$ coincides with the potential ϕ_0 of the inert polarization given by eq. (5.31), we have to choose $\tilde{\epsilon}$ according to eq. (5.49). It is to be stressed that $\tilde{\epsilon}$ must not be confused with the dielectric constant of a medium in which only the inert polarization exists. For the inert polarization is not independent of the active polarization, but both influence each other mutually. $\tilde{\epsilon}$ is, rather, the dielectric constant of a fictitious medium whose total polarization produced by the field of the charge density ρ, coincides with the inert polarization of the actual medium which is orientated in the field of the charge shielded by the active polarization. Choosing $\epsilon_\nu = 3.5$ (a mean value between 1.78 and 5.25, the dielectric constants of water in the visible and microwave regions), $\tilde{\epsilon} = 1.38$ is obtained from eq. (5.49).

In the approximation (5.22), the reaction potential of two point charges e' and e'', separated by a distance d, must be calculated. Here d is the separation of the two wells in the double-minimum potential $V(r_P)$. The radius of the spherical cavity around the midpoint of the potential is denoted by a. The simple electrostatic problem can be solved exactly in polar coordinates r, ϑ, φ by expanding the potential inside and outside the cavity in Legendre polynomials. The expansion coefficients are determined by boundary conditions at $r = a$, $r \to \infty$ and $a \to \infty$ (see for instance Böttcher [1952]). The reaction potential is then obtained by subtracting the potential of the same charges in vacuum from the electrostatic potential. The result is the following

$$\phi_R(r, \vartheta) = -\sum_{l=0}^{\infty} \frac{(l+1)(\tilde{\epsilon} - 1)}{l + (l+1)\tilde{\epsilon}} \frac{(-1)^l e' + e''}{a^{2l+1}} \left(\frac{rd}{2}\right)^l P_l(\cos\vartheta), \tag{5.51}$$

whereby the polar axis coincides with the axis of the H-bond, i.e. with the line connecting the two charges e' and e'' (at $r = \frac{1}{2}d$ and $\vartheta = \pi$ or $\vartheta = 0$, respectively). The energy difference of the two wells

$$\Delta V = e\,\Delta\phi_R = e\,\phi_R(\tfrac{1}{2}d, 0) - e\,\phi_R(\tfrac{1}{2}d, \pi) \tag{5.52}$$

follows from eq. (5.51) as

$$\Delta V = \frac{2e(e' - e'')}{a} \sum_{l\,\mathrm{odd}} \frac{(l+1)(\tilde{\epsilon} - 1)}{l + (l+1)\tilde{\epsilon}} \left(\frac{d}{2a}\right)^{2l}. \tag{5.53}$$

The potential of course remains symmetric if $e' = e''$ or $\tilde{\epsilon} = 1$. The maximum asymmetry ΔV_m is obtained if the proton is localized completely in one well (e' or $e'' = e$) and this well is in fact lowered.

In fig. 5.10, ΔV_m is plotted as a function of the radius of the cavity for various values of $\tilde{\epsilon}$ and $d = 1$ Å. With $\tilde{\epsilon} = 1.38$ and $a = 3$ Å, a maximum asymmetry of $\Delta V_m \approx 400\ \mathrm{cm}^{-1}$ results. The values of the parameters $\tilde{\epsilon}$, d and a depend of course on the particular system considered. In fig. 5.10, they were chosen with regard to the system $H_5O_2^+$, being of special importance in the hydration of protons. The value of a corresponds to the separation of the water molecules of the first hydration shell around the H-bond in $H_5O_2^+$.

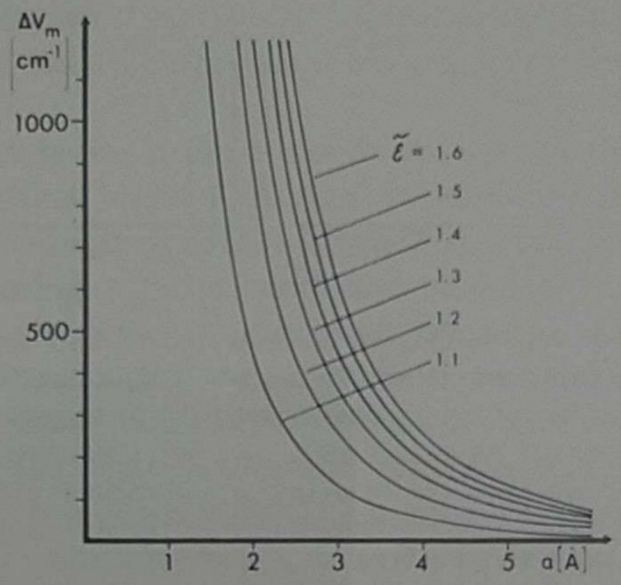

Fig. 5.10. Maximum energy difference ΔV_m of the wells in a double-minimum potential, as a function of cavity radius a, for various dielectric constants of the medium. The asymmetry is caused by the dipoles of a polar medium orientated with respect to a proton which is localized in one well.

5.4.6. Discussion of numerical results

Let us first consider a system of two H-bonds and two anions in a highly symmetric spatial configuration, as indicated in the upper right-hand corner of fig. 5.11. The lines represent the H-bonds, the small circles the

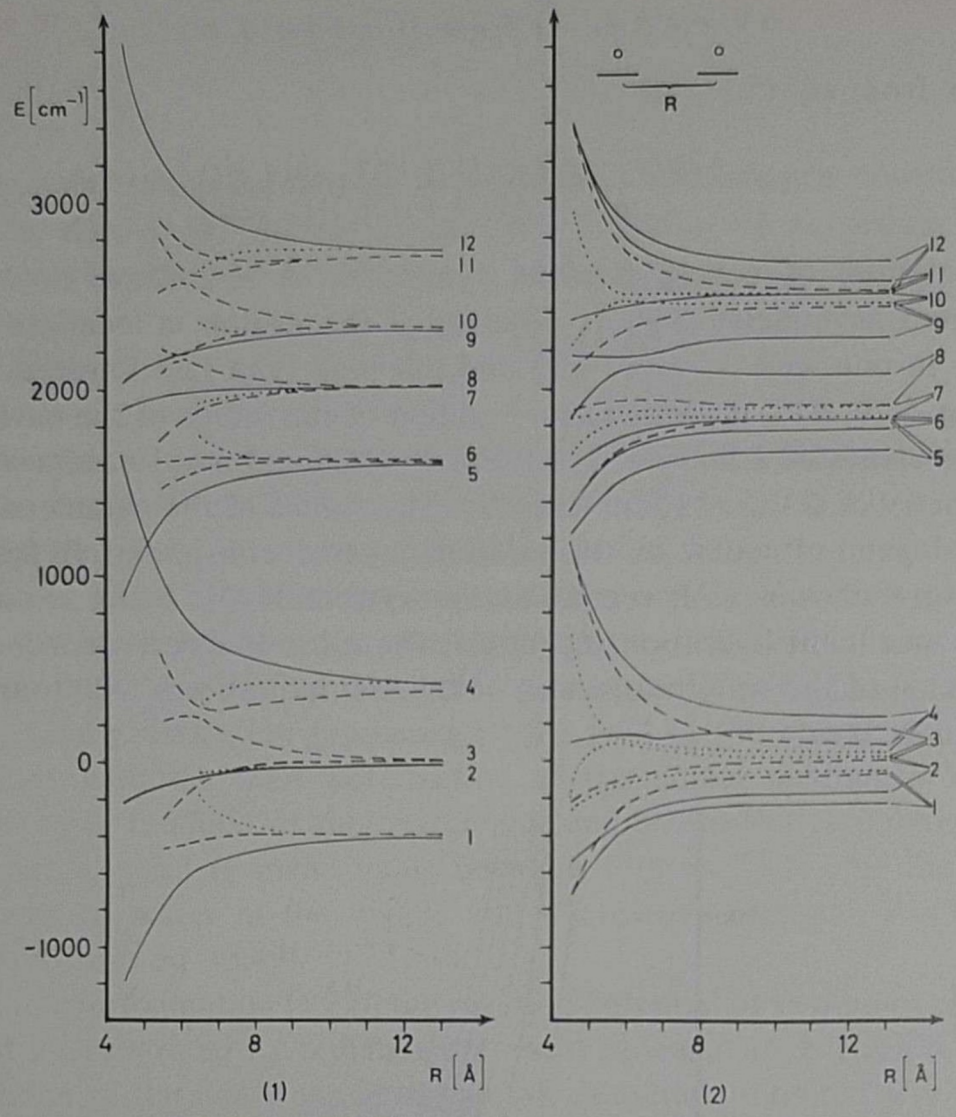

Fig. 5.11. Energy levels for two H-bonds and two anions with a spatial configuration as indicated in the upper right-hand corner, as a function of separation R of the centers of the H-bonds: (1) —— Dipoles of the medium orientated with respect to the mean charge distribution of the protons in the ground state; ------, ····· metastable states. (2) Dipoles of the medium orientated with respect to the mean charge distribution of the protons in the first (——), second (------) and third (·····) excited state.

anions. Since the anions are arranged vertically with respect to the bond axis and opposite to the centers of the bonds, the field of the left-hand ion influences the proton motion in the right-hand H-bond only and vice versa. However, the components of the anion fields in the direction of the H-bonds only partially compensate for the repelling field of one proton at the position of the other proton. Hence, it is to be expected that the same interaction effects occur if the anions are left out completely, but shifted to greater distances R between the H-bonds. This is confirmed by the

calculations (Pfeiffer et al. [1974]). Hence, the anions essentially compensate for the charges of the H-bonds, for the case considered here.

The solid lines in fig. 5.11.1 are the energy levels of the system as a function of the distance R between the H-bonds. They are the energy levels of the twelve lowest states, whereby the central level of the lower group and the four levels of the upper group are double degenerate. The degeneracy is a consequence of the symmetry of the geometrical configuration and is removed as soon as the symmetry is disturbed. In the four states of the lower level group, the protons are either in state $0+$ or $0-$, i.e. in the lower level doublet of fig. 5.1. In the upper group of levels, one proton is also in a state of this doublet, the other proton, however, is in a state $1+$ or $1-$, i.e. in a state of the upper level doublet of fig. 5.1. Both groups are treated independently; transitions between the groups brought about by the interaction between the H-bonds are hence neglected. As a consequence of this approximation, intersections of levels of different groups occur which do not in reality take place. The zero point of the ordinate was chosen in such a way that the sum of the energies of the lower level group vanishes. This statement is valid for all distances R since the trace of a matrix is invariant with respect to unitary transformations.

The interaction between the H-bonds show up if the distance of the bonds is smaller than about 12 Å. The interaction increases strongly at shorter distances. Frequency shifts in the IR spectra follow from the level shifts. The intensities of the bands are also influenced considerably because of the alteration of the wave functions. Since a statistical distribution of distances R occurs in fluids, a continuous absorption is to be expected in a broad range of wave numbers as a consequence of the superposition of the bands for various distances R.

Apart from the solid lines, fig. 5.11.1 contains broken and dotted lines corresponding to metastable states. In order to explain how these states come about, consider first the simple case of one H-bond and one anion at a distance R from the center of the bond on the bond axis. The level scheme is shown in fig. 15.21 for this case. At first, however, we are interested in the energy difference ΔV of the potential wells produced by the fields of the anion and of the dipoles of the polar medium, orientated with respect to the average charge distribution of the proton.

The solid lines in fig. 5.12 show ΔV plotted against the distance R of the anion for the ground state, i.e. for the case that the dipoles of the medium are orientated with respect to the mean charge distribution in the proton

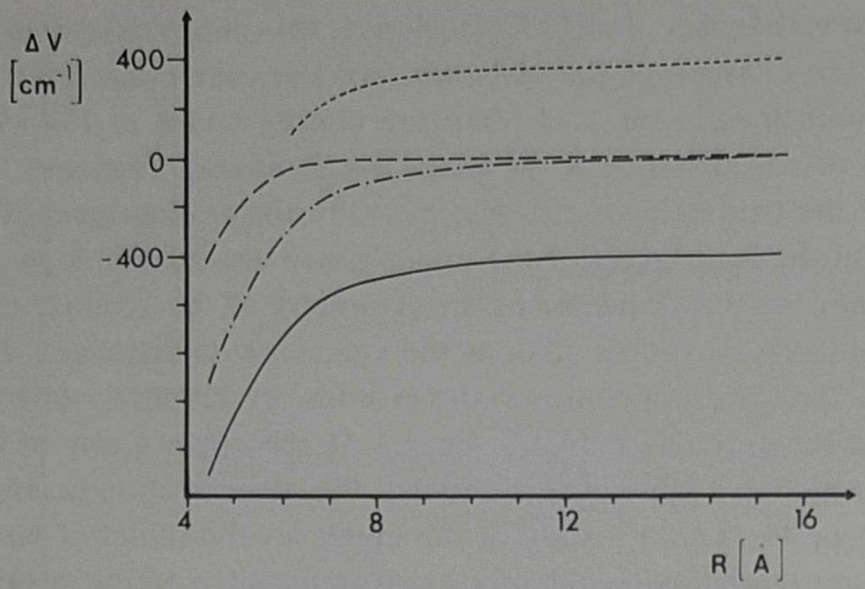

Fig. 5.12. Energy difference of the potential wells ΔV, caused by the field of an anion at separation R, and by the dipoles of the medium which are orientated with respect to the mean charge distribution of the proton in various states, plotted against R: —— ground state, –·–· ground state neglecting the reaction field, ------ first excited state, ····· metastable state.

ground state. The asymmetry is more pronounced as the ion approaches the H-bond. It does not, however, vanish with $R \to \infty$, since the symmetrical state is also unstable in the absence of the ion. The reason for the instability can easily be understood. A small asymmetry in the double-minimum potential caused by an external disturbance, effects a big change in the proton wave functions and gives rise to a highly asymmetrical mean charge distribution. In the ground state, the position probability in the deeper well is considerably greater than in the upper well. The dipoles of the medium orientate themselves preferably with respect to the deeper well and thereby enhance the asymmetry of the potential. The state becomes stable if the maximum asymmetry ΔV_m caused by the reaction field is nearly attained, i.e. if $e'' \ll e'$ in eq. (5.53). The value of $400\ \mathrm{cm}^{-1}$ for ΔV_m was obtained in section 5.4.5, a value which coincides with the asymptotic value of $\Delta V(R)$ in fig. 5.12. The second lowest curve in fig. 5.12 shows the direct influence of the ion field, neglecting the reaction field, i.e. without the influence of the third term in eq. (5.42) on the symmetry of the potential. It is evident that the reaction field merely displaces this curve downward by ΔV_m.

It should be noted that with small distances between the anion and the H-bond, the asymmetry becomes so high that the proton is captured completely in the deeper well. This is evident from fig. 15.14 showing that

the asymmetry has to be higher than about 1000 cm^{-1}, with the double-minimum potentials which come into question, in order to prevent the proton in the ground state from tunnelling into the upper well. With high asymmetry of the potential (but smaller than 1000 cm^{-1}), the average charge density in the upper well becomes indeed so small that e'' in eq. (5.53) is negligible and $\Delta V \approx \Delta V_m$. The small charge density in the upper well, however, is chiefly effected by the small lingering time in this well and not by the fact that the tunnelling motion ceases entirely.

The dashed curve in fig. 5.12 is calculated assuming that the dipoles of the medium are orientated with respect to the mean charge distribution of the proton in the first excited state. Hence, e' and e'' in eq. (5.53) are calculated by means of the proton wave function in the first excited state. Of course, the lifetime of the proton in this state has to be long enough, i.e. long compared with the relaxation times relevant to the reorientation of the dipoles. This condition will be realized in many media since the relaxation times relevant to the reorientation of small solvent molecules lie in the range of 10^{-9}–10^{-11} seconds. The dashed curve shows, contrary to the solid curve, that the potential becomes appreciably asymmetric only below 6 Å.

The differing polarization of a H-bond with a double-minimum potential in the ground state, and in the first excited state of the proton, is the reason for the totally different influence of the polar medium on the potential curve in the two cases in which the dipoles are orientated with respect to the different charge distributions. Whereas the proton occupies preferably the deeper well in the ground state, the position probability in the higher well prevails in the first excited state. Hence, the dipoles of the medium orientate themselves with respect to the higher well in the latter case, and lower this well. The reaction field of the polar medium thus diminishes the asymmetry of the potential caused by the ion field, if the dipoles are orientated with respect to the mean charge distribution of the proton in the first excited state. Hence, the symmetrical potential is stable for large separations in this case. An appreciable degree of asymmetry is generated by the ion field only if this field is so strong that the asymmetry produced thereby cannot be compensated by the reorientation of the dipoles of the medium.

Finally, the dotted curve in fig. 5.12 corresponds to a metastable state of the system comprising anion, proton and polar medium. The metastable state arises as follows: It was tacitly assumed in the discussion of the solid curve that the potential well turned toward the anion is lowered by

the polar medium, so that this well is lowered further if the ion approaches. A metastable state arises in the opposite situation, i.e. if the well turned away from the anion is initially lowered by the polar medium. In this case, the asymmetry of the potential will be diminished when the ion approaches. Such a state is of course unfavorable with respect to the energy compared with the state first discussed. It can, however, change to the other state only by repolarization of the medium and is, hence, relatively long-lived. It is stable with respect to small perturbations. Small changes of the asymmetry in both directions cause negligible modifications of the mean charge distribution of the proton and thereby no modifications of the polarization of the medium. Hence, the asymmetry retains its original value if the perturbation ceases. Therefore, the state is called metastable. It becomes unstable only if the ion field gets so strong that the effect of the reaction field is compensated and the potential thereby becomes almost symmetric. For in that case, small changes in the potential caused by a perturbation effect big changes in the mean charge distribution of the proton and thus in the polarization of the medium. Hence, the dotted curve ceases before it intersects the abscissa $\Delta V = 0$. The metastable state is obtained in the calculations by starting with an appropriate initial distribution in the iterative solution of the self-consistent eigenvalue problem, i.e. with a distribution in which the proton is localized in the well turned away from the anion. The instability of the metastable state with small separations R becomes perceptible on the convergence of the iterative solution into the stable solution, independent of the initial distribution.

In fig. 5.11.1, the energy levels of the metastable states are plotted as dashed and dotted lines for the case of two H-bonds and two anions in the particular spatial configuration sketched in the upper right-hand corner. They lie between the solid lines, which are the border lines in each level group. The transitions between the metastable states of the same group are thus displaced to smaller wave numbers compared with the transitions between the stable states. The metastable levels do not reach arbitrarily small values of the separation R because of the reason mentioned above; with a sufficiently strong interaction of the protons, the metastable states are no longer realized since the forces between the protons are stronger than the interaction with the dipoles of the medium.

In fig. 5.11.2, the level scheme is plotted for the same spatial configuration of H-bonds and anions, with the assumption, however, that the dipoles of the medium are not orientated with respect to the mean charge

distribution of the proton in the ground state, but in one of the three lowest excited states. These states can be realized only if the lifetime of the excited states is long compared with the relaxation time for the reorientation of the dipoles. If they were all realized, they would constitute a quasi continuum of energy levels by themselves, and they would give an essential contribution to the generation of the IR continuum observed. The question, to what extent these states are realized, is difficult to answer. In thermal equilibrium, the occupation number of a state, being a decisive factor for the intensities of the transitions from this state, depends only on the excitation energy of the state and of course on the partition function, the latter being irrelevant in the calculation of relative intensities. It is difficult to obtain the mutual position of the energy levels belonging to different polarization fields of the medium. In order to determine the mutual position, the energy necessary for polarizing the medium has to be calculated, this energy being given by the last three terms in eq. (5.48). Since this has not yet been possible, the intensity problem must be left open.

In order to demonstrate the influence of the polar medium on the position of the energy levels, the levels of the lower group of fig. 5.11.1 are redrawn in fig. 5.13 for the case that the dipoles of the medium are orientated with respect to the mean charge distribution of the protons in the ground state. Figure 5.13 also contains, as dashed lines, the lowest and highest levels of the group as they are obtained without the effect of the permanent dipoles of the medium, hence, in a medium with dielectric constant ϵ_∞. The dashed curves approach $\pm \bar{\nu}_0 = \pm 53\ \mathrm{cm}^{-1}$ in the limit $R \to \infty$, since all interactions between the H-bonds and the ions vanish in this limiting case because of the position of the ions perpendicular to the H-bonds. The corresponding solid curves, however, go to $\pm 2(\Delta V/2) \pm \bar{\nu}_0$ in the same limit, whereby ΔV is the energy difference of the two potential wells produced by the polarization of the medium, and given by eq. (5.53); hence, $\Delta V/2$ is the depression of one well compared with its position in the symmetrical case. Even in the limit $R \to \infty$, the protons are localized by means of the polarization in the outer wells in the ground state, but in the inner wells in the third excited state. Therefore the levels remain almost constant up to small separations, so that the range of the forces brought about by the interaction between the protons, is reduced by the influence of the polar medium. With small distances, the dashed and full lines approach each other, and hence the forces are not influenced appreciably in this range.

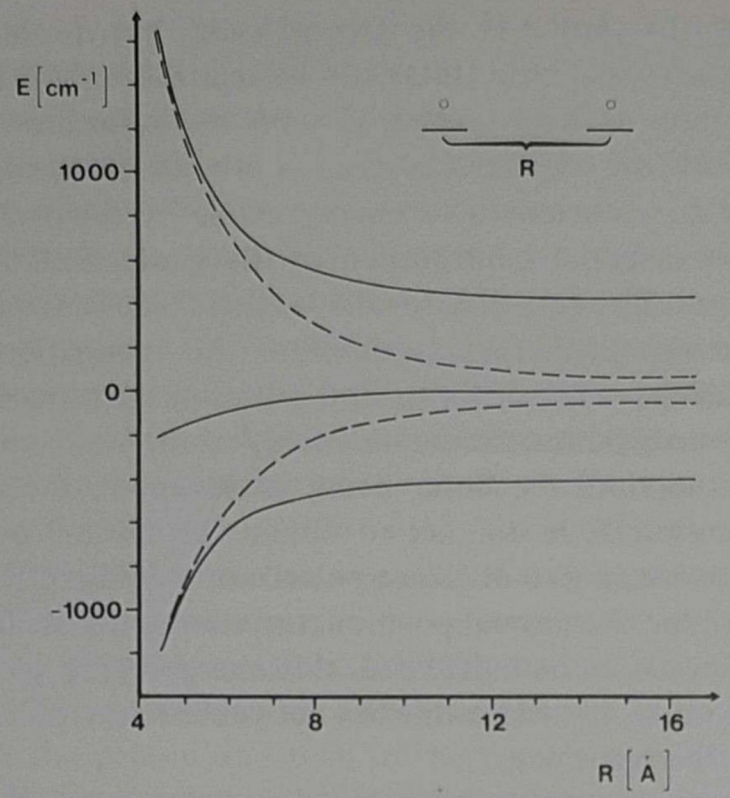

Fig. 5.13. Influence of a polar medium on the position of energy levels: —— levels of the four lowest states of fig. 5.11.1; ------ levels of the same states without the polar medium.

In the case of the first and second excited states, both being degenerate within the accuracy of the drawing, the dashed and solid curves coincide. Hence, the medium has no appreciable influence in these states. This can easily be understood by looking for the position probabilities in the various potential wells. All of the position probabilities are nearly equal to 1/2 in both states. Thus the dipoles of the medium orientate themselves to the same extent with respect to both wells of the two H-bonds, hence displacing the whole potential curves downward without changing their symmetry.

Until now, we have considered the H-bonds and the anions in a spatial configuration in which the influence of the ions on the proton motion is a minimum, and in which the correlation of the protons is disturbed as slightly as possible. To investigate the effect of the ion fields on the proton correlations, consider two H-bonds and two anions in the configuration indicated in fig. 5.14, with variation of the separation R_1 of the ion lying on the extension of the bond axis. Figure 5.14.1 shows the level scheme assuming that the dipoles of the medium are orientated with respect to the mean charge distribution of the protons in the ground state, and also the

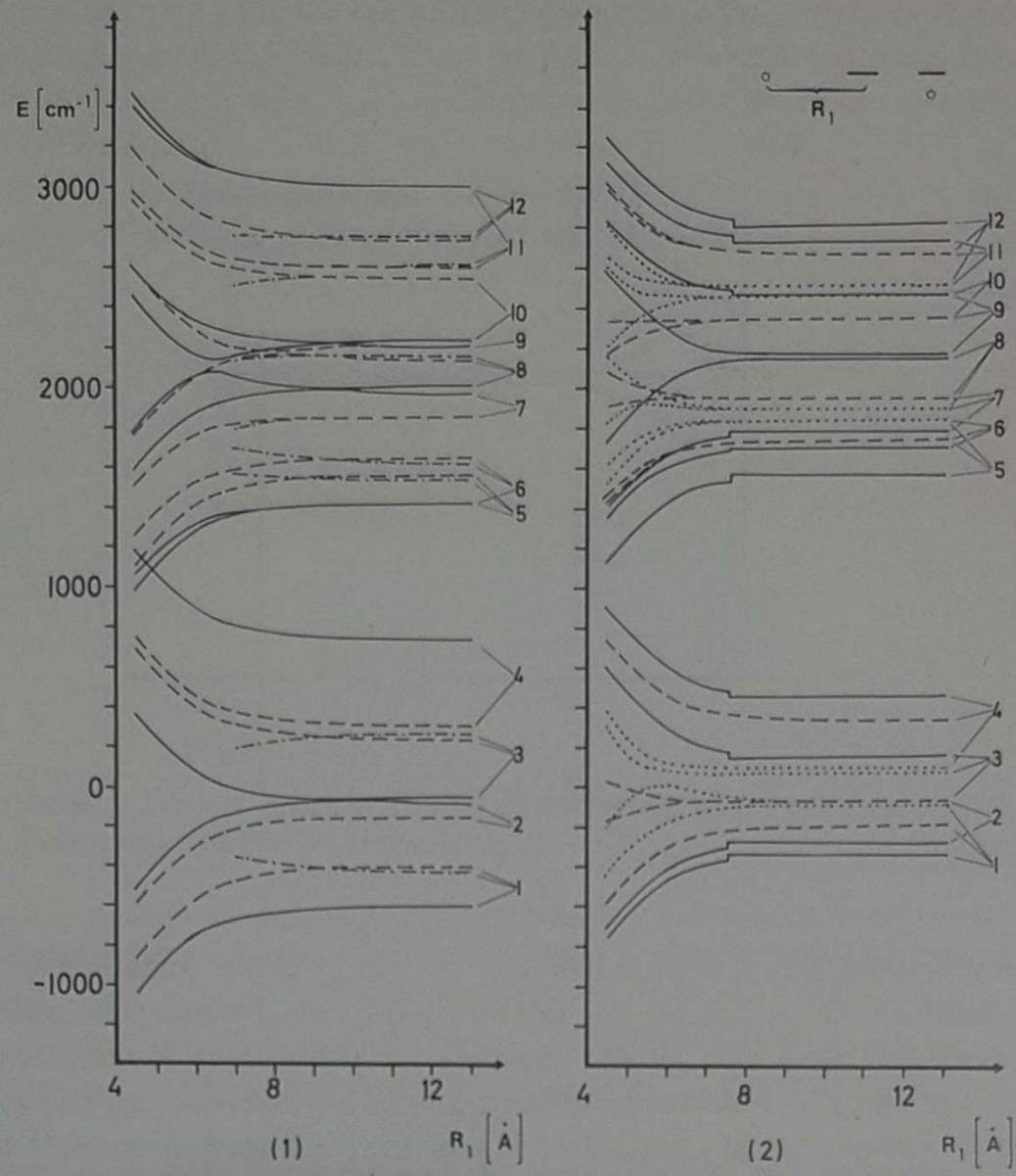

Fig. 5.14. Energy levels for two H-bonds and two anions, in the configuration indicated in the upper right-hand corner, as a function of the separation R_1 between anion and H-bond: (1) —— Dipoles of the medium orientated with respect to the mean charge distribution of the protons in the ground state; –·–·–, ------ metastable states. (2) Dipoles of the medium orientated with respect to the mean charge distribution of the protons in the first (——), second (------) and third (·····) excited state.

levels of the metastable states. Figure 5.14.2 shows the level scheme if the dipoles are orientated with respect to the charge distribution in the first, second or third excited state.

Of particular interest is the behavior of the two central levels of the lower group in fig. 5.14.1 or fig. 5.15. These levels are nearly degenerate in the case considered previously (fig. 5.11.1 or fig. 5.13). The degeneracy is

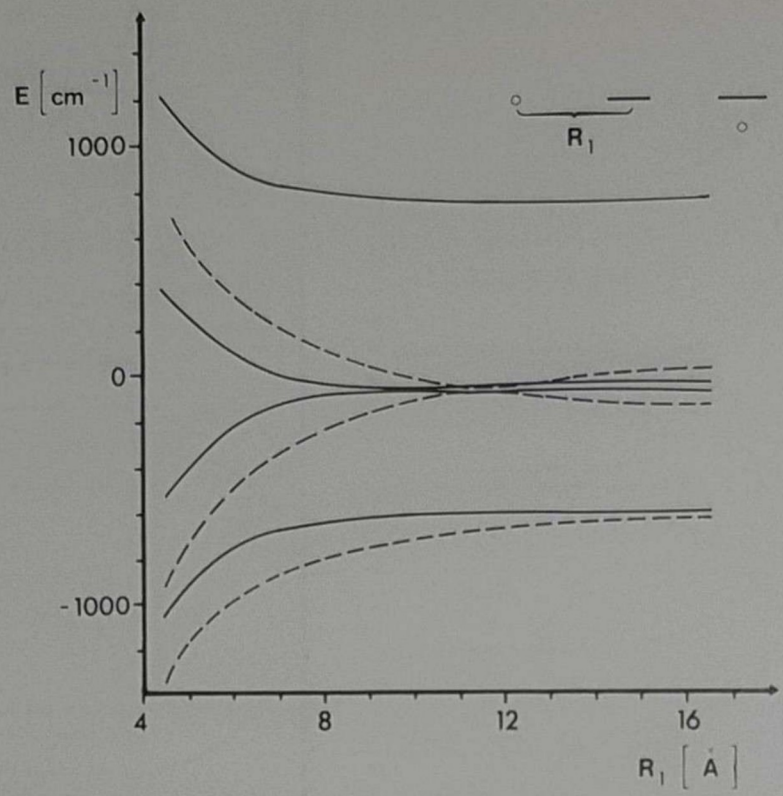

Fig. 5.15. Influence of a polar medium on the position of energy levels: —— levels of the four lowest states of fig. 5.14.1; ------ levels of the same states without the polar medium.

removed with large separations R_1, in fact, by the influence of the left-hand anion on the proton in the right-hand H-bond. The splitting between the two levels almost vanishes for separations R_1 between 9.5 and 10 Å, since with these separations the field of the left-hand anion and the field component of the right-hand anion in the direction of the H-bond just compensate each other. With smaller distances, the levels again split strongly by means of the ion fields. In fig. 5.15, the four lowest levels, in dashed lines, are obtained without the reorientation of the permanent dipoles of the medium, i.e. in a medium with dielectric constant ϵ_ν. With the configurations considered here, the picture is qualitatively the same as if the orientation polarization were taken into account and only shifted to larger separations. The reason for this displacement is that the charges are less strongly shielded by the smaller dielectric constant ϵ_ν.

Striking are the sudden changes of the energy levels in fig. 5.14.2 at $R_1 = 7.5$ Å, for the case that the dipoles of the medium are orientated with respect to the mean charge distribution in the first excited state. The reason for the appreciable changes in energy with very small alterations in the separation R_1 may be understood by considering the position prob-

abilities of the protons in the various potential wells. Figure 5.16 shows a sudden change in the mean charge distribution of both protons in the first excited state with $R_1 = 7.5$ Å. Whereas with large distances, the protons preferably occupy the wells situated on the right, the wells on the left are preferably occupied at smaller distances. The transition occurs abruptly because of the high polarizability of the H-bonds.

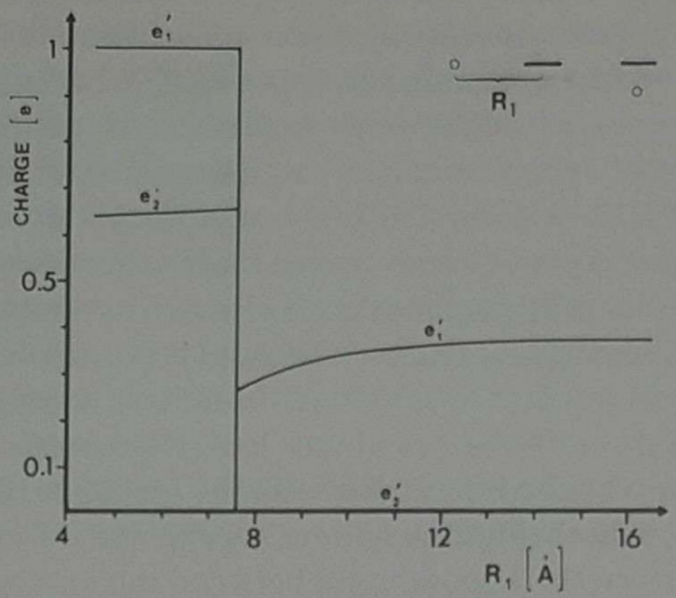

Fig. 5.16. Average proton charge in the left-hand potential wells of two H-bonds, in the configuration indicated above, as a function of the anion separation R_1 (1 left-hand H-bond, 2 right-hand H-bond).

5.4.7. Correlation of protons

What can be seen from the numerical results with regard to the correlation of protons in adjacent H-bonds? By investigating the position probabilities in the various potential wells, it can be stated that, to a large extent, the protons are localized in single wells. This implies that the potentials of each proton have become asymmetrical due to the interaction with the ions and the polar medium and the interaction between the H-bonds. The asymmetry is not necessarily very large since the proton wave functions in a double-minimum potential react very sensitively to small perturbations of the symmetry. As mentioned in the discussion of fig. 5.12 and in section 5.4.6, this does not at all imply that the tunnelling motion is suppressed completely; the lingering time in the higher well is only very small. Hence, in most cases the H-bonds are strongly polarized by the interactions, and the interactions result in a strong

correlation of the directions of polarization in the H-bonds. Expressed in another way, the interactions result in a correlation of the mean charge distributions in the H-bonds.

In these cases, however, one cannot speak of a correlation of the tunnelling motions of the protons. The probability for the correlated tunnelling motion of two protons is proportional to the probability of one proton passing on to the higher well, multiplied by the conditional probability that the other proton also performs a tunnelling motion during the lifetime of the first proton in the upper well. With largely asymmetric potentials, this process is highly improbable because of the short lingering time in the upper well. Correlated motion can be expected–with one exception which is discussed below–only if the potentials for both protons are almost symmetrical. It was shown in section 5.4.6 that the interaction with the polar medium gives rise to a symmetrical potential if the proton occupies the first excited state and if the dipoles of the medium are orientated with respect to this state. In fact, an asymmetry ΔV, being smaller than $\Delta V_m \approx 400\,\mathrm{cm}^{-1}$ without the polar medium, is removed almost completely by the interaction with the medium. Hence, symmetrical potentials for both protons are to be expected with not too small separations between the H-bonds and between the ions and the H-bonds, if both protons occupy the first excited state $0-$, or more precisely, if the probability amplitude of the state $|0-0-\rangle$ is high in an interacting state.

As an example of the occurrence of correlated tunnelling motions, consider two H-bonds and two anions in the spatial configuration indicated in fig. 5.11, and in particular the third excited state with a separation of $R = 10.5$ Å between the H-bonds. It is assumed that the dipoles of the medium are orientated with respect to the mean charge distribution in this state. Denoting the potential wells of each H-bond by right and left, the probabilities G_{rr}, G_{ll}, G_{rl} and G_{lr} can be calculated, i.e. the probabilities that the proton in the first H-bond (left-hand in fig. 5.11) occupies the right (left) well and that at the same time the proton in the second (right-hand) H-bond occupies the right (left) well. The result is $G_{rr} = 0.175$, $G_{ll} = 0.175$, $G_{rl} = 0.340$ and $G_{lr} = 0.310$ for the case considered here. The summation over the first or second index yields the probabilities that one proton is in a certain well, independent of the position of the other proton. Calling these probabilities w_{1r} and w_{1l} or w_{2r} and w_{2l}, respectively, the following relations are valid:

$$w_{1r} = G_{rr} + G_{rl} = 1 - w_{1l}, \qquad w_{2r} = G_{rr} + G_{lr} = 1 - w_{2l}. \tag{5.54}$$

Hence, the values $w_{1r} = 0.515$, $w_{1l} = 0.485$, $w_{2r} = 0.485$ and $w_{2l} = 0.515$ are obtained. If the tunnelling motions in the two H-bonds would occur statistically independent, the probabilities G_{ij} would be simply the products of the individual probabilities: $G_{ij} = w_{1i}w_{2j}$. In this case, the result would be $G_{rr} = 0.250$, $G_{ll} = 0.250$, $G_{rl} = 0.266$ and $G_{lr} = 0.234$. The evident differences between these and the actual values show that the tunnelling motions take place correlated in the two H-bonds.

In the example discussed above, the interaction with the polar medium is the reason for the high degree of symmetry of the potentials, and renders thereby the correlated proton motion. There is another case, however, in which correlated motions occur without the polar medium being of great importance–a case in which the potentials of both protons are highly unsymmetrical. This happens if the H-bonds and the anions are arranged so symmetrically in space that the excitation energies of both protons would be the same without the interaction between the protons. By means of this interaction, a resonance exchange of the excitation energy takes place starting from a state in which one proton occupies an excited state, e.g. state $0-$, and in which the other proton is in the ground state $0+$. A correlated tunnelling motion of both protons results from this energy exchange.

For example, in the case of the configuration shown in fig. 5.11 with a separation of $R = 10.5$ Å, assuming that the dipoles of the medium are orientated with respect to the mean charge distribution in the ground state, the probabilities $G_{rr} = 0.5$, $G_{ll} = 0.5$, $G_{rl} = 0$ and $G_{lr} = 0$ are obtained in the first excited state, and the probabilities $G_{rr} = 0.496$, $G_{ll} = 0.496$, $G_{rl} = 0.002$ and $G_{lr} = 0.006$ in the second excited state. Hence, in both states the probabilities are nearly equal to 1/2 when both protons occupy either the right-hand or the left-hand potential well, whereas the probability is almost zero when one proton is in the right-hand and the other in the left-hand well. In this case, it follows from eq. (5.54) that the probabilities w_{1r}, w_{1l}, w_{2r} and w_{2l} are all equal to 1/2 and hence, the products equal to 1/4. The deviations of the products from the actual probabilities G_{rr}, G_{ll}, G_{rl} and G_{lr} show that the correlation of the tunnelling motion is nearly perfect in this case.

Remarkably, the correlated proton motion takes place in very asymmetric potentials. This is shown by the probabilities with which the potential wells are occupied in the ground state at the same separation $R = 10.5$ Å: $G_{rr} = 0.004$, $G_{ll} = 0.004$, $G_{rl} = 0.000$ and $G_{lr} = 0.992$. From these values, the individual probabilities $w_{1r} = 0.004$, $w_{1l} = 0.996$, $w_{2r} =$

0.996 and $w_{21} = 0.004$ follow from eq. (5.54). Hence in the ground state, the charges are localized almost completely in the outer wells, as would be expected in light of the energy. The outer wells are lowered considerably, compared with the inner wells, by the repulsion of the protons. This effect is enhanced by the orientation of the dipoles of the medium with respect to the occupied wells. The correlated tunnelling motion in the two excited states discussed above, consists of a periodic transfer of one proton from the lower to the higher well and the simultaneous transfer of the other proton from the higher to the lower well. This process is possible if the excitation energies of both protons are equivalent, i.e. if both potentials have the same asymmetry.

5.4.8. Changes in tunnelling frequency

The calculations discussed thus far are based on the important assumption that the tunnelling frequency, i.e. the frequency of the proton transitions from one well to the other in the double-minimum potential, is so high that the dipoles of the polar medium cannot follow the proton motion and orientate themselves with respect to the mean charge distribution of the H-bonds. In this case, the value of the tunnelling frequency determines the strength of the interaction between the protons and between the polar medium and the protons by way of the dielectric constant ϵ_ν only (see eq. (5.48)). On the other hand, however, the tunnelling frequency is changed by the interactions. For, by means of the interactions, more or less unsymmetrical potentials result from the initially symmetrical potentials. Because the tunnelling frequency decreases thereby, there is the danger that the basic assumption becomes violated, even if valid in the case of the symmetrical potentials.

In fact, this problem is not as serious as it first seems, because of the high polarizability of the H-bonds with a double-minimum potential. A small asymmetry, changing the tunnelling frequency only slightly, is sufficient to polarize the H-bonds almost completely. The mean charge distribution of the protons, with respect to which the dipoles of the medium are orientated, is hence almost completely concentrated in one well before the tunnelling frequency is reduced so far that the dipoles start to follow the tunnelling motions of the protons. In fact, this case will not occur at all in the ground state, since the lingering time in the upper well is simultaneously reduced so considerably that the dipoles of the medium are no longer able to orientate themselves with respect to the protons occupying that well and, hence, only see the charge distribution in

the lower well. Therefore with increasing asymmetry, the orientation of the dipoles with respect to the charge distribution in both wells, changes to an orientation with respect to the charge distribution in the lower well. The difference, however, is negligible since the position probability in the upper well decreases rapidly. Hence, only a small error is introduced, assuming that the dipoles are always orientated with respect to the charge distribution in the entire potential. Corresponding considerations apply to the first excited state, too. In this case, the position probability in the upper well is almost equal to one, and the dipoles are mainly orientated with respect to this well. For higher excited states the change of tunnelling frequency, being much smaller, is hardly of importance, since few of the states are excited thermally. Finally, only an insignificant alteration of the tunnelling frequency by means of the interactions is to be expected for the state (discussed in section 5.4.7), in which the proton motion is correlated in adjacent H-bonds.

The problem of calculating the tunnelling frequency in a double-minimum potential was treated by several authors, starting with the discussion of the inversion vibration of the NH_3 molecule by Hund [1927]. The problem can be solved by considering the time development of a state in which the proton is localized in one of the two potential wells at a certain time. For the case of a symmetrical potential, the tunnelling frequency is well-known to be given by the splitting of the lowest level doublet. In the case of an unsymmetrical potential the splitting increases, whereas the tunnelling frequency decreases since, finally, with high asymmetry, the proton remains in the lower well in the ground state. For the latter case, the tunnelling frequency was calculated using various methods. Conway et al. [1965] treat the tunnelling motion semiclassically by means of the WKB method. Brickmann and Zimmermann [1966] divide the splitting of the level doublet into two parts: one part caused by the asymmetry of the potential and another part caused by the tunnelling motion, and yielding the tunnelling frequency. In a subsequent paper by the same authors (Brickmann and Zimmermann [1967]), the tunnelling frequency is calculated by solving the time-dependent Schroedinger equation numerically for various potentials.

In the two-level approximation, called tunnelling approximation, the time-dependent Schroedinger equation can of course be solved analytically. With some insignificant additional statistical assumptions, simple formulas can be derived for the lingering times in both wells which are in good agreement with the results of the laborious numerical calculations

(Weidemann and Zundel [1973]). Assuming that the left-hand well is higher than the right-hand one and denoting the lingering times in the two wells by τ_l and τ_r, the following formulas are obtained:

$$\tau_l = \frac{1}{\sqrt{1+\zeta^2}}\,\tau_0, \qquad \tau_r = \frac{1+2\zeta^2}{\sqrt{1+\zeta^2}}\,\tau_0. \tag{5.55}$$

Here, τ_0 is the lingering time in one well of the corresponding symmetrical potential and ζ is a dimensionless parameter being a measure of the asymmetry of the potential: $\zeta = \Delta V/(h\nu_0)$, whereby ΔV is the energy difference of the two wells, and $\nu_0 = 1/(2\tau_0)$ is the tunnelling frequency in the corresponding symmetrical potential with $\Delta V = 0$. If the asymmetry is produced by an electric field, ΔV is given by eq. (5.18) and ζ approximately by eq. (5.20).

In choosing $p = 2$ debye for the transition moment between the lowest level doublet and $\bar{\nu}_0 = 100\ \mathrm{cm}^{-1}$, a value of $\zeta = 0.606 \times 10^{-6}\,F$ is obtained. Here, F is the electric field strength in volt/cm. Hence, in an electric field of 10^7 volt/cm, the lingering time in the upper well is about 1/6 of the original value τ_0; the lingering time in the lower well is increased by a factor of 12; the tunnelling frequency $\nu = 1/(\tau_r + \tau_l)$ is diminished to about 1/6 of the value in the symmetrical potential.

It is noteworthy that the lingering time in the lower well increases almost twice as rapidly as the lingering time in the higher well decreases. Moreover, the ratio of the lingering times, and hence of the position probabilities in the two wells, increases much more rapidly than the tunnelling frequency decreases. Therefore, it cannot be concluded from highly diverse position probabilities that the tunnelling motion has come to an end. Of course, it must be borne in mind that eq. (5.55) is valid for small asymmetries only, because the higher states were neglected. Hence, the transition to the localized states in highly asymmetric potentials cannot be described by eq. (5.55).

By means of similar methods, one can calculate the change in tunnelling frequency caused by the interaction between two protons which are more or less correlated in adjacent H-bonds. This was calculated (Weidemann and Zundel [1973]) for the special case of two neutral H-bonds without dipole moment, using the dipole–dipole approximation for the interaction operator. In this case, no induced dipole interactions are possible, but rather dispersion and resonance interactions only. The calculation yields the remarkable result that the reduction of the tunnelling frequency can readily be seen in the level scheme of the interacting pair of H-bonds. In

fact, the tunnelling frequency is equal to the excitation energy of the first excited state divided by Planck's constant. Hence, in fig. 5.3, the reduction of the tunnelling frequency with increasing coupling of the protons is indicated by the narrowing separation between the levels 1 and 2 or 1 and 3.

5.5. Conclusion

The high polarizability is a characteristic property of H-bonds in which the protons move in a symmetrical potential with a double minimum or a very broad single minimum. Weak electric fields are sufficient to displace the proton considerably. The proton displacement causes a simultaneous shift of the electrons, whereby the center of the negative charges is usually shifted opposite to the field direction, enhancing the dipole moment. The high polarizability is the reason for several interaction effects: The fields of adjacent ions cause an induced dipole interaction with the H-bonds. In polar media the same is true for the fields of the dipoles surrounding the H-bonds. Moreover, the H-bonds polarize each other mutually, whereby a correlation of the directions of polarization is brought about. Finally, correlated fluctuations of the directions of polarization sometimes occur in adjacent H-bonds, i.e. correlated tunnelling motions of the protons take place.

In polar media unusual effects occur because the proton is shifted opposite to the field direction in the first excited state of a double-minimum potential, so that the polarizability is negative in this state. The dipoles of the polar medium orientate themselves with respect to the occupied well and lower the potential in that well thereby. In the first excited state, mainly the higher well is occupied, and hence is lowered by the dipoles of the medium. In this case, therefore, the interaction of the protons with the polar medium yields a largely symmetrical potential, whereas an already existing asymmetry is enhanced in the ground state. Hence, although the protons are mainly localized in one well in the ground state, in most cases, so that only correlations of the directions of polarization occur, the protons are often distributed over both wells in the first excited state. With two adjacent H-bonds in this latter state, correlated tunnelling motions of the protons occur. Even with highly unsymmetrical potentials, correlated proton motions are possible if only one of two adjacent H-bonds is excited and if a resonance exchange of the excitation energy takes place.

The coupling of the proton motion in H-bonds with the dipoles of a polar medium is an interesting problem, already treated frequently, in particular in connection with H-bonded ferroelectrics (see ch. 23). Nevertheless, many questions are still unanswered, in particular if the frequency of the tunnelling motion of the protons falls into the range of the reorientation frequencies of the dipoles of the polar medium.

References

Blinc, R. and M. Ribarič, 1963, Phys. Rev. **130**, 1816.

Böttcher, C. J. F., 1952, Theory of Electric Polarisation (Elsevier Publ. Comp., Amsterdam), section 16.

Brickmann, J. and H. Zimmermann, 1966, Ber. Bunsenges., Phys. Chem. **70**, 157.

Brickmann, J. and H. Zimmermann, 1967, Ber. Bunsenges., Phys. Chem. **71**, 160.

Brickmann, J. and H. Zimmermann, 1969, J. Chem. Phys. **50**, 1608.

Conway, B. E., J. O'M. Bockris and H. Linton, 1965, J. Chem. Phys. **24**, 834.

Dzyaloshinskii, I. Y., Y. M. Lifshitz and L. P. Pitayevskii, 1961, Advan. Phys. **10**, 165.

Fischer, S. F. and G. L. Hofacker, 1969, Phys. of Ice, Proc. Intern. Symp., Munich (Plenum Press, N.Y.), p. 369.

Fischer, S. F., G. L. Hofacker and J. R. Sabin, 1969a, Phys. kondens. Materie **8**, 268.

Fischer, S. F., G. L. Hofacker and M. A. Ratner, 1969b, Phys. of Ice, Proc. Intern. Symp., Munich (Plenum Press, N.Y.), p. 385.

Hayd, A., E. G. Weidemann and G. Zundel, 1974, in preparation.

Hund, F., 1927, Z. Phys. **43**, 805.

Janoschek, R., 1973, Theoret. Chim. Acta (Berlin) **29**, 57.

Janoschek, R., E. G. Weidemann, H. Pfeiffer and G. Zundel, 1972, J. Am. Chem. Soc. **94**, 2387.

Janoschek, R., E. G. Weidemann and G. Zundel, 1973, J. Chem. Soc., Faraday Trans. II **69**, 505.

Jehle, H., 1963, Proc. Natl. Acad. Sci. **50**, 516.

Jehle, H., 1969, Ann. N.Y. Acad. Sci. **158**, 240.

Jehle, H., J. M. Yos and W. L. Bade, 1958, Phys. Rev. **110**, 793.

Jehle, H., W. Parke and A. Salyers, 1965, Biophys. **9**, 433.

Kremer, F., E. G. Weidemann and G. Zundel, 1974, in preparation.

Kurz, J. L. and L. C. Kurz, 1972, J. Am. Chem. Soc. **94**, 4451.

Landis, D. H. and G. Schwarzenbach, 1969, Chimia **23**, 146.

Lifshitz, Y. M., 1955, J. Exptl. Theoret. Phys. **29**, 94.

Merlet, P., S. D. Peyerimhoff and R. J. Buenker, 1972, J. Am. Chem. Soc. **94**, 8301.

Narajanamurti, V. and R. O. Pohl, 1970, Rev. Mod. Phys. **42**, 201.

Pfeiffer, H., E. G. Weidemann and G. Zundel, 1974, in preparation.

Somorjai, R. L. and D. F. Hornig, 1962, J. Chem. Phys. **36**, 1980.

Tokunaga, M., 1966, Progr. Theor. Phys. **36**, 857.

Tokunaga, M. and T. Matsubara, 1966, Progr. Theoret. Phys. **35**, 1581.

Vorotyntsev, M. A., R. R. Dogonadze and A. M. Kuznetsov, 1973, Dokl. Akad. Nauk SSSR **209**, 1135.

Weidemann, E. G. and G. Zundel, 1967, Z. Phys. **98**, 288.
Weidemann, E. G. and G. Zundel, 1970, Z. Naturforsch. **A25**, 627.
Weidemann, E. G. and G. Zundel, 1973, Z. Naturforsch. **A28**, 236.
Will, G., 1969, Angew. Chem. **81**, Jahrg., 307.
Zundel, G., 1969, Hydration and Intermolecular Interaction (Academic Press., N.Y.).
Zundel, G. and E. G. Weidemann, 1970, Trans. Faraday Soc. **66**, 1941.

CHAPTER 6

DYNAMICAL PROPERTIES OF HYDROGEN BONDED SYSTEMS

G. L. HOFACKER

Lehrstuhl für Theoretische Chemie, Technische Universität München, D-8 München 2, West Germany

Y. MARECHAL

C.E.N. Grenoble, Lab. de Résonance Magnétique, 38041 Grenoble Cedex, France and Lab. de Spectrométrie Physique, B.P. 53,38041 Grenoble Cedex, France

AND

M. A. RATNER

Chemistry Department, Northwestern University, Evanston, Illinois 60201, U.S.A.

Contents

6.1. Introduction 297
6.2. Infrared spectra of hydrogen bonded systems 299
6.2.1. Previous qualitative models of hydrogen bond dynamics 302
6.2.1.1. Fermi resonance 302
6.2.1.2. Proton tunnelling 304
6.2.1.3. Combination with the $\nu_{X\cdots Y}$ mode 305
6.2.1.4. Strong-coupling theory of IR spectra 305
6.2.2. Strong-coupling Hamiltonian for a single hydrogen bond 306
6.2.2.1. Evaluation of optical absorption coefficient–golden rule and linear response formulations for a single linear hydrogen bond . 314
6.2.3. Smoothing of delta function spectrum within the strong-coupling model . 319
6.2.4. Discussion of the coupling mechanism for a single hydrogen bond . . 323
6.2.5. Solvent effects 325
6.2.6. Dynamics of two neighbor hydrogen bonds: carboxylic acid dimers . 330
6.2.7. Strong hydrogen bonds 337
6.3. Dynamical aspects of hydrogen bonds in solids 340
6.3.1. Theory of defect motion 341
6.3.2. Proton motion in ferroelectrics 346
6.3.3. Deuteration effects 349
6.4. Conclusions 351
Note added in proof 352
References 353

The hydrogen bond – recent developments in theory and experiments
Eds. P. Schuster et al. © *North-Holland Publ. Co., Amsterdam, 1976*

6.1. Introduction

The range of strength of H-bonds, intermediate between ordinary covalent bonds and Van der Waals-type forces, means that, as distinct from the usual covalent bond, it is strongly affected by weak environmental perturbations such as thermal motion and ionic or molecular interaction fields. The response of the H-bond to external mechanical forces, particularly electromagnetic fields varying sinusoidally in time, will be the primary concern of this review, as it has been the focal point of experimental work on H-bonded systems for the last forty years. This probe is of course dynamic, and by studying the response to these time-varying fields, we are able to draw information on nearly all forces acting within the system under study, provided, however, we can work from a proper theory. Since infrared spectroscopy is the simplest of these dynamic probes, we will devote most of our attention to the analysis of IR experiments, but several related topics will also be discussed.

Most descriptions of H-bonds attempt to simplify the problem to the extent that only the proton dynamics are detailed. The resulting predictions are nearly always at variance with experiment, due to the fact that the protonic and X···Y motions, at least, are strongly and ineluctably coupled. Attempts to include this coupling in simple Fermi resonance or anharmonic potential models have usually not been much more successful. The reason for this is simple: the coupling is too strong to be treated as a weak perturbation, and the anharmonic term linear in the X···Y displacement plays a dominant role in the dynamics. There have been two schemes developed which take this strong interaction into account. Almlöf [1972] and Janoschek et al. [1973] have treated the dynamics in a two-dimensional space. On the other hand, several workers (Witkowski [1968], Marechal and Witkowski [1968], Fischer et al. [1969] and Kubarev and Shedrin [1969]) have developed a strong-coupling picture, which retains a quasi-one-dimensional picture for the protonic motion, but

transforms the dynamical variables to take the strong interactions into account. This latter approach has the enormous advantage that additional couplings (e.g. radiation fields, heat bath, anharmonicities) can be incorporated.

It is this strong-coupling model which informs most of the discussion presented here. In section 6.2 some general aspects of the IR spectra are pointed out, and the inadequacy of such simplistic explanations as Fermi resonance or proton tunnelling is stressed. The strong-coupling Hamiltonian for an isolated H-bond is then developed, using both the first and second quantization notations. The golden rule and linear response formulae for the optical absorption coefficient are then given, followed by a discussion of the coupling mechanisms for a single H-bond; this also includes some remarks on environmental (heat bath) interaction. The next most complicated H-bonded systems, the carboxylic acid dimers, are considered in section 6.2.6; here both excitonic splitting and strong-coupling are important. In section 6.2.7, we discuss the case of strong H-bonds, and present a new interpretation of the A, B, C bands distinguished by Hadži [1965]. Section 6.3 is devoted to hydrogen bonding in solids. Proton mobility, spectra, the ferroelectrics and the Ubbelohde (bond-length change) effect are all discussed from a strong-coupling viewpoint, and a very brief summary is given in ch. 4.

It is perhaps useful to clarify two definitions at this point. In general, chemical bond strength is closely related to bond length. Thus long X–H$\cdots$Y H-bonds, such as that in solid NaOH (3.02 Å) or glycerol (2.96 Å), are generally considered weak. Shorter bonds, such as that in ice (2.76 Å), are called intermediate, while those of about 2.45–2.55 Å are called strong H-bonds. Thus, such systems as KH_2PO_4, trichloracetic acid-dimethyl sulfoxide or Ni-dimethylglyoxime are in the strong bond category (this nomenclature is common–for example, compare Hadži [1965]). There exist, of course, even shorter H-bonds, such as that in the bifluoride ion (2.32 Å). These are not overly common, and might be called super-strong H-bonds.

The other point of nomenclature has to do with the word "anharmonicity". As explained above, most of the interesting response phenomena of H-bonded systems are dominated by the term coupling the $\tilde{X}$–$\tilde{H}\cdots\tilde{Y}$ and the $\vec{X}\cdots\vec{Y}$ motions, which is proportional to the second power of the former and to the first power of the latter normal coordinate. This term is then formally a third-order anharmonicity. We will call its diagonal part the strong-coupling term, however, and will usually reserve the term (potential, or vibrational) anharmonicity for other third- and fourth-power

terms in the potential. Some of these can be quite important; in particular those leading to Fermi resonance. The term electrical anharmonicity, defined in section 6.2, is an altogether distinct concept dealing with that portion of the dipole moment of a H-bond which is not linear in the atomic coordinates.

6.2. Infrared spectra of hydrogen bonded systems

One of the most striking aspects of H-bonds is found in their dynamical behavior. More precisely, the high anharmonicity and asymmetry of the potential for the stretching motion $\nu_{X\text{-}H\cdots Y}$ in the H-bond X–H$\cdots$Y is the origin of most of the characteristic and unusual spectroscopic properties of H-bonds. It appears, therefore, to be of great interest to construct a precise, quantitative theory of the dynamics of the H-atom in H-bonds. Such a theory should be the basis for understanding spectroscopic investigations of H-bonds, not only in simple systems but also in highly structured liquids, solids, biological species, etc.

From the experimental point of view, the most general method for studying these dynamical aspects is infrared (IR) spectroscopy, which resolves directly the normal motions of the nuclei and some of their couplings. In H-bonds, the IR absorption band which corresponds to the $0 \rightarrow 1$ transition for the $\nu_{X\text{-}H\cdots Y}$ motion (X–$\ddot{\text{H}}\cdots$Y) is a characteristic one. This band will henceforth be called the $\nu_{X\text{-}H\cdots Y}$ band. It is subject to dramatic changes upon the formation of a H-bond, and is completely different from the band corresponding to the stretching motion $\nu_{X\text{-}H}$ in the X–H molecule. The other IR-transitions do not show such enormous changes when a H-bond is formed. Therefore, as a first objective, any dynamical theory of H-bonds should reasonably account for the effects showing up in the $\nu_{X\text{-}H\cdots Y}$ band which, as will be seen later, discloses much of the information obtainable about the dynamics of the system.

A typical IR spectrum of a H-bond is shown in fig. 6.1 representing the spectrum of acetic acid in the vapor phase. The broad band is the $\nu_{O\text{-}H\cdots O}$ band for the H-bonded cyclic dimers of acetic acid. The band at 3600 cm^{-1} is the $\nu_{O\text{-}H}$ band for the (non H-bonded) monomers. It is apparent that the $\nu_{O\text{-}H\cdots O}$ band is very broad and has a well-defined structure. Furthermore, it is much more intense than the $\nu_{O\text{-}H}$ band (some 30 times more in the case of acetic acid) and is shifted to lower wave numbers, compared to the position of the free $\nu_{O\text{-}H}$ band. These features are characteristic of most H-bonded species (Pimentel and McClellan [1960]). The intensifica-

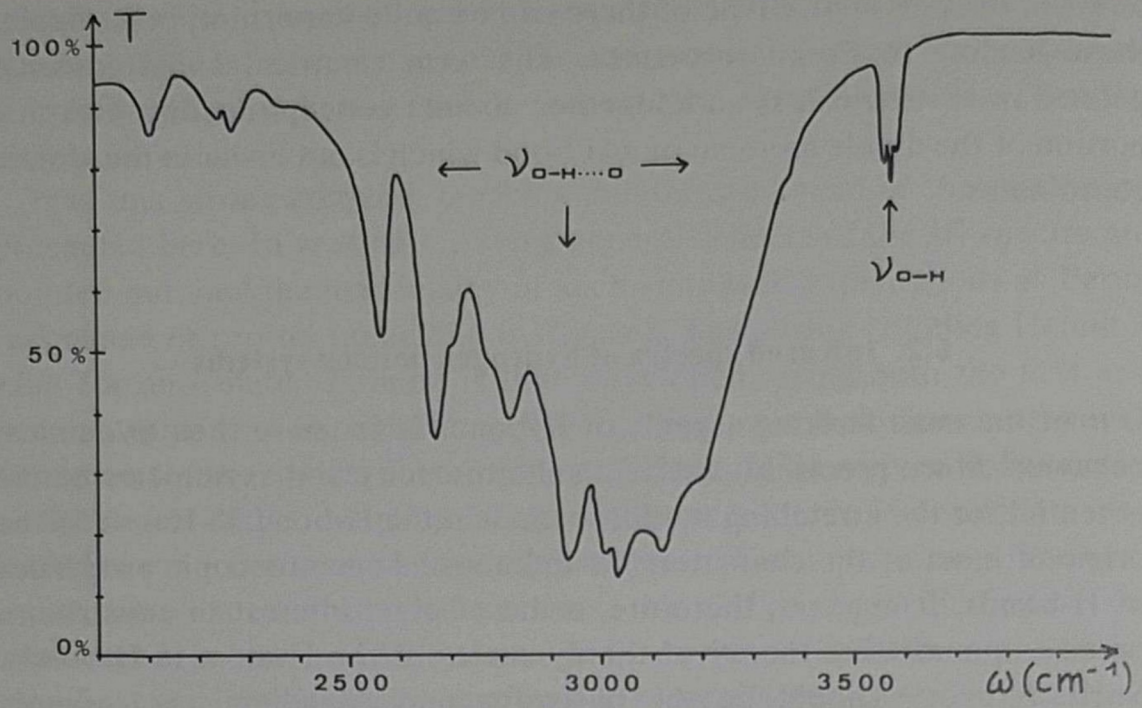

Fig. 6.1. Transmission spectrum of CD_3COOH vapor.

tion and the redshift seem to require for their quantitative explanation not only a knowledge of the electronic potential surface but also of the form of the electronic wave function, since they depend on the overall magnitude of the dipole moment, which includes the electron density. The broadening and the band shape, on the other hand, should be explicable in terms of the motions of the nuclei in the potential set up by the electrons; for the X–H···Y bond, in the center of mass system, this would be an energy surface in two dimensions q and Q, where q is the proton displacement and Q is the displacement of the X–Y distance from equilibrium (fig. 6.2). The further simplification is usually made that the q- and Q-motions can be separated, and that a cut of the (q, Q) surface for the equilibrium value $Q = Q_0$ is sufficient to explain the proton dynamics. We will show that this second simplification is not usually valid, and that the q-motion is strongly coupled to the Q-motion. There are then two approaches to the nuclear motion problem: the first is simply to solve for the two-dimensional dynamics. This has been done by Almlöf [1972] for HF_2^- and by Janoschek et al. [1973] for a model of $H_5O_2^+$. The second approach, which we will discuss at length, is the strong-coupling treatment which stems from polaron theory. For present purposes, the major point is that the surface is unavoidably two-dimensional; this precludes

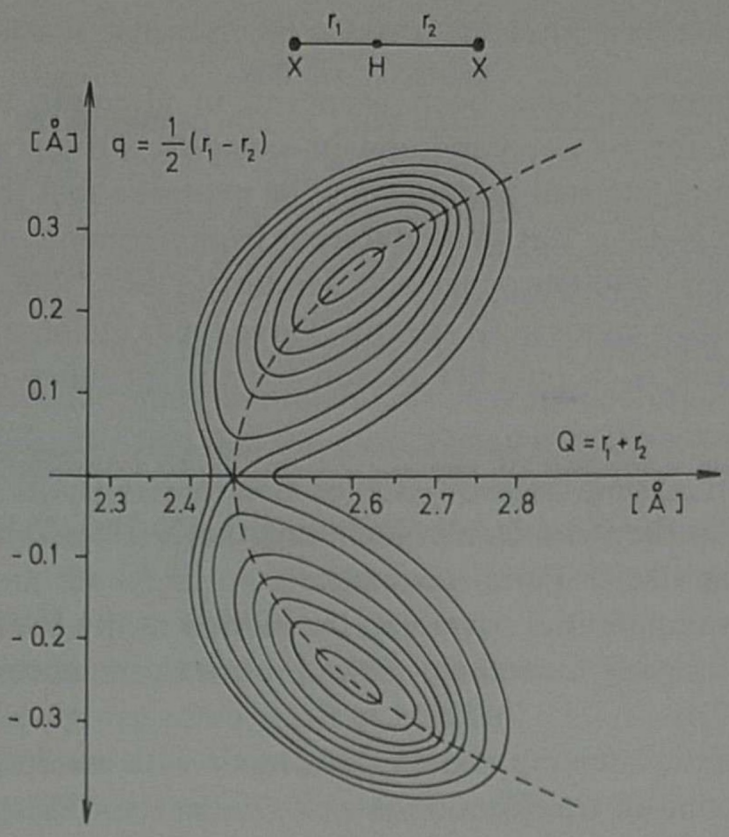

Fig. 6.2. Potential energy surface of symmetric H-bond (schematic).

simplistic interpretations in terms of one-dimensional model electronic potential energy surfaces (Fischer et al. [1970] and Rösch [1973]). On the contrary, the broadness and the rather complex structure of the band have their origin in rather complex couplings between modes, and will provide information primarily concerning dynamical properties. They will, moreover, constitute a very sensitive test for the various dynamical models and theories.

We can classify these models and theories as first and second generation. The first generation models were qualitative; they implemented several physical ideas to explain the peculiarities of the $\nu_{X-H\cdots Y}$ band. The second generation theories, which are still developing but have now reached a quantitative level, are largely an outgrowth of these previous propositions. We shall first briefly review the qualitative models and then describe the more quantitative theory based on the concept of strong coupling between modes. This theory seems to provide a sufficiently general description of the prevalent dynamic properties of the X–H $\cdots$ Y system.

6.2.1. Previous qualitative models of hydrogen bond dynamics

Several mechanisms have been proposed in attempts to explain the broadening of the $\nu_{X\text{-}H\cdots Y}$ band and its complex structure. First it was noticed that such unusual features may be evidence that the vibration of the H-atom in X–H···Y is quite different from harmonic motion (Bratož and Hadži [1957] and Durocher and Sandorfy [1965, 1966, 1967]) which would give narrow bands in IR spectra. Three types of anharmonicity have been considered as a possible reason for this peculiar motion of the H-atom:

1) Anharmonic coupling of the $\nu_{X\text{-}H\cdots Y}$ mode to combination modes of vibrations in the X molecule, including the $\overset{\downarrow}{X}\text{–}\overset{\uparrow}{H}\cdots\overset{\downarrow}{Y}$ bending mode, δ_{XHY}, giving rise to Fermi resonance;
2) a double-well potential governing the motion of the H-atom stretching vibration, causing tunnelling of the proton to the acceptor Y (Hadži [1965, 1972]);
3) an anharmonic coupling of the $\nu_{X\text{-}H\cdots Y}$ mode with low frequency modes of the H-bond of the form $\vec{X}\text{–}H\cdots\vec{Y}$ (Badger and Bauer [1937]). We shall briefly review these three anharmonic models.

6.2.1.1. *Fermi resonance*

Various authors (Bratož et al. [1956], Bratož and Hadži [1957] and Sheppard [1959]) have attributed the submaxima of the $\nu_{X\text{-}H\cdots Y}$ band to an anharmonic coupling with suitable binary combinations of modes in the X molecule, including particularly the X–H···Y bending mode. These modes, ν_{F1} and ν_{F2}, with frequencies ω_1 and ω_2 are chosen such that $\omega_1 + \omega_2$ is close to the value of the frequency ω_H of the $\nu_{X\text{-}H\cdots Y}$ mode. Then a small anharmonic coupling between $\nu_{X\text{-}H\cdots Y}$ and the ν_{F1} and ν_{F2} modes would give rise to a pronounced splitting of $\nu_{X\text{-}H\cdots Y}$. This is called Fermi resonance if $\omega_1 + \omega_2$ closely equals ω_H. Instead of having one band at ω_H, we would then have $N+1$ bands, if N is the number of binary combinations of modes with $\omega_1 + \omega_2 \approx \omega_H$. This mechanism enables one to "reasonably interpret the spectra" (Bellamy and Rogasch [1960], Bellocq et al. [1965], Haurie and Novak [1965], Perchard et al. [1965], Hall and Wood [1967] and Wolff and Wolff [1971]). Hall and Wood [1967] could show experimentally that the matching of binary frequency combinations had a pronounced effect on the $\nu_{X\text{-}H\cdots Y}$ line shape. In general, however, this interpretation, based solely on the combination of two frequencies, is ambiguous since for each maximum of the band of frequency ω_M quite a number of absorption frequencies ω_1 and ω_2 can usually be found in the

IR spectrum such that $\omega_1 + \omega_2 \approx \omega_M$, since there are many absorption bands in the region from 700 to 2000 cm^{-1} in an ordinary molecule. Furthermore, assignments of this kind cannot account for the intensities of the submaxima.

To illustrate the latter point we consider carboxylic acids as an example. In the gas phase, these acids form cyclic dimers held together by H-bonds. The $\nu_{O-H\cdots O}$ band has many submaxima, as shown in fig. 6.1. These submaxima have been attributed to Fermi resonance (Haurie and Novak [1965]) with binary combinations of frequencies. This interpretation was based on the fact that the $\nu_{O-H\cdots O}$ band was slightly changed when going from $(CH_3COOH)_2$ dimers to $(CD_3COOH)_2$ dimers. Recent calculations of the intensities for this mechanism, however, showed drastic deviations from the experimental intensity pattern (Marechal [1973]). It seems, therefore, that Fermi resonance is not the main mechanism responsible for the structure of the IR spectrum, though it certainly can not be completely neglected (Hall et al. [1967]).

In this mechanical analysis possible electrical anharmonicity, being of a fundamentally different nature, was not considered. We mean by electrical anharmonicity those important nonlinear terms which arise in the expression for the transition moment, represented as a product of the normal coordinates of the ν_{F1} and ν_{F2} modes. The occurrence of electrical anharmonicity does not require any mechanical coupling of $\nu_{X-H\cdots Y}$ with ν_{F1} and ν_{F2}. The two anharmonicities arise from different terms in the Hamiltonian for the external field-molecule system. If we write the overall Hamiltonian as

$$H = H_{\text{molecule}} + H_{\text{field}} + H_{\text{molecule/field}},$$

then the mechanical anharmonicity arises from terms in H_{molecule} of higher than quadratic order in the normal modes, while the electrical anharmonicity comes about from our way of writing $H_{\text{molecule/field}}$. This coupling term, for dipole transitions, is written as $-\boldsymbol{\mu} \cdot \boldsymbol{F}$, where $\boldsymbol{\mu}$ is the total molecular, or bond, dipole and $\boldsymbol{F}$ is the exciting field. This dipole is rigorously a one-particle term in both electrons and nuclei; that is

$$\boldsymbol{\mu} = \sum_{\substack{\text{nuclei} \\ \alpha}} Z_\alpha e \boldsymbol{r}_\alpha - \sum_{\substack{\text{electrons} \\ i}} e \boldsymbol{r}_i$$

(here Z_α is a nuclear charge and $\boldsymbol{r}$ is a coordinate vector). When we average over the electronic density and write $\boldsymbol{\mu}$ solely in the form of a Taylor expansion in the normal modes, terms of higher than linear order

arise; these constitute the electrical anharmonicity (Janoschek et al. [1973]). Electrical and mechanical anharmonicities can be distinguished only on the basis of a careful analysis including both anharmonicities, and requiring a very precise evaluation of the intensities of the $\nu_{X-H\cdots Y}$ submaxima.

6.2.1.2. *Proton tunnelling*

For an isolated X–H···Y bond, the potential function for motion of the hydrogen, assuming that X and Y remain stationary, may have the form of a symmetric or unsymmetric double minimum. No such potential has yet been found by Hartree–Fock type electronic calculations, but their existence, especially for H-bonds longer than 2.45 Å cannot yet be precluded; they certainly exist in networks of H-bonds. Several authors have pointed out that a double-minimum potential could mean a splitting of the infrared absorption fundamental, and in addition it has been claimed that the broadening of the IR spectrum upon formation of a H-bond can be understood in terms of this double minimum. Experimentally, the evidence for this splitting for a single H-bond has been very weak; instances have been adduced by Yenger and Barrow [1965] and by Hadži [1965, 1972].

Practically, in the H-bonding case, the manifestations of the double minimum in the IR spectrum will not be obvious as is shown later. The usually-invoked argument that a doublet peak requires a double minimum is clearly fallacious; an anharmonic single minimum can easily give a doublet IR spectrum.

As to the line broadening, most isolated true double minima show very sharp doublets–the NH_3 molecule is the classic example. There will be a linewidth corresponding to the tunnelling time in the excited state if the experimental timescale is such that the two possible upper states cannot be resolved: that is, if $\tau_{exp} T_{upper} \approx h$, where T_{upper} is the tunnelling energy splitting in the upper state, then the line will be broadened at least to $\Delta E \approx T_{upper}$, but in this case only a single peak will be observed. This may, however, be termed a "natural" linewidth and, on the basis again of experiments on molecules like NH_3, it is expected to be very small (of order 40 cm^{-1}; Herzberg [1945]), so that it cannot explain that linewidth for single bonds.

For the case of several neighboring H-bonds, a correlated tunnelling of the H-atoms through their bonds may occur. This would lead to subpeaks either in the $\nu_{X-H\cdots Y}$ band (when at least one $\nu_{X-H\cdots Y}$ vibration is excited) or in

the low frequency band corresponding to modes of the form $\vec{X}$–$\vec{H}\cdots\vec{Y}$. The former case might have been seen by Excoffon and Marechal [1972] who studied the spectrum of formic acid dimers. However, the crucial point of this dimer work is that the majority broadening comes from the strong coupling of $\nu_{X\text{–}H\cdots Y}$ with the $X\cdots Y$ displacement. The latter case has been considered by Ginn and Wood [1967] who have however discarded this hypothesis.

6.2.1.3. *Combination with the $\nu_{X\cdots Y}$ mode ($\vec{X}$–$\vec{H}\cdots\vec{Y}$)*

While potential functions for protonic motion in H-bonds are usually taken as one-dimensional, there is every reason to suppose that there is, in fact, substantial interaction between the $\nu_{X\text{–}H\cdots Y}$ mode and the $\nu_{X\cdots Y}$ mode. This suggestion was first made by Badger and Bauer [1937]; it was stressed by Batuev [1949] and Chulanovskii and Simova [1949], who called the resulting spectrum "frequency modulated", with the $\nu_{X\cdots Y}$ mode modulating $\nu_{X\text{–}H\cdots Y}$. The same idea, expressed more clearly underlies the potential function approaches of Lippincott and Schroeder [1956], and particularly of Reid [1959], who not only presents a model potential which is two-dimensional, but also stresses that in certain H-bonding situations the coupling can in fact become quite strong. According to this coupling or combination theory, the structure and width of the IR spectrum of H-bonded systems comes from the occurrence of side bands of Franck–Condon type appearing in addition to the fundamental $0\rightarrow 1$ transition of $\nu_{X\text{–}H\cdots Y}$.

The qualitative concept behind this idea of combinations seems, as Pimentel and McClellan [1960] remark, "most reasonable". Quantitatively, the idea of combinations could not be used to predict a spectral profile, until the advent of the strong-coupling approach.

6.2.1.4. *Strong-coupling theory of IR spectra*

The anharmonic coupling between the $\nu_{X\text{–}H\cdots Y}$ and the $\nu_{X\cdots Y}$ motions can be treated in a general theory, called the "strong-coupling theory". This theory treats the coupling of a rapid motion with a slow motion. It has often been used for the description of the coupling of an electron with nuclei and with field (Kuper and Whitefield [1963]). In our case, a strong-coupling theory of H-bonding, which seems capable of generally explaining the proton dynamics, has been developed by several workers (Marechal and Witkowski [1968], Marechal [1969], Ratner [1969], Fischer et al. [1969, 1970], Bournay and Marechal [1971], Leviel and Marechal

[1971], Witkowski and Wojcik [1971, 1973], Excoffon and Marechal [1972] and Ratner and Rösch [1974a, b]). The rapid motion in this case is the stretching motion $\nu_{X\text{-}H\cdots Y}$, the wave numbers of which drop to around $2800\,cm^{-1}$ for an intermediate strength H-bond. The slow motion is represented by the $\nu_{X\cdots Y}$ mode, of wave numbers around $150\,cm^{-1}$. The strong-coupling theory takes into account part of the coupling of these two motions, and treats this coupling, which is too large to be treated perturbatively, exactly. In this theory, we can also include other mechanisms. If, for instance, several H-bonds are considered, this theory can take into account the mode–mode coupling between the neighbor $\nu_{X\text{-}H\cdots Y}$ motions. It may also include the effects of tunnelling, Fermi resonance and so forth. The strong-coupling scheme thus can be thought of as a quantitative synthesis of the previous theories discussed above.

The strong-coupling Hamiltonian can be expressed in any of several notations. The most elegant and general of these involves the use of the occupation-number formalism (second quantization) for the vibrations of the heavy atoms ($X\cdots Y$, for a single bond). The calculation of transport properties, such as mobility or optical absorption probability, can also be expressed in various ways, of which the golden rule formula of first order perturbation theory is the most usual and the Kubo method of linear response is the most general and powerful (Kubo [1957, 1959]).

We present first, for illustrative purposes, a description of the strong-coupling procedure as applied to a single, linear $X\text{–}H\cdots Y$ bond. This treatment is outlined first using configuration space notation, then employing second-quantized notation. We then present applications of this method to carboxylic acids and to solids.

6.2.2. Strong-coupling Hamiltonian for a single hydrogen bond

We consider, as an illustration of the strong-coupling method, a single H-bond, and denote the $\nu_{X\text{-}H\cdots Y}$ mode by q and the $\nu_{X\text{-}Y}$ mode by Q. Then q will be the distance of the H-atom from its equilibrium position along the bond; Q will be the variation of the X–Y distance from its equilibrium value. We shall neglect, for the moment, the coupling of either of these two modes to the other modes of vibration in the X or Y subsystem, or any bending mode. The H describing these two motions is $H(q, Q)$, whose eigenfunctions will be $\psi(q, Q)$, with corresponding energies E. In a Born–Oppenheimer type picture, the two modes, q and Q, are coupled, but since the q-motion is fast compared to the Q-motion, we can assume, to define a basis representation, that the q-motion follows adiabatically

the Q-motion, just as electrons follow adiabatically the motions of the nuclei in the Born–Oppenheimer approximation. This is described by writing:

$$\psi(q, Q) = \phi(q, Q)\chi(Q). \tag{6.1}$$

$\phi(q, Q)$ is the wave function for the q-mode, which depends parametrically on Q. Its corresponding energy is $\epsilon(Q)$. We can write $H(q, Q)$ in the form: $H(q, Q) = P^2/2M_Q + h(q, Q)$, where P is the conjugate momentum of Q, M_Q is the $\nu_{X\cdots Y}$ mode effective mass, and $h(q, Q)$ is the Hamiltonian for the q-mode. We then have

$$\begin{aligned} h(q, Q)\phi_\alpha(q, Q) &= \epsilon_\alpha(Q)\phi_\alpha(q, Q) \\ [P^2/2M_Q + \epsilon_\alpha(Q)]\chi^i_\alpha(Q) &= E^i_\alpha\chi^i_\alpha(Q). \end{aligned} \tag{6.2}$$

These equations are a consequence of the adiabatic approximation. Just as is usual in the Born–Oppenheimer representation, there are perturbation terms which in this case, represent the change in protonic motion due to X$\cdots$Y velocity. These perturbation terms are nondiagonal in our basis $\psi(q, Q)$: That is, they induce transitions between the eigenstates $\psi(q, Q)$ of the adiabatic Hamiltonian. These nonadiabatic terms have been calculated in the case of the H-bonds of acetic acid dimers, and have been found to be negligibly small (Marechal and Witkowski [1968] and Marechal [1969]). We can thus rely on this approximation, at least for weak and intermediate H-bonds. The perturbation terms may become important for strong H-bonds, and are probably necessary for a proper explanation of proton mobility in solids. We shall be, more precisely, interested in the wave functions for the two lowest $\phi(q, Q)$ states. These will be denoted ϕ_0 and ϕ_1, with corresponding energies $\epsilon_0(Q)$ and $\epsilon_1(Q)$. Let us note that the neglected nonadiabatic terms (which can be important for strong H-bonds) would couple ϕ_0 with ϕ_1 through terms of the form $\langle\phi_0(q, Q)|P|\phi_1(q, Q)\rangle$. When q is in its ground state ϕ_0 (or excited state ϕ_1) the different possible wave functions for the Q-mode will be denoted by $\chi^i_0(Q)$ or $\chi^i_1(Q)$. They satisfy the equations:

$$\begin{aligned} [P^2/2M_Q + \epsilon_0(Q)]\chi^i_0 &= H_{(0)}\chi^i_0 = E^i_0\chi^i_0 \\ [P^2/2M_Q + \epsilon_1(Q)]\chi^i_1 &= H_{(1)}\chi^i_1 = E^i_1\chi^i_1, \end{aligned} \tag{6.3}$$

where $H_{(0)}$ and $H_{(1)}$ are the Hamiltonians for the Q-mode. Let us suppose that we know the different functions χ^i_0 which correspond to all the vibrational functions for the Q-mode, when the q-mode is in its ground

state. To a good approximation, these functions are harmonic, which means that $\epsilon_0(Q) = \frac{1}{2}M_Q\Omega^2Q^2$.* In a more precise description, the anharmonic terms of the Q-mode can be taken into account (Leviel and Marechal [1971]). We can expand $\epsilon_1(Q) - \epsilon_0(Q)$ in powers of Q:

$$\epsilon_1(Q) - \epsilon_0(Q) = \hbar\omega_H + BQ + \cdots. \tag{6.4}$$

We then have

$$H_{(1)} = P^2/2M_Q + \tfrac{1}{2}M_Q\Omega^2Q^2 + BQ + \hbar\omega_H + \cdots. \tag{6.5}$$

Here ω_H can be considered as the frequency of the q-modes while B may be a function of Q. At this point it is interesting to write $H_{(0)}$ and $H_{(1)}$ as functions of the dimensionless coordinate $\tilde{Q}$ (with conjugate momentum $\tilde{P}$) such that

$$\tilde{Q} = (M\Omega/\hbar)^{1/2}Q \tag{6.6}$$

$$H_{(0)} = \tfrac{1}{2}(\tilde{P}^2 + \tilde{Q}^2)\hbar\Omega \tag{6.7}$$

$$H_{(1)} = [\tfrac{1}{2}(\tilde{P}^2 + \tilde{Q}^2) + 2^{1/2}b\tilde{Q}]\hbar\Omega + \hbar\omega_H + \cdots \tag{6.8}$$

with $b = B/(2\hbar M_Q\Omega^3)^{1/2}$. This quantity b is the key parameter in the strong-coupling theory. We have here taken the X$\cdots$Y frequency Ω as constant in accordance with eq. (6.5). This restriction is only for illustrative purposes and can easily be relaxed. With this simple model, we can easily calculate the form of the $\nu_{X\text{-}H\cdots Y}$ absorption band. If f_m is the m-th harmonic oscillator wave function, we have

$$\chi_0^m = f_m(\tilde{Q}) \qquad \text{and} \qquad E_0^m = (m + \tfrac{1}{2})\hbar\Omega. \tag{6.9}$$

If only the constant and linear terms are retained in eq. (6.4), which is often quite a good approximation, we have

$$\chi_1^c = f_c(\tilde{Q} + 2^{1/2}b) \qquad \text{and} \qquad E_1^c = (c + \tfrac{1}{2} - b^2)\hbar\Omega + \hbar\omega_H. \tag{6.10}$$

The term proportional to $\tilde{Q}$ in $H_{(1)}$ is called the strong-coupling term. We proceed to consider its effects which are primarily responsible for many of the interesting properties of H-bonds. We thus must consider this term in an exact, nonperturbative way. In the strong-coupling method, this is done by performing a canonical transformation. That is, we write

$$\tilde{H}_{(1)} = e^S H_{(1)} e^{-S} = H_{(1)} + [S, H_{(1)}] + \tfrac{1}{2}[S, [S, H_{(1)}]] + \cdots. \tag{6.11}$$

S should be an anti-hermitian operator; $\tilde{H}_{(1)}$ and $H_{(1)}$ have identical

* For simplicity we have taken in this section, the origin of the Q-mode at the minimum of $\epsilon_0(Q)$. We shall take a more suitable origin in section 6.2.4.

eigenvalues. In our case, since $[\tilde{Q}, \tilde{P}] = \mathrm{i}$ we see that $S = 2^{1/2} b\tilde{P}/\mathrm{i}$ and

$$\tilde{H}_{(1)} = [\tfrac{1}{2}(\tilde{P}^2 + \tilde{Q}^2) - b^2]\hbar\Omega + \hbar\omega_{\mathrm{H}}. \tag{6.12}$$

We have also:

$$\chi_{\mathrm{i}}^{\mathrm{c}} = \exp(2^{1/2}\mathrm{i}b\tilde{P}) f_c(\tilde{Q}), \tag{6.13}$$

as $f_c(\tilde{Q})$ are the eigenfunctions of $\tilde{H}_{(1)}$, which is reduced to a harmonic oscillator Hamiltonian. (The transformation eq. (6.11) corresponds to a displacement of the oscillator, and the result eq. (6.12) is exact to all orders of perturbation.) Terms which correspond to changing the X···Y frequency in the state ϕ_1 can be included, and the transformation eq. (6.11), which will then become somewhat more clumsy, will still be exact (Fischer [1970]). This kind of canonical transformation can be performed even in the presence of other interactions (Fischer et al. [1970]) such as mode–mode coupling between different H-bonds, or anharmonic coupling with vibrations in the X-radical, Fermi resonance with the bending mode, etc. (Witkowski and Wojcik [1973]). The terms corresponding to these interactions will not be diagonalized, in general, by this unitary transformation. They will be treated as perturbations, or damping terms.

The essential idea underlying the strong-coupling model is a very simple one. In the case of, say, the electronic spectrum of a diatomic like HCl, the Born–Oppenheimer potential surface for the excited state has a different equilibrium point than that for the ground state. This means that the vibrational Hamiltonian for the excited state will contain a term linear in the displacement from the ground-state zero. That is, defining X as the H–Cl displacement from equilibrium, in harmonic approximation we can write

$$V_{\mathrm{vib}}(\text{ground}) = \tfrac{1}{2} k_0 X^2. \tag{6.14}$$

Then

$$V_{\mathrm{vib}}(\text{excited}) = \tfrac{1}{2} k_e (X + X_0)^2 \tag{6.15}$$

$$= \tfrac{1}{2} k_e X^2 + X_0 k_e X + \tfrac{1}{2} X_0^2 k_e$$

$$= \tfrac{1}{2} k_0 X^2 + X_0 k_e X + \tfrac{1}{2} X_0^2 k_e + \tfrac{1}{2}(k_e - k_0) X^2. \tag{6.16}$$

The third term of eq. (6.16) is a constant which can be put into the electronic energy. The first term is the same as V_{vib} (ground). Thus

$$V_{\mathrm{vib}}(\text{excited}) = V_{\mathrm{vib}}(\text{ground}) + X_0 k_e X + \tfrac{1}{2}(k_e - k_0) X^2. \tag{6.17}$$

If we utilize the second quantization representation for the vibrational displacement, and if we assume that the stretch frequency, or force

constant, is the same for the ground and excited states, we obtain*

$$V_{\text{vib}}\,(\text{excited}) = \hbar\Omega b^{\dagger}b + g\hbar\Omega(b^{\dagger} + b) + \text{const.} \tag{6.18}$$

where the coupling constant g is

$$g = X_0\sqrt{k/2\hbar\omega} \tag{6.19}$$

and is identical to b of eq. (6.8) if one sets $k = M_Q\Omega^2$. The second term of eq. (6.18) is the usual strong-coupling term, originally introduced by Fröhlich in the theory of solids (Kuper and Whitefield [1963]). It is proportional to X_0, the displacement of the vibrational zero in the excited state, away from that in the ground state. In this example case of the electronic spectrum of HCl, the vibrational and electronic frequencies are quite different, and the vibrational dynamics can be separated from the electronic motion (Franck–Condon principle) (Herzberg [1945]).

For a linear isolated X–H$\cdots$Y H-bonded system, the formal eqs. (6.14)–(6.19) still hold, if the protonic well can be assumed nearly harmonic. The difference is that the time scales for the two motions are now much closer than in the electronic spectra case. While a typical electronic to vibrational energy ratio may be 50:1, the ratio of X–H and X$\cdots$Y stretching frequencies is more like 10:1 or even less. Therefore, there is no perfect separation of the proton and heavy atom dynamics. However, an adiabatic separation of high and low frequencies of the type

$$H = H_{\text{proton}} + H_{\text{ion}} + H_{\text{coupling}} \tag{6.20}$$

still holds, and a basis for the protonic motion can be defined, giving rise to

$$H_{\text{proton}} = \sum_{\alpha} \epsilon'_{\alpha}|\alpha\rangle\langle\alpha| \tag{6.21}$$

and

$$H_{\text{vib}} = \hbar\Omega b^{\dagger}b \tag{6.22}$$

where Ω is the frequency of the X$\cdots$Y stretch and ϵ'_{α} is the protonic vibrational eigenenergies for the electronic energy surface at fixed (equilibrium) X$\cdots$Y separation. The values ϵ'_{α} include the zero-point energy of Ω. The difference is that the perturbation term

$$H_{\text{coupling}} = \sum_{\alpha} g_{\alpha}\hbar\Omega(b^{\dagger} + b)|\alpha\rangle\langle\alpha| \tag{6.23}$$

is so large that it cannot be treated in low order perturbation theory, and so constructed that it mixes the dynamics of the protonic and ionic

* The destruction operator b should not be confused with the parameter b of eq. (6.8).

motions. This will become clearer when we actually solve for the dynamic eigenstates below.

It should be noted that the neglect of the frequency change terms

$$H_{\Delta\omega} = \sum_{\alpha} \hbar\Omega_0(b^\dagger + b)^2|\alpha\rangle\langle\alpha| \frac{\Omega_e^2 - \Omega_0^2}{4\Omega_0^2} \tag{6.24}$$

may not always be justified. The situation when these terms are included is not more difficult in principle, and analogous terms have been included in the strong-coupling treatment of radiationless decay (Fischer [1970]) and bimolecular kinetics (Fischer and Ratner [1972]); we will neglect them here in the interests of clarity.

We thus have derived the basic Hamiltonian for the strong-coupling treatment of the vibrational spectrum of H-bonding. For a single linear X–H$\cdots$Y system with a nearly harmonic adiabatic fixed atom potential surface, this Hamiltonian is given by

$$H_{\text{isolated}} = \sum_{\alpha} \epsilon'_\alpha|\alpha\rangle\langle\alpha| + \hbar\Omega b^\dagger b + \sum_{\alpha} g_\alpha \hbar\Omega(b^\dagger + b)|\alpha\rangle\langle\alpha| \tag{6.25}$$

The formulation eq. (6.25) is identical to the formulation eqs. (6.7) and (6.8) if the sum over α in eq. (6.25) is restricted to $\alpha = 0, 1$. The second-quantized form, as noted above, is more general and more compact that the configuration space notation of eqs. (6.7) and (6.8). From now on we will thus use the second-quantized form, but it must be remembered that this is simply a great notational advantage: no new physical content is introduced by the use of this notation.

In fact, the protonic motion is also coupled, however weakly, to all of the other normal mode motions of the system. In the simple case of X–H$\cdots$Y, the doubly-excited bending mode will also couple to the protonic motion. This is the principal Fermi resonance which has very often been blamed for the peculiar nature of the H-bond spectrum. Indeed, we might expect this coupling to be fairly strong, though estimates are not too reliable. If the X–H$\cdots$Y system is coupled either to the rest of a molecular framework (as in, say, salicyclic acid or $H_5O_2^+$) or to a heat bath (as any system in condensed phase always is), we would expect terms like eq. (6.23), but with different frequencies and different coupling constants, to appear in H, describing these interactions. Such couplings, as long as they are linear, introduce no essential complication into the Hamiltonian, and we can therefore write the basic strong-coupling Hamiltonian for a single proton coupling with several ion normal

modes as:

$$H = \sum_{\alpha} \epsilon'_{\alpha} |\alpha\rangle\langle\alpha| + \sum_{i} \hbar\Omega_i b_i^{\dagger} b_i + \sum_{\alpha i} \hbar\Omega_i q_{\alpha}^{i} (b_i^{\dagger} + b_i) |\alpha\rangle\langle\alpha|. \quad (6.26)$$

Here we have included all zero-point vibrational energies in ϵ'_{α}. Generally, we expect one of the g_{α}^{i} to be much larger than any of the others. The coupling terms in eq. (6.26) correspond, in a configuration space notation, to anharmonic terms of the form $q^n Q_i$, for all i. We have thus included in eq. (6.26) a potential of the form

$$U = \sum_{n} \alpha_{n0} q^n + \sum_{i} a_{01}^{i} Q_i + \sum_{ij} \alpha_{02}^{ij} Q_i Q_j + \sum_{i} P(q) Q_i \quad (6.27)$$

where $P(q)$ is any polynomial in q. Higher order anharmonicities such as $Q_i^2 Q_j$ or $q Q_i Q_j$, must be treated perturbatively. However, the form eq. (6.26) can be treated to infinite order, and we now proceed with our treatment for the simplest illustrative case of one proton interacting with one vibration.

Our basic strong-coupling Hamiltonian is given by:

$$H = H^{(0)} + H^{(1)} \quad (6.28)$$

$$H^{(0)} = \sum_{\alpha} \epsilon'_{\alpha} |\alpha\rangle\langle\alpha| + \hbar\Omega(b^{\dagger} + b) \quad (6.29)$$

$$H^{(1)} = \sum_{\alpha} \hbar\Omega g_{\alpha} (b^{\dagger} + b) |\alpha\rangle\langle\alpha|. \quad (6.30)$$

Here we have taken the ϵ'_{α} as the protonic eigenvalues in a fixed heavy atom geometry. $\hbar\Omega$ is the eigenenergy of the bound degrees of freedom which should generally include both bends and stretches. The major contribution to the coupling should come from strong interaction with the X···Y stretch, as described above. The dimensionless coupling constant g_{α} is of order unity for this strong interaction. The problem is similar to the Franck–Condon problem for the electronic spectrum of a diatomic molecule, except that the coupling here is expected to be much stronger, since the Born–Oppenheimer (Born and Huang [1954]) mass factor $\kappa = (M_X/M_H)^{1/4}$, where M_X and M_H are the masses of the light and heavy atoms, respectively, is here about 0.5 whereas for a typical diatomic it is of order 0.1. We have here neglected the nondiagonal nonadiabatic coupling term

$$H_{(nd)} = \sum_{\alpha\beta} \hbar\Omega \Lambda_{\alpha\beta} (b^{\dagger} + b) |\alpha\rangle\langle\beta|. \quad (6.31)$$

This term was considered by Fischer, Hofacker and Sabin because of its role in providing virtual transitions and scattering effects in the protonic mobility problem (Fischer et al. [1969]). For our example of a single H-bond, we expect it to be much smaller than $H^{(1)}$, and so ignore it.

The $H^{(1)}$ term is too large to treat as a perturbation, so we took to a canonical transformation procedure, as is common in polaron theory. Physically, this has the effect of introducing a quasiparticle picture; the transformed Hamiltonian will look like a single proton form, but will contain exponential operators describing ionic vibrational motion. These operators describe the dynamic effects of heavy atom motion on the proton as it moves between its Born–Oppenheimer eigenstates. The usual language is that the "bare" proton is "dressed" in a cloud of virtual lattice vibrations. The actual transformation is

$$\tilde{H} = e^{S} H e^{-S} \tag{6.32}$$

$$S = \sum_{\alpha} g_{\alpha}(b^{\dagger} - b)|\alpha\rangle\langle\alpha| \tag{6.33}$$

$$\tilde{b} = b - \sum_{\alpha} g_{\alpha}|\alpha\rangle\langle\alpha| \tag{6.34}$$

$$\langle\tilde{\alpha}| = \langle\alpha|B_{\alpha} \tag{6.35}$$

$$B_{\alpha} = \exp\left[-g_{\alpha}(b^{\dagger} - b)\right] \tag{6.36}$$

$$|\tilde{\alpha}\rangle = B_{\alpha}^{\dagger}|\alpha\rangle \tag{6.37}$$

$$\tilde{H}^{(0)} = \hbar\Omega b^{\dagger} b + \sum_{\alpha} \tilde{\epsilon}_{\alpha}|\alpha\rangle\langle\alpha| - \sum_{\alpha} \hbar\Omega g_{\alpha}(b^{\dagger} + b)|\alpha\rangle\langle\alpha| \tag{6.38}$$

$$\tilde{H}^{(1)} = \sum_{\alpha} \hbar\Omega g_{\alpha}(b_{q}^{\dagger} + b_{q})|\alpha\rangle\langle\alpha| - 2\sum_{\alpha} g_{\alpha}^{2}\hbar\Omega|\alpha\rangle\langle\alpha| \tag{6.39}$$

$$\tilde{H} = \hbar\Omega b^{\dagger} b + \sum_{\alpha} \tilde{\epsilon}_{\alpha}|\alpha\rangle\langle\alpha| \tag{6.40}$$

where the shifted energy is given as

$$\tilde{\epsilon}_{\alpha} = \epsilon_{\alpha}' - g_{\alpha}^{2}\hbar\Omega. \tag{6.41}$$

This transformed Hamiltonian provides a simple description of the motion in a single H-bond. (The result eq. (6.39), if restricted to $\alpha = 0, 1$, is identical to the result eq. (6.12).) Conventionally, the zero of displacement is defined by the ground protonic state, so that

$$g_{\alpha} \to g_{\alpha} - g_{0}, \qquad g_{0} \equiv 0. \tag{6.42}$$

The shifted energies eq. (6.41) reflect the relaxation of the vibrational equilibrium position of the ions. Within a harmonic approximation, the B, $B^{\dagger}$ operators will give rise to Franck–Condon factors (see below), while such effects as Fermi resonance and strong anharmonicity will be dynamically modulated by these virtual vibrations. If the equilibrium displacements in the ground protonic state and in the α-th excited protonic state are identical, then

$$\tilde{\epsilon}_\alpha \to \epsilon_\alpha, \qquad B_\alpha \to 1 \quad (\text{if } g_\alpha = g_0) \tag{6.43}$$

and no strong-coupling effects would be expected in this approximation (in fact, for such a level the nondiagonal terms eq. (6.31) and/or coupling with other vibrational modes can become important).

The true excited states of the proton, within the strong-coupling model, can then be written as canonically transformed zero-order (virtual or BO) protonic states:

$$|\tilde{\alpha}\rangle = \mathrm{e}^{S}|\alpha\rangle. \tag{6.44}$$

The strong-coupling Hamiltonian eq. (6.39) is a good description of the true dynamics of the H-bonded system, and constitutes a good basis for the description of all response phenomena, including especially optical absorption and proton mobility.

6.2.2.1. *Evaluation of optical absorption coefficient – golden rule and linear response formulations for a single linear hydrogen bond*

The strong-coupling Hamiltonian eq. (6.25) which we have derived can be used to find the absorption spectrum in either of two standard ways. We first derive the spectrum for the illustrative case of a single H-bond using the standard golden rule expression, and then derive the same result, in the limit of zero temperature, using the more general and powerful linear response approach. The delta function which results from the simple golden rule expression is, of course, never observed in practice: the two modulating factors are further coupling of modes and statistical corresponding to interactions with a heat bath, which result in a damping of each individual subpeak in the spectrum. These modulating factors are most apparent in condensed phase or in larger molecules. We discuss these factors in qualitative fashion in section 6.2.5.

Under an applied external electromagnetic field $\boldsymbol{F}_0 \cos \omega t$, which is taken as coupling with the dipole moment of the H-bonded system by

means of the (weak) perturbation

$$V = -\boldsymbol{\mu} \cdot \boldsymbol{F}_0 \cos \omega t \tag{6.45}$$

the transition probability per unit time from an initial state $|i\rangle$ to a final state $|f\rangle$ is given by the golden rule as

$$w_{i\to f} = (2\pi/\hbar)|\langle i|\boldsymbol{\mu} \cdot \boldsymbol{F}_0|f\rangle\delta(E_f - E_i - \hbar\omega). \tag{6.46}$$

If we neglect, for the moment, electrical anharmonicity, and take the field to lie along the proton axis and the dipole moment $\boldsymbol{\mu}$ to be simply Zeq, where q is the proton displacement and Z is the effective charge on the proton, then the transition probability becomes

$$\begin{aligned} w_{i\to f} &= (2\pi/\hbar)F_0^2 Z^2 e^2 |\langle i|q|f\rangle|^2 \delta(E_f - E_i - \hbar\omega) \\ &= (2\pi/\hbar)F_0^2 |\mu_{if}|^2 \delta(E_f - E_i - \hbar\omega) \end{aligned} \tag{6.47}$$

where we have denoted the matrix element

$$\langle i|Zeq|f\rangle = \mu_{if}.$$

In fact, the role of electrical anharmonicity can, to some extent, be taken into account by taking the effective charge Z to be a function of q, but for our present illustrative purpose we take Z to be constant.

The energies E_i and E_f and the states $|i\rangle$ and $|f\rangle$ refer to the overall eigenstates of the basis: that is they correspond to our states $\psi(q, Q)$ and have two quantum numbers, one corresponding to q-motion, the other to Q-motion. If we take a general representation of the proton displacement in terms of the eigenstates of q-motion

$$q = \sum_{\alpha\beta} q_{\alpha\beta}|\alpha\rangle\langle\beta|. \tag{6.48}$$

Then the transition moment for the proton spectrum becomes

$$\mu_{0\to\gamma} = Ze\langle\tilde{0}|q|\tilde{\gamma}\rangle = Ze\langle 0|\sum_{\alpha\beta} q_{\alpha\beta}|\alpha\rangle\langle\beta|B_\gamma^\dagger \tag{6.49}$$

$$= Zeq_{0\gamma}\langle B_\gamma^\dagger\rangle. \tag{6.50}$$

We have taken Z as the effective charge on the proton; the averages in eq. (6.49) are taken over both heavy atom and protonic motion. In eq. (6.50) the average is taken over the vibrations. To evaluate the form eq. (6.50), we use the Bloch result that, for harmonic motion.

$$\langle e^{L(q,p)}\rangle = \exp\left[\tfrac{1}{2}\langle L^2(q, p)\rangle\right] \tag{6.51}$$

where $L(q, p)$ is any linear form in q, p. Then

$$\langle B_\gamma^\dagger \rangle = \langle \exp [g_\gamma (b^\dagger - b)] \rangle = \exp [\tfrac{1}{2} g_\gamma^2 (b^\dagger - b)^2]. \tag{6.52}$$

The evaluation of eq. (6.52) is facilitated by noting that

$$(b^\dagger - b)^2 = (2/M\hbar\Omega) P^2; \tag{6.53}$$

Where P is the momentum conjugate to normal mode Q. The square of the momentum is found using the equipartition result

$$\hbar\Omega(n + \tfrac{1}{2}) = P^2/M_Q. \tag{6.54}$$

(This statistical result can be rigorously justified–cf. Messiah [1961], ch. 12.) Thus we find, for the equilibrium thermal average

$$\langle B_\gamma^\dagger \rangle = \exp [\tfrac{1}{2} g_\gamma^2 \coth (\tfrac{1}{2}\beta\hbar\Omega)]. \tag{6.55}$$

Where

$$\beta^{-1} = k_B T. \tag{6.56}$$

(The Bose–Einstein-factor $\coth (\frac{1}{2}\beta\hbar\Omega)$ comes from taking the thermal equilibrium occupation number for n_Q, the number of excitations in normal mode Q.) At zero temperature, n_Q becomes zero and β becomes infinite, so that

$$\left.\begin{aligned} \coth (\tfrac{1}{2}\beta\hbar\Omega) &\to 1 \\ \langle B_\gamma^\dagger \rangle &\to \exp (\tfrac{1}{2} g_\gamma^2) \end{aligned}\right\} \quad \text{if } T = 0. \tag{6.57}$$

Thus the overall transition moment comes out as

$$\boldsymbol{\mu}_{\tilde{0} \to \tilde{\gamma}} = Ze\boldsymbol{q}_{0\gamma} \exp [\tfrac{1}{2} g_\gamma^2 \coth (\tfrac{1}{2}\beta\hbar\Omega)] \tag{6.58}$$

where the $\boldsymbol{q}_{0\gamma}$ is the matrix element in the adiabatic basis, and the vibrational factors describe the shift in the upper state due to the strong coupling. The exponential can be expanded:

$$\boldsymbol{\mu}_{\tilde{0} \to \tilde{\gamma}} = Ze\boldsymbol{q}_{0\gamma} \sum_{k=0}^{\infty} \frac{1}{k!} \left(\frac{g_\gamma^2}{2}\right)^k \coth^k (\tfrac{1}{2}\beta\hbar\Omega) \tag{6.59}$$

which gives rise to a progression of vibrational peaks separated by the harmonic frequency Ω of the vibrational mode. If we deal with, say, an O–H$\cdots$O bond, this would be the O$\cdots$O vibration. The form eq. (6.59) predicts a spectrum consisting of a set of delta function peaks with a distribution of intensities corresponding to the Franck–Condon factors in

eq. (6.55). This spectrum is illustrated in fig. 6.3 assuming:

$$\epsilon_1 - \epsilon_0 = 2500\ \mathrm{cm}^{-1}, \qquad g_1 - g_0 = 1.5, \qquad \Omega = 250\ \mathrm{cm}^{-1}, \tag{6.60}$$

which is a reasonable set of parameters for O–H $\cdots$ O bonds. We have *not* assumed a double-minimum potential for protonic motion. The envelope of the spectrum fig. 6.3, is the "broadened" spectrum observed upon H-bond formation. The overall width of the envelope is proportional to the square of the coupling constant g_α.

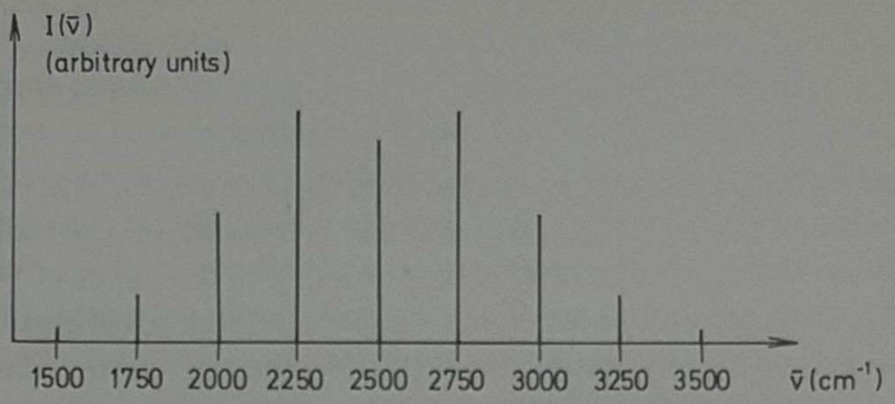

Fig. 6.3. δ function spectrum of $\nu_{X-H\cdots Y}$ with strong coupling in golden rule limit (eq. (2.59)).

The golden rule formulation which we have presented here has the advantage of familiarity and simplicity, but it can become quite tricky when there are random forces as well as the oscillatory applied field, and is essentially a low temperature approach. A more general scheme, called linear response theory, and based on a perturbation of the density matrix rather than the wave function, was first formulated generally by Kubo [1957, 1959]. For the special case of infrared absorption at zero temperature, a particularly clear and comprehensible treatment has been given by Gordon [1965] (compare also Bratož et al. [1970]). In the limit of zero temperature, the infrared band shape $I(\omega)$ is expressed, in the linear response scheme, as

$$I(\omega) = \frac{1}{2\pi} \int_{-\infty}^{\infty} \mathrm{e}^{-\mathrm{i}\omega t} \langle \boldsymbol{\mu}(0) \cdot \boldsymbol{\mu}(t) \rangle \, \mathrm{d}t \tag{6.61}$$

where the $\boldsymbol{\mu}(t)$ is the time-varying value of the dipole moment in the Heisenberg representation:

$$\boldsymbol{\mu}(t) = \mathrm{e}^{\mathrm{i}Ht/\hbar} \boldsymbol{\mu} \, \mathrm{e}^{-\mathrm{i}Ht/\hbar} \tag{6.62}$$

where H is the strong-coupling Hamiltonian. For our example case of the

single H-bond, the correlation function becomes

$$\langle \boldsymbol{\mu}(0) \cdot \boldsymbol{\mu}(t) \rangle = \sum_{\alpha,\beta,\gamma,\delta} Z^2 e^2 F_0^2 \boldsymbol{q}_{\alpha\beta} \cdot \boldsymbol{q}_{\gamma\delta} \langle |\alpha\rangle\langle\beta| e^{iHt/\hbar} |\gamma\rangle\langle\delta| e^{-iH/\hbar} \rangle. \quad (6.63)$$

If we now take the states $|\alpha\rangle$ as eigenstates of the Hamiltonian $\tilde{H}$ with eigenvalues $\tilde{\epsilon}_\alpha$, then we find, at zero temperature

$$\langle \boldsymbol{\mu}(t) \cdot \boldsymbol{\mu}(0) \rangle \to \langle 0 | \boldsymbol{\mu}(t) \cdot \boldsymbol{\mu}(0) | 0 \rangle \quad (6.64)$$

so that

$$\langle \boldsymbol{\mu}(t) \cdot \boldsymbol{\mu}(0) \rangle \to \sum_{\alpha,\beta,\gamma,\delta} Z e^2 F_0^2 \boldsymbol{q}_{\alpha\beta} \cdot \boldsymbol{q}_{\gamma\delta} \langle 0|\alpha\rangle\langle\beta| e^{-S}\, e^{i\tilde{H}t/\hbar}\, e^{S} |\gamma\rangle\langle\delta| e^{-S}\, e^{-i\tilde{H}t}\, e^{S} |0\rangle$$

$$= Z e^2 F_0^2 \sum_\beta |q_{0\beta}|^2 \exp[it(\tilde{\epsilon}_\beta - \tilde{\epsilon}_0)/\hbar] \langle B_\beta B_\beta^{\$}(t) B_0(t) B_0 \rangle_v \quad (6.65)$$

where the subscript v means averaged over the vibrations. The vibrational average of the shift operators, which is the last factor on the right side of eq. (6.65), is evaluated in several places, notably in the paper of Fischer et al. [1970]. It requires use of some single operator identities. At zero temperature, we simply quote the result for the correlator, which is

$$\langle \boldsymbol{\mu}(0) \cdot \boldsymbol{\mu}(t) \rangle = Z^2 e^2 F_0^2 \sum_\beta |q_{0\beta}|^2 \exp[it(\tilde{\epsilon}_\beta - \tilde{\epsilon}_0)/\hbar]$$

$$\times \exp[-(g_\beta^2 - g_0^2)] \exp[(g_\beta - g_0)^2 e^{i\Omega t}]. \quad (6.66)$$

The absorption spectrum for the single bond is then found by substituting the correlation function eq. (6.66) in the expression eq. (6.61) for the lineshape. We thus obtain:

$$I(\omega) = \frac{Z^2 e^2 F_0^2}{2\pi} \int_{-\infty}^{\infty} dt \sum_\beta |q_{0\beta}|^2 e^{i\omega t} \exp[it(\tilde{\epsilon}_\beta - \tilde{\epsilon}_0)/\hbar] \exp[-(g_\beta - g_0)^2$$

$$\times \exp[(g_\beta - g_0)^2 e^{i\Omega t}]. \quad (6.67)$$

If we now expand the last exponential, we find

$$I(\omega) = F_0^2 \sum_\beta |\mu_{0\beta}|^2 \exp[-(g_\beta - g_0)^2] \sum_m \frac{1}{m!} (g_\beta - g_0)^{2m}$$

$$\times \int_{-\infty}^{\infty} dt \exp[it(\tilde{\epsilon}_\beta - \tilde{\epsilon}_0 + \hbar\Omega m - \hbar\omega)/\hbar \quad (6.68)$$

or

$$I(\omega) = \sum_\beta |\mu_{0\beta}|^2 F_0^2 \sum_m f_{0\beta}^m \int_{-\infty}^{\infty} dt \exp[it(\tilde{\epsilon}_\beta - \tilde{\epsilon}_0 + \hbar\Omega m - \hbar\omega)/\hbar]. \quad (6.69)$$

The last factor is simply the integral representation of the delta function,

so that we finally obtain:

$$I(\omega) = \sum_m \sum_\beta |\mu_{0\beta}|^2 F_0^2 f_{0\beta}^m \hbar\delta(\tilde{\epsilon}_\beta - \tilde{\epsilon}_0 + \hbar\Omega m - \hbar\omega). \tag{6.70}$$

The function $f_{0\beta}^m$, which is defined here, is the generalized Franck–Condon factor

$$f_{0\beta}^m \equiv \exp[-(g_\beta - g_0)^2](1/m!)(g_\beta - g_0)^{2m}. \tag{6.71}$$

The expression eq. (6.70) is the same as the golden rule formulation eq. (6.47). The different values of m define the different subpeaks in the spectrum, corresponding to the excitation of $m = 0, 1, 2, 3 \ldots$ quanta in the normal mode $\nu_{X\cdots Y}$. $f_{0\beta}^m$ is strongly peaked at $m = (g_\beta - g_0)^2$. The correlation-function approach is thus seen for the simple illustrative limit of one H-bond interacting with one other vibration at absolute zero, to give the same result as the golden rule approach. The result of the correlation-function method is a bit more general, even in this supersimplified limit, since the expression eq. (6.70) includes all final states of the $\nu_{X\text{-}H\cdots Y}$ mode, rather than simply the one final state $|f\rangle$ of eq. (6.47). But the real advantages of the linear response scheme accrue when real systems at finite temperature are considered. Some particularly fascinating features occur at values of $(g_\beta - g_0)^2 \approx 6$ when the excited state decay effect can be seen (see section 6.2.3).

The delta function spectrum of eq. (6.70) is never actually observed in practice. There are always such factors as instrumental resolution, rotational structure and Doppler broadening which can smear out such spectra even in the most favorable cases (such as, say, the electronic spectrum of HCl vapor). In practice, for H-bonded systems, there is a series of more important broadening and smoothing mechanisms, all of which can be consistently included in a strong-coupling picture. We proceed with the general formalism, indicating how these broadening effects are included.

6.2.3. Smoothing of the delta function spectrum within the strong-coupling model

Even in the linear three-atom model system several dynamic broadening* mechanisms can occur, which lead to a smoothed absorption profile. For

* By "broadening" we mean both the broadening of the individual ion-vibrational subpeaks within the main H-bonded absorption and the usually described broadening upon formation of H-bonds (Pimentel and McClellan [1960], (section 6.3)). This latter broadening refers to the envelope of all the vibrational sublevels of eq. (6.70), or of fig. 6.3.

strong H-bonds, there is the possibility of a double-minimum potential for the BO basis. In this case, the final state $|f\rangle$ will be split by tunnelling through the barrier (the state $|0\rangle$ will also be split, but such splitting is usually too small to be observable). This will lead to a superposition of two bands such as those of eq. (6.70), whose origins will be displaced from one another by $\Delta\omega_{\text{tun}} = (T_0 + T_1)/\hbar$, where T_0 is the tunnelling (splitting) in state $|0\rangle$ and T_1 is the tunnelling in state $|f\rangle$. In the late 1950's, several investigations were undertaken in an attempt to observe this splitting as a double peak in the infrared spectrum. Few clear-cut cases of this splitting were ever observed, however, and the reason is quite clear: reasonable values for $\Delta\omega_{\text{tun}}$ are of the order 300 cm^{-1} (Ibers and Snyder's estimate for the $HCrO_2$ case, Snyder and Ibers [1962]), while for a coupling constant like $g_f = 1.5$, the half-width of the envelope for the individual bands (to the lower and to the upper levels of $|f\rangle$) is of the order 380 cm^{-1}, for an ionic stretch wave number of 250 cm^{-1}. If the ionic stretch frequency is increased, these half-widths will become even greater; the doublet will not be seen due to the strong-coupling line width.

Electronic structure calculations of the MO–SCF type indicate that a static double well (that is, a double well in the case of Born–Oppenheimer electron-nucleus separation as well as Born–Oppenheimer proton-ion separation) is nowhere near so common as once believed, but that, instead, most unsymmetrical H-bonds form broad, anharmonic single minima* (Kollman and Allen [1972] and Ratner and Sabin [1973]). In this case, the excited protonic state still couples with the lattice vibrations, but these lattice vibrations are now anharmonic. There are two ways of describing this anharmonicity. Rigorously, both third- and fourth-order anharmonicities should be included in the strong-coupling Hamiltonian H (eq. 6.28). These terms, which have been analyzed by Fischer [1971] for the related case of radiationless decay, are

$$\begin{aligned} H_{\text{anh}} = & \sum_{\alpha,\beta,q,q'} [\Gamma_1(\alpha, \beta, q, q') b_q^\dagger b_{q'} + \Gamma_2(\alpha, \beta, q, q') b_q^\dagger b_{q'}^\dagger] |\alpha\rangle\langle\beta| \\ & + \sum_{\alpha,\beta,q,q',q''} [\Gamma_3(\alpha, \beta, q, q', q'') b_q^\dagger b_{q'}^\dagger b_{q''} \\ & + \Gamma_4(\alpha, \beta, q, q', q'') b_q^\dagger b_{q'}^\dagger b_{q''}^\dagger] |\alpha\rangle\langle\beta| + \text{C.C.} \end{aligned} \tag{6.72}$$

* It is to be stressed that this is the Born–Oppenheimer potential in the absence of coupling. It may be called the static proton potential; a dynamic proton potential, including coupling effects, may also be defined, and such a potential may have a form quite different from the static potential; in particular, it may exhibit a double minimum.

We have written the most general form of these couplings; the Γ_1, Γ_2, Γ_3 and Γ_4 are coupling functions including the frequencies, with dimensions of energy. In the case of the X–H $\cdots$ Y three-atom strictly linear system, q, q', q'' must *all* be the X–Y vibration, so that eq. (6.72) simplifies to

$$H_{\text{anh}} = \sum_{\alpha} \hbar\Omega[\bar{\Gamma}_1(\alpha)b^{\dagger}b + \bar{\Gamma}_2(\alpha)b^{\dagger}b^{\dagger}]|\alpha\rangle\langle\alpha| + \sum_{\alpha} \hbar\Omega[\bar{\Gamma}_2(\alpha)b^{\dagger}b^{\dagger}b + \bar{\Gamma}_4(\alpha)b^{\dagger}b^{\dagger}b^{\dagger}]|\alpha\rangle\langle\alpha| + \text{C.C.} \quad (6.73)$$

We have here included only the diagonal components, and only the most important anharmonic terms. Nevertheless, when eq. (6.73) is added to the Hamiltonian, the canonical transformation eq. (6.11) no longer takes account of the entire interaction. Fischer has developed a Van Vleck transformation to remove these interactions to second order; his approach will be discussed further below. The most important effect of these anharmonicities is to induce decay in the Ω manifold. If there is any kind of heat bath coupled to our XHY network, this also will result in a finite lifetime for these vibrationally excited states. This may be represented by a damping of the frequency, as was first used by Weisskopf and Wigner [1930]. In that case, the delta function peaks which result from simple use of the golden rule are replaced by Lorentzian functions, whose width is equal to the damping (that is, to the inverse lifetime). The anharmonicity has other effects also, such as modifying selection rules, bringing in Fermi resonances, and, eventually, leading to bond dissociation. However, as a lowest approximation the major effect of anharmonicity is to introduce lifetimes, and therefore broadening, into the spectrum. It is clear how these lifetime effects come about: the anharmonicity terms correspond to destruction and creation of normal-mode excitations, and therefore the anharmonic terms of the Hamiltonian, which do not commute with the normal-mode number operator $b_q^{\dagger}b_q$, do not conserve the number of normal-mode excitations. Physically this is also clear: a highly excited state in a classical network of coupled springs will decay to equilibrium if the decay route is permitted. The route will only be permitted if there are anharmonic terms which allow transfer between normal modes.

Fermi resonances can appear as special cases of anharmonicity. In particular, for the X–H $\cdots$ Y system there may be a near-degeneracy of the doubly excited bending mode with the X–H stretch. This situation has long been cited as a possible contribution to the spectral broadening due to

H-bonding, and a treatment based on the strong-coupling picture, within the golden rule procedure, has very recently been given by Witkowski and Wojcik [1973]. Essentially, a third-order anharmonicity term is added to the Hamiltonian, of the form

$$H_{\text{Fermi}} = \hbar\Omega_{2\delta} \sum_{\alpha,\beta=0}^{1} \Gamma_{\alpha\beta}^{(2\delta)} b_{2\delta}^{\dagger} b_{2\delta} |\alpha\rangle\langle\beta| \tag{6.74}$$

where $b^{\dagger}$ creates an excitation of the local bending mode overtone of frequency $\Omega_{2\delta}$, while the $|\alpha\rangle\langle\alpha|$ are the projection operators for local proton stretching, and $\Gamma_{\alpha\beta}^{2\delta}$ is a coupling parameter. The crucial aspect of the Fermi resonance term is that, unlike the simple strong-coupling Hamiltonian eq. (6.20), the Fermi resonance interaction is *not* diagonal in the protonic motion operators. This means that when the canonical transformation is applied, the resulting term, $\tilde{H}_{\text{Fermi}}$, will contain exponential operators $B^{\dagger}B$. If this term is then considered as a perturbation to first order, the resulting transition moment will be modified:

$$\langle\tilde{0}|q|\tilde{\alpha}\rangle \rightarrow \langle\tilde{0}|q|\tilde{\alpha}\rangle + \sum_{\alpha\neq\beta} \frac{\langle\tilde{0}|q|\tilde{\beta}\rangle\langle\tilde{\beta}|\tilde{H}_{\text{Fermi}}|\tilde{\alpha}\rangle}{\tilde{\epsilon}_{\beta} - \tilde{\epsilon}_{\alpha}}; \tag{6.75}$$

but since $\langle\tilde{\beta}|\tilde{H}_{\text{Fermi}}|\tilde{\alpha}\rangle = \langle\beta|H_{\text{Fermi}}|\alpha\rangle$,

$$\langle\tilde{0}|\tilde{q}|\tilde{\alpha}\rangle \rightarrow \langle\tilde{0}|q|\alpha\rangle + \sum_{\alpha\neq b} \frac{\langle\tilde{0}|q|\tilde{\beta}\rangle\langle\beta|H_{\text{Fermi}}|\alpha\rangle}{\tilde{\epsilon}_{\beta} - \tilde{\epsilon}_{\alpha}}. \tag{6.76}$$

This results in a final state, $|\tilde{\alpha}\rangle$, which is mixed with several different states of bending modes (and also with higher virtual states of the protonic motion) by the (weak) Fermi resonance interaction. Witkowski and Wojcik [1971] have analyzed the resulting spectrum in the case of an isolated H-bond, and have presented the resulting delta function spectra for several values of the coupling parameter. This work shows that the Fermi resonance does indeed provide significant broadening, but that this can be neatly included within the strong-coupling description. It seems to us that an even more reasonable description will be provided by the use of the full correlation-function approach with the use of steepest-descent integration, since the interaction of three modes, while certainly not yet the statistical limit, does provide sufficient phase cancellation that a smoothing, such as is provided mathematically by the steepest-descent procedure, is the most reasonable approach.

6.2.4. Discussion of the coupling mechanism for a single hydrogen bonding

In this section, we shall discuss the origin of the coupling existing between $\nu_{X-H\cdots Y}$ and $\nu_{X\cdots Y}$. This coupling has been postulated for explaining the unusual features of the $\nu_{X-H\cdots Y}$ band. However, its importance may be estimated from data independent of IR spectroscopy. It is well known that the $X\cdots Y$ distance is different in the $X-H\cdots Y$ bond and in the $X-D\cdots Y$ bond (Pimentel and McClellan [1960], ch. 9). This difference $\Delta_{X\cdots Y}$ has been measured, mainly in crystals (Ubbelohde and Gallagher [1955], Hamilton and Ibers [1968]), but also in gases (Almenningen et al. [1970]). It can be taken as an evidence of the existence of a strong coupling between $\nu_{X-H\cdots Y}$ and $\nu_{X\cdots Y}$.

The origin of this coupling seems quite clear: the frequency of the $\nu_{X-H\cdots Y}$ mode is known to decrease rapidly with the strength of the H-bond. In the O–H group it is equal to 3600 cm^{-1}. For strong $O-H\cdots O$ bonds, it can decrease to 2000 cm^{-1} or less. Therefore, the force constant k for the $\nu_{X-H\cdots Y}$ mode will strongly depend on the $X\cdots Y$ distance. This dependence of k will create an anharmonic coupling between q and Q, as the potential for those two motions will then be of the form:

$$V(q, Q) = \tfrac{1}{2}k(Q)q^2 + U(Q) \tag{6.77}$$

where $U(Q)$ is the part of the potential which depends on Q only (it will be equal to $\frac{1}{2}M_Q\Omega^2Q^2$ in the harmonic approximation for the Q-motion*). The potential for motion along Q is then given by the sum of the energy for q-motion and the $X\cdots Y$ potential $U(Q)$

$$\epsilon_\alpha(Q) = W_\alpha(Q) + U(Q) \tag{6.78}$$

with

$$W_\alpha(Q) = (\alpha + \tfrac{1}{2})\hbar(k(Q)/m)^{1/2} = (\alpha + \tfrac{1}{2})\hbar\omega(Q) \tag{6.79}$$

where m is the proton mass.

If we develop $\omega(Q)$ in series of Q and limit ourselves to linear terms, we see that the strong-coupling coefficient b of eq. (6.8) is then equal to

$$b = (\hbar/2M_Q\Omega)^{1/2}\Omega^{-1}(d\omega/Q)_0 \tag{6.80}$$

where $(d\omega/dQ)_0$ is the value of $d\omega/dQ$ for Q equal to zero. This

* In this section, we have chosen the origin of Q as coinciding with the minimum of $U(Q)$. This is the more appropriate choice especially for comparing H-bonds with D-bonds (Marechal [1972]).

coefficient is chiefly responsible for the strong anharmonic coupling (Bertie and Millen [1965], Marechal and Witkowski [1968] and Marechal [1969]) between q and Q (it is anharmonic, because it is the coefficient of a term of degree higher than two of the form q^2Q). This term can formally be calculated in the Born–Oppenheimer representation. However, this is a difficult task using MO calculations. On the other hand, this quantity is proportional to $\Delta_{X\cdots Y}$ (Ibers [1964]) which is equal to (Marechal [1972]) $\Delta_{X\cdots Y} = [\frac{1}{2}(\sqrt{2}-1)b](\hbar/M_Q\Omega)^{1/2}$. As $\Delta_{X\cdots Y}$ is in principle experimentally measurable by X-ray diffraction (Pimentel and McClellan [1960] ch. 9, Ubbelohde and Gallagher [1955]) or electron diffraction (Almenningen et al. [1970]), b can be characterized independently of IR spectroscopy. Therefore, the constant b proves a direct correlation between $\Delta_{X\cdots Y}$ and the structure of the IR spectrum. This has been recognized by Ibers [1965] in the HF_2^--case as well as by Marechal [1972] for the formic-acid dimers. More recent work on the relationship of $\Delta_{X\cdots Y}$ to the length has been done by Ratner and Rösch [1974] (see section 6.3 on solids) and by Cummings and Wood [1974].

Perhaps the simplest way to express the coupling constant is in terms of the Taylor series expansion of the potential (Janoschek et al. [1973] and Ratner and Rösch [1974]). That is, if we write (again, for a single H-bond)

$$V(q, Q) = \sum_{ij} a_{ij} q^i Q^j, \tag{6.81}$$

then the terms break up as

$$U(Q) = \sum_j a_{0j} Q^j \tag{6.82}$$

$$h(q) - (\text{kinetic energy of } q) = \sum_i a_{i0} q^i \tag{6.83}$$

$$g_\alpha = \langle \alpha | \sum_i a_{i1} q^i | \alpha \rangle \tag{6.84}$$

and terms of type $\Sigma_i a_{i2} q^i Q^2$ correspond to frequency changes. The coupling constant g_α will be largest when a_{i1} is large and when the proton displacement is large enough to significantly sample the highly anharmonic region. Further discussion of the coupling constant is given in section 6.3 below, actual values have been found for certain systems (Gosar [1963], Fischer et al. [1969] and Ratner and Rösch [1974]).

Let us note that a particular requirement for the theory is to explain the deuteration effects on the spectrum. This can be simply predicted, if we look at eq. (6.80): if we replace the H-atom by a D-atom, the mass m will be replaced by $2m$. Therefore, b_H will become $b_D = b_H/\sqrt{2}$. More accurately, of course, the harmonic approximation for the q-motion breaks

down, and then the mass dependence of the coupling becomes more intricate.

In this strong-coupling representation Fermi resonance can be included. As this mechanism is thought to be quite general for H-bonds (Bratož et al. [1956], Bratož and Hadži [1957] and Sheppard [1959] p. 85), it should be an intrinsic property of the group X–H$\cdots$Y. The most probable origin of this mechanism should therefore be an anharmonic coupling between q and the bending mode Ω_δ of the H-atom in X–H$\cdots$Y, of the form qQ_δ^2. This latter term can be easily included, as has been shown by Witkowski and Wojcik [1971, 1973]. These authors have established the Hamiltonians $H_{(0)}$ and $H_{(1)}$ in the presence of this coupling. They have calculated the different transition probabilities $w_{\alpha\to\beta}$ given by eq. (6.46) and showed that this mechanism adds new features to the spectrum in some cases. Due to the strong coupling of $\nu_{\text{X–H}\cdots\text{Y}}$ with $\nu_{\text{X}\cdots\text{Y}}$, this mechanism involves not only binary combinations of states in q and Q_δ, but also tertiary combinations of states in q, Q_δ and Q. If $f_0(Q_\delta)$ is the ground state wave function for the Q_δ-mode and $f_2(Q_\delta)$ its second excited state, the total wave function of the first excited state of q should be linear combinations of functions of the form

$$\phi_1(q, Q)f_m(\tilde{Q} + b)f_0(Q_\delta) \quad \text{and} \quad \phi_0(q, Q)f_m(\tilde{Q})f_2(Q_\delta). \tag{6.85}$$

We then see that even in the case where only one mode is coupled to q, there should be more than one additional line and the test of Fermi resonance based on the addition of frequencies alone is no longer valid. This is due to the predominance of the strong coupling between $\nu_{\text{X–H}\cdots\text{Y}}$ and $\nu_{\text{X}\cdots\text{Y}}$, which specifies which Q-transitions take place, if a q-transition occurs. Furthermore, in the case of Fermi resonance considered above, even more additional lines should appear; the q- and Q-modes are normal modes to a good approximation, the bending motion Q_δ is not usually a normal mode (Fukushima and Zwolinski [1969]), which means that if one moves the H-atom of X–H$\cdots$Y perpendicularly to the bond, one also moves other atoms in the X radical. Therefore, all the normal modes which include Q_δ will participate in Fermi resonance. In actual molecules, this would give many additional lines. For a broader view on this problem, see Sandorfy [1972].

6.2.5. Solvent effects

When dissolved in nonpolar solvents such as CCl_4, most H-bonded systems exhibit no major qualitative changes, unless major temperature

changes also occur (see, for instance, the early work of Liddel and Becker [1956] on methanol in CCl_4). On the other hand, acidic or basic solvents can strongly alter the characteristics of the absorption spectrum; in particular, there can be pronounced broadening and redshifting, either of a proton donor, such as pure H_2O monomer (Greinacher et al. [1955]) or of an associated system. Leaving aside such obvious effects as the thermodynamic mass-action factors which would tend to favor one or another polymeric species in solution, there remains the question of the effect of solvent interactions of the acceptor ions on the spectrum of the X–H···Y bond. Schematically, we may represent such a bond by

$$S_1 \sim\sim X\text{–}H \cdots\cdots Y \sim\sim S_2 \tag{6.86}$$

where S_1 and S_2 are solvent molecules or groups (–SH, –OH, –NH etc.) and the wiggly lines indicate a weak interaction. The same picture can be applied even in interaction with quasi-inert solvents such as CCl_4, but then the coupling indicated by the wiggly lines would be expected to be even weaker, and nonspecific.

The analysis of the spectral behavior of system (6.86) is strongly dependent on the nature of S_1 and S_2, as well as on the wiggly line interaction. For the general solvent interaction problem, however, what is really desired is a treatment in which the solvent plays the role of a heat bath, whose coupling to the system may be frequency dependent, but which is large enough to be treated as a classical system unperturbed by its interaction with the H-bond. Rosenstein [1973] and Rösch [1973] have presented a discussion of the effect of such a coupling on the mobility problem for a proton in a symmetrical double-well potential; Rösch's approach, which employs both the correlation-function approach and the strong-coupling method, has not yet been applied to the spectroscopy problem, but clearly can be (Rösch and Ratner [1974]).

Rösch starts by adding to the usual strong-coupling Hamiltonian eq. (6.26) a term corresponding to the heat bath and another term describing the coupling of the bath to the ionic motion (the term corresponding to the wiggly lines in (6.86)). These terms are, respectively,

$$H_{\text{bath}} = \sum_{\omega,\lambda} \hbar\omega_\lambda C^\dagger_{\omega,\lambda} C_{\omega,\lambda} \tag{6.87}$$

$$H_{\text{bath/ion}} = \hbar \sum_{\omega,\lambda} G_{\omega,\lambda} C^\dagger_{\omega,\lambda} b + \text{C.C.} \tag{6.88}$$

where $C^\dagger_{\omega,\lambda}$ creates a vibration of frequency ω in the heat bath, and $G_{\omega,\lambda}$ is

a (weak) coupling constant. We have neglected zero-point energy in the bath, and taken the bath as a collection of harmonic oscillators at various frequencies, which is the usual assumption in statistical mechanics. We have also neglected, on physical grounds, direct coupling of the bath with the protonic motion. This assumption is valid for clear physical reasons, unless the solvent is sufficiently basic to cause either bifurcation or actual base replacement in the H-bond. We will neglect these latter eventualities, assuming that the coupling is fairly weak.

To solve the Hamiltonian eqs. (6.26), (6.87) and (6.88)

$$H_{\text{solvated}} = H_{\text{S-coup}} + H_{\text{bath}} + H_{\text{bath/ion}} \tag{6.89}$$

Rösch used a standard statistical mechanical trick for deriving a Fokker–Planck equation. That is, he wrote the coupled Heisenberg equations of motion of the $b^\dagger$ and $c^\dagger$ operators, and then replaced the $c^\dagger_{\omega,\lambda}$, which appeared in the equation for $\mathrm{d}b^\dagger/\mathrm{d}t$ by

$$\int^t \frac{\mathrm{d}C(\tau)}{\mathrm{d}\tau}\,\mathrm{d}\tau.$$

This yields a result which reads, schematically,

$$\frac{\mathrm{d}}{\mathrm{d}t} b^\dagger(t) = \mathrm{i}\Omega b^\dagger + \mathrm{i}\sum_{\omega,\lambda} G_{\omega,\lambda} C^\dagger_{\omega,\lambda}\, \mathrm{e}^{\mathrm{i}\omega t} - \int^t \mathrm{d}\tau \left\{ b^\dagger(\tau) - \sum_\alpha g^2_\alpha |\alpha\rangle\langle\alpha| \right\} \sum_{\omega,\lambda} G^2_{\omega,\lambda}\, \mathrm{e}^{\mathrm{i}\omega(t-\tau)}. \tag{6.90}$$

Now the physical nature of the bath must be built into the dynamics of the ionic motion. This is done by assuming that the energy levels of the bath form a continuum, that the coupling of the ionic motion to the bath is frequency independent, and that the net result of the bath should be a damping of motion in the X–H$\cdots$Y system. That is to say, the final term in eq. (2.40) is taken as

$$\sum_{\omega,\lambda} G^2_{\omega,\lambda}\, \mathrm{e}^{\mathrm{i}\omega(t-\tau)} \to \int_0^\infty \mathrm{d}\omega G^2_{\omega,\lambda}\, \mathrm{e}^{\mathrm{i}\omega(t-\tau)} = 2\kappa\delta(t-\tau), \tag{6.91}$$

where the constant κ is a measure of the net interaction strength of the X$\cdots$Y motion with the solvent. Since $\int_0^t \mathrm{d}\tau\delta(t-\tau) = \frac{1}{2}$ we find that eq. (6.90) becomes

$$\frac{\mathrm{d}}{\mathrm{d}t} b^\dagger = \mathrm{i}\Omega b^\dagger - \kappa b^\dagger + \kappa \sum_\alpha g_\alpha |\alpha\rangle\langle\alpha| + F(t), \tag{6.92}$$

where $F(t)$ is a fluctuating force term. The important, obvious fact is that even if the fluctuating force is neglected, the frequency becomes complex. That is, the solution of eq. (6.92), neglecting $F(t)$ and taking, momentarily, $g_\alpha = 0$ is

$$b^\dagger(t) = b^\dagger(0)\, e^{i\Omega t}\, e^{-\kappa t}. \tag{6.93}$$

We have therefore derived in eq. (6.92), a stochastic, Langevin-like equation for the X$\cdots$Y displacement. The presence of the damping term $e^{-\kappa t}$ in eq. (6.93), which is a direct result of the smoothing assumption (eq. (6.91)), will result in a finite lifetime (or a complex frequency $\Omega + i\kappa$) for the vibrations. This, in turn, can be substituted into the strong-coupling form eq. (6.26). That is: within the assumption that the solvent acts as a weakly-coupled heat bath with a white spectrum and smooth energy-independent coupling to the X–Y vibration, the major effect of the solvent is to introduce a damping into the normal mode frequency Ω. Of course, this conclusion is modified by the last two terms of eq. (6.92), which will tend to cause spectral shifts as well as broadening. This point has not been fully explored to date.

Rösch's treatment of solvent effects is very attractive; it is general, the assumptions and approximations are well-defined, and the final result, eq. (6.92) is in the form of an equation of motion for the ionic displacement; it can therefore be treated by any one of a number of techniques, either dynamic (correlation-function approach) or static (golden rule). In fact, the fully dynamic treatment is shown to its greatest advantage in systems such as this, in which the system of primary interest has a dynamics of its own. Handling the resulting coupled-mode problem, especially at finite temperatures and in the situation in which the frequencies of the system and the bath are of the same order, is very difficult using straightforward perturbation techniques. But there are also some serious drawbacks, the most important of which is that the entire scheme has thus far been applied only to the somewhat artificial symmetric double-well mobility problem. The important spectral applications have not yet been carried out, but the overall outlook seems clear: the eq. (6.92) provides, on a microscopic and easily characterized level, the damping required to smooth the envelope of delta function peaks which result from eq. (6.70). In addition, shift and intensification factors can come about from the last two terms in eq. (6.92). The interpretation is hardly clear yet, however, and several important questions remain. The most important of these probably are the sizes of the coupling constant G and the possible role of

resonances. In the analogous magnetic resonance problem, for instance, the density of states and the coupling at the Larmor frequency are the important terms in the system-bath interaction (Abragam [1961]). We might expect an analogous situation to occur in our H-bond-solvent system, and therefore that the flat coupling spectrum assumed in eq. (6.91) and indicated by the curve f of fig. 6.4 should be replaced by the Lorentzian shape s, which schematically indicates a coupling strongly

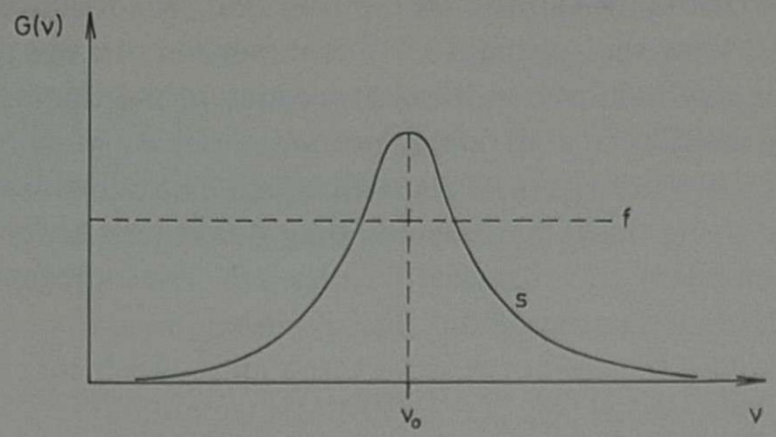

Fig. 6.4. Frequency independent (Rösch [1973]) vs. Lorentzian coupling (f resp. s).

peaked at the resonance-frequency Ω_0 of the unperturbed X–Y stretch. There is also the possibility of a difference frequency coupling corresponding to an anharmonic process like that described by eq. (6.93) $\Gamma_{\alpha,\omega} b c_\omega |\alpha\rangle\langle\alpha + 1|$ which could couple strongly at resonance [that is Γ may be large if $\epsilon_{\alpha+1} - \epsilon_\alpha \approx \hbar(\omega + \Omega_0)$]. The Lorentzian shape of fig. 6.4 would be expected to provide the same type of damping (or broadening) as the flat spectrum f, and in addition will be more physical, since the broadening will now be a frequency-dependent phenomenon. (In the same spirit, Gosar et al. [1968] has treated the transport phenomena in general electron-vibration systems by introducing a Gaussian width into the normal vibrations.) In addition, the possible appearance of anharmonic terms like eq. (6.93) might lead to the addition of ancillary subpeaks, especially if the solvent contains internal modes of the proper frequency. All of these conclusions are very tenuous, however, since no true calculation along these lines has yet been performed.

Janoschek et al. [1973] have attempted to describe the solvent effects by including an additional term

$$H_{\text{solvent}} = \boldsymbol{\mu} \cdot \boldsymbol{P} \tag{6.94}$$

where $\boldsymbol{P}$ is a local polarization field, caused by the electric charge distribution in the solvent and $\boldsymbol{\mu}$ is the dipole moment of the X–H···Y system (the electrical anharmonicity was specifically taken into account in this treatment). They then solve for the spectrum of the system, assuming a model potential surface. They obtain a large number of shifted bands, caused by the static perturbation eq. (6.94). While these shifted bands are important, the most important point seems to be that the true interactions with the solvent, as becomes manifestly clear from the NMR analogy, is dynamic in nature and the true line broadening cannot come from a static term such as eq. (6.94). Another way to see this is a time scale argument: the local electrical properties of the liquid change on a time scale at least as fast as that of protonic motion, so that a neglect of the dynamics of $\boldsymbol{P}$ in eq. (6.94) is unjustified. The same model has now been treated using the full strong-coupling dynamics (Rösch and Ratner [1974]) which allow calculation of shifts and linewidths, as well as a complete characterization of the time scale regimes.

6.2.6. Dynamics of two neighbor hydrogen bonds: carboxylic acid dimers

In this section, we examine the application of the strong-coupling theory to a real system of H-bonds. In most H-bonded species, there are several H-bonds which interact: single H-bonds are in fact rather scarce. In the spectrum of H_2O, for instance, H-bonded dimers, trimers, . . . , n-mers are present. With such mixtures, it is very hard to draw definite conclusions concerning the dynamical behavior of one H-bond. However, some systems are well defined, and can be taken as models. Examples include gaseous mixtures (Bertie and Millen [1965], Arnold and Millen [1965], Millen and Samsonov [1965] and Millen and Zabicky [1965]) of

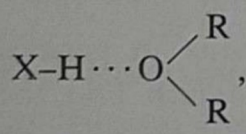

, and the carboxylic acid dimers. These latter species have the advantage of giving a very intense $\nu_{O\text{–}H\cdots O}$ band. In the vapor state, only monomers and H-bonded cyclic dimers exist at equilibrium. These dimers are centrosymmetric and have the form:

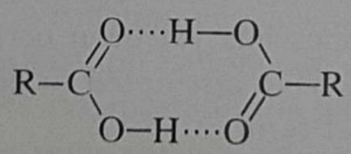

They constitute one of the simplest well-defined H-bonded systems: they

are gaseous, and thus can be considered as isolated molecules containing two ordered H-bonds (as the $\nu_{O\text{-}H\cdots O}$ band is intense, the spectra can be recorded at low pressure).

From the theoretical point of view, the Hamiltonian describing the motions of these two H-bonds will be the sum of the Hamiltonians of each individual H-bond, already described, plus an interaction term between the two H-bonds. This interaction term can be viewed as a term which gives an excitonic character to the H-bond (Witkowski [1968]); if one of the H-bonds is in the first vibrational excited state of the q-mode, this excitation will have a tendency to jump to the other H-bond, as a consequence of the interaction term. This term can also be viewed as a dipole–dipole interaction between the two H-bonds. Formally, this type of interaction adds terms of type discussed by Fischer et al. [1970], in their strong-coupling description of H-bonded crystals.

More precisely, let us call q_A, q_B the coordinates of the $\nu_{O\text{-}H\cdots Y}$ modes of the bonds A and B, and $\tilde{Q}_A$, $\tilde{Q}_B$, the corresponding dimensionless coordinates for the $\nu_{O\cdots O}$ modes. Just as in the case of a single H-bond, we can define a Hamiltonian $H_{(0)}$ for the $\tilde{Q}_A$, $\tilde{Q}_B$ modes, when the q_A, q_B modes are in their ground state, which will be equal to

$$H_{(0)} = \tfrac{1}{2}(\tilde{P}_A^2 + \tilde{P}_B^2)\hbar\Omega + U(\tilde{Q}_A, \tilde{Q}_B). \tag{6.95}$$

This Hamiltonian corresponds to a wave function of the form

$$\psi_0^m = \phi_0(q_A, \tilde{Q}_A)\phi_0(q_B, \tilde{Q}_B)\chi_0^m(\tilde{Q}_A, \tilde{Q}_B). \tag{6.96}$$

In the potential $U(\tilde{Q}_A, \tilde{Q}_B)$ anharmonic terms for the $\tilde{Q}_A$- and $\tilde{Q}_B$-motions can be included (Leviel and Marechal [1971]), in addition to the harmonic terms for the $\tilde{Q}_A$- and $\tilde{Q}_B$-motions.

When one mode q_A or q_B is in its first excited state, the total wave function for the q_A, q_B, $\tilde{Q}_A$, $\tilde{Q}_B$ modes can be resolved into two components, a totally symmetric one ψ_+^n and an antisymmetric one ψ_-^n, by taking the combinations:

$$\begin{aligned}\psi_\pm^n = {} & \phi_1(q_A, \tilde{Q}_A)\phi_0(q_B, \tilde{Q}_B)\chi_{1\pm}^n(\tilde{Q}_A, \tilde{Q}_B) \\ & \pm \phi_0(q_A, \tilde{Q}_A)\phi_1(q_B, \tilde{Q}_B)\mathscr{C}_2\chi_{1\pm}^n(\tilde{Q}_A, \tilde{Q}_B).\end{aligned} \tag{6.97}$$

Here $\mathscr{C}_2$ is the inversion operator, which is chosen such that $\mathscr{C}_2\tilde{Q}_A = \tilde{Q}_B$ and $\mathscr{C}_2\tilde{Q}_B = \tilde{Q}_A$. The ψ_+^n functions (or ψ_-^n) are then totally symmetric (or antisymmetric) with respect to inversion. Note that due to the coupling of the q, Q modes, the wave functions are no longer symmetric or antisymmetric with respect to each kind of mode separately, but instead

with respect to the whole set of modes. The Hamiltonians whose eigenfunctions are the χ^n_{1+} or the χ^n_{1-} are:

$$H^{\pm} = H_{(0)} + \hbar\Omega(b\tilde{Q}_A \pm V_0\mathscr{C}_2) + \hbar\omega_H \tag{6.98}$$

where V_0 is the interaction term between the two q-modes. Equations (6.96), (6.97) and (6.98) describe the system as being equal to the addition of the two single H-bonds A and B, plus an interaction between A and B. The Hamiltonians H^+ and H^- play the same role as $H_{(1)}$ in a single H-bond. An equation analogous to eq. (6.46) then defines the transition probabilities of the $\nu_{O\text{-}H\cdots O}$ band as:

$$w^{m\to n}_{\pm}(\nu) = |\langle\psi^m_0|q_A - q_B|\psi^n_{\pm}\rangle|^2\delta(\nu - (1/\hbar)(E^n_{\pm} - E^m_0)) \tag{6.99}$$

$E^n_{\pm}$ is the eigenvalue of H^+, which corresponds to $\psi^n_{\pm}$. E^m_0 is the eigenvalue of $H_{(0)}$, which corresponds to ψ^m_0. The dipole-moment operator $q_A - q_B$ is antisymmetric with respect to inversion. In the Franck–Condon approximation, where quantities such as $\langle\phi_0(q_A\tilde{Q}_A)|q_A|\phi_1(q_A\tilde{Q}_A)\rangle$ are taken as independent of Q_A and equal to a constant λ we then find:

$$w^{m\to n}_{\pm} = \lambda^2|\langle\chi^m_0|1 \mp \mathscr{C}_2|\chi^n_{1\pm}\rangle_{\tilde{Q}_A\tilde{Q}_B}|^2. \tag{6.100}$$

The factor $1 \mp \mathscr{C}_2$ shows that the transitions occur with a reversal of parity ($1 \mp \mathscr{C}_2$ are projection operators): if χ^m_0 is symmetric, the only allowed transitions are to states χ^n_{1-} of ψ^n_- and vice versa.

The functions χ^m_0, χ^n_{1+} and χ^n_{1-} have been computed, allowing the calculation of the different $w^{n\to m}_{\pm}$ (Bournay and Marechal [1971], Leviel and Marechal [1971] and Excoffon and Marechal [1972]). The result is shown in fig. 6.5 for acetic acid dimer. In the case of a gaseous system, we see that the calculation of the probabilities of the individual transitions gives a correct simulation. When replacing the H-atoms of the H-bonds by D-atoms, b should be divided by $\sqrt{2}$. (This result presupposes a harmonic well for the q-motion.) More generally, the potential for q-motion is highly anharmonic, and may even be a double-well. In these cases, the mass effects are more complicated–see section 6.2.7. The exciton term V_0 was originally thought not to vary under deuteration (Marechal and Witkowski [1968], Marechal [1969], Bournay and Marechal [1971], Leviel and Marechal [1971] and Excoffon and Marechal [1972]). It is most probable that this results from terms of the form $q_A \cdot q_B$ in the expansion of the full potential, and should therefore be divided by $\sqrt{2}$ under deuteration. However, the predominant term being the strong-

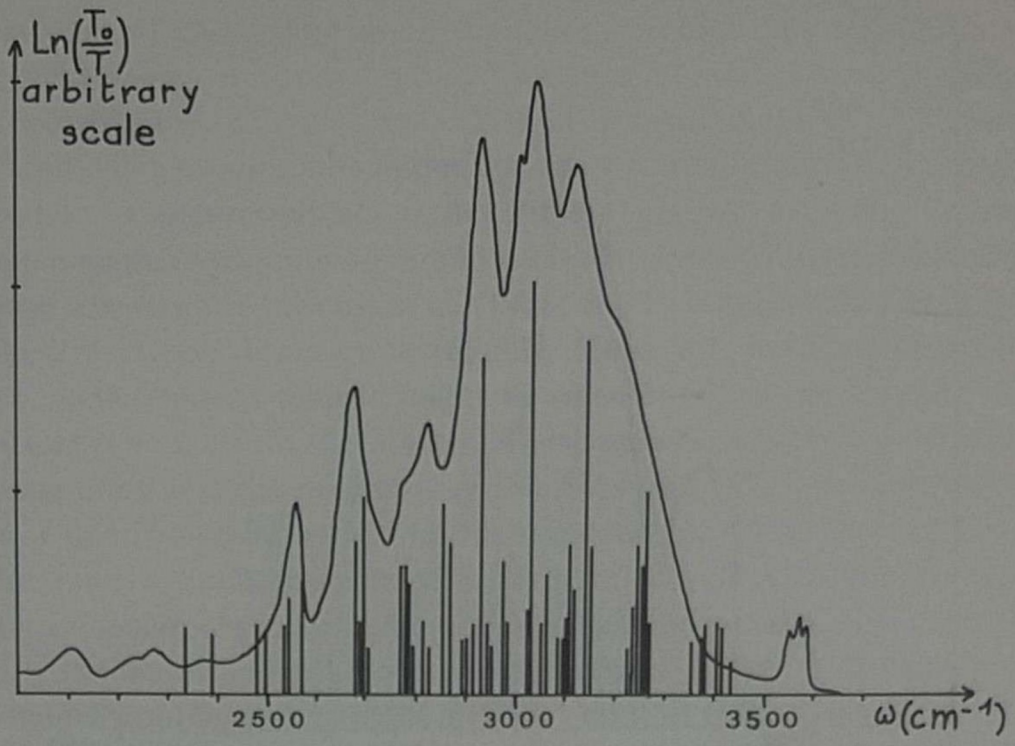

Fig. 6.5. Experimental absorption spectrum (optical density) and theoretical reconstitution of the CD_3COOH vapor spectrum.

coupling term b, both values of V_0 can fit rather well the spectrum of acetic acid D-bonds. In fig. 6.6, which shows the reconstitution for $(H_3CCOOD)_2$, this term has been divided by $\sqrt{2}$ after deuteration. The importance of this term has been recognized by Mikhailov et al. [1973], who explained the effect of isotopic dilution in a mixture of methanol and D-methanol by the existence of this Davydov splitting (the exciton term is responsible for a "Davydov splitting" in the case of crystals with several molecules in the unit cell, Davydov [1962]).

This simulation shows that the strong-coupling theory quantitatively predicts the important changes in the spectra of the H-bond upon deuteration. Furthermore, from the value of the strong-coupling coefficient b, the value $\Delta_{O\cdots O}$ of the difference in the $O\cdots O$ distances between H-bonds and D-bonds, could be calculated. This value has been experimentally measured by electron diffraction for formic acid (Almenningen et al. [1970]). In this case, the calculated and experimental values are the same (Marechal [1972]), which constitutes a fair support for the strong-coupling theory.

We can formulate several criticisms about these reconstitutions. Firstly, they constitute a four modes theory, in the sense that they consider only the motions of the two $O–H\cdots O$ groups. This leads to a

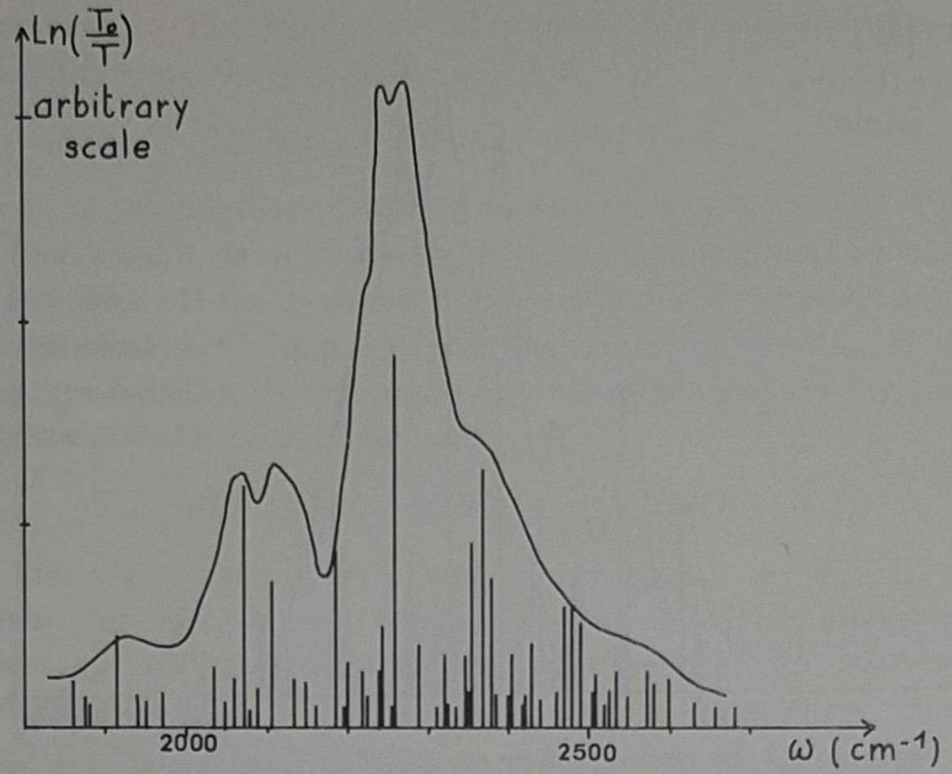

Fig. 6.6. Experimental absorption spectrum (optical density) and theoretical reconstitution of the CH_3COOD vapor spectrum.

complete neglect of the couplings of the $\nu_{O-H\cdots O}$ modes with other modes in the molecule, via anharmonic terms, including Fermi resonance. These couplings have most probably only a local influence on the bandshape. However, they are not completely negligible, as indicated by the fact that the $\nu_{O-H\cdots O}$ band in $(D_3CCOOH)_2$ is slightly different from the $\nu_{O-H\cdots O}$ band in $(H_3CCOOH)_2$. This difference has been taken as evidence of the importance of Fermi resonance in these dimers (Haurie and Novak [1965]). However, it could also find its origin in an electrical anharmonicity (Marechal [1973]). The second kind of criticism which can be formulated is that these reconstitutions are done on the basis of δ functions. This means that the line shape of the individual lines is not taken into account. These reconstitutions are indeed the first step only towards a complete understanding of the dynamics of the H-atom in H-bonds. The next step will be to find an expression for the line shape. In the case of carboxylic acid dimers, this step will mainly consist in examining the role of the rotations of the dimer, which seem to be the main cause of broadening of the individual transitions shown in figs. 6.5 and 6.6 (Lassegues [1972], Lascombe et al. [1973], Thomas and Thompson [1970] and Thomas [1971]). It might then be interesting to approach this problem dynamically in the scheme of the linear response theory.

In the case of carboxylic acids, the theory predicts some variations of the spectrum with the temperature T. Experimentally, these variations are, however, very difficult to measure: when heating, the H-bonds break down, and when cooling, the vapor condenses into liquid. Therefore, the T variation is experimentally rather difficult. However, some attempts have been made to trap the dimers in solid matrices of nitrogen and argon at helium temperature (Grenie et al. [1971] and Redington and Lin [1971]). The spectra obtained are quite reliable. However, it seems that other species, such as open dimers might be present. Furthermore, the solid matrix can interact with the dimers. These spectra are then most useful when one considers the positions of the lines only. They are not defined clearly if one is also interested in the intensities of the different lines. In fact, the matrices constitute a special type of solvent, and the line shape for matrix isolated species can perhaps best be handled by a strong-coupling theory of solvent interactions, such as Rösch [1973] has given for a model double-well system.

In the light of the preceding sections it seems that the strong-coupling interaction between the $\nu_{X-H\cdots Y}$ mode and the $\nu_{X\cdots Y}$ mode is an intrinsic property of most H-bonds. It is the predominant feature of their dynamical behavior. For an isolated system, such as carboxylic acid dimers or complexes of X–H with diethers, the role of other anharmonic couplings, like Fermi resonance or tunnelling, is reasonably well understood, even though a complete quantitative treatment still has its difficulties. For this reason small systems constitute ideal test cases from which generalizations to more complex systems can be drawn. In highly structured systems (macromolecules, liquids, solids) new effects, such as clustering, disorder and cooperativity can have important consequences; spectroscopically it is very often hard to distinguish these from other secondary anharmonic effects; their role in these systems is still open to discussion.

The theoretical discription of dynamical aspects of H-bonds now seems to be approaching the quantitative level. Previously, the complications of the spectra of H-bonded systems had been approached on one of two tracks. One was purely phenomenological and is represented by the effective potentials of Lippincott and Schroeder [1956] or of Reid [1959]. Although this approach is not satisfactory in its foundation, it permitted the interpretation of some experimental correlations (Lippincott [1957]) and indicated the importance of the $\nu_{X-H\cdots Y}$–$\nu_{X\cdots Y}$ coupling. The other approach consisted of qualitative definitions of the different coupling mechanisms of the $\nu_{X-H\cdots Y}$ mode with other modes. This approach, which

had a strong physical basis, has now been developed in the strong-coupling theory, which provides a unified, consistent scheme for these different mechanisms. Further work must now be quantitative, with emphasis on the estimation of potentials and the evaluation of coupling constants.

Similarly, the fact that the theory has reached a quantitative level will greatly influence the experimental work on H-bonds. In the preceding period, emphasis has been placed on the compilation of spectra. This line of work stems from the necessity to analyze and recognize H-bonded systems. Now, emphasis should be put on well-defined species, such as carboxylic acids or H-bonded simple crystals, which will serve as model systems and are being intensively studied with regard to their dependence on well-defined physical and chemical parameters, including deuteration (Falk and Ford [1966] and Ford and Falk [1968]), temperature (Lassegues [1972] and Zelsmann and Marechal [1974]), isotopic dilution (Lautie and Novak [1972]), mixed complexes etc. Studying spectra by simply examining the frequencies of the lines will no longer suffice since intensities and line shapes of the spectra are essential features to be explained by quantitative theories (Bournay and Marechal [1971] and Rösch and Ratner [1974]).

New physical methods are also appearing, which will bring additional information on H-bonds. These methods are often not so powerful as IR spectroscopy for the study of dynamical aspects, but they can give information which is not found in IR spectra. They include, for instance, neutron inelastic scattering (Hamilton and Ibers [1968], Collins and Haywood [1970] and Stiller [1974]), which provides information on the motions of nuclei in H-bonds. This technique is not parallel, but rather complementary, to IR and Raman spectroscopy. This is particularly true for solids, where the symmetry conditions are relaxed, which permits the determination, for instance, of the dispersion curve of strongly coupled phonons. This would be interesting for the low frequency motions $\nu_{X\cdots Y}$ of H-bonds in crystals, which may show renormalized frequencies due to the strong coupling. This inelastic neutron scattering technique is also complementary to neutron diffraction techniques, which have proved very useful for determining H-bond structures (Bacon et al. [1953, 1955], Delaplane et al. [1969] and Schlemper et al. [1971]).

The IR region might also be extended towards the study of the overtones of the $\nu_{X-H\cdots Y}$ mode. These overtones fall in the near IR region (Greinacher et al. [1955], Foldes and Sandorfy [1966] and Asselin et al.

[1969, 1971a, b]), which is rather easy to handle. These studies can be seen as complementary to the studies in the region of the $\nu_{X-H\cdots Y}$ band. However, due to the low intensities of these overtones, only their frequencies have been measured up to now, these yield only partial information on anharmonicity.

6.2.7. Strong hydrogen bonds

MO–SCF calculations for isolated small H-bonded systems seem to indicate that even for strong bonds, in most cases, no protonic double minimum potential will be present. This means that the $X\cdots Y$ distance has the tendency to become too small to permit a hump in the protonic potential. By the same token, we may expect protonic double minimum potentials in all those cases where repulsive forces between groups attached to the X and Y atoms, or crystal forces, keep the X–Y distance from attaining its minimal value. The latter type of H-bond is of particular interest for various reasons. We will confine ourselves here to the IR spectral properties which imply some truly amazing effects.

Most of the IR phenomenology was discovered by Hadži [1965, 1972] (see ch. 12). He noticed that three bands A, B and C, originating from ν_{X-H}, appeared in the spectra of strongly H-bonded complexes which were likely to possess protonic double minima. The three bands, however, could not originate from the split levels of an uncoupled protonic double well potential, as was quickly recognized from their changes with bond strength and deuteration. From our point of view the most striking experimental facts are:

1) The downward move of the frequencies A and (to a lesser degree) B, with C remaining constant, on increase of band strength. At the same time the intensity of A and B shifts to C.
2) On deuteration, instead of A and B a new band appears, whereas C drops in frequency and intensity.

It seems unlikely that this pattern can be attributed solely to Fermi resonance (some speculations regarding this mechanism are presented by Hadži in ch. 12) or to an Evans effect (Claydon and Sheppard [1969]).

Since strong coupling will prevail in these bonds we would like to interpret the phenomena cited above within the theoretical framework of Fischer, Hofacker and Ratner [1970], henceforth cited as FHR. This does not preclude that Fermi resonance might be involved in the strong-coupling setup. The results of the FHR theory, derived for symmetrical protonic potentials can, without changes in the formalism, be used for the

interpretation of strongly coupled non-symmetrical potentials. Fig. 6.7 shows a typical asymmetric potential for the proton with corresponding Born–Oppenheimer potentials for the X–Y motion. In a rather symmetric potential the transition $0 \rightarrow 1$ would have very little or no intensity whereas the splitting between the levels 2 and 3 becomes large so that these states will determine the spectral behavior.

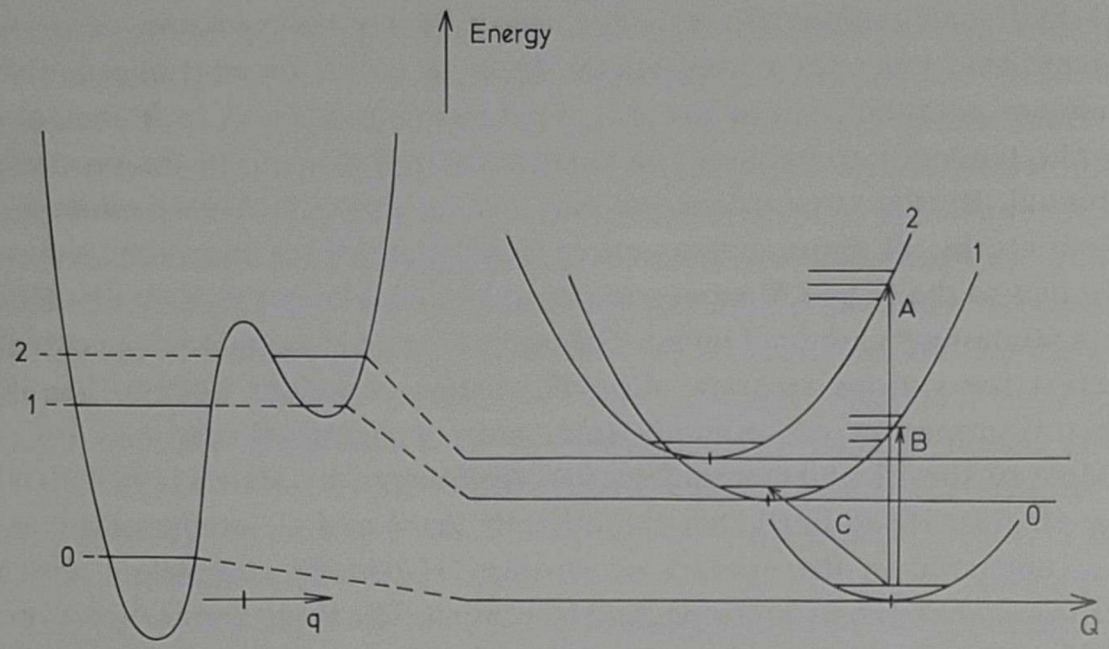

Fig. 6.7. Uncoupled protonic potential (left) and Born–Oppenheimer potential curves for X–Y motion (right). Transitions corresponding to Hadži's [1965, 1973] bands A, B, C are indicated.

The prediction of the FHR strong-coupling theory is, indeed, that the spectrum should be dominated by three peaks. Two of these (A and B) correspond to Franck–Condon transitions with a separation somewhat less than the hump-splitting, i.e. the energy difference between the two lowest states with non-zero wave amplitude in both wells of the protonic potential. If increase of bond strength means that the X–Y distance shortens somewhat (as it is strongly influenced by other repulsive forces) but the barrier decreases, band A, arising from the state closer to the barrier top, comes down the most, whereas B, originating from the state close to the bottom of the second minimum decreases less. On deuteration A and B can thus come near to coalescence; but the position of the joint band has to remain on the high frequency side of B in the undeuterated case.

The width of peaks A and B is determined by the strong-coupling

interaction which severely limits the lifetime in the upper states (like in Stepanov-predissociation); A and B are therefore very wide bands with as little temperature sensitivity as $T^{1/2}$, coming in through the T-dependence of the phonon spectrum. With increasing bond strength the lifetime, particularly of the highest state, decreases and band A becomes wider and less intense.

Bands A and B are thus recognized as strongly damped vertical transitions; in the FHR theory they come from the short time behavior of the correlation function for the protonic flux in the double well potential under the influence of the radiation field. Whereas in weak-coupling situations this is the only contribution to the absorption; for strongly coupled systems one may also obtain a sizable amount from the long time tail of the correlation function. This gives rise to bands which can be interpreted as the transitions to the relaxed Born–Oppenheimer potentials of A and B. Usually, only the lowest of these transitions is intense enough to be observed. It corresponds to the zero phonon line observed in polar semiconductors (e.g. Huybrechts et al. [1973]). We therefore consider Hadži's band C a zero phonon line, typically the one of the state related to the vertical transition B. Only if the upper B state is weakly coupled and A strongly (e.g. if the protonic potential suddenly widens near the energy of the A state) can the zero phonon line be related to A. When more than one zero phonon line is observed, the lower frequency line should be of considerably lower intensity. Being an adiabatic transition, band C may show phonon sidebands but no considerable broadening, except for anharmonicity. At low temperatures, C should become quite sharp, in contrast to A and B.

Most of the behavior of the zero phonon band is apparent from fig. 6.7. Increase in bond strength will tend to shift band C towards the red but, because the barrier becomes lower, transition moment and coupling will generally increase and provide more intensity for this band. Deuteration will shift C down in frequency, in highly asymmetric situations (like fig. 6.7) less than in the case of a near symmetric protonic potential. The loss in intensity is due to decrease in transition moment.

The relatively simple strong-coupling model evaluated by FHR, therefore, seems to provide a scheme in which the unusual IR spectroscopic phenomena of strong H-bonds can be rationalized with the aim to determine the importance of additional factors, mainly Fermi resonance, from experimental evidence. We have kept the discussion of the available data in rather general terms for that reason. It is our belief, however, that

the essential features of the FHR theory, particularly regarding the origin of band C, will remain valid for the interpretation of real spectra and the stage of quantitative predictions can be reached as soon as there are more data on the C band available, particularly on sidebands, low-temperature shapes and intensities, the question of additional C bands, shifts on deuteration.

6.3. Dynamical aspects of hydrogen bonds in solids

The H-bonded solids, especially ice and the ferroelectric (we use this generic term to include also antiferroelectric) crystals*, have been extensively investigated experimentally, and a good deal of theoretical work has gone into explaining certain of their properties, notably the dynamics of the ferroelectric phase transition and the proton mobility in ice and other "protonic semiconductors" (Onsager and Dupuis [1962]). Not a great deal of theory has been done on the vibrational IR spectrum of these systems, except in connection with the phase transition. We will therefore try to sketch the theoretical description of several phenomena, including mobility, spectra, and isotopic lattice distortion, which occur in associated solids.

In crystalline solids the translational invariance leads to Bragg-type reinforcive conditions, and therefore a whole series of experimental methods for investigation of structure and dynamics becomes available. These include oriented single crystal NMR, NQR, X-ray and neutron diffraction. The text by Hamilton and Ibers [1968] reviews the application of these methods to H-bonded solids. Most of these experiments have been interpreted in terms of simple potential-function models. Thus, for example, Ibers [1964] was able to explain the observed KHF_2 data by means of a simple single-minimum function with a large quartic contribution. For very short H-bonds (less than 2.3 Å) the negative anharmonicity does not lead to important dynamic coupling effects, and thus the success of Ibers' treatment of the acid fluorides is not surprising. For longer H-bonds, however, the coupling effects can become extremely important, and can lead to marked spectroscopic and structural peculiarities.

* Many good reviews on ferroelectrics exist (Jona and Shirane [1962], Cochran [1969], Mitsui [1969] and Blinc and Zeks [1972]), in particular, the discussion by Pepinsky et al. [1972] contains not only a critical evaluation of all the experimental results, but also some very germane observations from Mr. Lewis Carrol on the dangers of oversimplified theoretical discussion.

Most theoretical work on these solids has been in a one-dimensional approximation. While it is true that, even in solids, the extent of bifurcation in most H-bonds remains very small, nevertheless the transverse motions of the heavy ions can be very important in determining the overall proton dynamics, and the one-dimensional approximation is open to serious questions. Cases in point are provided by the importance of the 3-dimensional defect structure in ice, as shown by Godzik and Hofacker [1973] for H_3O^+ and, equally dramatically, by the fact that the coupled mode leading to the ferroelectric transition in KH_2PO_4 appears to be a transverse vibration. Nevertheless there are many systems, notably the chromous and cobaltous acids, in which an informed, quasi-one-dimensional treatment is probably justified. These particular crystals are discussed in greater detail below.

Marechal and Witkowski [1967] extended their strong-coupling approach to a model of a one-dimensional H-bonded solid (imidazole). They calculated a delta function spectrum, in which a large number of sidebands, coming from mode–mode coupling of the protons, appear; an envelope function can clearly be drawn over these peaks. This work could form the basis for extensive investigation of the IR spectrum of H-bonded solids, but it has not yet been extended to other systems. This work does not specifically evaluate coupling constants, deal with deuteration or momentum-dependence, or consider effects due to three-dimensionality.

6.3.1. Theory of defect motion

There has been some work on the transport phenomena associated with defect sites in associated solids. The most famous of these are the four defects, ionic and orientational, which are present in ice (Jaccard [1959], Gränicher [1963], Riehl et al. [1969] and Engelhard [1973]). The importance of these rare structures, which are local violations of the Bernal–Fowler rules for oxygen-proton coordination, was first pointed out by Bjerrum [1951]. Onsager and Dupuis [1962] and Onsager [1969] have discussed the dielectric properties of ice, and have shown that the defects are responsible for the protonic conductivity of ice and other "protonic semi-conductors". Gosar [1963] and Sussmann [1964, 1972] have investigated the protonic mobility problem; both include the strong coupling between protonic motion and lattice displacements. Gosar has used a rigid-ion approximation to evaluate the coupling strength. He then uses a temperature-dependent Green function technique to evaluate the mobility of an excess proton (the H_3O^+ defect). He contends that the

mobility is dominated by a virtual state in which the proton is promoted to an upper tunnelling level by the strong-coupling interaction. The actual strong-coupling treatment is done only to second order. He formally includes both transverse and longitudinal phonons, but his final result depends on a tunnelling energy in the ground level of $\sim 5\,\mathrm{cm}^{-1}$. Since electronic-structure Hartree–Fock calculations do not yield double-minimum potentials for the $H_5O_2^+$ complex, this would seem a major drawback of Gosar's approach. However, the proton–proton interactions in a chain do result in a local double minimum (Fischer and Hofacker [1969]), and Gosar's result thus becomes reasonable when reinterpreted as the motion of a kind of collective defect, rather than a single particle.

Perhaps a more serious drawback is the fact that Gosar (and also Sussmann) essentially considers a weak-coupling limit in which the defect motion is, still, essentially particle-like. Onsager [1963] as well as Jaccard [1959] and Gränicher [1963], have argued convincingly that protonic mobility in ice is a rather complicated process involving both protonic translation and molecular rotation, and that analogies to metallic or semiconductor systems are problematic. Kubarev and Shedrin [1969] have stated that the expected free path of protonic motion is far less than one bond length, so that the mobility process is closer to a hopping than to a band regime.

Sussmann has considered the motion of excess protons in ice as an example of the general phenomenon of phonon-induced tunnelling. He attempted to rationalize several measurements concerning proton mobility in ice, notably the observations of Eigen et al. [1964] that the proton mobility is larger than the deuteron mobility by about a factor of seven, and is in fact rather high and indicates a different activation energy for mobility. (Regarding these questions compare with Riehl et al. [1969] and Engelhard [1974].) Sussmann does not give any detailed treatment of the proton mobility problem, but does implicate phonon-assisted tunnelling as the mobility mechanism.

Fischer and Hofacker [1969], cited from here on as FH, using a one-dimensional model, were able to construct defect states (involving several protons), and to Fourier analyze them to find expressions for the defect bandwidth. This was found to be very small, and the effects of strong coupling with the vibrations of the lattice had to be taken into account. Fischer, Hofacker and Sabin [1969], henceforth cited as FHS, thereupon performed a model calculation to estimate the coupling strength. Although theirs is a one-dimensional treatment, it seemy to be the

first careful development of the strong-coupling method for associated solids, and is therefore worthy of further discussions as a prototype of such calculations.

They studied a one-dimensional model of the ice defects, assuming a Born–Oppenheimer separation of electronic and nuclear motion, and using a second-quantization formalism, with a Hilbert space basis consisting of the lowest three local vibrational states of the proton at each site. The defect quasiparticle was described simply by properly positioning the protons. For instance, the following graph shows the one-dimensional analog of the D-defect:

O–H O–H O–H H–O H–O H–O.

These defect states were then Fourier transformed, and the bare proton Hamiltonian written:

$$H_{\text{defect}} = \sum_{k} \sum_{\alpha=1}^{3} E_{\alpha}(k) a_{j\alpha}^{\dagger} a_{k\alpha} \tag{6.101}$$

where $E_\alpha(k)$ are the band energy and $a_{k\alpha}^{\dagger}$ creates a defect with quasimomentum k in the α band. The bandwidths are very small: if the local OHO bond is taken as a double minimum, then $E(k) = \epsilon_0 + T_0 \cos kd$, where d is the O–O bond length, ϵ_0 is the local ground state energy, and T_0 is the tunnelling matrix element (bandwidth) in the local lowest state.

FHS next considered the strong-coupling of the lattice vibrations with the protons. They used the formulation first given by Fröhlich [1957] for the electron–phonon coupling problem, and used by several authors in the analysis of polaron motions. That is, they considered the coupling of the local defect to a phonon mode:

$$H_{\text{coup}} = H_{\text{d}} + H_{\text{nd}} + H_{\text{int}} \tag{6.102}$$

$$H_{\text{d}} = \sum_{n,q} \sum_{\alpha=1}^{3} \hbar\omega_q g_{\alpha}^{q} \exp\left[iqR_n^0\right] a_{n\alpha}^{\dagger} a_{n\alpha} (b_q^{\dagger} + b_{-q}) \tag{6.103}$$

$$H_{\text{nd}} = \sum_{n,q} \hbar\omega_q \Lambda_0^q \exp\left[iqR_n^0\right] (a_{n0}^{\dagger} a_{n+1,0} + \text{c.c.})(b_q^{\dagger} + b_q) \tag{6.104}$$

$$H_{\text{int}} = \sum_{n,q} \hbar\omega_q \hat{g}^q \exp\left[iqR_n^0\right] (a_{n0}^{\dagger} a_{n1} + a_{n0}^{\dagger} a_{n2} + \text{c.c.})(b_q^{\dagger} + b_q). \tag{6.105}$$

Here g_α^q, Λ_0^q, $\hat{g}^q$ are coupling constants defining the local energy change due to phonons, the coupling of the phonons to proton–proton interaction,

and the coupling to interband transitions, respectively. The fermion operator $a^{\dagger}_{n\alpha}$ creates a proton in energy state $|\alpha\rangle$ at site n, while the boson operator $b^{\dagger}_{q}$ creates a phonon of wave vector q. There are several points of interest about the form chosen for H_{coup}. Firstly, while this form explicitly includes a sum over all lattice vibrations in actual calculation, only one vibrational mode was chosen for the coupling. This is an unnecessary simplification, and its use severely restricts the quantitative application of the FHS treatment. While it is true that a normal mode (say the O–O stretch, or the OH bend or the "wagging" vibrations) will couple more strongly to the proton motion than will the other modes, it is nevertheless so that other modes will couple, and that several dynamic consequences, such as Fermi resonance or increased density of states, can result from these weaker couplings*. Secondly, the interband coupling H_{int} was included. This does not occur in most treatments of the polaron problem, including Fröhlich's pioneer work. It leads to virtual transitions, and to phonon-assisted subpeaks in the absorption spectrum, but has not been studied extensively. Thirdly, there is the question of the identification of the mode q and of the evaluation of the coupling constants.

The identification of the mode q is a very tricky matter. In Fröhlich's original work, only acoustic modes were considered, and, in one dimension, there is then only one phonon branch, and this branch is to be identified with the $b^{\dagger}_{q}$. For a crystal made up of several kinds of atoms, such as ice, there are several modes, both optical and acoustic, which can couple to the proton. In the case of a localized proton (that is, in a system lacking translational invariance) such as the ice defects, the coupling should clearly be to a local mode rather than to the collective (phonon) modes of the lattice. In the case of real H-bonded crystals, the local modes can be created only by superposition of all the phonons: thus, even in the one-dimensional problem, we will have to couple the proton to all longitudinal modes at all wave vectors. If there are only two atoms (O and H) per unit cell, there are only two modes, one of which is the proton motion itself, and the FHS treatment again becomes valid: however, this is never the case in three dimensions.

* Indeed, one of the most useful advantages of the strong-coupling correlation-function approach, which is the use of a steepest-descents integration to provide an envelope of the delta function peaks (as is actually observed) works best when several modes are in fact coupled, so that the phase cancellation which underlies the steepest-descents can become large.

Thus, we again conclude that for realistic treatment of the three-dimensional problem, it will be necessary to really construct the particle picture of the defect, as FHS did, and include couplings with several modes.

The evaluation of the coupling constants q_α^q, Λ_0^q and $\hat{g}^q$ is a fairly complicated quantum chemical problem. Gosar evaluated the constant g_0^q for the local mode by a rigid-ion technique, and so did Godzik and Hofacker [1975] in a somewhat more sophisticated model. FHS found the $\hat{g}^q$ and g_0^q locally by performing SCF calculations using a Bloch representation for g_0^q and a Born–Oppenheimer expansion for $\hat{g}^q$. They found that $g_0^q(\mathrm{H}) = 3.4$; $g_0^q(\mathrm{D}) = 3.3$; $\hat{g}^q = 0.5$ and 0.6 respectively. While their values may not be very reliable due to the electronic basis set employed, as well as some assumptions on effective charges, the order of magnitude is probably correct.

Thus, the coupling is very large, and low-order perturbation theory is insufficient to describe the dynamics. Therefore, FHS used a canonical transformation (polaron picture) very similar to that of Marechal and Witkowski. The ensuing expressions for the transport coefficients involve exponential operators of the phonons, and their evaluation is a rather intricate matter. FH were interested in the protonic conductivity, which they evaluated using linear response theory. The final expression for the conductivity was evaluated using the steepest descents method, and the resultant expression qualitatively explains the defect conductivity.

Kubarev and Shedrin [1969] have given a treatment of the protonic mobility which is very similar to the FHS work, except that they ignore the interband coupling terms described by FH and Gosar [1963]. As a result they find that the overall mobility does have an activation form, but they argue that the large proton mass reduces the activation term to near-constant, so that the pre-exponential factor dominates the mobility, and therefore no important activation behavior is expected, as, in fact, none has been proven experimentally.

Fischer, Hofacker and Ratner [1969] have used the FHS method to discuss the absorption spectra of both the ice defects and general H-bonded solids. They use the same coupling terms and the canonical (dressing) transformation (for details see section 6.3.3). As a result they predict different conductivity changes, upon optical excitation of defects into the mode–mode (OH exciton) band, between ionic and orientational defects. In particular, the H_3O^+ mobility should decrease, whereas the D-mobility was to become larger. This has not yet been checked experimentally.

Other than the paper of Marechal and Witkowski, the work of Fischer, Hofacker and Ratner was the first strong-coupling approach to the spectra of associated solids, and it suffers from several oversimplifications. Firstly, only one mode was strongly coupled, thus making impossible the contribution of Fermi resonance with other lattice modes, or a fully quantitative calculation of the line width. Secondly, the q-dependence of the coupling g_q was not discussed. Fröhlich's continuum model yields a behavior $g_q \propto q^{-1}$ for small q. In a one-dimensional treatment, this gives a logarithmic divergence in the small q limit; in addition, the use of the Fröhlich form is clearly in error, since the coupling is not necessarily to a longitudinal acoustic mode, and since the one-dimensional model is in fact not a three-dimensional continuum. Dimensionality arguments would tend to favor g_q independent of q for small q, but this point is in need of clarification.

Despite these difficulties, the strong-coupling approach is as promising for H-bonded solids as the work of Witkowski, Marechal and coworkers has shown it to be for isolated dimeric systems. Indeed, it is probably even more important to use the strong-coupling (polaron) method for solids, since there is little hope for a direct model potential approach which has enjoyed some success for molecular systems; the number of states in a solid requires a treatment in terms of continuous variables (like q and k above), most conveniently handled in a quasiparticle method, which facilitates the necessary transformation and decoupling procedures. In addition it has been shown in the related problem of radiationless decay that the anharmonicity and the coupling of several modes can be treated by a finite variant of the canonical transform technique (Fischer [1972]). Clearly, this is the way to include Fermi resonance with other vibrations (Witkowski and Wojcik [1973]) into the proton–(strongly coupled)phonon system. Work is in progress on this generalization, but even on the basis of the work already done, the strong-coupling method seems promising even for two of the most celebrated and difficult of the problems of associated systems: the ferroelectrics and chromous and cobaltous acids.

6.3.2. Proton motion in ferroelectrics

The problem of H-bonded ferroelectrics, of which the best known is KH_2PO_4, has been extensively investigated, both experimentally and theoretically, in recent years, partly because of possible application as data-storage devices, partly because of general interest in the problem of

phase transitions. Slater [1941] pioneered the description of these systems. He treated the dynamics of the protons, and was able to conclude a spontaneous polarization at low temperatures. However, it soon became clear that a coupling of the protonic motion to the other vibrations of the crystal was necessary for interpreting both the phase transition and the vibrational spectrum of the ferroelectrics. The major spectroscopic work done in connection with the phase transition has been a series of Raman investigations on the oxygen–oxygen modes, since it is one of these which decreases in frequency and becomes "soft" as the transition is approached. There has also been a good deal of work on the IR spectrum; in particular, Barker and Tinkham [1963] have looked at KH_2PO_4 and KD_2PO_4 in the region 3–1500 cm^{-1}. They find an overdamped mode in KH_2PO_4 at about 50 cm^{-1} at room temperature, and they observe close similarity between the hydrogen and the deuterium crystals, which seem to weigh heavily against a tunnelling explanation of the ferroelectric mode.

The ferroelectrics are discussed at length in the contributions by Stiller, ch. 24, Schmidt, ch. 23 and Blinc, ch. 18. We simply wish to point out that the dramatic (100 K) change in critical temperature on isotopic substitution of H by D in KH_2PO_4 is firm evidence for strong coupling in these systems; Cochran [1969] has suggested that the oxygen soft mode is coupled to the protonic motion. In this way the observed correlation of the protonic disorder with the softening of the (ferroelectric) mode could be understood.

De Gennes [1963] introduced a quasi-spin formalism for calculating the collective mode behavior, but his model still contained no mode–mode coupling. The first important treatment of H-bonded ferroelectrics including strong coupling was given by Kobayashi [1968] (see also Stasyuk [1971]). For the most part, recent theoretical work on the spectroscopy of these crystals has, for temperatures above the Curie temperature, been based on anharmonic mode–mode coupling with complex frequency modes, as developed originally by Barker and Hopfield [1964] for the perovskites. The ferroelectric mode (proton) is then coupled strongly and anharmonically to a lattice mode (optical) and the resulting 2×2 matrix is diagonalized. Representative of work done in this area are papers by Scott [1968], Scott and Katiyar [1971]. Blinc and Ribaric [1963] have used an alternative coupled mode description. These treatments do describe fairly well the observed Raman line shape and lineshifts (as measured by Kaminow and Damen [1968], Wilson [1970], Wilson et al. [1971] or

She et al. [1972]). They are in error as to the predicted ferroelectric transition temperature, and leave as parameters to be fitted with the damping and coupling constants. In a typical analysis (She et al. [1972]) there are seven parameters characterizing the spectrum.

The De Gennes quasi-spin picture, which now is the most common language for describing the ferroelectric transition, takes the local protonic (one-dimensional) potential as being a symmetric double well, and considers the bare proton Hamiltonian to consist of the sum of a one-particle part, which corresponds to the tunnelling energy in the double well, and a two-particle part, which describes the dipole–dipole repulsion between neighboring sites. The dipole operator is taken as the protonic population difference between the right and left sides of the local double well (this is, again, a neglect of electrical anharmonicity). This Hamiltonian is then analyzed using the mean-field approach (a similar exposition is given by Fischer [1967], and the entire treatment is reviewed briefly by Stiller in ch. 24, and quite completely by Cochran [1969] and by Blinc and Zeks [1972]). The actual proton dynamics are rather well described by this simple picture.

On the other hand, the actual ferroelectric transition in these crystals is a displacive one, dominated by the motion of the K- and P-atoms. Since this actual lattice transition was fairly well characterized by the Slater–Takagi–De Gennes approaches, which considered only proton dynamics, and since there is such a dramatic change in critical point upon deuteration (T_c is raised by 91 K), it seems transparent, as was observed by Grindlay and Ter Haar [1959], that there is an extremely important coupling between protonic and ionic motions. This coupling was first included by Kobayashi, and his treatment characterizes quite well the phase transition, the mode softening, and the proton dynamics. The entire situation is described by Stiller in ch. 24. We wish only to make a few comments on the coupling problem.

The coupling considered by Kobayashi [1968] is the same as that considered by Gosar [1963] and by Sussmann [1964]. In the quasi-spin picture, it is essentially the linear displacement of the ionic lattice coupling with the H-bond dipole. This is clearly the mechanism for the interaction of the protonic order–disorder transition, which occurs largely in the *ab* crystal plane, and the displacive ferroelectric mode, which occurs along the 'easy' *c*-axis. On the other hand, the Kobayashi model, while very successful, does not really explain all of the interesting physics of the transition, notably the great mass effect. We would like to suggest

that this can be remedied by a treatment including not only the dipole coupling considered by Kobayashi, but also taking into account the (polaron-type) strong coupling which we have described in section 6.2. This coupling corresponds to the interaction of the lattice polarization field with the protonic density, rather than the protonic dipole, in the H-bonds. This coupling can account for the enormous sensitivity in the (effective one-dimensional proton potential to any change in the O–O distance, and describes the modification in tunnelling as the lattice vibrates. It appears that the inclusion of both this polaron-type coupling and Kobayashi's dipole coupling is necessary to provide a fully adequate model for the phase transition.

The ferroelectric situation is, clearly, immensely complicated, but the strong-coupling hypothesis, in one guise or another, has been quite successful in interpreting line shape and temperature dependence, which the uncoupled (pre-Kobayashi) treatments could not do. The plethora of parameters is annoying, but the inclusion of coupling to several lattice modes, whose coupling constants could be determined independently (by electronic calculation *à la* FHS or by lattice dynamic treatment) would probably reduce the parameter number.

6.3.3. Deuteration effects

The chromous and cobaltous acids, which have been extensively investigated by Ibers and coworkers, constitute a very special case, in which the strong coupling has pronounced effects not only on the spectral properties but also on the lattice geometry. The crystals are very poorly formed, and their investigation, in particular using diffraction techniques, is rather difficult. There are two startling effects which Ibers has noted. The first is that the IR spectra of the hydrogen and deuterium acids are quite different; the $HCrO_2$ shows a single broad absorption from 2300–700 cm^{-1}. This is split into two broad subpeaks. The low frequency lattice mode region in $HCrO_2$ contains two peaks, while it contains seven in $DCrO_2$. The overall O–H–O bond length, as determined from unit cell dimensions, increases upon deuteration from 2.49 Å to 2.56 Å. The neutron diffraction results indicate that in the deuterium system the deuterons are to one side of the O–D–O bond, while in $HCrO_2$ the location of H in the O–H–O bond remains uncertain.

Ibers explains the spectra of these systems by assuming that in the $HCrO_2$ crystal the proton sees a one-dimensional single minimum potential well, whereas in $DCrO_2$, due to the longer O–O distance, the effective

one-dimensional potential is a double well. The doublet IR peak for $DCrO_2$ is then explained as the two lowest allowed transitions ($0 \rightarrow 3$ and $1 \rightarrow 2$) in a symmetric double well. The lattice mode number changes because the selection rules for the $HCrO_2$ system refer to a system with an inversion center, which is missing in $DCrO_2$. This theoretical construction of Ibers resolves the experimental findings quite satisfactorily, and constitutes an immediate explanation for the observations, but the meaning of different potential functions for different masses is not readily clear. Ratner and Rösch [1974a] have considered these acids from the strong-coupling viewpoint, and have been able to reproduce both the experimental agreement of the Ibers method and the change in bond length using the usual strong-coupling Hamiltonian. The bond length change can be simply understood; again representing the proton displacement by q and the O–O displacement by Q, the electronic potential surface can be expanded in Taylor series as

$$V(q, Q) = \sum_{i,j} a_{ij} q^i Q^j. \tag{6.106}$$

Then the diagonal coupling constant in state $|\alpha\rangle$ is

$$g_\alpha = \langle \alpha | (\partial V(q, Q)/\partial Q)_{Q=0} | \alpha \rangle. \tag{6.107}$$

The state $|\alpha\rangle$, however, is dependent on the mass of the particle, as, therefore, is the coupling constant. If we then wish to find the change in O–O length, we must simply find the average value of Q when the proton is in state $|\alpha\rangle$, but remembering that we use the strongly coupled rather than the bare state $|\alpha\rangle$. Qualitatively, the argument is similar to one advanced long before by Rundle; that the proton sees a more anharmonic potential than the deuteron, and therefore couples more strongly. Since, in this case, strong coupling lowers bond length, the D-bond is larger than the H-bond.

The appearance of a doublet in the IR absorption spectrum of the deuterium compound is explained in the same way. The two upper states to which transition occurs will each be shifted downwards in energy by a factor $g_\alpha \Omega$ where Ω is the O–O frequency, which is about 300 cm^{-1} in these systems. Thus, if in going from H to D, the difference in the coupling constant in the two upper states changes by a factor of 0.5, it would bring the two peaks centroids together by 150 cm^{-1}, thus obliterating the splitting, due to the breadth of the two subpeaks. This is exactly what Rösch and Ratner found, using a model potential.

This unified explanation of the spectral and geometric properties of a very sensitive system seems to us to show the strong-coupling method to great advantage: the results for the spectra and the distortion are accurate, fairly easy to obtain, and simple to interpret physically. Rösch and Ratner also have investigated the general phenomenon of bond-length change upon deuteration (the so-called Ubbelohde effect), and have found, in general agreement with experiment, that the effect is largest for strong H-bonds of length near 2.50 Å such as those in $HCrO_2$. It is very much smaller, but still positive (OHO shorter than ODO) for intermediate bonds such as water, and larger but negative (OHO longer than ODO) for the bifluoride system (this last result was also found by Almlöf using a full two-dimensional treatment). The spectral changes on deuteration were not calculated by Rösch and Ratner, since satisfactory potential surfaces do not exist: this work remains to be done.

6.4. Conclusions

This article has attempted to discuss certain dynamic properties of H-bonds, in particular the IR spectrum, in terms of a strong-coupling model. The essential reasons for the presence of strong coupling in H-bonded systems are:

1) The anharmonicity in H-bonds, particularly of the $\nu_{X-H\cdots Y}$ vibration.
2) The large amplitude of hydrogenic displacement, if there is a double well potential.
3) The ratio of mass of the proton and the other nuclei, Cl, O, F, N, S.
4) The strong influence of the proton position on adjacent bonds.

This is borne out by various experimental findings, of which the most convincing are those associated with deuteration: the change in bond length and the marked spectral differences, and the huge deuteron effect in the H-bonded ferroelectrics.

The fact that there does exist strong coupling precludes simple one-dimensional potential function calculations of the dynamic (and some static) properties of H-bonded systems. This fact has become generally recognized, and two possible approaches have resulted:

1) Calculation of the vibrational eigenstates on the (many dimensional) electronic potential energy surface.
2) The canonical transformation technique applied to model systems.

The general procedure of fitting the entire potential surface by a wave

function $\psi(q, Q)$, while very successful in the simple linear three-atom system FHF (Almlöf [1972]), seems to suffer from several serious drawbacks. Firstly, there is the question of general applicability: if a larger system, such as acid dimers or, particularly, a solid is considered, the treatment clearly is impossible to carry out. Secondly, the electronic calculations which must be done are far more extensive than those needed for the (pseudo one-dimensional) strong-coupling procedure. Thirdly, the physical picture is not so readily grasped; indeed, there is, in a sense, no underlying physical picture for the motion of the proton, but only for the full vibrational dynamics of the nuclei. Finally, the interpretations of solvent and temperature effects is not transparent, as it is in the strong-coupling approach.

The strong-coupling model has been discussed at length in this article. We have attempted to show that it contains, potentially, the solution to most of the problems associated with proton dynamics in a H-bonded system. The essential idea of the strong-coupling approach is that there is an interaction between hydrogenic and heavy-atom motion, and that this interaction is too strong to be treated perturbatively. It leads to coupled motion of the hydrogenic and heavy-atom motion, which complicates the proton dynamics. On the other hand, the dominant part of the coupling can be treated exactly, by means of a canonical transformation, which corresponds to a dynamic readjustment of the heavy-atom motions as the proton is excited (spectra) or displaced (mobility). The strong-coupling method has proved very successful in the cases where it has been applied quantitatively, notably the carboxylic acid dimers and is both sufficiently general and elastic to include such other phenomena as tunnelling, Fermi resonance, and so forth. It seems the most general and applicable method for the discussion of the dynamic properties of H-bonded systems.

Note added in proof

1. (cf. section 6.2.6) – Since this paper has been written, a number of publications on the dynamical aspect of H-bonds have appeared. Novak [1974] has drawn a curve which correlates the $\nu_{X-H\cdots Y}$ mean frequency with the $X\cdots Y$ distance. If we calculate from this curve the value of the key parameter b [eq. (6.80)] we then find a value for carboxylic acid dimers which is consistent with the value determined to fit the IR spectra (figs. 6.5 and 6.6). In another paper Coulson and Robertson [1974] have definitely

ruled out the predissociation mechanism as a possible origin of the broadening of the $\nu_{X-H\cdots Y}$ band.

A new kind of dynamical effect has been measured: the ratio $P_{O-H\cdots O}/P_{O-D\cdots O}$ of the transition probabilities of the $\nu_{O-H\cdots O}$ band and of the corresponding $\nu_{O-D\cdots O}$ band is found equal to 2 in carboxylic acid dimers (Bournay and Marechal [1973, 1975]). This "anomalous" effect (the normally expected ratio is $\sqrt{2}$) is thought to be general for H-bonds and to stress the importance of electrical anharmonicity in H-bonds: it can be explained by supposing that besides the important dynamical coupling of the $\nu_{X-H\cdots Y}$ and $\nu_{X\cdots Y}$ modes presently described (mechanical anharmonicity), the electrical dipolar moment of the H-bond has also important non-linear cross terms in these two modes (Bournay and Marechal [1974]). This hypothesis seems to be corroborated by the difference between IR and Raman $\nu_{X-H\cdots Y}$ bands (Huong and Schlaak [1974]). These results indicate that the enhancement of the intensity of the $\nu_{X-H\cdots Y}$ band after the establishment of the H-bond is not only due to the peculiar electronic structure of the H-bond, but has also a vibrational or dynamical origin.

2. *(cf. section 6.3.2)* – Since this paper has been written, a publication by Godzik and Blumen [1974] appeared, which includes explicitly in a mixed mode model the coupling of the proton to the changes in O–O distance of its bond. Handling the Hamiltonian by a canonical transformation the authors are able to show that the model gives a very satisfactory description of the isotope effect on the transition temperature T_c since this coupling leads to a modification of the effective dipole–dipole interaction between different hydrogen bonds and the tunnelling frequency becomes renormalized.

References

Abragam, A., 1961, Principles of Nuclear Magnetic Resonance (Clarendon Press, Oxford).
Almenningen, A., O. Bastiansen and T. Motzfeld, 1970, Acta Chem. Scand. **24**, 747.
Almlöf, J., 1972, Chem. Phys. Letters **17**, 49; 1972, J. Mol. Struct. **14**, 427.
Anderson, G. R. and E. R. Lippincott, 1971, J. Chem. Phys. **55**, 4077.
Arnold, J. and D. J. Millen, 1965, J. Chem. Soc. 503, 509.
Asselin, M. and C. Sandorfy, 1971a, Can. J. Chem. **49**, 1539.
Asselin, M. and C. Sandorfy, 1971b, J. Mol. Struct. **8**, 145.
Asselin, M., G. Belanger and C. Sandorfy, 1969, J. Mol. Spectr. **30**, 96.
Bacon, G. E. and R. S. Pease, 1953, Proc. Roy. Soc. **A220**, 397; 1955, **A230**, 359.
Badger, R. M. and S. H. Bauer, 1937, J. Chem. Phys. **5**, 839.
Barker, A. S. and J. J. Hopfield, 1964, Phys. Rev. **135A**, 1732.

Barker, A. S. and M. Tinkham, 1963, J. Chem. Phys. **38**, 2257.
Batuev, M. I., 1949, Zhur. Khim. **23**, 1399.
Bellamy, L. J. and P. E. Rogasch, 1960, Proc. Roy. Soc. **A257**, 98.
Bellocq, A. M., Cl. Perchard, A. Novak and M. L. Josien, 1965, J. Chim. Phys. **62**, 1334.
Bertie, J. E. and D. J. Millen, 1965, J. Chem. Soc. **497**, 514.
Bjerrum, N., 1951, Kgl. Danske Videnskab. Mat. Phys. Medd. **27**, 1.
Blinc, R. and D. Hadži, 1958, Mol. Phys. **1**, 391.
Blinc, R. and H. Ribaric, 1963, Phys. Rev. **130**, 1816.
Blinc, R. and B Zeks, 1972, Adv. Phys. **21**, 693.
Born, M. and K. Huang, 1954, Dynamical Theory of Crystal Lattices (Clarendon Press, Oxford), Appendix 7.
Bournay, J. and Y. Marechal, 1971, J. Chem. Phys. **55**, 1230.
Bratož, S., 1967, Adv. Quant. Chem. **3**, 209.
Bratož, S. and D. Hadži, 1957, J. Chem. Phys. **27**, 991.
Bratož, S., D. Hadži and N. Sheppard, 1956, Spectrochim. Acta **8**, 249.
Bratož, S., J. Rios and Y. Guissani, 1970, J. Chem. Phys. **52**, 439.
Carbonell, R. G. and M. D. Kostin, 1973, Int. J. Quant. Chem. **7**, 319.
Chulanovskii, V. M. and P. D. Simova, 1949, Dokl. Akad. Nauk SSSR **68**, 1033.
Claydon, M. F. and N. Sheppard, 1969, Chem. Comm. **D23**, 1431.
Cochran, W., 1969, Adv. Phys. **18**, 157.
Collins, M. F. and B. C. Haywood, 1970, J. Chem. Phys. **52**, 5740.
Conway, B. E. and M. Salomon, 1966, in: Chemical Physics of Ionic Solutions, Eds. B. E. Conway and R. G. Barradas (Wiley, New York).
Coulson, C. A., 1959, in: Hydrogen Bonding, Eds. D. Hadži and A. W. Thomson (Pergamon, New York), p. 339.
Cummings, D. L. and J. L. Wood, 1974, J. Mol. Struct. **23**, 103.
Davydov, A. S., 1962, Theory of Molecular Excitons (McGraw-Hill, New York).
De Gennes, P. G., 1963, Solid State Comm. **1**, 132.
Delaplane, R. G., J. A. Ibers, J. R. Ferraro and J. J. Rush, 1969, J. Chem. Phys. **50**, 1920.
Devreese, J. T., Ed., 1972, Polarons in Ionic Crystals and Polar Semiconductors (North-Holland, Amsterdam).
Dreyfus, M., and A. Pullman, 1970, Theo. Chim. Acta **37**, 20.
Durocher, G. and C. Sandorfy, 1965, J. Mol. Spectroscopy **15**, 22; 1966, **20**, 262; 1967, **22**, 347.
Eigen, M. L., L. de Maeyer and H.-Ch. Spatz, 1964, Z. Elektrochem. Ber. Bunsenges. **68**, 19.
Engelhard, H., 1973, in: Physics and Chemistry of Ice, Eds. E. Whalley, S. J. Jones and L. W. Gold, Royal Soc. of Canada.
Excoffon, P. and Y. Marechal, 1972, Spectrochim. Acta **28A**, 269.
Falk, M. and T. A. Ford, 1966, Can. J. Chem. **44**, 1699.
Faure, P., 1970, J. Phys. **37**, 20.
Faure, P. and A. Kahane, 1967, J. Phys. **28**, 944.
Fischer, S. F., 1967, Int. J. of Quantum Chem. **IS**, 745.
Fischer, S. F., 1970, J. Chem. Phys. **53**, 3195.
Fischer, S. F., 1971, Chem. Phys. Letters **11**, 577.
Fischer, S. F., 1972, Chem. Phys. Lett. **17**, 25.

Fischer, S. F. and G. L. Hofacker, 1969, in: Physics of Ice, Eds. N. Riehl, B. Bullemer and H. Engelhard (Plenum Press, New York).
Fischer, S. F. and M. A. Ratner, 1972, J. Chem. Phys. **57**, 2769.
Fischer, S. F., G. L. Hofacker and J. R. Sabin, 1969, Phys. Condens. Materie **8**, 268.
Fischer, S. F., G. L. Hofacker and M. A. Ratner, 1970, J. Chem. Phys. **52**, 1934.
Foldes, A. and C. Sandorfy, 1966, J. Mol. Spectry **20**, 262.
Ford, T. A. and M. Falk, 1968, Can. J. Chem. **46**, 3579.
Fröhlich, H., 1957, Arch. Sci. (Geneva) **10**, 5.
Fukushima, K. and B. J. Zwolinski, 1969, J. Chem. Phys. **50**, 737.
Ginn, S. G. W. and J. L. Wood, 1967, J. Chem. Phys. **46**, 2735.
Godzik, K. and G. L. Hofacker, 1973, Ber. Bunsenges. **77**, 981.
Godzik, K, and G. L. Hofacker, 1975, (to be published).
Gordon, R., 1965, J. Chem. Phys. **43**, 1307.
Gosar, P., 1963, Nuovo Cimento **30**, 931.
Gosar, P. and Sang-Il Choi, 1968, in: Excitons, Magnons and Polarons in Molecular Crystals, Ed. A. B. Zahlan (Cambridge University Press).
Gränicher, H., 1963, Phys. Kondens. Materie **1**, 1.
Greinacher, E. G., W. Löttke and R. Mecke, 1955, Z. Elektrochem. **59**, 23.
Grenie, Y., J. C. Cornut and J. C. Lassegues, 1971, J. Chem. Phys. **55**, 5844.
Grindlay, J. and D. Ter Haar, 1959, Proc. Roy. Soc. **A250**, 266.
Hadži, D., 1965, Pure and Applied Chemistry **11**, 435.
Hadži, D., 1972, Chimia **26**, 7.
Hadži, D. and H. W. Thomson, Eds, 1959, in: Hydrogen Bonding (Pergamon Press, New York).
Hall, A. and J. L. Wood, 1967, Spectrochim. Acta **23A**, 1257; **23A**, 2657.
Hamilton, W. C. and J. A. Ibers, 1968, Hydrogen Bonding in Solids (Benjamin, New York).
Haurie, M. and A. Novak, 1965, J. Chim. Phys. **62**, 146; 1967, Spectrochim. Acta **21**, 1217.
Herzberg, G., 1945, Infrared and Raman Spectra of Polyatomic Molecules (Van Nostrand, New York).
Hofacker, G. L. and U. A. H. Hofacker, 1967, in: Proc. XIV-th Colloque Anpère, Ljubljana, Ed. R. Blinc (North-Holland, Amsterdam), p. 502.
Ibers, J. A., 1964, J. Chem. Phys. **41**, 25.
Ibers, J. A., 1965, Ann. Rev. Phys. Chem. **16**, 375.
Jaccard, C., 1959, Helv. Phys. Acta **32**, 89.
Janoschek, R., E. G. Weidemann, H. Pfeiffer and G. Zundel, 1972, J. Am. Chem. Soc. **94**, 2387.
Janoschek, R., E. G. Weidemann and G. Zundel, 1973, J. C. S. Faraday II, **69**, 505.
Jona, F. and G. Shirane, 1962, Ferroelectric Crystals (MacMillan, New York).
Kaminow, I. P. and T. C. Damen, 1968, Phys. Rev. Lett. **20**, 1105.
Kobayashi, K. K., 1968, J. Phys. Soc. Japan, **24**, 497.
Kollmann, P. A. and L. C. Allen, 1972, Chem. Rev. **72**, 283.
Kubarev, S. I. and M. I. Shedrin, 1969, Int. J. of Quant. Chem. **3**, 893.
Kubo, R., 1957, J. Phys. Soc. Japan **12**, 570.
Kubo, R., 1959, in: Lectures in Theoretical Physics, Vol. I, Boulder 1958, Eds. W. E. Brittin and L. G. Dunham (Interscience).

Kuper, C. G. and G. D. Whitefield, Eds., 1963, Polarons and Excitons (Oliver and Boyd, Edinburgh).
Lassegues, J. C., 1972, Thêse Université Bordeaux I.
Lautie, A. and A. Novak, 1972, J. Chem. Phys. **56**, 2479.
Lavrencie, B., I. Levstek, B. Zeks, R. Blinc and D. Hadži, 1970, Chem. Phys. Letters **5**, 441, and Ref. therein.
Leviel, J. L. and Y. Marechal, 1971, J. Chem. Phys. **54**, 1104.
Liddel, U. and J. D. Becker, 1956, J. Chem. Phys. **25**, 173.
Lippincott, E. R., 1957, J. Chem. Phys. **26**, 1678.
Lippincott, E. R. and R. Schroeder, 1956, J. Am. Chem. Soc. **78**, 5171.
Lippincott, E. R., J. N. Finch and R. Schroeder, 1959, in: Hydrogen Bonding, Eds. D. Hadži and H. W. Thomson (Pergamon, New York).
Marechal, Y., 1969, Commissariat â l'Energie Atomique, Rapport CEA R 3683.
Marechal, Y., 1972, Chem. Phys. Letters **13**, 237.
Marechal, Y., 1973, J. Phys. **B6**, L 188.
Marechal, Y. and A. Witkowski, 1967, Theor. Chim. Acta **9**, 116.
Marechal, Y. and A. Witkowski, 1968, J. Chem. Phys. **48**, 3697.
Messiah, A., 1961, Quantum Mechanics (North-Holland, Amsterdam).
Mikhailov, I. D., V. A. Savelev, N. D. Sokolov and N. G. Bokii, 1973, Phys. Stat. Sol. (b) **57**, 719.
Millen, D. J. and O. A. Samsonov, 1965, J. Chem. Soc., 3085.
Millen, D. J. and J. Zabicky, 1965, J. Chem. Soc., 3080.
Mitsui, T., Ed., 1969, Ferro- and Antiferroelectric Substances, Landolt–Bornstein Tables III, 3 (Springer, New York).
Morita, H. and S. Nagakura, 1972, J. Mol. Spectr. **41**, 54; **42**, 536.
Murthy, A. S. N. and C. N. R. Rao, 1972, J. Mol. Struct. **6**, 253.
Onsager, L., 1969, Science **166**, 3911.
Onsager, L. and M. Dupuis, 1962, in: Electrolytes (Pergamon, New York), p. 27.
Pepinsky, R., 1972, in: Physics of Electronic Ceramycs, Eds. L. L. Hench and D. B. Dove (Dekker, New York), p. 567.
Perchard, Cl., A. M. Bellocq and A. Novak, 1965, J. Chim. Phys. **62**, 1344.
Pimentel, G. C. and A. L. McClellan, 1960, The Hydrogen Bond (Freeman, San Francisco).
Pimentel, G. C. and A. L. McClellan, 1971, in: Annual Rev. of Chem. **22**, 347, Ed. H. Eyring.
Psenichnov, E. A. and N. D. Sokolov, 1961, Opt. Spektro. **11**, 16.
Ratajczak, H., W. J. Orville and J. Thomas, 1968, J. Mol. Struct. **1**, 449.
Ratner, M. A., 1969, Theses, Northwestern University, unpublished results.
Ratner, M. A. and N. Rösch, 1974a, J. Chem. Phys. **61**, 3344.
Ratner, M. A. and N. Rösch, 1974b, to be published.
Ratner, M. A. and J. R. Sabin, 1973, in: Wave Mechanics: The First Fifty Years, Eds. S. Chissick and W. C. Price (Butterworths).
Redington, R. L. and R. C. Lin, 1971, J. Chem. Phys. **54**, 4111.
Reid, C., 1959, J. Chem. Phys. **30**, 182.
Rice, S. A. and J. L. Wood, 1973, J. Chem. Soc. Faraday Trans. II **69**, 87.
Riehl, N., B. Bullemer and H. Engelhard, 1969, Physics of Ice (Plenum Press, New York).
Rösch, N., 1973, Chemical Physics, **1**, 220.
Rosenstein, R. A., 1973, Ber. Bunsenges. **77**, 494.

Sabin, J. R., 1972, J. Chem. Phys. **56**, 45.
Sandorfy, C., 1972, Can. J. of Spectroscopy **17**, 23.
Schlemper, E. L., W. C. Hamilton and S. J. La Placa, 1971, J. Chem. Phys. **54**, 3990.
Scott, J. F., 1968, Phys. Rev. Letters **21**, 907.
Scott, J. F. and R. Katiyar, 1971, Ind. J. Pure and Appl. Phys. **9**, 950.
Seszler, W. and G. Zundel, 1972, Chem. Phys. Letters **14**, 356.
Shakhparonov, M. I., 1964, Russian Journal of Physical Chemistry **38**, 137.
She, C. Y., T. W. Broberg, L. S. Wall and D. F. Edwards, 1972, Phys. Rev. **B6**, 1847.
Sheppard, N., 1959, in: Hydrogen Bonding, Eds. D. Hadži and H. W. Thomson (Pergamon, New York), p. 85.
Singh, T. R. and J. L. Wood, 1968, J. Chem. Phys. **48**, 4567.
Slater, J. C., 1941, J. Chem. Phys. **9**, 16.
Snyder, R. G. and J. A. Ibers, 1962, J. Chem. Phys. **36**, 1396.
Sokolov, N. D., 1965, Ann. Chim. (Paris) 10–487.
Somorjai, R. L. and D. F. Hornig, 1962, J. Chem. Phys. **36**, 1980.
Stasyuk I. V., 1971, Theor. Mat. Fiz. **9**, 431.
Stepanov, B. I., 1946, Nature 157, 808; 1945, Zhur. Fiz. Khim **19**, 507; 1946, Zhur. Fiz. Khim **20**, 907.
Stiller, H., 1974, ch. 24.
Sussmann, J. A., 1964, Phys. Kondens. Materie **2**, 146.
Sussmann, J. A., 1972, Mol Cryst. and Liquid Cryst. **18**, 39.
Thomas, R. K. and H. Thompson, 1970, Proc. Roy. Soc. **A316**, 303.
Thomas, R. K., 1971, Proc. Roy. Soc. **A325**, 133.
Tokonaga, M., 1966, Prog. Theor. Phys. **36**, 857.
Tokonaga, M. and T. Matsubara, 1966, Prog. Theor. Phys. **35**, 581.
Tubino, R. and G. Zerbi, 1970, J. Chem. Phys. **53**, 1428.
Ubbelohde, A. R. and K. J. Gallagher, 1955, Acta Cryst. **8**, 71.
Vinogradov, S. N. and R. H. Linnell, 1971, Hydrogen Bonding (Van Nostrand Reinhold Co).
Weisskopf, V. and E. Wigner, 1930, Z. Physik **63**, 54; **65**, 18.
Wilson, G. V. H., 1970, Solid State Comm. **8**, 125.
Wilson, G. V. H. and H. Z. Cummins, 1971, in: Light Scattering in Solids, Ed. M. Balkanski (Flammarion, Paris).
Witkowski, A., 1968, J. Chem. Phys. **47**, 3654.
Witkowski, A. and M. Wojcik, 1971, Bull. Acad. Pol. Sci. XIX, 577; 1973, J. Chem. Phys. **1**, 9.
Wolff, H. and E. Wolff, 1971, Spectrochim. Acta **27A**, 2109.
Yenger, E. A. and G. M. Barrow, 1955, J. Am. Chem. Soc. **77**, 6206.

Added in proof:

Bournay, J. and Y. Marechal, 1973, J. Chem. Phys. **59**, 5077; 1974, Chem. Phys. Letters 27, 180; 1975, Spectrochim. Acta, to be published.
Coulson, C. A. and G. N. Robertson, 1974, Proc. Roy. Soc. **A337**, 167.
Godzik, K. D. and A. Blumen, 1974, Phys. Stat. Sol. (b) **66**, 569.
Huong, P. V. and M. Schlaak, 1974, Chem. Phys. Letters **27**, 111.
Novak, A., 1974, Structure and Bonding **18**, 177.

CHAPTER 7

HYDROGEN BOND STATISTICS

J. W. PERRAM

Department of Applied Mathematics, Institute of Advanced Studies, Australian National University, P.O. Box 4, Canberra A.C.T. 2614, Australia

Contents

7.1. Introduction 361
7.1.1. General considerations 361
7.1.2. The residual entropy of ice 362
7.1.3. Speculations on the role of the hydrogen bond on the structure of water . 362
7.1.4. Hydrogen bonded ferroelectric crystals 362
7.2. The residual entropy of ice 363
7.2.1. The experiment of Giaque and Stout 363
7.2.2. The calculation of Pauling 363
7.2.3. The calculation of Nagle 365
7.2.4. Lieb's exact solution to the two-dimensional ice problem 366
7.3. Speculations on the role of the hydrogen bond in the structure of water 368
7.3.1. Four co-ordination in water 368
7.3.2. The bent bond concept 369
7.3.3. The co-operative hydrogen bond 370
7.3.4. Theories of water based on the Frank–Wen picture 370
7.3.5. Mathematical consequences of co-operative hydrogen bonding 372
7.3.6. Lattice theories of water 373
7.3.7. Recent continuum theories of water 375
7.3.8. Computer simulation of water 379
7.4. Hydrogen bonded ferroelectric crystals 382
7.4.1. Phase transitions in ferroelectric crystals 382
7.4.2. The eight-vertex problem 383
Acknowledgements 385
Note added in proof 385
References 387

The hydrogen bond – recent developments in theory and experiments
Eds. P. Schuster et al. © *North-Holland Publ. Co., Amsterdam, 1976*

7.1. Introduction

7.1.1. General considerations

In writing this review, we take as our terms of reference the statistical mechanical effects arising in a system where spatially extensive interactions of the hydrogen bonding type are possible. However, our discussion is by no means exhaustive and is indeed restricted to two main systems, where significant advances have been made in the past few years.

The first of these, namely the structure and thermodynamic properties of liquid water, has long been one of the most challenging and important problems in the field of chemical physics. The observation that the co-ordination number of water in the liquid is much lower (c.a. 4.5) than other fluids, and the possibility that the structure of the water molecule permits the formation of tetrahedral arrays of H-bonds, indicates that these highly directional forces play a key role in determining the structure of water. The change in emphasis from simple model theories to potentially less arbitrary continuum theories has altered considerably our view of the H-bond: it can be said to have lost some of the simple on–off switching character of the chemical bond with which it was formerly imbued. Recent results concerning both quantum mechanical and statistical theories are reviewed here.

The second field where some progress has been made to solving the statistical mechanical problems is the field of phase transitions in the H-bonded crystals. Here the long-range order associated with the lattice ensures that the statistical problems are rather well defined. In this situation we are dealing with H-bonds which are close to linear, so that the problems have a much simpler formulation. However, difficulties of no small mathematical complexity arise, and their resolution has provided a significant increase in the state of our knowledge of critical phenomena.

7.1.2. The residual entropy of ice

This phenomenon represents one of the few cases where statistical mechanics has been able to give a definitive explanation of an experimental observation. This observation is that ice at 0 K possesses a non-zero entropy of 0.82 cal deg^{-1} $mole^{-1}$ apparently due to the possibility of disorder in the position of the protons in the H-bonds. On the assumption that all allowable proton configurations had the same energy, Pauling [1933] estimated the value at 0.805 cal deg^{-1} $mole^{-1}$; later, Nagle [1966a] put narrow upper and lower bounds on the exact value which fell within the error estimate of the experiment. In solving the two-dimensional analogue of the ice problem, Lieb [1967a] introduced the transfer matrix technique which enabled exact solution of more complex problems in H-bond statistics.

7.1.3. Speculations on the role of the hydrogen bond on the structure of water

We review the various theoretical pictures of the H-bond prior to the direct calculation of the bond interaction by the methods of quantum mechanics. The bent bond concept of Pople [1951], the electrostatic models of Rowlinson [1951] and Bjerrum [1951], and the quasi-chemical bond ideas of Frank and Wen [1957] are compared with each other. The statistical consequences of the co-operative bonding envisaged by Frank and Wen are discussed with the conclusion that the flickering clusters that this was thought to imply, probably do not exist in water.

Various recent works on the statistical mechanics of systems acting through the electrostatic potentials, both by integral equation and computer simulation methods are reviewed. Recent extensive Hartree–Fock calculations on the potential surface for the water dimer are reviewed, as are computer simulations of the liquid using this potential.

7.1.4. Hydrogen bonded ferroelectric crystals

Certain H-bonded crystals, notably KH_2PO_4 (KDP) and $NH_4H_2PO_4$ (ADP) exhibit phase transitions resulting from ordered proton configurations. Various approximate theories (Slater [1941] and Rhys [1963]) indicated the origin of the transitions, but provided a somewhat incomplete picture as is usually the case with approximate methods in statistical mechanics (Domb [1960]). Lieb [1967b, c] solved exactly the statistical problems associated with ferroelectric and antiferroelectric behaviour in

two dimensions. These models turn out to have a much richer range of critical behaviour than hitherto exactly soluble models, such as the Ising model.

By studying a generalization of the ferroelectric models, Baxter [1972] solved the eight-vertex problem. Contrary to the law of Universality, the critical exponents, which dictate the behaviour of thermodynamic functions near the critical point, are not universal numbers, but functions of the interaction parameters. As the effective interactions in the eight-vertex model are not pairwise additive, but contain 4-body forces, it is now suspected that variations in critical indices between different systems result from non-additive intermolecular forces.

7.2. The residual entropy of ice

7.2.1. The experiment of Giaque and Stout

There are certain substances, of which water is the most common, for which the standard entropy S of the vapour at 298.1 K and 1 atm pressure, when calculated from different measurements, shows a discrepancy. Thus, when Giaque and Ashley [1933] computed this quantity, from the vibration spectrum and also from the specific heat C_p, different values of the entropy were obtained. The thermodynamic measurements (C_p) were then refined by Giaque and Stout [1936], and the difference ΔS of the spectral and thermodynamic values estimated as 0.82 ± 0.05 cal deg^{-1} mole^{-1}. The error bound indicated clearly that this was a real effect, so that some speculation on its origin then took place.

7.2.2. The calculation of Pauling

It was Pauling [1935] who pointed out that the directional nature of the H-bond in ice could give rise to residual disorder at 0 K. If a model of the crystal structure of ice is considered with all the protons removed, the lattice characteristic of diamond is obtained. Now the H-bond at low temperatures should be almost linear, i.e. the proton should lie on the O–O line. Moreover, for any bond, the proton does not lie in the symmetric position, but closer to one atom (the donor) than to the other (the acceptor) thus O–H$\cdots$O. At each vertex of the lattice, to preserve the structure of the water molecule, the oxygen atom will be acting as a proton donor in two of its bonds and a proton acceptor in the other two.

This constraint, that at each vertex, two of the O–H distances are short and two long, is the ice rule.

If we now take our proton-denuded lattice and attempt to replace the protons in accordance with the ice rule, it becomes clear that there is no unique way of doing so. Pauling set out to estimate the number of ways of arranging the protons in the crystal. Figure 7.1 shows schematically the six proton configurations at each vertex allowed by the ice rule. An outward arrow indicates proton donor behaviour and an outward one that of a proton acceptor.

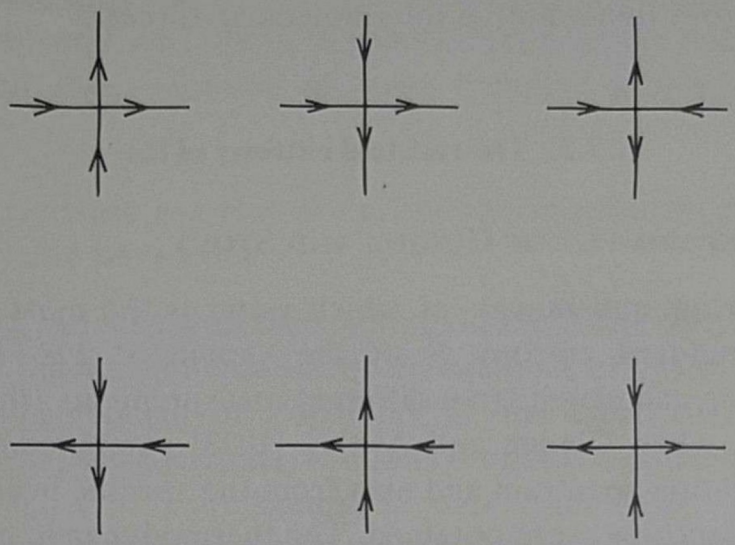

Fig. 7.1. Showing the six-vertex configurations allowed by ice rule.

If there were no constraint, the arrows on each bond could be arranged at random, in 2^{2N} ways, where N is the number of oxygens. However, at each vertex, only 6 of the 16 possible configurations are allowed (if neighbouring vertices are independent–which they are not). Thus, if we reduce the above estimate by a factor $(6/16)^N$, we obtain an estimate of W_N, the total number of configurations as

$$W_N = 2^{2N}(6/16)^N = (3/2)^N. \tag{7.1}$$

The residual entropy S^0 arising from this is $k \ln W_N$, so that for 1 mole

$$S^0 = R \ln 1.5 = 0.805 \text{ cal deg}^{-1} \text{ mole}^{-1} \tag{7.2}$$

which is within the error bound on the experimental value. As Lieb [1967a] remarks, this calculation represents one of the most successful applications of simple statistical mechanics to a real system.

7.2.3. The calculation of Nagle

There is a slight problem however. Pauling's result is not the exact answer nor do we know how accurate it is. (It is, in fact (Onsager and Dupuis [1960]) lower bound on S^0.) The calculation of narrow bounds on the exact answer was carried out by Nagle [1966a], which we now briefly describe. The six allowed configurations at vertex i are denoted ξ_i. The configurations on neighbouring vertices are either compatible or not, as shown for example in fig. 7.2. A compatibility function $A(\xi_i, \xi_j)$ is thus

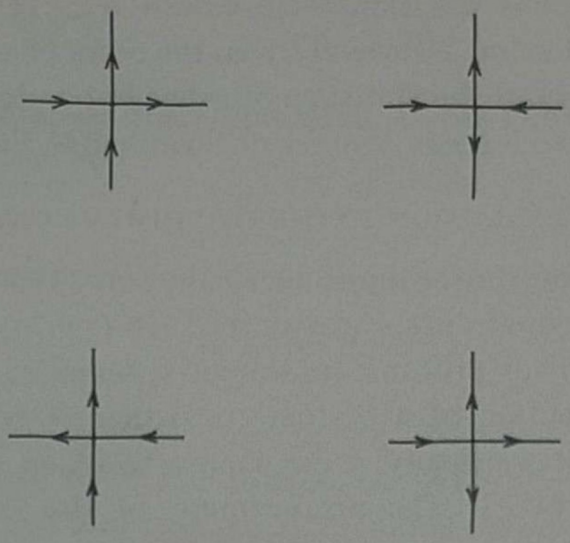

Fig. 7.2. Compatible (a) and incompatible (b) proton configurations at neighbouring vertices in ice.

defined for neighbouring vertices, with the property that it is unity if compatible and zero if not. Then W_N is given by

$$W_N = \sum_{[\xi]} \prod_{i<j}^{n \cdot n} A(\xi_i, \xi_j) \tag{7.3}$$

where the product is over all nearest neighbour pairs and the sum over all permissible vertex configurations. It is convenient to define a new function $a(\xi_i, \xi_j)$ by

$$a(\xi_i, \xi_j) = 2A(\xi_i, \xi_j) - 1 \tag{7.4}$$

so that a takes values ± 1. Nagle then wrote (7.3) as

$$W_N = (3/2)^N \sum_{[\xi]} \prod_{i<j}^{n \cdot n} 6^{-1/2}[1 + a(\xi_i, \xi_j)]. \tag{7.5}$$

By expanding the product and carrying out the sums, Nagle then generates a series for W_N, which is then extrapolated to give upper and lower bounds for $W = (W_N)^{1/N}$. He studied three different models for ice, cubic ice, hexagonal ice and square ice, the latter being in two dimensions. For real ice, he found

$$W = 1.50685 \pm 0.00015, \qquad S^0 = 0.845 \pm 0.0002$$

and for square ice

$$W = 1.540 \pm 0.001.$$

The result for real ice is remarkably close both to the result of Pauling and to the experimental value. However, from the point of view of providing a stimulus to the study of the statistics of other H-bonded crystal systems, the result for square ice has proved of inestimable value.

7.2.4. Lieb's exact solution to the two-dimensional ice problem

The statistical problem posed and numerically solved by Nagle [1966a] was attacked in a somewhat different way by Lieb [1967a]. He considered a typical arrangement of protons, as shown schematically in fig. 7.3, this diagram being a section of a system consisting of N water molecules horizontally and M vertically, wound on a torus so that row $N+1$ is co-incident with row 1. The arrangement of the N vertical arrows

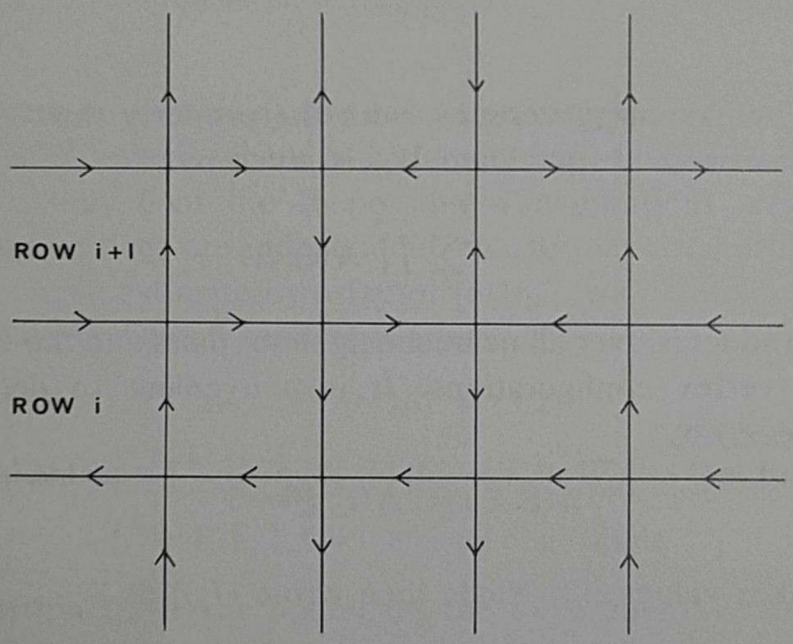

Fig. 7.3. Showing a typical configuration of protons on neighbouring rows used in the construction of the transfer matrix.

immediately above row i can be specified by an N-vector ϕ_i with 2^N possibilities. Consider also the corresponding vector ϕ_{i+1} for the next row of vertical bonds and let $A(\phi_i, \phi_{i+1})$ be the number of ways of arranging the intervening horizontal bonds consistent with the ice rule. Then the total number W_N of arranging the arrows (distributing H-bonds) is

$$W_{N,M} = \sum_{\phi_1} \dots \sum_{\phi_M} A(\phi_1, \phi_2)\, A(\phi_2, \phi_3) \dots A(\phi_N, \phi_1) \tag{7.6}$$

where each sum is over the 2^N states of the ϕ-vector. We can think of $A(\phi_1, \phi_2)$ say as $2^N \times 2^N$ matrix, known as the transfer matrix, so that

$$W_{N,M} = [\mathrm{Tr}(A)]^M \tag{7.7}$$

where Tr is the standard trace operation. In the limit $N,M \to \infty$, $W_{N,M}$ is asymptotically given by

$$W_N = \Lambda^M \tag{7.8}$$

where Λ is the largest eigenvalue of the transfer matrix. Thus W is

$$W = \lim_{N \to \infty} \Lambda^{-N}. \tag{7.9}$$

Fairly simple considerations show that n, the number of up (or down) arrows is conserved from row to row, i.e. $A(\phi_1, \phi_2) = 0$ unless $n_1 = n_2$. The matrix A is thus block diagonal, breaking up into N blocks of sizes $1, \mathrm{N}, \frac{1}{2}N(N-1) \dots N, 1$, corresponding to $n = 0, 1, \dots, N$. Lieb correctly guessed that the block corresponding to $n = N/2$ (assuming N even) contained the maximum eigenvalue Λ.

It proved convenient to reformulate the 2^N-vector ϕ as follows. The function $\phi(x_1, \dots, x_n)$ denotes ϕ for n upspins if x_i, in $1 \leqslant x_1 < x_2 < \dots < x_n \leqslant N$, denote the positions of those spins. If we write for an eigenvector Ψ of A

$$\Psi = \sum_{x_1 \dots x_n} f(x_1 \dots x_n)\, \phi(x_1 \dots x_n) \tag{7.10}$$

then the equation

$$A\Psi = \Lambda\Psi \tag{7.11}$$

enables us to find the ${}^NC_n$ coefficients f. The assumption that the dependence of f on the $x_1, \dots, x_n$ is exponential (the Bethe Ansatz) then permits the solution to the problem. After solving an integral equation, Lieb [1967a] found the remarkably simple result that

$$W = (4/3)^{3/2} = 1.5396007 \dots \tag{7.12}$$

for square ice, in agreement with Nagle's [1966a] result. However, far from merely being an elegant mathematical trick, the transfer matrix method introduced enabled the solution of a whole class of problems concerning H-bonded systems which have given considerable insight both into the phase behaviour of ferroelectrics and the fundamental behaviour of matter near phase transitions and critical points, reviewed in section 7.4.

7.3. Speculations on the role of the hydrogen bond in the structure of water

7.3.1. Four co-ordination in water

A consideration of the radial distribution function for water (Morgan and Warren [1938] and Narten et al. [1967]) with that of argon (Mikolaj and Pings [1967]) show similar features. Both indicate that molecular correlations die off in a distance of a few molecular diameters, but the average co-ordination number, as measured by the area under the first peak in $g(r)$ is about twice as big (c.a. 9) for argon as for water, where the value is 4.5 at room temperature. This is puzzling, as it is thought (Barker and Henderson [1967] and Andersen et al. [1972]) that the structure of liquids is largely determined by the hard-core of the repulsion. Clearly the highly directional forces between water molecules play an important role in the structure of water.

The idea that the approximate four co-ordination and the short-range retention of ice-like order in the liquid is responsible for most of the anomalous properties of water is an old one, originating with Bernal and Fowler [1933]. It is an idea that has been taken up by many authors in the field (e.g. Pople [1951], Frank and Wen [1957], Nemethy and Scheraga [1962], Gurikov [1965], Jhon et al. [1966], Perram [1971], Bell and Lavis [1970a, b] and Weres and Rice [1972]), the principal differences betwen theories being the detailed nature of the breakdown of the long-range order.

The near tetrahedral structure of the water molecule, with its two proton donor and two proton acceptor sites for H-bonds encourages the view that the short-range attractive forces between water molecules are narrowly constrained to the four bonding directions. How narrowly, is, of course, what the controversy over water has been all about.

The obvious method to settle the question is to perform direct quantum mechanical calculations on the interaction between two or more water molecules. The early attempts at this task are reviewed by Coulson [1959], but until the arrival of high-speed digital machines, little more progress

was possible. Molecular orbital calculations on water were reported by Hankins et al. [1970] and Del Bene and Pople [1970], although both calculations focused only on the most favourable (linear) H-bond configuration. However, the situation has been recently improved by the appearance of (Popkie et al. [1973]) extensive Hartree–Fock calculations of the water–water potential function. This calculation has been further improved by the inclusion of correlation energy corrections (Kistenmacher et al. [1974]), and the potential function studied by Monte Carlo methods. We take up these advances at greater length in section 7.3.8.

7.3.2. The bent bond concept

One of the earliest attempts to come to grips with the problem of retaining near four co-ordination in water, but not the long-range order of ice, was made by Pople [1951] who introduced the idea of bent H-bonds. The idea that the lowest energy configuration involved the linear O–H---O configuration, but that other configurations where the bonds were not linear were allowed, albeit weighted by an increased energy (fig. 7.4)

$$U(\theta_1, \theta_2) = - U_H[\cos \theta_1 + \cos \theta_2] \tag{7.13}$$

where θ_1, θ_2 measure the deviations of the O–H and H--O directions from the O----O line, which was kept at a fixed separation. The radial distribution function and density were calculated, and the higher density (than ice) interpreted by the partial collapse of second neighbours into the first shell of water molecules. The dielectric constant ϵ was also calculated, and although the absolute value was low, the temperature variation, measured by $d\epsilon/dT$ was in excellent agreement with experiment. The Pople theory was virtually the only one in the next 15 years to take account of deviations from H-bond linearity explicitly, although the form (7.13) of the potential function is certainly too simple.

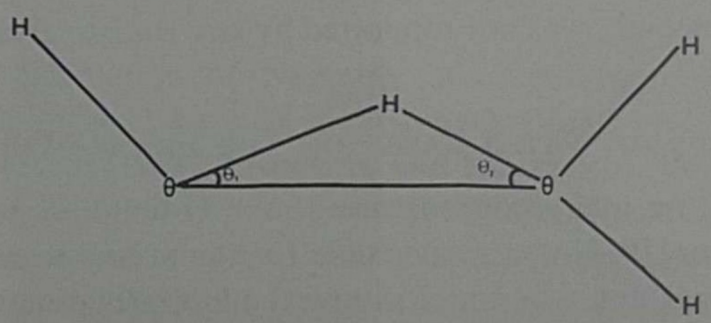

Fig. 7.4. Defining the angles θ_1 and θ_2 used by Pople to describe the energy of a bent H-bond configuration.

7.3.3. The co-operative hydrogen bond

The early valence-bond calculations of the water–water interaction (Hadži [1959]) predicted a significant contribution to the energy arising from various charge-transfer complexes. Thus, slight overlap of the proton of one molecule with the oxygen lone pair of a second would have the effect of a small transfer of electron density to the first. Frank and Wen [1957] pointed out that the first molecule could stabilise itself by acting as an electron donor for a second water molecule, to form the sequentially bonded configuration shown in fig. 7.5. This premise was later verified in the molecular orbital studies of Del Bene and Pople [1970], who showed that the bonds formed in this way were stronger than that in the water dimer. In modern statistical mechanical terms, this represents a recognition of the non-pairwise additivity (many-body nature) of the H_2O–H_2O interaction.

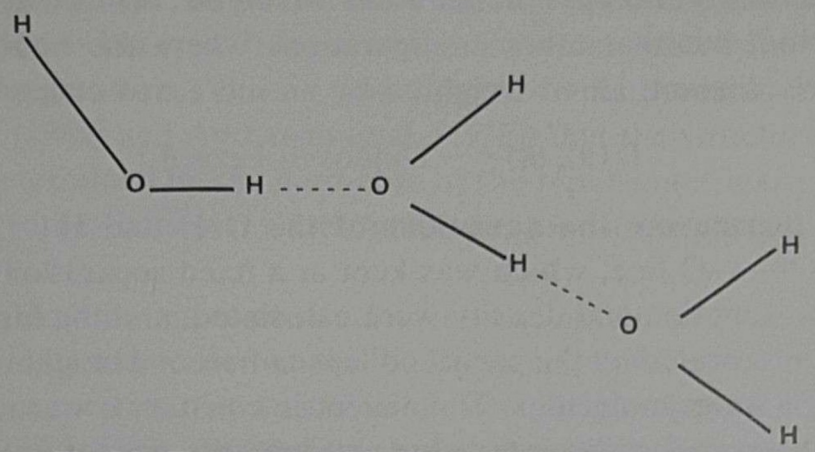

Fig. 7.5. Three sequentially H-bonded water molecules.

However, Frank and Wen pushed the concept a little further, surmising that such co-operative effects would be responsible for H-bond clustering in water, in view of exact results on the statistical mechanics of other co-operative systems (Onsager [1944] and Lee and Yang [1952]). This contention, however, was not supported by any statistical calculation (see section 7.3.5).

7.3.4. Theories of water based on the Frank–Wen picture

The idea that the many-body nature of the H-bond, as propounded by Frank and Wen [1957] was responsible for the presence of certain types of bond arrangement, was coupled with the interpretation of the infrared spectrum of water (Nemethy and Scheraga [1962] and Buijs and Choppin

[1964]) in terms of an interaction with a very sharp dependence on mutual orientation to provide an attractively simple view of the local states of association of water molecules in the liquid. Following the publication of the "significant structures" theory of Eyring et al. [1958], these two concepts were combined by many authors to construct so-called "mixture" theories of water. These theories were so-called because they view the principal contributions to the partition function, and hence the free energy, to come from a relatively small number of topologically distinct local structures.

If the water–water interaction has this quasichemical bond character, then it is meaningful to speak of the number i of H-bonds possessed by a particular molecule. In evaluating thermodynamic properties, it is necessary to perform sums over various sets $\{n_i\}$ where n_i is the number of molecules taking part in H-bonds. Those sets included in the sum are restricted to values of $\{n_i\}$ consistent with the topological structures assumed to dominate the partition function. The energy associated with a particular bond configuration $E\{n_i\}$ is then defined and the sum

$$Z_N = \sum_{(n_i)} g\{n_i\} \exp\left(-E\{n_i\}/kT\right) \tag{7.14}$$

defines the canonical configurational partition function. Here $g\{n_i\}$ is the number of arrangements of the bonds consistent with $\{n_i\}$. It is also usual to include the intramolecular partition functions f_i appropriate to a molecule with i bonds, so that (7.14) is generalized to

$$Z_N = \sum_{(n_i)} g\{n_i\} \left(\prod_{i=0}^{4} f_i^{n_i}\right) \exp\left(-E\{n_i\}/kT\right). \tag{7.15}$$

Discussions on the form of the various f_i have been given by Nemethy and Scheraga [1962], Vand and Senior [1965] and Perram and Levine [1971]. Apart from the initial choice of topological structures, the problem is reduced to the calculation of the combinatorial factor $g\{n_i\}$ and the form of $E\{n_i\}$.

The initial calculation of Nemethy and Scheraga [1962] has been commented upon elsewhere at great length (Vand and Senior [1965], Levine and Perram [1968], Eisenberg and Kauzmann [1969] and Perram [1974]), and we just note those comments here. There is disagreement over the assignment of the vibrational spectrum in the calculation of the f_i (Vand and Senior [1965]), the form of the $g\{n_i\}$ assumed was in error (Levine and Perram [1968]), the assumption that clusters were the result

of co-operative H-bonding is not supported by statistical calculations (Perram and Levine [1971]), an overabundance of adjustable parameters and the bond distributions $\{n_i\}$ at equilibrium are not consistent with molecular dynamics calculations (Rahman and Stillinger [1971]). This latter criticism applies to all such mixture theories.

Similar theories have been advanced by Vand and Senior [1965], Jhon et al. [1966] and Orentlicher and Vogelhut [1966]. On balance, in the light of subsequent developments, these theories do not provide a particularly useful or accurate picture of water, nor is any extension of them likely to.

7.3.5. Mathematical consequences of co-operative hydrogen bonding

One of the conceptual difficulties associated with the mixture theories discussed in the previous section is the assumption of favoured states of local association. This arises because once the energy $E\{n_i\}$ appropriate to a bond configuration $\{n_i\}$ is specified, these local states are determined by the principles of statistical mechanics. If $E\{n_i\}$ is a linear function of i, as assumed by Nemethy and Scheraga [1962], then there are no co-operative effects and the bond distribution is random. To include co-operative effects, it is necessary to go to more complicated functions. Unfortunately, if this is done, the statistical sums become much more difficult. However, there are two models, both in keeping with the spirit of Frank and Wen [1957] for which computations have been possible. The first is that $E\{n_i\}$ should be a quadratic function of i. This corresponds to assuming that the binding energy for a particular bond should increase with the number of other bonds formed by the two molecules participating in it (Levine and Perram [1968], Perram and Levine [1971] and Perram [1974]). Such a mechanism should favour densely bonded regions (clusters). However, it is possible to transform the statistical problem into an Ising problem (Onsager [1944]), for which certain exact results are known. The form of local order predicted is not consistent with flickering clusters.

A second model, based on the valence bond ideas of Frank and Wen [1957], infers that molecules forming even numbers of bonds should be favoured (this is partially confirmed by the molecular orbital calculations of Del Bene and Pople [1970]). It is also possible (Perram and Levine [1971]) to transform this to an Ising problem, with the same conclusions. The type of local ordering implied by these models is an extensive, disordered bond-structure, interrupted by small regions of less dense

bonding, the exact opposite to the flickering cluster hypothesis. These conclusions have been made the basis of the more successful lattice models reviewed in the next section.

7.3.6. Lattice theories of water

In more recent times, the concept that the anomalies in water arise from the disorder introduced into ice as molecules leave sites on the ice lattice and migrate into the interstices has been elaborated. Perram [1971] and Bell and Lavis [1970a] have considered the statistical mechanics of such systems and examined their predictions with regard to the density maximum observed in water. We delay a more detailed consideration of the interactions in such models and describe here only the simplest possible picture, that due to Bell and Lavis [1970a]. The N molecules are distributed over the N_0 lattice and $N_0/2$ interstitial sites of a triangular lattice, shown in fig. 7.6 with $N \leqslant 3N_0/2$. A molecule on a lattice site

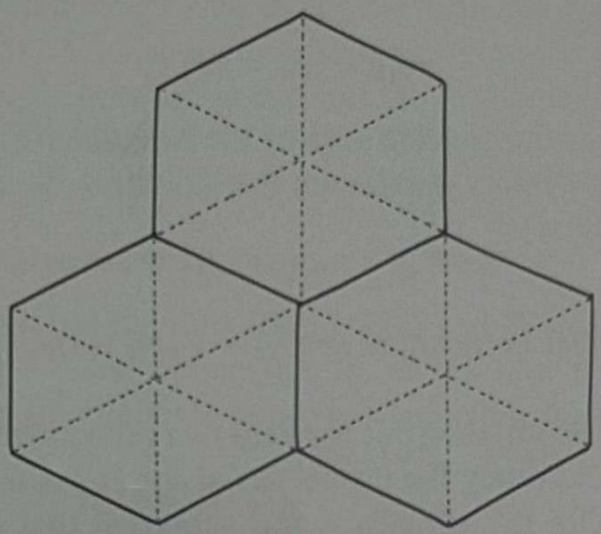

Fig. 7.6. The two-dimensional lattice model of Bell and Lavis. The heavy lines indicate bonds between lattice molecules and the dotted ones bonds between lattice and interstitial molecules.

interacts with one on a neighbouring interstitial site with energy $-\epsilon$, and with one on neighbouring lattice site with energy $-\epsilon - w$. A corresponding three-dimensional model, is shown in fig. 7.7 (Perram [1971]), where the lattice sites are the vertices of the ice I lattice, and the interstices are sites in the 12-member cage formed by 12 water molecules. With no other decorations, these models are conveniently studied in the random mixing approximation. For the two-dimensional case, it was shown (Bell and

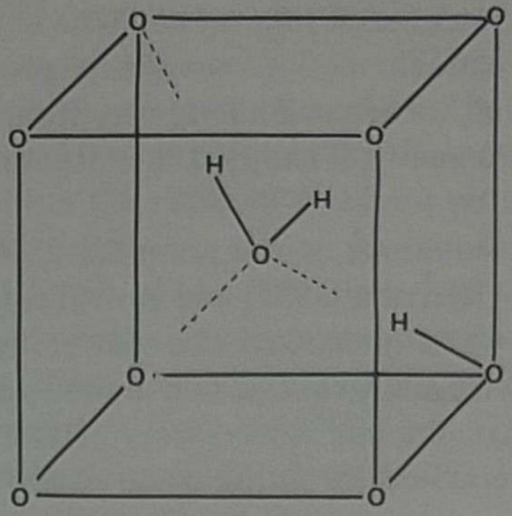

Fig. 7.8. The three-dimensional body-centred cubic model of Bell. H-bonds are formed along the diagonals and second-neighbour interactions take place along the edges.

neighbouring bonded molecules interact with energy $-w-\epsilon$ and energy $-\epsilon$ is unbonded. Bell weights close-packed molecules with an energy $\frac{1}{3}u$, which discriminates against such structures. A rather more complicated range of behaviour is now predicted, but the fundamental features are as before. A density maximum is predicted, which disappears above a characteristic pressure determined by the strength of the interactions.

7.3.7. Recent continuum theories of water

Although the structural theories (Bell [1972] and Weres and Rice [1972]) have been of some value in enabling us to see how the open structure encouraged by the directional H-bonds is responsible for such behaviour as the observed density maximum (Perram [1971, 1974]), they do not totally amount to a complete statistical theory. Such a theory should start from a given potential function

$$U(1,2) = U(r_{12}, \Omega_1, \Omega_2) \tag{7.16}$$

between molecules 1 and 2 with 3- and 4-body corrections for non-additive effects. The thermodynamic functions should then be calculated from the partition function Q_N, given by

$$Q_N = \frac{\Lambda^N}{N!} \int \ldots \int \exp\left[-\sum_{i<j} u(i,j)\right] \mathbf{d}_1 \mathbf{d}_2 \ldots \mathbf{d}_N \tag{7.17}$$

where Λ is the momentum integral (and the internal partition function), and the integrals $\int \mathbf{d}_1$ etc. must be carried out over all orientations and positions of particle 1. The structural theories set out from the premise

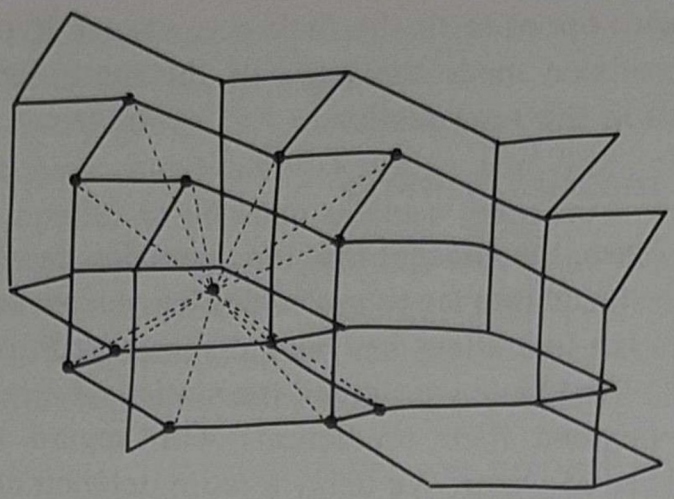

Fig. 7.7. The three-dimensional ice I model of Perram. The heavy lines indicate bonds between lattice molecules and the dotted ones interactions between lattice and interstitial molecules.

Lavis [1970a]) that if $(w - 3\epsilon)$ was positive, and the two-dimensional pressure p satisfied

$$pa_0 < \tfrac{3}{2}(w - 3\epsilon)$$

where $a_0 = A/N_0$ is the specific area of the hexagonal sublattice, then the model predicted a density maximum. For the three-dimensional case, the analogous inequality is

$$pv_0 < 2(w - 5\epsilon)$$

where $(w - 5\epsilon)$ must be positive and $v_0 = V/N_0$ is the specific volume of the ice I lattice.

Bell and Lavis [1970b] then put forward two refinements of the model to represent more accurately the properties of the H-bond potential. Firstly, they dispensed with the sublattice and supposed that a water molecule had three bonding and three non-bonding directions. They analysed the system using the quasi-chemical approximation and found results similar to those given above. Bell [1972] has also recently extended the above considerations to a three-dimensional model. Molecules which exhibit directional interactions are distributed about the vertices of a body-centred cubic lattice, of the type shown in fig. 7.8. Such a lattice is typical of ice I(c) or ice VII, as given by Fletcher [1971]. This is a novel feature, as most other structural models of water involve ice I structures (Nemethy and Scheraga [1962] and Gurikov [1965]). The b.c.c. lattice allows the possibility of ordered open, intermediate and close-packed structures, with fractions $\frac{1}{2}$, $\frac{3}{4}$ and 1 of sites occupied respectively. As before, a pair of

that the form of the potential (7.16), if it could be determined, is such that the co-ordination assumed in the theories is produced. It should be stressed, however, that we are still a long way from carrying out the task dictated by eqs. (7.16) and (7.17) so that the structural theories still have much to contribute.

The earliest representations of the potential (7.16) were the so-called point-charge models (Bjerrum [1951] and Rowlinson [1951]) in which the interaction between water molecules was viewed as mainly electrostatic and completely pairwise additive. The two models for the charge distributions are shown in figs. 7.9 and 7.10 respectively. The various distances and charges are determined by fitting some easily measurable quantity

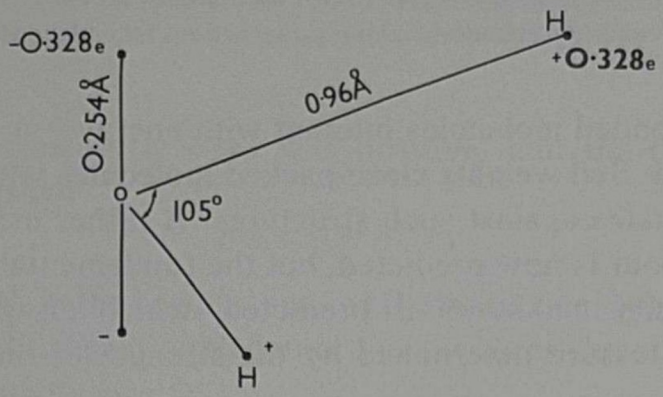

Fig. 7.9. The arrangement of the charges in the Rowlinson point-charge model of the water molecule.

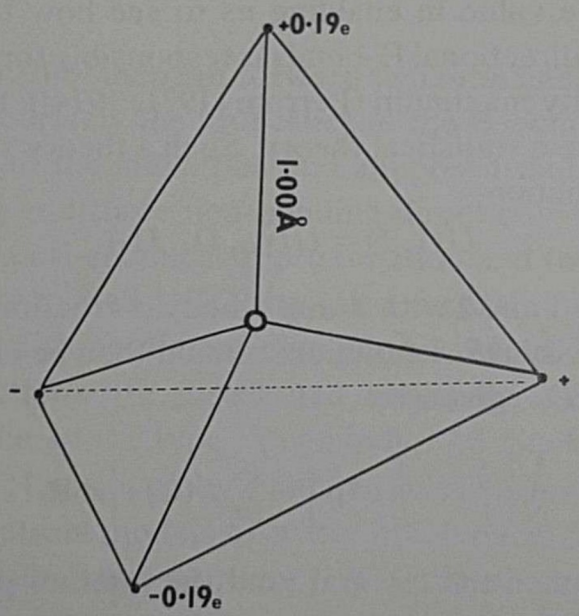

Fig. 7.10. The arrangement of charges in the modified Bjerrum (Ben-Naim–Stillinger) picture of the water molecule.

such as dipole moment (gas phase) and latent heat of sublimation. The potentials were then employed (Rowlinson [1951]) to compute the second and third virial co-efficients of steam, B_2 and B_3. The agreement with B_2 is respectable, but B_3 has the wrong sign indicating an oversimplification. It is interesting to note that the value of the third virial co-efficient will be affected by non-additive forces.

More sophisticated liquid state calculations had to await the development of techniques to handle angle-dependent potentials of the form (7.16). The first series of such calculations were by Ben-Naim [1970] and Ben-Naim and Stillinger [1971] who derived and attempted to solve the Percus–Yevick equation for a fluid of water-like particles, choosing a potential of the form

$$V(\boldsymbol{X}_1, \boldsymbol{X}_2) = V_{\mathrm{LJ}}(R_{12}) + S(R_{12}) V_{\mathrm{HB}}(\boldsymbol{X}_1, \boldsymbol{X}_2) \tag{7.18}$$

where $\boldsymbol{X}_1$ is the generalized co-ordinate of molecule 1 specifying the position and orientation of that particle. $V_{\mathrm{LJ}}(R_{12})$ is a Lennard-Jones 6 : 12 potential with parameters for Neon, which is iso-electronic with water, and V_{HB} a slight variant of the Bjerrum [1951] 4-point charge model. The function $S(R_{12})$ is a switching function to give small weight to configurations in which the two-point charges on neighbouring molecules overlap. The generalized direct correlation function $c(\boldsymbol{X}_1, \boldsymbol{X}_2)$ and total correlation function $h(\boldsymbol{X}_1, \boldsymbol{X}_2)$ are connected by the generalized Ornstein–Zernike relation

$$h(\boldsymbol{X}_1, \boldsymbol{X}_2) = c(\boldsymbol{X}_1, \boldsymbol{X}_2) + (\rho/8\pi^2) \int h(\boldsymbol{X}_1, \boldsymbol{X}_3) c(\boldsymbol{X}_3, \boldsymbol{X}_2)\, \mathrm{d}\boldsymbol{X}_3 \tag{7.19}$$

where ρ is the number density. In the usual way, h is defined in terms of $g(\boldsymbol{X}_1, \boldsymbol{X}_2)$ the pair correlation function by

$$h(\boldsymbol{X}_1, \boldsymbol{X}_2) = g(\boldsymbol{X}_1, \boldsymbol{X}_2) - 1 \tag{7.20}$$

and the function $Y(\boldsymbol{X}_1, \boldsymbol{X}_2)$ by

$$Y(\boldsymbol{X}_1, \boldsymbol{X}_2) = g(\boldsymbol{X}_1, \boldsymbol{X}_2) \exp[\beta V(\boldsymbol{X}_1, \boldsymbol{X}_2)]. \tag{7.21}$$

Then the Percus–Yevick equation is obtained by setting

$$c(\boldsymbol{X}_1, \boldsymbol{X}_2) = y(\boldsymbol{X}_1, \boldsymbol{X}_2)\{\exp[-\beta V(\boldsymbol{X}_1, \boldsymbol{X}_2)] - 1\}. \tag{7.22}$$

A further assumption was made, namely that, if Q is defined by

$$g(\boldsymbol{X}_1, \boldsymbol{X}_2) = \exp\{-\beta[V(\boldsymbol{X}_1, \boldsymbol{X}_2) + Q(\boldsymbol{X}_1, \boldsymbol{X}_2)]\} \tag{7.23}$$

then $Q(\boldsymbol{X}_1, \boldsymbol{X}_2) \equiv Q(R_{12})$, i.e. is a function of separation only.

In a later calculation, Ben-Naim [1970] considered a two-dimensional water-like system very similar to that studied by Bell and Lavis [1970a, b] but with a continuum interaction. The calculated pair correlation function had a geometrical interpretation which seems to mirror the expected short-range order in water. Ben-Naim [1970] also applied the method to a mixture of the two-dimensional water-like particles and a non-polar solute in an attempt to give a theoretical view of the hydrophobic interaction.

A method related to the Percus–Yevick equation has been of considerable value in the study of angle-dependent potentials. This is the mean spherical model (MSM) of Lebowitz and Percus [1966] which replaces the closure (7.22) by the equation

$$c(\boldsymbol{X}_1, X_2) = -\beta V(X_1, X_2). \tag{7.24}$$

In addition, it is necessary to impose a hard-sphere cutoff at some separation R, so that

$$V(\boldsymbol{X}_1, \boldsymbol{X}_2) = \infty \tag{7.25}$$

$$g(\boldsymbol{X}_1, \boldsymbol{X}_2) = 0 \tag{7.26}$$

if $R_{12} = R$. Wertheim [1971] was able to obtain the exact solution to eq. (7.19) with these conditions, for the case when the potential (7.18) is that between permanent dipoles. This solution relies on the symmetry properties of the spherical harmonics, and Blum and Torruella [1972] and Blum [1972, 1973] have generalized this to include an arbitrary number of multipoles, but no numerical calculations have as yet appeared for water-like potentials. One drawback of this equation is that although an explicit expression for the full angle-dependent pair correlation function $g(\boldsymbol{X}_1, X_2)$ is obtained, the radial distribution function

$$g(R_{12}) = \int\int g(\boldsymbol{X}_1, \boldsymbol{X}_2)\, \mathrm{d}\boldsymbol{\Omega}_1\, \mathrm{d}\boldsymbol{\Omega}_2 \tag{7.27}$$

is the radial distribution function for hard spheres. Thus it is difficult to see how the MSM will predict the loose packing characteristic of water in the liquid state. Adelman and Deutch [1973, 1974] have generalized the MSM solution to mixtures of dipoles, and to a system of equal numbers of positive and negative ions embedded in hard spheres dissolved in a system of dipoles.

There have been several perturbation theories of non-simple fluids which merit attention. The theories of Gubbins and Gray [1972] and Stell et al. [1972] make use of the cumulant expansion, reminiscent of the

Barker–Henderson [1967] theory. The thermodynamic properties and distribution functions are obtained as a series of terms involving the hierarchy of distribution functions for a suitable reference fluid, in these cases, a system of hard spheres. Numerical results have been obtained for the Stell theory and are discussed in the next section. However, $g(R_{12})$ is, like the MSM, that of the reference system.

Another approach is the expansion introduced by Perram and White [1972, 1974]. In this, the Boltzmann factor for a pair of particles is expanded as a series of spherical harmonics*

$$\exp[-\beta V(\boldsymbol{X}_1, \boldsymbol{X}_2)] = \sum_{l,l'} b_{l,l'} f_l(\Omega_1) f_{l'}(\Omega_2). \tag{7.28}$$

The $b_{l,l'}$ are functions of separation only and are readily calculated. In particular, the first term is $b_{0,0}(R_{12})$ and is independent of angles, giving rise to an effective angle-independent potential $\bar{u}(R_{12})$ which is included in the reference system. Thus for the case when dipoles or whatever are embedded in hard spheres, $g(R_{12})$ is not that of the hard-sphere system. For the case of two-dimensional dipoles embedded in hard discs, the radial distribution function is in good agreement with Monte Carlo calculations (Perram and White [1974]).

Some recent work has gone into the determination of potential functions for the water dimer. The earlier quantum mechanical calculations of Del Bene and Pople [1970] and Hankins et al. [1970] had looked only at linear H-bonds, although the interaction of several particles was considered. Recently, however (Popkie et al. [1973], Kistenmacher et al. [1974] and Watts [1974]) extensive Hartree–Fock determinations of the potential energy surface of a water dimer have become available. In the later paper (Kistenmacher et al. [1974]), correlation energy corrections have been included. The potential surfaces calculated in this way have been compared with the Bjerrum [1951] and Rowlinson [1951] point-charge models, and would seem to be more consistent with the former. Kistenmacher et al. [1974] have also reported Monte Carlo simulations of a system acting through the Hartree–Fock potential, and these are reviewed in section 7.3.8.

7.3.8. Computer simulation of water

With the advent of high-speed digital computers, direct calculation of the multi-dimensional integral has become possible, and is now one of our

* Or Wigner functions if the molecule has no axis of symmetry.

most powerful techniques for evaluating liquid structure. A system of between 30 and 500 particles is placed in a "box" of suitable dimensions in the computer memory. "Suitable dimensions" implies that the mean free path at that density is small compared to the length of the box. Periodic boundary conditions are then imposed and the direct calculation of the integrals commenced.

Two methods are available for the generation of configurations. The Monte Carlo technique relies on the fact that the Boltzmann factor, suitably normalized, is the probability measure of a Markov chain. Thus "moves" are generated using a random number generator, a move being accepted or rejected on some energetic or geometric condition. Usually 10^5 to 10^6 moves are required for a calculation. The molecular dynamics method generates configurations by stepwise numerical integration of the equations of motion. This method has the advantage of actually following the movement of the particles, and so enables calculation of transport as well as equilibrium properties. Both methods have the disadvantage that for angle-dependent potentials, they consume a large amount of computer time.

The first computer simulation of a water-like potential was done by Barker and Watts [1969] using the Monte Carlo method for 64 particles interacting via the Rowlinson potential. This was followed by the much more extensive molecular dynamics study of Rahman and Stillinger [1971] on 216 particles interacting through the modified Bjerrum potential (7.18). Because of the computer time involved, extensive tabulation of thermodynamic functions was not possible, although both works reported reasonably good values of specific heat. The really interesting feature of both studies was the observation of low co-ordination numbers and the open structure characteristic of water. However, none of the characteristic local structures of the mixture models was observed, although there are conceptual difficulties of defining what constitutes a H-bond in a continuum picture.

However, difficulties arise in the simulation of water, or other systems with long-range dipolar forces, from one of the more technical features of the simulation methods, namely the requirement to truncate the potential beyond some finite distance (usually half the box size). Barker and Watts [1973] indicated the difficulties arising from the finite sample size in predicting the dielectric constant. The dipole–dipole correlation function $g_\mu(R)$, defined by

$$g_\mu(R) = \langle \boldsymbol{\mu}(0) \cdot \boldsymbol{\mu}(R, R + \mathrm{d}R) \rangle / (2\pi\rho\mu^2 R^2 \mathrm{d}R) \qquad (7.29)$$

measures the average correlation between a dipole $\boldsymbol{\mu}(0)$ at the origin and one in a spherical shell of thickness $\mathrm{d}R$ a distance R from the origin. This quantity is a sensitive function of box size, and determines whether or not an Onsager-type correction for the finite size of the sample is considered. This last technique is unsatisfactory in that, to some extent, to calculate the dielectric constant, one has to assume a value for the quantity one is trying to find. Jansoone [1974] has attempted to get around this problem by performing the lattice sums over the array of duplicated Monte Carlo boxes, but this requires even more computer time for a given simulation.

Popkie et al. [1973] and Kistenmacher et al. [1974] have reported Monte Carlo calculations for molecules acting through the Hartree–Fock potential discussed in section 7.3.7. Good agreement with the experimental O–O, O–H and H–H distribution functions of Narten [1972] are obtained, especially in the latter study, but thermodynamic functions are not as impressive. The predicted internal energy in particular appears sensitive to the box size.

Further studies have recently been reported by Watts [1974], comparing the predictions of the Rowlinson [1951] and Ben-Naim and Stillinger [1971] (modified Bjerrum) potentials. Particular attention was paid to the influence of box size and reaction field corrections. Systems of 64 and 216 particles were considered at 25°C at the experimental density for both potentials. The Ben-Naim and Stillinger potential was studied with 500 particles. The dielectric properties predicted by both potentials are poor, and there are significant differences between distribution functions predicted for both potentials and the experimental ones. However, Watts points out that there are assumptions made in constructing the distribution functions from the X-ray scattering data, namely the use of atomic form factors, which may not be valid. Monte Carlo results on water have also been reported by Sarkisov and Dashevskii [1972].

Patey and Valleau [1973] report Monte Carlo simulations on the dipole–hard-sphere system. The results are compared to the MSM solution of Wertheim [1971] and to results obtained from a Padé approximant of the Stell et al. [1972] perturbation theory. The agreement with free energy is good in the case of the perturbation theory, but poor in the case of the MSM.

7.4. Hydrogen bonded ferroelectric crystals

7.4.1. Phase transitions in ferroelectric crystals

Apart from ice (see section 7.2), there are other bonded systems where the arrangement of bonds can give rise to interesting thermodynamic behaviour, and, in particular, phase transitions. Two of the most widely studied systems are potassium dihydrogen phosphate KH_2PO_4, (hereafter KDP) and ammonium dihydrogen phosphate $NH_4H_2PO_4$, (hereafter ADP). Both substances form H-bonded crystals of co-ordination number 4, for which the ice rule (section 7.2) applies. However, unlike ice, not all the six vertices have the same energy associated, and possibilities for long-range order, analogous to that observed for ferromagnetic materials occur.

The theoretical model for KDP was put forward by Slater [1941] who proposed vertex energies as shown in fig. 7.11. With this assignment a degenerate ordered configuration, stable at 0 K, with a permanent electric

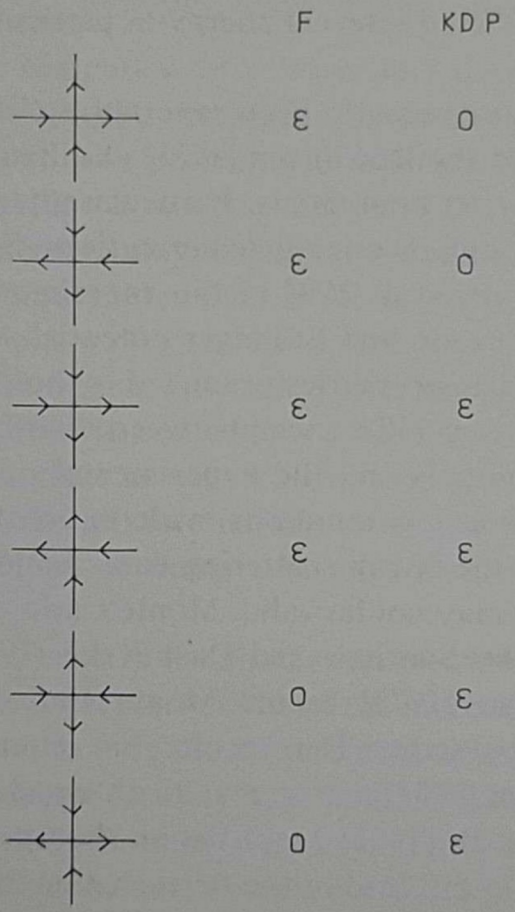

Fig. 7.11. Showing the assignments of the six-vertex energies for the F and KDP model ferroelectrics.

moment, is possible. Thus, in line with analogous considerations on ferromagnetics (Domb [1960]), an order–disorder transition in zero external field is possible. By treating the problem in mean field theory, Slater predicted a transition of first order. The actual transition is of second order however (Takagi [1948] and Nagle [1966b]).

The assignment of vertex energies appropriate to ADP was made by Rhys [1963], the so-called F-model, as shown in fig. 7.11. Here the ground states have no permanent electric moment, but, by analogy with the theory of antiferromagnetics (Domb [1960]) a transition is still possible. However, the theory of Rhys failed to predict a transition.

Nagle [1966b] constructed the series expansions for the free energy of both models, and was able to make some conclusions. He firstly demonstrated the transition in KDP, but the results for ADP were inconclusive.

Lieb [1967b, c] applied the transfer matrix technique used to solve the ice model, and was able to solve both the KDP model [1967b] and the F-model [1967c] exactly in two dimensions. In fact, both cases are included in a more general soluble problem, the six-vertex model, so called because it corresponds to the statistical problem of evaluating the free energy in the case when the six-vertex configurations allowed by the ice rule (see fig. 7.11) are given arbitrary energies. The result of these calculations shows a bewildering range of phase behaviour (Lieb and Wu [1972]). The solution to these problems represented the first qualitative advance in the theory of phase transitions since the classic work of Onsager [1944] on the Ising problem. However, the range and nature of the singularities of the ice-type models is very much richer than that for the ferromagnets.

7.4.2. The eight-vertex problem

With the solution of the six-vertex models, and the refinement of thermodynamic measurements, interest began to centre on the behaviour of thermodynamic functions near a critical point. Such functions either vanish, e.g. the surface tension, or approach infinity, e.g. specific heat, as the critical point is approached. This interest has focused not so much on the location of the critical temperature T_c, but on the form of the leading term in the expansion (Laurent series) about T_c. For instance, we expect the specific heat of a ferromagnet (or gas) to have a singularity of the form

$$C_V \sim A(T - T_c)^{-\alpha} \tag{7.30}$$

for T near T_c. Also, the difference $\Delta\rho$ between liquid and gaseous phases,

vanishes as

$$\Delta\rho \sim A'(T - T_c)^{\beta} \tag{7.31}$$

as we approach the critical point. Other exponents, such as that governing the divergence of the correlation length, and the susceptibility (in the magnetic case) may also be defined. It is possible, by making plausible assumptions about the free energy near the critical point, to derive relations between the various exponents (Widom [1965]), the so-called scaling laws.

Based on the correspondence between the lattice gas and the Ising model ferromagnet, the exponent β in eq. (7.31) should also govern the disappearance of spontaneous magnetization in a ferromagnet. Experimental studies suggest that this is indeed the case, and also that the corresponding exponents for a whole class of systems are more or less universal numbers. This observation led to the principle of Universality (Kadanoff [1967, 1972]), which may be stated (Barber [1974]) as "All phase transition problems can be divided into a small number of different classes depending on the dimensionality of the system and the symmetries of the ordered state. Within each class, all phase transitions have identical behaviour in the critical region, only the names of the thermodynamic variables are changed".

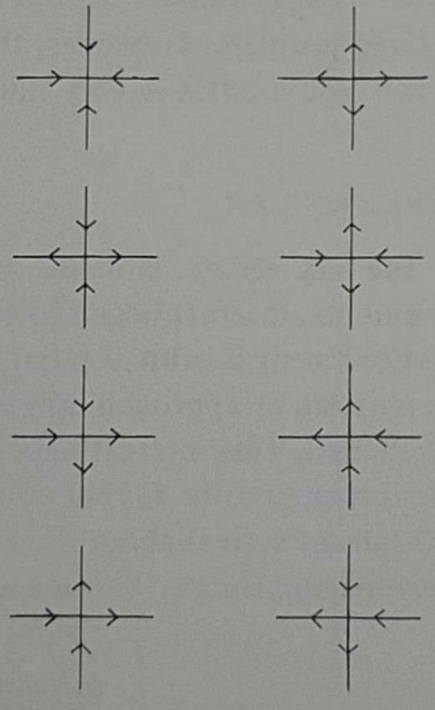

Fig. 7.12. Showing the allowed vertex configurations for the eight-vertex model.

The solution of the eight-vertex problem by Baxter [1972] thus came as somewhat of a surprise. This model supplements the six vertices permitted by the ice rule by two further ones, all eight allowed configurations being shown in fig. 7.12. The weights given the various vertices are arbitrary. The critical exponents for this model are *not* unique numbers, but rather complicated functions of the vertex energies. However, there is strong evidence (Barber and Baxter [1973]) that although the indices are continuously varying, they satisfy the thermodynamic scaling laws.

The conceptual problem posed by these exponents has been the subject of some consideration. It is possible (Wu [1971]) to case the eight-vertex problem into more familiar ferromagnetic notation. If this is done, then the interactions are not pairwise, but contain a four-body term. Under these conditions, the "symmetry of the ordered phase" is difficult to interpret. This idea of the role of three-body forces is strengthened by (Baxter and Wu [1974]) the solution to the Ising model with a three-spin interaction, which has different exponents from the standard two-dimensional Ising problem. There is, however, a growing interest in the more accurate experimental determination of critical exponents to test whether many-body forces are of any significance (see for example, preprints of the Van der Waals Centennial, Amsterdam [1973]).

Acknowledgements

The author wishes to express his gratitude to a number of people: firstly to Professors F. Kohler and P. Schuster of the University of Vienna for their hospitality during my stay there when some of the work contained herein was performed. Secondly, I am grateful to Drs. R. O. Watts, J. P. Valleau, R. J. Baxter, M. N. Barber, B. Freasier and J. N. Deutch for kindly providing details and preprints of work prior to publication.

Note added in proof

Since commencing this review, significant progress has been made in the theory of non-simple fluids, with relevance to hydrogen bonded systems. Jansoone [1974] has taken account of the corrections in computer simulations of polar fluids due to the long-range nature of the dipole–dipole potential. Smith and Perram have given improved numerical methods for the computation of the lattice sums [1975a] and a proof that the free energy of the periodic system studied in computer simulations need not be the

same as for the real system [1974]. There is evidence that these effects are non-trivial (Watts [1974]) by the observation that some of the molecular dynamics configurations obtained by Stillinger and Rahman [1974a] were ferroelectric. The failure to take proper account of the Lorentz reaction field (Smith and Perram [1975a, b]), to which the Onsager reaction field (Watts [1974]) is an approximation, may invalidate some aspects of these calculations. Similar comments apply to simulations of the hard sphere-dipole model (Patey and Valleau [1973] and McDonald [1974]). Stillinger and Rahman [1974b] have published a molecular dynamics simulation of water at high pressures.

Considerable progress has been made in the application of perturbation theory and the mean spherical model to non-simple fluids. Rushbrooke et al. [1973] and Verlet and Weis [1974] have given numerical estimates of the thermodynamic perturbation theory applied to the dipolar system. The general (unequal radii) solution of the M.S.M. for dipolar mixtures has been given by Isbister and Bearman [1974]. Smith [1974] has given the general expression for the perturbation theory of non-simple mixtures.

The perturbation theory for short range orientational forces has been intensely studied of late. Steele and Sandler [1974] have given a method for the solution of the Percus–Yevick (P.Y.) equation for systems with anisotropic exclusion forces. Similar results are obtained by applying the P.Y. approximation (Kohler and Perram [1975]) to the reference system of the orthogonal function expansion (Perram and White [1972, 1974]). Smith [1974] has related these methods to the "blip" function method (Verlet and Weis [1974] and Sung and Chandler [1972]). Freasier et al. [1975] have performed Monte Carlo calculations on dumbbells.

A very promising approach to the study of these forces has been given by Chandler and Andersen [1972] and Chandler [1973] extended by Lowden and Chandler [1973, 1974]. This, the R.I.S.M. (reference interaction site model) is a Percus–Yevick like integral equation for the correlation functions of systems composed of molecules constructed from fused hard spheres. Thus far it has been applied to N_2, CCl_4, CS_2, and CSe_2 with considerable success.

Andersen [1973, 1974] has applied cluster theory to hydrogen bonded systems. Utilizing the highly directional nature of the H-bond, many diagrams are shown to make negligible contribution. Using graph-theoretic techniques, a renormalized potential is obtained, to which more familiar techniques can be applied.

The problem of electrolytes in hydrogen bonded systems is much more

complex, but Watts et al. [1974] have made a start by performing Monte Carlo calculations of water molecules in the presence of ions (Li^+F^-) at various separations. This is undoubtedly the way in which the very obscure question of hydration and solvation will eventually be resolved.

To conclude, the study of non-simple fluids and water has now attained considerable momentum and answers to many of the basic problems of aqueous chemical physics can be expected over the next few years.

References

Adelman, S. A. and J. N. Deutch, 1973, J. Chem. Phys. **59**, 3971.
Adelman, S. A. and J. N. Deutch, 1974, J. Chem. Phys. **60**, 3935.
Andersen, H. C., D. Chandler and J. D. Weeks, 1972, J. Chem. Phys. **56**, 3812.
Barber, M. N., 1974, Lectures on Critical Phenomena, A.N.U.
Barber, M. N. and R. J. Baxter, 1973, J. Phys. **C6**, 2913.
Barker, J. A. and D. Henderson, 1967, J. Chem. Phys. **47**, 4714.
Barker, J. A. and R. O. Watts, 1969, Chem. Phys. Letters **3**, 144.
Barker, J. A. and R. O. Watts, 1973, Mol. Phys. **26**, 789.
Baxter, R. J., 1971, Phys. Rev. Letters **26**, 832.
Baxter, R. J., 1972, Ann. Phys. **70**, 193.
Baxter, R. J. and F. Y. Wu, 1974, Aust. J. Phys. **27**, 357.
Bell, G. M., 1972, J. Phys. **C5**, 889.
Bell, G. M. and D. A. Lavis, 1970a, J. Phys. **A3**, 427.
Bell, G. M. and D. A. Lavis, 1970b, J. Phys. **A3**, 568.
Ben-Naim, A., 1970, J. Chem. Phys. **52**, 5531.
Ben-Naim, A. and F. H. Stillinger, 1971, in: Structure and Processes in Water and Aqueous Solutions, Ed. R. A. Horne (Wiley, New York).
Bernal, J. D. and R. A. Fowler, 1933, J. Chem. Phys. **1**, 515.
Bjerrum, N., 1951, Kgl. Danske Videnskab Selskab, Mat.-Fis., Med. **27**, 1.
Blum, L., 1972, J. Chem. Phys. **57**, 1862.
Blum, L., 1973, J. Chem. Phys. **58**, 3295.
Blum, L. and Torruella, 1972, J. Chem. Phys. **56**, 303.
Buijs, K. and G. R. Choppin, 1964, J. Chem. Phys. **39**, 2035.
Coulson, C. A., 1959, in: Hydrogen Bonding, Ed. D. Hadži (Pergamon).
Del Bene, J. and J. A. Pople, 1970, J. Chem. Phys. **52**, 4858.
Domb, C., 1960, Adv. Phys. **9**, 149.
Eisenberg, D. and W. Kauzmann, 1969, "The Structure and Properties of Water", O.U.P.
Eyring, H., T. Ree, and N. Hirai, 1958, Proc. Natl. Acad. Sci. (U.S.) **44**, 683.
Fletcher, N. H., 1971, Rep. Prog. Phys. **34**, 913.
Frank, H. S. and W. Y. Wen, 1957, Disc. Faraday Soc. **24**, 133.
Giaque, W. F. and M. Ashley, 1933, Phys. Rev. **43**, 81.
Giaque, W. F. and J. W. Stout, 1936, J. Am. Chem. Soc. **58**, 1144.
Gubbins, K. E. and Gray, C. G., 1972, Mol. Phys. **23**, 187.
Gurikov, Yu. V., 1965, Zh. Strukt. Khimi **6**, 817.

Hankins, D., J. W. Moskowitz and F. H. Stillinger, 1970, J. Chem. Phys. **53**, 4544.
Jhon, M. S., J. Grosh, T. K. Ree and H. Eyring, 1966, J. Chem. Phys. **44**, 1465.
Kadanoff, L. P., 1972, in: Proc. 51st Enrico Fermi Summer School, Varenna, Italy, Academic Press, N.Y.
Kistenmacher, H., H. Popkie, E. Clementi and R. O. Watts, to be published.
Lee, T. D. and C. N. Yang, 1952, Phys. Rev. **87**, 404, 410.
Lebowitz, J. L. and J. K. Percus, 1966, Phys. Rev. **144**, 251.
Levine, S. and J. W. Perram, 1968, in: Hydrogen Bonded Solvent Systems, Eds. Covington and Jones, Taylor and Francis.
Lieb, E. H., 1967a, Phys. Rev. **162**, 162.
Lieb, E. H., 1967b, Phys. Rev. Letters **18**, 1046.
Lieb, E. H., 1967c, Phys. Rev. Letters **19**, 108.
Mikolaj, P. G. and C. J. Pings, 1967, J. Chem. Phys. **46**, 1601.
Morgan, J. and B. E. Warren, 1938, J. Chem. Phys. **6**, 666.
Nagle, J. F., 1966a, J. Math. Phys. **7**, 1484.
Nagle, J. F., 1966b, J. Math. Phys. **7**, 1492.
Narten, A. H., M. D. Danford and H. A. Levy, 1967, Disc. Faraday Soc. **43**, 97.
Narten, A. H., 1972, J. Chem. Phys. **56**, 5681.
Nemethy, G. and H. A. Scheraga, 1962, J. Chem. Phys. **36**, 3382.
Onsager, L., 1944, Phys. Rev. **65**, 117.
Onsager, L. and M. Dupuis, 1960, Rc. Scu. int. Fis. "Enrico Fermi" **10**, 294.
Orentlicher, N. and P. O. Vogelhut, 1966, J. Chem. Phys. **45**, 4719.
Patey, N. and J. D. Valleau, 1973, Chem. Phys. Letts. **21**, 2971.
Pauling, L., 1935, J. Am. Chem. Soc. **57**, 2680.
Perram, J. W., 1971, Mol. Phys. **22**, 1077.
Perram, J. W., 1974, Adv. Molec. Relaxation Processes. **6**, 85.
Perram, J. W. and S. Levine, 1967, Disc. Faraday Soc. **43**, 131.
Perram, J. W. and S. Levine, 1971, Mol. Phys. **21**, 101.
Perram, J. W. and L. R. White, 1974, Mol. Phys. **28**, 527.
Popkie, H., H. Kistenmacher and E. Clementi, 1973, J. Chem. Phys. **59**, 1325.
Pople, J. A., 1951, Proc. Roy. Soc. **A205**, 163.
Rahman, A. and F. H. Stillinger, 1971, J. Chem. Phys. **55**, 3336.
Rhys, F., 1963, Helv. Phys. Acta **36**, 537.
Rowlinson, J. S., 1951, Trans. Faraday Soc. **47**, 120.
Sarkisov, G. N. and Dashevskii, 1972, Zh. Strukt. Khimi, **13**, 199.
Slater, J. C., 1941, J. Chem. Phys. **9**, 16.
Stell, G., J. Rasiah and H. Narang, 1972, Molec. Phys. **23**, 393.
Takagi, Y., 1948, J. Phys. Soc. (Japan) **3**, 273.
Vand, V. and W. A. Senior, 1965, J. Chem. Phys. **43**, 1878.
Watts, R. O., 1974, Mol. Phys. **28**, 1069.
Weres, O. and S. A. Rice, 1972, J. Am. Chem. Soc. **94**, 8983.
Wertheim, M. S., 1971, J. Chem. Phys. **55**, 4291.
Widom, B., 1965, J. Chem. Phys. **43**, 3898.
Wu, F. Y., 1971, Phys. Rev. **34**, 2312.

Added in proof:

Andersen, H. C., 1973, J. Chem. Phys. **59**, 4714.
Andersen, H. C., 1974, J. Chem. Phys. **61**, 4985.
Chandler, D. and H. C. Andersen, 1972, J. Chem. Phys. **57**, 1930.
Chandler, D., 1973, J. Chem. Phys. **59**, 2742.
Freasier, B., D. Jolly and R. J. Bearman, 1975 (manuscript).
Isbister, D. and R. J. Bearman, 1974, Mol. Phys. **28**, 1297.
Jansoone, V. M., 1974, Chem. Phys. **3**, 79.
Kohler, F. and J. W. Perram, 1975 (to be published).
Lowden, L. W. and D. Chandler, 1973, J. Chem. Phys. **59**, 6587.
Lowden, L. J. and D. Chandler, 1974, J. Chem. Phys. **61**, 5228.
McDonald, I.R., 1974, J. Phys. **C7**, 1225.
Patey, G. N. and J. P. Valleau, 1973, Chem. Phys. Letts. **21**, 297.
Rushbrooke, G. S., G. Stell and J. S. Høye, 1973, Mol. Phys. **26**, 1199.
Smith, W. R., 1974, Can. J. Phys. **52**, 2022.
Smith, E. R. and J. W. Perram, 1974, Phys. Letts. **50A**, 294.
Smith, E. R. and J. W. Perram, 1975, Mol. Phys. (in press).
Smith, E. R. and J. W. Perram, 1975, J. Phys. A (submitted).
Steele, W. A. and I. Sandler, 1974, J. Chem. Phys. **61**, 1315.
Stillinger, F. H. and A. Rahman, 1973, J. Chem. Phys. **60**, 1545.
Stillinger, F. H. and A. Rahman, 1974, J. Chem. Phys. **61**, 4973.
Sung, S. and P. C. Chandler, 1972, J. Chem. Phys. **56**, 4989.
Verlet, L. and J.-J. Weis, 1974, Mol. Phys. **28**, 665.
Watts, R. O., 1974, Mol. Phys. **28**, 1069.
Watts, R. O., E. Clementi and J. Fromm, J. Chem. Phys. **61**, 2550.

SUBJECT INDEX TO VOLUMES I – III

Ab initio calculations 34 ff, 61f, 65f, 73, 75f, 94 ff, 101, 108ff, 117, 120, 147, 183, 186, 188, 191, 199, 210, 220, 379, 415, 425, 438, 517, 723 ff
  method 30 ff, 167, 175
Acceptor atom 401, 736
Acetic acid 932, 1099, 1100
  cyclic dimer 92f, 735
  trichloroacetic acid, mixed cyclic dimer 93
  trifluoroacetic acid, mixed cyclic dimer 93
Acetoaceticacidester 5
Acetone 942
  adsorbed on silica 1274, 1275, 1279
  adsorption on oxides 1274, 1275, 1279, 1344, 1349
  complexes of 119
Acetonitrile 8
  complex with hydrogenfluoride 642
Acetylacetone, enol 125, 127
Acetylene, complexes with polar molecules 94ff, 104ff
Acids 687, 689ff, 742ff, 750ff, 1414
  conductivity of solids 979ff
  conductivity of solutions 757ff
  dissociation process 753
  salt effects on polarizable H-bonds 744f
  solvate structures 689ff, 753ff
Acid salts 422, 427, 429
  of carboxylic acids 587, 597ff
Acoustic phonon branches 902
Acrolein, complexes of 145
Acridine 10
Activation energy 693, 966, 1113, 1121, 1123, 1126, 1146, 1149, 1155
  of the viscosity of H_2O 1402
Activation enthalpy 917, 972
Activation entropy 917
Activity coefficients 1227ff
  of H^+ and neutral salts 744f
  of variously deuterated methylamines and methanols in solutions with *n*-hexane 1239
Additivity, pairwise in intermolecular forces 132ff, 136, 140, 142
Adiabatic approximation 174, 180
Adiabatic photoreaction 14ff
Adsorbed molecules 1263ff
  polarizable H-bonds between 717
  tetrahydrofuran 784
  water, on zeolite 785, 786
Adsorbed water 998ff, 1303ff, 1333ff
Aggregates of molecules 1040
Aging effects 966
Alcohol spectra 1378
Alcohols 540, 942, 1070, 1092, 1093, 1096
  adsorbed on alumina 1337ff
    adsorption isotherms 1338
    autophobicity 1338, 1339
    coordinately bonded 1339, 1341
    heats of adsorption 1338, 1342
    IR fundamentals 1339ff
    NMR chemical shifts 1339
  adsorbed on oxides 1318ff, 1337ff, 1343ff
  adsorbed on silica 1318ff
    adsorption isotherms 1322
    cluster formation 1320, 1321ff
    deuterium NMR 1328
    deuterium quadrupole coupling constant 1328
    dielectric behavior 1322, 1328
    dynamic behavior 1327ff
    electrical conductivity 1328
    entropy of adsorption 1327
    equation of state 1329
    heat of adsorption 1319, 1321, 1322, 1327, 1328
    IR fundamental 1320ff
    IR overtone 1322ff
    NMR chemical shifts 1319
    NMR relaxation 1327
    proton transfer in 1328
    self association 1320
    surface diffusion 1327, 1328, 1329
Alcohols, H-bonding in 622ff

with acid IR continuum 694, 704
with base IR continuum 705
Aldehydes, adsorption on oxides 1279, 1343
Aliphatic dialcohols 542
Alkene–HI complexes 1102, 1103
Alumina
adsorption on 1329ff
hydroxyl group on 1330ff
characterization of surface 1329ff
LEED pf-surface 1332
surface structure 1329ff, 1332
Alums
methylammonium aluminum sulfate dodecahydrate, ferric ammonium sulfate dodecahydrate 1146f, 1159
Amides 85, 89, 109, 111, 632
adsorption on oxides 1349
Amines 627ff
adsorbed on oxides 1274, 1278, 1281, 1286, 1289, 1301, 1344ff, 1349
adsorbed on silica 1274, 1278, 1281, 1286, 1289
Amino acids 459ff
Ammonia 414, 932
adsorbed on alumina 1342
adsorbed on silica 1274, 1295ff
continuous absorption 717ff, 1301
dielectric behavior 1298
electrical conductivity 1299
heat of adsorption 1298
IR spectra of 1295
length changes of adsorbent 1296ff
NMR chemical shifts 1299ff
NMR relaxation time 1298ff
NMR wide line 1297
proton transfer 1299
adsorption on oxides 1274, 1295ff, 1341ff
water complex 64, 68, 89, 109, 131
dimer 92, 108
complexes of 108ff, 131, 150
Ammonium
azide 931
berylliumtetrafluoride 931
bisulfate 1146, 1159
bromide 931
cadmium sulfate 1145f
carbonate 931
chromate 932
chloride 16, 17, 40, 906
compounds 930
dichromate 931
dihydrogen arsenate 1117, 1123, 1155
dihydrogen phosphate 362, 382f, 1119, 1122, 1124f
fluoberyllate (AFE) 1145
fluoride 931
hydrogensulfate 931
hydroxide 5
iodide 901, 931
ion, complex with ammonia 120, 150, 718, 1295
nitrate 931
perchlorate 931
phosphorhexafluoride 931
Rochelle salt (ARS) 1142, 1158
silicohexafluoride 931
sulfate 908, 912, 918, 920, 926, 931, 1145, 1159
thiocyanate 931
trihydrogen periodate 1141, 1136
vanadate 932
Anatase, adsorption on 1335, 1342, 1344
Anesthetic effect 559
Angle dependence of H-bond 403ff, 528ff, 536, 545, 1081, 1087, 1095
energy 533, 536
Anharmonic coupling 213, 305, 353, 347, 315, 571, 593
Angle dependent potential 1377
Anharmonicity 570, 571, 589, 592, 614–652
constants 616, 624, 625, 633
electrical 177
mechanical 177, 204
of alcohols 622ff, 1386
oscillator
diatomic 615
triatomic 618
Aniline, adsorbed on silica 1281, 1301
Anions 1404
Anionic H-bonds 7
'Anomalous' water 1317
Anisole, adsorbed on silica 1277, 1279, 1281
Antiferroelectrics 1114ff, 1136, 1139, 1141, 1142, 1148–1155
Apparent hydration numbers per ion pair 1410

Association constants
from vapor pressure measurements 1234
of variously deuterated alcohols, amines and methanethiols in solutions with *n*-hexane 1236, 1238
Association energies from vapor pressure measurements 1235
Association equilibria 1231, 1234ff
Association models 1231, 1233, 1235, 1253
Asymmetry parameter, definition 835
Atomic
charges 73
displacements 1176, 1180, 1184, 1190
units 30
ATP hydrolysis 760f
Auto-correlation function 901
Average degree of association 1235
^{75}As quadrupole coupling and electrical field gradient (EFG) tensor
temperature dependence 865
in antiferroelectric $NH_4H_2AsO_4$ 863
in ferroelectric KH_2AsO_4 863
effect of proton ordering 864
effect of formation of clusters of polarized H-bonds 866

Badger–Bauer relationship 575
Badger–Bauer rule 543, 563, 1379
Band broadening 577ff, 637ff, 750, 1099
Band shape 577, 588
Band width 577ff, 588ff, 637ff
Band splitting pattern 577ff, 1080
Bare proton model 178
Barium chlorate hydrate 930
Barium chloride dihydrate 930
Barker method 1228
Barrier height 904, 905, 908, 918, 926
Bases 687, 693ff, 742ff, 1414
conductivity base solutions 689, 757ff
salt effects on polarizable H-bonds 744f
solvate structures 693ff, 753ff
Basis sets (in MO calculations) 31ff, 46, 56, 59ff, 63ff, 70, 106, 112f, 139, 176
Bending vibration (*see also* H-bond bending mode) 175, 594ff
Ben-Naim–Stillinger Potential 1374
Bent H-bonds 362, 369, 401ff, 466, 529ff, 1079
Benzene, adsorption on oxides 1273, 1274, 1276ff, 1286, 1291ff, 1342, 1343, 1346
Benzene, adsorption on silica 1273, 1274, 1276ff, 1286, 1291ff
dielectric behavior 1292
electronic spectra 1292
entropy of adsorption 1293ff
intramolecular vibrations 1292
NMR relaxation times 1294ff
set diffusion coefficients 1294ff
Benzene HI complexes 1102
Benzoic acids 533
Beryllium oxide, adsorption on 1343
Beryllium sulfate tetrahydrate 930
$BeHBe^+$ 182
BET monolayer 1008, 1015
Bichloride ion ($ClHCl^-$) 186, 697
Bifluoride ion, *see* Hydrogen fluoride ion
Bifurcated H-bonds 408
Bigeleisen equation 1244
Binding energy, H-bond 182
Biological membranes 558, 760
Biopolymers 759ff, 1012
Bjerrum faults 966
Boltzmann distribution 230
Bond angles in hydrates 530
Bond energy analysis (BEA) 58
Bond length 401ff, 574, 1113, 1118, 1121, 1125, 1132f, 1137, 1140
Bond orbital analysis 71
Bond polarity 77
Born approximation 1173
Born–Oppenheimer approximation 30, 168
Born–von Karman periodic boundary condition 142
Boundary structures of proton 692, 693, 706 and structure diffusion 757f
Brillouin scattering 1125, 1156, 1158
Brillouin zone 893, 909
Buckingham's theory 616
1,4-Butanediol 543
β-Naphthol 10
β-Naphthylamine 10
β-Quinol 1420

Calcium oxide, adsorption on 1343
Calcium sulfate dihydrate 930
Carbocations 131

Carbonyl groups as H-bond acceptor 417
Carboxyl group 467, 1011
Carboxylic acids 303, 307, 330, 923, 1070, 1089, 1099, 1100
  adsorption on oxides 1344, 1349
Carboxylic acid dimers 5ff, 577ff, 735, 779f
Cartesian coordinates 170
Centered H-bonds 426, 428, 503
Cesium dihydrogen arsenate 1117, 1124, 1131f, 1154–56
Cesium dihydrogen phosphate 1117, 1121
Cesium trihydrogen selenite 1121, 1136, 1139
$CsHCl_2$ 932
Change of dielectric constant by ions 1408
Channel adducts 1420
Charge transfer 73ff, 88, 92, 129
  complex 942ff
    dipole moments of 942ff
  effects 6, 9ff
  energy 40, 44, 59, 89f, 97
  model 1286ff
Chemical potentials of binary mixtures of a selfassociating compound and an inert solvent 1234
Chemical shifts 809ff, 1208ff
  ^{13}C 822, 825
  ^{19}F 809, 826
  ^{14}N and ^{15}N 823
Chloride anion, complex with water 119
Chromia, adsorption on 1345
Critical and tricritical points 1119f, 1130, 1153, 1154
Critical exponents 363, 383–385
Critical fluctuations 1115, 1119, 1121f, 1123f, 1129f, 1135, 1140, 1141, 1144, 1149, 1158, 1160
Cross-over of the vapor pressure ratios 1243
Cross section 896
Cross section for neutron scattering 894, 909, 926
Cryogenic temperatures 1067
Crystallites 1080
Crystal orbital method 142f
Clays, adsorption on 1348ff
Clathrates 964, 985ff
Cluster approximation 1128, 1131, 1140, 1157, 1158
Clusters 1393f
  in water 1053, 1393f
Coercive field 1119, 1152
Colemanite 1149, 1160
Collision complexes 573
Collisional interactions 581
Colloid effects 1404
Combination tones 583, 619, 633, 635
Combination transitions 181, 199
Complete neglect of differential overlap (CNDO) 37–40, 51ff, 70, 83, 113, 116ff, 123ff, 129ff, 135ff, 141ff, 143ff, 146f
Complexes
  free radical 819, 826
  bihalide 820
  vapor 818
  higher order 824, 826, 942, 944, 949, 952, 955
Conductivity, anomalous proton 757ff, 973ff
  salt effects on 758
Configuration interaction 33, 49f, 70, 143, 148, 182
Conformation of biopolymers 786f
Conjugate–chelate H-bonds 603ff
Consistent force field 85ff
Constant of ionization 12ff
Content
  of free OH groups 1378
  of non-H-bonded OH groups in water 1378
  of non-bonded OH groups of H_2O 1405, 1406
Continuous association 1231
Continuous IR absorption (*see* IR continuum)
Continuous rotational diffusion 914
Continuum model 1373
Continuum (*see* IR continuum)
Coordinate systems, for molecular interactions 128f
Coordination numbers 1372, 1386
Coordination number in a liquid model 1371
Coordination numbers of the first next neighbours 1374
Cooperative bonds 362–372
Cooperative effects 1335
Cooperative mechanism 553f, 1388, 1405
Copper (II) chloride dihydrate 930
Copper formate tetrahydrate 1148, 1160
Copper (II) sulfate pentahydrate 930

Correlation
energy 33, 49, 97ff
function 591, 895, 1171, 1173, 1313
Correlations 407ff, 557ff, 1209ff
between N–H-bond length and N···O distance 412
between N–H-bond length and H···O distance 412
between O–H-bond length and H···O distance 410, 411
between O–H-bond length and O···O distance 410, 411
between N–H···O angle and H···O distance 407
between O–H···O angle and H···O distance 406
bond length and wave number shifts 574
IR intensity and bond strength 576
of protons in H-bonds 248, 253, 259ff
spectroscopic shifts and enthalpy 1209ff
wave number shift and bond energy 574f
Correlation time 591
rotational 1032ff
Coulomb energy 42, 47, 52, 59, 63
Coulomb integral 37, 52f
Counterpoise method (correction of basis set error) 63
Coupled electron pair approximation (CEPA) 35, 36, 66f, 70, 148
Coupled equilibrium of cyclic dimers and trimers 534
Coupled equilibrium of different aggregates 541
Coupled mode theories: Kobayashi, etc. 1128f, 1131, 1133f, 1155f
Coupling constants 329, 345, 346
Coupling
electrical 201
mechanical 201
of vibrations and IR continuum 728, 731
Covalent energy 88
Covalent H-bond contributions 1216–1219
4-Cyanopyridine, adsorbed on silica 1282
Cycle structures 537ff, 1074ff
Cyclic aggregates of methanol, water 547
Cyclic dimers 531, 535, 550
Cyclic structures 537ff, 1074ff
Cyclohexanone oxime 535
Cyclopentanone oxime 538, 539
Curie point, T_c (ferroelectric transition temperature) 1114, 1116f, 1125, 1135–1151, 1153, 1159
Curie–Weiss law 1117, 1119, 1120, 1132, 1136, 1142–51, 1153, 1159
Coumarin dyes 16
^{13}C chemical shift tensors
for solid acetic and thioacetic acid 881
^{35}Cl quadrupole coupling
NMR frequency 854
temperature dependence 856
and the strength of the H-bond 855
theory of 855
in $NH_4H(ClCH_2COO)_2$ 856, 857
C_{2v} symmetry of liquid water 554

Damped proton motion in H-bonds 233
Debye–Hückel theory 1414
Debye–Waller factor 898
Defects in H-bonded networks 341ff, 345
Deformation modes 594ff
Delocalization energy 55, 91
Density of vibrational states 897
Desalination processes of water 1420
DNA 759ff, 1012
Deuteration 181
Deuteration shift of γ_{AH} 572, 600
Deuterated compounds 186, 205, 421ff, 690f, 696, 844, 847, 848, 850, 926, 927, 967, 1009, 1071, 1077, 1082, 1084–87, 1090, 1094, 1095, 1099, 1102, 1230, 1235–40, 1242–1244, 1251, 1254–57, 1380, 1381
Deutero-acetic acid 1099
Deutero-bifluoride ion 186
Deutero-methanol 1094, 1095
Deuteron dynamics
and the form of the potential surface 842–846
and ferroelectric phase transition 845–846
and spin lattice relaxation 847–849
Deuteron quadrupole coupling and electric field gradient tensor
theory of 838, 841, 842
proportionality of deuteron quadrupole coupling to square of OH stretching frequency 889
deuteron dynamics 843–849

in KD_2PO_4, KD_2AsO_4 and CsD_2AsO_4 844
and strength of H-bond 838–842
and the strength of the O–H···O bond 838, 840, 841
and the strength of the N–D···O bond 841
and the strength of the O–D···Cl bond 841
and the strength of the B–D···Cl bond 841
Deuteron quadrupole coupling in symmetric H-bonds 838, 842
Deuterium bonding 1227ff
Deuterium chloride 696, 1077, 1082, 1102
Deuterium cyanide 1084, 1085
D-defects 965, 966, 969
Deuterium halides 1071, 1077
Deuterium isotope shift 572, 600, 1085, 1095
Deuterium oxide 967, 1009, 1086, 1087
Deuterium sulphide 1090
Dialcohols 544
Diborane 7
Diaquahydrogen ion (*see* $H_5O_2^+$ *and* Hydronium hydrates)
Diaquaoxonium ion
structure 481, 507, 674ff
theoretical studies 520
Dielectric absorption in adsorbates 998ff, 1292, 1298, 1313, 1314, 1315ff, 1322, 1328, 1335, 1343, 1345, 1347ff
Dielectric constant in ice 1402
Dielectric constant of H_2O 1399
Dielectric dispersion 967ff
Dielectric polarization 940, 963
Dielectric relaxation 1113, 1119, 1127f, 1129f, 1134
Dielectric susceptibility 1118, 1126, 1129f, 1132, 1137, 1139, 1142–43, 1145, 1147–48, 1150–52, 1156–59
Dielectric titration 955, 956
Diethylamine $(C_2H_5)_2NH$ 1230, 1236, 1237, 1243
Diethylamine $(C_2H_5)_2ND$ 1230, 1238, 1239, 1243
Difference map 398
Diffusion 910, 912, 913
Dihydrated proton ($H_5O_2^+$) (*see* Hydronium hydrates *and* $H_5O_2^+$)
Dihydrated deuteron 203, 696
Dihydrate of polyethylene oxide derivatives 557
Diisopropyl phenol 647
Dimensions of the area of H-bonded molecules 1394f
Dimers 531ff, 537, 539, 1068, 1069, 1073–75, 1078, 1083–90, 1092, 1096, 1098, 1104
open chain 1074, 1076, 1084, 1087, 1088, 1090–92, 1095, 1096, 1098, 1099, 1104
cyclic 107, 116ff, 531ff, 1074, 1075, 1079, 1086, 1088, 1091, 1094, 1096, 1104
pseudodimers 1081
linear 107ff, 129
bifurcated 107
Dimethylamine $(CH_3)_2NH$ 627, 1230, 1236, 1237, 1243ff
Dimethylamine $(CH_3)_2ND$ 1230, 1238, 1239, 1243ff
Dimethylamine $(CD_3)_2NH$ 1230, 1236, 1237, 1243ff
Dimethylamine $(CD_3)_2ND$ 1230, 1237, 1238, 1243ff
DMSO with acid, IR continuum 694, 704, 735
Dioxane 942
Dioxane effect 940
Dipole–dipole interactions 552, 1081
Dipole energy 950
Dipole–quadrupole interactions 1081
Dipole moment 32, 33, 36, 49, 64, 65, 77, 85, 89, 98ff, 107, 139, 169, 177, 940, 942, 950, 954, 960, 962, 969
of $H_5O_2^+$ 175, 724
of hydrogen bonds 946ff
of alcohols 541
Dispersion energy 40, 44, 45, 56, 97ff
Displacive transition 113f, 1128, 1144–1145, 1150, 1160
Dissociation of acids
true degree of 689
processes with 753ff
Distance criterion for H-bonding 401f
Domain walls 1119, 1129, 1135, 1153, 1160
Dopant molecules (in matrices) 1101
Double hydrates 1419
Double minimum potential well 3, 172, 175, 196, 220f, 240, 247, 249, 261, 263, 266,

279, 288f, 291, 692ff, 917, 918, 920, 921, 923, 925, 928
and polarizability of H-bonds 706f, 722ff
Double perturbation theory 49, 56
Double scale enthalpy equation 1212, 1216
Dynamic reorientation (*see also* Molecular dynamics studies) 4
Dynamic structure factor 1176, 1189, 1190
DL-serine 462

Effective potential depth in water 1054, 1055
Effects of H-bonding on vibrational modes 568ff, 620ff, 1209ff
Eight-vertex problem 363, 383–385
Elastic incoherent neutron scattering 908, 910f, 921, 923
Electrical anharmonicity 299, 303, 315, 353, 620, 648
Electronic spectra of adsorbates 1290, 1292ff
Electrical (protonic) conductivity
proton interbond jumps 757ff, 761ff, 973ff
of adsorbates 1299ff, 1313ff, 1327, 1330, 1336, 1347ff
Electric field gradient tensor
definition 835
relation to electronic structure 835
relation to point symmetry at nuclear site 839
Electric quadrupole moment of the nucleus 834
Electrolyte solutions 1403
Electron affinity 10
Electron correlation 33, 47, 49, 70, 130, 148, 151
intramolecular 49, 64
intermolecular 64
Electron density 73, 74, 81, 82, 149, 187
Electron density difference function 73, 74
Electron exchange 41, 47
Electron excitation spectra 143ff
Electron nuclear double resonance (ENDOR) 1155, 1223
Electron hole potential theory 145
Electron pair theory 36
Electron paramagnetic resonance 1122f
Electron excited states 8ff
Electrostatic fields 179, 187
effects on H-bonds 724ff
Electrostatic H-bond contributions 1216–1219
Electrostatic energy (*see also* Coulomb energy) 42, 49, 51, 56, 59, 107, 119, 129
Electrostatic potential, molecular 81ff
Enclathration 1420
Energetically unfavoured H-bonds 1381
Energy levels 199, 249, 253ff
continuous distribution of 720ff
shifts due to electrical fields 202, 724ff
shifts due to interactions 728ff
Energy partitioning 46, 50, 52, 57ff
Energy in intramolecular H-bonds 124ff
Energy resolution 896, 898, 904, 910, 911, 916, 918, 921
Energy surface (*see also* Potential energy function) 25ff, 168, 183, 188, 199, 210, 220, 301, 379, 693, 736ff, 842ff
Entropy change at the transition 920
Entropy of adsorption 1293ff, 1305, 1315, 1327, 1343, 1345, 1348
Equilibrium constant 814, 826, 951, 1397
of ethanol aggregation 1397
of water aggregation 1397
Equilibrium geometry 28, 34, 35, 39, 40, 56, 68, 77, 82, 88, 94ff, 107, 108ff, 112, 114, 117, 120f, 125, 129ff, 140, 144, 403ff, 530ff
Ethane thiol 1097, 1098
Ethanol C_2H_5OH 926, 927, 932, 1069, 1230, 1236, 1243ff, 1378
Ethanol CH_3CD_2OH 926
Ethanol C_2H_5OD 926, 1230, 1238, 1243ff
Ethanol C_2D_5OD 1230, 1238, 1243ff
Ethanol C_2D_5OH 1230, 1236, 1243f
Ethanol CD_3CH_2OH 926
Ethers, adsorbed on silica 1277, 1279, 1281, 1291
Ether hydrogen chloride 635
Ether hydrogen fluoride 634
Ethyl alcohol (*see* Ethanol)
Ethylamine $C_2H_5NH_2$ 1230, 1236
Ethylamine $C_2H_5ND_2$ 1230, 1238
Ethylene, complexes with polar molecules 95ff, 104ff
Ethylenoxide derivatives 1404
Ethyl methylamine $CH_3C_2H_5NH$ 1230, 1236
Ethyl methylamine $CH_3C_2H_5ND$ 1230, 1238
Evans effect 592, 599, 602

Exchange energy 41, 42, 52, 59, 97
Exchange, slow and fast 1041f, 1048, 1054
Exciplexes 10
Excited states, H-bonds in 143ff
Expansion of the areas of H-bonded molecules of H_2O 1393
Expansion of H-bonded aggregates of electrolyte solutions 1407
Eyring formula 917
E and *C* parameters 1212, 1217

Fermi interaction 19
Fermi resonance 181, 201, 256, 261f, 302, 303, 325, 346, 571, 586, 590, 592, 632, 639, 643, 732
Ferroelectricity and ferroelectric substances 326, 340, 346, 382–385, 908, 920, 924, 965, 1113ff, 1178ff
and polarizability of H-bonds 748
First hydration shell 748ff, 1413
Fissure plains 1394
Five-membered rings of water 558f
Flickering clusters 370–372, 1053, 1393f
Fluctuating potential 225, 233
Fluctuation of proton 693
and $H_7O_4^-$ 753ff
and $H_9O_4^+$ 753ff
charge fluctuation forces 729
Fluorescence quenching 10
Fluoride anion
complex with water 119ff, 203
complex with monodeuterated water 205
Fluorine bridging 7
Fluorine hydroxide, complex of 108ff
Fluoro alcohols 1096
Fluoro carbon solvents 621, 628
Förster cycle 13
Force constants 33ff, 39, 66, 77, 170, 174, 178, 902, 909, 910, 943, 1080
Formaldehyde 9
complex of 108ff, 125, 127, 131, 135, 143ff
Formamide
cyclic dimer 209, 116f
hydration 85, 86, 109
linear dimer 111
two-dimensional networks 142
translatory and rotatory modes 772–774
far infrared dipole correlation function and phonon lifetimes 775
Formic acid 932, 1099
dimer (vapor)
structure 771
infrared relaxation 778–780
proton tunneling in H-bonds 779–780
cyclic dimer 116f, 150f
Fourier map 398
Franck–Condon state 13
Franck–Condon transitions 316, 338
Freon solvents 621, 628
Frequency distribution 897, 898
Frequency spectrum 893, 901, 902, 906
Frost damage 1317
Fundamental spectrum of water in solid argon 548
Fundamental stretching vibration of HOD 1381
Furan, adsorbed on silica 1277, 1281

Gas hydrates 559, 1415, 1419
Gas phase 19
H-bonding in 634ff
Gaussian approximation 915
Gaussian distribution 227
Geometrical requirements in H-bond formation 413
Geometry of water in hydrates 436
Germanium oxide, adsorption on 1342, 1343
Gibbs energy of binary mixtures from a self associating component and an inert solvent 1232
Gibbs–Helmholtz equation 1392
Glycerol 932
Glycole 548
Grotthus conductivity (*see also* Electrical (protonic) conductivity) 757ff, 979ff
salt effects on 759
Guanine–cytosine base pair 116, 118, 759f

Hall effect 997
Harmonic approximation 169, 170, 182, 205
Hartree equations 182
Hartree–Fock approximation 31, 379
Hartree–Fock limit 32, 33, 37
Hartree–Fock orbitals 33
Heat bath of harmonic oscillators 225

Heat capacity of adsorbates 1306, 1309ff, 1342, 1345
Heat content of the intermolecular degrees of freedom in a liquid 1391
Heats of adsorption 1273ff, 1285ff, 1291, 1298, 1319, 1322, 1327, 1328, 1333, 1335, 1338, 1342, 1343, 1345ff
Heats of immersion 1309, 1343, 1345, 1349
Heat of melting of H_2O, CH_3OH, C_2H_5OH 1379
Heat of sublimation of ice 1369
Heat of vaporization of H_2O, CH_3OH, C_2H_5OH 1379
Helium dimer 54
Helium, complexes with polar molecules 93ff
Hemoglobin 1015
Heptakaidecahedron cage of water molecules 1416
Hetero-associated species 1100–1102
Hetero excimer 10
Hexafluoroacetyl acetone, enol 125, 127
Hexafluoro propanol 1096
High resolution NMR in solids
  Hamiltonian 842
  experimental technique 874, 881–882
  in oxalic acid dihydrate 877
  in malonic acid 879
  proton chemical shift tensors 878
  carbon-13 chemical shift tensors 881
  chemical shift tensor and the strength of the H-bond 880
Hindered rotation 1122, 1146f, 1149, 1159
H_3O^+ (*see* Hydronium ion)
$H_3O_2^-$ (*see also* Hydroxyde hydrate) 120, 688, 693ff, 753ff
  concentration and IR continuum 742ff
$H_5O_2^+$ (*see also* Hydronium hydrates) 474f, 498ff, 667ff, 687, 689ff, 753ff
  concentration and IR continuum 742
  dipole moment 195, 250, 724
  Grotthus conductivity 757f
  polarizability 722
  potential energy surface in 194, 726
  salt effects on 744f
  SCF calculations 191ff, 723ff
  structure and spectra, solid state 474f, 498ff, 667ff
  structure diffusion 692
$H_7O_4^-$ 688, 753ff
$H_9O_4^+$ (*see also* Hydroniumtrihydrate) 510ff, 677ff, 688, 753ff
  fluctuating structure 753ff
  structure and spectra, solid state 510ff, 677ff
Hofmeister ion series 1404
Hole defects 1387
Hole-defect model 1371
Hot bands 640, 641
Hybridization of lone pairs 129
Hydrated proton (*see* Hydronium ion)
Hydrates 433, 902, 964
Hydrate structures 593, 1414
  H^+ and OH^- 491ff, 659ff, 753ff
Hydration 998ff, 1000
  and polarizability of H-bonds 748
Hydrazoic acid 1090, 1091
Hydrocarbons 85
Hydrocyanic acid (*see* Hydrogen cyanide)
H-bond
  angle 128ff, 549
  angle distribution 404
  bending mode 175, 594ff, 1074, 1076, 1084, 1086–1088, 1091, 1094, 1095, 1100, 1102
  content during ice melting 1371
  definition 3, 401
  disorder 667, 673, 674
  energies 539, 1092, 1395
  energy per OH group 1369
  geometry 401ff, 529ff
  in ice 1425ff
  infrared force constants 658
  linearity 403, 434, 529ff
  proton transfer in (*see* Proton transfer)
  polarizable (*see* Polarizable H-bonds, Polarizability of H-bonds)
  potential function (*see also* Potential energy functions) 220, 693, 736ff, 842ff, 1085
  rupture and molecular mobility 25ff
    of NH_3^+ in L-alanine 776
    of glycerol 777
  shift and anharmonicity 644
  temperature and shift 646
  and weakness of overtones 648
H-bonded crystals 395ff, 1425ff
H-bonded cyclic dimers 303, 307, 330, 531ff, 735, 1074ff

H-bonding conferences 6
Hydrogen
  cyanide 1083–1085
    complex of 108ff, 112, 135, 141
    complex with hydrogen fluoride 642
  chloride 909, 932, 1071, 1072, 1075, 1080, 1083, 1101, 1102, 1103
    complexes 107, 108, 110, 112
  difluoride anion 431, 118, 120, 183
  fluoride 932, 1071
    crystal 141ff
    dimer 27, 55, 57, 60, 61, 64–67
    molecule 35, 89
    oligomers 135f
  fluoronium cation, complex with hydrogen fluoride 121
  halides, HCl, HBr, HI 1147f, 1160, 1071, 1072, 1073, 1100, 1103
  iodide 1071, 1073, 1075, 1080, 1101–1103
  maleate anion 125, 127
  molecule, complexes with polar molecules 93ff
  peroxide, complexes of 108ff
  position from X-ray and neutron diffraction 398, 399, 400
  sulphide 1087–1090, 1103
    anion, complex with hydrogen sulfide 120
    dimer 107, 108
Hydrolysis of H_2O due to ions 749
Hydronium
  compounds 930
  hydrates (*see also* $H_5O_2^+$, $H_9O_4^+$ *and* Diaquaoxonium ion) 118ff, 150f, 190, 474f, 498ff, 659ff, 667f, 687, 689ff, 753ff
    structure and spectra (liquid state) 687, 689ff, 753ff
    structure and spectra (solid state) 474f, 498ff, 667ff
  ion (H_3O^+) 472ff, 480, 659ff, 691f
    dissociation of 148ff
    fundamental vibrational modes 665
    NMR 476, 497f
    structure and spectra (solid state) 477f, 491ff, 661ff
    theoretical studies 517f
    X-ray 485ff
  dihydrate (solid state) 507ff, 674ff
  nitrate 930
  perchlorate 903ff, 911, 915, 930
  polyhydrates 139ff, 753ff
  trihydrate (*see also* $H_9O_4^+$)
    fluctuating structure 753ff
    structure and spectra (solid state) 677ff
Hydrophobic
  forces 1418
  groups 1418
  hydration 1056
  side 1416
Hydroxide hydrates (*see also* $H_3O_2^-$ *and* $H_7O_2^-$) 120, 688, 693ff, 753ff
Hydroxide, polyhydrates 139ff, 753ff
Hydroxonium hydrate (*see* Hydronium hydrate)
Hydroxonium ion (*see* Hydronium ion)
Hydroxylamine, complexes of 108ff
Hydroxyl groups, on alumina 1328ff
Hydroxyl groups, on silica (*see* Silanol groups)
3-Hydroxy propionic aldehyde 124ff
Hyperpolarizability 193
  of $H_5O_2^+$ 725, 727
  of H-bonds 725, 727
Hysteresis 1151–1152, 1158

Ice 138, 141f, 634, 898ff, 902, 929, 964, 966ff, 1425ff
  bending vibrations 1461ff
  doped with HF 1403
  dissociation energy 1453ff
  geometries 1430ff
  nucleation of, on surfaces 1311, 1316, 1317, 1336
  OH stretching vibrations 1458ff
  residual entropy of 363, 368
  rotational vibrations 1461
  iceberg forming 1418
Iceberg structure 1418
Iceberg-like structure of water 558f
Ideal associated solutions 1229
Ideal liquid 1387
Imidazole solutions 708f
  Grotthus conductivity of semi-protonated 761ff
Imperfections 967

Improper ferroelectrics 1139–1140, 1143, 1145, 1146, 1158
Impurities 983
Incoherent scattering 893ff, 1177, 1179, 1181, 1190
Independent electron pair approximation 34–36, 66ff, 70, 98, 103, 147
Induced bands 1101, 1102
Induced dipole interactions 688, 729ff
  and IR continuum 731ff
Induced dipole moment 179, 197
Inductive effects 945
Induction effects in H-bonds 248, 252, 270, 291, 688, 729ff
  and IR continuum 731ff
Inelastic neutron scattering 18, 893ff, 1177ff
IR absorption intensities 77, 78, 80, 177, 178, 200, 256ff, 576, 648
Infrared bandshapes 314, 319, 337, 577, 583, 637ff
  of adsorbed molecules 1290
IR continuous absorption (*see* IR continuum)
IR continuum 247, 277, 281, 687ff
  a more general effect 694
  and polarizability of H-bonds 728ff
  dependence on concentration of polarizable H-bonds 742f
  $H_3O_2^-$ 693ff, 753ff
  $H_5O_2^+$ 689ff, 753ff
  $H_9O_4^+$ 753ff
  influence of temperature 693, 745ff
  non-aqueous systems 694ff
  reasons for 731f
  salt effect on 744f
  table for systems with 646–703
  wave number dependence 734ff
  with adsorbed molecules 717, 1301ff
  with asymmetrical H-bonds 718ff
  with dissolved molecules 707ff
Infrared shift techniques 1207
IR spectra 537ff, 566ff, 614ff, 684ff, 689ff, 768ff, 945, 972, 979, 1134, 1145, 1148, 1159, 1377ff
IR transitions, intensity of (*see* IR absorption intensities)
Initial proton states 227
Initial wave packet 223
Intensity of γ_{AH} (*see also* IR absorption intensities) 576
Interaction energy of water 1369
Interaction potential 1080, 1081
Interaction between H-bond protons 253ff, 272, 276f, 281ff, 290, 687f, 729f
Interaction of H-bonds with environment and IR continuum 728ff
  induced dipole 688, 729
  proton dispersion forces (*see also* Interaction between H-bond protons) 687f, 729f
Intermediate neglect of differential overlap (INDO) 37–40, 71, 83, 123ff
Intermediate scattering function 895
Intermolecular relaxation rate 1032, 1046, 1048
Internal coordinates 169, 170
Internal energies of liquid water 1369
Intramolecular degrees of freedom 224
Intramolecular H-bonds 3, 123ff, 542, 544, 603, 720, 953
  ortho-halophenols, torsional vibrations and electronegativities of halogen substituents 780f
  polarizable 720
  saccharides 781
Intramolecular relaxation rate 1031, 1047, 1050
Inverse vapor pressure isotope effect 1240ff
Iodoalkane–HI complexes 1102f
Ion exchange resins 1010
  polarizable H-bonds in 689ff
Ionization potential 10
Iron oxide, adsorption on 1336, 1345
Ising model 1131, 1148, 1152
Isomerization 220
Isomerization rates 219
Isosbestic points 140
Isotope effect 324, 333, 338, 348, 350, 420, 507, 600, 1113, 1116f, 1124, 1127, 1129, 1132, 1133, 1135–40, 1141, 1143–51, 1154, 1155, 1157, 1159
  IR continuum 690
  on γ_{AH} 572, 600
Isotopic isolation 581, 624, 635, 638

Jacobian coordinates 171
Jump diffusion 914f

Jump length 919
Jump rotation 911, 912, 916–19, 923

Kaolinite, adsorption on 1349

Lactams 531
Lactim–lactam equilibrium 12
Lagrange equations 169, 170
Laser pulses
  intensity effects 15
  ultrashort, and time resolved spectra 15
Latent heat, entropy of transition 1120, 1129, 1134f, 1137, 1141, 1145, 1147
Lattice modes of
  solid formamide 772
  solid methanol 778
  biopolymer model substances 786
$La_2Mg_3(NO_3)_{12}\cdot 24H_2O$ 930
Lead monetite 1159
Lecontite 1146, 1159
Lennard-Jones potential 86ff
Librational levels 1082
Librational mode 1076, 1085, 1088
Libration band (*see also* Torsional vibrations) 1383
Lifetimes of H-bonds 4, 1035, 1041f, 1046f, 1053, 1415
Lifetime of proton in XH group 1030, 1050, 1052, 1055
Linear combination 173
Linear enthalpy, spectroscopic shift relations 1209, 1210
Linear H-bond 403ff, 530ff, 1079, 1379
Line profile 893
Lingering times in potential wells 247, 266, 279, 285, 288f
Lippincott–Schröder model 1214
Lithium
  ammonium tartrate 1143, 1158
  chloride hydrate 930
  hydrazinium sulfate 1151
  perchlorate trihydrate 930
  sulphate hydrate 930
  thallium tartrate 1143
  trihydrogen selenite 1121, 1138, 1140, 1136
Localized molecular orbitals (LMOs) 68, 141
Lone pair electrons 5, 413
Lorentzian–Gaussian convolution 910, 911
Low temperature effects 582, 587
Lyotropic ion series 1409
L-defects 965f, 969

Manganese oxide, adsorption on 1345
Magnesium oxide, adsorption on 1342, 1343
Magnetic dipole–dipole interaction 1030
Magnetic ferroelectrics 1148, 1151
Magnetic susceptibility of H_2O 1398
Malonic dialdehyde, enol 124ff, 150, 151
Malonic acid difluoride, enol 125ff
Mass tensor 898
Matrices
  noble gases 1067, 1069
  nitrogen 79, 1067
  carbon monoxide 1067
Matrix isolation technique 545ff, 580, 582f, 603, 1067ff
Maxwell – Wagner dispersion 998, 1006, 1009, 1013
Mean association number 543
Mean field theories (Slater, Tagaki et al.) 1126f, 1129f, 1132f, 1134, 1137, 1143, 1144, 1148, 1153f, 1157
Mechanical anharmonicity 177, 204, 298, 303, 321, 614-42
Melting heat of water 1387
Membranes 558
  proton conductivity with 761ff
Membrane mechanism 558
Mesomorphism 19
Metastable proton states in H-bonds 279f, 755
Methanethiol CH_3SH 1097, 1098, 1103, 1230, 1236, 1243
Methanethiol CH_3SD 1230, 1238, 1243
Methanethiol dimer 108
Methanol (CH_3OH) 545, 546, 926ff, 927, 932, 1093, 1094-96, 1103, 1230, 1236, 1243ff, 1378, 1379
  complexes of 108ff, 143ff, 1230, 1234f, 1238
  protonated and deprotonated 694f, 704f
  trideuterated 926, 927, 1230, 1236, 1243ff
2-Methoxypyridine, adsorbed on silica 1278, 1279, 1282
Methyl alcohol (*see* Methanol)
Methylamine 1230, 1238ff, 1280, 1236, 1239

Methylchloroform 8
4-Methyl umbelliferone 16ff
Methylmercaptane (*see* Methanethiol)
Micelle building 1409
Microviscosity 1039
Microwave spectroscopy 115
Minerals 999, 1003
Minimum energy pathway 151
Minimum of dipole moment 541
Minimum of the specific heat of water 1389
Mixed association 3
Mixed hydrates 1419
Mixture models 1373
  of certain species 1373
  of water 1401
Molar surface tension 1391
Molecular clusters 1103
Molecular dynamics calculation 380, 902
Molecular dynamics studies
  of collective proton motion 1178ff
  with dielectric methods 938ff
  with inelastic neutron scattering 901, 915
  with nuclear magnetic resonance relaxation 1028ff
Molecular liquids 911
Molecules-in-molecules (MIM) method 67ff
Modulation method 18
Monomers of H_2O 1394
Monte-Carlo calculations 380f
Montmorillonite, adsorption on 1348ff
Morse curve 172
Morse potential 88ff, 615
Multimers 1068-70, 1075, 1080, 1084, 1089, 1090, 1092-95, 1098f
Multipole site trapping 1084, 1086, 1095
Multipole expansion 83

N–H distances 456, 466
N–H · · · O bonds 464–467
N–Methylacetamide 632
N–Methylaniline 631
N–Methylpivalamide 632
^{14}N quadrupole coupling
  NQR frequency 858
  and the strength of the NH · · · N bond 859
  and the N–H bond stretching frequency 859
  temperature dependence 860-862
  effect of deuteration 862
  theory of 859
  in TGS 860f
Neutron elastic incoherent scattering 908, 910f, 921, 923
Neutron inelastic scattering 892ff, 1169ff
  coherent 895, 902, 906, 908, 921, 928, 1169
  incoherent 893ff, 1177, 1179, 1181, 1190f
  of adsorbates 1305, 1333, 1347
Neutron diffraction 395, 459, 494, 502, 510, 1113, 1118, 1121, 1134
Neutron momentum transfer 893
Neutron scattering (*see also* Neutron elastic and neutron inelastic scattering) 597, 1113, 1123f, 1153, 1155
Nickel sulphate heptahydrate 930
Nickel sulphate hexahydrate 930
Nitriles, adsorption on oxides 1278, 1344, 1346ff
Nitrogen, adsorbed on silica 1276, 1280
Noble gases 1067
Noble-gas atoms, complexes 54, 93ff
Non-additivity of intermolecular energies 132ff, 136, 140, 142
Non-H-bonded liquids, correlation time for 1036
Non-H-bonded OH groups 1373, 1415
Non-linear effects 959
Non-stationary proton states 227
Normal coordinates 169, 171
Normal coordinate analysis 568
Normal modes of vibration, computer drawn 664, 666
Normal vapor pressure isotope effect 1240ff
Nuclear double resonance
  in the laboratory frame 853
  in the rotating frame 861
Nuclear magnetic resonance NMR
  adsorption line shape
    in case of an axially symmetric chemical shift tensor 876
    in case of a non-axially symmetric chemical shift tensor 875, 876
    dipolar line shape of an A_3B_2 ion 871
    of KH_2F_3 868
  chemical shifts 77, 81, 139

of H_2O 1398
of adsorbates 1299, 1319, 1339, 1244, 1346, 1347
deuterium pulsed 1328
in solids
wide line 867
high resolution 872
proton resonance shifts 1208
quadrupole interactions, spin–lattice relaxation 1113, 1120f, 1127, 1129f, 1132, 1137f, 1140, 1141, 1143, 1145-50, 1153-54, 1157-60
relaxation times
of adsorbed molecules 1305, 1306, 1311, 1316, 1327ff, 1336, 1347ff, 1391, 1394ff, 1398ff
wide line of adsorbates 1297, 1343, 1345ff
Number of non-H-bonded OH groups 1415
Nuclear quadrupole resonance (NQR) 834-848
Nuclear quadrupole interaction 1034
Nylon 558

Octet theory 5
o-hydroxyphenanthrene aldehydeanil 11
Olefins, adsorption on oxides 1346, 1348
Oleic acid 932
One-minimum potential 3
One-phonon approximation 897
Optical properties (*see also* Brillouin and Raman scattering, *and* Infrared spectra) 1113, 1139, 1151
^{17}O quadrupole coupling
dependence of the transition frequencies on the asymmetry parameter 852
and the strength of the O–H···O bond 850
effect of proton ordering 851
in ice, HDO and KH_2PO_4 850
Orbital basis set (*see also* Basis set) 32, 59ff
Order–disorder transition 1113f, 1115, 1119, 1122, 1126, 1128f, 1131, 1137, 1138f, 1141, 1144, 1150f, 1152-53, 1158-60
Organic hydrates 558
Orientation defects 1387, 1394
Oscillator function 173, 176
Overlap integral 37, 42, 47, 52ff, 56
Overtones 185, 205, 207, 616, 621, 625, 648
IR continuum 687
of HOD 1380
Oxalic acid dihydrate 555
Oxygen, adsorbed on silica 1276, 1280
Oxonium ion (*see* Hydronium ion)

π-bonded complexes 1102, 1103
π-electron systems, H-bonds to 104ff
$\pi^* \rightarrow n$ states 5, 9
Pair interacting potential 906
Pair natural orbitals 36
Pair potential of water 1373
Parabolic potential 921
Paraelectric phase 908, 920, 922, 924
Partial molar volume
of electrolyte solutions 1412
of salts 1413
of water 1413
Partial pressure ratio (*see also* Vapor pressure ratio) 1240ff
Partition coefficient 1408, 1411
Pentagon–dodecahedron 558f, 1416
Pentakaidecahedral cage of water molecules 1416
Peptide 91, 124
Perovskites, two–dimensional 1151
Perturbation theory
intermolecular 39, 99, 129, 137
second order 167, 177, 180, 204
Phase transitions 382-85
Phenol 942
Phenol + 3,6-aminoacridine 10
Phonon dispersion curves 906, 908
Phonon dispersion relations 902
Phosphate ion as H-bond acceptor 419, 718
Phosphatidyl serine 760
Phosphoric acid, polarizable H-bonds 718, 751
Point charge model 84
p-iso-octylphenol 1404
Poisson equation 83
pK_a
and acid water bonds 750
and formation of polarizable H-bonds 708
and potential well 736ff, 750
Plastic crystals 911

Plutonium oxide, adsorption on 1346
Polar solvents, influence on proton motion in H-bonds 248, 265f, 270, 272, 277ff, 281f, 284, 291f, 754ff
Polarity 940, 947, 951
Polarizability 37, 63, 98ff, 102
of H-bonds (*see also* Polarizable H-bonds) 180, 197, 247, 249ff, 253, 263ff, 285, 291, 688, 722ff
and IR continuum 731ff
Polarizable H-bonds
alcohols
with acids 694, 704
with bases 705
and continuum, (*see* IR continuum)
and ferroelectricity 748
and Grotthus conductivity 757f
asymmetrical 718ff, 738ff
biological systems 759ff
between adsorbed molecules 717ff
between dissolved molecules 707ff
DMSO with acids 694, 704, 735
$H_3O_2^-$ 639
$H_5O_2^+$ 689ff, 723ff, 750ff, 753ff
imidazole semi-protonated 705ff
interaction with environment 728ff, 753ff
salt effects on 744f
table of systems with 696-703
with crystals 747
Polarization 942, 945, 946
Polarization energy 44, 50, 59, 63, 91, 97ff
Polarization factor 897
Polarization of H-bonds in the first excited proton state 249, 264, 279, 286, 289, 291, 755f
Polarization of water by cations 748ff
Polarized IR spectra 586
Polyelectrolytes 687, 689ff
acidic 689ff
basic 693ff
Polyethylene oxide derivatives 556
Polyhistidine 761f
polarizable H-bonds 761f
proton conductivity 761f
Polynomial representation 173, 175
Polynucleotides 759f
Polypeptide 558
Positions, of hydrogens within bonds 397ff, 1113, 1116f, 1124, 1126, 1137-38, 1141, 1142
Potassium
bifluoride 932
dihydrogen arsenate 1117, 1119f, 1122f, 1129f, 1132, 1154, 1155, 1157
dihydrogen phosphate 362, 382f, 908, 912, 920-22, 924f, 932, 1115, 1116f, 1123f, 1132–1157
ferrocyanide trihydrate 1149, 1160
fluoride dihydrate 930
hexacyanoferrate (II)-trihydrate 930
trihydrogen selenite 1121, 1138, 1140, 1136
Potential barrier 222
and OO distance with $H_5O_2^+$ 194, 729
Potential energy surfaces 169, 172, 196, 199, 221, 228, 249, 338, 420, 570, 590, 596, 614ff, 692, 724ff
and environment of H-bonds 737, 754ff
and nature of acceptors 736
and polarizability of H-bonds 722ff
and wave number regions of continua 736f
calculated $H_5O_2^+$ 194, 723ff
with acid water bonds 750ff
Potential parameters 221, 238, 614ff
Predissociation theory of band width 589
Preference for angle 0° for H-bonds 403ff, 559
Pressure effects 1113, 1117, 1125, 1128, 1135–38, 1140, 1149, 1151, 1154, 1156–59
Primary hydrates of organic molecules 558
Probability density 223, 231
Probability distribution function 234
for a proton in a symmetrical H-bond 232
for a proton in a weakly unsymmetrical H-bond 233
Projection operators 228
Properties of water 1387
Propionic acid 533
Proteins 91, 124, 1013, 1015
Protomeric structures (*see also* Proton boundary structures) 219f, 223, 227f, 235, 241
Proton (*see also* Hydronium ion, Hydronium hydrates, $H_5O_2^+$ and $H_9O_4^+$) 687f, 689ff
boundary structures 692f, 706
catalytic activities and salt effects 744f
formation of easily polarizable H-bonds 684ff

fluctuation of 693, 753ff
tunneling (*see also* Tunneling of protons) 693
Proton acceptors 736f, 942
Proton affinities 113, 146ff
Protonation site 81
Proton chemical shift tensors
and the strength of the H-bond 879-880
in solid malonic acid 848-879
in oxalic acid dihydrate 874
Protonic conduction (*see also* Electrical (protonic) conductivity) 757ff, 761ff, 973ff
Proton dispersion forces 248, 254, 687, 729f
Proton donors 941
Proton donor–acceptor complexes
electronic effects on H-bond stretching frequencies 782-783
Proton hyperfine coupling tensors
in X-irradiated KH_2AsO_4 883
and the covalent character of the O–H···O bonds 884
and proton dynamics in O–H···O bonds 885
Proton intrabond jumps 1121f, 1123, 1127, 1130, 1132, 1134f, 1138, 1142, 1144, 1158
Proton jump mechanism of ice 979ff, 1403
Proton mobility (*see* Proton motion)
Proton motion in H-bonds (*see also* Proton intrabond jumps) 173, 217, 225, 231, 246ff, 692ff, 757ff, 761ff, 979ff
Proton states 175, 196, 221, 223, 720
Proton transfer 146ff, 219, 224, 235, 723, 946ff, 956
and dipole moment of H-bonds 946ff
and $H_5O_2^+$ dipole moment 195, 250, 723
with carboxylic acid N-base bonds 737, 949
in H-bonded adsorbates 718, 1299ff, 1301ff, 1311, 1313, 1318, 1328, 1336
mechanisms in ice 979ff, 1414
Proton wave functions 173f, 249f, 921
and polarizability of H-bonds 722f
Pseudodimers 1081
Pseudo spins 1181–1183
tunneling models 1127f, 1133
Purine bases 86, 698, 759f
Pyrazole 536, 698
Pyridine 10, 942
adsorbed on oxides 1273, 1274, 1277, 1281, 1282, 1286ff, 1289, 1301ff, 1334, 1344ff, 1348
adsorbed on silica 718, 740f, 1273, 1274, 1277, 1281, 1286ff, 1289, 1301ff
complexes of 131
bases 85
Pyroelectricity 1114, 1139, 1152
Pyrrole 631, 942
Pyrrolidone 532
Pyrromethene 124ff

Quadrupole coupling constant 1035, 1051f
definition 835
relation to electronic structure 835-37
deuteron QCC 838-42, 844
^{17}O QCC 850
^{35}Cl QCC 857
^{14}N QCC 859
^{75}As QCC 862
deuterium 1328
Quadrupole moment 101
Quadrupole–quadrupole interactions 1081
Quantum–mechanical tunneling 222, 228, 693
Quasielastic neutron scattering 893ff
Quasistationary state 228f
Quasiclassical WKB approximation 237, 240

Raman scattering 1124, 1131, 1134, 1145, 1156, 1157
continuum 689f
broadening of excitation line 732
Raman spectra, of adsorbates 1335, 1343, 1345, 1346
Raman transitions 179, 187
Rate of proton transfer 233, 236, 946ff
Reaction potential 271, 274
Rearrangement coordinate 220
Redlich–Kister equations 1228
Reduced masses 171
Reduplication of DNA 219
Relation
bond energy and wave number shift 574ff
H-bond length and wave number shift 574
spectroscopic shifts and enthalpy 1209ff
Relaxation mechanisms in ice 1414
Relaxation rate, nuclear magnetic 1030

Relaxation time T_1 of ^{13}C 824
Relaxation time of H_2O (*see also* Relaxation times) 1394, 1401
Relaxation times
  dielectric measurements 967ff, 971, 998
  inelastic neutron scattering 893
  nuclear magnetic resonance 1030
Reoccurrence time 224, 235
Reorientation time (*see also* Relaxation times) 1032, 1054
Resonance interaction 259, 287f, 291
Resonance interaction model 1073
Rigid glasses 621
Rigid ion model 906
Rochelle salt (RS) 1142f, 1158
Rocking 903
Rotational diffusion 915
Rotational freedom 905, 906, 926
Rubidium
  bisulfate 1146, 1159
  dihydrogen arsenate 1117, 1122, 1130, 1154, 1155
  dihydrogen phosphate 1116, 1117, 1121, 1130, 1155–57
  trihydrogen selenite 1139, 1140, 1136
Rutile, adsorption on 1335, 1343

Salt effects on polarizable H-bonds 745f
Salt-in effects, in water 1408
  on the solubility in water 1403
Salt-out effects, in water 1408
  on the solubility in water 1403
Salts, adsorption on 1350
Saturation effects 959
Scattering 396, 397
  function 895, 910, 915f
  law 915
Secondary hydration sphere 1413
Second moment of the NMR absorption line
  definition 867f
  in KH_2F_3 869
  of H_3O^+ ions 872
Second relaxation time of H_2O 1402
Second row elements, H-bonds to 107f, 112
Self association 3
  in alcohols 622, 626, 795
  in amides 632, 805
  in thiols 632
  carboxylic acid 806
  water 813
Self-consistent field (SCF) 31, 33, 57ff, 94ff, 100
SCF perturbation theory 50, 51
  for molecular crystals 141
SCF calculations $H_5O_2^+$ 118ff, 190ff, 723ff
Self-correlation function 896, 915
Self-diffusion coefficient 1031, 1050f
  of adsorbed molecules 1291, 1294, 1327, 1328, 1329, 1345f
Semi-carbazide hydrochloride 1150
Semi-clathrates 1418
Semi-empirical MO theories 37, 40, 70, 113f, 116f, 123, 129, 141f
Shear mode, spontaneous shear 1125, 1156
Shell model 906, 908
Shift of AH stretching band 569ff
Short H-bonds 426, 432, 503, 587
Silica-alumina, adsorption on 1346
Silica-chromia, adsorption on 1346
Silanol groups 633, 1266ff
  geminal 1271ff
  IR combination bands 1267
  IR fundamental 1266ff, 1270, 1271, 1274, 1275ff, 1282ff
  IR overtone bands 1267, 1290
  isolated 1271, 1272, 1274
  NMR of 1268, 1270
  number of 1269ff
  perturbation of 1274ff, 1296ff, 1303ff, 1319
  pK_a value of 1269, 1288
  vicinal 1271, 1274
Silver trihydrogen periodate 1136, 1141
Simultaneous excitation 622
Simultaneous proton motion (*see also* Proton motion in H-bonds) 220
Single scale enthalpy equations 1220
Site splitting 1095
Six-vertex problem 364, 382
Slater groups 1126, 1129, 1133-35, 1154, 1155, 1157
Slater rules 1178, 1181
Soap micelles 1419
Sodium bifluoride 909, 932

Sodium trihydrogen selenite 1121, 1136–38, 1140, 1157
Soft modes, ferroelectric mode 1113, 1115f, 1122-1125, 1128f, 1131f, 1134, 1140, 1154, 1156, 1158f
SO_2 gas hydrate 1416
Solids 936
Solubility in H_2O 1408
Solution calorimetry 1202
Solvation energy from vapor pressure measurements 1239
Solvent effects 821
  on band shift 572
  on polarizable H-bonds 737
  on proton transfer 737, 940ff
Space charge effects 967, 997
Specific effects in biochemistry 529
Specific heat 899, 901, 1120, 1126, 1129, 1137, 1139, 1147, 1151
  of H_2O 1401, 1388
Spin–lattice relaxation of water 1403
Spin–lattice relaxation time
  of deuterons in KD_2PO_4 847-848
  and deuteron dynamics 847-848
Spontaneous polarization 1114, 1117, 1119, 1120, 1126, 1128f, 1130, 1133, 1136, 1138f, 1142–44, 1146f, 1149, 1153–1159
Stark effect 180
Statistical mechanics approach 1373
Stereochemistry 71, 82, 401ff, 466, 529ff
Sterically hindered alcohols 626
Steric restrictions 1289ff, 1303
Stochastic
  function 591
  motions 893
  tunneling 1194
  variable 226
Stockmayer potential 92
Strong coupling theory 300, 305, 306ff, 338
Strong electric fields 959
Strontium chloride hexahydrate 930
Structure breakers 1408
Structure breaking effect 1055
Structural description of hydrogen bond networks 1116f, 1137, 1138-42, 1147-48, 1151-1152
Structure diffusion 692
  and Grotthus conductivity 757f
Structure makers 1408
Structure reinforcement 1057
Structure temperature of an electrolyte solution 1403
Substituted acetates 1150, 1160
Sulfate ion as H-bond acceptor 419
Supercooled water 1386
Surface
  energy of H_2O, alcohols 1391
  enthalpy H_σ of alcohols 1394
  tension 1391
Symmetrical double well potential (*see also* Double minimum potential well) 231f
Symmetrical H-bond 3, 171, 178, 231f, 426, 428, 503ff, 587, 596ff, 604, 605
  influence of environment on 275ff, 724ff, 754ff
Synthetic troegerite 1149

Tagaki groups 1126, 1130, 1132, 1134f, 1157
Tautomeric equilibria 11
T_c of alcohols 1385
T_c of water 1385
Temperature dependence of $\Delta\gamma$ 573
Terminal OH group 1095, 1099
Tetraaquahydrogen ion (*see* $H_9O_4^+$ *and* Hydronium hydrates) 1279, 1281
Tetrahydrofuran, adsorbed on silica 1279, 1281
Tetramers 1073–1075, 1080, 1089, 1092, 1094
Thermal expansion coefficient of H_2O 1401
Thermally stimulated polarization 995
Thermal motion, effect on bond lengths 400f
Thermodynamic analysis 115, 1157, 1158
Thermodynamic initial state 230
Thiols 632, 1097
Thiourea 1150
Thorium oxide, adsorption on 1345
Tight binding approximation 142
Time–dependent Schrödinger equation 223, 225
Time–energy uncertainty relation 239
Time evolution of a quantum system 223
Time-of-flight spectra 898
Time-of-flight technique 896, 904, 908, 918
Torsional frequency 904, 906, 912, 926
Torsional mode 1076, 1091, 1099

Torsional vibrations 901-8, 911
Total compressibility of H_2O 1401
Total energy 168
Total neutron scattering 925, 927
Transfer matrix 362, 367, 383
Transition moments 177, 198
Transition polarizability (*see also* Polarizable H-bonds) 177ff
Transition temperature 1179, 1193
Translational motions 898, 902, 903, 905, 906, 915
Translatory diffusion 911
Translatory jump 914
Translatory mode 901
Translatory peaks 904-6
Transmission coefficients 239
Transport theory 225
Transversal nuclear magnetic relaxation 1030
Transverse optical (TO) phonons 1123f, 1128, 1131, 1135, 1196
Triaquahydrogen ions 481, 674
Triaquaoxonium ion 481, 753ff, 766ff
  structure 510f
Trichloroacetic acid 10
  acetic acid, mixed cyclic dimer 117
Triethylamine 10ff
Trifluoroacetic acid 1099, 932
  cyclic dimer 116f
  mixed cyclic dimer with acetic acid 117
Trifluoroethanol 1096
Trifluoropropanol 1096
Trifurcated H-bond 408
Triglycine
  fluoberyllate 1144
  selenate 1144, 1158
  sulfate 1144, 1150, 1158, 1160
Trimers 537, 539, 1086, 1073-78, 1080, 1083
  cyclic 537ff, 1075, 1077, 1078f, 1094
Tunneling
  approximation 248, 251, 259ff, 263, 289, 723
  frequency 173, 199, 247, 279, 285, 288ff, 291f, 1183, 1193
  mode 1181, 1183, 1184, 1186, 1190, 1191-1193
  of protons 222, 247ff, 304, 349, 693, 1113, 1124, 1127f, 1131, 1132, 1135, 1143, 1154, 1155, 1157, 1178ff
  time 236, 238
Twisting 903
Two-constant model of alcohol and amine association 1235
Two-level approximation 240
Two-level system 230
Two-minimum potential (*see* Double-minimum potential well)
Two-state function of the vapor pressure ratio 1250

Ultrasonic absorption of H_2O 1400
Ultrasonic attenuation and velocity measurements 1120, 1125, 1130, 1131, 1160, 1172
Univalent redox reactions 10
Unrestricted Hartree–Fock method (UHF) 143

Valence electron distribution 416
Vanadium oxide, adsorption on 1344
Van der Waals forces 964
Van der Waals radii 28, 87, 401
Vaporization energies of variously deuterated alcohols, amines and methanethiols 1235ff
Vaporization heat of H_2O 1390
Vapor phase
  chemical shifts 819
Vapor pressure isotherms 1227, 1231ff, 1247
Vapor pressure isotope effect 1240ff
  concentration dependence of 1240
  frequency dependence of 1247ff
  temperature dependence of 1242
Vapor pressure ratios
  of chloroform and deuterochloroform on dilution with acetone 1256
  of highly diluted ammonia and trideuterated ammonia 1254
  of hydrogen fluoride and deuterium fluoride 1257
  of H_2O and D_2O, ice and water 1251
  of H_2O and D_2O on dilution with pyridine 1255
  of solid and liquid ammonia and trideuteroammonia 1254
  of variously deuterated carboxylic acids 1256

of variously deuterated dimethylamines 1244
of variously deuterated ethanols 1243
of variously deuterated methanols 1243
of variously deuterated methylamines 1240, 1242
Variational method 173
Velocity of sound 556
Vermiculite, adsorption on 1349
Very weak H-bonding 7
Vibrational
coupling 174, 196, 224, 731, 1082, 1096, 1098, 1099
frequencies of water 540
mode 169, 568
normal coordinates 221
splitting 1095
Virial coefficients, second 92

Water 415, 433, 748ff, 898, 911-913ff, 928, 929, 1049, 1070, 1086, 1087, 1103, 1368ff
H-bonds in clathrate hydrates 1415
H-bonds in electrolyte solutions 748ff, 1403ff
H-bonds in ice 1426ff
H-bonds in liquid water 1369ff
adsorbed on alumina 1333
cooperative effects 1335
coordinately bonded 1333
dielectric behavior 1335
electrical conductivity 1336
heat of adsorption 1333, 1335
neutron inelastic scattering 1333
NMR relaxation 1336
proton transfer 1336
Raman scattering 1335
adsorption on oxides 1285, 1303ff, 1333ff, 1343ff
adsorbed on silica 1285, 1303
cluster formation 1306ff
correlation function 1313
dielectric behavior 1313, 1314, 1315ff
electrical conductivity 1313ff
entropy of adsorption 1305, 1314
far IR 1308
frost damage 1317
heat capacity 1306, 1309ff
heat of immersion 1309
IR fundamental bands 1303, 1306
IR overtone and combination bands 1306ff
neutron inelastic scattering 1305, 1306
NMR relaxation 1305, 1306, 1311ff, 1316
nucleation of ice 1311, 1316, 1317
proton transfer 1311, 1313ff
computer simulation 372, 379-81
complexes of 108ff, 131, 143ff
continuum theories 375-79, 1368ff
dielectric constant 369, 381
dimer $(H_2O)_2$ 27, 46-48, 50, 55, 57, 59, 60, 62, 73ff, 78, 85, 109, 115, 129, 206
film 1005
intermolecular potential 368, 371, 375-81
lattice theories 371, 373, 375
molecule 34, 84, 89, 146
tetrahedral clusters 137f
of cristallization 902, 930
of oligomers 133ff
perturbation theories 379
Wave number shifts 172, 180, 213
and anharmonicity 644f
and bond energy 574f
and bond enthalpy 1209ff
and bond length 574
with polarizable H-bonds due to electrical fields 202, 724ff
Wave packet 220ff, 227
Waving 903
Wideline NMR and H-bonding 867
determination of proton–proton or proton–fluorine distances 867-872
in KHF_2 867
in KH_2F_3 868-871
in H_3O^+ ions 872
in $H_5O_2^+$ ions 872
Wien effect 966
Wilson equations 1228
Wilson parameters, physical interpretation 1229

X–N difference maps 416f
X–N maps 503

X-ray diffraction 395, 1113, 1118, 1138f, 1146, 1147, 1154, 1159
X-ray studies, adsorbed systems 1348, 1349

Zeolites, adsorption on 1346ff
Zero differential overlap (ZDO) 37, 52, 55
Zero phonon line 339
Zinc oxide, adsorption on 1345
Zirconium oxide, adsorption on 1344
Zwitterion 461

1407-in.
ЦНИИБ
БИБЛИОТЕКА

Volume II: Structure and Spectroscopy
CONTENTS: **Part B. Investigations on Structure and Stereochemistry.** 8. X-Ray and neutron diffraction studies of hydrogen bonded systems *(I. Olovsson and P.-G. Jönsson).* 9. Neutron diffraction studies of hydrogen bonding in α-amino acids *(Th.F. Koetzle and M.S. Lehmann).* 10. The hydrated proton in solids *(J.-O. Lundgren and I. Olovsson).* 11. The angular dependence of hydrogen bond interactions *(W.A.P. Luck).* **Part C. Vibrational and Resonance Spectroscopic Studies.** 12. Vibrational spectroscopy of the hydrogen bond *(D. Hadži and S. Bratos).* 13. Anharmonicity and hydrogen bonding *(C. Sandorfy).* 14. Spectroscopic studies of hydrated proton species, $H^+(H_2O)_n$, In crystalline compounds *(J.M. Williams).* 15. Easily polarizable hydrogen bonds - their interactions with the environment - IR continuum and anomalous large proton conductivity *(G. Zundel).* 16. Long wave length vibrational spectroscopy of hydrogen bonding *(W.G. Rothschild).* 17. High resolution nuclear magnetic resonance studies of hydrogen bonding *(E.E. Tucker and E. Lippert).* 18. Magnetic resonance studies of hydrogen bonding in solids *(R. Blinc).*

Volume III: Dynamics, Thermodynamics and Special Systems
CONTENTS: **Part D. Dynamics of Hydrogen Bonded Systems.** 19. Incoherent neutron scattering experiments on hydrogen bonded systems *(J.A. Janik).* 20. Dielectric properties of hydrogen bonded systems *(L. Sobczyk, H. Engelhardt and K. Bunzl).* 21. Nuclear magnetic relaxation in hydrogen bonded liquids *(H.G. Hertz and M.D. Zeidler).* **Part E. Matrix Isolation Technique.** 22. Matrix-isolation studies of hydrogen bonding *(H.E. Hallam).* **Part F. Investigations on Ferroelectrics with Hydrogen Bonds.** 23. Ferroelectric hydrogen bonded systems *(V.H. Schmidt).* 24. Coherent neutron scattering for observations on collective proton motions in systems of hydrogen bonds *(H. Stiller).* **Part G. Thermodynamics of Hydrogen Bonded Systems.** 25. Spectroscopic and calorimetric studies of hydrogen bonding *(A.D. Sherry).* 26. Vapor pressure studies on hydrogen and deuterium bonding *(H. Wolff).* **Part H. Hydrogen Bonding and Adsorption on Surfaces.** 27. Hydrogen bonds in systems of adsorbed molecules *(H. Knözinger).* **Part I. Water and Ice.** 28. Hydrogen bonds in liquid water *(W.A.P. Luck).* 29. The hydrogen bond in ice *(E. Whalley).*